University of Southampton
Faculty of Engineering, Science and Mathematics
School of Electronics and Computer Science

Near-Capacity MIMOs Using Iterative Detection

by

Mohammed H. El-Hajjar
BEng., MSc

A Doctoral thesis submitted in partial fulfilment of the requirements for the award of Doctor of Philosophy at the University of Southampton

28 September 2008

SUPERVISOR: *Professor Lajos Hanzo*
FREng, FIEEE, FIET, DSc
Chair of Telecommunications
School of Electronics and Computer Science
University of Southampton
Southampton SO17 1BJ
United Kingdom

This thesis is dedicated to

my beloved mother Afaf and father Hilmi

for their tremendous patience and care

with all my love and respect $\cdots$

UNIVERSITY OF SOUTHAMPTON

ABSTRACT

FACULTY OF ENGINEERING, SCIENCE AND MATHEMATICS
SCHOOL OF ELECTRONICS AND COMPUTER SCIENCE

Doctor of Philosophy

Near-Capacity MIMOs Using Iterative Detection

by

Mohammed El-Hajjar

In this thesis, Multiple-Input Multiple-Output (MIMO) techniques designed for transmission over narrowband Rayleigh fading channels are investigated. Specifically, in order to provide a diversity gain while eliminating the complexity of MIMO channel estimation, a Differential Space-Time Spreading (DSTS) scheme is designed that employs non-coherent detection. Additionally, in order to maximise the coding advantage of DSTS, it is combined with Sphere Packing (SP) modulation. The related capacity analysis shows that the DSTS-SP scheme exhibits a higher capacity than its counterpart dispensing with SP. Furthermore, in order to attain additional performance gains, the DSTS system invokes iterative detection, where the outer code is constituted by a Recursive Systematic Convolutional (RSC) code, while the inner code is a SP demapper in one of the prototype systems investigated, while the other scheme employs a Unity Rate Code (URC) as its inner code in order to eliminate the error floor exhibited by the system dispensing with URC. EXIT charts are used to analyse the convergence behaviour of the iteratively detected schemes and a novel technique is proposed for computing the maximum achievable rate of the system based on EXIT charts. Explicitly, the four-antenna-aided DSTS-SP system employing no URC precoding attains a coding gain of 12 dB at a BER of 10^{-5} and performs within 1.82 dB from the maximum achievable rate limit. By contrast, the URC aided precoded system operates within 0.92 dB from the same limit.

On the other hand, in order to maximise the DSTS system's throughput, an adaptive DSTS-SP scheme is proposed that exploits the advantages of differential encoding, iterative decoding as well as SP modulation. The achievable integrity and bit rate enhancements of the system are determined by the following factors: the specific MIMO configuration used for transmitting data from the four antennas, the spreading factor used and the RSC encoder's code rate.

Additionally, multi-functional MIMO techniques are designed to provide diversity gains, multiplexing gains and beamforming gains by combining the benefits of space-time codes, V-BLAST and beamforming. First, a system employing N_t=4 transmit Antenna Arrays (AA) with L_{AA} number of elements per AA and N_r=4 receive antennas is proposed, which is referred

to as a Layered Steered Space-Time Code (LSSTC). Three iteratively detected near-capacity LSSTC-SP receiver structures are proposed, which differ in the number of inner iterations employed between the inner decoder and the SP demapper as well as in the choice of the outer code, which is either an RSC code or an Irregular Convolutional Code (IrCC). The three systems are capable of operating within 0.9, 0.4 and 0.6 dB from the maximum achievable rate limit of the system. A comparison between the three iteratively-detected schemes reveals that a carefully designed two-stage iterative detection scheme is capable of operating sufficiently close to capacity at a lower complexity, when compared to a three-stage system employing a RSC or a two-stage system using an IrCC as an outer code. On the other hand, in order to allow the LSSTC scheme to employ less receive antennas than transmit antennas, while still accommodating multiple users, a Layered Steered Space-Time Spreading (LSSTS) scheme is proposed that combines the benefits of space-time spreading, V-BLAST, beamforming and generalised MC DS-CDMA. Furthermore, iteratively detected LSSTS schemes are presented and an LLR post-processing technique is proposed in order to improve the attainable performance of the iteratively detected LSSTS system.

Finally, a distributed turbo coding scheme is proposed that combines the benefits of turbo coding and cooperative communication, where iterative detection is employed by exchanging extrinsic information between the decoders of different single-antenna-aided users. Specifically, the effect of the errors induced in the first phase of cooperation, where the two users exchange their data, on the performance of the uplink in studied, while considering different fading channel characteristics.

Acknowledgements

Numerous people supported and helped me during the development of my thesis. A few words' mention here cannot adequately capture all my appreciation.

First and foremost, I am truly and deeply indebted to my supervisor Professor Lajos Hanzo, for his exceptional supervision, insightful guidance and overall for his supreme friendship. His utmost kindness and encouragement have greatly benefited me and he managed to cultivate in me the desire to be a good researcher through his enthusiasm and perseverance in research. I can never forget the patience Lajos explained the problems and listened to my un-mature ideas, the way he worked so hard and carefully to develop our research ideas so that we submit high quality papers. I have learned from Prof. Hanzo not only the views to see and solve the problem, but also his attitude of conducting high quality research and his way of living. All I want to say is I cannot ask for any more from a supervisor and I am very glad to have such a chance to work with such a good researcher and excellent supervisor.

I am also grateful to Dr. Lie-Liang Yang, Professor Sheng Chen, Dr. Soon (Michael) Ng and Dr. Robert Maunder for the numerous discussions I had with them and for their invaluable comments and suggestions. I also gratefully acknowledge all my former and present colleagues in the communications research group for creating such a wonderful work environment and for the numerous useful discussions. Special thanks to my colleague Dr. Osamah Alamri for his invaluable support and encouragement, his utmost kindness and overall for his friendship. I would also like to express my gratitude to Dr. Salam Zummo and all my colleagues whose names appear in my list of publications.

The Financial support of Vodafone under the auspices of the Dorothy Hodgkin Postgraduate Award as well as that of the School of Electronics and Computer Science in the University of Southampton is gratefully Acknowledged.

My past four years in Southampton wouldn't nearly be as much enjoyable without my incredible friends, to whom I owe all of my good memories from this time. I thank each and every one of them for their trust and friendship.

Last but not least, I would like to dedicate this thesis to my Family. My parents, who, from the day I came to the world, have provided me with tremendous support and constant encouragement. My mother with her love and prayers backed me up and helped me to reach my goal. My father taught me the respect of science and encouraged me to seek knowledge. The love and support of my three sisters Hiba, Aya and Lina are always the greatest inspiration to me, and without these, it would not have been possible for me to complete this work.

To all these wonderful people, many thanks again.

DECLARATION OF AUTHORSHIP

I, **Mohammed El-Hajjar**,

declare that the thesis entitled

Near-Capacity MIMOs Using Iterative Detection

and the work presented in the thesis are both my own, and have been generated by me as the result of my own original research. I confirm that:

- this work was done wholly or mainly while in candidature for a research degree at this University;
- where any part of this thesis has previously been submitted for a degree or any other qualification at this University or any other institution, this has been clearly stated;
- where I have consulted the published work of others, this is always clearly attributed;
- where I have quoted from the work of others, the source is always given. With the exception of such quotations, this thesis is entirely my own work;
- I have acknowledged all main sources of help;
- where the thesis is based on work done by myself jointly with others, I have made clear exactly what was done by others and what I have contributed myself;
- parts of this work have been published as: [1–22].

Signed: *M. El-Hajjar*
Date: 28 September 2008

List of Publications

Book:

1. Lajos Hanzo, Osamah Alamri, **Mohammed El-Hajjar** and Nan Wu, "Advanced Space-Time Coding: Near-Capacity Sphere Packing, Multi Functional MIMOs and Cooperative Space-Time Processing", John-Wiley & Sons IEEE-Press (in preparation).

Journal Papers:

1. **Mohammed El-Hajjar** and Lajos Hanzo, "Layered Steered Space-Time Codes and Their Capacity", Electronics Letters, vol. 43, issue 12, pp. 680-682, June 2007.

2. **Mohammed El-Hajjar**, Bin Hu, Lie-Liang Yang and Lajos Hanzo, "Coherent and Differential Downlink Space-Time Steering Aided Generalised Multicarrier DS-CDMA", IEEE Transactions on Wireless Communications, vol. 6, issue 11, pp.3857-3863, November 2007.

3. **Mohammed El-Hajjar**, Osamah Alamri, Soon Ng and Lajos Hanzo, "Turbo Detection of Precoded Sphere Packing Modulation Using Four Transmit Antennas For Differential Space-Time Spreading", IEEE Transactions on Wireless Communications, vol. 7, issue 3, pp. 943-952, March 2008.

4. **Mohammed El-Hajjar**, Osamah Alamri, Jin Wang, Salam Zummo and Lajos Hanzo, "Layered Steered Space-Time Codes Using Multi-dimensional Sphere-Packing Modulation", to appear in IEEE Transactions on Wireless Communications.

5. Noor Othman, **Mohammed El-Hajjar**, Osamah Alamri and Lajos Hanzo, "Iterative AMR-WB Source and Channel-Decoding of Differential Space-Time Spreading Assisted Sphere Packing Modulation", to appear in IEEE Transactions on Vehicular Technology.

6. **Mohammed El-Hajjar**, Osamah Alamri, Robert Maunder and Lajos Hanzo, "Layered Steered Space-Time Spreading Aided Generalised MC DS-CDMA", submitted to IEEE Transactions on Vehicular Technology.

7. **Mohammed El-Hajjar** and Lajos Hanzo, "Diversity and Multiplexing Tradeoffs in Multi-functional MIMO Systems", submitted to IEEE Communications Magazine.

8. Lajos Hanzo, **Mohammed El-Hajjar** and Osamah Alamri, "Near-Capacity Wireless Communications in The MIMO Era", to be submitted to Proceedings of the IEEE.

Conference Papers:

1. **Mohammed El-Hajjar**, Osamah Alamri and Lajos Hanzo, "Differential Space-Time Spreading using Iteratively Detected Sphere Packing Modulations and Two Transmit Antennas", in Proceeding of IEEE Wireless Communications and Networking Conference, vol.3, pp. 1664-1668, April 2006.

2. **Mohammed El-Hajjar**, Osamah Alamri and Lajos Hanzo, "Differential Space-Time Spreading using Four Transmit Antennas and Iteratively Detected Sphere Packing Modulations", in Proceedings of the IEEE ninth International Symposium on Spread Spectrum Techniques and Applications, pp. 322-326, August 2006.

3. **Mohammed El-Hajjar**, Osamah Alamri and Lajos Hanzo, "Adaptive Differential Space-Time-Spreading-Assisted Turbo-Detected Sphere Packing Modulation", in the Proceedings of the IEEE Wireless Communications and Networking Conference, pp. 645-649, March 2007.

4. **Mohammed El-Hajjar**, Salam Zummo and Lajos Hanzo, "Near-Instantaneously Adaptive Cooperative Schemes Based on Space-Time Block Codes and V-BLAST", in Proceedings of the IEEE Vehicular Technology Conference (VTC2007-Spring), pp. 2200-2204, April 2007.

5. Noor Othman, **Mohammed El-Hajjar**, Osamah Alamri and Lajos Hanzo, "Soft-Bit Assisted Iterative AMR-WB Source-Decoding and Turbo-Detection of Channel-Coded Differential Space-Time Spreading Using Sphere Packing Modulation", in Proceedings of the IEEE Vehicular Technology Conference (VTC2007-Spring), pp. 2010-2014, April 2007.

6. **Mohammed El-Hajjar**, Ronald Y. S. Tee, Hu Bin, Lie-Liang Yang and Lajos Hanzo, "Downlink Steered Space-Time Spreading Assisted Generalised Multicarrier DS-CDMA Using Sphere-Packing-Aided Multilevel Coding", in Proceedings of the IEEE Vehicular Technology Conference (VTC2007-Fall), pp.472-476, September 2007.

7. **Mohammed El-Hajjar**, Robert G. Maunder, Osamah Alamri, Soon X. Ng and Lajos Hanzo, "Iteratively Detected Irregular Variable Length Coding and Sphere-Packing Modulation Aided Differential Space-Time Spreading", in Proceeding of the IEEE Vehicular Technology Conference (VTC2007-Fall), pp. 1238-1242, September 2007.

8. **Mohammed El-Hajjar**, Osamah Alamri and Lajos Hanzo, "Layered Steered Space-Time Codes Using Iterative Detection", in Proceedings of the IEEE Workshop on Signal Processing Systems (SIPS), pp. 35-39, October 2007.

9. Nazar Sahal, **Mohammed El-Hajjar** and Lajos Hanzo, "Downlink Steered Space-Time Spreading For Multi-Carrier Transmission Over Frequency Selective Channels", in Proceeding of the IEEE Vehicular Technology Conference (VTC-2008 Spring), pp. 943-947, May 2008.

10. Raja Ali Riaz, **Mohammed El-Hajjar**, Qasim Z. Ahmed, Soon Xin Ng, Sheng Chen and Lajos Hanzo, "Convergence Analysis of Iteratively Detected Time Hopping and DS-CDMA Ultrawide Bandwidth Systems by EXIT Charts", in Proceeding of the IEEE Vehicular Technology Conference (VTC-2008 Spring), pp. 1127-1131, May 2008.

11. Noor Othman, **Mohammed El-Hajjar**, Anh Q. Pham, Osamah Alamri, Soon Xin Ng and Lajos Hanzo, "Over-Complete Source-Mapping Aided AMR-WB MIMO Transceiver Using Three-Stage Iterative Detection", in Proceeding of the IEEE International Conference on Communications (ICC), pp. 751-755, May 2008.

12. Tanh Dang Nguyen, **Mohammed El-Hajjar**, Lie-Liang Yang and Lajos Hanzo, "Systematic Luby Transform coded V-BLAST System", in Proceeding of the IEEE International Conference on Communications (ICC), pp. 775-779, May 2008.

13. Lei Xu, **Mohammed El-Hajjar**, Osamah Alamri, Sheng Chen and Lajos Hanzo, "Iteratively Detected Sphere Packing Modulated OFDM: An EXIT Chart Perspective", in Proceeding of the IEEE International Conference on Communications (ICC), pp. 631-635, May 2008.

14. Nasruminallah, **Mohammed El-Hajjar**, Noor S. Othman, Anh P. Quang and Lajos Hanzo, "Over-Complete Mapping Aided, Soft-Bit Assisted Iterative Unequal Error Protection H.264 Joint Source and Channel Decoding", in Proceedings of the IEEE Vehicular Technology Conference (VTC-2008 Fall), September 2008.

15. Raja A. Riaz, **Mohammed El-Hajjar**, Qasim Z. Ahmed, Soon X. Ng, Sheng Chen and Lajos Hanzo, "EXIT Chart Aided Design of DS-CDMA UltraWideBand Systems Using Iterative Decoding", in Proceedings of the IEEE Vehicular Technology Conference (VTC-2008 Fall), September 2008.

16. **Mohammed El-Hajjar**, Osamah Alamri and Lajos Hanzo, "Distributed Turbo Coding in the Presence of Inter-User Channel Impairment", submitted to IEEE Vehicular Technology Conference (VTC-2009 Spring).

17. **Mohammed El-Hajjar**, Osamah Alamri, Robert G. Maunder and Lajos Hanzo, "Iteratively Detected Generalised MC DS-CDMA Using Layered Steered Space-Time Spreading", submitted to IEEE International Conference on Communications 2009.

18. Noor Othman, **Mohammed El-Hajjar**, Osamah Alamri, Soon X. Ng and Lajos Hanzo, "Over-Complete Source-Mapping Aided AMR-WB Using Iteratively Detected Differential Space-Time Spreading", submitted to IEEE Vehicular Technology Conference (VTC-2009 Spring).

19. Noor Othman, **Mohammed El-Hajjar**, Osamah Alamri, Soon X. Ng and Lajos Hanzo, "Three-Stage Iterative Detection of a Precoded AMR-WB for Speech MIMO Transceiver", submitted to IEEE Vehicular Technology Conference (VTC-2009 Spring).

Contents

List of Symbols

General notation

- The superscript * is used to indicate complex conjugation. Therefore, a^* represents the complex conjugate of the variable a.
- The superscript ^{T} is used to indicate matrix transpose operation. Therefore, $\mathbf{a}^T$ represents the transpose of the matrix $\mathbf{a}$.
- The superscript † is used to indicate complex conjugate transpose operation. Therefore, $\mathbf{a}^\dagger$ represents the complex conjugate transpose of the matrix $\mathbf{a}$.
- The notation $\tilde{x}$ represents the estimate of x.

Special symbols

$a_{l,i}$: The ith coordinate of the lth SP symbol.

$\mathcal{A}$: The area under an EXIT curve.

B: The number of binary bits corresponding to a constellation symbol.

B_{sp}: The number of binary bits corresponding to a sphere packing constellation symbol.

$\mathbf{b}$: The input bit stream.

b_i: The binary bit at position i in the bit stream $\mathbf{b}$.

$\mathbf{c}$: The outer channel coded bit stream.

$\bar{\mathbf{c}}$: The spreading code.

$\mathbf{C}_l$: The sphere packing signal mapping to the DSTS signal.

C: The channel capacity in [bits/sym].

$\mathbb{C}^n$: The n-dimensional complex space.

d: The received and despread DSTS signal.

D: The constellation dimension.

D_{int}: The depth of the random interleaver.

$E[k]$: The expected value of a variable k.

$E[k|a]$: The expected value of a variable k given variable a.

E_b: The bit energy.

E_s: The symbol energy.

E_{total}: The total energy of a constellation set.

f_D: The normalised Doppler frequency.

f_d: The Doppler frequency.

G: The feedforward generator polynomial of a recursive systematic convolutional code.

G_r: The feedback generator polynomial of a recursive systematic convolutional code.

h_i: The channel impulse response from transmit antenna i for single-receive antenna systems.

$h_{i,j}$: The channel impulse response from transmit antenna i to receive antenna j.

$\mathbf{H}$: The channel matrix whose jith element is $h_{i,j}$.

I: The number of decoding iterations.

$I_{k,a}(\mathbf{b})$: The mutual information associated with the *a apriori* information of the bit stream $\mathbf{b}$ in decoder k.

$I_{k,e}(\mathbf{b})$: The mutual information associated with the *extrinsic* information of the bit stream $\mathbf{b}$ in decoder k.

$\mathbf{I}_n$: The identity matrix of size $(n \times n)$.

$Imag\{.\}$: The imaginary part of a complex number.

K: The constraint length of a recursive systematic convolutional code.

L: The size of the legitimate modulation constellation $\mathbf{S}$.

L_{AA}: The number of elements per antenna array.

$L(\mathbf{b})$: The LLR of the bit stream $\mathbf{b}$.

$L_{k,a}(.)$: The *a priori* LLR values of the decoder k.

$L_{k,e}(.)$: The *extrinsic* LLR values of the decoder k.

$L_{k,p}(.)$: The *a posteriori* LLR values of the decoder k.

n: The additive White Gaussian noise.

n_I: The in-phase additive White Gaussian noise.

n_Q: The quadrature-phase additive White Gaussian noise.

N_0: The noise power spectral density.

N_t: The number of transmit antennas.

N_r: The number of receive antennas.

$P\{.\}$: The probability density function.

$p\{A|B\}$: The probability density function of variable A given variable B.

$\mathbf{Q}$: The orthonormal basis matrix for the left null space of a channel matrix $\mathbf{H}$.

r_t^i: The received signal at time instance t at receive antenna i.

R: The coding rate.

$R_{DSTS-SP}$: The coding rate of the DSTS-SP scheme.

$Re\{.\}$: The real part of a complex number.

$\mathbb{R}^n$: The n-dimensional real-valued Euclidean space.

$\mathbf{s}$: The sphere packing symbol.

$\mathbf{S}$: The legitimate SP constellation set.

$\mathbf{S}_0^k$: The subset of the legitimate constellation set $\mathbf{S}$ that contains all symbols having $b_k = 0$.

$\mathbf{S}_1^k$: The subset of the legitimate constellation set $\mathbf{S}$ that contains all symbols having $b_k = 1$.

T_s: The symbol duration.

$T_{sp}\{.\}$: The transfer function from SP to complex signals.

$T_{sp}^{-1}\{.\}$: The inverse transfer function from complex signals to SP signal.

v_t: The differentially encoded symbol at time instant t.

W: The channel bandwidth.

$\mathbf{w}_{nm}$: The L_{AA}-dimensional weight vector for the mth beamformer antenna array and the nth receive antenna.

$\mathbf{W}$: The diagonal transmit antenna array weight matrix.

x_t: The modulated symbol at time instant t.

y_t^i: The transmitted signal at time instance t from transmit antenna i.

Π: The interleaver.

Π^{-1}: The deinterleaver.

σ_n^2: The complex AWGN variance.

η: The bandwidth efficiency in [bits/sec/Hz].

η_{max}: The maximum achievable bandwidth efficiency in [bits/sec/Hz].

χ_i^2: The Chi-square distributed random variable having i degrees of freedom.

λ: The carrier's wavelength.

ψ_{nm}: The nmth link direction of arrival.

Chapter 1

Introduction

Since Shannon quantified the capacity of a wireless communications system in 1948 [23], the researchers endeavoured to devise high-speed, high-quality wireless communication systems exhibiting both high bit rate and a low error rate. The hostile wireless channel characteristics make it challenging to simultaneously accomplish both objectives.

The demand for high-rate wireless communication systems driven by cellular mobile and wireless multimedia services has been rapidly increasing worldwide. However, the available radio spectrum is limited and the associated bandwidth demands cannot be readily met without a significant increase in the achievable spectral efficiency [24]. Furthermore, the system capacity is interference limited and hence cannot be readily increased by simply increasing the transmitted power. Therefore, against the explosive expansion of the Internet and the continued dramatic increase in demand for high-speed multimedia wireless services, there is an urging demand for flexible and bandwidth-efficient transceivers. Advances in coding made it feasible to approach Shannon's capacity limit in systems equipped with a single antenna [25–27], but fortunately these capacity limits can be further extended with the aid of multiple antennas. Hence, their employment in most future communication systems seems to be inevitable [28, 29]. Multiple-Input Multiple-Output (MIMO) wireless communication systems have recently attracted considerable attention as one of the most significant technical breakthroughs in modern communications [30].

Recent advances in wireless communications have increased both the attainable throughput and reliability of systems communicating over wireless channels. The main driving force behind the advances in wireless communications is the promise of seamless global mobility and ubiquitous accessibility, while meeting the following challenges [30]: supporting a high data rate, maintaining the required quality of service, supporting high vehicular speeds, tolerating the interference imposed by other users, while maintaining privacy and security. For exam-

ple, the requirement of tetherless operation results in the use of batteries, which necessitates the employment of power-efficient algorithms to extend the battery life. Another important challenge is the co-channel interference caused by other users, which can be counteracted by sophisticated transceiver designs. Additionally, the available bandwidth is limited, while there is a demand for high data rates and low error rates.

Therefore, in this dissertation we present several wireless transceiver designs that satisfy the data rate and performance expectations for transmission over wireless channels. We first design a Differential Space-Time Spreading (DSTS) scheme that is capable of achieving a diversity gain and hence resulting in an improved BER performance, while at the same time eliminating the potentially high-complexity MIMO channel estimation. Additionally, we propose a near-capacity DSTS scheme using iterative detection. Then we develop two different multi-functional MIMO schemes that are capable of simultaneously providing a high throughput and a good performance, which are capable of benefitting from employing a higher number of antennas than the DSTS scheme. Finally, in order to mitigate the effects of large-scale shadow fading on the performance of MIMO systems, we design a cooperative communication system that is capable of providing substantial diversity-, throughput- as well as coding-gains, while using single-antenna-aided mobile stations.

1.1 The Wireless Channel

The wireless channel imposes fundamental limitations on the attainable performance of wireless communication systems [31]. The key characteristics of the wireless channel in contrast to the Gaussian channel are small-scale fading and multi-path propagation [31], which is based on the fact that there are many different paths between the transmitter and the receiver, as exemplified in Figure 1.1. This results in the destination receiving different versions of the same transmitted signal, where these received versions experience different path loss and phase rotations [30]. The received versions of the transmitted signal randomly combine either constructively or destructively at the receiver, resulting in substantial fluctuation of both the amplitude and phase of the resultant received signal [27].

There are two general aspects characterising a wireless channel. The first is referred to as large-scale fading that corresponds to the effect of the channel on the signal power over large distances, which is directly related to the path loss and shadow fading. The other aspect is the small-scale fading that is characteristic of the rapid fluctuation in the amplitude and phase of the signal. The main mechanisms affecting the transmitted signal's propagation can generally be considered to be reflection, diffraction and scattering, as shown in Figure 1.1. The

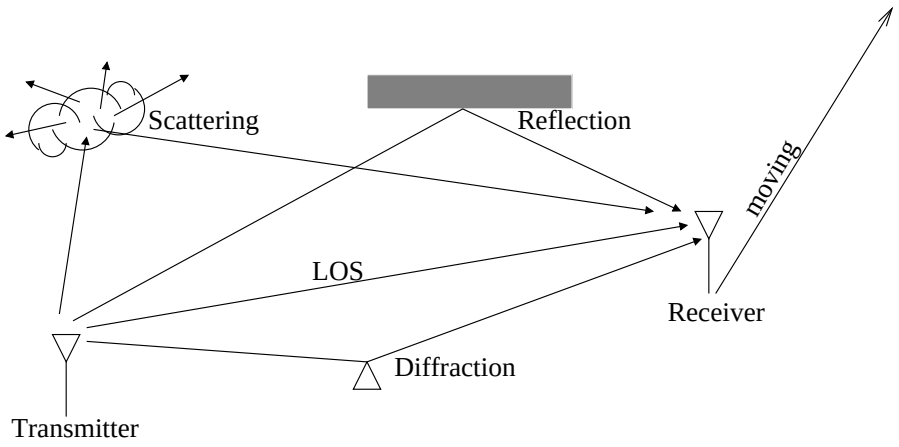

Figure 1.1: An example of different paths in a wireless channel, © Jafarkhani [30], 2005.

direct path between the transmitter and receiver of Figure 1.1 is referred to as the Line Of Sight (LOS) path, where the received signal propagating through the LOS path is typically the strongest signal. The transmitted signal can also be reflected by objects that are larger than its wavelength, before reaching the receiver. On the other hand, electromagnetic waves can also be diffracted by the sharp edges of objects having irregular surfaces. Finally, as shown in Figure 1.1, scattering results in several copies of the wave propagating in different directions. These factors result in attenuation of the amplitude as well as of the phase of the signal, when the received signals are superimposed at the receiver. Additionally, when the transmitter or receiver is moving, the resultant channel becomes a time varying channel, where the amplitude and phase attenuation fluctuate with time. Other factors that influence the small-scale fading include the velocity of both the mobile as well as of the surrounding objects and the transmission bandwidth of the signal [31].

1.2 Multiple-Input Multiple-Output Systems

A MIMO system employs $N_t \geq 1$ transmit antennas and $N_r \geq 1$ receive antennas. A wireless system employing a MIMO scheme transmits the signals $\mathbf{C}_{t,n}, n = 1, 2, \ldots, N_t$, simultaneously from the N_t transmit antennas at time instant t. Each signal transmitted from each of the N_t antennas propagates through the wireless channel and arrives at each of the N_r receive antennas. In a wireless system equipped with N_r receive antennas, each received signal is constituted by a linear superposition of the faded versions of the transmitted signal perturbed by noise. Of particular interest is the specific propagation scenario, where the individual channels between given pairs of transmit and receive antennas may be accurately modelled by independent Rayleigh fading channels. As a result, the signal corresponding to every transmit antenna has a distinct spatial signature, i.e. impulse response, at a receive antenna. The independent

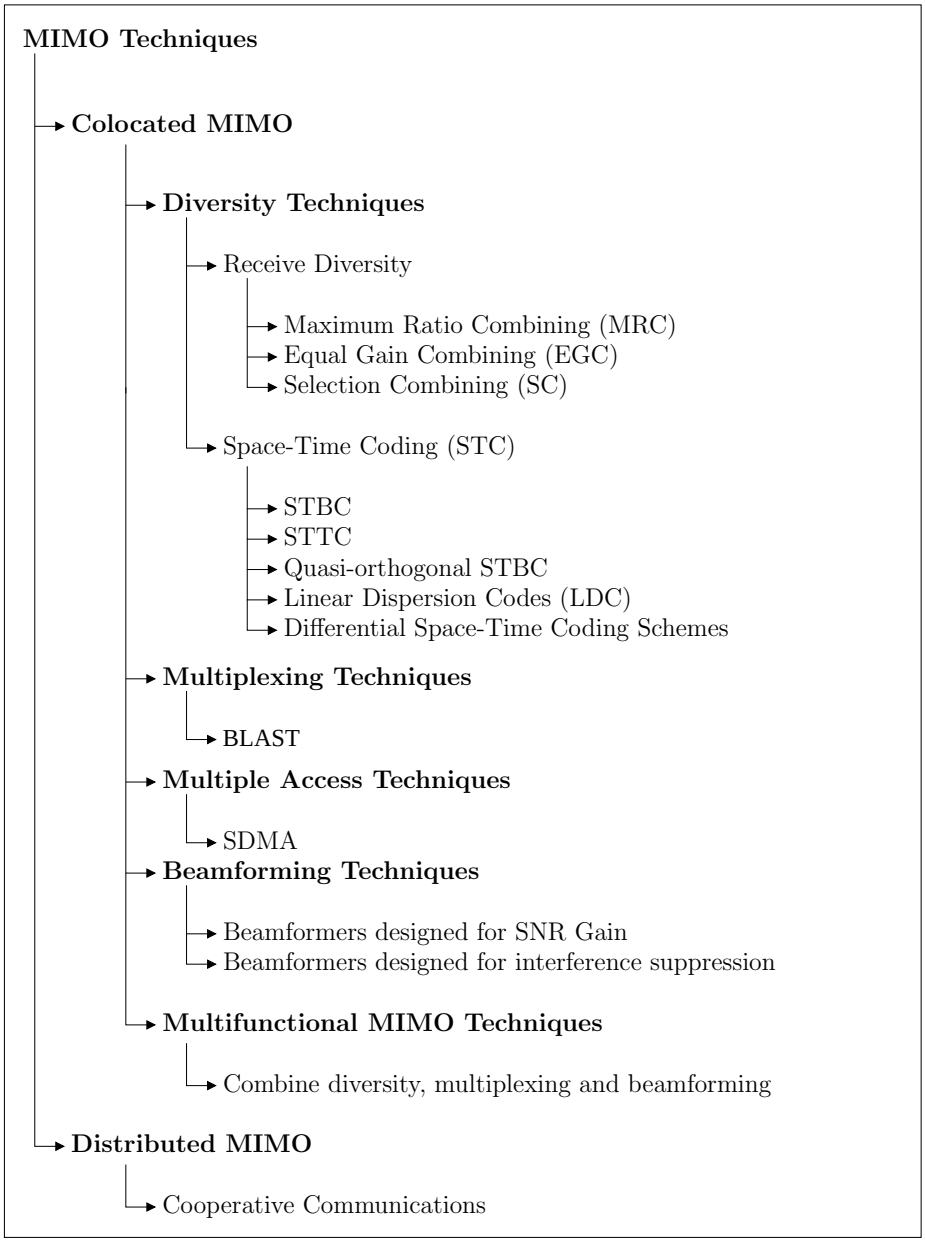

Figure 1.2: Classification of MIMO techniques.

Rayleigh fading model can be assumed in MIMO channels, where the antenna spacing is considerably higher than the carrier's wavelength. As a result, the signal corresponding to every transmit antenna has a distinct spatial signature at a receive antenna.

The information-theoretic aspects of MIMO systems were considered by several authors [32–34]. It was demonstrated that MIMO systems exhibit capacity gains in comparison to the employment of a single antenna at both the transmitter and receiver. In [33,34], it was demonstrated that the capacity of a MIMO system increases linearly with the number of transmit antennas when communicating over an independent and identically distributed (i.i.d.) flat Rayleigh fading channel, provided that the number of receive antennas is equal to or greater than the number of transmit antennas. Explicitly, information theoretic studies [34] have shown

that in contrast to the logarithmic Shannon-Hartley law [35], MIMO schemes increase the systems' capacity linearly with the number of transmit antennas. Hence, when the extra power is assigned to additional antennas, it may be argued that the capacity increases also linearly with the transmit power.

The classification of different MIMO systems is summarised in Figure 1.2, which can be classified as colocated MIMOs and distributed MIMOs. The colocated MIMO can be also categorised as diversity techniques, multiplexing techniques, multiple access methods, beamforming as well as multi-functional MIMO techniques as shown in Figure 1.2. The concept of distributed MIMOs is also often referred to as cooperative communications [36, 37].

1.2.1 Colocated MIMO Techniques

MIMO systems exhibit higher capacity than single-antenna-aided systems. Multiple antennas can be used to provide diversity gains and hence a better BER performance or multiplexing gains, in order to attain a higher throughput. Additionally, multiple antennas can be used at the transmitter or receiver in order to attain a beamforming gain. On the other hand, multiple antennas can be employed in order to attain diversity gains, multiplexing gains as well as beamforming gains as shown in Figure 1.2. The terminology of colocated MIMOs refers to the systems, where the multiple antennas are located at the same transmitter or receiver station. In the sequel, we give an overview of the family of multiple antennas, when used for achieving diversity, multiplexing or beamforming gains.

1.2.1.1 Diversity Techniques

Communication in the presence of channel fading has been one of the grand research challenges in recent times. In a fading channel, the associated severe attenuation often result in decoding errors. A natural way of overcoming this problem is to allow the receiver to have several replicas of the same transmitted signal, while assuming that at least some of them are not severely attenuated. This technique is referred to as diversity, where it is possible to attain diversity gains by creating independently fading signal replicas in the time, frequency or spatial domain.

Spatial diversity can be attained by employing multiple antennas at the transmitter or the receiver. Multiple antennas can be used to transmit and receive the same information sequence in order to achieve diversity and hence to obtain an improved BER performance. A simple spatial diversity technique, which does not involve any loss of bandwidth, is constituted by the employment of multiple antennas at the receiver. In case of narrowband frequency-flat fading,

Year	Author(s)	Contribution
1959	Brennan [38]	introduced and provided analysis for the three combining techniques: selection combining, maximum ratio combining and equal gain combining.
1991	Wittneben [39]	proposed a bandwidth-efficient transmit diversity technique, where different base stations transmit the same signal.
1993	Wittneben [40]	proposed a modulation diversity scheme in a system equipped with multiple transmit antennas.
	Seshadri *et al.* [41]	proposed a transmit diversity scheme that was inspired by the delay diversity design of Wittneben [40].
1994	Winters [42]	proved that the diversity advantage of the scheme proposed in [39] is equal to the number of transmit antennas.
1996	Eng *et al.* [43]	Compared several diversity combining techniques in a Rayleigh fading transmission with coherent detection and proposed a new second order selection combining technique.
1998	Alamouti [44]	discovered a transmit diversity scheme using two transmit antennas with simple linear processing at the receiver.
	Tarokh *et al.* [45]	proposed a complete study of design criteria for maximum diversity and coding gains in addition to the design of space-time trellis codes.
1999	Tarokh *et al.* [46, 47]	generalised Alamouti's diversity scheme [44] to more than two transmit antennas.
	Guey [48]	derived the criterion for designing the maximum transmit diversity gain.
2001	Hochwald *et al.* [49]	proposed the twin-antenna-aided space-time spreading scheme.
	Jafarkhani *et al.* [50]	designed rate-one STBC codes which are quasi-orthogonal and provide partial diversity gain.
2002	Hassibi *et al.* [51]	proposed the LDCs that provide a flexible trade-off between space-time coding and spatial multiplexing.
	Stoica *et al.* [52]	compared the performance of STBC when employing different estimation/detection techniques and proposed a blind detection scheme dispensing with the pilot symbols transmission for channel estimation.

Table 1.1: Major coherent spatial diversity techniques (Part 1).

Year	Author(s)	Contribution
2003	Wang *et al.* [54]	derived upper bounds for the rates of complex orthogonal STBCs.
	Su *et al.* [55]	introduced the concept of combining orthogonal STBC designs with the principle of sphere packing.
2005	Zhang *et al.* [56]	derived the capacity and probability of error expressions for PSK/PAM/QAM modulation with STBC for transmission over Rayleigh-, Ricean- and Nakagami-fading channels.
2006	Liew *et al.* [57]	studied the performance of STTC and STBC in the context of wideband channels using adaptive orthogonal frequency division multiplex modulation.
2007	Alamri *et al.* [58]	modified the SP demapper of [55] for the sake of accepting the *a priori* information passed to it from the channel decoder as extrinsic information.
2008	Luo *et al.* [59]	combined orthogonal STBCs with delay diversity and designed special symbol mappings for maximising the coding advantage.

Table 1.2: Major coherent spatial diversity techniques (Part 2).

the optimum combining strategy in terms of maximising the SNR at the combiner output is Maximum Ratio Combining (MRC) [26, 38, 53]. Additionally, other combining techniques have been proposed in the literature, as shown in Figure 1.2, including Equal Gain Combining (EGC) [38] and Selection Combining (SC) [26]. All the three combining techniques are said to achieve full diversity order, which is equal to the number of receive antennas [43].

On the other hand, the idea of transmit diversity corresponds to the transmission of the same signal over multiple transmit antennas at the same time within the same bandwidth. The first bandwidth-efficient transmit diversity scheme was proposed in [39] and it was shown that the diversity advantage of this scheme is equal to the number of transmit antennas [30, 42, 60]. In [44] Alamouti discovered a witty transmit diversity technique using two transmit antennas, whose key advantage was the employment of simple linear processing at the receiver, which is based on Maximum-Likelihood (ML) detection. The decoding algorithm proposed in [44] can be generalised to an arbitrary number of receive antennas using MRC, EGC or SC. Alamouti's achievement inspired Tarokh *et al.* [46, 47] to generalise the transmit diversity scheme to more than two transmit antennas, contriving the concept of Space-Time Block Codes (STBC). The family of STBCs is capable of attaining the same diversity gain as Space-Time Trellis Codes (STTC) [45, 61] at lower decoding complexity, when employing the same number of transmit antennas. However, a disadvantage of STBCs when compared to STTCs is that they provide no coding gain [26], as documented for example in [57].

Inspired by the philosophy of STBCs, Hochwald *et al.* [49] proposed the transmit diversity concept known as Space-Time Spreading (STS) for the downlink of Wideband Code Division Multiple Access (WCDMA) [25] that is capable of achieving the highest possible transmit diversity gain. The STBC and STS designs contrived for higher number of transmit antennas results in a reduction of the achievable transmission rate and hence in a reduction of the attainable bandwidth efficiency. An alternative idea for constructing full-rate STBCs for complex modulation schemes and more than two antennas was pursued in [30, 50]. Here the strict constraint of perfect orthogonality was relaxed in favour of a higher data rate. The resultant STBCs were referred to as quasi-orthogonal STBCs [50].

The STBC and STS designs offer at best the same data rate as an uncoded single-antenna system, but they provide an improved BER performance as compared to the family of single-antenna-aided systems by providing diversity gains. In contrast to this, several high-rate space-time transmission schemes having a normalised rate higher than one have been proposed in the literature. For example, high-rate space-time codes that are linear in space and time, namely the so-called Linear Dispersion Codes (LDC), were proposed in [51]. LDCs provide a flexible trade-off between achieving space-time coding and spatial multiplexing.

Additionally, the concept of combining orthogonal transmit diversity designs with the principle of Sphere Packing (SP) was introduced by Su *et al.* [55] in order to maximise the achievable coding advantage, where it was demonstrated that the proposed SP aided STBC scheme was capable of outperforming the conventional orthogonal design based STBC schemes of [44, 46]. A further advance was proposed in [58], where the SP demapper of [55] was modified for the sake of accepting the *a priori* information passed to it from the channel decoder as extrinsic information. The major coherent spatial diversity techniques are summarised in Tables 1.1 and 1.2.

A common feature of all the above-mentioned schemes is that they use coherent detection, which assumes the availability of accurate Channel State Information (CSI) at the receiver. In practice, the CSI of each link between each transmit and each receive antenna pair has to be estimated at the receiver either blindly or using training symbols. However, channel estimation invoked for all the antennas substantially increases both the cost and complexity of the receiver. Furthermore, when the CSI fluctuates dramatically from burst to burst, an increased number of training symbols has to be transmitted, potentially resulting in an undesirably high transmission overhead and wastage of transmission power. Therefore, it is beneficial to develop low-complexity techniques that do not require any channel information and thus are capable of mitigating the complexity of MIMO-channel estimation.

A detection algorithm designed for Alamouti's scheme [44] was proposed in [62], where the

Year	Author(s)	Contribution
1998	Tarokh *et al.* [62]	proposed a detection algorithm for the Alamouti scheme [44] dispensing with channel estimation.
1999	Tarokh *et al.* [63]	proposed a differential encoding/decoding of Alamouti's scheme [44] with PSK constellations.
2000	Hochwald *et al.* [64]	proposed a differential modulation scheme for transmit diversity based on unitary space-time codes.
	Hughes [65]	proposed a differential modulation scheme that is based on group codes.
2001	Jafarkhani *et al.* [66]	proposed a differential detection scheme for the multiple antenna STBC [46].
2002	Schober *et al.* [67]	proposed non-coherent receivers for differential space-time modulation (DSTM) that can provide satisfactory performance in fast fading unlike the conventional differential schemes that perform poorly in fast fading.
2003	Hwang *et al.* [68, 69]	extended the scheme of [66] to QAM constellations.
2004	Nam *et al.* [70]	extended the scheme of [68, 69] to four transmit antennas and QAM constellations.
2005	Zhu *et al.* [71]	proposed a differential modulation scheme based on quasi-orthogonal STBCs, which when compared with that of [66] results in a lower BER and provides full diversity.
2007	Song *et al.* [72]	proposed a new class of quasi-orthogonal STBCs and presented a simple differential decoding scheme for the proposed structures that avoids signal constellation expansion.

Table 1.3: Major differential spatial diversity techniques.

channel encountered at time instant t was estimated using the pair of symbols detected at time instant $t-1$. The algorithm, nonetheless, has to estimate the channel during the very first time instant using training symbols and hence is not truly differential. Tarokh and Jafarkhani [63,73] proposed a differential encoding and decoding algorithm for Alamouti's scheme [44] using real-valued phasor constellations and hence the transmitted signal can be demodulated both with or without CSI at the receiver. The resultant differential decoding aided non-coherent receiver performs within 3 dB from the coherent receiver assuming perfect channel knowledge at the receiver. The differential scheme of [63] was restricted to complex-valued PSK modulation. The twin-antenna-aided differential STBC scheme of [63] was extended to QAM constellations in [68, 69].

Differential STBC (DSTBC) schemes designed for multiple antennas were proposed in [66]

for real-valued constellations. Afterwards, the authors of [68, 70] developed a DSTBC scheme that supports non-constant modulus constellations combined with four transmit antennas. This extension, however, requires the knowledge of the received power in order to appropriately normalise the received signal. The received power was estimated blindly using the received differentially encoded signals without invoking any channel estimation techniques or transmitting any pilot symbols. In [64], a differential modulation scheme was proposed for the sake of attaining transmit diversity based on unitary space-time codes [74]. The proposed scheme can be employed in conjunction with an arbitrary number of transmit antennas. Around the same time, a similar differential scheme was also proposed in [65] based on the employment of group codes.

Zhu *et al.* [71] proposed a differential modulation scheme based on quasi-orthogonal STBCs, which were compared to that of [66] and resulted in a reduced BER as a benefit of providing full diversity. Additionally, a new class of quasi-orthogonal STBCs was proposed in [72], which presented a simple differential decoding scheme that avoids signal constellation expansion. The major contributions on differential spatial diversity techniques are summarised in Table 1.3.

1.2.1.2 Multiplexing Techniques

STBC and STTC are capable of providing diversity gains for the sake of improving the achievable system performance. However, this BER performance improvement is often achieved at the expense of a rate loss since the STBC and STTC may result in a throughput loss compared to single-antenna-aided systems. As a design alternative, a specific class of MIMO systems was designed for improving the attainable spectral efficiency of the system by transmitting the signals independently from each of the transmit antennas, hence resulting in a multiplexing gain.

The basic principle of spatial multiplexing can be summarised as follows. The source bit sequence at the transmitter side is split into N_t sequences, which are modulated and then transmitted simultaneously from the N_t transmit antennas using the same carrier frequency. At the receiver side, interference cancellation is employed in order to separate the different transmitted signals. In the case of narrowband frequency flat fading, there are several decoding algorithms designed for interference cancellation at the receiver side of the spatial multiplexing systems. The different receivers can be characterised by a tradeoff between the achievable performance and the complexity imposed. A low-complexity receiver is constituted by the Zero-Forcing (ZF) or the Minimum Mean Square Error (MMSE) technique [75, 76]. However, when we employ the ZF receiver, the attainable BER performance is typically poor in addition to imposing the condition that the number of receive antennas should be at least equal to

the number of transmit antennas. The optimum receiver is the Maximum Likelihood (ML) receiver [35], which is capable of achieving full diversity gain, i.e. the same diversity order, as the number of receive antennas. However, a major drawback of the ML receiver is its complexity that grows exponentially with the number of transmit antennas and the number of bits per symbol employed by the modulation scheme. Fortunately, the complexity of the ML decoders can be reduced by employing sphere decoders [77–79] that are capable of achieving a similar performance to the ML decoders at a fraction of their complexity.

In [80] Foschini proposed a multi-layer MIMO structure, known as the Diagonal Bell Labs Layered Space-Time (D-BLAST) scheme[1], which is in principle capable of approaching the substantial capacity of MIMO systems. The D-BLAST signal may be subjected to low-complexity linear processing for decoding the received signals. However, the diagonal approach suffers from a potentially high implementation complexity that led Wolniansky *et al.* to propose another version of BLAST, which is known as Vertical BLAST (V-BLAST) [81]. In V-BLAST, each transmit antenna simultaneously transmits independent data over the same carrier frequency band. At the receiver side, provided that the number of receive antennas is higher than or equal to the number of transmit antennas, a low complexity *serial* decoding algorithm may be applied to detect the transmitted data. The V-BLAST transceiver is capable of providing a substantial increase of a specific user's effective bit-rate without the need for any increase in the transmitted power or the system's bandwidth. However, its impediment is that it was not designed for exploiting transmit diversity. Furthermore, the decision errors of a particular antenna's detector propagate to other bits of the multi-antenna symbol, when erroneously cancelling the effects of the sliced bits from the composite signal. The V-BLAST detector first selects the layer[2] with the largest SNR and estimates the transmitted bits of that layer, while treating the other layers as interference. The detected symbol is then subtracted from the received signal and then the layer with the second highest SNR is selected for decoding. The procedure is repeated for all the layers. The BER performance of each layer is different and it depends on the received SNR of each layer. The first decoded layer has the highest SNR, while the layers detected later have a higher diversity order, since they suffer from less interference.

The BLAST detection algorithm is based on Successive Interference Cancellation (SIC), which was originally proposed for multiuser detection in CDMA systems [88]. Several BLAST detectors have been proposed in the literature for either reducing the complexity [89–94] or for improving the attainable BER performance [85, 95–100]. An alternative design approach

[1]The diagonal approach implies that the signal mapped to the consecutive antenna elements is delayed in time, which has the potential of subjecting the delayed signal components of a space-time symbol to more independent fading, hence leading to a potential diversity gain.

[2]The layer in the case of the V-BLAST corresponds to each of the transmit antennas.

Year	Author(s)	Contribution
1996	Foschini *et al.* [80]	studied the encoding and decoding of the diagonal BLAST structure.
1998	Wolniansky *et al.* [81]	introduced the vertical BLAST architecture for reducing the implementation complexity of the diagonal approach.
1999	Golden *et al.* [82]	provided the first real-time BLAST demonstrations.
2001	Benjebbour *et al.* [83]	introduced the minimum mean square error receiver for V-BLAST and introduced an ordering scheme for improving the attainable performance.
2002	Sellathurai *et al.* [84]	studied the combination of BLAST architecture with that of a turbo code to improve its performance.
2003	Wubben *et al.* [85]	proposed a detector for improving the attainable performance of V-BLAST.
2004	Zhu *et al.* [86]	proposed a complexity-reduction algorithm for BLAST detectors.
2005	Huang *et al.* [87]	proposed a new detection algorithm for BLAST based on the concept of particle filtering and provided a near ML performance at a reasonable complexity.

Table 1.4: Major spatial multiplexing techniques.

contrived for spatial multiplexing using less receive antennas than transmit antennas was proposed in [101] based on group Maximum A Posteriori (MAP) detection. In [84, 102] a spatial multiplexing scheme referred to as Turbo-BLAST was proposed, which uses quasi-random interleaving in conjunction with an iterative receiver structure, in order to separate the individual layers. The major spatial multiplexing techniques are summarised in Table 1.4.

1.2.1.3 Beamforming Techniques

According to Sections 1.2.1.1 and 1.2.1.2, it becomes clear that multiple antennas can be used for the sake of attaining either spatial diversity or spatial multiplexing gains. However, multiple antennas can also be used in order to improve the Signal-to-Noise Ratio (SNR) at the receiver or the Signal-to-Interference-plus-Noise Ratio (SINR) in a multi-user scenario. This can be achieved by employing beamforming techniques [103,104]. Beamforming constitutes an effective technique of reducing the multiple access interference, where the antenna gain is increased in the direction of the desired user, whilst reducing the gain towards the interfering users.

In a wireless communications scenario the transmitted signals propagate via several paths and hence are received from different directions/phases at the receiver. If the directions of the

different propagation paths are known at the transmitter or the receiver, then beamforming techniques can be employed in order to direct the received beam pattern in the direction of the specified antenna or user [105,106]. Hence, significant SNR gains can be achieved in comparison to a single antenna system. On the transmitter side, when the Direction of Arrival (DOA) of the dominant paths at the receiver is known for the transmitter, then the transmit power is concentrated in the direction of the target user, where less power is wasted in the other directions.

On the other hand, beamforming can be used in order to reduce the co-channel interference or multiuser interference. When using beamforming, each user adjusts his/her beam pattern to ensure that there are nulls in the directions of the other users, while there is a high directivity in the direction of the desired receiver [103, 107]. Hence, the system attains an SINR gain.

1.2.1.4 Multi-functional MIMO Techniques

V-BLAST is capable of achieving full multiplexing gain, while STBC can achieve full antenna diversity gain. Hence, it was proposed in [108] to combine the two techniques to provide both antenna diversity and spectral efficiency gains. More specifically, it was proposed that the antennas at the transmitter be partitioned into layers, where each layer uses STBC. At the receiver side, successive group interference cancellation can be applied to each layer before decoding the signals using ML STBC decoding. Therefore, by combining V-BLAST and STBC, an improved transmit diversity gain can be achieved as compared to pure V-BLAST, while ensuring that the overall bandwidth efficiency is higher than that of pure STBC due to the independence of the signals transmitted by different STBC layers. Furthermore, the combined array processing proposed in [108] was improved in [109] by optimising the decoding order of the different antenna layers. An iterative decoding algorithm was proposed in [109] that results in a full receive diversity gain for the combined V-BLAST STBC system.

In [113] the authors presented a transmission scheme referred to as Double Space-Time Transmit Diversity (D-STTD), which consists of two STBC layers at the transmitter that is equipped with four transmit antennas, while the receiver is equipped with two antennas. The decoding of D-STTD presented in [113] is based on a linear decoding scheme presented in [123], where the authors provided a broad overview of space-time coding and signal processing designed for high data rate wireless communications. A two-user scheme was presented in [123], where each user is equipped with a twin-antenna-aided STBC scheme transmitting at the same carrier frequency and in the same time slot. A two-antenna-aided receiver was implemented for the sake of decoding the two users' data, while eliminating the interference imposed by the users on each others' data. An extension to the idea of combining interference cancellation with

Year	Author(s)	Contribution
1998	Naguib *et al.* [110]	presented a multi-user scenario where each user employs STBC and the receiver applies interference cancellation for eliminating the co-channel interference and then uses ML decoding for the STBC of each user.
1999	Tarokh *et al.* [108]	proposed to combine STBC with V-BLAST in order to provide both antenna diversity and spectral efficiency gains.
2000	Huang *et al.* [111]	extended the idea of combining interference cancellation with STBC to multiuser scenarios using CDMA.
2001	Stamoulis *et al.* [112]	proposed a simple decoder for the two-user system, where each user employs STBC and showed how the decoder can be extended to more users and then extended the results for frequency-selective channels.
2002	Onggosanusi *et al.* [113]	presented the Double Space-Time Transmit Diversity scheme, which consists of two STBC blocks at the transmitter that is equipped with four antennas, while the receiver is equipped with two antennas.
	Jongren *et al.* [114]	combined conventional transmit beamforming with STBC assuming that the transmitter has partial knowledge of the channel and derived a performance criteria for improving the system performance.
	Huang *et al.* [115]	introduced a transmission scheme that can achieve transmit diversity and spatial separation and proposed a generalisation of the V-BLAST detector for CDMA signals.
	Soni *et al.* [116]	designed a hybrid downlink technique for achieving both transmit diversity and transmit beamforming combined with DS-CDMA.
2003	Liu *et al.* [117]	combined the twin-antenna-aided Alamouti STBC with ideal beamforming in order to show that the system can attain a better performance while keeping full diversity and unity rate.
2004	Tao *et al.* [109]	improved the design of [108] by optimising the decoding order of the different antenna layers. Also proposed an iterative decoder than can achieve full diversity.
	Zhu *et al.* [118]	compared the performance of two systems combining beamforming with STBC, while using a single or two antenna arrays and studied the effect of the DOA on the performance of the two schemes.

Table 1.5: Major multi-functional MIMO techniques (Part 1).

Year	Author(s)	Contribution
2005	Zhao *et al.* [119]	compared the performance of the combined diversity and multiplexing systems while employing ZF, QR and MMSE group interference cancellation techniques.
	Lee *et al.* [120]	proposed a computationally efficient ZF decoder for the double space-time transmit diversity scheme [113] that achieves similar performance to the conventional ZF decoder but with less complexity.
2007	Sellathurai *et al.* [121]	investigated the performance of multi-rate layered space-time coded MIMO systems and proposed a framework where each of the layers is encoded independently with different rates subject to equal per-layer outage probabilities.
2008	Ekbatani *et al.* [122]	combined STBC and transmit beamforming while using limited-rate channel state information at the transmitter. Also proposed a combined coding, beamforming and spatial multiplexing scheme over multiple-antenna multi-user channels that enables a low-complexity joint interference cancellation.
	Luo *et al.* [59]	considered a new class of full-diversity STCs that consist of a combination of delay transmit diversity with orthogonal STBCs and specially designed symbol mappings.

Table 1.6: Major multi-functional MIMO techniques (Part 2).

STBC techniques was presented in [111,115], where the STBC and interference cancellation arrangements were combined with CDMA for the sake of increasing the number of users supported by the system. A zero-forcing decoder designed for the D-STTD was presented in [120] for the sake of reducing the decoding complexity. Finally, the authors of [112, 124] presented further results that compare the performance of STBC versus D-STTD and extended the applicability of the D-STTD scheme to more than two STBC layers.

Furthermore, in order to achieve additional performance gains, beamforming has been combined with spatial diversity as well as spatial multiplexing techniques. STBC has been combined with beamforming in order to attain a higher SNR gain in addition to the diversity gain [114, 117, 118, 125–127]. In [114], the authors combined conventional transmit beamforming with STBC, assuming that the transmitter has partial knowledge of the channel and derived a performance criterion for a frequency-flat fading channel. In addition, a particularly efficient solution was developed in [114] for the specific case of independently fading channel coefficients. More explicitly, the transmission scheme of [114] combines the benefits of conventional beamforming with those of orthogonal STBC. Furthermore, in [118] the performance of combined

beamforming and STBC has been analysed as a function of the number of antenna array groups. Explicitly, Zhu *et al.* [118] compared the performance of the system combining beamforming with STBC, while using either a single or two antenna arrays and studied the effect of the DOA on the attainable system performance. Finally, multiplexing techniques have been combined with beamforming techniques in [128–130]. The major multi-functional MIMO techniques are summarised in Tables 1.5 and 1.6.

1.2.2 Distributed MIMO Techniques

Wireless channels suffer from multipath propagation of the signals that results in channel fading, as discussed in Section 1.1. Employing multiple transmit antennas is a beneficial method that can be used for counteracting the effects of the channel fading by providing diversity gains. Transmit diversity results in a significantly improved BER performance, when the different transmit antennas are spatially located so that the paths arriving from each transmit antenna to the destination experience independent fading, which can be achieved by having a distance between the different antennas, which is significantly higher than the carrier's wavelength. However, considering a handheld mobile phone, it is not a feasible option to position the transmit antennas far enough in order to achieve independent fading. On the other hand, the spatial fading correlation caused by insufficiently high antenna spacing at the transmitter or receiver of a MIMO system results in a degradation of both the achievable capacity and the BER performance of MIMO systems. The problem of correlation of the transmit signals can be circumvented by introducing a new class of MIMOs also referred to as distributed MIMOs or cooperative communications [36, 37].

The basic idea behind cooperative communications can be traced back to the idea of the relay channel which was introduced in 1971 by Van der Meulen [131]. Cover and El Gamal [132] characterised the relay channel from an information theoretic point of view. In [134] Sendonaris *et al.* generalised the conventional relay model, where there is one source, one relay and one destination, to multiple nodes that transmit their own data as well as serve as relays for each other. The scheme of [134] was referred to as "user cooperation diversity". Sendonaris *et al.* presented in [36, 37] a simple user-cooperation methodology based on a Decode-and-Forward (DF) signalling scheme using CDMA. In [135] the authors reported data rate gains and a decreased sensitivity to channel variations, where it was concluded that cooperation effectively mimics the multi-antenna scenario with the aid of single-antenna terminals. Dohler *et al.* [137] introduced the concept of Virtual Antenna Arrays (VAA) that emulates Alamouti's STBC for single-antenna-aided cooperating users. Space-time coded cooperative diversity protocols for exploiting spatial diversity in a cooperative scenario was proposed in [138].

Year	Author(s)	Contribution
1971	Meulen [131]	investigated a simple 3-node relay channel incorporating a transmitter, a relay and a receiver using a time-sharing approach.
1979	Cover *et al.* [132]	characterised the relay channel from an information theoretic point of view.
1983	Willems [133]	introduced a partially cooperative communications scenario where the encoders are connected by communication links with finite capacities, which permit both encoders to communicate with each other. The paper also established the capacity region of the multiple access channel with partially cooperating encoders.
1998	Sendonaris *et al.* [134]	generalised the relay model to multiple nodes that transmit their own data as well as serve as relays for each other.
2001	Laneman *et al.* [135]	built upon the classical relay channel and exploited space diversity available at distributed antennas through coordinated transmission and processing by cooperating radios.
2002	Hunter *et al.* [136]	proposed a user cooperation scheme for wireless communications in which the idea of cooperation was combined with the existing channel coding methods.
	Dohler *et al.* [137]	introduced the concept of virtual antenna arrays that emulates Alamouti's STBC for single-antenna-aided cooperating users.
2003	Sendonaris *et al.* [36, 37]	presented a simple user-cooperation methodology based on a DF signalling scheme using CDMA.
	Laneman *et al.* [138]	developed space-time coded cooperative diversity protocols for exploiting spatial diversity in a cooperation scenario, which can also be used for higher spectral efficiencies than repetition-based schemes.
	Valenti and Zhao [139, 140]	proposed a turbo coding scheme in a relay network.
2004	Laneman *et al.* [141]	developed and analysed cooperative diversity protocols and compared the DF, AF, selection relaying and incremental relaying.
	Nabar *et al.* [142]	analysed the spatial diversity performance of various signalling protocols.
	Janani *et al.* [143]	presented two extensions to the coded cooperation framework [136]: increased the diversity of coded cooperation via ideas borrowed from space-time codes and applied turbo codes in the proposed relay framework.

Table 1.7: Major distributed MIMO techniques (Part 1).

Year	Author(s)	Contribution
2004	Stefanov *et al.* [144]	analysed the performance of channel codes that are capable of achieving the full diversity provided by user cooperation in the presence of noisy interuser channels.
2005	Azarian *et al.* [145]	proposed cooperative signalling protocols that can achieve the diversity-multiplexing tradeoff.
	Sneessens *et al.* [146]	proposed a soft decode-and-forward signalling strategy that can outperform the conventional DF and AF.
	Hu *et al.* [147]	proposed Slepian-Wolf cooperation that exploits distributed source coding technologies in wireless cooperative communication.
	Yu [148]	compared the AF and DF signalling schemes in practical scenarios.
2006	Hunter *et al.* [149, 150]	developed the idea of coded cooperation [136] by computing BER and FER bounds as well as the outage probability of coded cooperation.
	Li *et al.* [151]	employed soft information relaying in a BPSK modulated relay system employing turbo coding.
	Hu *et al.* [152]	proposed Wyner-Ziv cooperation as a generalisation of the Slepian-Wolf cooperation [147] with a compress-and-forward signalling strategy.
	Hϕst-Madsen [153]	derived upper and lower bounds for the capacity of four-node ad hoc networks with two transmitters and two receivers using cooperative diversity.
2007	Bui *et al.* [154]	proposed soft information relaying where the relay LLR values are quantised, encoded and superimposedly modulated before being forwarded to the destination.
	Khormuji *et al.* [155]	improved the performance of the conventional DF strategy by employing constellation rearrangement in the source and the relay.
	Bao *et al.* [156]	combined the benefits of AF and DF and proposed a new signalling strategy referred to as decode-amplify-forward.
	Xiao *et al.* [157]	introduced the concept of network coding in cooperative communications.

Table 1.8: Major distributed MIMO techniques (Part 2).

Year	Author(s)	Contribution
2008	Yue *et al.* [158]	compared the multiplexed coding and superposition coding in the coded cooperation system.
	Zhang *et al.* [159]	proposed a distributed space-frequency coded cooperation scheme for communication over frequency-selective channels.
	Wang *et al.* [160]	introduced the complex field network coding approach that can mitigate the throughput loss in the conventional signalling schemes and attain full diversity gain.

Table 1.9: Major distributed MIMO techniques (Part 3).

Cooperative communications has been shown to offer significant performance gains in terms of various performance metrics, including diversity gains [138, 141, 161] as well as multiplexing gains [145]. Hunter *et al.* [136] proposed the novel philosophy of coded cooperation schemes, which combine the idea of cooperation with the classic channel coding methods. Extension to the framework of coded cooperation was presented in [143], where the diversity gain of coded cooperation was increased with the aid of ideas borrowed from the area of space-time codes. Additionally, a turbo coded scheme was proposed in [143] in the framework of cooperative communications. Furthermore, the analysis of the performance benefits of channel codes in a coded cooperation aided scenario was performed in [144]. Laneman *et al.* [141] developed and analysed cooperative diversity protocols and compared the DF, Amplify-and-Forward (AF), selection relaying and incremental relaying signalling strategies.

Recently, there has been substantial research interest in the idea of soft relaying, where the relay passes soft information to the destination. In [146], it was argued that the DF signalling loses soft information and hence, it was proposed to use soft DF signalling, where all operations are performed using the Log-Likelihood Ratio (LLR) based representation of soft information. It was shown in [146] that the soft DF philosophy outperforms the DF and the AF signalling strategies. In [154] soft DF was also used, where the soft information was quantised, encoded and superimposed before transmission to the destination. In [151] soft information based relaying was employed in a turbo coding scheme, where the relay derives parity checking BPSK symbol estimates for the received source information and forwards the symbols to the destination. In [146, 151, 154] soft information relaying has been used, where it was shown that soft DF attains a better performance than hard DF. Furthermore, in [147, 152] distributed source coding techniques have been adopted for employment in wireless cooperative communications in order to improve the attainable performance. The major distributed MIMO techniques are summarised in Tables 1.7, 1.8 and 1.9.

1.3 Iterative Detection Schemes and Their Convergence Analysis

The concept of concatenated codes has been proposed in [162]. However, at the time of its conception it was deemed to have an excessive complexity and hence it failed to initiate immediate research interest. It was not until the discovery of turbo codes [163] that efficient iterative decoding of concatenated codes became a reality at a low complexity by employing simple constituent codes. Since then, the appealing iterative decoding of concatenated codes has inspired numerous researchers to extend the technique to other transmission schemes consisting of a concatenation of two or more constituent decoding stages [164–180].

For example, in [171] iterative decoding was invoked for exchanging extrinsic information between a soft-output symbol detector and an outer channel decoder in order to combat the effect of Inter-Symbol Interference (ISI). In [172] iterative decoding was carried out by exchanging information between an outer convolutional decoder and an inner Trellis Coded Modulation (TCM) decoder. The authors of [173, 174] presented a unified theory of Bit-Interleaved Coded Modulation (BICM). On the other hand, the employment of the iterative detection principle in [175] was considered for iterative soft demapping in the context of BICM, where a soft demapper was used between the multilevel demodulator and the channel decoder. In addition, iterative multiuser detection and channel decoding was proposed in [179] for CDMA schemes. Finally, in [180] an iteratively detected scheme was proposed for the Rayleigh fading MIMO channel, where an orthogonal STBC scheme was considered as the inner code combined with an additional block code as the outer channel code.

It was shown in [198] that a recursive inner code is needed in order to maximise the interleaver gain and to avoid the average BER floor, when employing iterative decoding. This principle has been adopted by several authors designing serially concatenated schemes, where unity-rate inner codes were employed for designing low complexity iterative detection aided schemes suitable for bandwidth- and power-limited systems having stringent BER requirements [184, 185, 187, 195, 199].

Semi-analytical tools devised for analysing the convergence behaviour of iteratively decoded systems have attracted considerable research attention [184,186,189–192,196,200,201]. In [186], ten Brink proposed the employment of the so-called EXtrinsic Information Transfer (EXIT) characteristics for describing the flow of extrinsic information between the soft-in soft-out constituent decoders. The computation of EXIT charts was further simplified in [191] to a time averaging, when the PDFs of the information communicated between the input and output of the constituent decoders are both symmetric and consistent. A tutorial introduction to EXIT charts can be found in [200]. The concept of EXIT chart analysis has been extended to three-

Year	Author(s)	Contribution
1966	Forney [162]	promoted concatenated codes.
1974	Bahl *et al.* [181]	invented the Maximum A-Posteriori (MAP) algorithm.
1993	Berrou *et al.* [163]	invented the turbo codes and showed that the iterative decoding is an efficient way of improving the attainable performance.
1995	Robertson *et al.* [182]	proposed the log-MAP algorithm that results in similar performance to the MAP algorithm but with significantly lower complexity.
	Divsalar *et al.* [164]	extended the turbo principle to multiple parallel concatenated codes.
1996	Benedetto *et al.* [165]	extended the turbo principle to serially concatenated block and convolutional codes.
1997	Benedetto *et al.* [172]	proposed an iterative detection scheme where iterations were carried out between the outer convolutional code and an inner TCM decoders.
	Caire *et al.* [173, 174]	presented the BICM concept with its design rules.
	Li *et al.* [176–178]	presented the BICM with iterative detection scheme.
1998	Benedetto *et al.* [166, 183]	studied the design of multiple serially concatenated codes with interleavers.
	Brink *et al.* [175]	introduced a soft demapper between the multilevel demodulator and the channel decoder in an iteratively detected coded system.
1999	Wang *et al.* [179]	proposed iterative multiuser detection and channel decoding for coded CDMA systems.
2000	Divsalar *et al.* [184, 185]	employed unity-rate inner codes for designing low-complexity iterative detection schemes suitable for bandwidth and power limited systems having stringent BER requirements.
	ten Brink [186]	proposed the employment of EXIT charts for analysing the convergence behaviour of iteratively detected systems.
2001	Lee [187]	studied the effect of precoding on serially concatenated systems with ISI channels.
	ten Brink [188, 189]	extended the employment of EXIT charts to three-stage parallel concatenated codes.
	EL Gamal *et al.* [190]	used SNR measures for studying the convergence behaviour of iterative decoding.

Table 1.10: Major concatenated schemes and iterative detection (Part 1).

Year	Author(s)	Contribution
2002	Tüchler *et al.* [191]	simplified the computation of EXIT charts.
	Tüchler *et al.* [192]	compared several algorithms predicting the decoding convergence of iterative decoding schemes.
	Tüchler *et al.* [193]	extended the EXIT chart analysis to three-stage serially concatenated systems.
2003	Sezgin *et al.* [180]	proposed an iterative detection scheme where a block code was used as an outer code and STBC as an inner code.
2004	Tüchler *et al.* [194]	proposed a design procedure for creating systems exhibiting beneficial decoding convergence depending on the block length.
2005	Lifang *et al.* [195]	showed that non-square QAM can be decomposed into parity-check block encoder having a recursive nature and a memoryless modulator. Iterative decoding was implemented with an outer code for improving the system performance.
	Brännström *et al.* [196]	considered EXIT chart analysis for multiple concatenated codes using 3-dimensional charts and proposed a way for finding the optimal activation order.
2008	Maunder *et al.* [197]	designed irregular variable length codes for the near-capacity design of joint source and channel coding aided systems.

Table 1.11: Major concatenated schemes and iterative detection (Part 2).

stage concatenated systems in [188, 193, 196]. The major contributions on iterative detection and its convergence analysis are summarised in Tables 1.10 and 1.11.

1.4 Novel Contributions

This dissertation is based on the following publications and manuscript submissions [1–22], where the main contributions can be summarised as follows:

- A Differential Space-Time Spreading (DSTS) scheme is proposed, which is advocated for the sake of achieving a high transmit diversity gain in a multi-user system, while eliminating the complexity of MIMO channel estimation. Additionally, the system is combined with multi-dimensional Sphere Packing (SP) modulation, which is capable of maximising the coding advantage of the transmission scheme by jointly designing and detecting the sphere-packed DSTS symbols. The capacity of the DSTS-SP scheme is quantified analytically, where it is shown that the DSTS-SP system attains a higher capacity than its counterpart dispensing with SP [1, 7, 8].

- Iteratively detected DSTS-SP schemes are designed for near-capacity operation, where EXIT charts are used for analysing the convergence behaviour of the iterative detection. The outer code used in the iterative detection aided systems is a Recursive Systematic Convolutional (RSC) code, while the inner code is SP mapper in the first system and a Unity Rate Code (URC) in the second system, where the URC is capable of eliminating the error floor present in the BER performance of the system dispensing with URC [1,5,11,17].

- An algorithm is devised for computing the maximum achievable rate of the DSTS system using EXIT charts, where the maximum achievable rate obtained using EXIT charts matches closely with the analytically computed capacity [1].

- An adaptive DSTS-SP scheme is proposed in order to maximise the system's throughput. The adaptive scheme exploits the advantages of differential encoding, iterative decoding as well as SP modulation. The achievable integrity and bit rate enhancements of the system are determined by the following factors: the specific transmission configuration used for transmitting data from the four antennas, the spreading factor used and the RSC encoder's code rate [9].

- The merits of V-BLAST, STC and beamforming are amalgamated in a Layered Steered Space-Time Coded (LSSTC) multi-functional MIMO scheme for the sake of achieving a multiplexing gain, a diversity gain as well as a beamforming gain. Additionally, the capacity of the LSSTC-SP scheme is quantified analytically [2].

- Furthermore, in order to characterise the LSSTC scheme, three iteratively detected LSSTC-SP receiver structures are proposed, where iterative detection is carried out between the outer code's decoder, the intermediate code's decoder and the LSSTC-SP demapper. The three systems are capable of operating within 0.9, 0.4 and 0.6 dB from the maximum achievable rate limit of the system. A comparison between the three iteratively detected schemes reveals that a carefully designed two-stage iterative detection aided scheme is capable of operating sufficiently close to capacity at a lower complexity, when compared to a three-stage system employing RSC or a two-stage system employing an Irregular Convolutional Code (IrCC) as the outer code [4, 14].

- A multi-functional MIMO combining STS, V-BLAST and beamforming with generalised MC DS-CDMA is proposed and referred to as Layered Steered Space-Time Spreading (LSSTS). The LSSTS scheme is capable of achieving a spatial diversity gain, frequency diversity gain, multiplexing gain as well as beamforming gain.The number of users supported can be extended by employing combined time- and frequency-domain spreading [6].

- A novel LLR post-processing technique is devised for improving the iteratively detected LSSTS system's performance [6].
- Finally, ideas from cooperative communications and turbo coding are combined to form a Distributed Turbo Code (DTC), where turbo coding is employed by exchanging extrinsic information between the outer codes' decoders in the two cooperating users' handsets.

1.5 Outline of Thesis

This thesis is organised as follows.

■ **Chapter 2: Differential Space-Time Spreading**

The DSTS design is presented and combined with SP modulation. The chapter commences with a review of the differential modulation concept in Section 2.2, where it is shown that differential encoding requires no channel information for decoding and thus eliminates the complexity of channel estimation at the expense of a 3 dB performance loss compared to the coherently detected system assuming perfect channel knowledge at the receiver. In Section 2.3, the encoding and decoding algorithms of the DSTS scheme are presented, when combined with conventional modulation schemes, such as PSK and QAM, as well as with sphere packing modulation. Afterwards, the capacity of the DSTS scheme employing $N_t = 2$ transmit antennas is derived in Section 2.3.6, followed by the performance characterisation of a twin-antenna-aided DSTS scheme in Section 2.3.7, demonstrating that the DSTS scheme is capable of providing full diversity. Our results demonstrate that DSTS-SP schemes are capable of outperforming DSTS schemes dispensing with SP.

The four-antenna-aided DSTS design is characterised in Section 2.4, where it is demonstrated that the DSTS scheme can be combined with conventional real- and complex-valued modulated constellations as well as with SP modulation. It is also shown that the four-dimensional SP modulation scheme is constructed differently in the case of two transmit antennas than when employing four transmit antennas. The capacity of the four-antenna-aided DSTS-SP scheme is also derived for systems having different bandwidth efficiency, while employing a variable number of receive antennas in Section 2.4.5. Finally, Section 2.4.6 presents the simulation results obtained for the four-antenna-aided DSTS scheme, when combined with conventional as well as SP modulation schemes.

■ **Chapter 3: Iterative Detection of Channel-Coded DSTS Schemes**

Two realisations of a novel iterative detection aided DSTS-SP scheme are presented, namely an iteratively detected RSC-coded DSTS-SP scheme as well as an iteratively

detected RSC-coded and URC precoded DSTS-SP arrangement. The iteratively detected RSC-coded DSTS-SP scheme is described in detail in Section 3.2. Afterwards, the concept of EXIT charts is introduced in Section 3.2.2 as a tool designed for studying the convergence behaviour of iterative detection aided systems. Then, a novel technique devised for computing the maximum achievable bandwidth efficiency of the system based on EXIT charts is proposed in Section 3.2.3, followed by a discussion of the iteratively detected RSC-coded DSTS-SP system's performance.

In Section 3.3 an iteratively detected RSC-coded and URC-precoded DSTS-SP scheme is proposed that is capable of eliminating the error floor exhibited by the system of Section 3.2, which was hence capable of operating closer to the system's achievable bandwidth efficiency. In Section 3.3.1 we present an overview of the system, followed by a discussion of the results in Section 3.3.2.

■ **Chapter 4: Adaptive DSTS-Assisted Iteratively-Detected SP Modulation**

An adaptive DSTS aided system that exploits the advantages of differential encoding, iterative decoding as well as SP modulation is presented. The adaptive DSTS-SP scheme adapts the system parameters for the sake of achieving the highest possible bandwidth efficiency, while maintaining a given target BER. The proposed adaptive DSTS-SP scheme benefits from a substantial diversity gain, while using four transmit antennas without the need for pilot-assisted channel estimation and coherent detection. The proposed scheme reaches the target BER of 10^{-3} at an SNR of about 5 dB and maintains it for SNRs in excess of this value, while increasing the effective throughput. The system's bandwidth efficiency varies from 0.25 bits/sec/Hz to 16 bits/sec/Hz. The achievable integrity and bit rate enhancements of the system are determined by the following factors: the specific transmission configuration used for transmitting data from the four antennas, the spreading factor used and the RSC encoder's code rate.

■ **Chapter 5: Layered Steered Space-Time Codes**

A multi-functional MIMO scheme is proposed, that combines the benefits of V-BLAST, STBC and beamforming. The proposed system is characterised by a multiplexing gain, a diversity gain and a beamforming gain. The multi-functional MIMO scheme is referred to as a Layered Steered Space-Time Code (LSSTC). In Section 5.2 the encoding and decoding processes of the LSSTC scheme are outlined, when combined with conventional as well as SP modulation schemes. Then, in Section 5.3 the capacity of the proposed LSSTC scheme is quantified, where the capacity limits for a system employing $N_t = 4$ transmit Antenna Arrays (AA), $N_r = 4$ receive antennas and a variable number L_{AA} of elements per AA are presented.

On the other hand, in order to further enhance the attainable system performance, the

LSSTC scheme is serially concatenated with both an outer code and a URC, where three different receiver structures are presented by varying the iterative detection configuration of the constituent decoders/demapper. In Section 5.4.1 we provide a brief description of the iteratively detected two-stage RSC-coded LSSTC-SP scheme, where extrinsic information is exchanged between the outer RSC decoder and the inner URC decoder, while no iterations are carried out between the URC decoder and the SP demapper. In Section 5.4.1.2, we employ the powerful technique of EXIT tunnel-area minimisation, for the sake of achieving a near-capacity operation using IrCCs [191, 194]. In Section 5.4.2 an iteratively detected three-stage RSC-coded LSSTC scheme is presented, where extrinsic information is exchanged between the three constituent decoders, namely the outer RSC decoder, the inner URC decoder and the demapper. Finally, in Section 5.5 we discuss our performance results and characterise the three proposed iteratively detected LSSTC schemes.

■ **Chapter 6: Downlink LSSTS Aided Generalised MC DS-CDMA**

A multi-functional multiuser MIMO scheme that combines the benefits of V-BLAST, of STS, of generalised MC DS-CDMA as well as of beamforming is presented. The proposed system is referred to as Layered Steered Space-Time Spreading (LSSTS) aided generalised MC DS-CDMA, which benefits from a multiplexing gain, a spatial diversity gain, a frequency diversity gain and a beamforming gain.

In Section 6.2 the proposed LSSTS scheme's transmitter structure is characterised and then the decoding process is illustrated. Afterwards, in order to increase the number of users supported by the system, Frequency Domain (FD) spreading is applied in the generalised MC DS-CDMA in addition to the Time Domain (TD) spreading action of the STS. A user-grouping technique is employed that minimises the FD interference coefficient for the users in the same TD group.

To further enhance the achievable system's performance, the proposed MIMO scheme is serially concatenated with an outer code combined with a URC, where three different iteratively detected systems are presented in Section 6.4. EXIT charts are used to study the convergence behaviour of the proposed systems and in Section 6.4.1 we propose an LLR post-processing technique for the soft output of the QPSK demapper in order to improve the achievable system performance. In Section 6.5 we discuss our performance results and characterise the three proposed iteratively detected schemes, while employing N_t=4 transmit AAs, N_r=2 receive antennas, L_{AA} number of elements per AA and V number of subcarriers supporting K users.

■ **Chapter 7: Distributed Turbo Coding**

A cooperative communication scheme referred to as Distributed Turbo Coding (DTC) is

presented. In the proposed scheme, two users are cooperating, where each user's transmitter is constituted by an RSC code and an interleaver followed by a SP mapper. In Section 7.2 we provide an overview of cooperative communications and the background of the major cooperative signalling strategies including AF, DF and coded cooperation. In Section 7.3 the DTC scheme is presented, where a two-phase cooperation scheme is proposed. In the first phase, the two users exchange their data, while in the second phase the two users simultaneously transmit their data to the base station. In Section 7.4 we characterise the attainable system performance and study the effects of varying the inter-user channel characteristics on the performance of the uplink DTC scheme.

■ **Chapter 8: Conclusions and Future Research**

This chapter summarises the main findings of our research and suggests some future research ideas.

Chapter 2

Differential Space-Time Spreading

2.1 Introduction

An effective and practical way of counteracting the effect of wireless channels is to provide diversity, which can be achieved by employing space-time coding [28,30,44,46,202–208]. Space-time coding employs multiple transmit antennas, where coding is performed in both the spatial and temporal domains in order to introduce correlation between signals transmitted from the multiple antennas in different time slots. The spatial-temporal correlation is imposed in order to exploit the fact that the individual MIMO links are likely to experience independent fading and hence to mitigate the effects of transmission errors at the receiver. Space-time coding can achieve a substantial transmit diversity and power gain over its spatially uncoded counterpart without bandwidth expansion. There are numerous well established coding structures, including Space-Time Block Codes (STBC) [44,46], Space-Time Trellis Codes (STTC) [203] and Layered Space-Time (LST) codes [80]. A central issue in designing all these schemes is the exploitation of multi-path effects in order to achieve diversity performance gains [24].

In practice, the Channel State Information (CSI) of each link between each transmit and each receive antenna pair has to be estimated at the coherent receiver either blindly or using training symbols. In such a coherent system, it is assumed that the channel does not change dramatically during a transmitted frame of data [30]. However, channel estimation invoked for all the transmit and receive antennas substantially increases both the cost and complexity of the receiver. Furthermore, when the CSI fluctuates dramatically from burst to burst, an increased number of training symbols has to be transmitted, potentially resulting in an undesirably high transmission overhead and wastage of transmission power.

Alternatively, it is beneficial to develop low-complexity techniques that do not require any channel information at the receiver. For a single transmit antenna, it is well known that dif-

ferential schemes, such as Differential Phase-Shift Keying (DPSK) [27], can be demodulated without the use of channel estimates. Differential schemes have been widely used in practical cellular mobile communication systems [24,27,35]. It is natural to consider extensions of differential schemes to MIMO systems. A detection algorithm designed for Alamouti's scheme [44] was proposed in [62], where the channel encountered at time instant t was estimated using the pair of symbols detected at time instant $t-1$. The algorithm, nonetheless, has to estimate the channel during the very first time instant using training symbols and hence is not truly differential. Tarokh *et al.* [63, 73] proposed a differential encoding and decoding technique for Alamouti's scheme [44] using real-valued phasor constellations and hence the transmitted signal can be demodulated both with or without CSI at the receiver. The resultant differential decoding aided non-coherent receiver performs within 3 dB from the coherent receiver assuming perfect knowledge of the channel impulse response (CIR) at the receiver. The complex constellation was also restricted to Phase-Shift Keying (PSK) schemes, which was extended to Quadrature Amplitude Modulation (QAM) constellations in [68, 69]. This extension, however, requires the knowledge of the channel power in order to appropriately normalise the received signal. The channel power in [68, 69] was estimated blindly using the received differentially encoded signals without invoking any channel estimation techniques or transmitting any pilot symbols. The proposed differential space-time block code was then extended to multiple antennas [66] using a real-valued phasor constellation. Afterwards, the authors of [68, 70] developed a Differential Space-Time Block Coding (DSTBC) scheme that supports non-constant modulus constellations combined with four transmit antennas.

The novelty and rationale of this chapter can be summarised as follows:

1. *Differential Space-Time Spreading (DSTS) is a MIMO-aided scheme, which is advocated for the sake of achieving a high transmit diversity gain. This facilitates low-complexity differential detection, rather than using a more complex receiver employing both channel estimation [209] for all MIMO links and coherent detection. Moreover, the system benefits from the multi-user support capability of the STS scheme. Furthermore, the high diversity order of the system results in a Gaussian-like channel error distribution as a function of time, i.e. the bit index, which improves the attainable system performance.*

2. *Additionally, the system is combined with multi-dimensional SP modulation [55, 58], which is capable of maximising the coding advantage of the transmission scheme by jointly designing and detecting the sphere-packed DSTS symbols.*

3. *We quantify the capacity of the DSTS-SP scheme for transmission over both Rayleigh as well as Gaussian channels.*

The rest of the chapter is organised as follows. First, differential encoding designed for a

single transmit antenna is briefly described in Section 2.2. Then, the encoding and decoding processes of the DSTS scheme employing two transmit antennas is carried out in Section 2.3 for both conventional as well as for SP modulation. Section 2.3.6 presents the capacity analysis of the sphere packing modulation aided DSTS (DSTS-SP) scheme employing two transmit antennas and a variable number of receive antennas, while in Section 2.3.7 we present our comparative study of the various twin-antenna-aided DSTS schemes. In Section 2.4 we demonstrate how a four-antenna-aided DSTS scheme can be combined with conventional real- and complex-valued as well as sphere packing modulation schemes and quantify the attainable capacity of the four-antenna-aided DSTS-SP scheme. Our conclusions are presented in Section 2.5, followed by a chapter summary in Section 2.6.

2.2 Differential Phase Shift Keying

Before presenting the details of DSTS designed for multiple transmit antennas, we review the concept of differential encoding/decoding for a single transmit antenna. To be more precise, the following section presents the details of Differential Phase Shift Keying (DPSK) modulation and captures the main ideas behind it [27].

In DPSK modulation, the demodulator does not have to perform channel estimation. The two consecutive transmitted symbols depend on each other and the demodulator detects the transmitted data symbol by observing two successive symbols. It is assumed that the channel has a phase response that is approximately constant for two symbol periods and this is approximately valid for the case of slow fading channels. The information is essentially transmitted by first providing a single dummy reference symbol, followed by differentially phase-modulated symbols [24].

Let us assume that we transmit the modulated symbol v_t at time instant t, when the CIR between the transmitter and receiver is h_t and that the noise sample is n_t with a variance of σ_n^2. Therefore, the received signal at time instant t is:

$$r_t = h_t \cdot v_t + n_t. \tag{2.1}$$

For DPSK modulation, the transmitted symbol v_t at time instant t is obtained from $v_t = x_t \cdot v_{t-1}$, as shown in Figure 2.1, where x_t is a non-differentially PSK modulated symbol and v_{t-1} is the symbol transmitted at time instant $t-1$. To detect the signal transmitted at time instant t, the receiver computes $r_t \cdot r_{t-1}^*$, where * represents the complex conjugate operation. Then the receiver finds the legitimate symbol of the QPSK constellation closest to $r_t \cdot r_{t-1}^*$ as the estimates of the transmitted symbol [30]. To further augment the rationale behind the

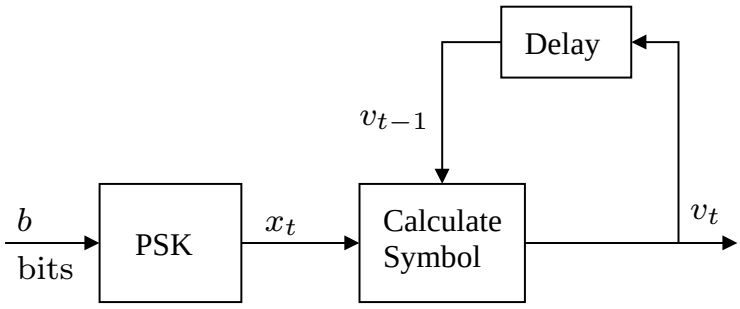

Figure 2.1: Transmitter block diagram for DPSK modulation.

above scheme and taking into consideration the assumption that the channel encountered is a slow fading one, i.e. that we have $h_t \approx h_{t-1} = h$, we arrive at:

$$\begin{aligned} r_t \cdot r_{t-1}^* &= (h_t \cdot v_t + n_t) \cdot (h_{t-1} \cdot v_{t-1} + n_{t-1})^* \\ &= |h|^2 \cdot v_t \cdot v_{t-1}^* + h \cdot v_t \cdot n_{t-1}^* + n_t \cdot h^* \cdot v_{t-1}^* + n_t \cdot n_{t-1}^* \\ &= |h|^2 \cdot x_t \cdot |v_{t-1}|^2 + N \\ &= |h|^2 \cdot x_t + N, \end{aligned} \tag{2.2}$$

where $|v_{t-1}|^2 = 1$, N is a Gaussian noise process having a variance of $\sigma_N^2 \approx 2 \cdot h \cdot \sigma_n^2$ and the path gain h is assumed to be constant during the modulation instants of $t-1$ and t. Therefore, the optimal estimate of x_t is given by:

$$\tilde{x}_t = \arg \min_{x_t} |r_t \cdot r_{t-1}^* - |h|^2 \cdot x_t|^2. \tag{2.3}$$

Based on Equation (2.3), it becomes clear that the decoded output does not depend on either earlier demodulation decisions or on the channel state information, rather it depends only on the received symbols of two consecutive symbol periods. The noise power experienced by the receiver of the differential decoding scheme is $\sigma_N^2 \approx 2 \cdot h \cdot \sigma_n^2$, which is about twice that of the coherent scheme. Therefore, for the same transmission power, the received SNR of the differential detection scheme is approximately half of that of the coherent detection scheme using perfect channel knowledge at the receiver. This translates to a 3 dB SNR difference for the performance of these two systems, i.e. the coherently detected system using perfect channel knowledge at the receiver outperforms the differentially detected scheme by 3 dB.

2.3 DSTS Design Using Two Transmit Antennas

As widely recognised, coherent detection schemes require CSI, which is acquired by transmitting training symbols. However, high-accuracy MIMO channel estimation imposes a high complexity

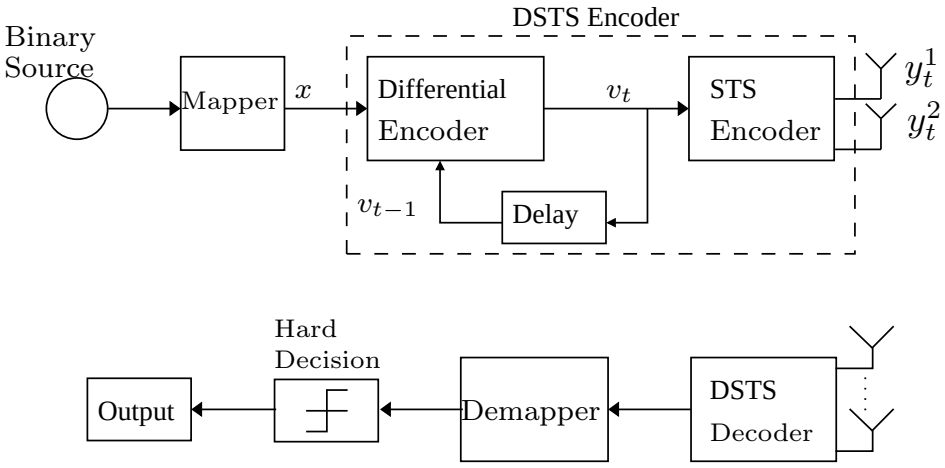

Figure 2.2: The twin-antenna-aided DSTS system block diagram.

on the receiver. This renders differential encoding and decoding an attractive design alternative, despite the associated E_b/N_0 loss.

The transmitted and received DSTS symbols are encoded and decoded based on the differential relationship among subsequent symbols as illustrated in Section 2.2 for classic DPSK. For the sake of simplicity, in what follows we consider having a single receive antenna, although the extension to systems having more than one receive antenna is straightforward.

2.3.1 Twin-Antenna Aided DSTS Encoding Using Conventional Modulation

According to Figure 2.2, it becomes clear that the DSTS encoder can be divided into two main stages. The differential encoding takes place before space-time spreading and the differentially encoded symbols are then spread as exemplified in simple graphical terms in Figure 2.3 [25], where 2 symbols are transmitted using 2 transmit antennas within 2 time slots.

The DSTS encoding algorithm operates as follows. At time instant $t = 0$, the arbitrary dummy reference symbols v_0^1 and v_0^2 are passed to the STS encoder for transmission from antennas one and two, respectively. The dummy symbols v_0^1 and v_0^2 usually carry no information. At time instants $t \geq 1$, a block of $2B$ bits arrive at the mapper, where each set of B bits is mapped to a symbol x_t^k, $k = 1, 2$, selected from a 2^B-ary constellation. Assume that v_t^1 and v_t^2 are the differentially encoded symbols, then differential encoding of Figure 2.2 is carried out as follows:

$$v_t^1 = \frac{(x_t^1 \cdot v_{t-1}^1 + x_t^2 \cdot v_{t-1}^{2*})}{\sqrt{(|v_{t-1}^1|^2 + |v_{t-1}^2|^2)}} \tag{2.4}$$

$$v_t^2 = \frac{(x_t^1 \cdot v_{t-1}^2 - x_t^2 \cdot v_{t-1}^{1*})}{\sqrt{(|v_{t-1}^1|^2 + |v_{t-1}^2|^2)}}, \tag{2.5}$$

where the superscript * represents the complex conjugate operation.

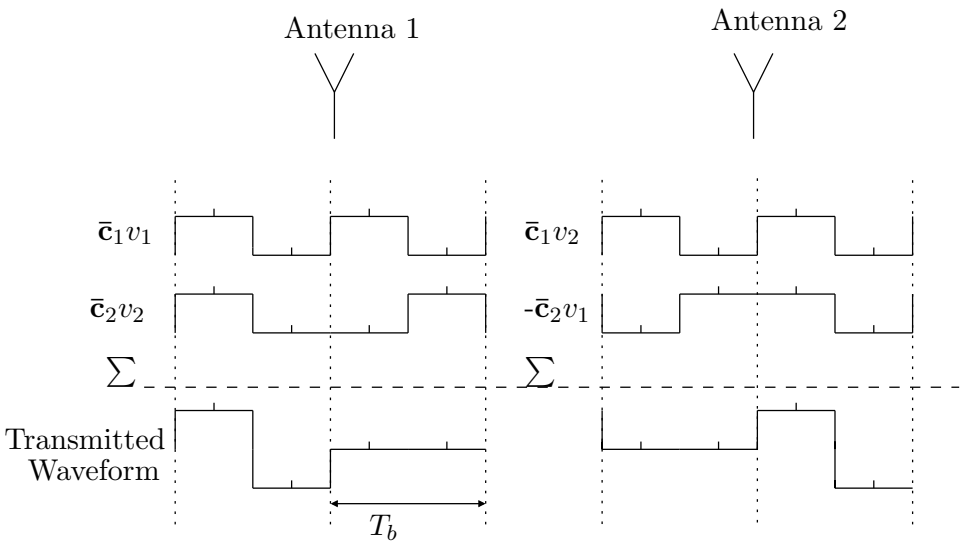

Figure 2.3: Illustration of STS using two transmit antennas transmitting 2 bits within $2T_b$ duration. $v_1 = v_2 = 1$ were assumed and $\bar{\mathbf{c}}_1 = [+1+1-1-1+1+1-1-1]$ and $\bar{\mathbf{c}}_2 = [+1+1-1-1-1-1+1+1]$.

The differentially encoded symbols are then spread with the aid of the spreading codes $\bar{\mathbf{c}}_1$ and $\bar{\mathbf{c}}_2$ to both transmit antennas, where $\bar{\mathbf{c}}_1$ and $\bar{\mathbf{c}}_2$ are generated from the same user-specific spreading code $\bar{\mathbf{c}}$ by ensuring that the two spreading codes $\bar{\mathbf{c}}_1$ and $\bar{\mathbf{c}}_2$ become orthogonal using the simple code-concatenation rule of Walsh-Hadamard codes, yielding longer codes and hence a proportionately reduced per antenna throughput according to:

$$\bar{\mathbf{c}}_1 = [\bar{\mathbf{c}} \quad \bar{\mathbf{c}}] \tag{2.6}$$

$$\bar{\mathbf{c}}_2 = [\bar{\mathbf{c}} \quad -\bar{\mathbf{c}}]. \tag{2.7}$$

The differentially encoded data is then divided into two half-rate substreams and the two consecutive symbols are then spread to both transmit antennas using the mapping of:

$$\mathbf{y}_t^1 = \frac{1}{\sqrt{2}}(\bar{\mathbf{c}}_1 \cdot v_t^1 + \bar{\mathbf{c}}_2 \cdot v_t^{2*}) \tag{2.8}$$

$$\mathbf{y}_t^2 = \frac{1}{\sqrt{2}}(\bar{\mathbf{c}}_1 \cdot v_t^2 - \bar{\mathbf{c}}_2 \cdot v_t^{1*}), \tag{2.9}$$

which is exemplified in simple graphical terms in Figure 2.3.

2.3.2 Receiver and Maximum Likelihood Decoding

Assuming that the channel is modelled as a temporally correlated narrowband Rayleigh fading channel, where the channel coefficients are spatially independent, associated with a normalised Doppler frequency of $f_D = f_d T_s = 0.01$, where f_d is the Doppler frequency and T_s is the symbol duration. The complex Additive White Gaussian Noise (AWGN) of $n = n_I + jn_Q$ contaminates the received signal, where n_I and n_Q are two independent zero-mean Gaussian

random variables having a variance of $\sigma_n^2 = \sigma_{n_I}^2 = \sigma_{n_Q}^2 = N_0/2$ per dimension, with $N_0/2$ representing the double-sided noise power spectral density expressed in W/Hz.

The received signal at the output of the single receiver antenna can be represented as:

$$\mathbf{r}_t = h_1 \cdot \mathbf{y}_t^1 + h_2 \cdot \mathbf{y}_t^2 + \mathbf{n}_t, \tag{2.10}$$

where h_1 and h_2 denote the narrowband complex-valued CIRs corresponding to the first and second transmit antennas respectively, where it is assumed that the channel coefficients remain unchanged for two consecutive transmitted vectors $\mathbf{y}^k$, while $\mathbf{n}_t$ is a complex-valued Gaussian random variable with a covariance matrix of $\sigma_n^2 \cdot \mathbf{I}_{SF}$, with SF representing the spreading factor of the spreading codes $\bar{\mathbf{c}}_1$ and $\bar{\mathbf{c}}_2$ and $\mathbf{I}_{SF}$ is the identity matrix of size $SF \times SF$.

The received signal $\mathbf{r}_t$ is then correlated with $\bar{\mathbf{c}}_1$ and $\bar{\mathbf{c}}_2$ according to the following operations:

$$d_t^1 = \bar{\mathbf{c}}_1^\dagger \cdot \mathbf{r}_t = \frac{1}{\sqrt{2}} \cdot h_1 \cdot v_t^1 + \frac{1}{\sqrt{2}} \cdot h_2 \cdot v_t^2 + \bar{\mathbf{c}}_1^\dagger \cdot \mathbf{n}_t \tag{2.11}$$

$$d_t^2 = \bar{\mathbf{c}}_2^\dagger \cdot \mathbf{r}_t = \frac{1}{\sqrt{2}} \cdot h_1 \cdot v_t^{2*} - \frac{1}{\sqrt{2}} \cdot h_2 \cdot v_t^{1*} + \bar{\mathbf{c}}_2^\dagger \cdot \mathbf{n}_t, \tag{2.12}$$

where the superscript † represents the Hermitian or the conjugate transpose operation.

Following the received signal's correlation with $\bar{\mathbf{c}}_1$ and $\bar{\mathbf{c}}_2$, we arrive at two data symbols that are then differentially decoded by using the received data of two consecutive time slots as follows:

$$\begin{aligned} \tilde{x}_t^1 &= d_t^1 \cdot d_{t-1}^{1*} + d_t^{2*} \cdot d_{t-1}^2 \\ &= \frac{1}{2} \cdot (|h_1|^2 + |h_2|^2) \cdot \sqrt{|v_{t-1}^1|^2 + |v_{t-1}^2|^2} \cdot x_t^1 + N_1 \end{aligned} \tag{2.13}$$

$$\begin{aligned} \tilde{x}_t^2 &= d_t^1 \cdot d_{t-1}^{2*} - d_t^{2*} \cdot d_{t-1}^1 \\ &= \frac{1}{2} \cdot (|h_1|^2 + |h_2|^2) \cdot \sqrt{|v_{t-1}^1|^2 + |v_{t-1}^2|^2} \cdot x_t^2 + N_2, \end{aligned} \tag{2.14}$$

where N_1 and N_2 are zero-mean complex-valued Gaussian random variables having variances of $\sigma_N^2 = \sigma_{N_1}^2 = \sigma_{N_2}^2 \approx 2 \cdot \chi_{2N_t}^2 \cdot \sigma_n^2$, with $N_t = 2$ is the number of transmit antennas and $\chi_{2N_t}^2 = \frac{1}{2} \cdot (|h_1|^2 + |h_2|^2) \cdot \sqrt{|v_{t-1}^1|^2 + |v_{t-1}^2|^2}$ representing a chi-squared distributed random variable having $2N_t = 4$ degrees of freedom.

We can observe from Equations (2.13) and (2.14) that the proposed method guarantees achieving a diversity gain, since the two transmit antennas' signals are independently faded according to the values of h_1 and h_2, while using a low-complexity decoding algorithm. Moreover, since $\bar{\mathbf{c}}_1$ and $\bar{\mathbf{c}}_2$ are derived by appropriately concatenating the user-specific code $\bar{\mathbf{c}}$, no extra spreading codes are required for carrying out the STS operation and the two symbols of the two transmit antennas are transmitted in two time slots.

The previous decoding operation has been carried out for the case of constant modulus constellations such as PSK. Non-constant modulus constellations [27] can also be transmitted

using the proposed DSTS scheme. According to Equations (2.13) and (2.14), the DSTS decoded signal has a multiplicative factor of $\chi^2_{2N_t} = \frac{1}{2} \cdot (|h_1|^2 + |h_2|^2) \cdot (\sqrt{|v^1_{t-1}|^2 + |v^2_{t-1}|^2})$ as compared to the original transmitted symbols regardless of the effect of noise. Therefore, in order to obtain the original transmitted multi-level constellation symbols, the multiplicative factor must be compensated for by estimating the channel's output power $(|h_1|^2 + |h_2|^2)$ as well as the power of the previously transmitted symbols $(\sqrt{|v^1_{t-1}|^2 + |v^2_{t-1}|^2})$. The power of the previously transmitted symbols can be estimated from that of the symbols received during the previous time slot. Furthermore, to estimate the channel's output power, the following simple computation can be carried out:

$$d^1_{t-1} \cdot d^{1*}_{t-1} + d^2_{t-1} \cdot d^{2*}_{t-1} = \frac{1}{2} \cdot (|h_1|^2 + |h_2|^2) \cdot (|v^1_{t-1}|^2 + |v^2_{t-1}|^2) + w, \tag{2.15}$$

where w is a zero-mean complex-valued Gaussian random variable having a variance of $\sigma^2_w \approx 2 \cdot \chi^2_{2N_t} \cdot \sigma^2_n$. Therefore, using the estimate of the signal power of the previous transmitted symbols, i.e. $(|v^1_{t-1}|^2 + |v^2_{t-1}|^2)$, as well as the result of Equation (2.15), the channel's power transfer function of $(|h_1|^2 + |h_2|^2)$ can be calculated. Then the received signal can be normalised by the channel's power transfer function and the transmitted signal power estimates, before the demodulation process takes place.

The above encoding/decoding operations have been carried out for the case of a single receive antenna, but these arguments may be readily extended to an arbitrary number of receive antennas, where the resultant signals are appropriately combined, before passing them to the differential detector.

Therefore, to further augment the rationale behind the above arguments, we contrast the decoding processes of both the coherent and differentially encoded STS schemes, while employing non-constant modulus constellations.

1. The coherently decoded signal can be represented as $\tilde{x}_t = \frac{1}{2} \cdot (|h_1|^2 + |h_2|^2) \cdot x_t + N_{coh}$, while the differentially decoded signal is given by Equation (2.13) as $\tilde{x}_t = \frac{1}{2} \cdot (|h_1|^2 + |h_2|^2) \cdot \sqrt{|v^1_{t-1}|^2 + |v^2_{t-1}|^2} \cdot x_t + N_{diff}$.

2. The coherent decoder has to estimate the CIR and hence it has full knowledge of h_1 and h_2, which is required for normalising the decoded signal and estimating the transmitted symbol x_t. By contrast, the differential encoding aided receiver does not employ channel estimation, although it is required to estimate $(|h_1|^2 + |h_2|^2)$ and $(\sqrt{|v^1_{t-1}|^2 + |v^2_{t-1}|^2})$ for demodulating the non-constant modulus transmitted symbol x.

3. To elaborate a little further, the differential decoder does not employ any channel estimation for quantifying $(|h_1|^2 + |h_2|^2)$. First, the differential decoder estimates $(\sqrt{|v^1_{t-1}|^2 + |v^2_{t-1}|^2})$

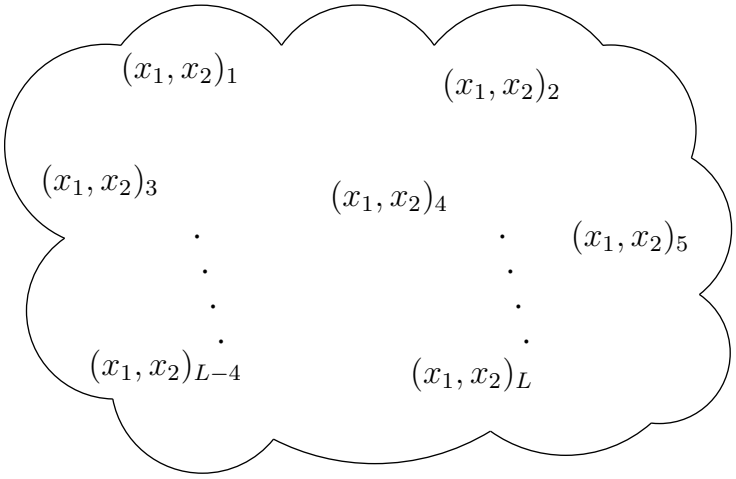

Figure 2.4: The L legitimate two-dimensional complex vectors.

from the symbols received during the previous time slot and then employs Equation (2.15) for estimating the channel's output power by using the received signal only.

2.3.3 Design Using Sphere Packing Modulation[1]

The design concept of maximising the diversity product[2] [64, 212] was generalised in [55] in order to account for the effects of the temporal correlation exhibited by the fading channel. In order to maximise the achievable coding advantage for DSTS signals that attain full diversity, we construct a class of DSTS signals in conjunction with SP modulation [58, 213], which is referred to as DSTS-SP.

According to Equations (2.13) and (2.14), the DSTS-decoded symbols $\tilde{x}^1$ and $\tilde{x}^2$ represent scaled versions of the transmitted symbols x^1 and x^2 corrupted by the complex-valued AWGN. Assuming that there are L legitimate SP-modulated signals, which the DSTS encoder can choose from, this observation implies that the diversity product is determined by the Minimum Euclidean Distance (MED) of the L number of the two-dimensional complex-valued vectors $(x_1, x_2)_l \in \mathbb{C}^2$, $l = 0, \ldots, L-1$. Therefore, in order to maximise the diversity product, the L number of the two-dimensional complex vectors must be designed by ensuring that they have the best MED in the two-dimensional complex-valued space $\mathbb{C}^2$, as illustrated in Figure 2.4. If each of the L number of two-dimensional complex vectors is expressed using its real and imaginary components, then we have

$$(x_1, x_2)_l \Longleftrightarrow (a_1 + ja_2, a_3 + ja_4)_l. \tag{2.16}$$

[1] This section is based on the design of the sphere packing modulation of [210, 211].

[2] The diversity product or coding advantage is defined as the estimated SNR gain over an uncoded system having the same diversity order as the coded system [46].

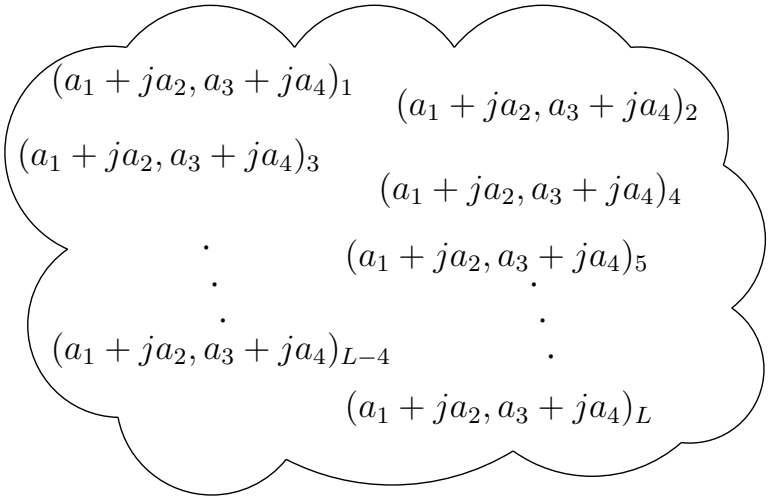

Figure 2.5: The L legitimate two-dimensional complex vectors represented by their real and imaginary components.

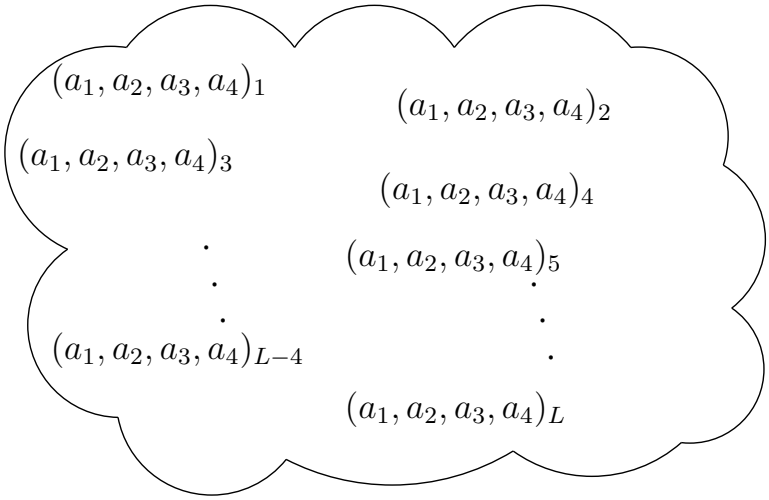

Figure 2.6: The L legitimate four-dimensional real-valued vectors.

Hence, each of these complex vectors can be represented as shown in Figure 2.5. It may be directly observed from Figure 2.5 that the design problem can be readily transformed from the two-dimensional complex-valued space $\mathbb{C}^2$ to the four-dimensional real-valued Euclidean space $\mathbb{R}^4$, as portrayed in Figure 2.6. It was proposed in [55] to use SP for combining the individual antennas signals into a joint design, since SP modulated symbols have the best known MED in the $2(k+1)$-dimensional real-valued Euclidean space $\mathbb{R}^{2(k+1)}$ [213], which directly maximises the diversity product.

To summarise, according to Section 2.3.1, x^1 and x^2 represent independent conventional PSK/QAM modulated symbols transmitted from the first and second transmit antenna and no effort is made to jointly design a signal constellation for the various combinations of x^1 and x^2. By contrast, in the case of SP, these symbols are designed jointly, in order to further increase the attainable Euclidean distance and hence the resultant diversity product or coding

advantage, as suggested previously. Assuming that there are L legitimate vectors $(x^{l,1}, x^{l,2})$, $l = 0, 1, \ldots, L-1$, where L represents the number of sphere-packed modulated symbols, the transmitter then has to choose the modulated signal from these L legitimate symbols to be transmitted over the two DSTS antennas, where the twin-antenna-aided DSTS-SP bandwidth efficiency is given by $(\log_2 L/2)$ bits-per-channel-use.

In contrast to the independent transmitted signal design of Section 2.3.1, the aim is to design $x^{l,1}$ and $x^{l,2}$ jointly, so that they have the best minimum Euclidean distance from all other $(L-1)$ legitimate SP symbols, since this minimises the system's SP symbol error probability. Let $(a^{l,1}, a^{l,2}, a^{l,3}, a^{l,4})$, $l = 0, 1, \ldots, L-1$, be legitimate phasor points of the four-dimensional real-valued Euclidean space $\mathbb{R}^4$, hence the two time-slot's complex-valued phasor points $x^{l,1}$ and $x^{l,2}$ may be written as

$$\begin{aligned} \{x^{l,1}, x^{l,2}\} &= T_{sp}(a^{l,1}, a^{l,2}, a^{l,3}, a^{l,4}) \\ &= \left\{a^{l,1} + ja^{l,2}, a^{l,3} + ja^{l,4}\right\}, \end{aligned} \tag{2.17}$$

where the SP-function T_{sp} represents the mapping of the SP symbols $(a^{l,1}, a^{l,2}, a^{l,3}, a^{l,4})$ to the complex-valued symbols $x^{l,1}$ and $x^{l,2}$, $l = 0, \ldots, L-1$.

In the four-dimensional real-valued Euclidean space $\mathbb{R}^4$, the lattice D_4 is defined as a SP having the best minimum Euclidean distance from all other $(L-1)$ legitimate constellation points in $\mathbb{R}^4$ [213]. More specifically, D_4 may be defined as a lattice that consists of all legitimate sphere packed constellation points having integer coordinates $(a^{l,1}, a^{l,2}, a^{l,3}, a^{l,4})$, $l = 0, \ldots, L-1$, uniquely and unambiguously describing the L legitimate combinations of the two time-slots' modulated DSTS symbols, but subjected to the SP constraint of [213]

$$a^{l,1} + a^{l,2} + a^{l,3} + a^{l,4} = \kappa_l, \qquad l = 0, \ldots, L-1, \tag{2.18}$$

where κ_l may assume any even integer value. Alternatively, D_4 may be defined as the integer span of the vectors $\mathbf{u}_1$, $\mathbf{u}_2$, $\mathbf{u}_3$ and $\mathbf{u}_4$ that form the rows of the following generator matrix [213]

$$\begin{bmatrix} \mathbf{u}_1 \\ \mathbf{u}_2 \\ \mathbf{u}_3 \\ \mathbf{u}_4 \end{bmatrix} \triangleq \begin{bmatrix} 2 & 0 & 0 & 0 \\ 1 & 1 & 0 & 0 \\ 1 & 0 & 1 & 0 \\ 1 & 0 & 0 & 1 \end{bmatrix}. \tag{2.19}$$

We may infer from the above definition in Equation (2.19) that D_4 contains the centres $(2, 0, 0, 0)$, $(1, 1, 0, 0)$, $(1, 0, 1, 0)$ and $(1, 0, 0, 1)$. It also contains all linear combinations of these points [213].

Assuming that $\mathbf{S} = \{\mathbf{s}^l = [a^{l,1}, a^{l,2}, a^{l,3}, a^{l,4}] \in \mathbb{R}^4 : 0 \leq l \leq L-1\}$ constitutes a set of L

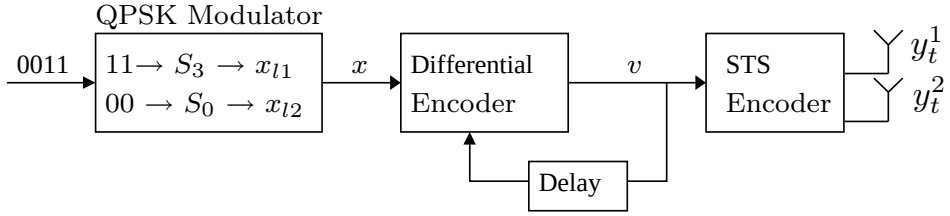

Figure 2.7: Transmission of two QPSK symbols using two-antenna-aided DSTS system.

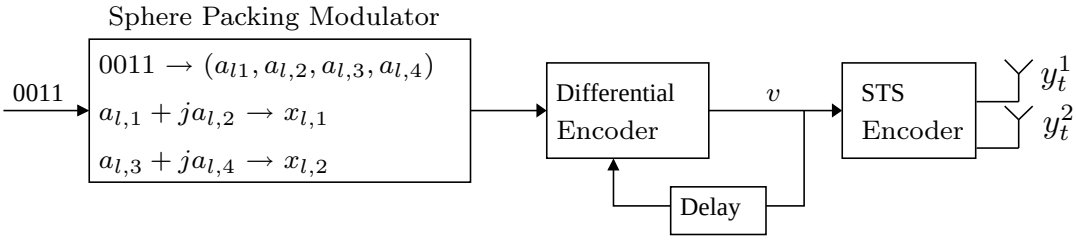

Figure 2.8: Transmission of sphere-packed symbols using two-antenna-aided DSTS system.

legitimate constellation points from the lattice D_4 having a total energy of

$$E_{total} \triangleq \sum_{l=0}^{L-1} \left(|a^{l,1}|^2 + |a^{l,2}|^2 + |a^{l,3}|^2 + |a^{l,4}|^2 \right), \tag{2.20}$$

and upon introducing the notation

$$\begin{aligned} \mathbf{C}_l &= \sqrt{\frac{2L}{E_{total}}} \left(x^{l,1}, x^{l,2} \right) \\ &= \sqrt{\frac{2L}{E_{total}}} \left(a^{l,1} + ja^{l,2}, a^{l,3} + ja^{l,4} \right), \qquad l = 0, 1, \ldots, L-1, \end{aligned} \tag{2.21}$$

we have a set of complex SP constellation symbols, $\{\mathbf{C}_l \colon 0 \leq l \leq L-1\}$, whose diversity product is determined by the MED of the set of L legitimate SP constellation points in $\mathbf{S}$.

The following example illustrates how SP modulation is combined with the twin-antenna-aided DSTS scheme as compared to the conventionally modulated DSTS system.

Example 2.3.1 *Assume that there are $L = 16$ different legitimate signals $(x^{l,1}, x^{l,2})$, $l = 0, 1, \ldots, 15$, that can be transmitted by the DSTS encoder. We will compare two modulation schemes, namely conventional QPSK and SP modulation.*

- **Conventional QPSK Modulation:**
  There are four legitimate complex-valued QPSK symbols (S_0, S_1, S_2, S_3) that can be used to represent independently any of the $x^{l,1}$ and $x^{l,2}$ symbols, $l = 0, 1, \ldots, 15$. The transmission scheme using two consecutive time slots is portrayed in Figure 2.7.

- **Sphere Packing Modulation:**
  We need $L = 16$ SP phasor points $(a^{l,1}, a^{l,2}, a^{l,3}, a^{l,4})$ from the lattice D_4 in order to jointly

represent each pair of signals $(x^{l,1}, x^{l,2})$, $l = 0, 1, \ldots, 15$ *according to Equation (2.21) as depicted in Figure 2.8.*

2.3.4 Sphere Packing Constellation Construction[3]

Since the signal constructed from the sphere packing scheme of Equation (2.21) is multiplied by a factor that is inversely proportional to $\sqrt{E_{\text{total}}}$, namely by $\sqrt{\frac{2L}{E_{total}}}$, it is desirable to choose a specific subset of L SP constellation points from the entire set of legitimate SP constellation points hosted by D_4, which results in the minimum total energy E_{total}, while maintaining a certain minimum Euclidean distance amongst the SP symbols. Viewing this design trade-off from a different perspective, if more than L SP points satisfy the minimum total energy constraint, an exhaustive computer search is carried out for determining the optimum choice of the L SP constellation points out of all possible points, which possess the highest MED, hence minimising the SP-symbol error probability. The legitimate constellation points hosted by D_4 are categorised into layers or shells based on their Euclidean norms or energy (i.e. the distance from the origin) as seen in Table 2.1. For example, it was shown in [213] that the first layer consists of 24 legitimate constellation points hosted by D_4 having an identical minimum energy of $E_{total} = 2$. In simple terms, it may be readily verified that the SP symbol centred at $(0, 0, 0, 0)$ has 24 minimum-distance or closest-neighbour SP symbols around it, centred at the points $(+/-1, +/-1, 0, 0)$, where any choice of signs and any ordering of the coordinates is legitimate [213].

Table 2.1 provides a summary of the constellation points hosted by the first 10 SP layers in the four-dimensional lattice D_4. In order to generate the full list of SP constellation points for a specific layer, we have to apply all legitimate permutations and signs for the corresponding constellation points given in Table 2.1.

2.3.5 Bandwidth Efficiency of the Twin-Antenna-Aided DSTS System

In the two-antenna-aided DSTS encoder, the data is serial-to-parallel converted to two sub-streams. The new bit duration of each parallel substream, or equivalently the symbol duration becomes T_s=2T_b as illustrated in [25, 49] and as exemplified in simple graphical terms in Figure 2.3. According to Section 2.3.1, the DSTS transmitter using two transmit antennas transmits two real- or complex-valued conventional modulated symbols in two time slots. Therefore, the two transmit antenna DSTS code rate is $2/2 = 1$ and then according to the number of bits-per-symbol (BPS) B, the system's bandwidth efficiency becomes equal to B

[3]This section is based on the design of the sphere packing modulation of [210, 211].

Layer	Constellation Points				Norm	Number of Combinations
0	0	0	0	0	0	1
1	+/-1	+/-1	0	0	2	24
2	+/-2	0	0	0	4	8
	+/-1	+/-1	+/-1	+/-1	4	16
3	+/-2	+/-1	+/-1	0	6	96
4	+/-2	+/-2	0	0	8	24
5	+/-2	+/-2	+/-1	+/-1	10	96
	+/-3	+/-1	0	0	10	48
6	+/-3	+/-1	+/-1	+/-1	12	64
	+/-2	+/-2	+/-2	0	12	32
7	+/-3	+/-2	+/-1	0	14	192
8	+/-2	+/-2	+/-2	+/2	16	16
	+/-4	0	0	0	16	8
9	+/-4	+/-1	+/-1	0	18	96
	+/-3	+/-2	+/-2	+/-1	18	192
	+/-3	+/-3	0	0	18	24
10	+/-4	+/-2	0	0	20	48
	+/-3	+/-3	+/-1	+/-1	20	96

Table 2.1: The first 10 layers of the lattice D_4.

bits-per-channel-use. For example, in the case of QPSK we have $B = 2$ BPS, which results in an effective system bandwidth efficiency of 2 bits-per-channel-use. Table 2.2 presents the bandwidth efficiency of the twin-antenna-aided DSTS system for different conventional modulated constellation sizes.

On the other hand, for two transmit antenna system using SP modulation, one SP symbol is transmitted in two time slots. Therefore, the DSTS-SP code rate is 1/2 and then according to the number of BPS B_{sp}, the SP system's bandwidth efficiency becomes equal to $B_{sp}/2$ bits-per-channel-use. For example, in the case of SP with $L = 16$ constellation, we have $B_{sp} = 4$ BPS, which results in an effective system's bandwidth efficiency of 2 bits-per-channel-use, which is identical to the system's bandwidth efficiency of the QPSK modulated twin-antenna-aided DSTS system. Table 2.3 presents the bandwidth efficiency of the twin-antenna-aided DSTS-SP system for different constellation sizes.

Modulation	BPS	Bandwidth Efficiency (bits-per-channel-use)
BPSK	1	1
QPSK	2	2
8PSK	3	3
16-QAM	4	4
64-QAM	6	6

Table 2.2: Bandwidth efficiency of twin-antenna-aided DSTS systems for different conventional modulation signal sets.

L	BPS	Bandwidth Efficiency (bits-per-channel-use)
4	2	1
8	3	1.5
16	4	2
32	5	2.5
64	6	3
128	7	3.5
256	8	4
512	9	4.5
1024	10	5
2048	11	5.5
4096	12	6

Table 2.3: Bandwidth efficiency of twin-antenna-aided DSTS-SP systems for different SP signal set sizes L.

2.3.6 Capacity of the Two-Antenna-Aided DSTS-SP Scheme

The capacity of a single-input-single-output AWGN channel was quantified by Shannon in 1948 [23, 214]. Since then, substantial research efforts have been invested in finding channel codes that would produce an arbitrarily low probability of error. Shannon's channel capacity was only defined for continuous-input continuous-output memoryless channel (CCMC) [35], where the channel input is continuous-amplitude discrete-time Gaussian-distributed signal and the capacity is only restricted by either the signalling energy or the bandwidth [215]. By contrast, in the context of discrete-amplitude QAM [27] and PSK [35] signals, we encounter a discrete-input continuous-output memoryless channel (DCMC) [35].

With the Advent of MIMO systems, the MIMO channel capacity is of immediate interest. Thus, the channel capacity of MIMO systems was found for CCMC in [24, 33, 34, 216] and then Ng *et al.* [215] developed the DCMC channel capacity of the STBC-aided MIMO system combined with multi-dimensional signal sets. In this section, we present the CCMC and DCMC

capacities of the twin-antenna-aided DSTS system using multi-dimensional SP modulation and employing N_r receive antennas. The same analysis can be performed to generate the capacity of the DSTS system employing two-dimensional conventional modulation schemes.

The complex-valued channel output symbols received during two consecutive DSTS time slots at receive antenna r, $r \in [1, \cdots, N_r]$, are DSTS decoded in order to extract the estimates $\tilde{x}^1$ and $\tilde{x}^2$ of the most likely transmitted symbols x^1 and x^2 resulting in:

$$\begin{aligned} \tilde{x}^1_{t,r} &= \frac{1}{2} \cdot (|h_{1,r}|^2 + |h_{2,r}|^2) \cdot \sqrt{|v^1_{t-1}|^2 + |v^2_{t-1}|^2} \cdot x^1_t + N_{1,r} \\ &= \chi^2_{2N_t,r} \cdot x^1_t + N_{1,r} \qquad (2.22) \\ \tilde{x}^2_{t,r} &= \frac{1}{2} \cdot (|h_{1,r}|^2 + |h_{2,r}|^2) \cdot \sqrt{|v^1_{t-1}|^2 + |v^2_{t-1}|^2} \cdot x^2_t + N_{2,r} \\ &= \chi^2_{2N_t,r} \cdot x^2_t + N_{2,r}, \qquad (2.23) \end{aligned}$$

where $h_{1,r}$ and $h_{2,r}$ denote the narrowband complex-valued CIRs corresponding to the first and second transmit antennas and the rth receive antenna, respectively. $N_{1,r}$ and $N_{2,r}$ are zero-mean complex-valued Gaussian random variables having variances of $\sigma^2_N = \sigma^2_{N_{1,r}} = \sigma^2_{N_{2,r}} \approx 2 \cdot \chi^2_{2N_t,r} \cdot \sigma^2_n$ and $\chi^2_{2N_t,r} = \frac{1}{2} \cdot (|h_{1,r}|^2 + |h_{2,r}|^2) \cdot \sqrt{|v^1_{t-1}|^2 + |v^2_{t-1}|^2}$ represents the chi-squared distributed random variable having $2N_t = 4$ degrees of freedom.

The received sphere-packed symbol $\tilde{\mathbf{s}}_r$ at receive antenna r is then constructed from the estimates $\tilde{x}^1_{t,r}$ and $\tilde{x}^2_{t,r}$ using the inverse function of T_{sp} introduced in Equation (2.17) as

$$\tilde{\mathbf{s}}_r = T^{-1}_{sp}(\tilde{x}^1_{t,r}, \tilde{x}^2_{t,r}), \qquad (2.24)$$

where we have $\tilde{\mathbf{s}} = [\tilde{a}^1 \ \tilde{a}^2 \ \tilde{a}^3 \ \tilde{a}^4] \in \mathbb{R}^4$. Therefore, the received sphere-packed symbol $\tilde{\mathbf{s}}_r$ at receive antenna r can be written as

$$\tilde{\mathbf{s}}_r = \chi^2_{2N_t,r} \cdot \mathbf{s}^l + \acute{\mathbf{N}}_r, \qquad (2.25)$$

where we have $\mathbf{s}^l = [a^{l,1} \ a^{l,2} \ a^{l,3} \ a^{l,4}] \in S$, $0 \leq l \leq L-1$. Furthermore, $\acute{\mathbf{N}}_r = [\acute{N}_{1,r} \ \acute{N}_{2,r} \ \acute{N}_{3,r} \ \acute{N}_{4,r}] \in \mathbb{R}^4$ is a four-dimensional real-valued Gaussian random variable having a covariance matrix of $\sigma^2_{\acute{N}} \cdot \mathbf{I}_D = \sigma^2_N \cdot \mathbf{I}_D = 2 \cdot \chi^2_{2N_t,r} \cdot \sigma^2_n \cdot \mathbf{I}_D = 2 \cdot \chi^2_{2N_t,r} \cdot \frac{N_0}{2} \cdot \mathbf{I}_D$, where we have $D = 4$, since the SP symbol constellation $\mathbf{S}$ is four-dimensional.

Therefore, the received sphere packed symbol $\tilde{\mathbf{s}}$ can be written as

$$\tilde{\mathbf{s}} = \sum_{r=1}^{N_r} \chi^2_{2N_t,r} \cdot \mathbf{s}^l + \acute{\mathbf{N}}. \qquad (2.26)$$

The conditional probability of receiving a four-dimensional signal $\tilde{\mathbf{s}}$, given that a four-dimensional L-ary signal $\mathbf{s}^l \in \mathbf{S}$, $l \in [0, \cdots, L-1]$, was transmitted over the Rayleigh channel

of Equation (2.26), is given by the following probability density function [35]:

$$\begin{aligned} p(\tilde{\mathbf{s}}|\mathbf{s}^l) &= \frac{1}{\prod_{d=1}^{D=4}\sqrt{\pi N_0 \sum_{r=1}^{N_r}\chi^2_{2N_t,r}[d]}} \cdot \exp\left(\sum_{d=1}^{D=4}\sum_{r=1}^{N_r}\frac{-\left(\tilde{\mathbf{s}}_r[d]-\chi^2_{2N_t,r}[d]\cdot\mathbf{s}^l[d]\right)^2}{\chi^2_{2N_t,r}[d]\cdot N_0}\right) \\ &= \frac{1}{\prod_{d=1}^{D=4}\sqrt{\pi N_0 \sum_{r=1}^{N_r}\chi^2_{2N_t,r}[d]}} \cdot \exp\left(\sum_{d=1}^{D=4}\sum_{r=1}^{N_r}\frac{-\left(\tilde{a}^d_r-\chi^2_{2N_t,r}[d]\cdot a^{l,d}\right)^2}{\chi^2_{2N_t,r}[d]\cdot N_0}\right). \end{aligned} \tag{2.27}$$

The channel capacity for the DSTS MIMO system employing D-dimensional L-ary SP signalling over the DCMC [35] can be derived from that of the discrete memoryless channel [217] as

$$\begin{aligned} C_{\text{DCMC}} &= \max_{p(\mathbf{s}^0),\ldots,p(\mathbf{s}^{L-1})} \sum_{l=0}^{L-1} \underbrace{\int_{-\infty}^{\infty}\cdots\int_{-\infty}^{\infty}}_{D\text{–fold}} p\left(\tilde{\mathbf{s}}|\mathbf{s}^l\right)\cdot p\left(\mathbf{s}^l\right) \\ &\quad \cdot \log_2\left(\frac{p\left(\tilde{\mathbf{s}}|\mathbf{s}^l\right)}{\sum_{k=0}^{L-1} p\left(\tilde{\mathbf{s}}|\mathbf{s}^k\right)\cdot p\left(\mathbf{s}^k\right)}\right) \mathrm{d}\tilde{\mathbf{s}} \quad \text{[bit/symbol]}, \end{aligned} \tag{2.28}$$

where $p(\mathbf{s}^l)$ is the probability of occurrence for the transmitted SP symbol $\mathbf{s}^l$ and $p(\tilde{\mathbf{s}}|\mathbf{s}^l)$ is expressed in Equation (2.27). The right-hand side of Equation (2.28) is maximised, when the transmitted SP symbols are equiprobably distributed, i.e. when we have $p(\mathbf{s}^l) = \frac{1}{L}$, $l = 0,\ldots,L-1$, which leads to achieving the full capacity [217]. The right-hand side of Equation (2.28) may be further simplified as follows [215]:

$$\begin{aligned} \log_2\left(\frac{p\left(\tilde{\mathbf{s}}|\mathbf{s}^l\right)}{\sum_{k=0}^{L-1} p\left(\tilde{\mathbf{s}}|\mathbf{s}^k\right)\cdot p\left(\mathbf{s}^k\right)}\right) &= -\log_2\left(\frac{1}{L}\sum_{k=0}^{L-1}\frac{p\left(\tilde{\mathbf{s}}|\mathbf{s}^k\right)}{p(\tilde{\mathbf{s}}|\mathbf{s}^l)}\right) \\ &= \log_2(L) - \log_2\sum_{k=0}^{L-1}\exp(\Psi_{l,k}), \end{aligned} \tag{2.29}$$

where $\Psi_{l,k}$ is expressed as [215]:

$$\begin{aligned} \Psi_{l,k} &= \sum_{d=1}^{D=4}\sum_{r=1}^{N_r}\left(\frac{-\left(\tilde{a}^d_r-\chi^2_{2N_t,r}[d]\cdot a^{k,d}\right)^2}{\chi^2_{2N_t,r}[d]\cdot N_0} + \frac{\left(\tilde{a}^d_r-\chi^2_{2N_t,r}[d]\cdot a^{l,d}\right)^2}{\chi^2_{2N_t,r}[d]\cdot N_0}\right) \\ &= \sum_{d=1}^{D=4}\sum_{r=1}^{N_r}\left(\frac{-\left(\chi^2_{2N_t,r}[d]\cdot\left(a^{l,d}-a^{k,d}\right)+\acute{N}_{d,r}\right)^2+\left(\acute{N}_{d,r}\right)^2}{\chi^2_{2N_t,r}[d]\cdot N_0}\right). \end{aligned} \tag{2.30}$$

Now, substituting Equation (2.29) into Equation (2.28) and observing that we have $p(\mathbf{s}^l) = \frac{1}{L}$, yields [215]

$$\begin{aligned} C_{\text{DCMC}} &= \frac{\log_2(L)}{L} \sum_{l=0}^{L-1} \underbrace{\int_{-\infty}^{\infty} \cdots \int_{-\infty}^{\infty}}_{D\text{–fold}} p\left(\tilde{\mathbf{s}}|\mathbf{s}^l\right) \, \mathrm{d}\tilde{\mathbf{s}} \\ &- \frac{1}{L} \sum_{l=0}^{L-1} \underbrace{\int_{-\infty}^{\infty} \cdots \int_{-\infty}^{\infty}}_{D\text{–fold}} p\left(\tilde{\mathbf{s}}|\mathbf{s}^l\right) \log_2 \sum_{k=0}^{L-1} \exp\left(\Psi_{l,k}\right) \, \mathrm{d}\tilde{\mathbf{s}} \\ &= \log_2(L) - \frac{1}{L} \sum_{l=0}^{L-1} E\left[\log_2 \sum_{k=0}^{L-1} \exp\left(\Psi_{l,k}\right) \middle| \mathbf{s}^l\right] \quad [\text{bit/sym}], \end{aligned} \tag{2.31}$$

where $E[A|B]$ is the expectation of A conditioned on B. The expectation in Equation (2.31) can be estimated using a sufficiently high number of h and $\acute{\mathbf{N}}_r$ realisations with the aid of Monte Carlo simulations for $r = 1, \ldots, N_r$.

The bandwidth efficiency η_{DCMC} of the DCMC is computed by normalising the DCMC capacity C_{DCMC} with respect to the product of W and T, where W is the bandwidth and T is the signalling period of the finite-energy signalling waveform. Furthermore, it was reported in [218][pp. 348-351] that the constellation dimension D is given by $D = 2WT$. Explicitly, the bandwidth efficiency as a function of the capacity is given by [215, 218, 219]:

$$\eta_{\text{DCMC}}(\text{SNR}) = \frac{C_{\text{DCMC}}(\text{SNR})}{WT} = \frac{C_{\text{DCMC}}(\text{SNR})}{D/2} \quad [\text{bits/sec/Hz}]. \tag{2.32}$$

For multiple-antenna aided transmitter using N_r coherent detectors provided with perfect knowledge of the channel coefficients at the receiver, the CCMC's [35] bandwidth efficiency can be formulated as follows [33]:

$$\eta_{\text{CCMC}}^{\text{coherent}}(SNR) = E\left[\log_2\left(1 + \sum_{r=1}^{N_r} \chi_{2N_t,r}^2 \frac{SNR}{N_t}\right)\right] \quad [\text{bits/sec/Hz}], \tag{2.33}$$

where the expectation $E[.]$ is taken over $\chi_{2N_t,r}^2$.

Figures 2.9, 2.10 and 2.11 show the DCMC capacity evaluated from Equation (2.31) for the four-dimensional SP modulation assisted DSTS as well as STS schemes for $L = 4$, 16 and 64, when employing $N_t = 2$ transmit antennas as well as $N_r = 1$, 2 and 4 receive antennas, respectively. The CCMC [35] capacity of the MIMO scheme was also plotted for comparison in Figures 2.9, 2.10 and 2.11 based on [33].

Figures 2.12, 2.13 and 2.14 quantify and compare the achievable bandwidth efficiency of both various SP modulated DSTS schemes and that of their identical-throughput conventionally modulated DSTS counterparts. The specific modulation type employed by the various schemes is outlined in Table 2.4. The figures explicitly illustrate that a higher bandwidth efficiency

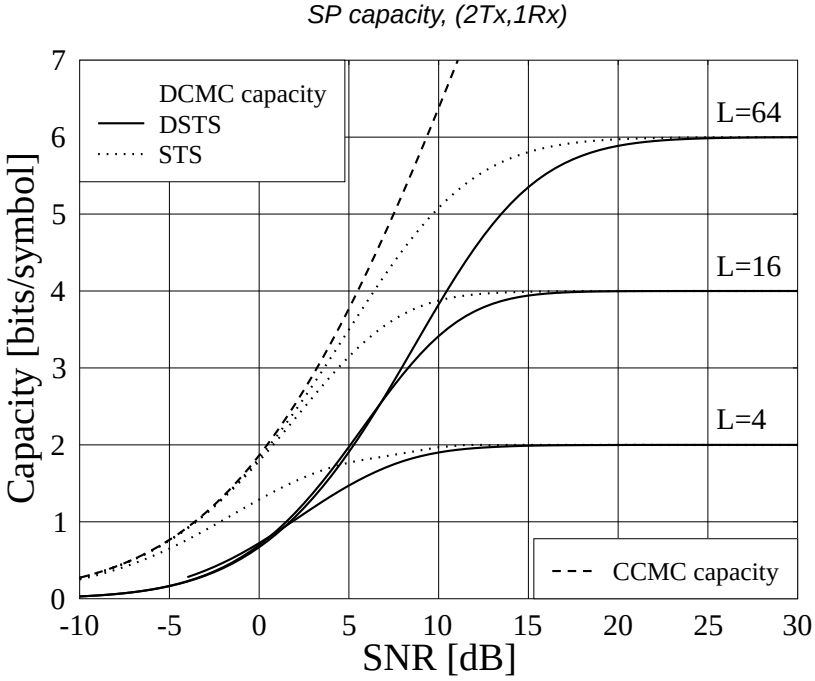

Figure 2.9: Capacity comparison of coherent and differential STS-SP based schemes evaluated from Equation (2.31) and using $L = 4$, 16 and 64, when employing $N_t = 2$ transmit and $N_r = 1$ receive antenna for communicating over a correlated Rayleigh fading channel having a normalised Doppler frequency of $f_D = 0.01$.

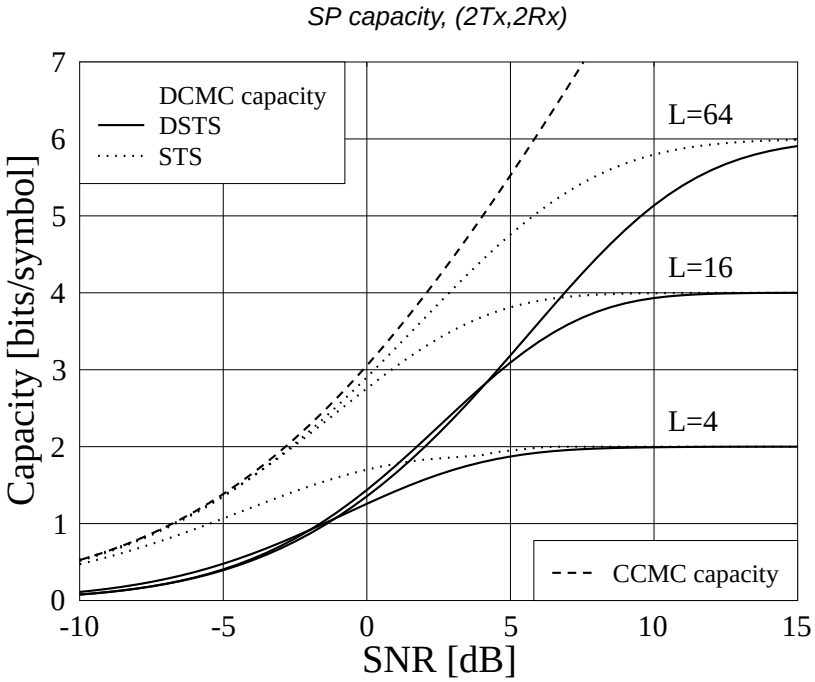

Figure 2.10: Capacity comparison of coherent and differential STS-SP based schemes evaluated from Equation (2.31) and using $L = 4$, 16 and 64, when employing $N_t = 2$ transmit and $N_r = 2$ receive antennas for communicating over a correlated Rayleigh fading channel having a normalised Doppler frequency of $f_D = 0.01$.

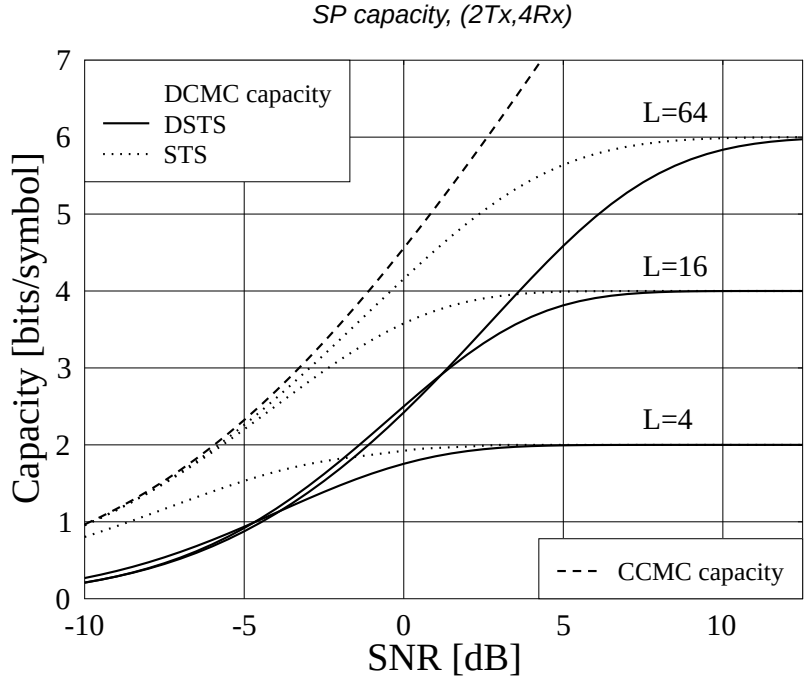

Figure 2.11: Capacity comparison of coherent and differential STS-SP based schemes evaluated from Equation (2.31) and using $L = 4$, 16 and 64, when employing $N_t = 2$ transmit and $N_r = 4$ receive antennas for communicating over a correlated Rayleigh fading channel having a normalised Doppler frequency of $f_D = 0.01$.

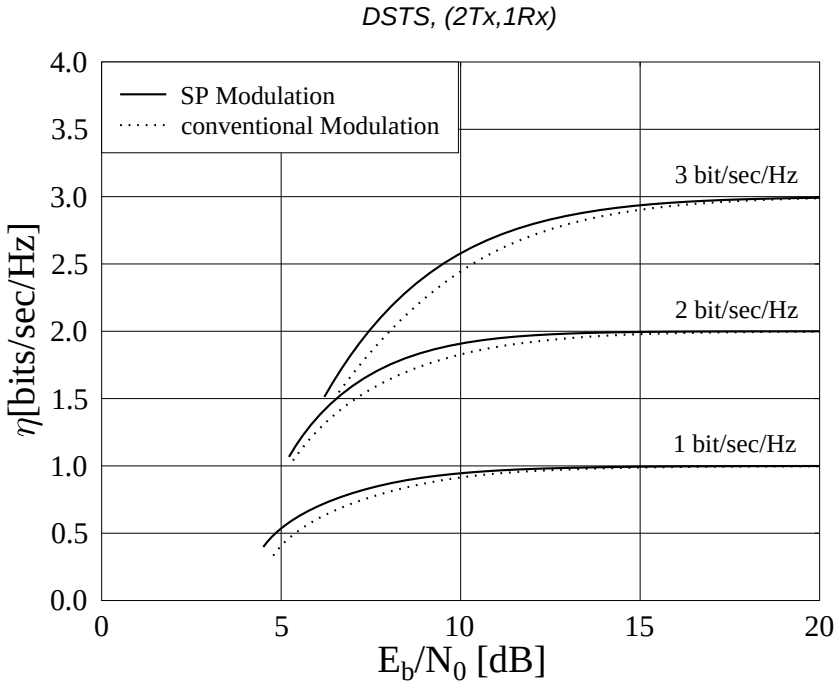

Figure 2.12: Bandwidth efficiency comparison of SP and conventional modulation aided DSTS schemes evaluated from Equation (2.32), when employing $N_t = 2$ transmit and $N_r = 1$ receive antenna for communicating over a correlated Rayleigh fading channel having a normalised Doppler frequency of $f_D = 0.01$.

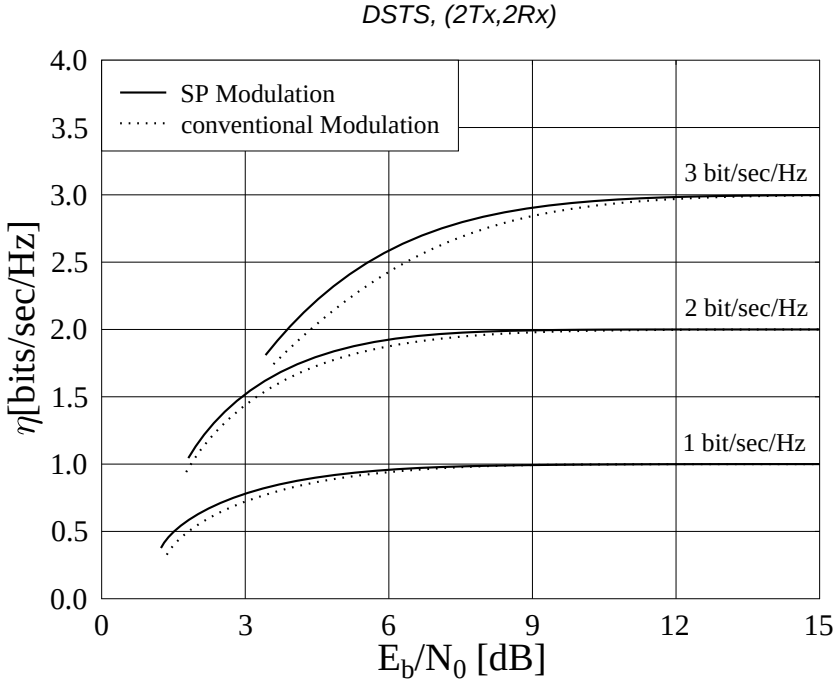

Figure 2.13: Bandwidth efficiency comparison of SP and conventional modulation aided DSTS schemes evaluated from Equation (2.32), when employing $N_t = 2$ transmit and $N_r = 2$ receive antenna for communicating over a correlated Rayleigh fading channel having a normalised Doppler frequency of $f_D = 0.01$.

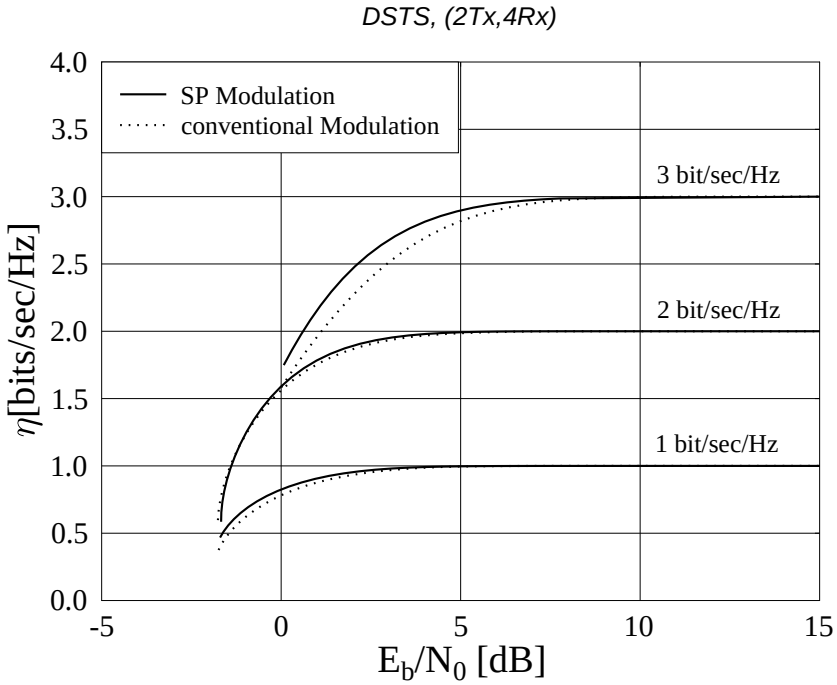

Figure 2.14: Bandwidth efficiency comparison of SP and conventional modulation aided DSTS schemes evaluated from Equation (2.32), when employing $N_t = 2$ transmit and $N_r = 4$ receive antenna for communicating over a correlated Rayleigh fading channel having a normalised Doppler frequency of $f_D = 0.01$.

Bandwidth Efficiency	Conventional Modulation	Sphere Packing Modulation
1	BPSK	$L = 4$
2	QPSK	$L = 16$
3	8-PSK	$L = 64$
4	16-PSK	$L = 256$

Table 2.4: Conventional and sphere packing modulation employed for different bandwidth efficiency rates.

may be attained, when employing SP modulation in conjunction with DSTS schemes having $N_t = 2$ transmit antennas as compared to an equivalent system employing conventional PSK modulation.

2.3.7 Performance of the Two-Antenna-Aided DSTS System

In this section, the two-antenna-aided DSTS schemes of Sections 2.3.1 and 2.3.3 are considered. Simulation results are provided for systems having different bandwidth efficiencies in conjunction with appropriate conventional and sphere packing modulation schemes, as outlined in Table 2.4. Observe that *two* consecutive time slots are required for transmitting a *single* SP symbol when using the two-antenna-aided system. By contrast, *two* conventionally modulated symbols are transmitted during the same time period. Therefore, the bandwidth efficiency of the sphere packing modulation scheme has to be twice as high as that of the conventional modulation scheme in order to compensate for the potential rate loss and to produce systems having an identical overall bandwidth efficiency. This explains the specific choices of L in Table 2.4. Our results are presented in terms of the Bit Error Ratio (BER) and Sphere Packing Symbol Error Ratio (SP-SER) performance curves for various systems employing $N_r = 1, 2, 3$, and 4 receive antennas for communication over a temporally correlated narrowband Rayleigh fading channel having a normalised Doppler frequency of $f_D = 0.01$.

Figures 2.15 and 2.16 compare the BER performance of both the differentially encoded as well as of the coherently detected space-time spreading while using BPSK modulated signals, two transmit antennas, a spreading factor of four in conjunction with one and four receive antennas, respectively. The coherent STS results are generated for the idealised scenario, where perfect channel knowledge is assumed at the receiver. As shown in Figures 2.15 and 2.16, the error doubling induced by the differential decoding results in a 3 dB performance loss as compared to coherent detection aided STS benefiting from perfect channel knowledge at the receiver. Again, this is mainly due to the fact that according to Equation (2.13) differential decoding results in doubling the noise power as compared to the coherently detected signals. However, the differential encoding/decoding process eliminates the complexity of channel es-

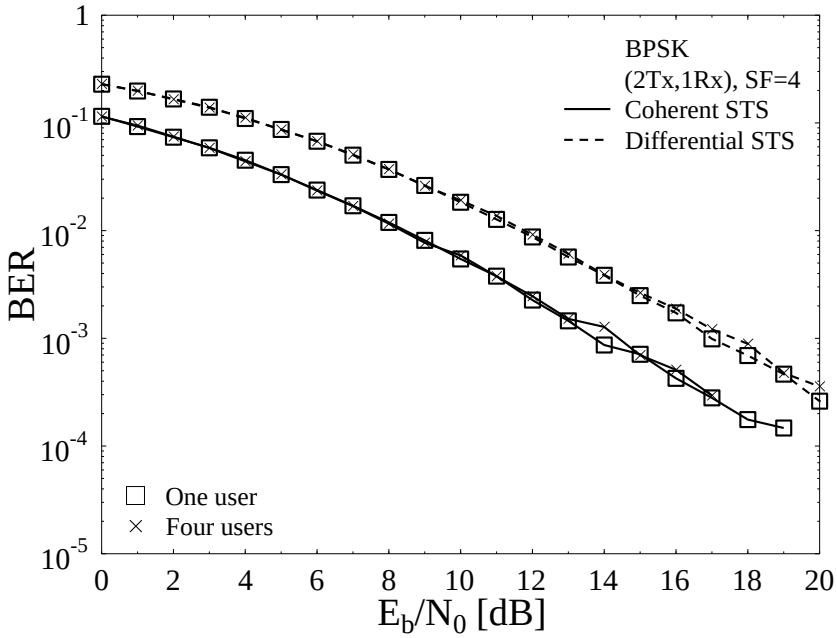

Figure 2.15: Comparison of the BER performance of coherent and differential space-time spreading, while using a BPSK modulated signal, two transmit antennas, one receive antenna, a spreading factor of 4 and a variable number of users.

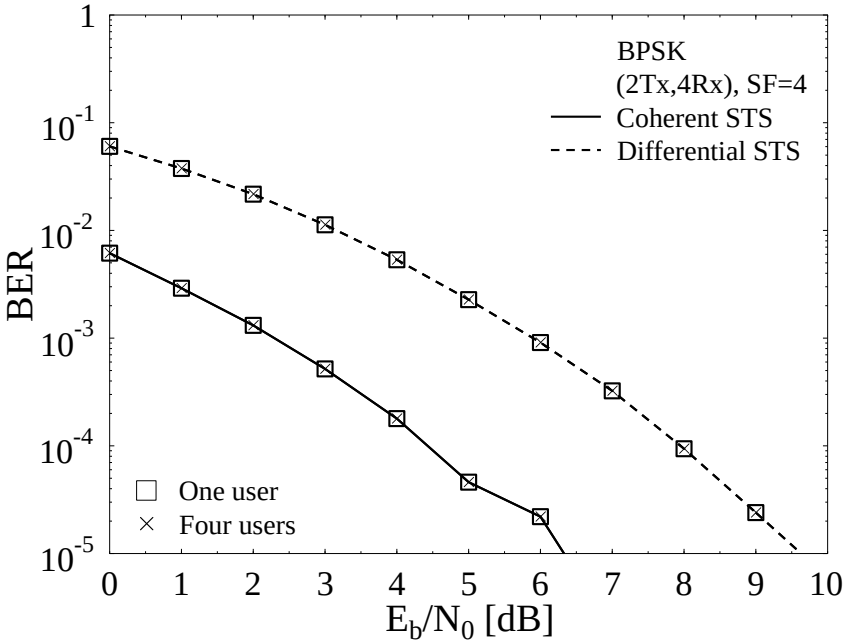

Figure 2.16: Comparison of the BER performance of coherent and differential space-time spreading, while using a BPSK modulated signal, two transmit antennas, four receive antennas, a spreading factor of 4 and a variable number of users.

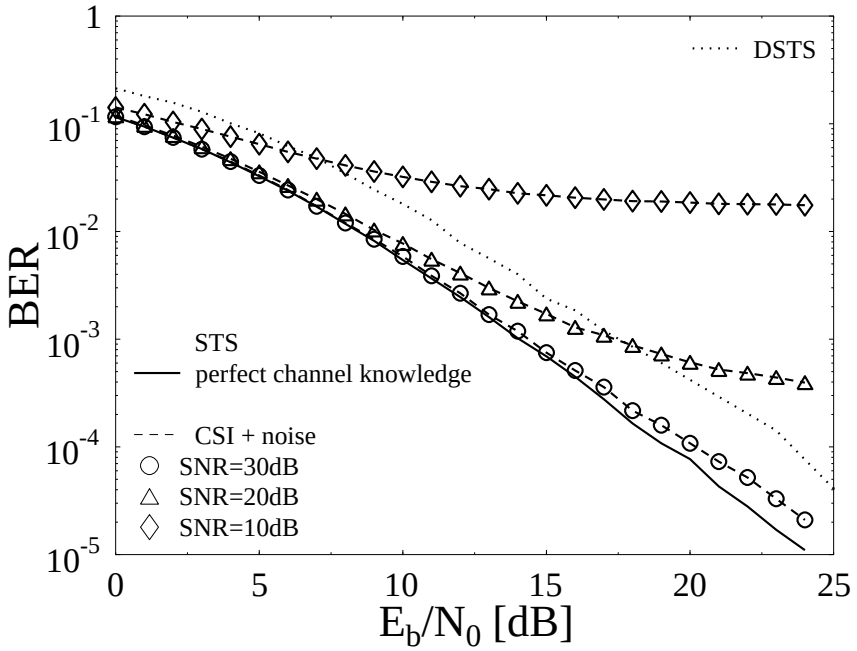

Figure 2.17: Comparison of the BER performance of coherent and differentially encoded non-coherent space-time spreading, while using a BPSK modulated signal, two transmit antennas, one receive antenna, a spreading factor of four for supporting a single user. The CSI in the coherent STS is contaminated with AWGN in order to compare the performance, when there is a channel estimation error.

timation required in coherent detection aided schemes, which is directly proportional to the product of the number of transmit and receive antennas and also depends on the characteristics of the channel. Additionally, it becomes clear from Figures 2.15 and 2.16 that the BER performance of both the DSTS and STS schemes is independent of the number of users in the system, which is a benefit of the fact that the spreading codes used are orthogonal and the channel is frequency-flat faded.

Furthermore, in order to study the effect of channel estimation error on the performance of the coherently detected STS signals, we contaminate the channel information at the receiver side with noise. We add AWGN to the channel information at the receiver side to model the effect of errors that may occur due to the channel estimation. Although the channel estimation error typically does not obey a Gaussian distribution, this simplified investigation gives us an insight concerning the effects of channel estimation errors on the system performance degradation of coherent systems. Figure 2.17 compares the BER performance of the DSTS and the STS scheme, while using two transmit antennas, one receive antenna, BPSK modulation, a spreading factor of four and a single user. As discussed previously, coherent systems assuming perfect channel knowledge at the receiver outperform their differentially encoded, non-coherently detected counterpart by about 3 dB. However, when we add noise to the CSI used by the coherent STS scheme, we see that the performance degrades, as shown in Figure 2.17. More quantita-

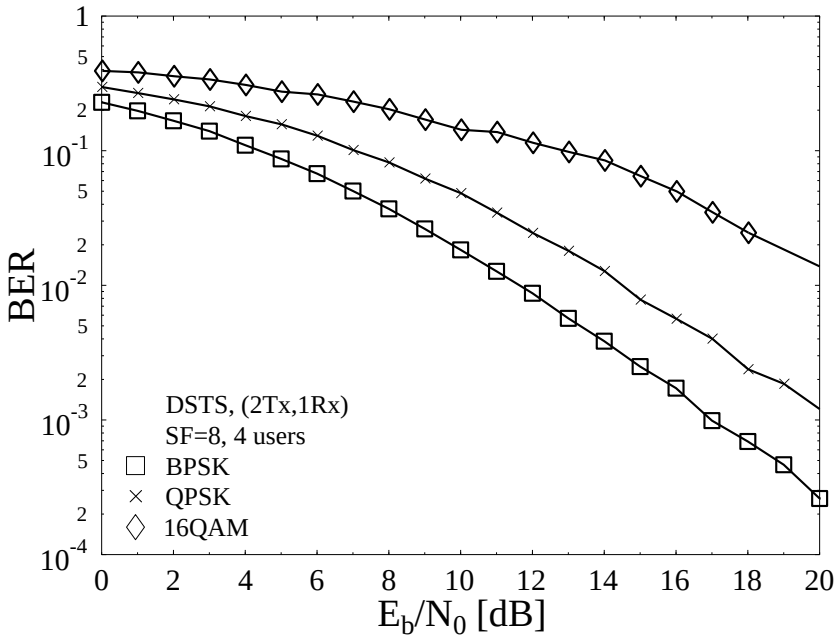

Figure 2.18: Comparison of the BER performance of differential space-time spreading while using PSK and QAM modulated signals, two transmit antennas, one receive antenna, a spreading factor of 4 and two users.

tively, Figure 2.17 shows that when the power of the channel estimation noise added to the CSI is increased and hence the corresponding CSI SNR is 20 dB or less, the performance of the coherent STS scheme tends to exhibit an error floor and its BER curve crosses the BER curve of the DSTS scheme. Beyond this cross-over point the DSTS outperforms the STS. Therefore, the DSTS constitutes a convenient and low-complexity design alternative to the coherent STS scheme, since the DSTS scheme eliminates the complexity of channel estimation and also results in a better performance when the channel estimation error is high.

On the other hand, Figure 2.18 compares the BER performance of the DSTS scheme using BPSK, QPSK as well as 16-QAM signals. Moreover, a comparison between the BER performance of both the differentially and coherently detected STS when using SP modulation is provided in Figure 2.19. As for the conventional modulation schemes, the differentially decoded system performs within 3 dB from the coherently detected one using perfect channel knowledge at the receiver.

Furthermore, in order to understand the effects of varying the Doppler frequency on the performance of the DSTS system, Figure 2.20 shows the attainable BER performance of the QPSK modulated system using two transmit antennas, one receive antenna and a spreading factor of four, while communicating over a temporally correlated narrowband Rayleigh fading channel and varying the Doppler frequency. As shown in the figure, when the normalised Doppler frequency increases from $f_D = 0.0001$ to 0.01, the system's performance remains similar. However, as the Doppler frequency increases beyond 0.01, the achievable BER performance substantially

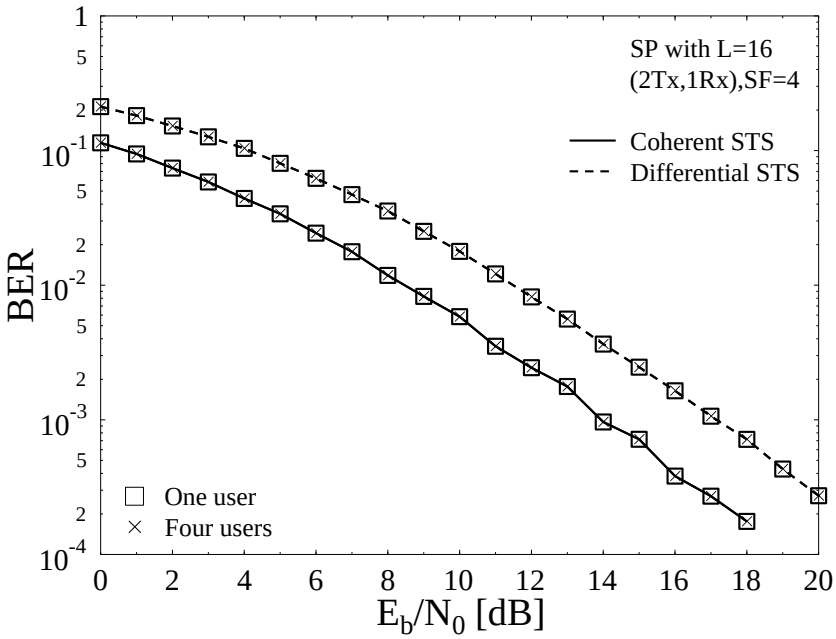

Figure 2.19: Comparison of the BER performance of coherent and differential space-time spreading, while employing SP modulated signal with L=16, two transmit antennas, one receive antenna, a spreading factor of 4 and a variable number of users.

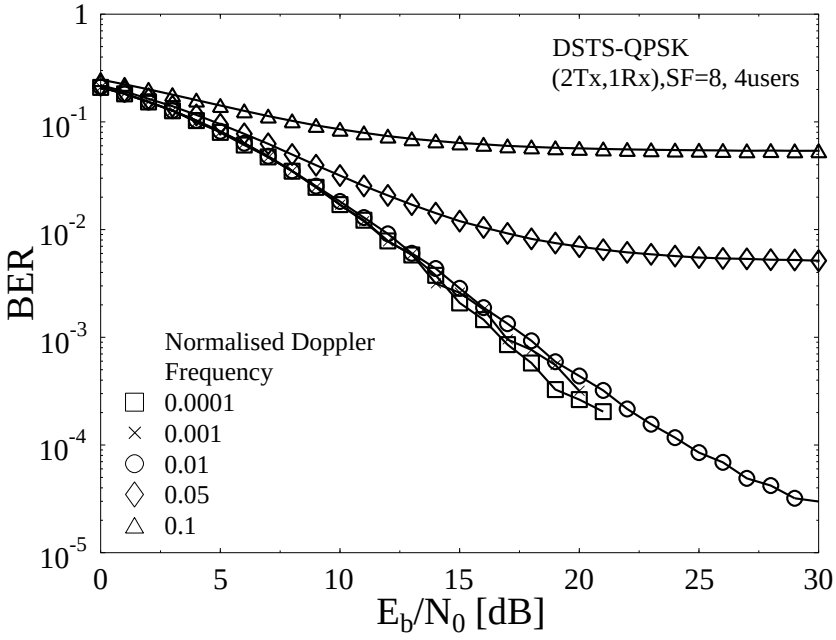

Figure 2.20: Comparison of the BER performance of differential space-time spreading while employing SP modulated signal with L=16, two transmit antennas, one receive antenna, a spreading factor of 4 and two users for a different normalised Doppler frequency values.

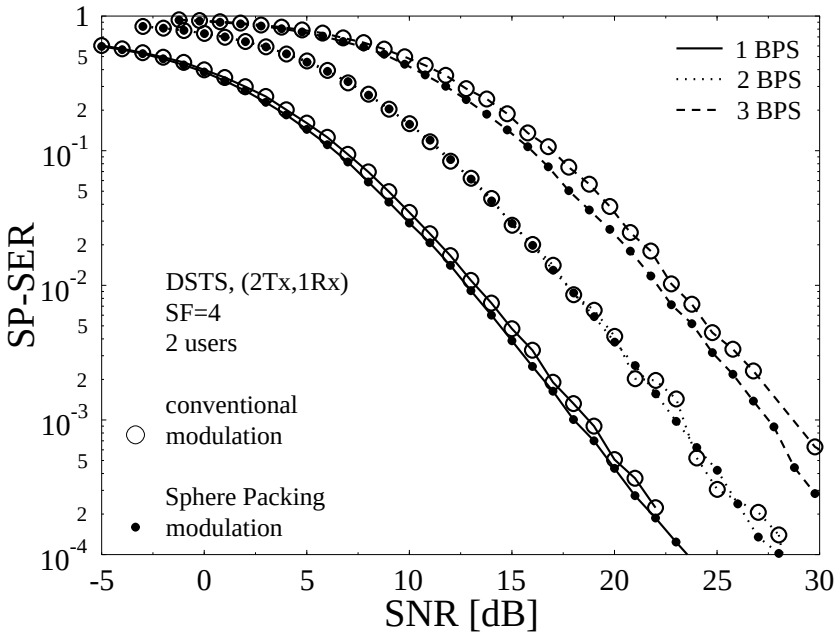

Figure 2.21: Performance comparison of the SP-SER of DSTS in combination with conventional modulation and sphere packing modulation for different bandwidth efficiency rates as outlined in Table 2.4 while employing two transmit antennas, one receive antenna, a spreading factor of four, two users and communicating over a correlated Rayleigh fading channel associated with $f_D = 0.01$.

degrades. This is predominantly due to the fact that increasing the Doppler frequency makes the channel fast fading and thus the differential decoding scheme, which relies on the fact that the subsequent symbols experience similar fading, performs poorly.

Figure 2.21 shows the SP-SER performance curves of the DSTS scheme in conjunction with different conventional as well as SP modulations at various bandwidth efficiency values, as outlined in Table 2.4. All systems employ two transmit antennas for communication over a correlated Rayleigh fading channel associated with $f_D = 0.01$. Moreover, the system uses a spreading factor of four and here accommodates two users. It is evident from Figure 2.21 that for a particular bandwidth efficiency, the two curves corresponding to the conventional modulation and to the SP modulation schemes have the same asymptotic slope (i.e. diversity order). This observation is based on the fact that the DSTS scheme is capable of achieving full diversity, similar to Alamouti's STBC scheme [44]. Accordingly, it is not expected that the asymptotic slope of the performance curves would improve by merely employing new modulation schemes without introducing another level of channel coding. The resultant BER performance curves are shown in Figure 2.22. Notice that SP modulation attains a better SP-SER performance than the conventionally modulated DSTS scheme and this is expected, since SP was specifically designed for improving the DSTS-SP-SER as compared to conventional DSTS schemes. However, observe in Figure 2.22 that the BER performances of SP modulation and conventional modulation are identical for systems having a bandwidth efficiency of 2 bits-per-channel-use because it can

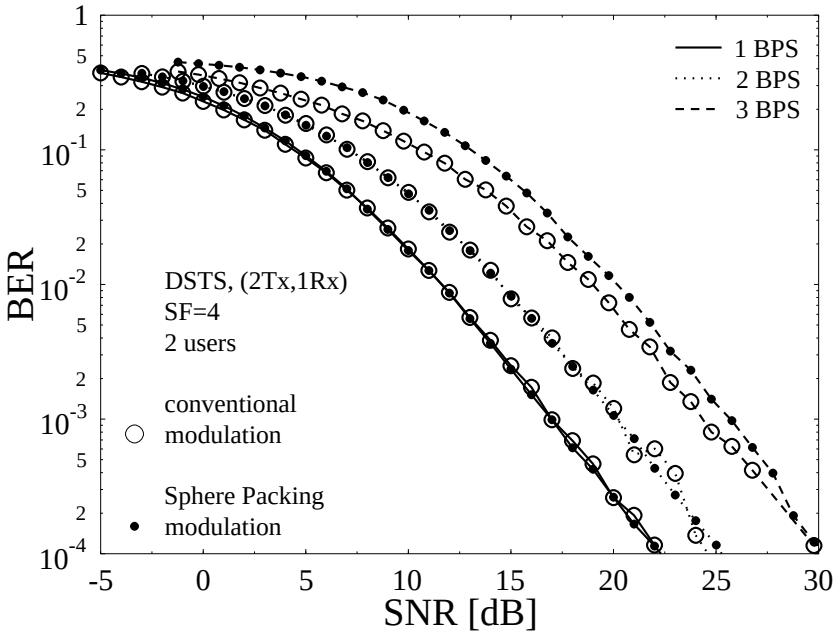

Figure 2.22: Performance comparison of the BER of DSTS in combination with conventional modulation and sphere packing modulation for different bandwidth efficiency rates as outlined in Table 2.4 while employing two transmit antennas, one receive antenna, a spreading factor of four, two users and communicating over a correlated Rayleigh fading channel associated with $f_D = 0.01$.

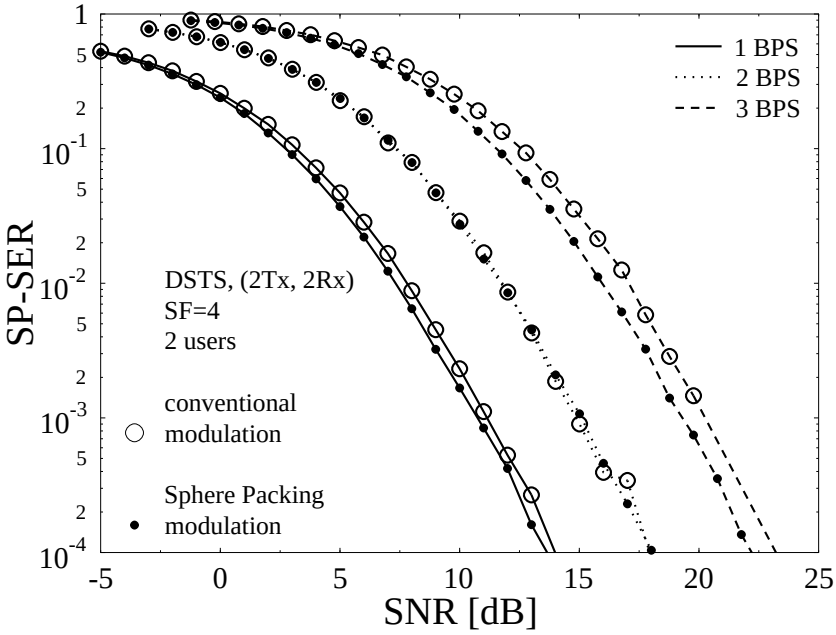

Figure 2.23: Performance comparison of the SP-SER of DSTS in combination with conventional modulation and sphere packing modulation for different bandwidth efficiency rates as outlined in Table 2.4 while employing two transmit antennas, two receive antenna, a spreading factor of four, two users and communicating over a correlated Rayleigh fading channel associated with $f_D = 0.01$.

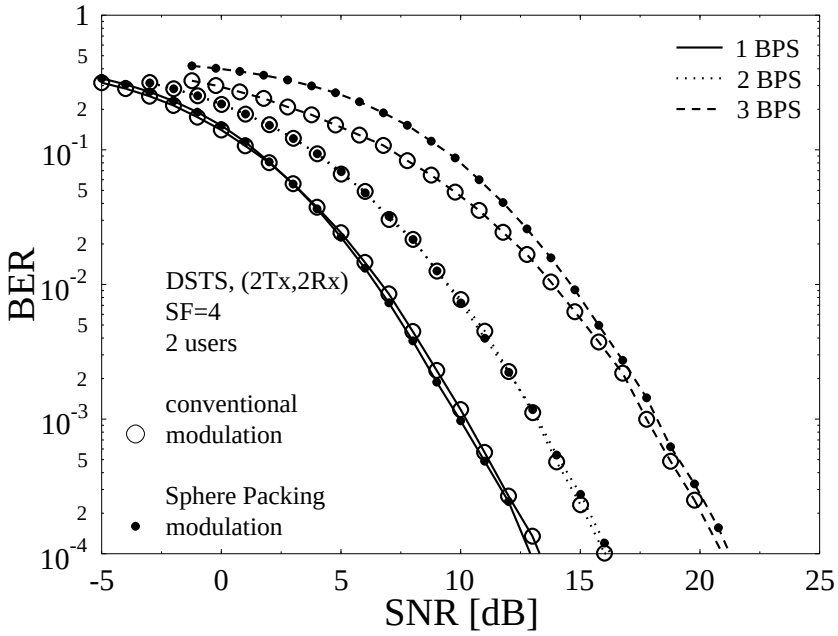

Figure 2.24: Performance comparison of the BER of DSTS in combination with conventional modulation and sphere packing modulation for different bandwidth efficiency rates as outlined in Table 2.4 while employing two transmit antennas, two receive antenna, a spreading factor of four, two users and communicating over a correlated Rayleigh fading channel associated with $f_D = 0.01$.

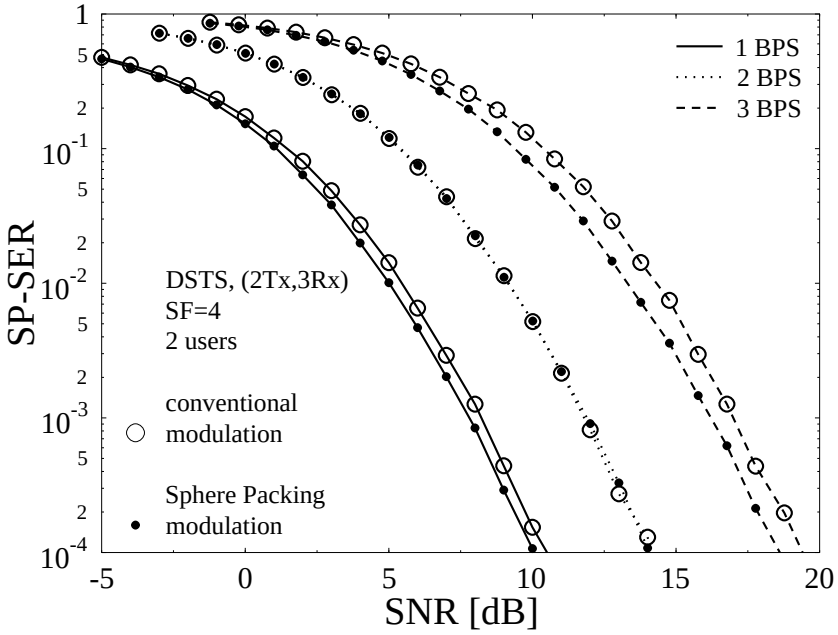

Figure 2.25: Performance comparison of the SP-SER of DSTS in combination with conventional modulation and sphere packing modulation for different bandwidth efficiency rates as outlined in Table 2.4 while employing two transmit antennas, three receive antenna, a spreading factor of four, two users and communicating over a correlated Rayleigh fading channel exhibiting $f_D = 0.01$.

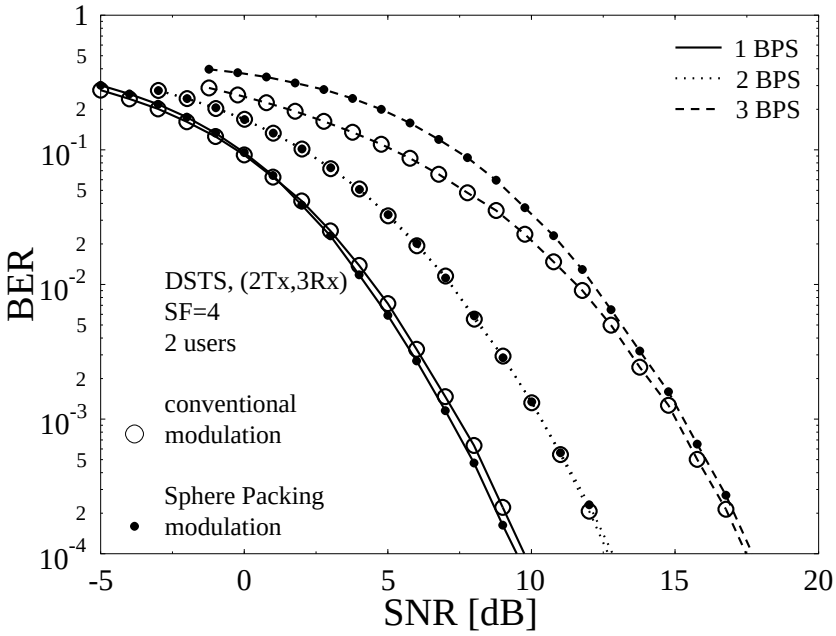

Figure 2.26: Performance comparison of the BER of DSTS in combination with conventional modulation and sphere packing modulation for different bandwidth efficiency rates as outlined in Table 2.4 while employing two transmit antennas, three receive antenna, a spreading factor of four, two users and communicating over a correlated Rayleigh fading channel exhibiting $f_D = 0.01$.

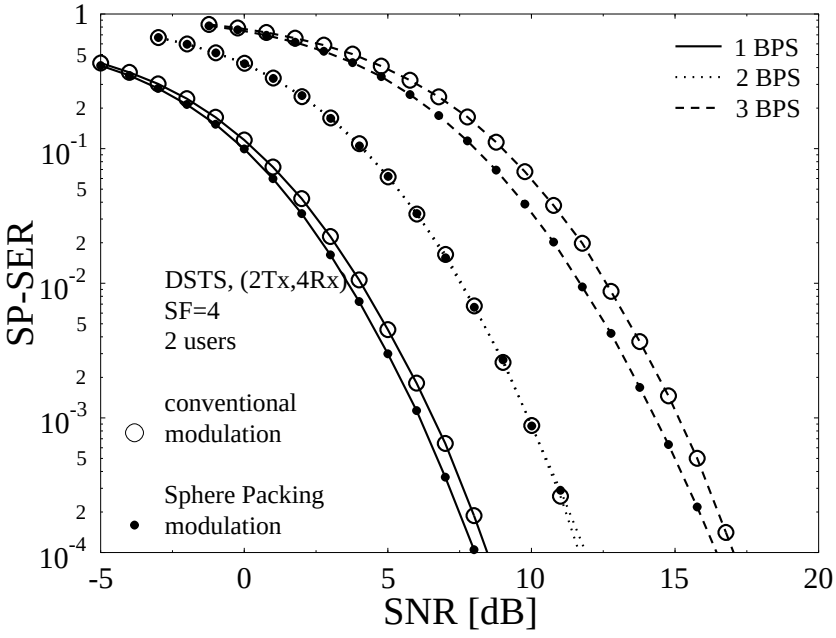

Figure 2.27: Performance comparison of the SP-SER of DSTS in combination with conventional modulation and sphere packing modulation for different bandwidth efficiency rates as outlined in Table 2.4 while employing two transmit antennas, four receive antenna, a spreading factor of four, two users and communicating over a correlated Rayleigh fading channel exhibiting $f_D = 0.01$.

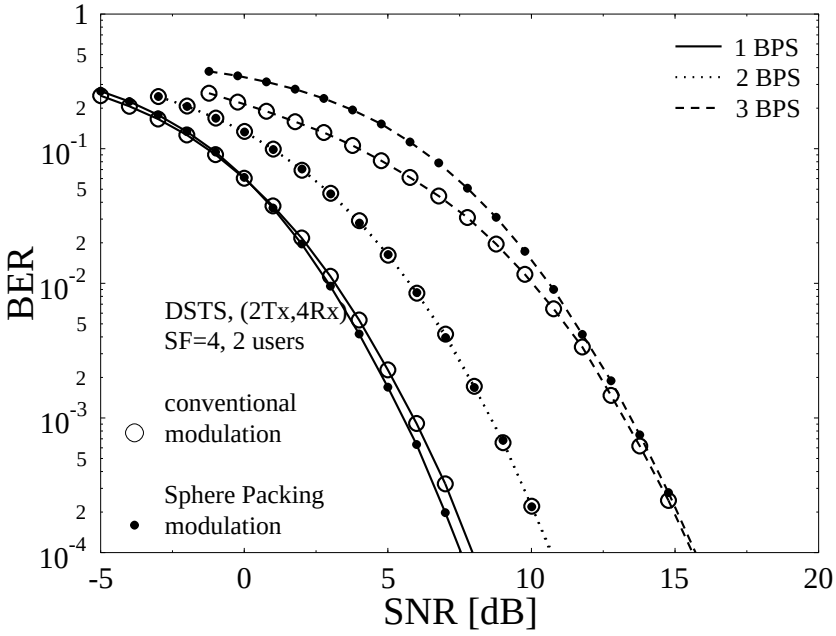

Figure 2.28: Performance comparison of the BER of DSTS in combination with conventional modulation and sphere packing modulation for different bandwidth efficiency rates as outlined in Table 2.4 while employing two transmit antennas, four receive antenna, a spreading factor of four, two users and communicating over a correlated Rayleigh fading channel exhibiting $f_D = 0.01$.

be shown [58] that at this throughput they constitute specific manifestation of each other. By contrast, the DSTS-SP BER performance recorded for 3 bits-per-channel-use is marginally worse than that of the conventionally modulated DSTS schemes, as shown in Figure 2.22, which demonstrates that the marginal advantage of conventional modulation over SP modulation diminishes at high SNRs.

Figures 2.23 to 2.28 illustrate the beneficial effect of increasing the number of receive antennas from two to four, respectively. Observe in Figures 2.24, 2.26 and 2.28 that the BER performance of SP modulation improves in comparison to that of conventional modulation upon increasing the number of receive antennas, especially for schemes having bandwidth efficiencies of 1 and 3 bits-per-channel-use. Observe, however, in Figures 2.21 to 2.28 that both the BER and SP-SER performance curves of QPSK modulation as well as those of the identical-throughput SP modulation having L=16 are identical. Again, this phenomenon is due to the fact that QPSK modulation is a special case of the SP modulation constellation, when combined with DSTS. More specifically, let us consider the DSTS signal, when $x_{l,1}$ and $x_{l,2}$ are chosen independently from the QPSK modulation constellation, then the 16 legitimate combined signals produced will be identical to the 16 legitimate signals constructed using Equation (2.21), where $(a_{l,1}, a_{l,2}, a_{l,3}, a_{l,4})$, $l = 0, \ldots, 15$, correspond to the L=16 SP constellation points hosted by D_4.

Finally, the attainable coding gains of SP modulation over conventional modulation are

	1 BPS	2 BPS	3 BPS
$1Rx$	0.20 dB	0.0 dB	0.70 dB
$2Rx$	0.25 dB	0.0 dB	0.90 dB
$3Rx$	0.30 dB	0.0 dB	0.95 dB
$4Rx$	0.30 dB	0.0 dB	1.00 dB

Table 2.5: Coding gains of SP modulation over conventional modulation at SP-SER of 10^{-4} for the schemes of Figures 2.21, 2.23, 2.25 and 2.27, when communicating over a correlated Rayleigh fading channel associated with $f_D = 0.01$.

summarised in Table 2.5 for the schemes characterised in Figures 2.21 to 2.28 at an SP-SER of 10^{-4}, when communicating over a correlated Rayleigh fading channel associated with $f_D = 0.01$.

2.4 DSTS Design Using Four Transmit Antennas

In the following section, we present the design of the DSTS system using four transmit antennas that can be implemented together with real- and complex-valued phasor constellations as well as with SP modulation.

2.4.1 Design Using Real-Valued Constellations

A high level block diagram of the four-antenna-aided DSTS scheme in shown in Figure 2.29, where the DSTS encoder is divided into two main stages. The differential encoding takes place after which the differentially encoded symbol matrices are space-time spread. Moreover, the basic principle of the four-antenna-aided STS is exemplified in simple graphical terms in Figure 2.30, where a 8-chip orthogonal spreading code was used for spreading each bit of duration T_b to an interval of $T_s = 4T_b$.

The DSTS encoding and decoding algorithms operate as follows. At time instant $t = 0$, the arbitrary dummy reference *real-valued* symbols v_0^1, v_0^2, v_0^3 and v_0^4 are transmitted from antennas one, two, three and four, respectively. At time instants $t \geq 1$, a block of $4B$ bits arrives at the modulator of Figure 2.29, where each set of B bits is mapped to a real-valued modulated symbol x_t^k, $k = 1, 2, 3, 4$, selected from a 2^B-ary constellation.

Assuming v_t^k to be the symbol transmitted from antenna k, $k = 1, 2, 3, 4$, at time instant t, differential encoding is carried out as follows:

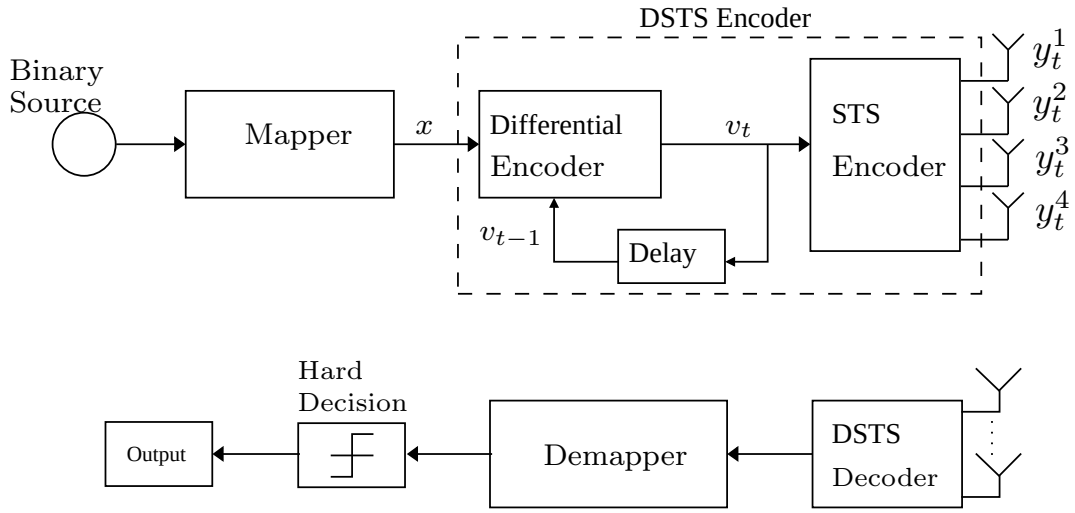

Figure 2.29: The four transmit antenna differential space-time spreading system block diagram.

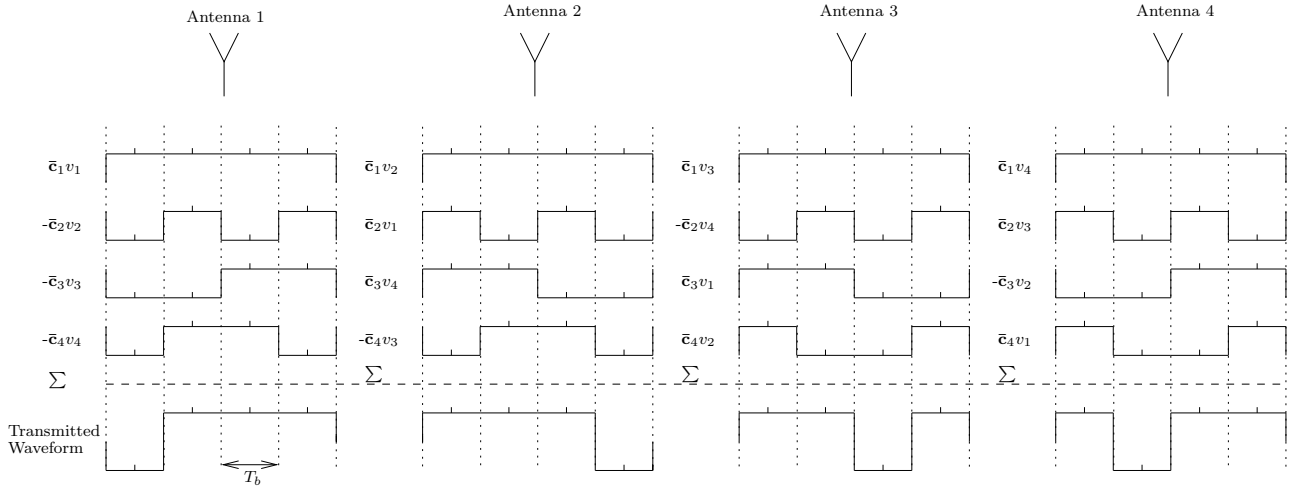

Figure 2.30: Illustration of STS using four transmit antennas transmitting 4 bits within $4T_b$ duration. v_1=v_2=v_3=v_4=1 were assumed and $\bar{\mathbf{c}}_1 = [+1+1+1+1+1+1+1+1]$, $\bar{\mathbf{c}}_2 = [+1+1-1-1+1+1-1-1]$, $\bar{\mathbf{c}}_3 = [+1+1+1+1-1-1-1-1]$ and $\bar{\mathbf{c}}_4 = [+1+1-1-1-1-1+1+1]$.

$$\mathbf{V_t} = \begin{pmatrix} v_t^1 \\ v_t^2 \\ v_t^3 \\ v_t^4 \end{pmatrix} = x_t^1 \cdot \begin{pmatrix} v_{t-1}^1 \\ v_{t-1}^2 \\ v_{t-1}^3 \\ v_{t-1}^4 \end{pmatrix} + x_t^2 \cdot \begin{pmatrix} v_{t-1}^2 \\ -v_{t-1}^1 \\ v_{t-1}^4 \\ -v_{t-1}^3 \end{pmatrix} + x_t^3 \cdot \begin{pmatrix} v_{t-1}^3 \\ -v_{t-1}^4 \\ -v_{t-1}^1 \\ v_{t-1}^2 \end{pmatrix} + x_t^4 \cdot \begin{pmatrix} v_{t-1}^4 \\ v_{t-1}^3 \\ -v_{t-1}^2 \\ -v_{t-1}^1 \end{pmatrix}. \tag{2.34}$$

The vector $\mathbf{V_t}$ of Equation (2.34) is normalised by the magnitude of the previously computed vector $\mathbf{V_{t-1}}$ before transmission in order to limit the peak power and hence the out-of-band power emissions.

The differentially encoded symbols are then spread with the aid of the spreading codes $\bar{\mathbf{c}}_1$, $\bar{\mathbf{c}}_2$, $\bar{\mathbf{c}}_3$ and $\bar{\mathbf{c}}_4$, which are generated from the same user-specific spreading code $\bar{\mathbf{c}}$ by ensuring that they are orthogonal using the simple code-concatenation rule of Walsh-Hadamard codes,

yielding longer codes and hence a proportionately reduced per antenna throughput according to:

$$\bar{\mathbf{c}}_1^T = [\bar{\mathbf{c}} \quad \bar{\mathbf{c}} \quad \bar{\mathbf{c}} \quad \bar{\mathbf{c}}] \tag{2.35}$$

$$\bar{\mathbf{c}}_2^T = [\bar{\mathbf{c}} \quad -\bar{\mathbf{c}} \quad \bar{\mathbf{c}} \quad -\bar{\mathbf{c}}] \tag{2.36}$$

$$\bar{\mathbf{c}}_3^T = [\bar{\mathbf{c}} \quad \bar{\mathbf{c}} \quad -\bar{\mathbf{c}} \quad -\bar{\mathbf{c}}] \tag{2.37}$$

$$\bar{\mathbf{c}}_4^T = [\bar{\mathbf{c}} \quad -\bar{\mathbf{c}} \quad -\bar{\mathbf{c}} \quad \bar{\mathbf{c}}]. \tag{2.38}$$

The differentially encoded data is then divided into four quarter-rate substreams and the four consecutive symbols are then spread to the four transmit antennas as shown in Figures 2.29 and 2.30 using the mapping of:

$$\mathbf{y}_t^1 = \frac{1}{\sqrt{4}}\left(\bar{\mathbf{c}}_1 \cdot v_t^1 - \bar{\mathbf{c}}_2 \cdot v_t^2 - \bar{\mathbf{c}}_3 \cdot v_t^3 - \bar{\mathbf{c}}_4 \cdot v_t^4\right) \tag{2.39}$$

$$\mathbf{y}_t^2 = \frac{1}{\sqrt{4}}\left(\bar{\mathbf{c}}_1 \cdot v_t^2 + \bar{\mathbf{c}}_2 \cdot v_t^1 + \bar{\mathbf{c}}_3 \cdot v_t^4 - \bar{\mathbf{c}}_4 \cdot v_t^3\right) \tag{2.40}$$

$$\mathbf{y}_t^3 = \frac{1}{\sqrt{4}}\left(\bar{\mathbf{c}}_1 \cdot v_t^3 - \bar{\mathbf{c}}_2 \cdot v_t^4 + \bar{\mathbf{c}}_3 \cdot v_t^1 + \bar{\mathbf{c}}_4 \cdot v_t^2\right) \tag{2.41}$$

$$\mathbf{y}_t^4 = \frac{1}{\sqrt{4}}\left(\bar{\mathbf{c}}_1 \cdot v_t^4 + \bar{\mathbf{c}}_2 \cdot v_t^3 - \bar{\mathbf{c}}_3 \cdot v_t^2 + \bar{\mathbf{c}}_4 \cdot v_t^1\right). \tag{2.42}$$

Assuming the channel to be temporally correlated narrowband Rayleigh fading, the received signal at the output of the single receive antenna can be represented as:

$$\mathbf{r}_t = h_1 \cdot \mathbf{y}_t^1 + h_2 \cdot \mathbf{y}_t^2 + h_3 \cdot \mathbf{y}_t^3 + h_4 \cdot \mathbf{y}_t^4 + \mathbf{n}_t, \tag{2.43}$$

where h_1, h_2, h_3 and h_4 denote the narrowband complex-valued CIRs corresponding to the four transmit antennas, while $\mathbf{n}_t$ is a complex-valued Gaussian random variable having a covariance matrix of $\sigma_n^2 \cdot \mathbf{I}_{SF}$, where SF is the spreading factor of the per-antenna spreading code $\bar{\mathbf{c}}_k$, $k = 1, 2, 3, 4$.

The received signal $\mathbf{r}_t$ is then correlated with $\bar{\mathbf{c}}_1$, $\bar{\mathbf{c}}_2$, $\bar{\mathbf{c}}_3$ and $\bar{\mathbf{c}}_4$ according to the following operation: $d_t^k = \bar{\mathbf{c}}_k^\dagger \cdot \mathbf{r}_t$, $k \in [1, \cdots, 4]$. After the correlation operation we arrive at four data symbols represented by:

$$d_t^1 = \frac{1}{\sqrt{4}} \cdot h_1 \cdot v_t^1 + \frac{1}{\sqrt{4}} \cdot h_2 \cdot v_t^2 + \frac{1}{\sqrt{4}} \cdot h_3 \cdot v_t^3 + \frac{1}{\sqrt{4}} \cdot h_4 \cdot v_t^4 + \bar{\mathbf{c}}_1^\dagger \cdot \mathbf{n}_t \tag{2.44}$$

$$d_t^2 = -\frac{1}{\sqrt{4}} \cdot h_1 \cdot v_t^2 + \frac{1}{\sqrt{4}} \cdot h_2 \cdot v_t^1 - \frac{1}{\sqrt{4}} \cdot h_3 \cdot v_t^4 + \frac{1}{\sqrt{4}} \cdot h_4 \cdot v_t^3 + \bar{\mathbf{c}}_2^\dagger \cdot \mathbf{n}_t \tag{2.45}$$

$$d_t^3 = -\frac{1}{\sqrt{4}} \cdot h_1 \cdot v_t^3 + \frac{1}{\sqrt{4}} \cdot h_2 \cdot v_t^4 + \frac{1}{\sqrt{4}} \cdot h_3 \cdot v_t^1 - \frac{1}{\sqrt{4}} \cdot h_4 \cdot v_t^2 + \bar{\mathbf{c}}_3^\dagger \cdot \mathbf{n}_t \tag{2.46}$$

$$d_t^4 = -\frac{1}{\sqrt{4}} \cdot h_1 \cdot v_t^4 - \frac{1}{\sqrt{4}} \cdot h_2 \cdot v_t^3 + \frac{1}{\sqrt{4}} \cdot h_3 \cdot v_t^2 + \frac{1}{\sqrt{4}} \cdot h_4 \cdot v_t^1 + \bar{\mathbf{c}}_4^\dagger \cdot \mathbf{n}_t. \tag{2.47}$$

To derive the decoder equations of the DSTS receiver, the received signals in Equations (2.44)-(2.47) are rearranged in vectorial form as follows:

$$\mathbf{R}^1_{t-1} = \left(d^1_{t-1}, d^2_{t-1}, d^3_{t-1}, d^4_{t-1}\right) \quad (2.48)$$

$$\mathbf{R}^2_{t-1} = \left(-d^2_{t-1}, d^1_{t-1}, d^4_{t-1}, -d^3_{t-1}\right) \quad (2.49)$$

$$\mathbf{R}^3_{t-1} = \left(-d^3_{t-1}, -d^4_{t-1}, d^1_{t-1}, d^2_{t-1}\right) \quad (2.50)$$

$$\mathbf{R}^4_{t-1} = \left(-d^4_{t-1}, d^3_{t-1}, -d^2_{t-1}, d^1_{t-1}\right) \quad (2.51)$$

$$\mathbf{R}_t = \left(d^1_t, d^2_t, d^3_t, d^4_t\right). \quad (2.52)$$

To decode the transmitted symbols x^k_t, $k = 1, 2, 3, 4$, the decoder uses Equations (2.48)-(2.52) and computes:

$$\begin{aligned} \tilde{x}^k_t = Re\{\mathbf{R}_t \cdot \mathbf{R}^k_{t-1}\} &= \frac{1}{4} \cdot \sum_{i=1}^{4} |h_i|^2 \cdot \sqrt{\sum_{j=1}^{4} |v^j_{t-1}|^2} \cdot x^k_t + N_k \\ &= \chi^2_{2N_t} \cdot x^k_t + N_k, \end{aligned} \quad (2.53)$$

where $Re\{\cdot\}$ denotes the *real* part of a complex number, $\chi^2_{2N_t}$ represents a chi-squared random variable having $2N_t = 8$ degrees of freedom and N_k denotes the noise term having a variance of $\chi^2_{2N_t} \cdot N_0/2$. The receiver estimates x^k_t based on Equation (2.53) by employing a Maximum Likelihood decoder.

According to Equation (2.53), the receiver only has to estimate $\sum_{i=1}^{4} |h_i|^2$ in order to decode non-constant modulus real-valued constellations, such as Pulse Amplitude Modulation (PAM). In other words, the receiver does not have to estimate the individual CIR tap values of h_i, $i = 1, 2, 3, 4$, only $\sum_{i=1}^{4} |h_i|^2$ and $\sqrt{\sum_{j=1}^{4} |v^j_{t-1}|^2}$ has to be estimated in order to recover PAM modulated information from the received signal of Equation (2.53). A simple channel power estimator may be derived by computing the autocorrelation of the received signal as follows [68]:

$$E\{d^i_t \cdot d^i_t\} = \sum_{i=1}^{4} |h_i|^2 + \sigma^2_n \,. \quad (2.54)$$

The power of the previously transmitted symbols $\sqrt{\sum_{j=1}^{4} |v^j_{t-1}|^2}$ can be estimated from the previous output of the decoder [68].

We can observe from Equation (2.53) that the proposed method guarantees achieving a full diversity gain, while using a low-complexity decoding algorithm. Since $\bar{\mathbf{c}}_k$, $k = 1, 2, 3, 4$, are derived by appropriately concatenating the user-specific code $\bar{\mathbf{c}}$, no extra spreading codes are required for carrying out the STS operation and the four symbols of the four transmitters are transmitted in four time slots.

2.4.2 Design Using Complex-Valued Constellations

Quadrature Amplitude Modulated (QAM) signals represented by complex-valued constellations can also be transmitted using the proposed four-antenna-aided DSTS scheme. Accordingly, we assume that at time instant t, a block of $4B$ bits arrives at the encoder, where each $2B$ bits are modulated using an M-ary complex-valued constellation, so that we have $2B = \log_2 M$. The modulator outputs the two complex symbols x_{tc}^1 and x_{tc}^2, conveying the original $4B$ bits, where the postscript c is used to denote complex symbols. Now x_{tc}^1 and x_{tc}^2 are mapped to x_t^k, $k = 1, 2, 3, 4$, defined in the previous section as follows

$$(x_t^1, x_t^2, x_t^3, x_t^4) = (Re\{x_{tc}^1\}, Im\{x_{tc}^1\}, Re\{x_{tc}^2\}, Im\{x_{tc}^2\}). \tag{2.55}$$

Similarly to real-valued constellations, $\tilde{x}_t^k$, $k = 1, 2, 3, 4$, can be estimated using Equation (2.53), which is then used to recover the original complex symbols $\tilde{x}_{tc}^1$ and $\tilde{x}_{tc}^2$ as follows:

$$(\tilde{x}_{tc}^1, \tilde{x}_{tc}^2) = (\tilde{x}_t^1 + j\tilde{x}_t^2, \tilde{x}_t^3 + j\tilde{x}_t^4). \tag{2.56}$$

2.4.3 Design Using Sphere Packing Modulation

According to Equation (2.53), the decoded signals represent scaled versions of x_t^1, x_t^2, x_t^3 and x_t^4 corrupted by the complex-valued AWGN. This observation implies that the diversity product of the four-antenna-aided DSTS scheme is determined by the minimum Euclidean distance of all legitimate vectors (x_t^1, x_t^2, x_t^3, x_t^4). The idea is to jointly design the legitimate four-component vectors (x_t^1, x_t^2, x_t^3, x_t^4) so that they are represented by a single phasor point selected from a sphere packing constellation corresponding to a four-dimensional real-valued lattice having the best known minimum Euclidean distance in the four-dimensional real-valued space $\mathbb{R}^4$. For the sake of generalising our treatment, let us assume that there are L legitimate vectors ($x^{l,1}$, $x^{l,2}$, $x^{l,3}$, $x^{l,4}$), $l = 0, 1, \ldots, L-1$, where L represents the number of four-component sphere-packed modulated symbols. The transmitter, then, has to choose the modulated signal from these L legitimate symbols, which have to be differentially space-time spread and transmitted from the four transmit antennas. The bandwidth efficiency of the four-antenna-aided DSTS-SP system is $(\log_2 L)/4$ bits-per-channel-use.

In contrast to the independent transmitted signal design of Section 2.4.1, the aim is to design $x^{l,1}$, $x^{l,2}$, $x^{l,3}$, $x^{l,4}$ jointly, so that they have the best minimum Euclidean distance from all other $(L-1)$ legitimate SP symbols, since this minimises the system's SP symbol error probability. Let $(a^{l,1}, a^{l,2}, a^{l,3}, a^{l,4})$, $l = 0, 1, \ldots, L-1$, be legitimate phasor points of the four-dimensional

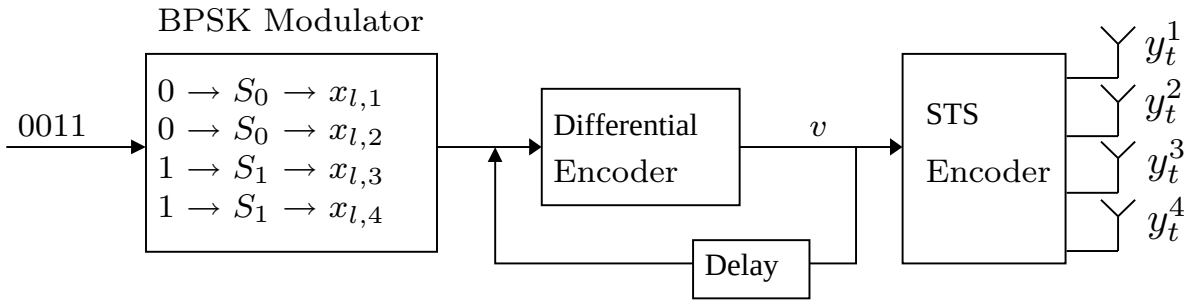

Figure 2.31: Transmission of four BPSK symbols using a four-antenna-aided DSTS scheme.

real-valued Euclidean space $\mathbb{R}^4$. Hence, $x^{l,1}$, $x^{l,2}$, $x^{l,3}$, $x^{l,4}$ may be written as

$$\begin{aligned} \{x^{l,1}, x^{l,2}, x^{l,3}, x^{l,4}\} &= T_{sp}(a^{l,1}, a^{l,2}, a^{l,3}, a^{l,4}) \\ &= \left\{a^{l,1}, a^{l,2}, a^{l,3}, a^{l,4}\right\}. \end{aligned} \tag{2.57}$$

Assuming that $\mathbf{S} = \{\mathbf{s}^l = [a^{l,1}, a^{l,2}, a^{l,3}, a^{l,4}] \in \mathbb{R}^4 : 0 \leq l \leq L-1\}$ constitutes a set of L legitimate constellation points from the lattice D_4 having a total energy of

$$E_{total} \stackrel{\triangle}{=} \sum_{l=0}^{L-1} (|a^{l,1}|^2 + |a^{l,2}|^2 + |a^{l,3}|^2 + |a^{l,4}|^2), \tag{2.58}$$

and upon introducing the notation

$$\begin{aligned} \mathbf{C}_l &= \sqrt{\frac{2L}{E_{total}}}(x^{l,1}, x^{l,2}, x^{l,3}, x^{l,4}) \\ &= \sqrt{\frac{2L}{E_{total}}}(a^{l,1}, a^{l,2}, a^{l,3}, a^{l,4}), \qquad l = 0, 1, \ldots, L-1, \end{aligned} \tag{2.59}$$

we have a set of constellation symbols, $\{\mathbf{C}_l\colon\ 0 \leq l \leq L-1\}$, leading to the design of DSTS signals, whose diversity product is determined by the minimum Euclidean distance of the set of L legitimate constellation points in $\mathbf{S}$.

The following example illustrates how SP modulation is implemented in combination with the four-antenna-aided DSTS scheme as compared to the conventionally modulated DSTS scheme.

Example 2.4.1 *Assume that there are $L = 16$ different legitimate symbols $(x^{l,1}, x^{l,2}, x^{l,3}, x^{l,4})$, $l = 0, 1, \ldots, 15$, that can be used by the encoder. We will compare three modulation schemes, namely conventional BPSK, QPSK and SP modulation.*

- **Conventional BPSK Modulation:**
  There are two real-valued legitimate symbols (S_0, S_1) that can be used to independently represent any of the $x^{l,1}$, $x^{l,2}$, $x^{l,3}$ and $x^{l,4}$, $l = 0, 1, \ldots, 15$ symbols. The transmission scheme processing the signals in four consecutive time slots is outlined in Figure 2.31.

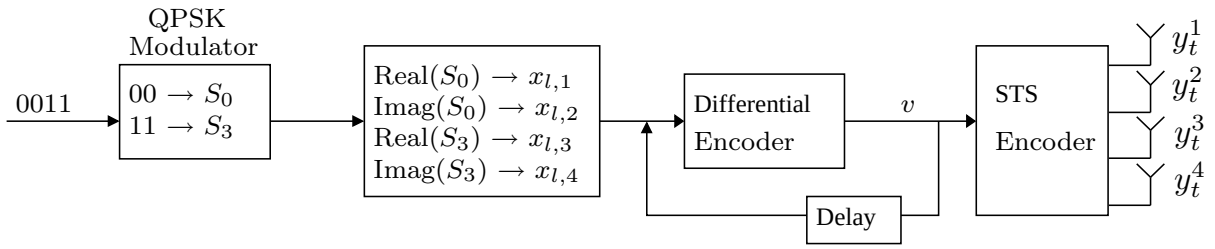

Figure 2.32: Transmission of two QPSK symbols using a four-antenna-aided DSTS scheme.

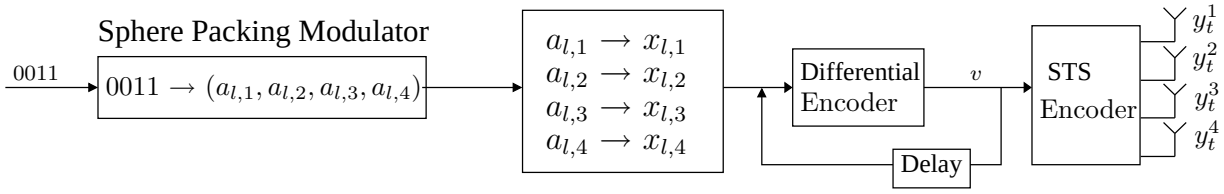

Figure 2.33: Transmission of a SP symbol using a four-antenna-aided DSTS scheme.

- **Conventional QPSK Modulation:**
  There are four complex-valued legitimate symbols (S_0, S_1, S_2, S_3) that can be used to independently represent any of the $x^{l,1}$, $x^{l,2}$, $x^{l,3}$ and $x^{l,4}$, $l = 0, 1, \ldots, 15$ symbols. The transmission scheme processing the signals of four consecutive time slots is highlighted in Figure 2.32.

- **Sphere Packing Modulation:**
  We need $L = 16$ SP phasor points $(a^{l,1}, a^{l,2}, a^{l,3}, a^{l,4})$ from the lattice D_4 in order to jointly represent each signal $(x^{l,1}, x^{l,2}, x^{l,3}, x^{l,4})$, $l = 0, 1, \ldots, 15$ according to Equation (2.59), as depicted in Figure 2.33.

2.4.4 Bandwidth Efficiency of the Four-Antenna-Aided DSTS Scheme

In the four-antenna-aided DSTS encoder, the data is serial-to-parallel converted to four substreams. The new bit duration of each parallel substream or equivalently the symbol duration becomes T_s=4T_b as illustrated in Figure 2.30. According to Section 2.4.3, the DSTS transmitter using four transmit antennas transmits one SP symbol in four time slots. Therefore, the DSTS-SP code rate becomes 1/4 and then according to the number of BPS B_{sp}, the DSTS-SP system's bandwidth efficiency becomes $B_{sp}/4$. For example, in the case of SP using L=16, we have B_{sp}=4 BPS, which results in an effective bandwidth efficiency of 1 bit-per-channel use. Table 2.6 presents the bandwidth efficiency of the four-antenna-aided DSTS system for different SP modulated constellation sizes.

The effective bandwidth efficiency for the DSTS-SP system is different from that of conventionally modulated DSTS schemes, which can be also categorised as real- and complex-valued.

L	BPS	Bandwidth Efficiency (bits-per-channel-use)
4	2	0.5
8	3	0.75
16	4	1
32	5	1.25
64	6	1.5
128	7	1.75
256	8	2
512	9	2.25
1024	10	2.5
2048	11	2.75
4096	12	3

Table 2.6: Bandwidth efficiency of four-antenna-aided DSTS-SP systems for different SP signal set sizes L.

Modulation	BPS	Bandwidth Efficiency (bits-per-channel-use)
BPSK	1	1
QPSK	2	1
8PSK	3	1.5
16-QAM	4	2
64-QAM	6	3

Table 2.7: Bandwidth efficiency of four-antenna-aided DSTS systems for different conventional modulation signal sets.

For the case of real-valued modulation constellations, the DSTS system using four transmit antennas transmits four symbols in four time slots, which gives an effective bandwidth efficiency of B bits-per-channel-use. However, for complex-valued constellations such as QPSK for example, the DSTS scheme transmits two complex-valued symbols, each conveying one bit per inphase plus one bit per quadrature component in four time slots. This also results in an effective system bandwidth efficiency of 1 bit-per-channel use, which is identical to that of the four-antenna-aided DSTS-SP system in conjunction with $L = 16$. Table 2.7 presents the bandwidth efficiency of the four-antenna-aided DSTS system for different conventional modulated constellation sizes.

2.4.5 Capacity of the Four-Antenna-Aided DSTS-SP Scheme

According to Equation (2.53), the DSTS-SP decoded signal can be modelled as:

$$\tilde{\mathbf{s}}_r = \chi^2_{2N_t,r} \cdot \mathbf{s}^l + \acute{\mathbf{N}}_r, \tag{2.60}$$

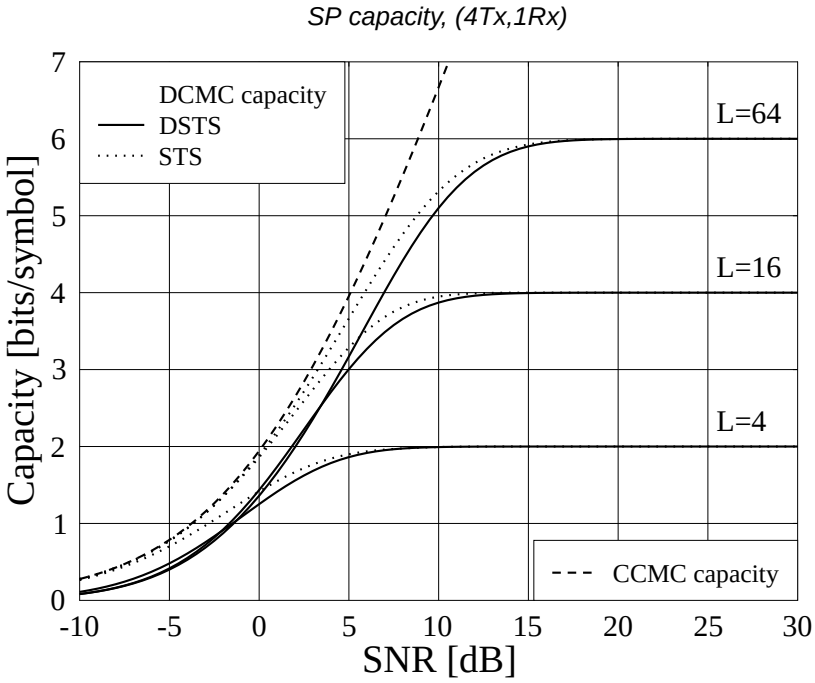

Figure 2.34: Capacity comparison of coherent and differential STS-SP based schemes using $L = 4$, 16 and 64, when employing $N_t = 4$ transmit and $N_r = 1$ receive antennas for communicating over a correlated Rayleigh fading channel having a normalised Doppler frequency of $f_D = 0.01$.

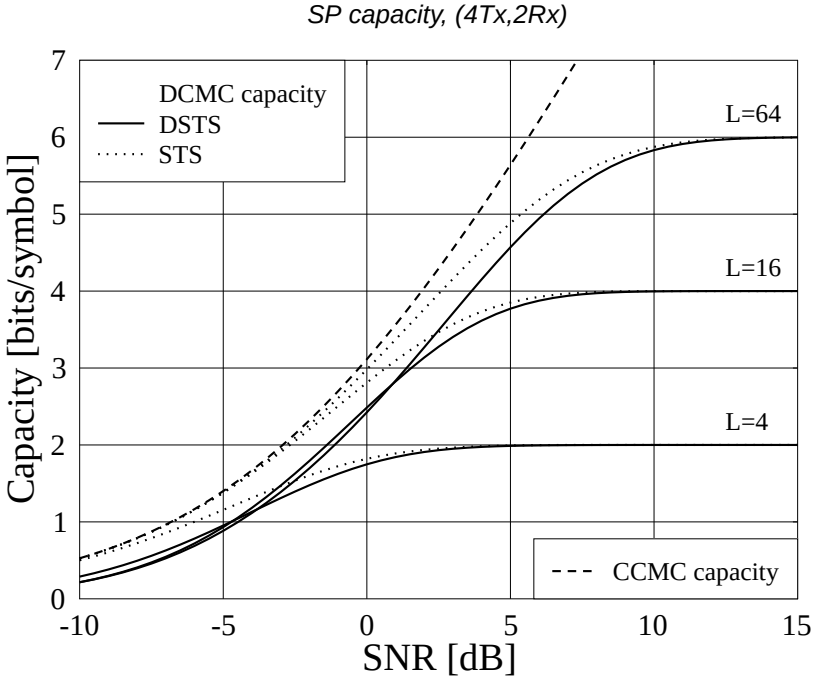

Figure 2.35: Capacity comparison of coherent and differential STS-SP based schemes using $L = 4$, 16 and 64, when employing $N_t = 4$ transmit and $N_r = 2$ receive antennas for communicating over a correlated Rayleigh fading channel having a normalised Doppler frequency of $f_D = 0.01$.

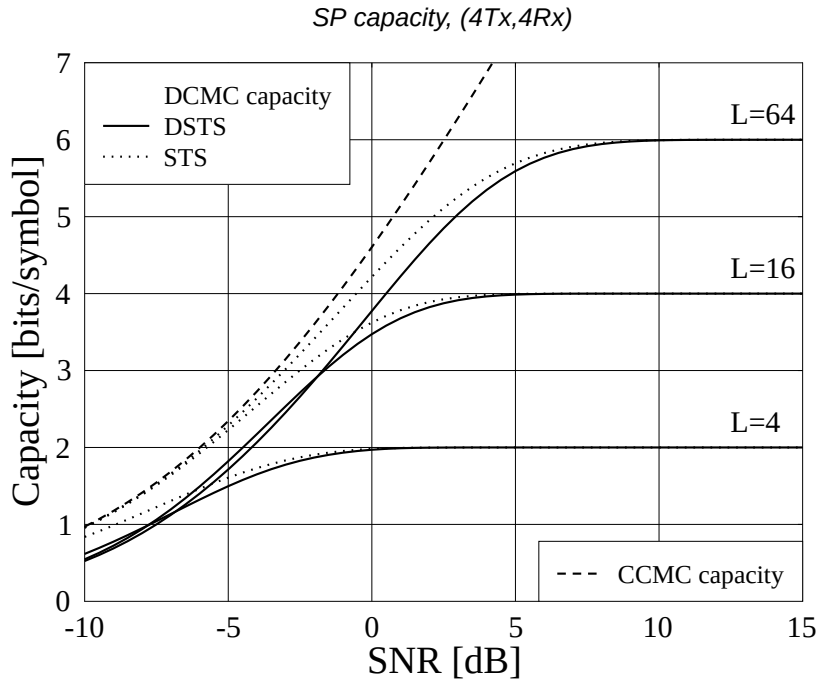

Figure 2.36: Capacity comparison of coherent and differential STS-SP based schemes using $L = 4$, 16 and 64, when employing $N_t = 4$ transmit and $N_r = 4$ receive antennas for communicating over a correlated Rayleigh fading channel having a normalised Doppler frequency of $f_D = 0.01$.

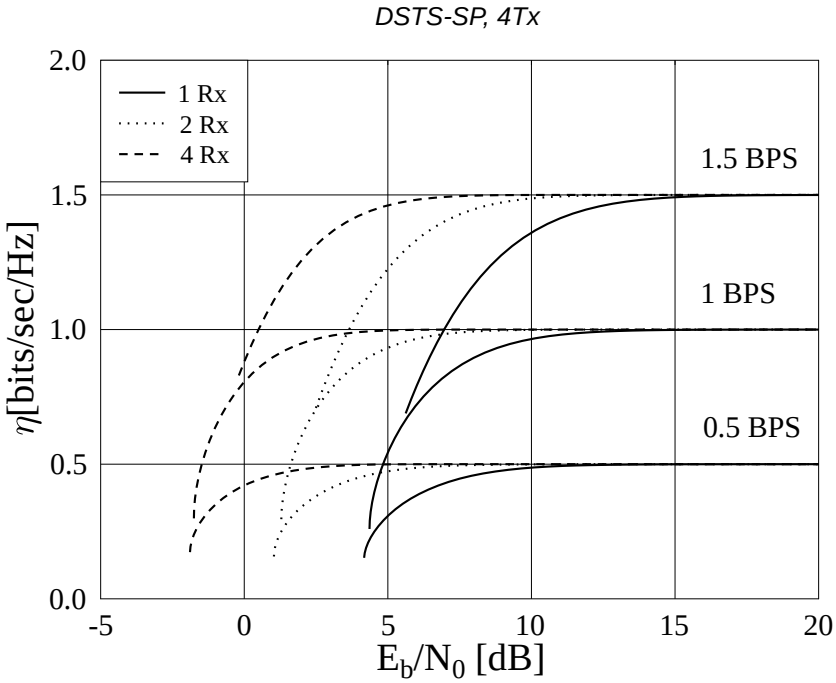

Figure 2.37: Bandwidth efficiency of DSTS based schemes employing SP modulation scheme for $L = 4$, 16 and 64, when employing $N_t = 4$ transmit and $N_r = 1,\ 2$ and 4 receive antenna for communicating over a correlated Rayleigh fading channel having a normalised Doppler frequency of $f_D = 0.01$.

where we have $\mathbf{s}^l = [a^{l,1}\ a^{l,2}\ a^{l,3}\ a^{l,4}] \in S$, $0 \leq l \leq L-1$, $\chi^2_{2N_t,r} = \frac{1}{4} \cdot \sum_{i=1}^{4} |h_{ir}|^2 \cdot \sqrt{\sum_{j=1}^{4} |v_t^j|^2}$. Therefore, the capacity of the four-antenna-aided DSTS-SP scheme can be derived using the same method as that in Section 2.3.6 to arrive at Equation (2.31).

Figures 2.34, 2.35 and 2.36 show the DCMC capacity evaluated from Equation (2.31) for the four-dimensional SP modulation assisted DSTS as well as STS schemes for $L = 4$, 16 and 64, when employing $N_t = 4$ transmit antennas as well as $N_r = 1$, 2 and 4 receive antennas, respectively. The CCMC [35] capacity of the MIMO scheme was also plotted for comparison in Figures 2.34, 2.35 and 2.36 based on [33].

Figure 2.37 compares the achievable bandwidth efficiency of various SP modulated DSTS schemes, while employing $N_t = 4$ transmit antennas and $N_r = 1,\ 2$ and 4 receive antennas. The figures explicitly illustrate that a higher bandwidth efficiency may be attained when employing SP modulation in conjunction with DSTS schemes having $N_t = 4$ transmit antennas, as the the number N_r of receive antennas increases.

2.4.6 Performance of the Four-Antenna-Aided DSTS Scheme

In this section, the four-antenna-aided DSTS scheme is considered. Simulation results are provided for systems having different bandwidth efficiencies in conjunction with appropriate real- and complex-valued conventional as well as SP modulation, when communicating over a correlated narrowband Rayleigh fading channel having a normalised Doppler frequency of $f_D = 0.01$.

Figure 2.38 compares the BER performance of both the differentially encoded and of the coherently detected STS scheme, while using BPSK, four transmit antennas, one receive antenna, a spreading factor of four and supporting two users. Again, coherent detection requires channel state information at the receiver for decoding the received signal, however in this case we assumed that the CIR is perfectly known at the receiver side. As shown in Figure 2.38, differential encoding results in a 3 dB performance loss compared to coherent detection, when assuming perfect channel knowledge. This is mainly due to the fact that differential decoding results in doubling the noise power compared to that recorded for coherently detected signals. However, using the differential encoding results in eliminating the complexity of channel estimation required by coherent detection schemes, where in this case the receiver is expected to estimate $4 \times N_r$ channel links. Furthermore, Figures 2.39 and 2.40 compare the BER performance of the DSTS encoded BPSK and QPSK modulated signals, while using two and four transmit antennas, one receive antenna, a spreading factor of four and supporting two users. It transpires from the figure that increasing the diversity order of the system by increasing

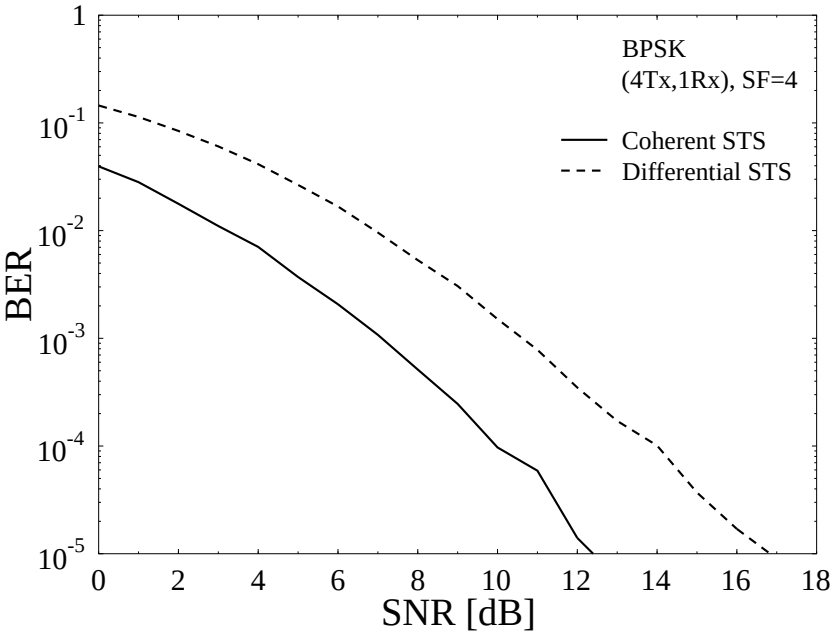

Figure 2.38: Comparison of the BER performance of coherent and differential space-time spreading, while using a BPSK modulated signal, four transmit antennas, one receive antenna, a spreading factor of four and supporting two users for communicating over a correlated Rayleigh fading channel having a normalised Doppler frequency of $f_D = 0.01$.

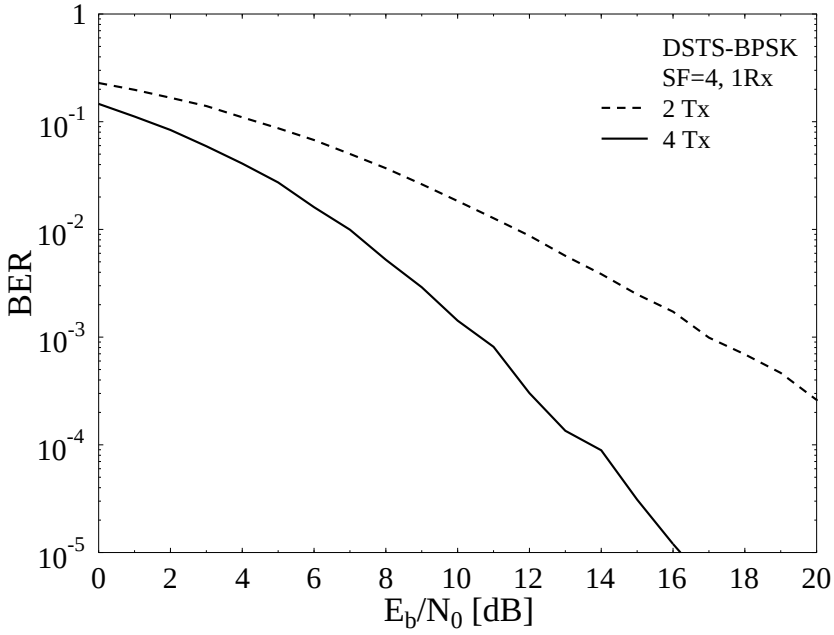

Figure 2.39: Comparison of the BER performance of differential space-time spreading assisted BPSK modulated signal while using two and four transmit antennas, one receive antenna, a spreading factor of four and supporting two users for communicating over a correlated Rayleigh fading channel having a normalised Doppler frequency of $f_D = 0.01$.

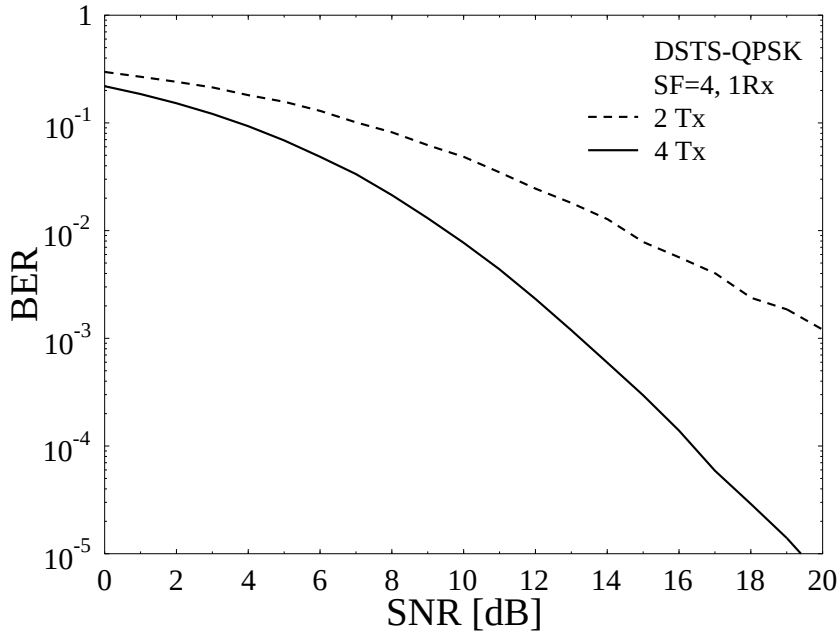

Figure 2.40: Comparison of the BER performance of differential space-time spreading aided QPSK modulated signal while using two and four transmit antennas, one receive antenna, a spreading factor of four and supporting two users for communicating over a correlated Rayleigh fading channel having a normalised Doppler frequency of $f_D = 0.01$.

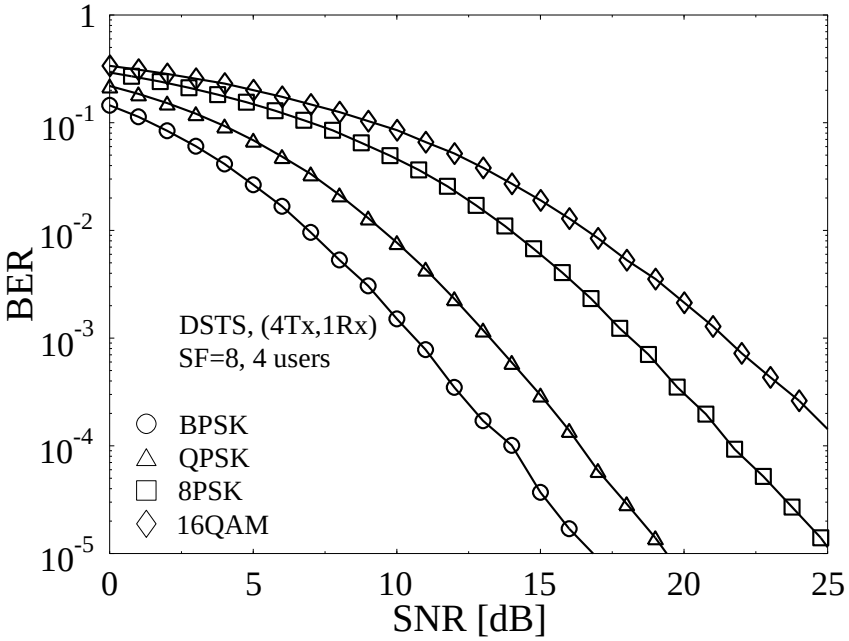

Figure 2.41: Comparison of the BER performance of differential space-time spreading while using BPSK, QPSK, 8PSK and 16QAM modulated signals, four transmit antennas, one receive antenna, a spreading factor of four and supporting two users for communicating over a correlated Rayleigh fading channel having a normalised Doppler frequency of $f_D = 0.01$.

the number of transmit antennas improves the attainable system performance. For the case of BPSK modulation, the system performance improves by almost E_b/N_0=10 dB at a BER of 10^{-5}. Figure 2.41 compares the BER performance of the DSTS system using BPSK, QPSK, 8PSK, as well as 16QAM signals.

Figure 2.42 shows the SP-SER performance curves of the DSTS scheme in conjunction with different conventional as well as SP modulation schemes at various bandwidth efficiency values, as outlined in Table 2.4. However, the figure does not show a comparison between the BPSK modulated and the SP modulated signals using $L = 4$, due to the fact that the two systems have different bandwidth efficiencies, when combined with four-antenna-aided DSTS. All systems employ four transmit antennas for communication over a correlated narrowband Rayleigh fading channel associated with $f_D = 0.01$. Moreover, the system uses a spreading factor of four, while supporting two users. Figure 2.42 suggests that the SP-SER performance of DSTS schemes may be improved by employing SP modulation. The resultant BER performance curves are shown in Figure 2.43. The BER performances of SP modulation and conventional modulation are identical for systems having a bandwidth efficiency of 1 BPS, but as suggested in Figure 2.43 is different for the higher bandwidth efficiency schemes. As depicted in Figure 2.43, the BER performance of the conventional modulation based four-antenna-aided DSTS scheme is better than that of the SP aided system and this is due to the fact that SP modulation was specifically designed for improving the SP-SER, rather than the BER and this explains the advantage of SP modulation in Figure 2.42.

To elaborate a little further, Figures 2.44 to 2.49 illustrate the beneficial effect of increasing the number of receive antennas from *two* to $four$ respectively. Observe in Figures 2.45, 2.47 and 2.49 that as expected, the BER performance of SP modulation improves in comparison to that of conventional modulation, when increasing the number of receive antennas, especially, for schemes having a bandwidth efficiency of 1.5 bit-per-channel-use. Observe however in Figures 2.43 to 2.48 that both the BER and SP-SER performance curves of QPSK modulation as well as those of the identical-throughput SP modulation having $L = 16$ are identical. This phenomenon is due to the fact that QPSK modulation is a special case of the sphere packing modulation as discussed in Section 2.3.7.

Finally, the attainable coding gains of sphere packing modulation over conventional modulation are summarised in Table 2.8 for the schemes characterised in Figures 2.42 to 2.49 at an SP-SER of 10^{-4}, when communicating over a correlated Rayleigh fading channel associated with $f_D = 0.01$.

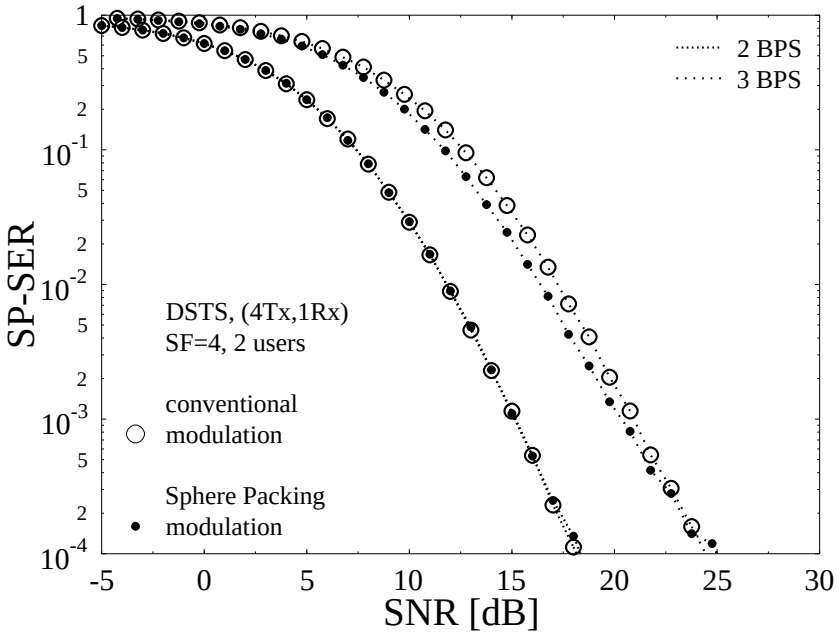

Figure 2.42: Performance comparison of the SP-SER of DSTS in combination with conventional modulation and sphere packing modulation for different bandwidth efficiency values as outlined in Table 2.4 while employing four transmit antennas, one receive antenna, a spreading factor of four and two users, when communicating over a correlated Rayleigh fading channel associated with $f_D = 0.01$.

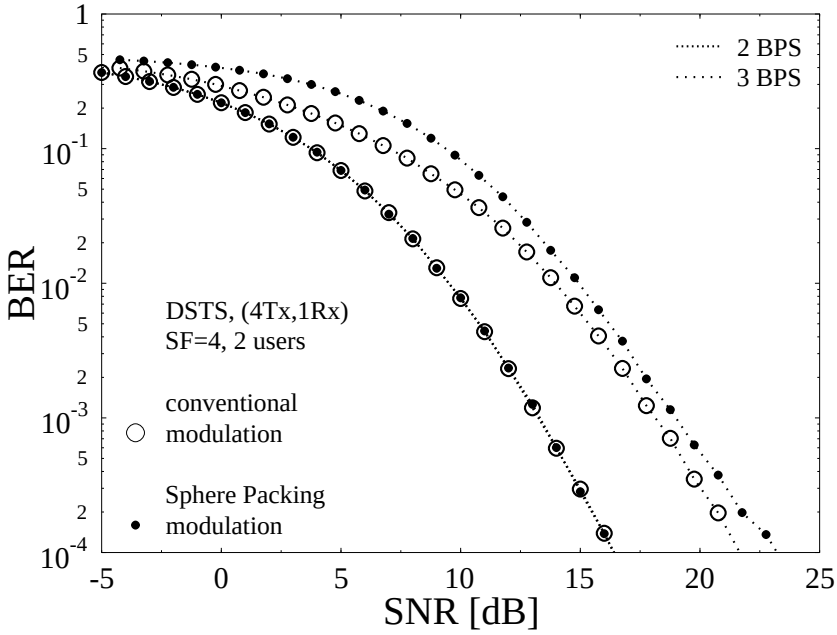

Figure 2.43: Performance comparison of the BER of DSTS in combination with conventional modulation and sphere packing modulation for different bandwidth efficiency values as outlined in Table 2.4 while employing four transmit antennas, one receive antenna, a spreading factor of four and two users, when communicating over a correlated Rayleigh fading channel associated with $f_D = 0.01$.

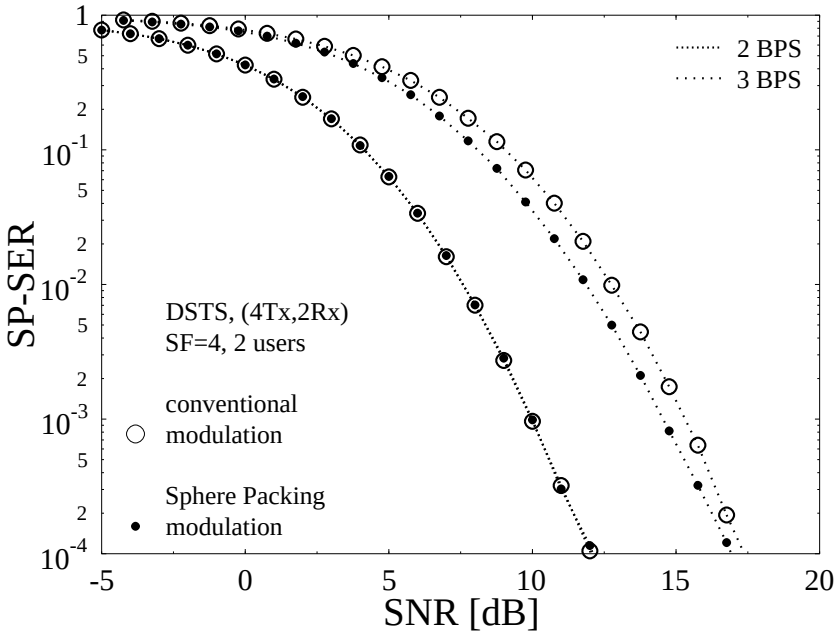

Figure 2.44: Performance comparison of the SP-SER of DSTS in combination with conventional modulation and sphere packing modulation for different bandwidth efficiency values as outlined in Table 2.4 while employing four transmit antennas, two receive antennas, a spreading factor of four and two users, when communicating over a correlated Rayleigh fading channel associated with $f_D = 0.01$.

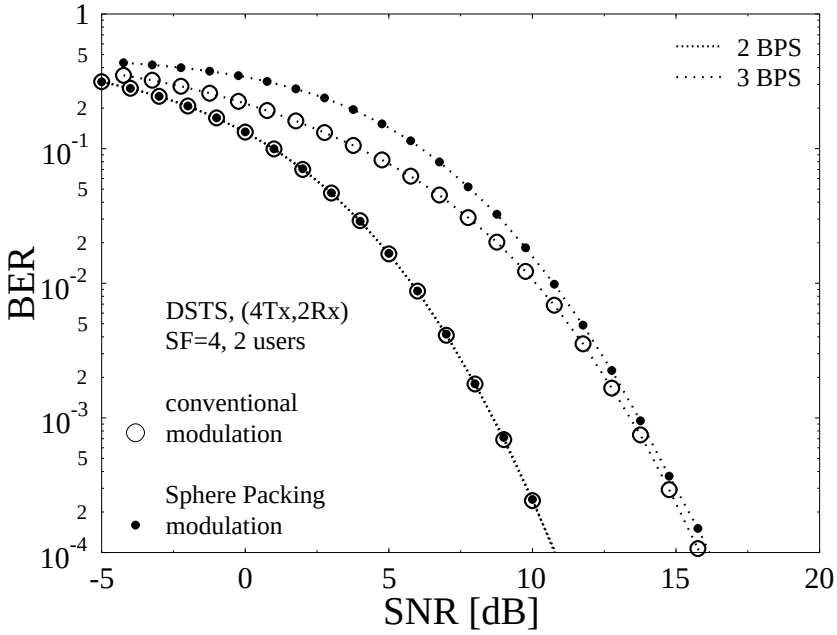

Figure 2.45: Performance comparison of the BER of DSTS in combination with conventional modulation and sphere packing modulation for different bandwidth efficiency values as outlined in Table 2.4 while employing four transmit antennas, two receive antennas, a spreading factor of four and two users, when communicating over a correlated Rayleigh fading channel associated with $f_D = 0.01$.

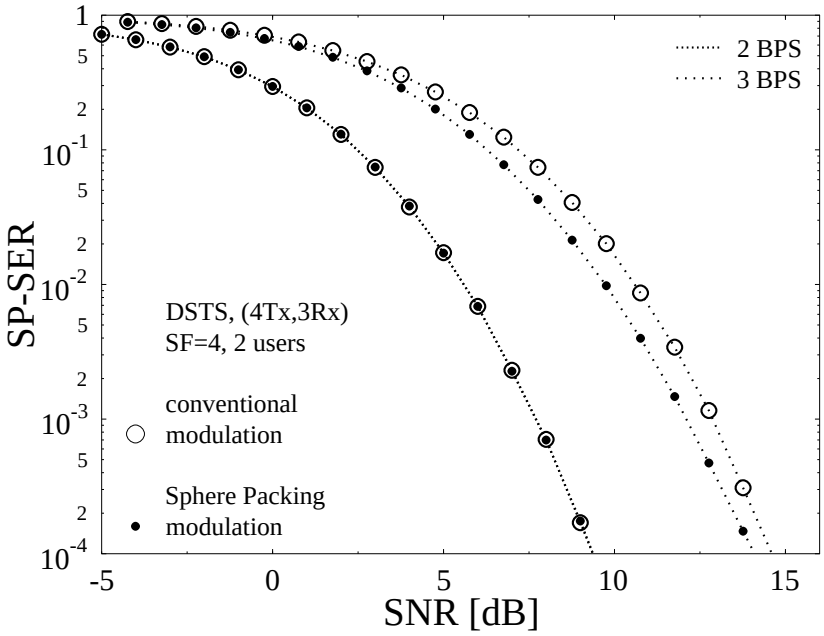

Figure 2.46: Performance comparison of the SP-SER of DSTS in combination with conventional modulation and sphere packing modulation for different bandwidth efficiency values as outlined in Table 2.4 while employing four transmit antennas, three receive antennas, a spreading factor of four and two users, when communicating over a correlated Rayleigh fading channel associated with $f_D = 0.01$.

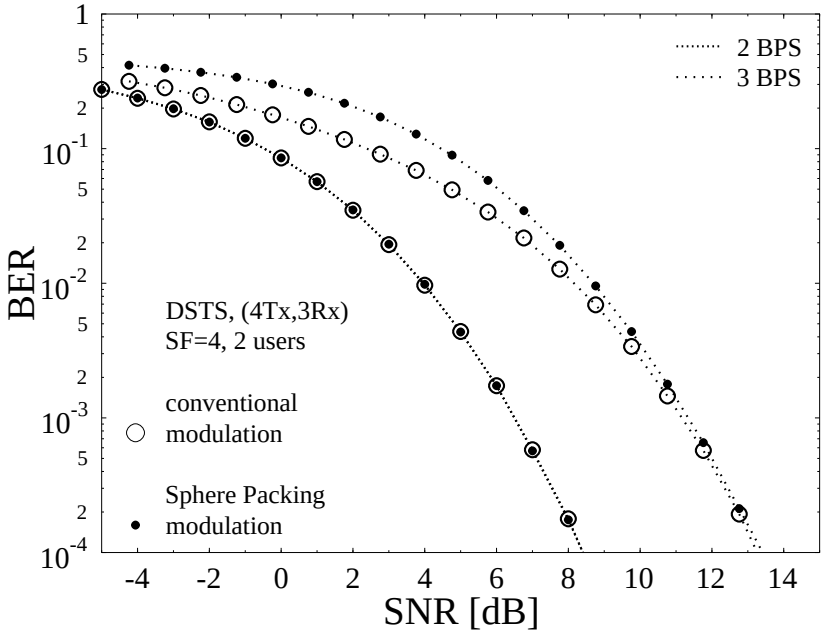

Figure 2.47: Performance comparison of the BER of DSTS in combination with conventional modulation and sphere packing modulation for different bandwidth efficiency values as outlined in Table 2.4 while employing four transmit antennas, three receive antennas, a spreading factor of four and two users, when communicating over a correlated Rayleigh fading channel associated with $f_D = 0.01$.

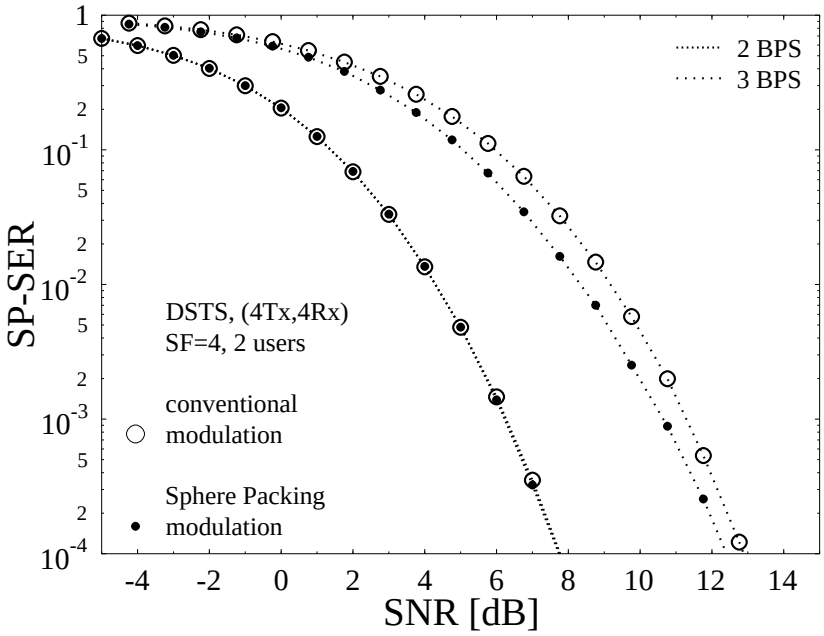

Figure 2.48: Performance comparison of the SP-SER of DSTS in combination with conventional modulation and sphere packing modulation for different bandwidth efficiency values as outlined in Table 2.4 while employing four transmit antennas, four receive antennas, a spreading factor of four and two users, when communicating over a correlated Rayleigh fading channel associated with $f_D = 0.01$.

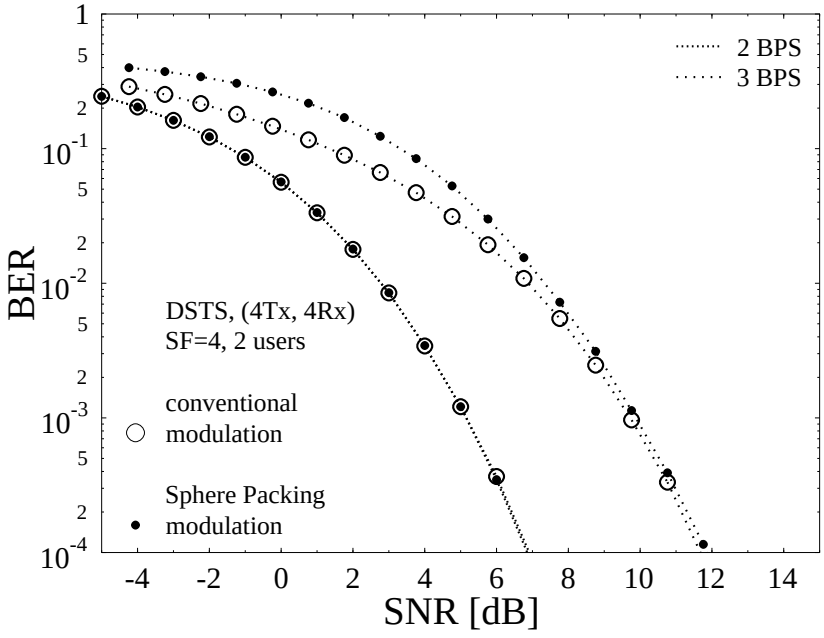

Figure 2.49: Performance comparison of the BER of DSTS in combination with conventional modulation and sphere packing modulation for different bandwidth efficiency values as outlined in Table 2.4 while employing four transmit antennas, four receive antennas, a spreading factor of four and two users, when communicating over a correlated Rayleigh fading channel associated with $f_D = 0.01$.

	2 BPS	3 BPS
$1Rx$	0.0 dB	0.00 dB
$2Rx$	0.0 dB	0.40 dB
$3Rx$	0.0 dB	0.80 dB
$4Rx$	0.0 dB	0.85 dB

Table 2.8: Coding gains of sphere packing modulation over conventional modulation at SP-SER of 10^{-4} for the schemes of Figures 2.42, 2.44, 2.46 and 2.48, when communicating over a correlated Rayleigh fading channel associated with $f_D = 0.01$.

2.5 Chapter Conclusion

In this chapter, we introduced the concept of differential space-time spreading employing two and four transmit antennas and demonstrated that the systems can be combined with conventional real- and complex-valued constellations. Furthermore, in order to maximise the diversity product, we combined the DSTS with sphere packing modulation, that has the best known MED in the $2(k+1)$-dimensional real-valued Euclidean space $\mathbb{R}^{2(k+1)}$ [213]. The capacity analysis provided in Sections 2.3.6 and 2.4.5 demonstrated that the DSTS-SP design is capable of attaining potential performance improvements over a conventionally modulated DSTS design. The simulation results presented in Sections 2.3.7 and 2.4.6 demonstrated that the DSTS system is capable of providing a full diversity gain, while employing two and four transmit antennas. Tables 2.5 and 2.8 summarise the coding gains of the SP modulation aided DSTS schemes over conventional modulated DSTS schemes at an SP-SER of 10^{-4}, when communicating over a correlated narrowband Rayleigh fading channel and employing two and four transmit antennas, respectively.

2.6 Chapter Summary

This chapter first reviewed the concept of differential encoding in Section 2.2. It was shown that differential encoding requires no channel state information at the receiver and thus eliminates the complexity of channel estimation at the expense of a 3 dB performance loss compared to the coherently detected system assuming perfect channel knowledge at the receiver. In Section 2.3, we outlined the encoding and decoding processes of the differential space-time spreading scheme, when combined with conventional modulation, such as PSK and QAM. In Section 2.3.3, the philosophy of DSTS using sphere packing modulation was introduced based on the fact that the diversity product of the DSTS design is improved by maximising the MED of the DSTS symbols, which is motivated by the fact that SP has the best known MED in the real-valued

space. Section 2.3.4 discussed the problem of constructing a sphere packing constellation having a particular size L. The constellation points were first chosen based on the minimum energy criterion. Then, an exhaustive computer search was conducted for all the SP symbols having the lowest possible energy, in order to find the specific set of L points having the best MED from all the other constellation points satisfying the minimum energy criterion. The capacity of DSTS-SP schemes employing $N_t = 2$ transmit antennas was derived in Section 2.3.6 followed by the performance characterisation of a twin-antenna-aided DSTS scheme in Section 2.3.7 demonstrating that the DSTS scheme is capable of providing full diversity. In addition to that, the results demonstrated that DSTS-SP schemes are capable of outperforming DSTS schemes that employ conventional modulation (PSK, QAM), when comparing the SP-SER performance.

The four-antenna-aided DSTS design was characterised in Section 2.4, where it was demonstrated how the DSTS scheme can be combined with conventional real- and complex-valued constellations as well as with SP modulation. It was also demonstrated that the four-dimensional SP modulation scheme is constructed differently in the case of two transmit antennas than when employing four transmit antennas. The capacity analysis of the four-antenna-aided DSTS-SP scheme was also derived for different bandwidth efficiency systems, while employing a variable number of receive antennas in Section 2.4.5. Finally, Section 2.4.6 presented the simulation results obtained for the four-antenna-aided DSTS scheme when combined with conventional as well as SP modulations.

Tables 2.5 and 2.8 summarise the coding gains of sphere packing modulation aided DSTS schemes over conventional modulated DSTS schemes at an SP-SER of 10^{-4}, when communicating over a correlated narrowband Rayleigh fading channel and employing two and four transmit antennas, respectively.

In the next chapter, we will demonstrate that further performance improvement can be attained by the concatenation of these schemes with channel codes and performing iterative detection by exchanging extrinsic information between the different component decoders/demapper at the receiver side. The convergence behaviour of the iteratively detected system will be studied using Extrinsic Information Transfer (EXIT) charts.

Chapter 3

Iterative Detection of Channel-Coded DSTS Schemes

3.1 Introduction

In Chapter 2, a Differential Space-Time Spreading (DSTS) scheme has been proposed for transmission over temporally correlated narrowband Rayleigh fading channels using conventional PSK and QAM modulations as well as Sphere Packing (SP) modulation scheme. The DSTS arrangement is a Multiple-Input Multiple-Output (MIMO) scheme, that is capable of attaining a full diversity gain as well as exploiting the combined advantages of differential encoding and multi-user support capability of space-time spreading [49]. The performance of the DSTS scheme can be enhanced by combining it with iterative detection aided schemes, where iterative decoding is carried out by exchanging extrinsic information between the different constituent decoders and demappers.

The turbo principle of [163] was extended to multiple parallel concatenated codes in [164], to serially concatenated codes in [165] and to multiple serially concatenated codes in [166]. In [175], the employment of the turbo principle was considered for iterative soft demapping in the context of multilevel modulation schemes combined with channel decoding, where a soft symbol-to-bit demapper was used between the multilevel demodulator and the binary channel decoder. The iterative soft demapping principle of [175] was extended to SP-aided STBC schemes in [58], where the SP demapper of [55] was modified in [58] for the sake of accepting the *a priori* information passed to it from the channel decoder as extrinsic information.

Furthermore, it was shown in [183] that a recursive inner code is needed in order to maximise the interleaver gain and to avoid the formation of a BER floor when employing iterative decoding. In [185], unity-rate inner codes were employed for designing low complexity iterative

detection aided schemes suitable for bandwidth and power limited systems having stringent BER requirements.

Recently, studying the convergence behaviour of iterative decoding has attracted considerable research attention [58, 184, 186, 189, 190, 192, 200, 220–223]. In [186], ten Brink proposed the employment of the so-called Extrinsic Information Transfer (EXIT) characteristics between a concatenated decoder's output and input for describing the flow of extrinsic information through the soft-in soft-out constituent decoders.

Motivated by the performance improvements reported in the previous chapter and in [55, 58, 224], the novelty and rationale of this chapter can be summarised as follows:

1. *The bit-to-SP-symbol mapper is designed using an EXIT-chart based procedure, which allows us to achieve diverse design objectives. For example, we can design a system having the lowest possible turbo-cliff-SNR, but tolerating the formation of an error floor. Alternatively, we can design a system having a low error floor, but exhibiting a slightly higher turbo-cliff-SNR.*

2. *A unity-rate precoder is introduced, which is capable of completely eliminating the system's error-floor as well as operating at the lowest possible turbo-cliff SNR without significantly increasing the associated complexity or interleaver delay.*

3. *We propose a novel technique for computing the maximum achievable rate of the system using EXIT charts and we show that the achievable rate obtained using EXIT charts closely matches the capacity limits computed in Section 2.3.6.*

4. *As a benefit of the proposed solution, it will be demonstrated in Section 3.2.4 that the iteratively detected twin-antenna-aided DSTS-SP scheme is capable of providing an E_b/N_0 gain of at least 14.9 dB at a BER of 10^{-5} over the equivalent bandwidth efficiency uncoded DSTS-SP scheme. Furthermore, the AGM-1 based iteratively detected twin-antenna-aided DSTS-SP scheme is capable of performing within 2.3 dB from the maximum achievable rate limit obtained using EXIT charts at BER=10^{-5}.*

5. *A Unity-Rate Code (URC) is amalgamated with the iteratively detected four-antenna-aided DSTS-SP system in order to eliminate the error floor and to operate as close as possible to the system's capacity. Explicitly, the system employing no URC precoding in conjunction with AGM-1 attains a coding gain of 12 dB at a BER of 10^{-5} and performs within 1.82 dB from the maximum achievable rate limit. By contrast, the URC precoded system outperforms its non-precoded counterpart and operates within 0.92 dB from the maximum achievable rate limit obtained using EXIT charts.*

The rest of the chapter is organised as follows. An overview of the iterative detection based

DSTS scheme is presented in Section 3.2 for systems employing two and four transmit antennas as well as conventional and sphere packing modulation schemes. In Section 3.2.2 we introduce the EXIT chart analysis technique and illustrate how to generate the EXIT charts for visualising the interaction of the inner as well as outer codes. Our performance results and discussions of the iteratively detected DSTS scheme are presented in Section 3.2.4. In Section 3.3 unity-rate inner code is combined with the iterative detection based system in order to eliminate the error floor and perform as close as possible to the system's capacity. Our conclusions are presented in Section 3.4, followed by the chapter's summary in Section 3.5.

3.2 Iterative Detection of RSC-Coded DSTS Schemes

A block diagram of the iterative-detection-aided DSTS system is shown in Figure 3.1, where the transmitted source bit stream $\mathbf{u}$ is convolutionally encoded by a 1/2-rate Recursive Systematic Convolutional (RSC) code and then interleaved by a random bit interleaver Π. After bit interleaving, the conventional mapper first maps B channel-coded bits $\mathbf{b} = b_0, \ldots, b_{B-1} \in \{0, 1\}$ to a conventionally modulated PSK or QAM symbol x. On the contrary, the SP mapper maps B_{sp}[1] channel-coded bits $\mathbf{b} = b_0, \ldots, b_{B_{sp}-1} \in \{0, 1\}$ to a sphere packing symbol $\mathbf{s}^l \in \mathbf{S}$, $l = 0, 1, \ldots, L-1$ as described in Chapter 2, such that we have $\mathbf{s}^l = \text{map}_{sp}(\mathbf{b})$, where B_{sp}=$\log_2 L$ and L represents the number of modulated symbols in the sphere-packed signalling alphabet, as described in Chapter 2. Subsequently, we have a set of symbols that can be transmitted using differential space-time spreading.

In this chapter, we consider transmission over a temporally correlated narrowband Rayleigh fading channel, associated with a normalised Doppler frequency of $f_D = f_d T_s = 0.01$, where f_d is the Doppler frequency and T_s is the symbol duration, while the spatial channel coefficients are independent. The complex AWGN of $n = n_I + jn_Q$ contaminates the received signal, where n_I and n_Q are two independent zero-mean Gaussian random variables having a variance of $\sigma_n^2 = \sigma_{n_I}^2 = \sigma_{n_Q}^2 = N_0/2$ per dimension, with $N_0/2$ representing the double-sided noise power spectral density expressed in W/Hz.

In the receiver, the soft-in soft-out RSC decoder iteratively exchange extrinsic information with the soft demapper, as shown in Figure 3.1. The RSC decoder invokes the Bahl-Cocke-Jelinek-Raviv (BCJR) algorithm [181] on the basis of bit-based trellis [225]. All BCJR calculations are performed in the logarithmic probability domain and using a lookup table for correcting the Jacobian approximation in the Log Maximum Aposteriori Probability (Log-MAP) algorithm [26, 182].

[1] Note that the notation B_{sp} is used for the SP modulation to differentiate it from that for the conventional modulation, as illustrated in Chapter 2.

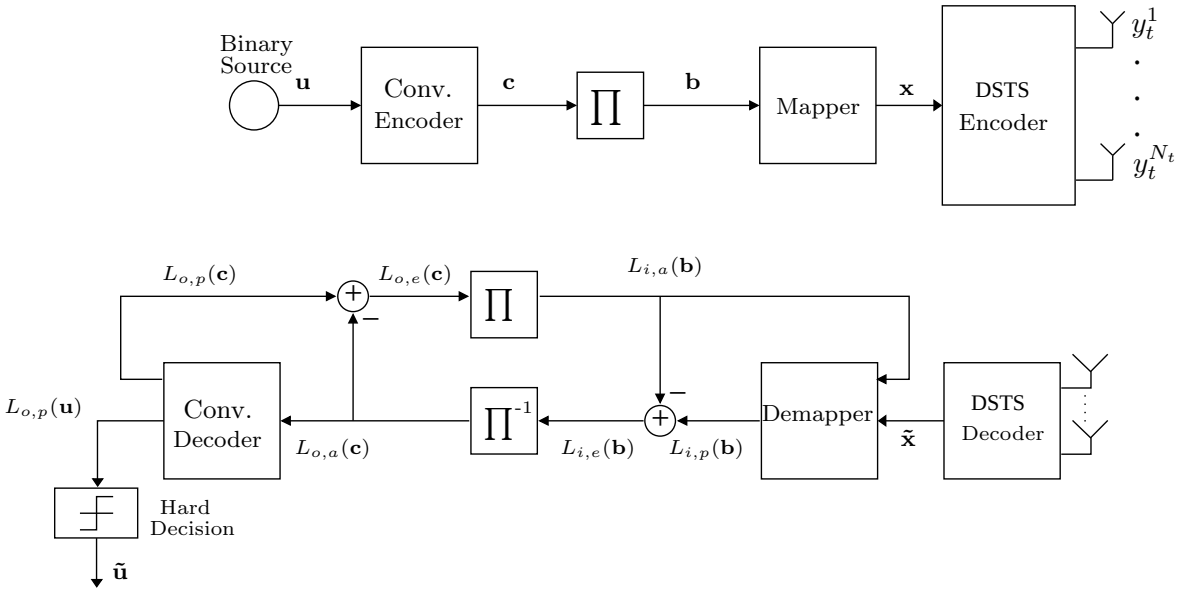

Figure 3.1: Iteratively-detected DSTS system block diagram.

The extrinsic soft information, represented in the form of Logarithmic Likelihood Ratios (LLR) [226], is iteratively exchanged between the demapper and the RSC decoder for the sake of assisting each other's operation, as detailed in [227]. In Figure 3.1, $L(\cdot)$ denotes the LLRs of the bits concerned, where the subscript i indicates the inner demapper, while o corresponds to outer RSC decoding. Additionally, the subscripts a, p and e denote the dedicated role of the LLRs with a, p and e indicating *a priori*, *a posteriori* and extrinsic information, respectively.

As shown in Figures 3.1, the received and DSTS-decoded complex-valued symbols $\tilde{\mathbf{x}}$ are demapped to their LLR representation for each of the channel-coded bits per symbol. The *a priori* LLR values $L_{i,a}(\mathbf{b})$ of the demapper are subtracted from the *a posteriori* LLR values $L_{i,p}(\mathbf{b})$ for the sake of generating the extrinsic LLR values $L_{i,e}(\mathbf{b})$ and then the LLRs $L_{i,e}(\mathbf{b})$ are deinterleaved by a soft-bit deinterleaver, as seen in Figure 3.1. Next, the soft bits $L_{o,a}(\mathbf{c})$ are passed to the RSC decoder in order to compute the *a posteriori* LLR values $L_{o,p}(\mathbf{c})$ provided by the Log-MAP algorithm [182] for all the channel-coded bits. During the last iteration, only the LLR values $L_{o,p}(\mathbf{u})$ of the original uncoded systematic information bits are required, which are passed to the hard decision decoder of Figure 3.1 in order to determine the estimated transmitted source bits. As seen in Figure 3.1, the extrinsic information $L_{o,e}(\mathbf{c})$, is generated by subtracting the *a priori* information from the *a posteriori* information according to $(L_{o,p}(\mathbf{c}) - L_{o,a}(\mathbf{c}))$, which is then fed back to the demapper as the *a priori* information $L_{i,a}(\mathbf{b})$ after appropriately reordering them using the interleaver of Figure 3.1. The demapper of Figure 3.1 exploits the *a priori* information for the sake of providing improved *a posteriori* LLR values, which are then passed to the channel decoder and then back to the demapper for further iterations.

3.2.1 Iterative Demapping[2]

For the sake of simplicity, we consider a system having a single receive antenna, although its extension to several receive antennas is feasible. As discussed in Section 2.3.6, the received channel output symbols are first DSTS-decoded and diversity-combined in order to extract the estimates $\tilde{\mathbf{x}}$ of the most likely transmitted symbols $\mathbf{x}$:

$$\tilde{x}_t = \chi^2_{2N_t} \cdot x_t + N, \tag{3.1}$$

where $\chi^2_{2N_t}$ represents a chi-squared distributed random variable having $2N_t$ degrees of freedom, as defined in Section 2.3.2 and Section 2.4.1. Furthermore, N_t is the number of transmit antennas and N is a zero-mean complex-valued Gaussian random variable having a variance of $\sigma_N^2 \approx 2 \cdot \chi^2_{2N_t} \cdot \sigma_n^2 = 2 \cdot \chi^2_{2N_t} \cdot N_0/2$.

3.2.1.1 Conventional Modulation

The decoded symbol $\tilde{x}$ can be written as

$$\tilde{x} = \chi^2_{2N_t} \cdot x + N. \tag{3.2}$$

According to Equation(3.2), the conditional Probability Density Function (PDF) $p(\tilde{x}|x)$ of receiving a symbol $\tilde{x}$, given that symbol x was transmitted is given by

$$p(\tilde{x}|x) = \frac{1}{\prod_{d=1}^{D} \sqrt{\pi \cdot N_0 \cdot \chi^2_{2N_t}[d]}} \cdot \exp\left(\sum_{d=1}^{D} \frac{-\left(\tilde{x}[d] - \chi^2_{2N_t}[d] \cdot x[d]\right)^2}{\chi^2_{2N_t}[d] \cdot N_0} \right), \tag{3.3}$$

where D represents the dimension of the symbol constellation used. Hence, we have D=1 for real-valued constellations and D=2 for complex-valued constellations.

The received symbol $\tilde{x}$ carries B channel-coded and interleaved bits $\mathbf{b} = b_0, \ldots, b_{B-1} \in \{0, 1\}$. The LLR-value of bit b_k for $k = 0, \ldots, B-1$ can be written as [224]

$$L(b_k|\tilde{x}) = L_a(b_k) + \ln \frac{\sum_{x \in S_{1k}} p(\tilde{x}|x) \cdot \exp\left(\sum_{j=0, j \neq k}^{B-1} b_j L_a(b_j) \right)}{\sum_{x \in S_{0k}} p(\tilde{x}|x) \cdot \exp\left(\sum_{j=0, j \neq k}^{B-1} b_j L_a(b_j) \right)}, \tag{3.4}$$

where S_{1k} and S_{0k} are subsets of the symbol constellation $\mathbf{S}$, so that $\mathbf{S}_{1k} \triangleq \{x \in \mathbf{S} : b_k = 1\}$ and likewise, $\mathbf{S}_{0k} \triangleq \{x \in \mathbf{S} : b_k = 0\}$. In other words, S_{ik} represents all symbols of the set S, where we have $b_k \in \{0, 1\}$, $k = 0, \ldots, B-1$. Using Equation (3.3), we can write Equation (3.4)

[2]Parts of this section are based on [210, 211].

as

$$\begin{aligned} L(b_k|\tilde{x}) &= L_a(b_k) \\ &+ \ln \frac{\sum_{x\in S_{1k}} \exp\left[\left(\sum_{d=1}^{D} \frac{-\left(\tilde{x}[d]-\chi^2_{2N_t}[d]\cdot x[d]\right)^2}{\chi^2_{2N_t}[d]\cdot N_0}\right) + \sum_{j=0,j\neq k}^{B-1} b_j L_a(b_j)\right]}{\sum_{x\in S_{0k}} \exp\left[\left(\sum_{d=1}^{D} \frac{-\left(\tilde{x}[d]-\chi^2_{2N_t}[d]\cdot x[d]\right)^2}{\chi^2_{2N_t}[d]\cdot N_0}\right) + \sum_{j=0,j\neq k}^{B-1} b_j L_a(b_j)\right]} \\ &= L_{i,a} + L_{i,e}. \end{aligned} \tag{3.5}$$

3.2.1.2 Sphere Packing Modulation

As detailed in Chapter 2, the mapping of the SP symbols to the DSTS scheme's antennas is different for two and four transmit antennas. A received sphere-packed symbol $\tilde{\mathbf{s}}$ is constructed from the estimates $\tilde{x}$ as

$$\tilde{\mathbf{s}} = T_{sp}^{-1}(\tilde{x}^1, \tilde{x}^2), \tag{3.6}$$

for the case of two transmit antennas according to Equation (2.24). By contrast, for the case of four-antenna-aided DSTS-SP, $\tilde{\mathbf{s}}$ is constructed from the estimates $\tilde{x}$ as

$$\tilde{\mathbf{s}} = T_{sp}^{-1}(\tilde{x}^1, \tilde{x}^2, \tilde{x}^3, \tilde{x}^3), \tag{3.7}$$

where $\tilde{\mathbf{s}} = \{[\tilde{a}^1, \tilde{a}^2, \tilde{a}^3, \tilde{a}^4] \in \mathbb{R}^4\}$. However, for both two- and four-antenna-aided DSTS schemes, the received sphere-packed symbol $\tilde{\mathbf{s}}$ can be written as

$$\tilde{\mathbf{s}} = \chi^2_{2N_t} \cdot \mathbf{s}^l + \mathbf{N}, \tag{3.8}$$

where we have $\mathbf{s}^l \in \mathbf{S}$, $0 \leq l \leq L-1$, and $\mathbf{N}$ is a four-dimensional Gaussian random variable having a covariance matrix of $\sigma_N^2 \cdot \mathbf{I}_4 \approx 2 \cdot \chi^2_{2N_t} \cdot \sigma_n^2 \cdot \mathbf{I}_4$, since the SP symbol constellation $\mathbf{S}$ is four-dimensional.

The conditional probability of receiving a four-dimensional signal $\tilde{\mathbf{s}}$, given that a four-dimensional L-ary signal $\mathbf{s}^l \in \mathbf{S}$, $l \in [0, \cdots, L-1]$, was transmitted over the Rayleigh channel of Equation (3.8) is given by Equation (2.27) and repeated here for convenience

$$p(\tilde{\mathbf{s}}|\mathbf{s}^l) = \frac{1}{\prod_{d=1}^{D=4} \sqrt{\pi \cdot N_0 \cdot \chi^2_{2N_t}[d]}} \cdot \exp\left(\sum_{d=1}^{D=4} \frac{-\left(\tilde{a}_r^d - \chi^2_{2N_t}[d] \cdot a^{l,d}\right)^2}{\chi^2_{2N_t}[d] \cdot N_0}\right), \tag{3.9}$$

where D=4 is used, since a four-dimensional SP symbol constellation is employed.

The SP symbol $\tilde{\mathbf{s}}$ carries B_{sp} channel-coded bits $\mathbf{b} = b_0, \ldots, b_{B_{sp}-1} \in \{0, 1\}$. The LLR-value of bit b_k for $k = 0, \ldots, B_{sp}-1$ can be written as [224]

$$L(b_k|\tilde{\mathbf{s}}) = L_a(b_k) + \ln \frac{\sum_{\mathbf{s}^l \in \mathbf{S}_{1k}} p(\tilde{\mathbf{s}}|\mathbf{s}^l) \cdot \exp\left(\sum_{j=0,j\neq k}^{B_{sp}-1} b_j L_a(b_j)\right)}{\sum_{\mathbf{s}^l \in \mathbf{S}_{0k}} p(\tilde{\mathbf{s}}|\mathbf{s}^l) \cdot \exp\left(\sum_{j=0,j\neq k}^{B_{sp}-1} b_j L_a(b_j)\right)}, \tag{3.10}$$

where $\mathbf{S}_{1k}$ and $\mathbf{S}_{0k}$ are subsets of the symbol constellation $\mathbf{S}$, so that $\mathbf{S}_{1k} \triangleq \{\mathbf{s}^l \in \mathbf{S} : b_k = 1\}$ and likewise, $\mathbf{S}_{0k} \triangleq \{\mathbf{s}^l \in \mathbf{S} : b_k = 0\}$. In other words, $\mathbf{S}_{ik}$ represents all symbols of the set $\mathbf{S}$, where we have $b_k \in \{0, 1\}$, $k = 0, \ldots, B_{sp} - 1$. Using Equation (3.9), we can write Equation (3.10) as

$$\begin{aligned} L(b_k|\tilde{\mathbf{s}}) &= L_a(b_k) \\ &+ \ln \frac{\sum_{\mathbf{s}^l \in \mathbf{S}_{1k}} \exp\left[\left(\sum_{d=1}^{D=4} \frac{-\left(\tilde{a}_r^d - \chi_{2N_t}^2[d] \cdot a^{l,d}\right)^2}{\chi_{2N_t}^2[d] \cdot N_0}\right) + \sum_{j=0, j\neq k}^{B_{sp}-1} b_j L_a(b_j)\right]}{\sum_{\mathbf{s}^l \in \mathbf{S}_{0k}} \exp\left[\left(\sum_{d=1}^{D=4} \frac{-\left(\tilde{a}_r^d - \chi_{2N_t}^2[d] \cdot a^{l,d}\right)^2}{\chi_{2N_t}^2[d] \cdot N_0}\right) + \sum_{j=0, j\neq k}^{B_{sp}-1} b_j L_a(b_j)\right]} \\ &= L_{i,a} + L_{i,e}. \end{aligned} \tag{3.11}$$

3.2.2 EXIT Chart Analysis

The concept of EXIT charts was proposed in [186,189] for predicting the convergence behaviour of iterative decoders, where the evolution of the input/output mutual information exchange between the inner and outer decoders in consecutive iterations was examined. The application of EXIT charts is based on two main assumptions, which are realistic when using long interleavers, namely that the *a priori* LLR values are fairly uncorrelated and that the Probability Density Function (PDF) of the *a priori* LLR values is Gaussian distributed.

The following analysis will be presented for the sphere packing modulation case and the same analysis can be extended for the conventional modulation with the difference of mapping the constellation points to the transmit antennas as discussed in Chapter 2.

3.2.2.1 Transfer Characteristics of the Demapper

As seen in Figure 3.1, the inputs of the demapper are the DSTS-decoded and diversity-combined data stream $\tilde{\mathbf{x}}$ and the *a priori* information $L_{i,a}(\mathbf{b})$ generated by the outer channel decoder. The demapper outputs the *a posteriori* LLR $L_{i,p}(\mathbf{b})$ then subtracts the *a priori* LLR and hence produces the extrinsic LLR $L_{i,e}(\mathbf{b})$. Based on the previously-mentioned two assumptions, the *a priori* input $L_{i,a}(\mathbf{b})$ can be modelled by applying an independent zero-mean Gaussian random variable having a variance of σ_a^2.

In conjunction with the outer channel coded and interleaved bits $b \in \{0, 1\}$ of Figure 3.1 or equivalently $d \in \{-1, +1\}$, the *a priori* input $L_{i,a}(\mathbf{b})$ can be written as [186]

$$L_{i,a} = \frac{\sigma_a^2}{2} \cdot d + n_a, \tag{3.12}$$

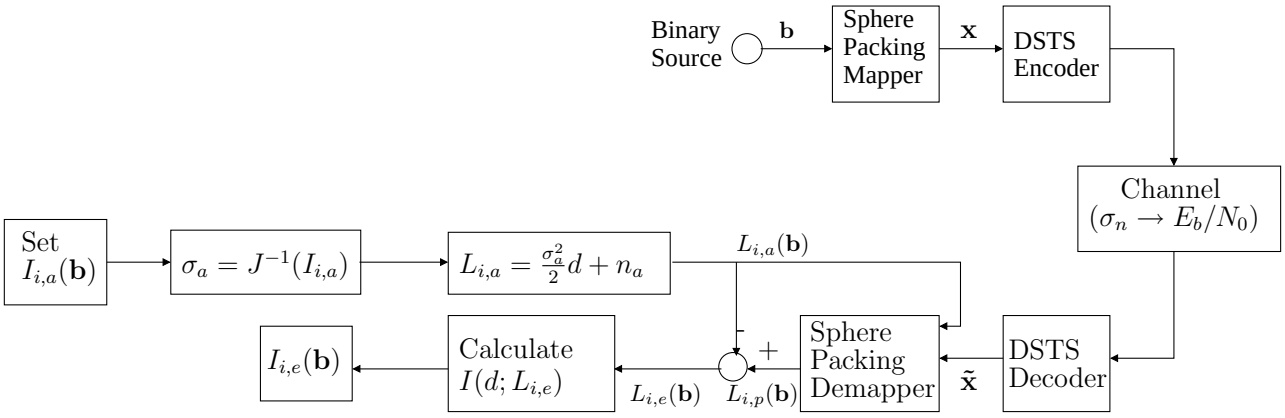

Figure 3.2: Demapper's transfer characteristics evaluation procedure block diagram.

since $L_{i,a}$ is an LLR-value obeying the Gaussian distribution [226]. Accordingly, the conditional PDF of the *a priori* input $L_{i,a}(\mathbf{b})$ is

$$p_a(\zeta|d) = \frac{1}{\sqrt{2\pi}\sigma_a} \cdot \exp\left(-\frac{(\zeta - \frac{\sigma_a^2}{2} \cdot d)^2}{2\sigma_a^2}\right). \tag{3.13}$$

The mutual information $I_{i,a}(\mathbf{b}) = I(\mathbf{b}; L_{i,a}(\mathbf{b}))$ or equivalently $I_{i,a}(\mathbf{b}) = I(\mathbf{d}; L_{i,a}(\mathbf{b}))$, $0 \leq I_{i,a} \leq 1$, between the outer coded and interleaved bit stream $\mathbf{b}$ and the *a priori* LLR values $L_{i,a}(\mathbf{b})$ is used to quantify the information content of the *a priori* knowledge [228]:

$$I_{i,a}(\mathbf{b}) = \frac{1}{2} \cdot \sum_{d=-1,+1} \int_{-\infty}^{+\infty} p_a(\zeta|d) \cdot \log_2 \frac{2 \cdot p_a(\zeta|d)}{p_a(\zeta|d=-1) + p_a(\zeta|d=+1)} d\zeta. \tag{3.14}$$

Using Equation (3.13), Equation (3.14) can be expressed as

$$I_{i,a}(\sigma_a) = 1 - \frac{1}{2\sigma_a^2} \int_{-\infty}^{+\infty} \exp\left(-\frac{(\zeta - \frac{\sigma_a^2}{2})^2}{2\sigma_a^2}\right) \cdot \log_2[1 + e^{-\zeta}] d\zeta. \tag{3.15}$$

It was shown in [191] that the mutual information between the equiprobable bits $\mathbf{d}$ and their respective LLRs L for *symmetric* and *consistent*[3] L-values always simplifies to

$$\begin{aligned} I(d; L) &= 1 - \int_{-\infty}^{+\infty} p(L|d=+1) \cdot \log_2\left[1 + e^{-L}\right] \mathrm{d}L \\ I(d; L) &= 1 - E_{d=+1}\{\log_2\left[1 + e^{-L}\right]\}. \end{aligned} \tag{3.16}$$

In order to quantify the information content of the extrinsic LLR values $L_{i,e}(\mathbf{b})$ at the output of the demapper, the mutual information $I_{i,e}(\mathbf{b}) = I(\mathbf{b}; L_{i,e}(\mathbf{b}))$ can be used, which is computed as in (3.14) using the PDF p_e of the extrinsic output.

[3]The LLR values are symmetric if their PDF is symmetric $p(-\zeta/d=+1) = p(\zeta/d=-1)$. Additionally, all LLR values with symmetric distributions satisfy the consistency condition [191] $p(-\zeta/d) = e^{-d\zeta}p(\zeta/d)$.

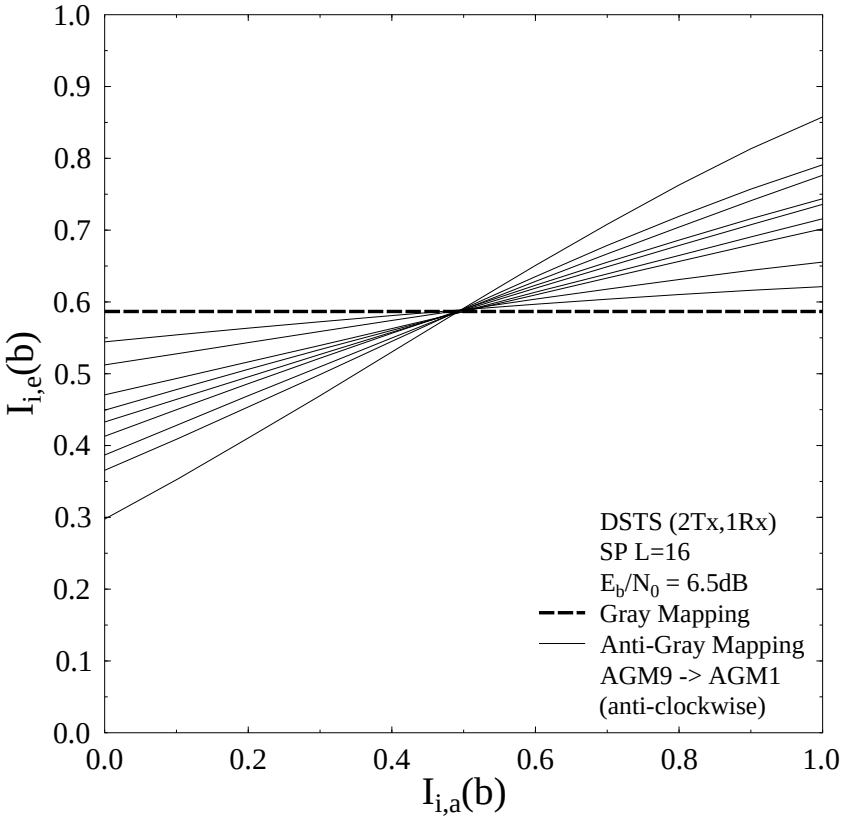

Figure 3.3: SP demapper extrinsic information transfer characteristics for different bits to SP symbol mappings at E_b/N_0=6.5 dB for L=16, while using the twin-antenna-aided DSTS scheme for transmission over temporally correlated Rayleigh fading channels.

Considering $I_{i,e}(\mathbf{b})$ as a function of both $I_{i,a}(\mathbf{b})$ and the E_b/N_0 value encountered, the demapper's extrinsic information transfer characteristic is defined as [186, 189]:

$$I_{i,e}(\mathbf{b}) = T_i(I_{i,a}(\mathbf{b}), E_b/N_0). \tag{3.17}$$

Figure 3.2 illustrates how the EXIT characteristic $I_{i,e}(\mathbf{b})$ is calculated for a specific ($I_{i,a}(\mathbf{b})$, E_b/N_0) input combination. First, the wireless channel noise variance σ_n is computed according to the specific E_b/N_0 value considered. Then, a specific value of $I_{i,a}(\mathbf{b})$ is selected to compute σ_a, where the EXIT curve has to be evaluated using $\sigma_a = J^{-1}(I_{i,a})$. Afterwards, Equation (3.12) is used to generate $L_{i,a}(\mathbf{b})$, as shown in Figure 3.2, which is applied as the *a priori* LLR input of the demapper. Finally, the mutual information of $I_{i,e}(\mathbf{b}) = I(\mathbf{b}; L_{i,e}(\mathbf{b}))$, $0 \leq I_{i,e}(\mathbf{b}) \leq 1$, between the outer coded and interleaved bit stream $\mathbf{b}$ and the LLR values $L_{i,e}(\mathbf{b})$ is calculated with the aid of the PDF p_e of the extrinsic output $L_{i,e}(\mathbf{b})$. This requires the determination of the distribution p_e by means of Monte Carlo simulations. However, according to [200] the mutual information can be estimated using sufficiently large number of samples even for non-Gaussian

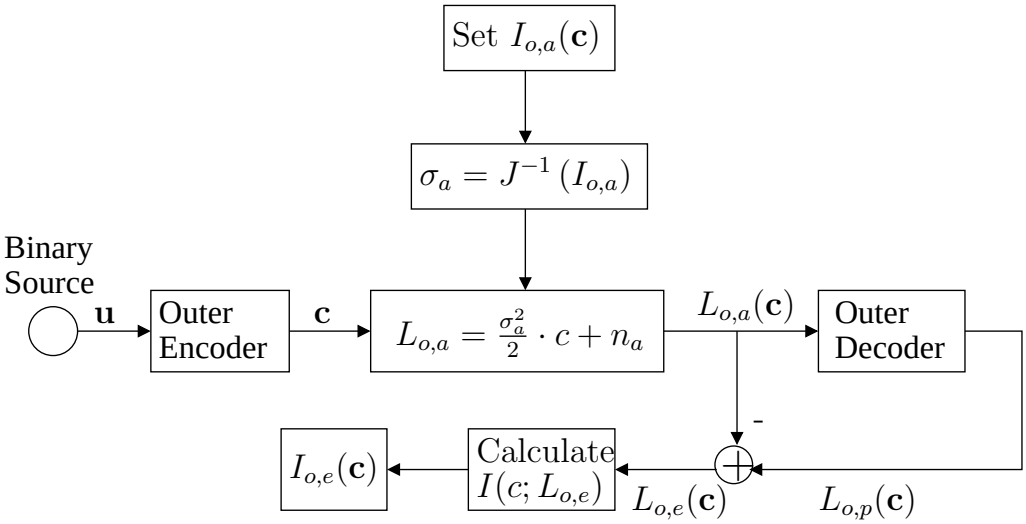

Figure 3.4: Evaluation of the outer channel decoder transfer characteristics.

or unknown distributions, which may be expressed as [200]:

$$\begin{aligned} I(\mathbf{b}; L_{i,e}(\mathbf{b})) &= 1 - E_{d=+1}\{\log_2[1 + \exp(-L_{i,e}(\mathbf{b}))]\} \\ &\approx 1 - \frac{1}{B_{sp}} \sum_{i=1}^{B_{sp}} \log_2[1 + \exp(-\mathbf{b}(i) \cdot L_{i,e}(\mathbf{b}(i)))]. \end{aligned} \tag{3.18}$$

Figure 3.3 shows the extrinsic information transfer characteristics of the SP demapper in conjunction with L=16 and various SP mapping schemes, while using the twin-antenna-aided DSTS scheme for transmission over temporally correlated Rayleigh fading channels. As seen Figure 3.3, Gray Mapping (GM) does not provide any iteration gain upon increasing the mutual information at the input of the demapper. However, using a variety of different Anti-Gray Mapping (AGM) schemes [58, 224] results in different extrinsic information transfer characteristics, as illustrated by the different slopes seen in Figure 3.3. Any mapping, which is different from the classic Gray mapping, may be referred to as AGM. The nine different AGM mapping schemes characterised in Figure 3.3 are specifically selected from all the possible mapping schemes for L=16 in order to demonstrate the different extrinsic information transfer characteristics associated with different bit-to-symbol mappings. We tested the performance of all legitimate AGM schemes in order to find the best performer. The GM and AGM schemes considered in this thesis are listed in Appendix A.

3.2.2.2 Transfer Characteristics of the Outer Decoder

The relationship between the outer channel decoder LLR input $L_{o,a}(\mathbf{c})$ and extrinsic output $L_{o,e}(\mathbf{c})$ can be described by the extrinsic transfer characteristic of the outer channel decoder. According to Figure 3.1, the input of the outer channel decoder consists only of the *a priori* input $L_{o,a}(\mathbf{c})$ provided by the SP demapper after appropriately reordering the corresponding

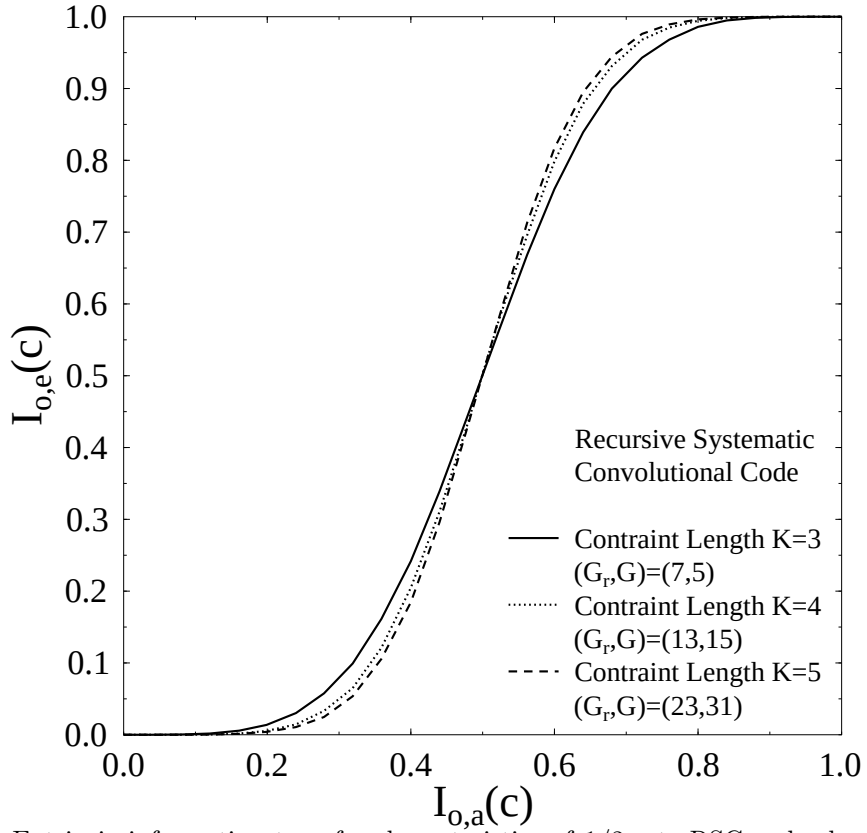

Figure 3.5: Extrinsic information transfer characteristics of 1/2-rate RSC codes having different constraint lengths.

extrinsic LLR $L_{i,e}(\mathbf{b})$. Therefore, the extrinsic information transfer characteristics of the outer channel decoder is independent of the E_b/N_0 value and hence $I_{o,e}(\mathbf{c})$ may be written as

$$I_{o,e}(\mathbf{c}) = T_o\left(I_{o,a}(\mathbf{c})\right), \tag{3.19}$$

where $I_{o,a}(\mathbf{c}) = I(\mathbf{c}; L_{o,a}(\mathbf{c}))$, $0 \leq I_{o,a} \leq 1$, is the mutual information between the outer channel coded bit stream $\mathbf{c}$ and the *a priori* LLR values $L_{o,a}(\mathbf{c})$ and similarly $I_{o,e}(\mathbf{c}) = I(\mathbf{c}; L_{o,e}(\mathbf{c}))$, $0 \leq I_{o,e} \leq 1$, is the mutual information between the outer channel coded bit stream $\mathbf{c}$ and the extrinsic LLR values $L_{o,e}(\mathbf{c})$. The computational model of evaluating the EXIT characteristics of the outer channel decoder is shown in Figure 3.4. As seen in the figure, the procedure is similar to that of the sphere-packing demapper shown in Figure 3.2, except that its value is independent of the E_b/N_0 value. Again, $I_{o,e} = I(\mathbf{c}; L_{o,e}(\mathbf{c}))$ can be computed either by evaluating the histogram approximation of p_e [186, 189] and then applying Equation (3.14) or, more conveniently, by the time averaging method [200] of Equation (3.18) as

$$\begin{aligned} I(\mathbf{c}; L_{o,e}(\mathbf{c})) &= 1 - E\{\log_2[1 + \exp(-L_{o,e})]\} \\ &\approx 1 - \frac{1}{B_{sp}} \sum_{i=1}^{B_{sp}} \log_2[1 + \exp(-\mathbf{c}(i) \cdot L_{o,e}(\mathbf{c}_i))]. \end{aligned} \tag{3.20}$$

The extrinsic transfer characteristics of various 1/2-rate Recursive Systematic Convolutional

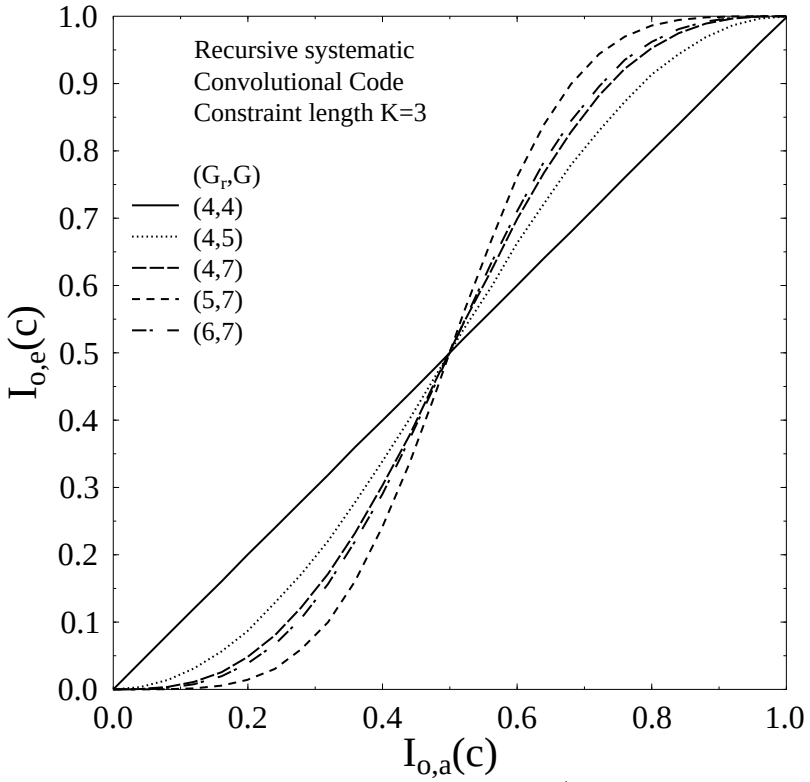

Figure 3.6: Extrinsic information transfer characteristics of 1/2-rate RSC codes with constraint length K=3 and different generator polynomials.

(RSC) codes having different constraint lengths K are shown in Figure 3.5. The generator polynomials employed are given in the figure's legend in octal form, where G_r is the feedback polynomial and G is the feed-forward polynomial. Figure 3.5 demonstrates that for $I_{o,a} > 0.5$, the set of RSC codes having higher constraint lengths converge faster upon increasing $I_{o,a}$ than the RSC codes having smaller constraint lengths. Furthermore, it is noticed that the extrinsic characteristics of the RSC codes having constraint lengths of K=4 and K=5 are close to each other and that they depend on the generator polynomial used.

Moreover, the extrinsic transfer characteristics of several 1/2-rate RSC codes having a constraint length of K=3 and variable generator polynomials are shown in Figure 3.6. All the possible generator polynomials having a constraint length of K=3 are employed. Explicitly, we have $(G_r, G) = (4, 4)$ to $(G_r, G) = (7, 7)$, where the generator polynomial is presented in octal form. According to Figure 3.6, the code having a generator polynomial $(G_r, G) = (5, 7)$ converges faster than the other codes.

3.2.2.3 Extrinsic Information Transfer Chart

The exchange of extrinsic information in the system of Figure 3.1 can be visualised by plotting the extrinsic information characteristics of the inner demapper and the outer RSC decoder in EXIT chart [186, 189]. The outer RSC decoder's extrinsic output information $I_{o,e}(\mathbf{c})$ becomes

the demapper's *a priori* input information $I_{i,a}(\mathbf{b})$, which is represented on the x-axis of the EXIT chart. Similarly, on the y-axis we plot the demapper's extrinsic output information $I_{i,e}(\mathbf{b})$, which becomes the outer RSC decoder's *a priori* input information $I_{o,a}(\mathbf{c})$. The EXIT curves presented in this section correspond to the system employing a 1/2-rate RSC code having constraint length K=3, denoted as RSC(2,1,3), in conjunction with an octal generator polynomial $(G_r, G) = (7, 5)$.

Figure 3.7 shows the EXIT chart of an iteratively detected RSC-coded DSTS-SP scheme employing two transmit antennas and Anti-Gray mapping AGM-1 of Figure 3.3 when communicating over a temporally correlated Rayleigh fading channel having a normalised Doppler frequency f_D=0.01. Ideally, in order for the exchange of extrinsic information between the SP demapper and the outer RSC decoder to converge at a specific E_b/N_0 value, the EXIT curve of the SP demapper at the E_b/N_0 value of interest and the extrinsic transfer characteristics curve of the outer RSC decoder should only intersect at the $(1.0, 1.0)$ point. If this condition is satisfied, then a so-called *convergence tunnel* [186, 189] appears on the EXIT chart. The narrower the tunnel, the more iterations are required for reaching the $(1.0, 1.0)$ point and the closer the performance is to the channel capacity. If however the two extrinsic transfer characteristics intersect at a point close to the line at $I_{o,e}(\mathbf{c}) = 1.0$ rather than at the $(1.0, 1.0)$ point, then a moderately low BER may be still achieved, although it will remain higher than the schemes where the intersection is at the $(1.0, 1.0)$ point. These types of tunnels are referred to here as *semi-convergent tunnels*. Observe in Figure 3.7 that a semi-convergent tunnel exists at E_b/N_0=7.0 dB. This implies that according to the predictions of the EXIT chart seen in Figure 3.7, the iterative decoding process is expected to converge at an E_b/N_0 value between 6.5 dB and 7.0 dB. These EXIT chart based convergence predictions are usually verified by the actual iterative decoding trajectory, as will be discussed shortly in Section 3.2.4.

After analysing the EXIT chart of the DSTS-SP scheme employing two transmit antennas and the optimum[4] SP Anti-Gray mapping AGM-1 of Figure 3.3, it is worth investigating the effect of employing different constellations. Figure 3.8 shows the EXIT chart of the system employing AGM-3 of Figure 3.3. As seen in the figure, a semi-convergent tunnel exists at an E_b/N_0 value of 6.0 dB, which is lower than that recorded for the optimum AGM mapping AGM-1. However, the intersection between the EXIT curve of the SP demapper employing AGM-3 at E_b/N_0=6.0 dB and that of the outer RSC decoder is almost at $I_{i,e}(\mathbf{b})$=0.75, while the SP AGM-1 demapper's extrinsic transfer characteristic and the outer RSC decoder's extrinsic transfer curve intersect at $I_{i,e}(\mathbf{b})$=0.85 for E_b/N_0=7.0 dB. Therefore, the iterative detection of the DSTS-SP

[4]The optimum SP Anti-Gray Mapping is selected from Figure 3.3 as the mapping that results in the highest intersection point between the EXIT curve of the SP demapper and the EXIT curve of the outer RSC decoder at a specific E_b/N_0 value.

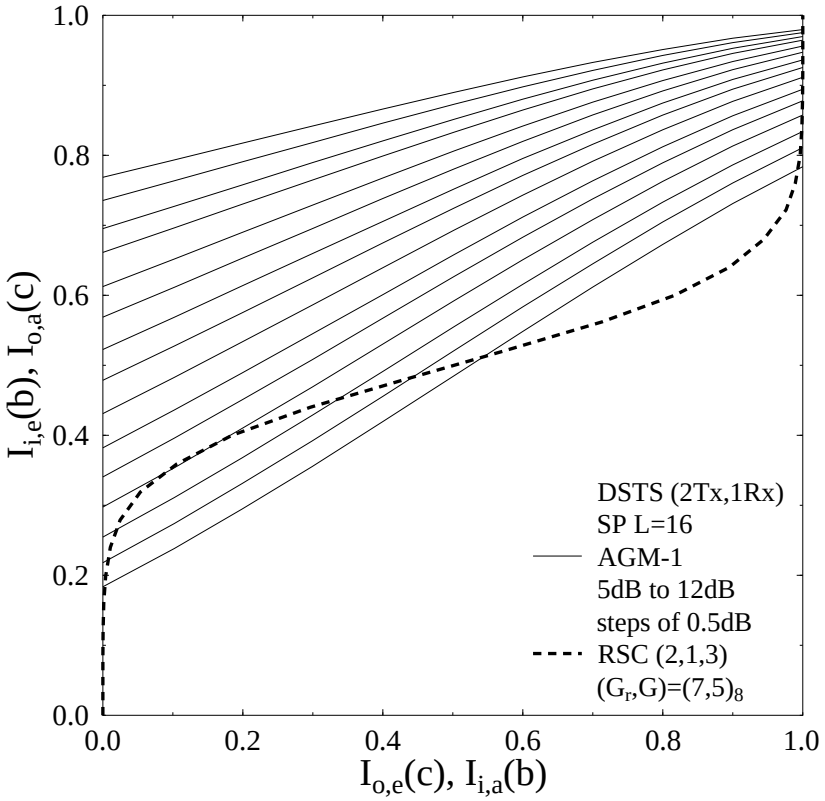

Figure 3.7: EXIT chart of an iteratively detected RSC-coded DSTS-SP scheme employing two transmit antennas and AGM-1 of Figure 3.3 in combination with the outer RSC(2,1,3) code, while communicating over a temporally correlated Rayleigh fading channel exhibiting f_D=0.01.

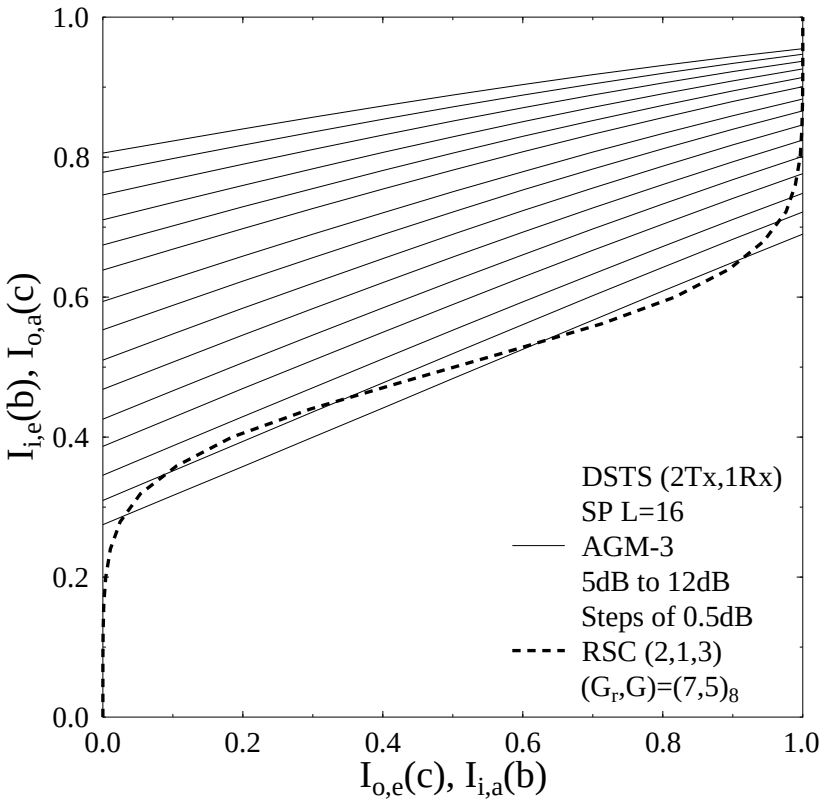

Figure 3.8: EXIT chart of an iteratively detected RSC-coded DSTS-SP scheme employing two transmit antennas and AGM-3 of Figure 3.3 in combination with the outer RSC(2,1,3) code, while communicating over a temporally correlated Rayleigh fading channel associated with f_D=0.01.

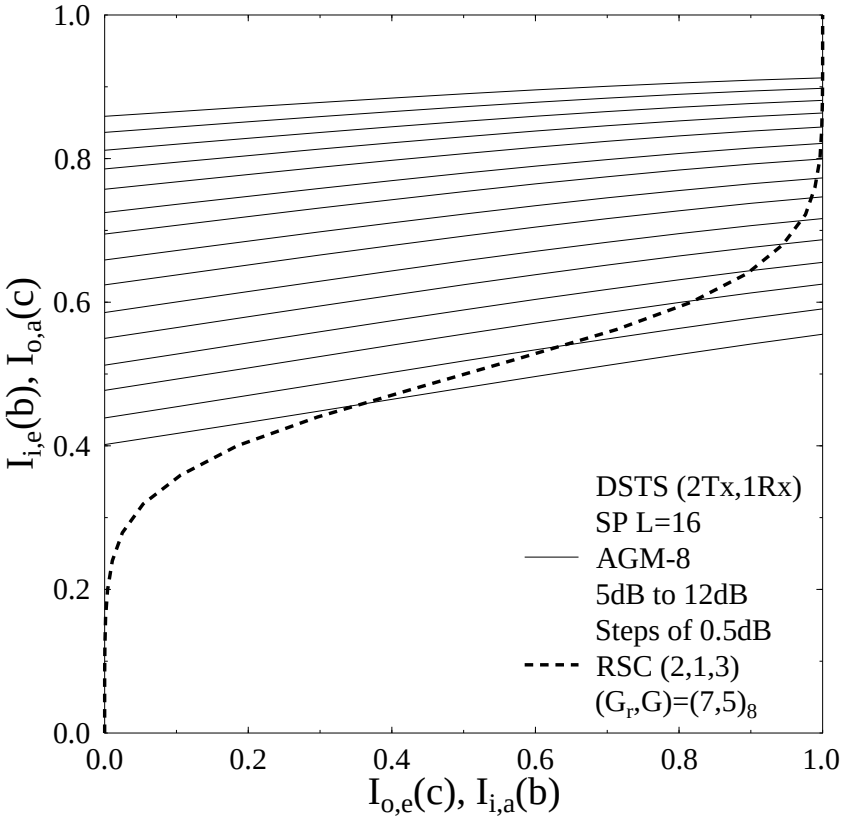

Figure 3.9: EXIT chart of an iteratively detected RSC-coded DSTS-SP scheme employing two transmit antennas and AGM-8 of Figure 3.3 in combination with the outer RSC(2,1,3) code, while communicating over a temporally correlated Rayleigh fading channel associated with f_D=0.01.

system employing AGM-3 converges at a lower E_b/N_0 than that of the AGM-1 aided system, although the AGM-1 based system converges to a lower BER value. Their difference becomes more explicit as we move towards higher index AGMs such as AGM-8 shown in Figure 3.9. In Figure 3.9 a semi-convergent tunnel exists at E_b/N_0=5.0 dB. However, the SP AGM-8 demapper's EXIT curve and the outer RSC decoder's EXIT curve intersect near $I_{i,e}(\mathbf{b})$=0.4 at E_b/N_0=5.0 dB, i.e. the BER performance dramatically improves at E_b/N_0=5.0 dB, but fails to decay to an infinitesimally low BER value, as will be shown shortly in Section 3.2.4.

Figure 3.10 depicts the EXIT chart of the iteratively detected RSC-coded DSTS-QPSK scheme employing two transmit antennas and Anti-Gray mapping in combination with outer RSC code having constraint lengths K=3 when communicating over a correlated Rayleigh fading channel having f_D=0.01. Observe in Figure 3.10 that a semi-convergent tunnel exists at E_b/N_0=5.0 dB, however the extrinsic transfer characteristic curve of the QPSK demapper and that of the outer RSC decoder intersect at almost $I_{i,e}(\mathbf{b})$=0.55 at E_b/N_0=5.0 dB, i.e. the performance curve converges at E_b/N_0=5.0 dB but not to a very low BER value compared to the DSTS-SP system employing AGM-1.

Finally, the EXIT chart of the iteratively detected RSC-coded DSTS-SP scheme employing four transmit antennas and AGM-1 of Figure 3.3 in combination with outer RSC code having

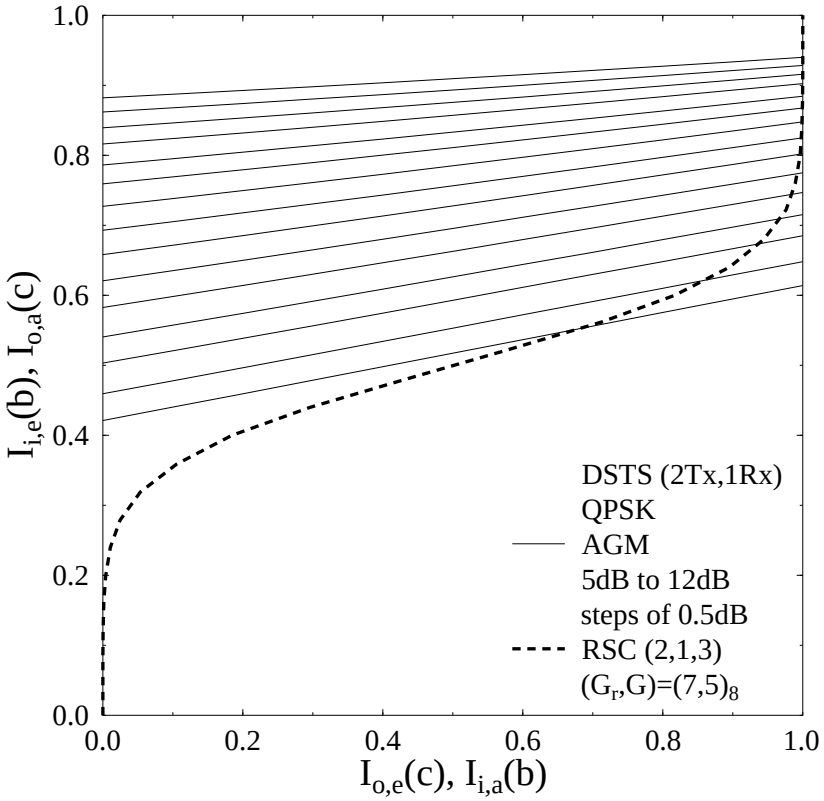

Figure 3.10: EXIT chart of an iteratively detected RSC-coded DSTS-QPSK scheme employing two transmit antennas and Anti-Gray mapping in combination with the outer RSC(2,1,3) code, while communicating over a temporally correlated Rayleigh fading channel associated with f_D=0.01.

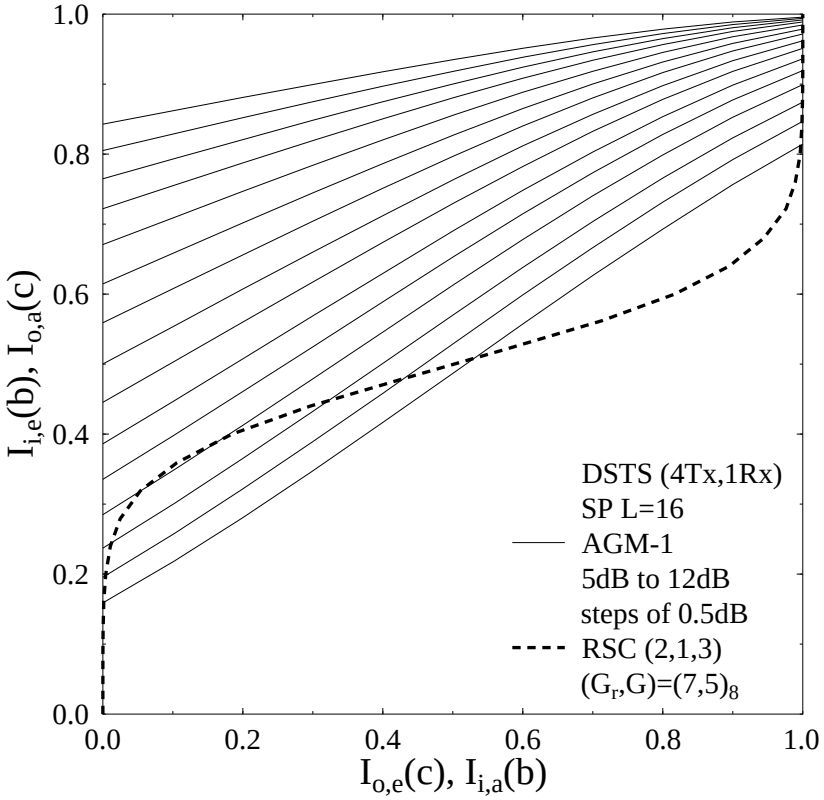

Figure 3.11: EXIT chart of an iteratively detected RSC-coded DSTS-SP scheme employing four transmit antennas and AGM-1 of Figure 3.3 in combination with the outer RSC(2,1,3) code, while communicating over a temporally correlated Rayleigh fading channel associated with f_D=0.01.

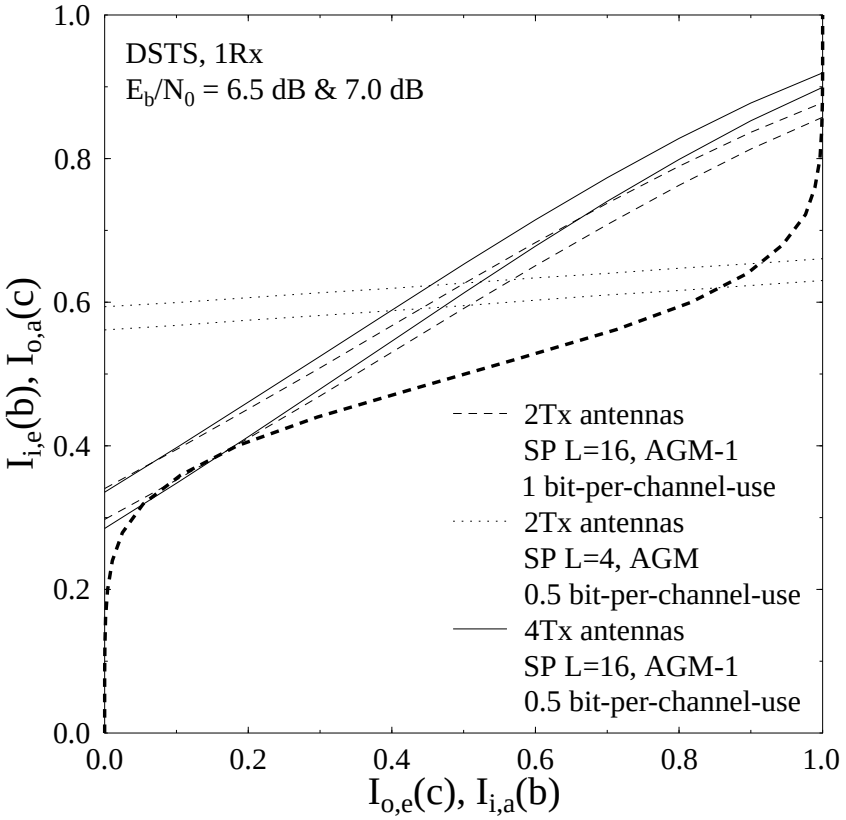

Figure 3.12: Comparison of the EXIT charts of an iteratively detected RSC-coded DSTS-SP scheme employing two and four transmit antennas in conjunction with L=16 and AGM-1 together with the two-antenna-aided DSTS-SP scheme employing L=4 and AGM.

constraint length K=3 is shown in Figure 3.11. Observe in the figure that a semi-convergent tunnel exists at E_b/N_0=7.0 dB, which is similar to the behaviour of the system employing two transmit antennas as characterised in Figure 3.7. However, note that the DSTS-SP schemes employing two and four transmit antennas have different bandwidth efficiencies. Therefore, we plot in Figure 3.12 the EXIT curves of the 1 bit-per-channel-use bandwidth efficiency two-antenna-aided DSTS-SP scheme in conjunction with L=16 and AGM-1 together with the 0.5 bit-per-channel-use two-antenna-aided DSTS-SP scheme employing L=4 and AGM as well as with the 0.5 bit-per-channel-use four-antenna-aided DSTS-SP scheme employing L=16 and AGM-1. Figure 3.12 shows the EXIT curves of the demapper for E_b/N_0=6.5 dB and 7.0 dB. As shown in the figure, the four-antenna-aided system has a higher intersection point between the SP AGM-1 demapper extrinsic transfer characteristics curve and the outer RSC decoder extrinsic transfer characteristics curve compared to the equivalent-bandwidth-efficiency system employing two transmit antennas as well as to the higher-bandwidth-efficiency system employing two transmit antennas.

3.2.3 Maximum Achievable Bandwidth Efficiency

In Section 2.3.6 we derived the capacity and bandwidth efficiency of the DSTS-SP scheme. In this section, a procedure for computing an upper limit on the maximum achievable bandwidth efficiency of the system is proposed. It was argued in [194, 229] that the maximum achievable bandwidth efficiency of the system is equal to the area under the EXIT curve of the inner code provided that the bit stream $\mathbf{b}$ has independently and uniformly distributed bits, the channel is an erasure channel, the inner code is unity-rate and the MAP algorithm is used for decoding. Assuming that the area under the EXIT curve of the inner decoder, i.e. the SP demapper in this case, is represented by $\mathcal{A}_i$, the *maximum* achievable rate for the outer code is given by R_{max}=$\mathcal{A}_i(E_b/N_0)$ [194] at a specific E_b/N_0 value. In other words, if $\mathcal{A}_i$ is calculated for different E_b/N_0 values, the maximum achievable bandwidth efficiency may be formulated as a function of the E_b/N_0 value as follows

$$\begin{aligned} \eta_{max}(\underline{E_b/N_0}) &= B_{sp} \cdot R_{DSTS-SP} \cdot R_{max} \\ &\approx B_{sp} \cdot R_{DSTS-SP} \cdot \mathcal{A}_i(E_b/N_0) \quad \text{[bit/sec/Hz]}, \end{aligned} \tag{3.21}$$

where B_{sp}=$\log_2(L)$ is the number of bits per SP symbol, $R_{DSTS-SP}$=1/2 for the N_t=2 transmit antennas case and $R_{DSTS-SP}$=1/4 for the N_t=4 transmit antennas case. Additionally, $\underline{E_b/N_0}$ and E_b/N_0 are related as follows

$$\underline{E_b/N_0} = E_b/N_0 + 10\log\left(\frac{R_o}{\mathcal{A}_i(E_b/N_0)}\right) \quad \text{[dB]}, \tag{3.22}$$

where R_o is the original outer code rate used for generating the EXIT curve of the inner decoder/demapper corresponding to the different $\mathcal{A}_i$ values. A simple procedure may be used to calculate the maximum achievable bandwidth efficiency of Equation (3.21) for $E_b/N_0 \in [\rho_{min}, \rho_{max}]$, assuming that $R_{arbitrary}$ is an arbitrary rate and ϵ is a small constant.

Algorithm 3.1 *Maximum Achievable Bandwidth Efficiency using EXIT Charts:*

Step 1: Let $R_o = R_{arbitrary}$.

Step 2: Let $E_b/N_0 = \rho_{min}$ dB.

Step 3: Calculate N_0.

Step 4: Let $I_{i,a}(\mathbf{b}) = 0$.

Step 5: Activate the SP demapper.

Step 6: Save $I_{i,e}(\mathbf{b}) = T_i(I_{i,a}(\mathbf{b}), E_b/N_0)$.

Step 7: Let $I_{i,a}(\mathbf{b}) = I_{i,a}(\mathbf{b}) + \epsilon$.

If $I_{i,a}(\mathbf{b}) \leq 1.0$, go to **Step 5**.

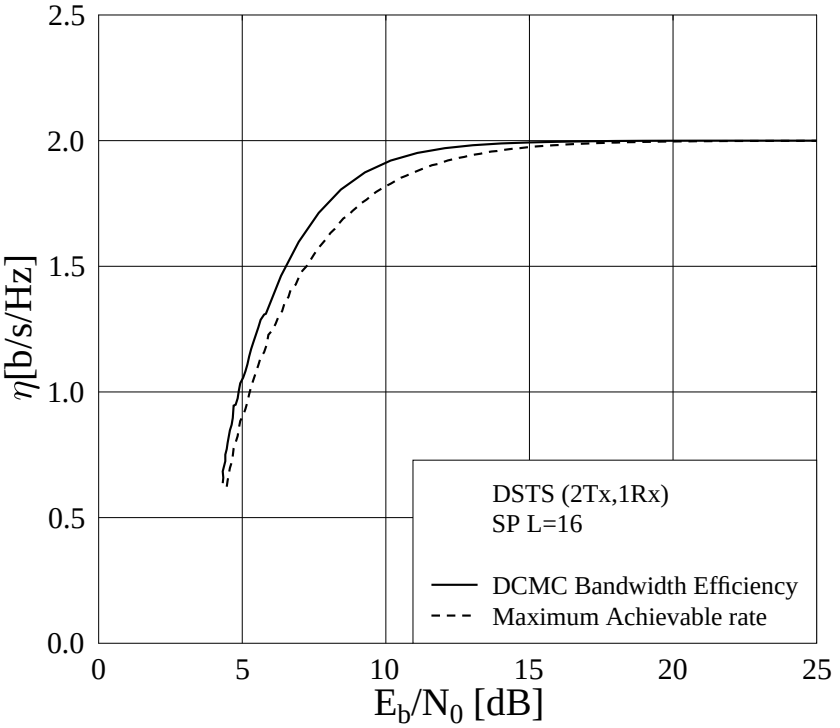

Figure 3.13: Comparison of the DCMC bandwidth efficiency and the maximum achievable rate obtained using EXIT charts of the two-antenna-aided DSTS-SP in conjunction with L=16.

Step 8: Calculate $\mathcal{A}_i(E_b/N_0) = \int_0^1 T_i(i, E_b/N_0)\ \mathrm{d}i$.

Step 9: Calculate $\underline{E_b/N_0}$ using Equation (3.22).

Step 10: Save $\eta_{max}(\underline{E_b/N_0})$ of Equation (3.21).

Step 11: Let $E_b/N_0 = E_b/N_0 + \epsilon$.

If $E_b/N_0 \leq \rho_{max}$ dB, go to **Step 3**.

Step 12: Output $\eta_{max}(\underline{E_b/N_0})$ from **Step 10**.

Observe that ρ_{min} and ρ_{max} are adjusted accordingly in order to produce the desired range of the resultant $\underline{E_b/N_0}$ values. Furthermore, the output of Algorithm 3.1 is independent of the specific choice of R_o, since Equation (3.22) would always adjust the E_b/N_0 values, regardless of R_o.

The MIMO channel capacity curves of the four-dimensional SP modulation assisted DSTS scheme in conjunction with L=16 are shown in Figures 3.13 and 3.14 for two and four transmit antennas respectively. The two figures portray both the DCMC bandwidth efficiency curve as well as the maximum achievable rate of the system derived from the EXIT curves according to Algorithm 3.1. Observe in Figures 3.13 and 3.14 that the maximum achievable rate of the system derived from the EXIT curves is quite close to the DCMC bandwidth efficiency. Note that the maximum achievable rate obtained from the EXIT charts and the bandwidth efficiency limit calculated using Equation (2.32) were only proven to be equal for the family

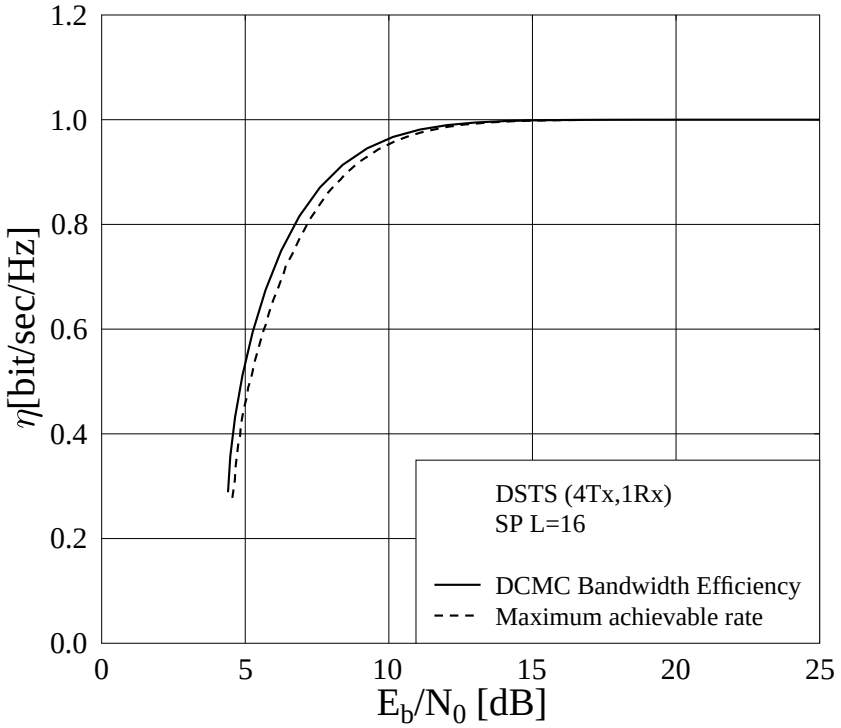

Figure 3.14: Comparison of the DCMC bandwidth efficiency and the maximum achievable rate obtained using EXIT charts of the four-antenna-aided DSTS-SP in conjunction with L=16.

of binary erasure channels [229]. Nonetheless, similar experimentally verified trends have been observed for both AWGN and Inter-Symbol-Interference (ISI) channels [191, 194], when APP-based decoders are used for all decoder blocks [229]. However, our DSTS decoder employs a very simple decoding algorithm that utilises only two or four consecutively received symbols, despite the fact that all the symbols are interdependent. Therefore, the decoder employed is suboptimum and if a trellis based DSTS decoder -such as the MAP algorithm [181]- is employed, then the maximum achievable rate obtained from the EXIT chart might match the capacity limit computed. Nevertheless, the complexity of the MAP algorithm is high in return to a modest gain of 0.35 dB observed in Figure 3.13 and the 0.2 dB gain seen in Figure 3.14.

At a bandwidth efficiency of η=1 bit/sec/Hz, the DCMC capacity limit of the two-antenna-aided DSTS-SP scheme is $E_b/N_0 \approx 4.85$ dB. Furthermore, at a bandwidth efficiency of η=1 bit/sec/Hz, the maximum achievable rate of the same scheme derived from the EXIT curves is E_b/N_0=5.2 dB. On the other hand, the DCMC capacity limit of the four-antenna-aided DSTS-SP scheme is $E_b/N_0 \approx 4.95$ dB at a bandwidth efficiency of 0.5 bits/sec/Hz, while the maximum achievable rate limit derived from the EXIT curves at the same bandwidth efficiency is E_b/N_0=5.18 dB.

SP modulation	L=16
Number of transmit antennas N_t	2 and 4
Number of receive antennas N_r	1
Channel	Correlated Rayleigh fading
Normalised Doppler frequency	0.01
Outer channel code	RSC(2,1,3)
Generator polynomial	$(G_r, G)=(7,5)_8$
Spreading code	Walsh-Hadamard code
Spreading factor	8
Number of users	4

Table 3.1: Iteratively-detected RSC-coded DSTS-SP system parameters.

3.2.4 Results and Discussions

In this section, we consider a DSTS system employing two and four transmit antennas and a single receive antenna in order to demonstrate the performance improvements achieved by the proposed iteratively detected SP-aided system. All simulation parameters are listed in Table 3.1.

As mentioned in Section 3.2.2.3, the EXIT chart based convergence predictions can be verified by the actual iterative decoding trajectory. Figure 3.15 records the trajectory of the iteratively detected RSC-coded DSTS-SP scheme in conjunction with two transmit antennas and AGM-1 of Figure 3.3 in combination with the system parameters outlined in Table 3.1, while operating at E_b/N_0=7.0 dB and employing interleaver depth of D_{int}=1,000,000 bits. The steps seen in the figure represent the actual extrinsic information transfer between the demapper and the outer RSC channel decoder. Since a long interleaver is employed, the assumptions outlined at the beginning of Section 3.2.2 are justified and hence the EXIT chart based convergence prediction becomes accurate.

Moreover, Figures 3.16, 3.17 and 3.18 record the trajectory of the iteratively detected RSC-coded DSTS-SP scheme in conjunction with two transmit antennas and AGM-1 of Figure 3.3 in combination with the system parameters outlined in Table 3.1, while operating at E_b/N_0=7.0 dB associated with interleaver depths of D_{int}=100,000 bits, D_{int}=10,000 bits and D_{int}=1,000 bits, respectively. The decoding trajectory in Figure 3.16 employs an interleaver depth of D_{int}=100,000 bits, as seen in the figure, the decoding trajectory is different from that observed in Figure 3.15. In other words, the system employing a shorter interleaver requires more iterations to reach the highest intersection point between the EXIT curves of the demapper

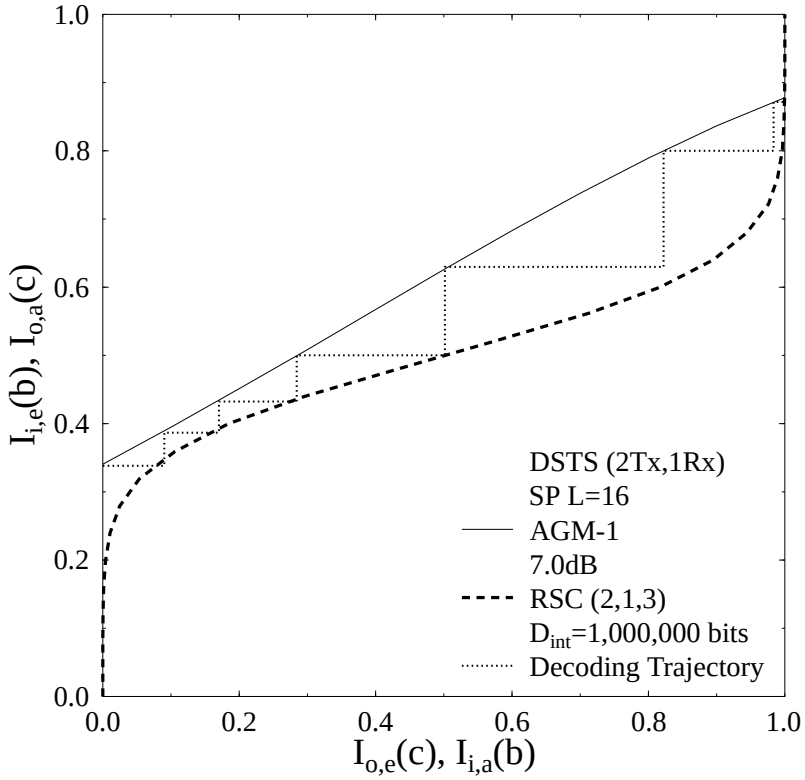

Figure 3.15: Decoding trajectory of the iteratively detected 1/2-rate RSC-coded DSTS-SP scheme in conjunction with two transmit antennas and AGM-1 of Figure 3.3 employing the system parameters outlined in Table 3.1, while operating at E_b/N_0=7.0 dB with an interleaver depth of D_{int}=1,000,000 bits.

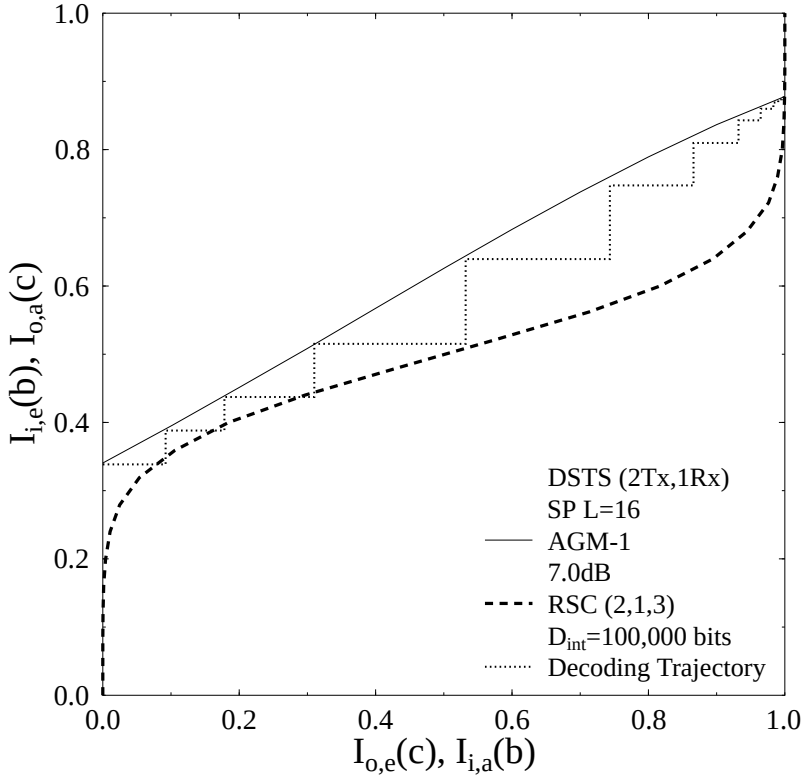

Figure 3.16: Decoding trajectory of the iteratively detected 1/2-rate RSC-coded DSTS-SP scheme in conjunction with two transmit antennas and AGM-1 of Figure 3.3 employing the system parameters outlined in Table 3.1, while operating at E_b/N_0=7.0 dB with an interleaver depth of D_{int}=100,000 bits.

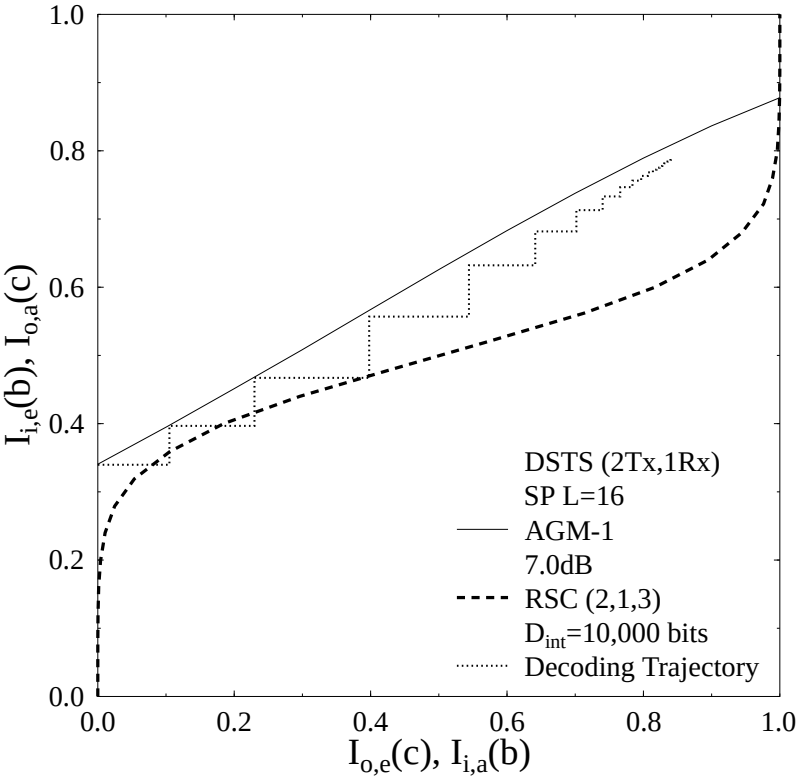

Figure 3.17: Decoding trajectory of the iteratively detected 1/2-rate RSC-coded DSTS-SP scheme in conjunction with two transmit antennas and AGM-1 of Figure 3.3 employing the system parameters outlined in Table 3.1, while operating at E_b/N_0=7.0 dB with an interleaver depth of D_{int}=10,000 bits.

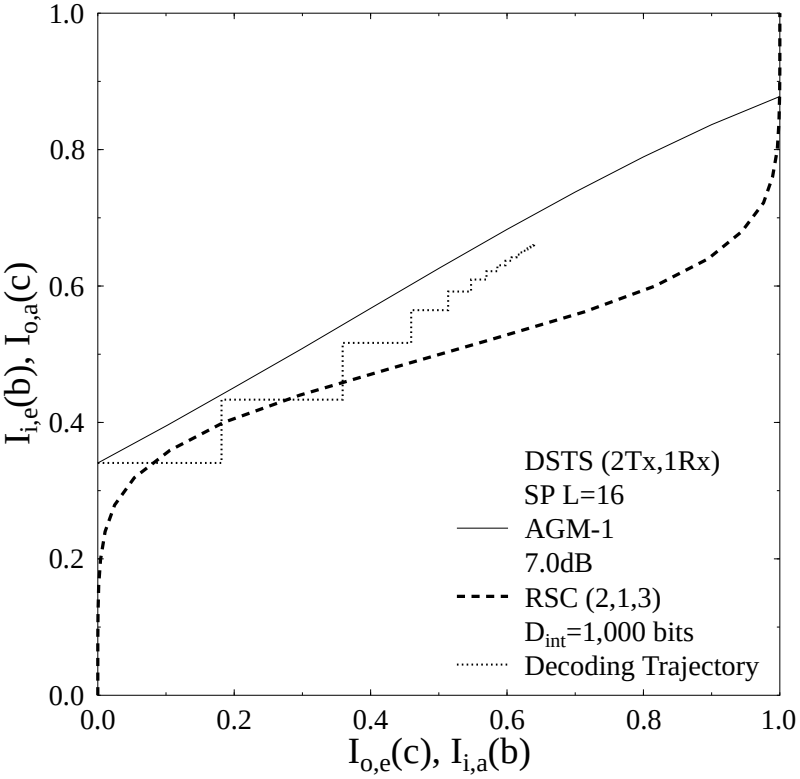

Figure 3.18: Decoding trajectory of the iteratively detected 1/2-rate RSC-coded DSTS-SP scheme in conjunction with two transmit antennas and AGM-1 of Figure 3.3 employing the system parameters outlined in Table 3.1, while operating at E_b/N_0=7.0 dB with an interleaver depth of D_{int}=1,000 bits.

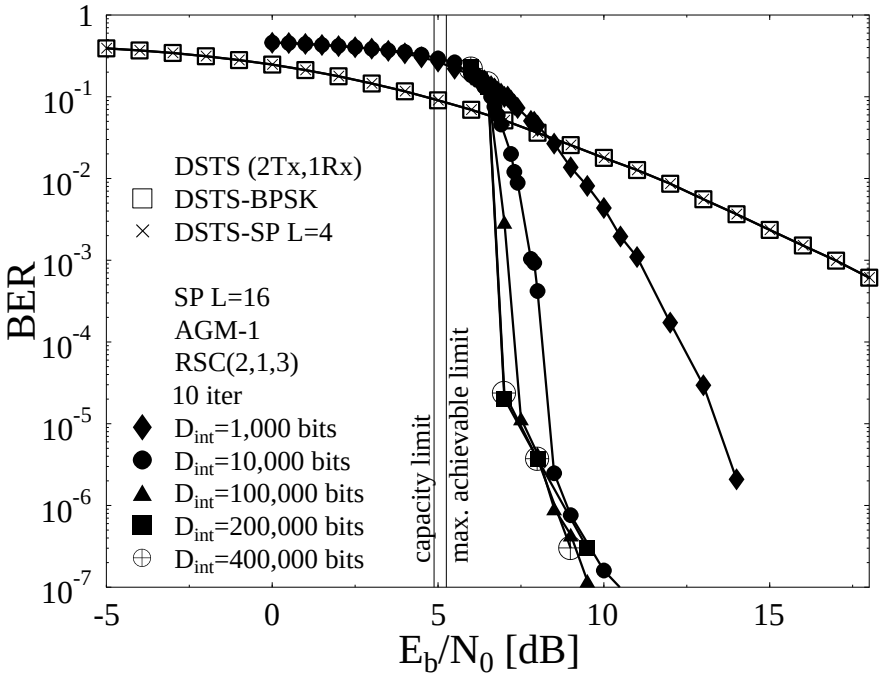

Figure 3.19: Performance comparison of the AGM-1 based RSC-coded two transmit antennas DSTS-SP schemes in conjunction with L=16 against an identical bandwidth efficiency of 1 bit-per-channel-use uncoded DSTS-SP scheme using L=4 and against the conventional DSTS-BPSK scheme, when employing the system parameters outlined in Table 3.1 and using different interleaver depths after I=10 iterations.

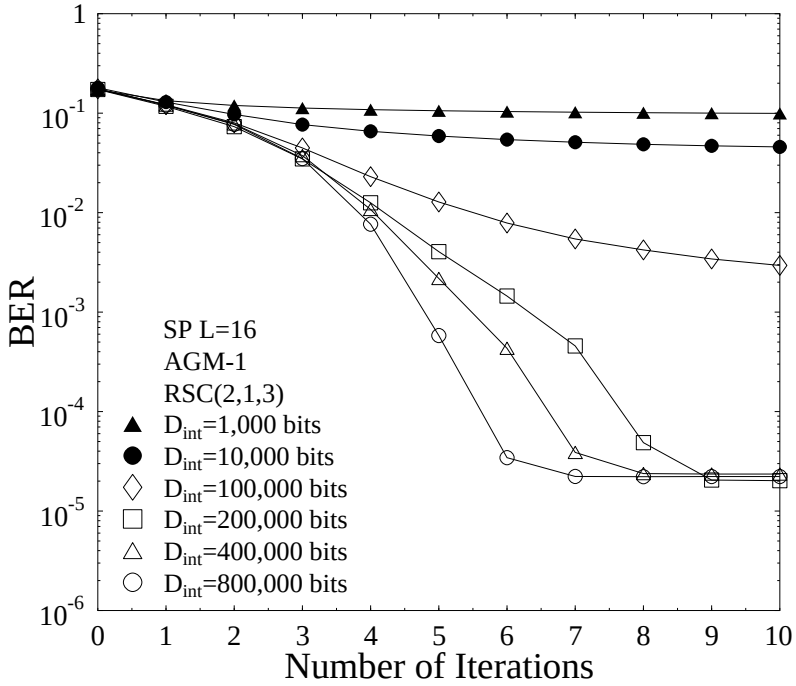

Figure 3.20: Comparison of the BER performance versus the number of iterations for the iteratively detected 1/2-rate RSC-coded DSTS-SP scheme in conjunction with two transmit antennas and AGM-1 of Figure 3.3, while employing the system parameters outlined in Table 3.1 for different interleaver depths recorded at E_b/N_0 of 7.0 dB.

and the outer RSC code, in addition to the fact that as $I_{i,a}(\mathbf{b})$ increases, the trajectory does not match the EXIT curve of the RSC decoder and this might be due to the fact that in conjunction with an interleaver depth of D_{int}=100,000 bits, the LLR distribution is no longer Gaussian for high $I_{i,a}(\mathbf{b})$ values.

On the other hand, the decoding trajectories shown in Figures 3.17 and 3.18 are different from the EXIT chart prediction because shorter interleavers are used and thus the assumptions at the beginning of Section 3.2.2 are not valid. The BER performance of the iteratively detected RSC-coded DSTS-SP scheme in conjunction with two transmit antennas and AGM-1 in combination with the system parameters outlined in Table 3.1 is shown in Figure 3.19 when using I=10 iterations and varying the interleaver depth. As seen in the figure, upon increasing the interleaver depth from D_{int}=1,000 bits to D_{int}=10,000 bits, the system's performance dramatically improves. Upon further increasing the interleaver depth from D_{int}=10,000 bits to D_{int}=100,000 bits, the attainable performance improves, but not as much as increasing it from 1,000 to 10,000 bits. Furthermore, increasing the interleaver depth beyond D_{int}=200,000 bits does not significantly improve the achievable system performance. Additionally, observe that a turbo cliff appears at E_b/N_0=8.5 dB upon increasing the interleaver depth to D_{int}=10,000 bits, while a turbo cliff occurs at E_b/N_0=7.5 dB, when using an interleaver depth of D_{int}=100,000 bits. Additionally, the system employing an interleaver depth of $D_{int} \geq 200,000$ bits converges at E_b/N_0=7.0 dB, as predicted by the EXIT curve of Figure 3.7. Furthermore, as the interleaver depth increases, the system's performance approaches the capacity limit, as shown in Figure 3.19. However, due to the error floor observed for the BER curves in Figure 3.19, as the E_b/N_0 increases, the system's BER curve diverges from the capacity limit. Explicitly, the system performs within 2.3 dB from the maximum achievable rate limit at BER=10^{-5} and within 3.3 dB from the same limit at BER=10^{-6}.

Figure 3.20 plots the BER performance of the iteratively detected RSC-coded DSTS-SP scheme employing AGM-1 versus the number of iterations while using different interleaver depths ranging from D_{int}=1,000 bits to D_{int}=800,000 bits in combination with the system parameters outlined in Table 3.1, while operating at E_b/N_0=7.0 dB. The plot investigates the BER performance versus the complexity of the system quantified in terms of the number of iterations. As shown in the figure, when using short interleavers, increasing the number of iterations results in no significant BER performance improvement, which is the case for the interleavers with depths of D_{int}=1,000 bits and D_{int}=10,000 bits. However, as the interleaver becomes longer, the achievable system performance improves upon increasing the number of iterations. Moreover, as the interleaver depth increases, the system requires less iterations to saturate, as shown in Figure 3.20. For example, for the case of an interleaver depth of D_{int}=800,000 bits, it is shown in Figure 3.20 that after I=7 iterations, there is no more improvement in the

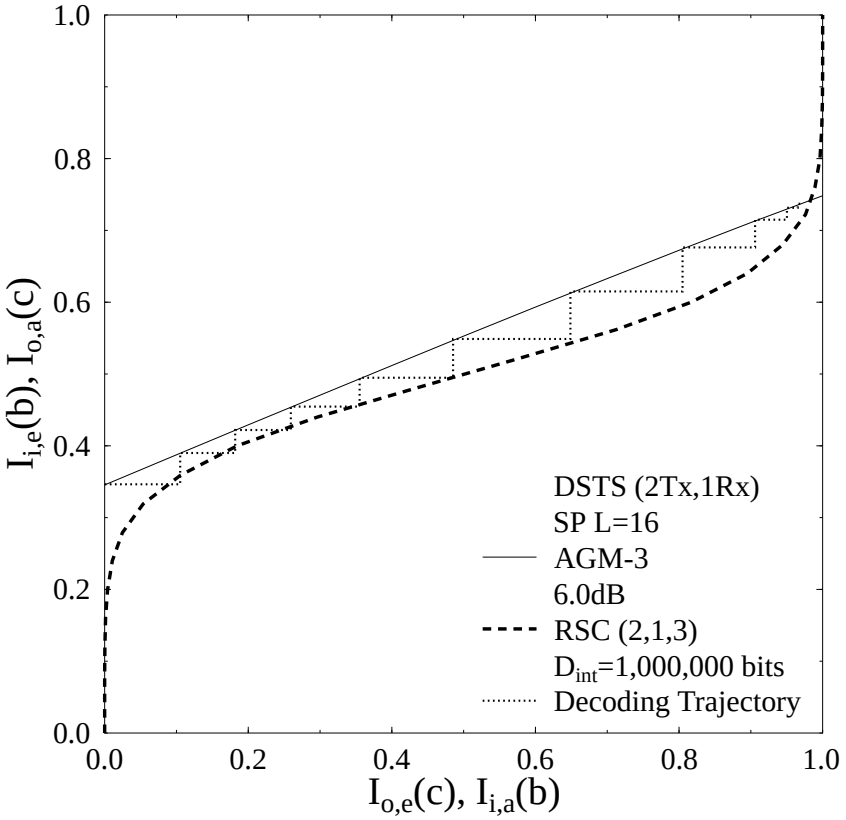

Figure 3.21: Decoding trajectory of the iteratively detected 1/2-rate RSC-coded DSTS-SP scheme in conjunction with two transmit antennas and AGM-3 of Figure 3.3 employing the system parameters outlined in Table 3.1, while operating at E_b/N_0=6.0 dB with an interleaver depth of D_{int}=1,000,000 bits.

attainable system performance, while the system employing D_{int}=400,000 bits requires one more iteration, before the system's performance saturates according to Figure 3.20.

Figures 3.21 and 3.22 record the trajectories of the iteratively detected RSC coded DSTS-SP schemes in conjunction with two transmit antennas and the system parameters outlined in Table 3.1 while employing AGM-3 and AGM-8, respectively. Figure 3.21 records the trajectory of the system employing AGM-3 while operating at E_b/N_0=6.0 dB, while Figure 3.22 records the trajectory of the system employing AGM-8 while operating at E_b/N_0=5.5 dB, when considering an interleaver depth of D_{int}=1,000,000 bits. The BER performance of the iteratively detected 1/2-rate RSC-coded DSTS-SP scheme recorded in conjunction with two transmit antennas and different GM and AGM mapping schemes, while using the system parameters outlined in Table 3.1 is shown in Figure 3.23, when applying I=10 iterations. Figure 3.23 also plots the performance curves for the equivalent bandwidth efficiency of 1 bit-per-channel-use employing uncoded DSTS in conjunction with SP L=4 and BPSK. Observe in Figure 3.23 that the GM and AGM-8 based systems have a similar performance and this can be justified by referring to the EXIT chart of Figure 3.3, where the EXIT curves of the GM and AGM-8 based systems have similar slopes. More explicitly, the system employing AGM-8 outperforms that employing

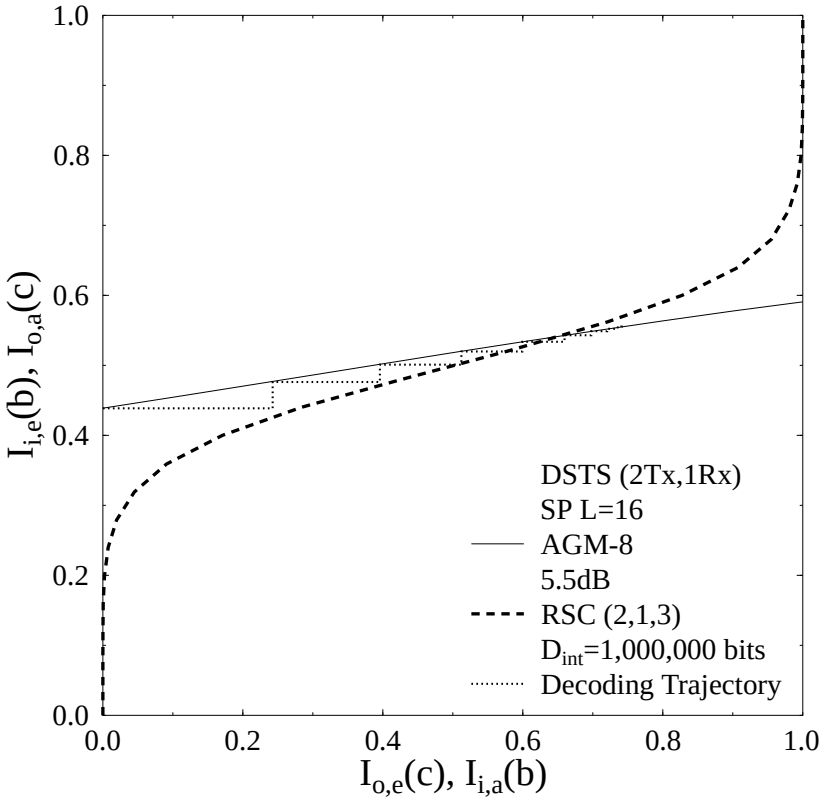

Figure 3.22: Decoding trajectory of the iteratively detected 1/2-rate RSC coded DSTS-SP scheme in conjunction with two transmit antennas and AGM-8 of Figure 3.3 employing the system parameters outlined in Table 3.1, while operating at E_b/N_0=5.5 dB with an interleaver depth of D_{int}=1,000,000 bits.

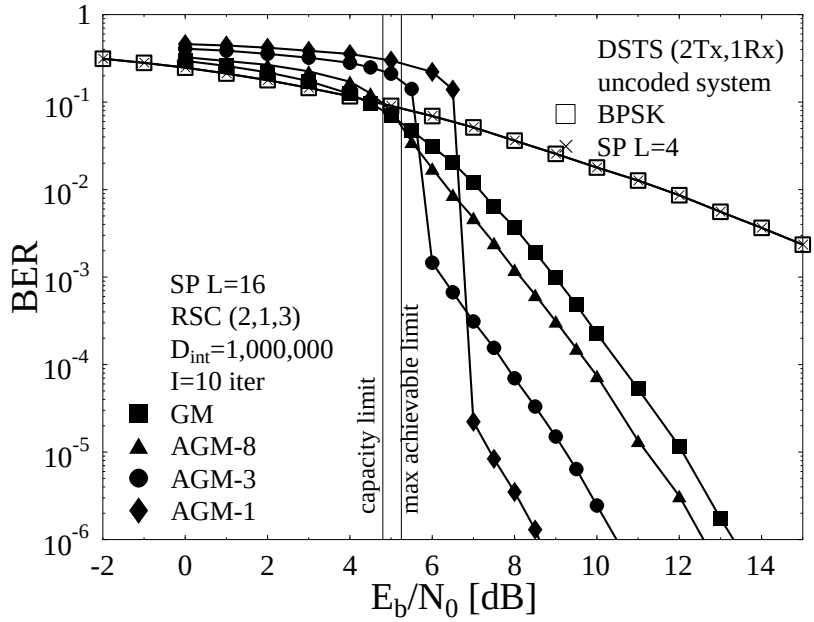

Figure 3.23: Performance comparison of different AGM- and GM-based iteratively detected RSC-coded two transmit antennas DSTS-SP schemes in conjunction with L=16 against an identical bandwidth efficiency of 1 bit-per-channel-use uncoded DSTS-SP scheme using L=4 and against the conventional DSTS-BPSK scheme, when employing the system parameters outlined in Table 3.1 with an interleaver depth of D_{int}=1,000,000 bits after I=10 iterations.

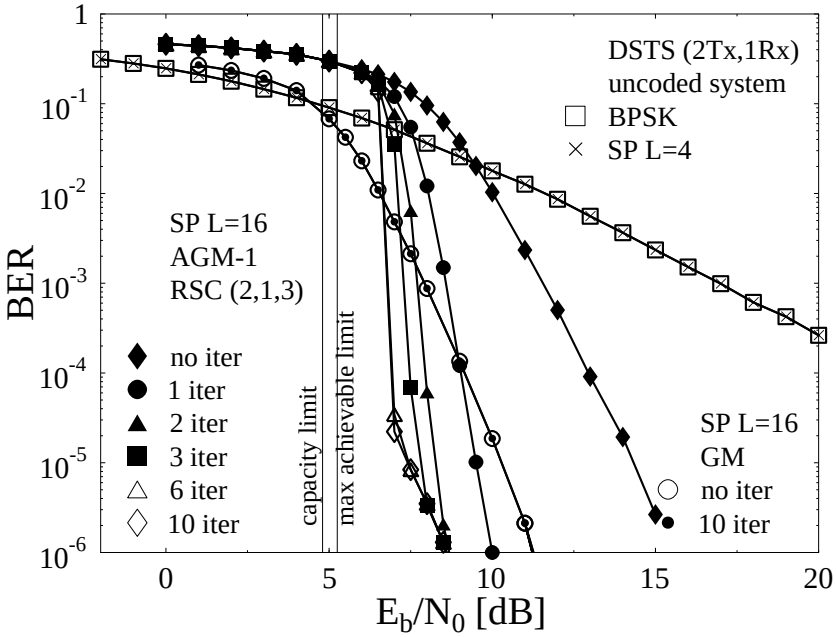

Figure 3.24: Performance comparison of AGM-1 and GM-based RSC-coded two transmit antennas DSTS-SP schemes in conjunction with L=16 against an identical bandwidth efficiency of 1 bit-per-channel-use uncoded DSTS-SP scheme using L=4 and against conventional DSTS-BPSK scheme, when employing the system parameters outlined in Table 3.1 and using an interleaver depth of D_{int}=1,000,000 bits for a variable number of iterations I.

GM by an E_b/N_0 of 0.6 dB at BER=10^{-6}, while the system employing AGM-3 outperforms that employing GM by an E_b/N_0 of 2.7 dB at BER=10^{-6}. Additionally, the AGM-1 aided systems outperform the GM-based system by an E_b/N_0 of 4.7 dB at BER=10^{-6}.

According to the EXIT chart predictions of Section 3.2.2.3, the system employing AGM does not reach the $I_{i,e}(\mathbf{b})$=1.0 point and thus must have an error floor, which clearly appears in Figure 3.23. Moreover, it is clear from the figure that the AGM-3 aided system converges at a lower E_b/N_0 value as compared to the AGM-1 based system, which implies that at lower E_b/N_0 values it is better to use AGM-3 rather than AGM-1. However, as the E_b/N_0 value increases, the AGM-1 based system starts to outperform that employing AGM-3; therefore whether to use AGM-1 or AGM-3 depends on the application or on the range of E_b/N_0 values of interest for the specific application considered. Furthermore, the performance results of Figure 3.23 match with the EXIT chart predictions of Section 3.2.2. In addition to that, it is obvious from Figure 3.23 that at low E_b/N_0 values, the system employing AGM-3 approaches the system capacity more closely than the AGM-1 based system. However, as the E_b/N_0 value increases, the AGM-3 based system exhibits an error floor and thus moves away from the capacity limit at lower BER values. On the other hand, the AGM-1 based system's performance is closer to the capacity limit than that of the AGM-3, AGM-8 or GM based systems' performance at low BER values, although there is an error floor.

Figure 3.24 compares the attainable performance of the proposed RSC-coded DSTS-SP

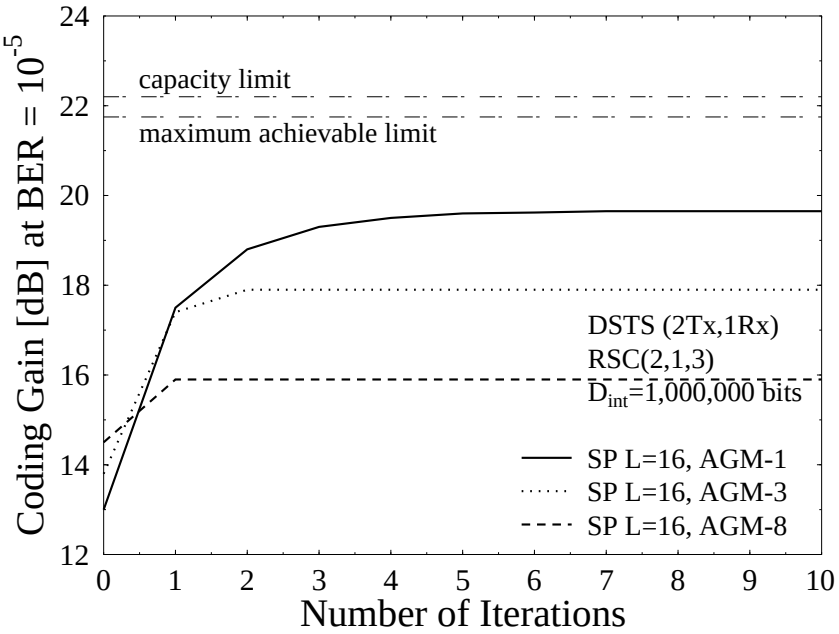

Figure 3.25: Coding gain of the iteratively detected 1/2-rate RSC-coded two transmit antennas DSTS-SP scheme against the number of iterations employed at a BER of 10^{-5} when employing AGM-1, AGM-3 and AGM-8 with an interleaver depth of D_{int}=1,000,000 bits.

scheme employing both AGM-1 and GM of the bits to the SP symbol, which are also contrasted to that of an identical bandwidth efficiency 1 bit-per-channel-use uncoded DSTS-SP scheme using L=4 and a conventional DSTS-BPSK design transmitting two independent BPSK symbols over the two antennas, when communicating over a correlated Rayleigh fading channel and employing the system parameters of Table 3.1. In Figure 3.24, an interleaver depth of D_{int}=1,000,000 bits was employed and a normalised Doppler frequency of f_D=0.01 was used. Observe in the figure that the two GM based DSTS-SP BER curves are exactly the same, when I=0 as well as I=10 iterations were employed, which is evident from the flat curve of the GM in Figure 3.3. By contrast, AGM-1 achieved a substantial performance improvement in conjunction with iterative demapping and decoding. Explicitly, Figure 3.24 demonstrates that a coding advantage of about 22.5 dB was achieved at a BER of 10^{-6} after I=10 iterations by the convolutional-coded AGM-based DSTS-SP system over both the uncoded DSTS-SP and over the DSTS-BPSK schemes for transmission over the correlated Rayleigh fading channel considered. Additionally, a coding advantage of approximately 4.7 dB was attained over the RSC-coded GM-based DSTS-SP scheme. Finally, the AGM-1 based system performs within 2.3 dB from the maximum achievable rate limit at BER of 10^{-5} and within 3.3 dB from the same limit at BER of 10^{-6}.

The coding gain of the iteratively detected DSTS-SP systems employing AGM-1, AGM-3 and AGM-8 is monitored in Figures 3.25 against the number of iterations employed at BER of 10^{-5} for an interleaver depth of D_{int}=1,000,000 bits. The coding gain is measured versus

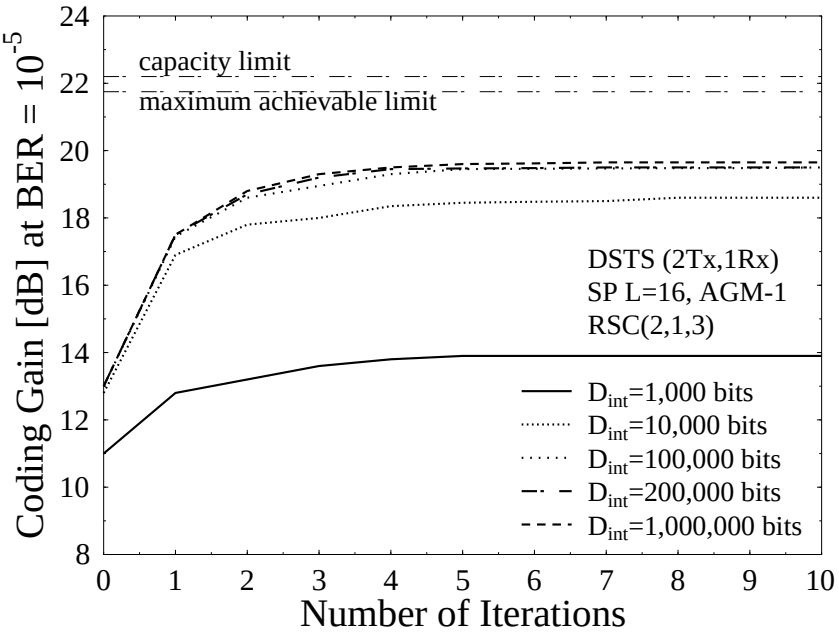

Figure 3.26: Coding gain of the iteratively detected 1/2-rate RSC-coded two transmit antennas DSTS-SP scheme against the number of iterations employed at a BER of 10^{-5} when employing AGM-1 and varying the interleaver depth D_{int} between $1,000$ and $1,000,000$ bits.

the performance of the uncoded equivalent bandwidth efficiency system employing DSTS-SP in conjunction with L=4 and GM. Figure 3.25 shows that increasing the number of iterations tends to attain a gradually eroding coding gain. Furthermore, it is observed that the coding gain of the AGM-1 based system is higher than that employing AGM-3 at BER=10^{-5} and this is verified by the performance curves of Figure 3.23. Moreover, notice that when no iterations are employed, the AGM-8 based system has a higher coding gain than the other two systems.

Figure 3.26 depicts the coding gain of the iteratively detected DSTS-SP systems employing AGM-1 versus the number of iterations employed at BER of 10^{-5} for different interleaver depths D_{int}. It is becomes explicit from the figure that as the interleaver depth increases, the coding gain increases and the system performance approaches the maximum achievable rate limit. Moreover, increasing the interleaver depth beyond D_{int}=$100,000$ bits results in a modest improvement in the system's performance.

A comparison between the performance of the SP aided and that of the equivalent bandwidth efficiency conventionally modulated iteratively detected two-antenna-aided DSTS system is shown in Figure 3.27. The proposed iteratively detected two-antenna-aided DSTS-SP scheme provides an improved performance over an equivalent-throughput DSTS scheme dispensing with SP modulation, as evidenced in Figure 3.27, demonstrating that the AGM-1 aided DSTS-SP scheme using L=16 exhibits an E_b/N_o gain of around 3.4 dB at a BER of 10^{-6} over the identical bandwidth efficiency 1 bit-per-channel-use DSTS-QPSK scheme.

Figure 3.28 records the trajectory of the iteratively detected RSC-coded DSTS-SP scheme

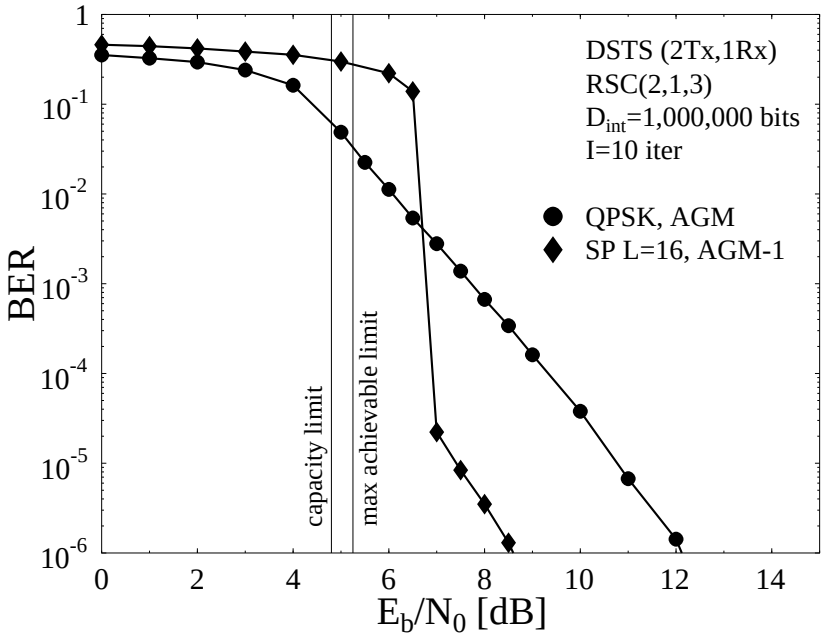

Figure 3.27: Performance comparison of an AGM-1 based iteratively detected RSC-coded two-antenna-aided DSTS-SP scheme in conjunction with L=16 and the equivalent bandwidth efficiency of 1 bit-per-channel-use AGM-based iteratively detected RSC-coded DSTS-QPSK scheme, while using an interleaver depth of D_{int}=1,000,000 bits for I=10 iterations and using the system parameters outlined in Table 3.1.

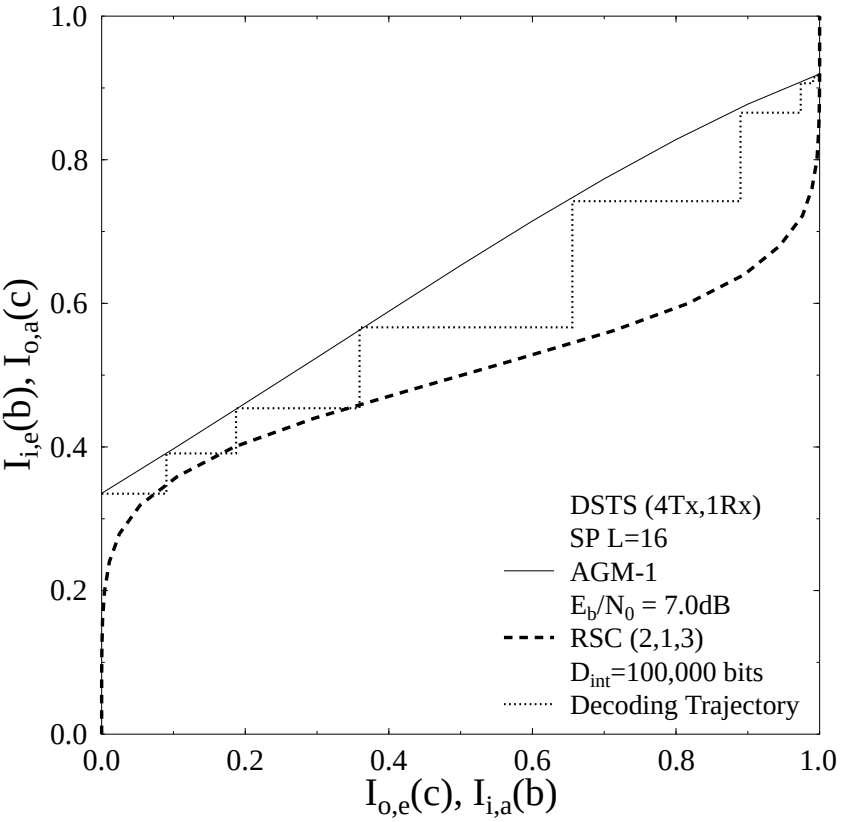

Figure 3.28: Decoding trajectory of the iteratively detected 1/2-rate RSC-coded DSTS-SP scheme in conjunction with four transmit antennas and AGM-1 of Figure 3.3 employing the system parameters outlined in Table 3.1, while operating at E_b/N_0=7.0 dB with an interleaver depth of D_{int}=100,000 bits.

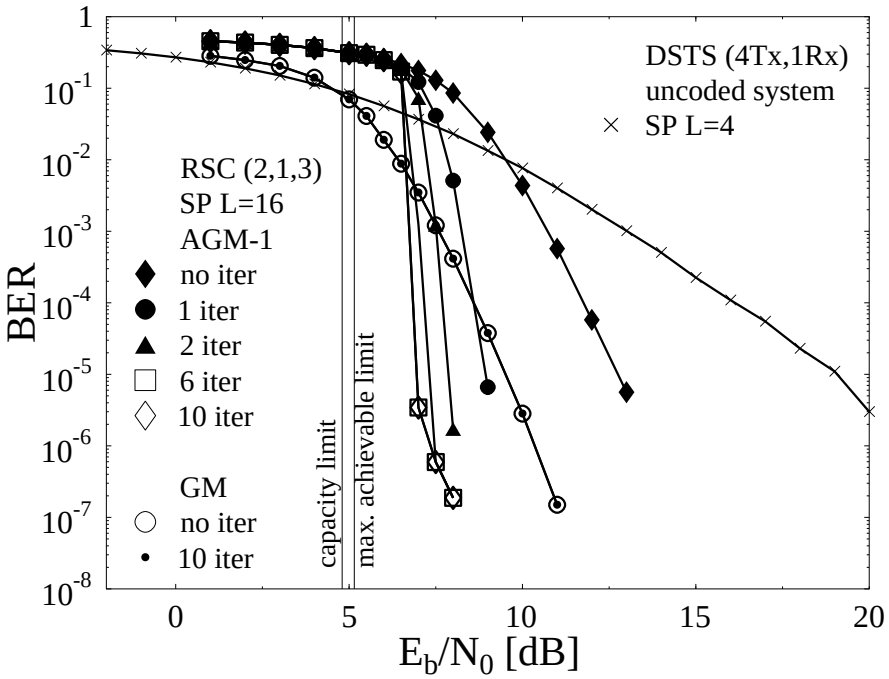

Figure 3.29: Performance comparison of AGM-1 and GM-based RSC-coded four-antenna-aided DSTS-SP scheme in conjunction with L=16 against an identical bandwidth efficiency of 1/2 bit-per-channel-use uncoded DSTS-SP L=4 scheme when employing the system parameters outlined in Table 3.1 and using an interleaver depth of D_{int}=1,000,000 bits for a variable number of iterations I.

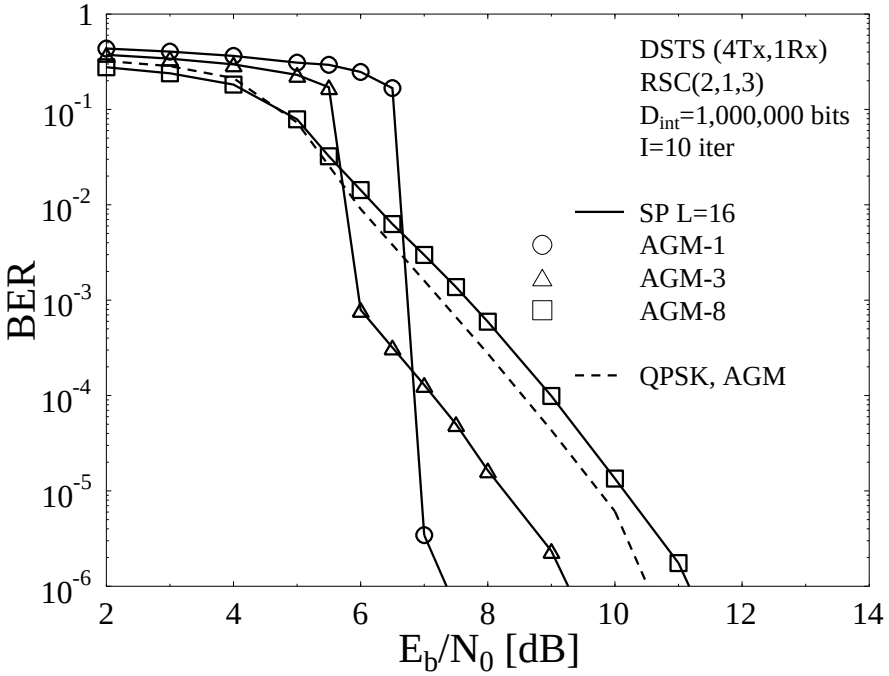

Figure 3.30: Performance comparison of different AGM-based RSC-coded four-antenna-aided DSTS-SP scheme in conjunction with L=16 and AGM-based RSC-coded DSTS-QPSK scheme, while using an interleaver depth of D_{int}=1,000,000 bits for I=10 iterations and using the system parameters outlined in Table 3.1.

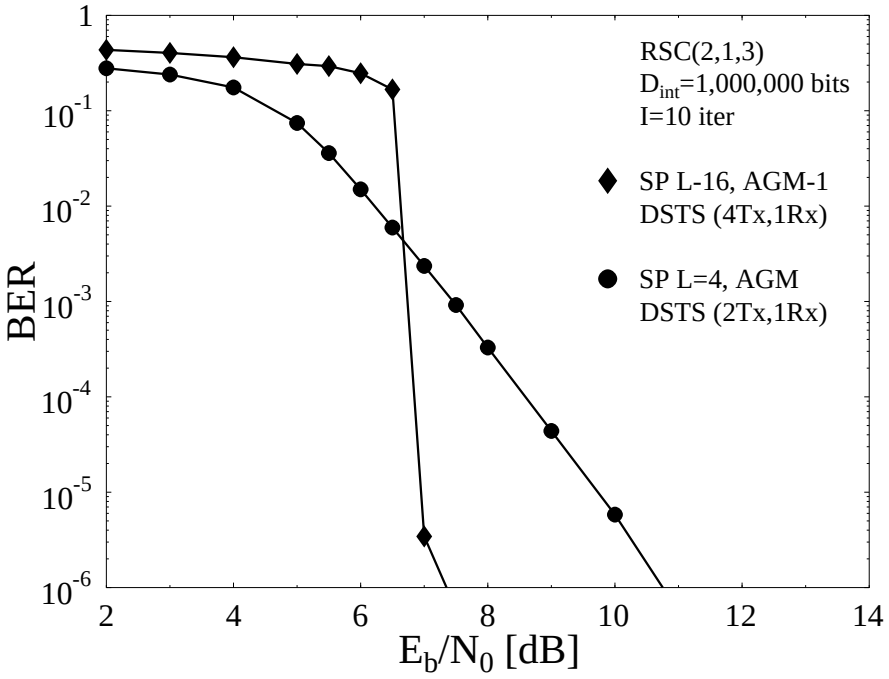

Figure 3.31: Performance comparison of AGM-1 based RSC-coded four-antenna-aided DSTS-SP scheme in conjunction with L=16 against an equivalent bandwidth efficiency two-antenna-aided DSTS-SP scheme employing L=4, while using an interleaver depth of D_{int}=1,000,000 bits after I=10 iterations and using the system parameters outlined in Table 3.1.

in conjunction with four transmit antennas and AGM-1 in combination with the system parameters of Table 3.1 while operating at E_b/N_0=7.0 dB with interleaver depth of D_{int}=100,000 bits. The decoding trajectories shown in Figures 3.28 matches with the EXIT chart prediction of Figure 3.11

Figure 3.29 compares the attainable performance of the proposed RSC-coded four-antenna-aided DSTS-SP scheme employing both AGM-1 and GM of the bits to the SP symbol, which are also contrasted to that of an identical bandwidth efficiency 0.5 bit-per-channel-use uncoded DSTS-SP scheme using L=4, when communicating over a correlated Rayleigh fading channel. In Figure 3.29, an interleaver depth of D_{int}=1,000,000 bits was employed in conjunction with the system parameters of Table 3.1. Observe in the figure that the two GM-based DSTS-SP BER curves are exactly the same, regardless whether no iterations or I=10 iterations were employed similarly to the two transmit antennas case and as exemplified in Figure 3.3. By contrast, the AGM-based system achieves a substantial performance improvement in conjunction with iterative demapping and decoding. Explicitly, Figure 3.29 demonstrates that a coding advantage of about 16.7 dB was achieved at a BER of 10^{-6} after I=10 iterations by the RSC-coded AGM-1 based DSTS-SP system over the uncoded DSTS-SP scheme. Additionally, a coding advantage of approximately 3 dB was attained over the 0.5 BPS-throughput RSC-coded GM-based DSTS-SP scheme. Finally, after I=10 iterations, the AGM-1 based four-antenna-aided

system performs within 1.82 dB from the maximum achievable rate limit at BER of 10^{-5} and within 2.12 dB from the same limit at BER of 10^{-6}.

Furthermore, Figure 3.30 provides a performance comparison of the iteratively detected RSC-coded four-antenna-aided DSTS scheme in conjunction with SP L=16 employing AGM-1, AGM-3 and AGM-8 as well as the identical-bandwidth-efficiency QPSK-aided scheme. As evidenced in Figure 3.30, the AGM-1 aided system outperforms the QPSK aided system by 3.2 dB at BER of 10^{-6} and the AGM-3 assisted system outperforms the QPSK-aided system by 1.3 dB at the same BER. However, the QPSK-aided scheme outperforms its identical-bandwidth-efficiency AGM-8 aided counterpart by almost 0.6 dB at BER of 10^{-6}.

Finally, Figure 3.31 compares the performance of the AGM-1 based RSC-coded DSTS-SP scheme in conjuction with L=16, when employing four transmit antennas and that of the AGM-based system employing two transmit antennas as well as SP in conjunction with L=4, while using an interleaver depth of D_{int}=1,000,000 bits, I=10 iterations and the system parameters outlined in Table 3.1. The four-antenna-aided system outperforms its two-antenna-aided counterpart by approximately 3.2 dB at a BER of 10^{-6}.

3.2.5 Application: Soft-Bit Assisted Iterative AMR-WB Source-Decoding and Iterative Detection of Channel-Coded DSTS-SP System[5]

The classic Shannonian source and channel coding separation theorem [214] has limited applicability in the context of finite-complexity, finite-delay lossy speech [230] and video [231] codecs, where the different encoded bits exhibit different error sensitivity. These arguments are particularly valid, when the limited-complexity limited-delay source encoders fail to remove all the redundancy from the correlated speech or video source signal. Fortunately, this residual redundancy may be beneficially exploited for error protection by intelligently exchanging soft information amongst the various receiver components.

These powerful iterative decoding principles may be further enhanced by exploiting the innovative concept of soft speech bits, which was developed by Vary and his team [232, 233], culminating in the formulation of iterative source and channel decoding (ISCD) [234]. More explicitly, in ISCD the source and channel decoders iteratively exchange *extrinsic* information for the sake of improving the overall system performance. As a further development, in [175] the turbo principle [26] was employed for iterative soft demapping in multilevel modulation [27] schemes combined with channel coding which resulted in an enhanced BER performance. Thus, ISCD may be beneficially combined with iterative soft demapping in the context of multilevel

[5]This work has been made possible by collaboration with my colleague Noor Othman, who generously offered her AMR-WB source-codec C++ code and her time for the numerous discussions.

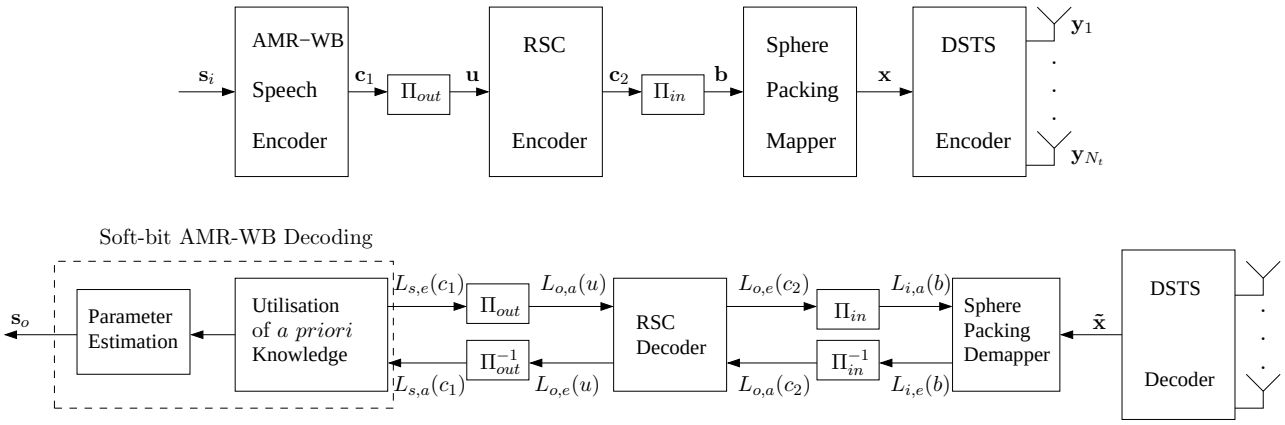

Figure 3.32: Block diagram of the DSTS-SP-RSC-AMRWB scheme.

modulation and amalgamated with a number of other sophisticated wireless transceiver components. In the resultant multi-stage scheme, *extrinsic* information is exchanged amongst three receiver components, namely the demapper, the channel decoder and the soft-input soft-output source decoder in the spirit of [235].

Explicitly, we propose and investigate the jointly optimised ISCD scheme of Figure 3.32 invoking the Adaptive Multi-rate-Wideband (AMR-WB) speech codec [236], which is protected by an RSC code. The resultant bit stream is transmitted using DSTS amalgamated with SP modulation [7] over a temporally correlated narrowband Rayleigh fading channel. An efficient iterative turbo-detection scheme is utilised for exchanging *extrinsic* information between the constituent decoders. Figure 3.32 shows the schematic of the proposed arrangement, referred to as DSTS-SP-RSC-AMRWB, where the *extrinsic* information gleaned is exchanged amongst all three constituent decoders namely the SP demapper, the RSC decoder and the AMR-WB decoder.

The AMR-WB speech encoder produces a frame of speech coded parameters, namely $\{\mathbf{v}_{1\tau}, \mathbf{v}_{2\tau}, \cdots, \mathbf{v}_{\kappa\tau}, \cdots, \mathbf{v}_{36,\tau}\}$, where $\mathbf{v}_{\kappa,\tau}$ denotes an encoded parameter, with $\kappa \in [1, \cdots, K_\kappa]$ denoting the index of each parameter in the encoded speech frame and $K_\kappa = 36$, whilst τ denotes the time index referring to the current encoded frame index. Then, $\mathbf{v}_{\kappa,\tau}$ is quantised and mapped to the bit sequence $\mathbf{c}_{1,\kappa\tau} = [c(1)_{1,\kappa\tau}\ c(2)_{1,\kappa\tau}, \cdots, c(M)_{1,\kappa\tau}]$, where M is the total number of bits assigned to the κth parameter. Then, the outer interleaver Π_{out} permutes the bits of the sequence $\mathbf{c}_1$ yielding $\mathbf{u}$ of Figure 3.32. Afterwards, the interleaved bit stream $\mathbf{u}$ is RSC encoded to produce the bit stream $\mathbf{c}_2$ which is then interleaved by the interleaver Π_{in} of Figure 3.32. After bit interleaving, the SP mapper maps blocks of B_{sp} channel-coded bits $\mathbf{b} = b_0, \ldots, b_{B_{sp}-1} \in \{0, 1\}$ to the L number of legitimate four-dimensional SP modulated symbols $\mathbf{s}^l \in \mathbf{S}$. The SP modulated symbols $\mathbf{x}$ are then transmitted using the DSTS scheme of Section 2.3.3.

At the receiver side, as shown in Figure 3.32, the received complex-valued symbols are first

Source coding	AMR-WB
Bit rates (kbit/s)	15.85
Speech frame length (ms)	20
Sampling rate (kHz)	16
Channel coding	RSC code
Code rate	1/2
Code memory	K=7
Code generator (G_r, G)	$(217, 110)_8$
Modulation scheme	Sphere Packing (L=16)
MIMO scheme	DSTS
Number of transmitters, N_t	2
Number of receivers, N_r	1
Spreading code	Walsh-Hadamard Code
Spreading factor	8
Number of users	4
Channel	Correlated Rayleigh fading
Normalised Doppler frequency	0.01
System bandwidth efficiency	1 bit-per-channel-use

Table 3.2: DSTS-SP-RSC-AMRWB system parameters.

decoded by the DSTS decoder in order to produce the received SP soft-symbols $\tilde{\mathbf{x}}$. Then, iterative demapping/decoding is carried out between the SP demapper, the RSC Decoder and the soft-input soft-output AMR-WB speech decoder, where extrinsic information is exchanged between the three constituent demapper/decoders. In the speech decoder, the residual redundancy[6] is exploited as *a priori* information in computing the *extrinsic* LLR values and estimating the speech parameters. During the last iteration, speech parameter estimation is carried out in the AMR-WB speech decoder in order to generate the transmitted source data estimate $\mathbf{s}_o$.

In the following, we characterise the attainable performance of the proposed DSTS-SP-RSC-AMRWB scheme using both the BER and the Segmental Signal to Noise Ratio (SegSNR) [230] evaluated at the speech decoder's output as a function of the channel SNR. All simulation parameters are listed in Table 3.2. In our simulations we employed one inner iteration between the SP demapper and the RSC decoder followed by one outer iteration between the RSC decoder and the AMR-WB decoder. The system performance is compared versus a benchmark scheme where no outer iterations are carried out between the AMR-WB decoder and the RSC decoder.

[6]For a detailed discussion about the residual redundancy, please refer to [11].

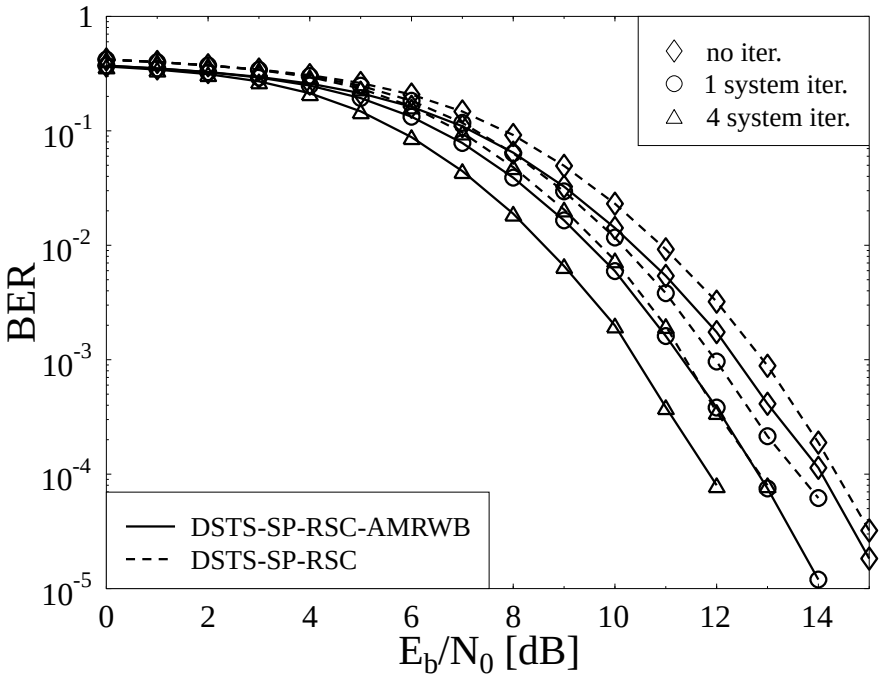

Figure 3.33: BER performance of the jointly optimised DSTS-SP-RSC-AMRWB scheme of Figure 3.32 employing the system parameters of Table 3.2, when communicating over temporally correlated narrowband Rayleigh fading channel.

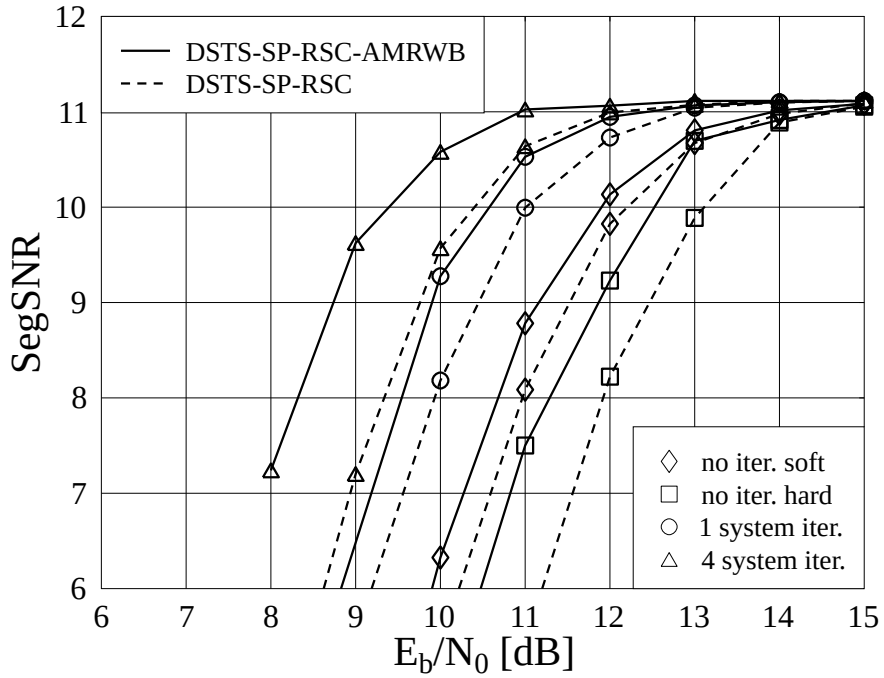

Figure 3.34: Average SegSNR performance of the jointly optimised DSTS-SP-RSC-AMRWB scheme of Figure 3.32 employing the system parameters of Table 3.2 in comparison to the DSTS-SP-RSC benchmark scheme, when communicating over temporally correlated narrowband Rayleigh fading channel.

Figure 3.33 depicts the BER performance of the DSTS-SP-RSC-AMRWB scheme and that of its corresponding DSTS-SP-RSC benchmark counterpart. It can be seen from Figure 3.32 that the DSTS-SP-RSC-AMRWB scheme outperforms the DSTS-SP-RSC benchmark scheme by about 1 dB at BER=10^{-4} after I_{sys}=4 system iterations, where we define a system iteration cycle as having an inner iteration followed by a single outer iteration, which is referred to as I_{sys}. The AMR-WB-decoded scheme has a lower BER at its speech-decoded output than its benchmark dispensing with speech decoding, because the *extrinsic* information exchange between the AMR-WB decoder and the RSC decoder has the potential of improving the attainable BER. Notice that the turbo effect of the BER figures seen in Section 3.2.4 is absent in Figure 3.33. This is due to the fact that the system employs a short interleaver depth of D_{int}=317 bits, which corresponds to a delay of 20 ms in speech transmission. This result is similar to that using an interleaver depth of D_{int}=1,000 bits in Figure 3.19.

Figure 3.34 depicts the speech SegSNR performance of the proposed DSTS-SP-RSC-AMRWB scheme together with that of the benchmark scheme. In this context the residual redundancy inherent in the encoded source is exploited twice, firstly during computing the *extrinsic* information and secondly during the Markov-model-based parameter estimation [237]. It can be seen from Figure 3.34 that the exploitation of the residual redundancy inherent in the encoded source during the decoding process benefitting from zero-order Markov-model-based parameter estimation performs approximately 0.5 dB better in terms of the required channel E_b/N_0 value, than its corresponding hard speech decoding based counterpart, when allowing a SegSNR degradation of 1.0 dB in comparison to the maximum attainable SegSNR maintained over perfectly error-free channels. Additionally, iteratively exchanging the soft-information amongst the three receiver components of the amalgamated DSTS-SP-RSC-AMRWB scheme results in a further E_b/N_0 gain of about 2.6 dB after I_{sys}=4 system iterations, when tolerating a SegSNR degradation of 1 dB.

3.3 Iterative Detection of RSC-Coded and Unity-Rate Precoded Four-Antenna-Aided DSTS-SP System

As mentioned in Section 3.1, it was shown in [183] that a recursive inner code is needed in order to maximise the interleaver gain and to avoid the formation of a BER floor, when employing iterative decoding. In [185], unity-rate inner codes were employed for designing low complexity iterative detection aided schemes suitable for bandwidth and power limited systems having stringent BER requirements. In this section we consider an iteratively detected RSC-coded and unity-rate precoded DSTS-SP scheme, where iterative detection is carried out between the

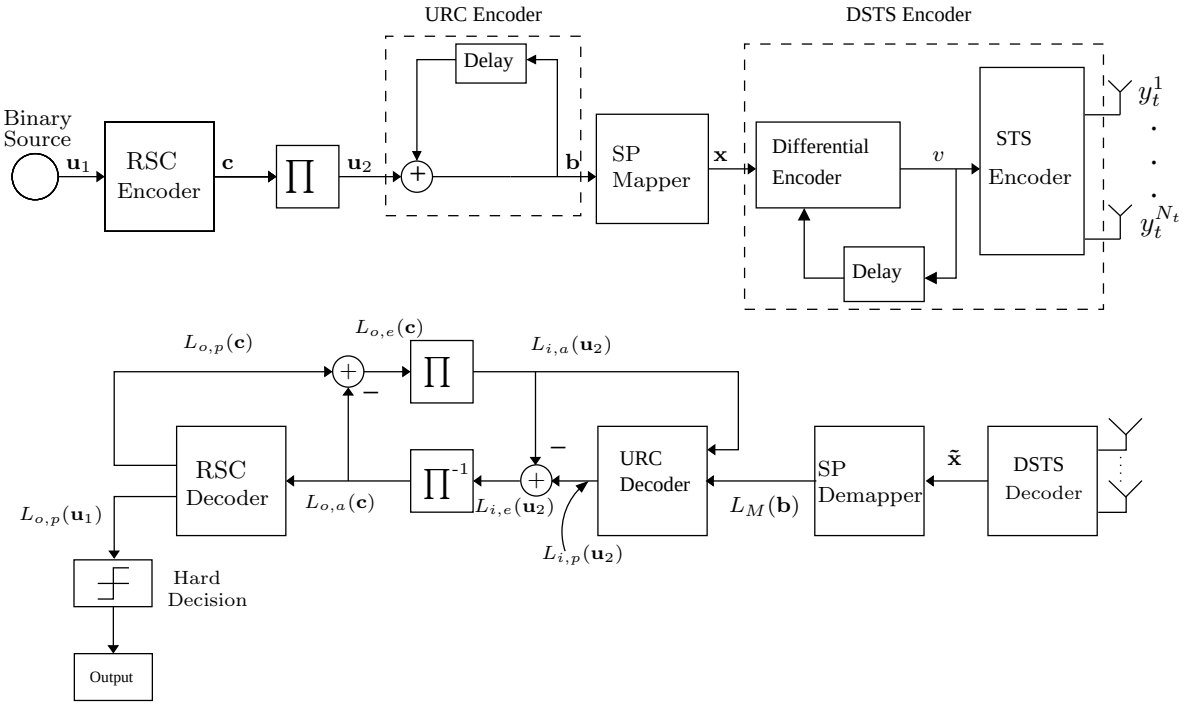

Figure 3.35: The iteratively detected RSC-coded and URC precoded DSTS-SP system block diagram.

outer RSC decoder and the inner URC decoder.

3.3.1 System Overview

The schematic of the proposed DSTS system is shown in Figure 3.35, where the transmitted source bits are convolutionally encoded and then interleaved by a random bit interleaver. A 1/2-rate memory-2 RSC code was employed having a generator polynomial with octal representation of $(G_r, G)=(7,5)_8$. After channel interleaving the symbols are precoded by a URC encoder. The SP mapper of Figure 3.35 maps B_{sp} channel-coded and precoded bits $\mathbf{b} = b_0, \ldots, b_{B_{sp}-1} \in \{0,1\}$ to a sphere packing symbol $\mathbf{s}^l \in S$, $l = 0, 1, \ldots, L-1$, so that we have $\mathbf{s}^l = \text{map}_{sp}(\mathbf{b})$, where $B_{sp} = \log_2 L$ and L represents the number of modulated symbols in the sphere-packed signalling alphabet. Subsequently, each of the four components of a SP symbol is transmitted using DSTS via four transmit antennas, as detailed in the Section 2.4.3.

In the following, we consider transmission over a temporally correlated narrowband Rayleigh fading channel associated with a normalised Doppler frequency of f_D=$f_d T_s$=0.01. The complex AWGN of $n = n_I + jn_Q$ contaminates the received signal, where n_I and n_Q are two independent zero-mean Gaussian random variables having a variance of $\sigma_{n_I}^2 = \sigma_{n_Q}^2 = N_0/2$ per dimension and N_0 represents the double-sided noise power spectral density expressed in W/Hz.

As shown in Figure 3.35, the received complex-valued symbols are first decoded by the DSTS decoder to produce a received SP symbol $\tilde{\mathbf{x}}$, which is fed into the SP demapper. The output

of the demapper represents the LLR metric $L_M(\mathbf{b})$ passed from the SP demapper to the URC decoder. As seen in Figure 3.35, the URC decoder processes the information forwarded by the demapper in conjunction with the *a priori* information $L_{i,a}(\mathbf{u}_2)$ passed from the RSC decoder, in order to generate the *a posteriori* probability. The *a priori* LLR values of the URC decoder are subtracted from the *a posteriori* LLR values for the sake of generating the extrinsic LLR values $L_{i,e}(\mathbf{u}_2)$ and then the LLRs $L_{i,e}(\mathbf{u}_2)$ are deinterleaved by a soft-bit deinterleaver, as seen in Figure 3.35. Next, the soft bits $L_{o,a}(\mathbf{c})$ are passed to the RSC decoder of Figure 3.35 in order to compute the *a posteriori* LLR values $L_{o,p}(\mathbf{c})$ for all the channel-coded bits $\mathbf{c}$. During the last iteration, only the LLR values $L_{o,p}(\mathbf{u}_1)$ of the original uncoded systematic information bits are required, which are passed to the hard decision decoder of Figure 3.35 in order to determine the estimated transmitted source bits. As seen in Figure 3.35, the extrinsic information $L_{o,e}(\mathbf{c})$, is generated by subtracting the *a priori* information from the *a posteriori* information according to $(L_{o,p}(\mathbf{c}) - L_{o,a}(\mathbf{c}))$, which is then fed back to the URC decoder as the *a priori* information $L_{i,a}(\mathbf{u}_2)$ after appropriately reordering them using the interleaver of Figure 3.35. The URC decoder of Figure 3.35 exploits the *a priori* information for the sake of providing improved *a posteriori* LLR values, which are then passed to the 1/2-rate RSC decoder and then back to the URC decoder for further iterations.

3.3.2 Results and Discussions

In this section, we consider a DSTS-SP scheme using four transmit antennas and a single receive antenna in order to demonstrate the performance improvements achieved by the proposed system of Figure 3.35. All simulation parameters are listed in Table 3.3.

Figure 3.36 depicts the EXIT chart for the iterative-detection aided channel-coded DSTS-SP system employing L=16 and GM in conjunction with the 1/2-rate RSC outer code, URC inner code and the system parameters outlined in Table 3.3 for different E_b/N_0 values. The GM was used in this case because no iterations are invoked between the SP demapper and the decoders and thus, in this case, it is better to use GM that results in a higher initial mutual information and hence a higher starting point in the EXIT curve. Ideally, in order for the exchange of extrinsic information between the URC decoder and the RSC decoder to converge at a specific E_b/N_0 value, the EXIT curve of the URC decoder and that of the outer RSC decoder should only intersect at a point near the $I_{o,e}(\mathbf{c})$=1.0 line. If this condition is satisfied, then a so-called *convergence tunnel* [186, 189] appears in the EXIT chart. It is plausible that the narrower the tunnel, the more iterations are required for reaching the $I_{o,e}(\mathbf{c})$=1.0 line. Observe from the figure that a convergence tunnel is formed at an E_b/N_0 of 6.5 dB. This implies that according to the predictions of the EXIT chart seen in Figure 3.36, the iterative decoding

Sphere Packing modulation	L=16
Number of transmit antennas N_t	4
Number of receive antennas N_r	1
Channel	Temporally correlated Rayleigh fading
Normalised Doppler frequency	0.01
Outer channel Code Generator	RSC $(2,1,3)$ $(G_r, G)=(7,5)_8$
Precoder Generator	URC $(G_r, G)=(3,2)_8$
Spreading Code	Walsh-Hadamard Code
Spreading Factor	8
Number of users	4

Table 3.3: RSC-coded and URC precoded DSTS-SP system parameters.

process is expected to converge at $E_b/N_0 \in [6.0, 6.5]$ dB. The EXIT chart based convergence predictions can be verified by the actual iterative decoding trajectory of Figure 3.37, where the trajectory at E_b/N_0=6.5 dB is recorded while using an interleaver depth of D_{int}=1,000,000 bits. The steps seen in the figure represent the actual extrinsic information transfer between the URC decoder and the outer RSC channel decoder. Since a long interleaver is employed, the assumptions outlined at the beginning of Section 3.2.2 are justified and hence the EXIT chart based convergence prediction becomes accurate.

Furthermore, a comparison between the convergence behaviour of the precoded and the non-precoded systems has been shown in Figure 3.38 for E_b/N_0=6.0 dB and E_b/N_0=6.5 dB as well as an interleaver depth of D_{int}=1,000,000 bits. The non-precoded system corresponds to the iterative-detection aided system of Section 3.2. Observe in Figure 3.38 that the precoded system's EXIT curve emerges from a higher point than that of both the AGM-1 and AGM-3 aided non-precoded systems. On the other hand, the precoded system's EXIT curve reaches the $(1.0, 1.0)$ point $\forall$ E_b/N_0, as compared to $I_{o,e}(\mathbf{c})$=0.9 for the AGM-1 based system and $I_{o,e}(\mathbf{c})$=0.81 for the AGM-3 based system for E_b/N_0=6.5 dB. Furthermore, note that the precoded system has a convergence tunnel at an E_b/N_0 value, which is only slightly higher than 6.0 dB as compared to having a convergence tunnel at $E_b/N_0 > 6.5$ dB for the AGM-1 aided non-precoded system and an E_b/N_0=6.0 dB for the AGM-3 aided non-precoded system. Hence, the precoded system converges at an E_b/N_0 value lower than that of the AGM-1 aided non-precoded system, which is close to that of the AGM-3 based non-precoded system. However, the precoded system reaches the point of $(1.0, 1.0)$ in the EXIT curve resulting in an infinites-

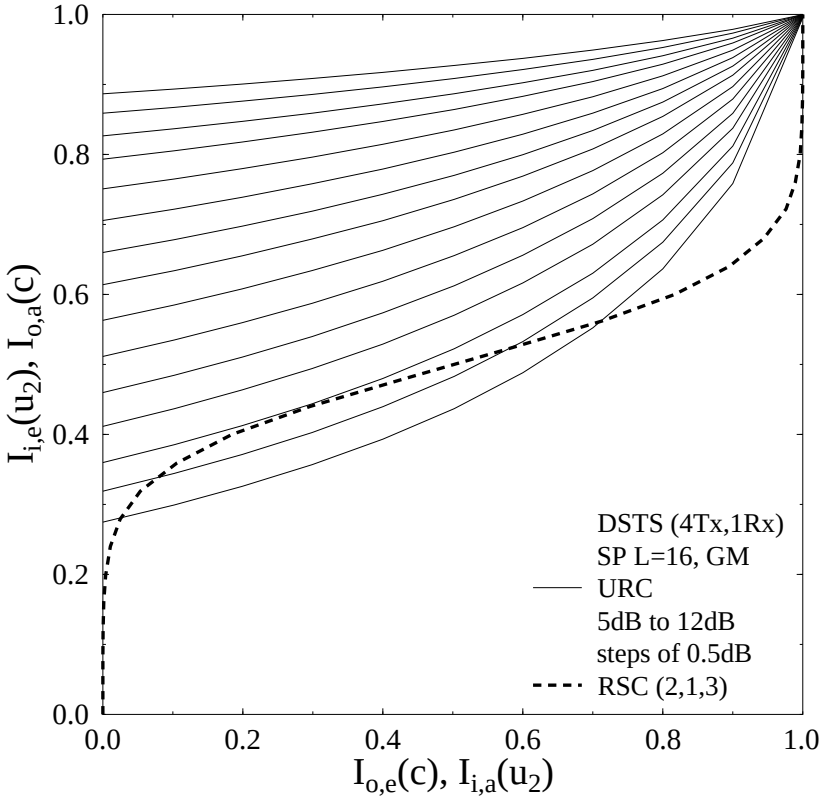

Figure 3.36: EXIT chart of a RSC-coded and URC-precoded DSTS-SP scheme employing GM in conjunction with L=16, while using an interleaver depth of D_{int}=1,000,000 bits and the system parameters outlined in Table 3.3.

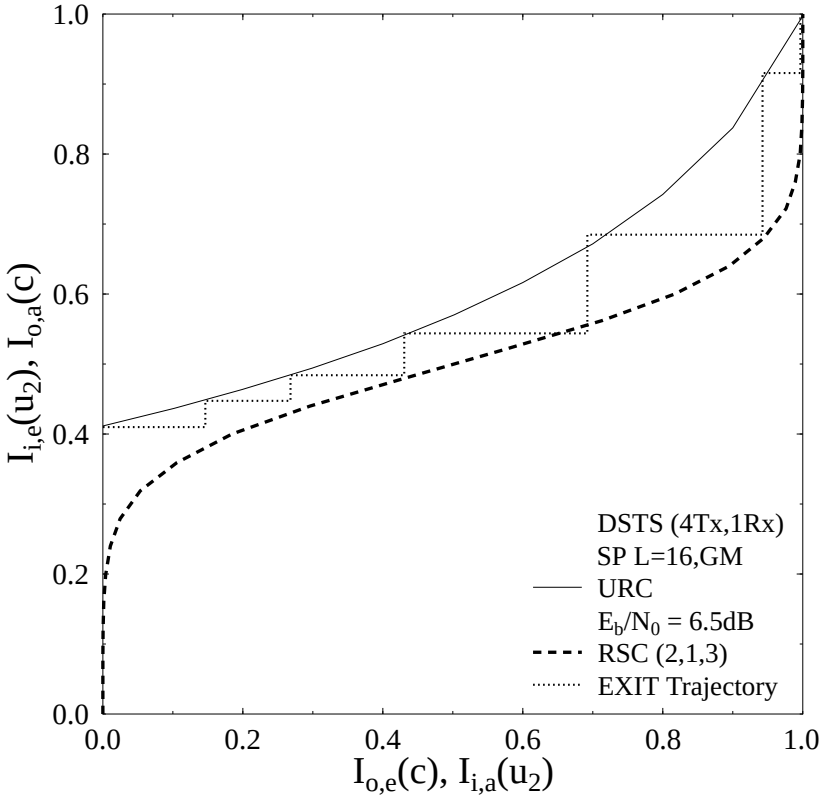

Figure 3.37: Decoding trajectory of the iteratively detected RSC-coded and URC-precoded DSTS-SP scheme employing GM in conjunction with L=16 and the system parameters outlined in Table 3.3 while operating at E_b/N_0=6.5 dB.

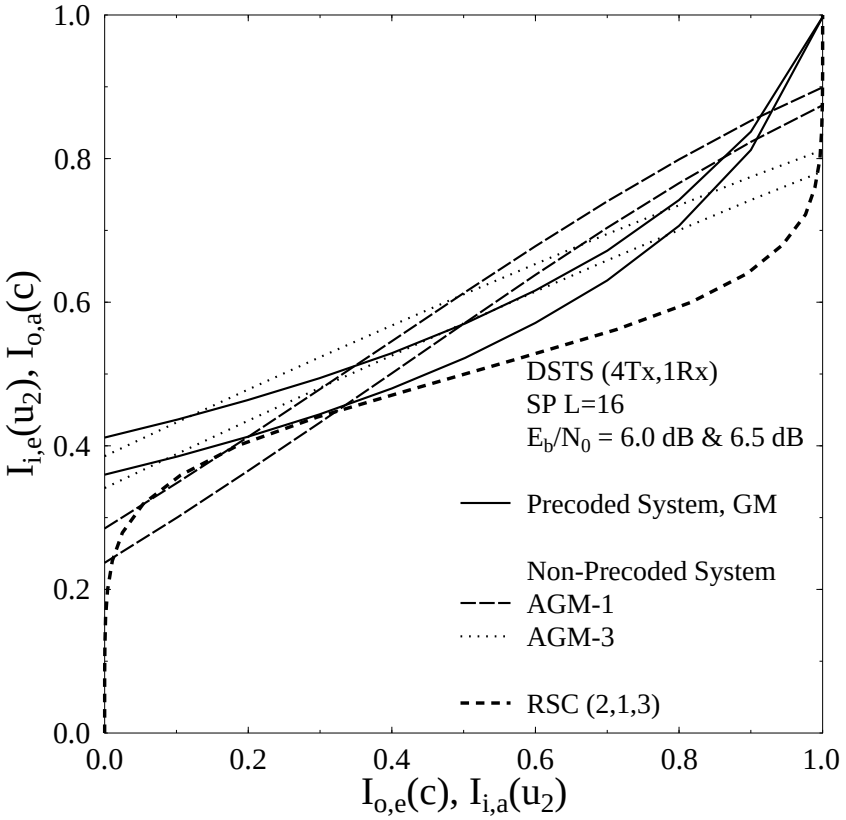

Figure 3.38: Comparison of the convergence behaviour of both the precoded and non-precoded DSTS-SP systems employing GM and AGM in conjunction with L=16, based on their EXIT characteristics while using an interleaver depth of D_{int}=1,000,000 bits and the system parameters outlined in Table 3.3 and operating at E_b/N_0 of 6 dB and 6.5 dB.

imally low BER. By contrast, the non-precoded systems do not reach the $(1.0, 1.0)$ point, as shown in Figure 3.38, which results in achieving only a modest BER performance associated with an error floor as E_b/N_0 increases.

Figure 3.39 compares the attainable performance of the RSC-coded four-antenna-aided DSTS-SP scheme employing GM of the bits to the SP symbol while using the URC precoder together with the non-precoded system, which are also contrasted to that of an identical bandwidth efficiency 0.5 bit-per-channel-use uncoded DSTS-SP scheme using L=4, when communicating over a temporally correlated Rayleigh fading channel and employing the system parameters of Table 3.3. In Figure 3.39, an interleaver depth of D_{int}=1,000,000 bits was employed. Observe in the figure that the two GM-based non-precoded DSTS-SP BER curves are exactly the same, regardless whether no iterations or I=10 decoding iterations were employed similarly as discussed in Section 3.2.4. By contrast, the precoded DSTS-SP system employing GM achieves a substantial performance improvement in conjunction with iterative demapping and decoding. That is due to the fact that no iteration was employed between the demapper and the decoder, while the iteration were employed between the RSC decoder and the URC decoder. Explicitly, the figure demonstrates that a coding advantage of about 4.2 dB was achieved at a

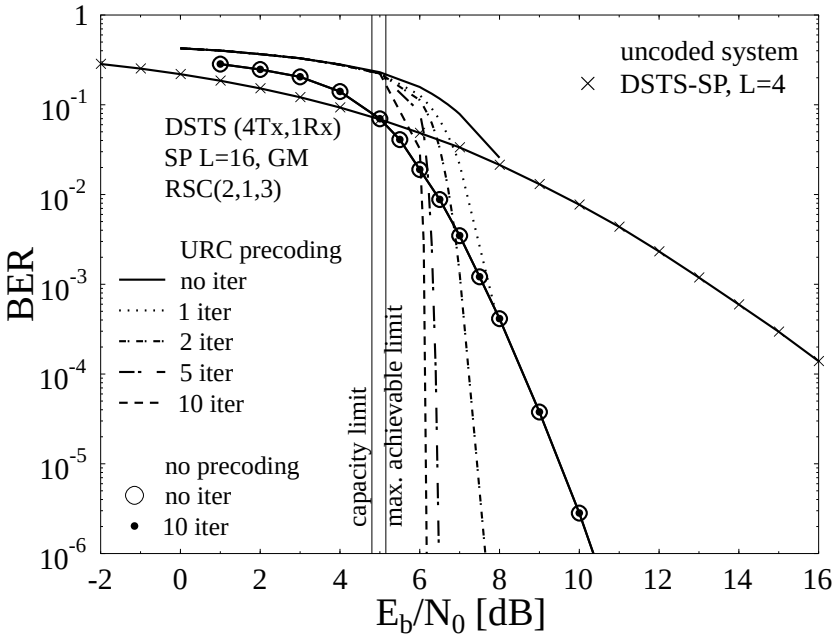

Figure 3.39: Performance comparison of URC-precoded and non-precoded GM-based RSC-coded four-antenna-aided DSTS-SP schemes in conjunction with L=16 against an identical bandwidth efficiency 1/2 bits-per-channel-use uncoded DSTS-SP in conjunction with L=4 when employing the system parameters outlined in Table 3.3 and using an interleaver depth of D_{int}=1,000,000 bits for a variable number of iterations.

BER of 10^{-6} after I=10 iterations by the RSC-coded and URC-precoded GM-based DSTS-SP system over the non-precoded RSC-coded and GM-based DSTS-SP scheme.

Additionally, Figure 3.40 depicts our performance comparison between two iteratively detected DSTS schemes, namely that of the non-precoded system employing AGM-1, AGM-3 and AGM-8 constellation mapping as well as the performance of the precoded systems in conjunction with GM, while employing an interleaver depth of D_{int}=1,000,000 bits, I=10 iterations and using the system parameters of Table 3.3. The results of Figure 3.40 demonstrate that the non-precoded system employing AGM-3 has approached the system capacity quite closely. However, as the E_b/N_0 value increases we notice in Figure 3.40 that the BER performance reaches a point, where further BER improvements require a more substantial E_b/N_0 increase and this is justified by the EXIT chart predictions of Figure 3.38. Moreover, the non-precoded system employing AGM-1 converges at E_b/N_0=7.0 dB to a lower BER than the AGM-3 based system. Similarly to the AGM-3 based result, the BER performance of the AGM-1 aided non-precoded system converges to a low BER value at E_b/N_0 of 7.0 dB, after which the system's BER performance exhibits an error floor, as shown in Figure 3.40. Furthermore, Figure 3.40 demonstrates that the proposed precoded system converges at E_b/N_0=6.1 dB and exhibits an infinitesimally low BER, as suggested by the EXIT chart of Figure 3.37. More explicitly, the URC precoded DSTS-SP scheme of Figure 3.40 using L=16 and GM exhibits an E_b/N_0 gain of 1.2 dB at a BER of 10^{-6} over the AGM-1 based non-precoded system and 3.1 dB at a BER

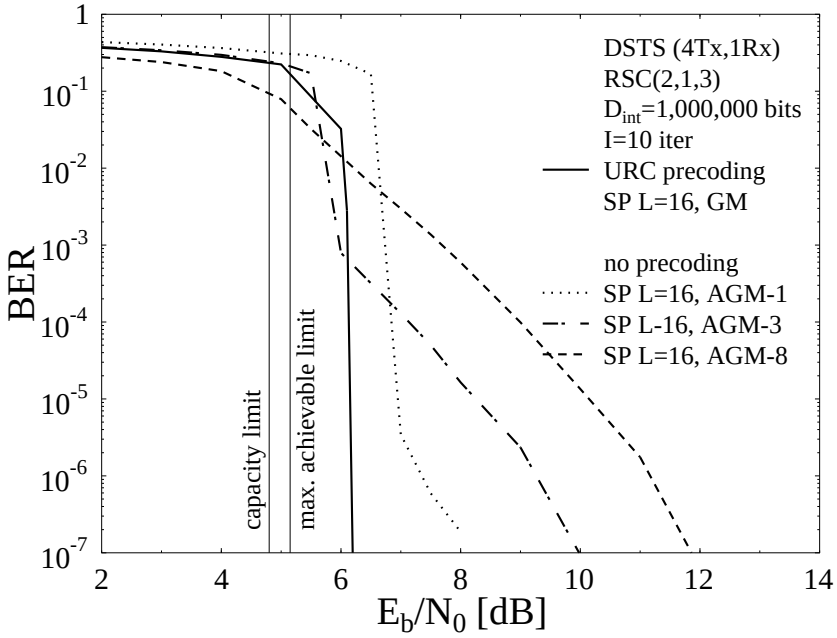

Figure 3.40: Performance comparison of different AGM-based 1/2-rate RSC-coded and GM-based 1/2-rate RSC-coded and URC precoded four-antenna-aided DSTS-SP schemes in conjuction with L=16 while using an interleaver depth of D_{int}=1,000,000 bits, I=10 iterations and the system parameters outlined in Table 3.3.

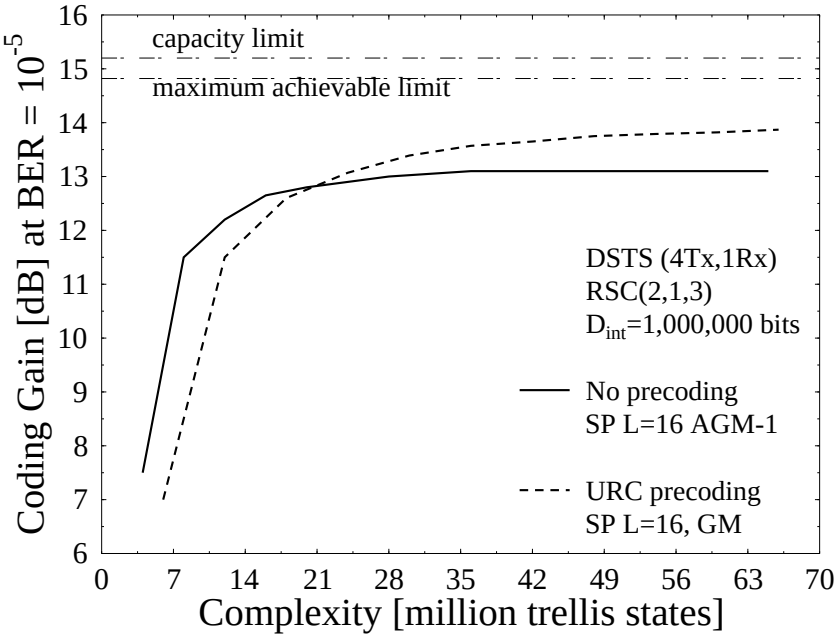

Figure 3.41: Coding gain comparison of the non-precoded and the URC-precoded iteratively detected RSC-coded four-antenna-aided DSTS-SP schemes plotted versus the number of trellis states at a BER of 10^{-5} when employing an interleaver depth of D_{int}=1,000,000 bits.

of 10^{-6} over the AGM-3 based non-precoded system. Finally, the iteratively detected RSC-coded and URC-precoded DSTS-SP system employing L=16 in conjunction with GM performs within 0.92 dB from the maximum achievable rate limit and within 1.3 dB from system capacity limit at BER=10^{-6}. By contrast, the non-precoded system employing AGM-1 performs within 2.12 dB from the maximum achievable rate limit at the same BER and the non-precoded system employing AGM-3 performs within 4.02 dB from the same limit at the same BER.

Finally, Figure 3.41 compares the coding gain achieved for the iteratively detected RSC-coded four-antenna-aided DSTS-SP system when no-precoding is employed and that when URC precoding is used. The figure plots the coding gain versus the number of trellis states, rather than versus the number of iterations as in Figure 3.25, since the two systems compared in Figure 3.41 have different number of trellis states, while that in Figure 3.25 employed the same trellis structure. Observe in Figure 3.41 that the non-precoded system has a lower complexity than the precoded one at a distance of 1.82 dB from the maximum achievable rate limit, where the non-precoded system approaches an infinitesimally low BER. The precoded system is capable of performing equally well in BER terms, while operating about 1 dB closer to the maximum achievable rate limit than the non-precoded system. However, this is achieved at the cost of almost doubling the complexity, as seen in Figure 3.41.

3.3.3 Application: Iteratively Detected Irregular Variable Length Coded and Unity-Rate Precoded DSTS-SP Schemes[7]

The schematic of the iteratively detected Irregular Variable Length Coded (IrVLC) and Unity-Rate Precoded DSTS-SP system is shown in Figure 3.42, where the VLC-encoded bits $\mathbf{c}_1$ are interleaved by a random bit interleaver and then the interleaved bit stream $\mathbf{u}_2$ is encoded by a URC encoder. After URC encoding, the DSTS-SP modulator maps B_{sp} number of coded bits $\mathbf{b} = b_0, \ldots, b_{B_{sp}-1} \in \{0, 1\}$ to a SP symbol $\mathbf{x}$ as discussed in Section 2.4.3. Subsequently, we have a set of SP symbols that can be transmitted with the aid of DSTS within two time slots using two transmit antennas. The schemes considered in this section differ from those in Section 3.3.1 in their choice of the outer source codec. Specifically, we consider an IrVLC codec and an equivalent-rate regular VLC-based benchmark scheme. We refer to these two schemes as the IrVLC- and VLC-DSTS-SP arrangements, as appropriate.

The schemes considered are designed for facilitating the near-capacity transmission of source symbol sequences over a correlated narrowband Rayleigh fading channel. We consider K=16-ary source symbol values that have the probabilities of occurrence resulting from the Lloyd-Max

[7]This work has been made possible by collaboration with my colleague Robert G. Maunder, who generously offered his IrVLC C++ code and his time for the numerous discussions.

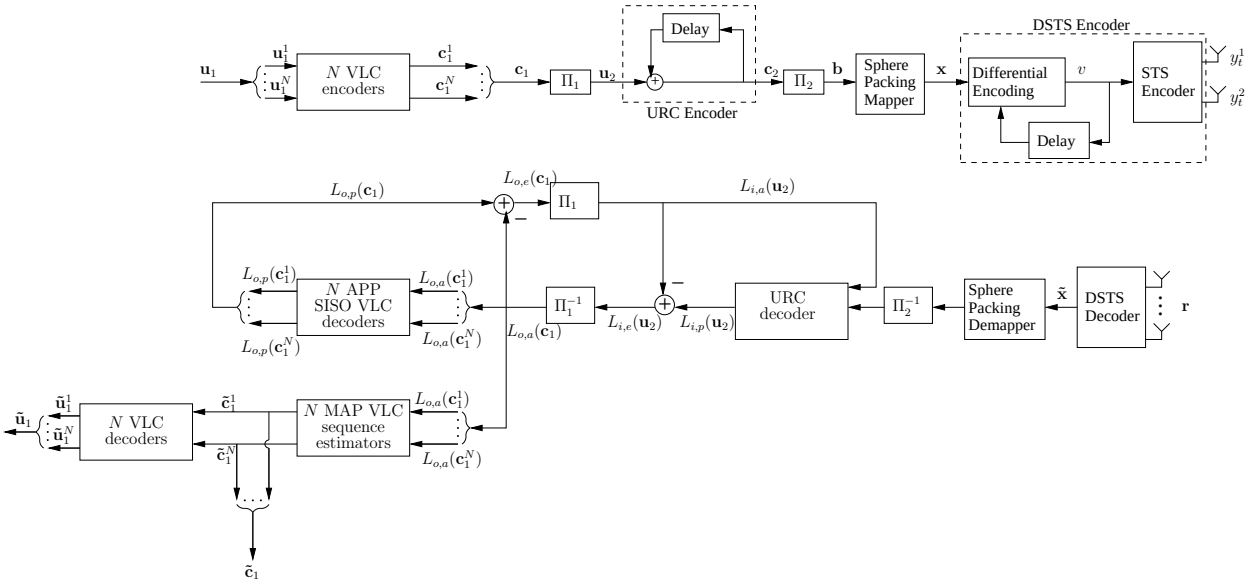

Figure 3.42: Schematic of the IrVLC- and VLC-DSTS-SP schemes. In the IrVLC-DSTS-SP scheme we have N=15 different irregularly encoded protection classes, whilst N=1 in the VLC-DSTS-SP scheme.

(LM) quantisation [238] of independent Gaussian distributed source samples. More explicitly, we consider the 4-bit LM quantisation of a Gaussian source. Note that these occurrence probabilities vary by more than an order of magnitude between 0.0082 and 0.1019. These probabilities correspond to entropy or average informations values between 3.29 bits and 6.93 bits, motivating the application of VLC and giving an overall source entropy of E=3.77 bits/VLC-symbol.

In the transmitter shown in Figure 3.42, the source symbol frame $\mathbf{u}_1$ comprises J=15,000 4-bit source symbols having the K=16-ary values $\{u_{1,j}\}_{j=1}^{J} \in [1 \dots K]$. These 4-bit source symbols are decomposed into N number of different protection classes $\{\mathbf{u}_1^n\}_{n=1}^{N}$, where we opted for N=15 in the case of the IrVLC-DSTS-SP scheme and N=1 in the case of the VLC-DSTS-SP scheme. The number of symbols in the source symbol frame $\mathbf{u}_1$ that are decomposed into the source symbol frame component $\mathbf{u}_1^n$ is specified as J^n, where we have $J^1 = J$ in the case of the VLC-DSTS-SP scheme. By contrast, in the case of the IrVLC-DSTS-SP scheme, the specific values of $\{J^n\}_{n=1}^{N}$ may be chosen in order to shape the EXIT curve of the IrVLC codec, so that it does not cross the EXIT curve of the precoder.

Each of the N number of source symbol frame components $\{\mathbf{u}_1^n\}_{n=1}^{N}$ is VLC-encoded using the corresponding codebook from the set of N number of VLC codebooks $\{\mathbf{VLC}^n\}_{n=1}^{N}$, having a range of coding rates $\{R^n\}_{n=1}^{N} \in [0, 1]$. The specific source symbols having the value of $k \in [1 \dots K]$ and encoded by the specific VLC codebook $\mathbf{VLC}^n$ are represented by the codeword $\mathbf{VLC}^{n,k}$, which has a length of $I^{n,k}$ bits. The J^n number of VLC codewords that represent the J^n number of source symbols in the source symbol frame component $\mathbf{u}_1^n$ are concatenated to provide the transmission frame component $\mathbf{c}_1^n = \{\mathbf{VLC}^{n,u^n_{1,j^n}}\}_{j^n=1}^{J^n}$.

Owing to the variable length of the VLC codewords, the number of bits comprised by each transmission frame component $\mathbf{c}_1^n$ will typically vary from frame to frame. In order to facilitate the VLC decoding of each transmission frame component $\mathbf{c}_1^n$, it is necessary to explicitly convey its length $I^n = \sum_{j^n=1}^{J^n} I^{n,u_{1,j^n}^n}$ to the receiver with the aid of side information. Furthermore, this highly error sensitive side information must be reliably protected against transmission errors. This may be achieved using a low rate block code or repetition code, for example. For the sake of avoiding obfuscating details, this is not explicitly shown in Figure 3.42.

In the transmitter of Figure 3.42, the N number of transmission frame components $\{\mathbf{c}_1^n\}_{n=1}^N$ are concatenated. As shown in Figure 3.42, the resultant transmission frame $\mathbf{c}_1$ has a length of $\sum_{n=1}^N I^n$ bits. Following interleaving Π_1, the transmission frame $\mathbf{u}_2$ is precoded [185] by the URC and then interleaved again before being SP modulated for transmission using DSTS.

In the receiver, the URC-decoder and the VLC-decoder iteratively exchange extrinsic information, as shown in Figure 3.42. In parallel to the formation of the bit-based transmission frame $\mathbf{c}_1$ from N number of components, the *a priori* LLRs $L_{o,a}(\mathbf{c}_1)$ are decomposed into N number of components, as shown in Figure 3.42. Each of the N number of VLC decoding processes is provided with the *a priori* LLR sub-frame $L_{o,a}(\mathbf{c}_1^n)$ and in response it generates the *a posteriori* LLR sub-frame $L_{o,p}(\mathbf{c}_1^n)$, $n \in [1 \dots N]$. These *a posteriori* LLR sub-frames are concatenated in order to provide the *a posteriori* LLR frame $L_{o,p}(\mathbf{c}_1)$, as shown in Figure 3.42.

During the final decoding iteration, N number of bit-based MAP VLC sequence estimation processes are invoked instead of soft-in soft-out VLC decoding, as shown in Figure 3.42. In this case, each transmission frame component $\mathbf{c}_1^n$ is estimated from the corresponding *a priori* LLR frame component $L_{o,a}(\mathbf{c}_1^n)$. The resultant transmission frame component estimates $\tilde{\mathbf{c}}_1^n$ may be concatenated to provide the transmission frame estimate $\tilde{\mathbf{c}}_1$. Additionally, the transmission frame component estimates $\tilde{\mathbf{c}}_1^n$ may be VLC decoded to provide the source symbol frame component estimates $\tilde{\mathbf{u}}_1^n$.

3.3.3.1 IrVLC Design Using EXIT Chart Analysis

The IrVLC-DSTS-SP scheme employs N=15 component VLC codebooks $\{\mathbf{VLC}^n\}_{n=1}^N$ having approximately equally spaced coding rates in the range $[0.26, 0.95]$. In each case, we employ a Variable Length Error Correcting (VLEC) codebook [239] that is tailored to the source symbol values' probabilities of occurrence and having the maximum minimum free distance that can be achieved at the particular coding rate considered. By contrast, in the VLC-DSTS-SP scheme, we employ just N=1 VLC codebook, which is identical to the VLC codebook $\mathbf{VLC}^{10}$ of the IrVLC-DSTS-SP scheme, having a coding rate of R=0.5, as shown in Figure 3.43. Note that this coding rate results in an average interleaver length of $J \cdot E/R$=113,100 bits and a

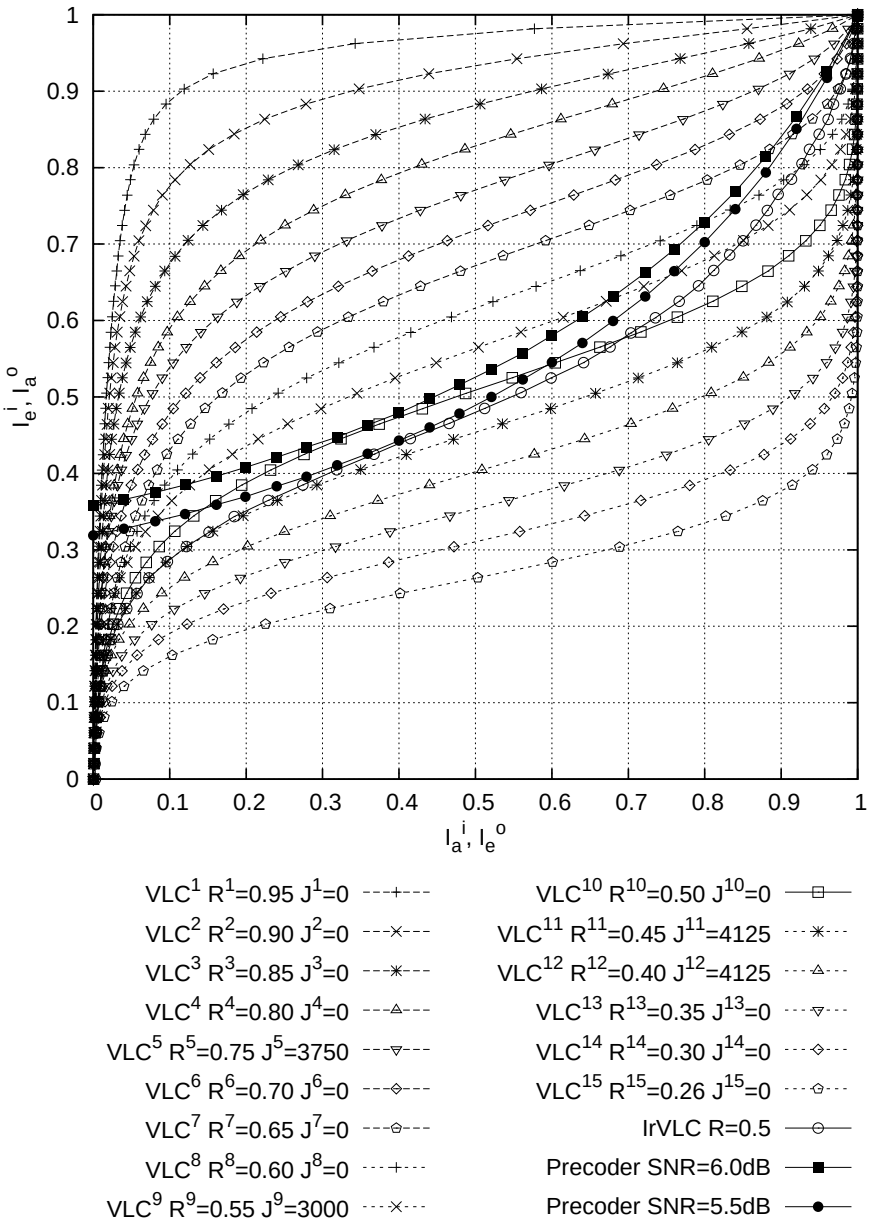

Figure 3.43: VLC EXIT curves and URC-precoded DSTS-SP EXIT curves.

bandwidth efficiency of 1 bit-per-channel-use, if we ignore the negligible overhead of conveying the side information and assume ideal Nyquist filtering having a zero excess bandwidth. We note furthermore that for the proposed DSTS-SP system, this bandwidth efficiency is associated with an E_b/N_0 maximum achievable rate bound of 5.2 dB as described in Section 3.2.3.

Figure 3.43 shows the EXIT curves that characterise the VLC decoding of the VLC codebooks together with the precoder's EXIT curves recorded for E_b/N_0 values of 5.5 and 6.0 dB. Figure 3.43 also shows the EXIT curve of the IrVLC scheme. This is obtained as the appropriately weighted superposition of the N=15 unequal protection component VLC codebooks' EXIT curves, where the weight applied to the EXIT curve of the component VLC codebook **VLC^n** is related to the number of source symbols that it is employed for encoding J^n [191]. Using the approach of [191], the values of $\{J^n\}_{n=1}^N$ given in Figure 3.43 were designed for en-

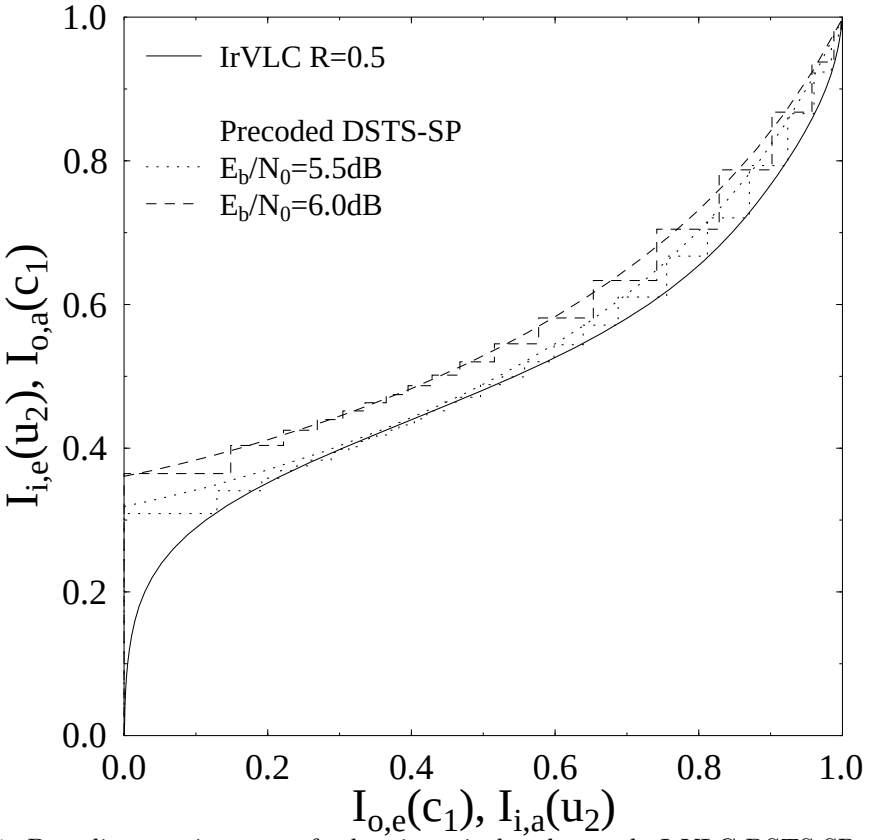

Figure 3.44: Decoding trajectory of the iteratively detected IrVLC-DSTS-SP scheme operating at E_b/N_0=5.5 dB and E_b/N_0=6.0 dB.

suring that the IrVLC coding rate matches that of our regular VLC scheme, namely VLC[10], and so that the IrVLC EXIT curve does not cross the precoder's EXIT curve at an E_b/N_0 value of 5.5 dB. We note that only four out of the N=15 VLC components were chosen by the proposed EXIT-chart matching procedure for encoding a non-zero number of source symbols. As shown in Figure 3.43, the presence of the resultant open EXIT chart tunnel implies that an infinitesimally low Symbol Error Ratio (SER) may be achieved by the IrVLC-DSTS-SP scheme for E_b/N_0 values in excess of 5.5 dB, which is just 0.3 dB from the maximum achievable rate bound of 5.2 dB. By contrast, no open EXIT chart tunnel is maintained for E_b/N_0 values below 6.0 dB in the case of the VLC-DSTS-SP benchmark scheme. This value of E_b/N_0 is 0.8 dB from the DSTS-SP capacity bound, representing a discrepancy that is 2.67 times that of the IrVLC-DSTS-SP scheme.

3.3.3.2 Performance Results

We consider a SP modulation scheme associated with L=16 in conjunction with GM for assigning the source bits to the SP symbols, while employing twin-antenna-aided DSTS system and a single receiver antenna in order to demonstrate the performance improvements achieved by the proposed system.

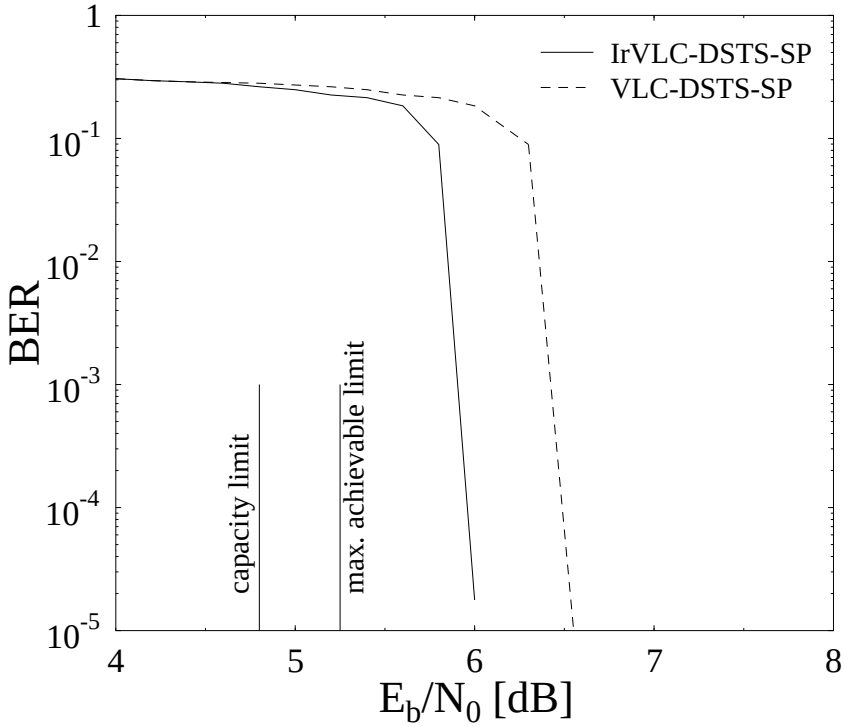

Figure 3.45: Performance comparison of the IRVLC- and VLC-DSTS-SP systems while employing an average interleaver length of 113100 bits and 40 iterations.

Figure 3.44 shows the EXIT curve of the IrVLC scheme employed as well as the EXIT curves of the precoded DSTS-SP system together with the decoding trajectories at both E_b/N_0 values of 5.5 dB and 6.0 dB. The system communicates over a correlated narrowband Rayleigh fading channel associated with a normalised Doppler frequency of f_D=0.01 and employs a random interleaver having an average depth of D_{int}=113, 100 bits. The decoding trajectory recorded for E_b/N_0=6.0 dB and shown in Figure 3.44 is the one we obtained from simulations, where the system did not converge below an E_b/N_0 value of 6.0 dB, although the EXIT curve of Figure 3.43 predicted an open tunnel at E_b/N_0 of 5.5 dB. The EXIT-chart predictions are accurate, if we employ a specially designed interleaver that is capable of removing the correlation of the data imposed by both the correlated channel employed as well as by the differential encoding that introduces more correlation to the data. Figure 3.44 also shows the decoding trajectory at E_b/N_0=5.5 dB. However, this trajectory was generated by simulating the effect of a random interleaver capable of eliminating the correlation, i.e. by generating uncorrelated LLRs at the input of the precoder's decoder. Therefore, the EXIT curve predictions can be fulfilled, if we succeed in designing an interleaver having a reasonable length that can be used for eliminating the correlation imposed by the DSTS scheme and by the channel employed. The performance of the IrVLC-aided system did not match with the EXIT chart prediction of Figure 3.43, while the performance of the system employing the RSC as an outer code did match with the EXIT chart prediction of the system. This might be due to the fact that the IrVLC scheme is more sensitive to the correlation exhibited by the data than the RSC code.

Figure 3.45 compares the attainable performance of the IrVLC-aided and of the VLC-aided DSTS-SP systems, when communicating over a correlated narrowband Rayleigh fading channel with a normalised Doppler frequency of f_D=0.01. The EXIT analysis of Figure 3.43 predicted a difference of 0.5 dB between the performance of the two systems. In Figure 3.45 we present the corresponding BER curves having the same E_b/N_0 difference as the EXIT curve prediction, however with a shift of 0.5 dB from the prediction. In other words, as mentioned in the previous paragraph, owing to the employment of an interleaver that is incapable of eliminating the effect of correlation, the IrVLC-aided system converges at E_b/N_0=6.0 dB and the VLC-aided system at E_b/N_0=6.5 dB. The BER curves presented in Figure 3.44 were recorded after 40 decoding iterations between the VLC decoder and the precoder's decoder, as shown in Figure 3.42.

3.4 Chapter Conclusion

In this chapter, we proposed a novel system that exploits the advantages of both iterative detection [224] as well as those of the DSTS schemes employing two and four transmit antennas [7,8]. The proposed DSTS scheme benefits from a substantial diversity gain without the need for any CSI. Moreover, our investigations demonstrated that significant performance improvements may be achieved, when the Anti-Gray mapping DSTS-SP is combined with outer channel decoding and iterative detection exchanging extrinsic information between the decoder and the demapper, as compared to the Gray-Mapping based systems. Subsequently, EXIT charts were used to search for bit-to-symbol mapping schemes that converge at lower E_b/N_0 values. Several DSTS-SP mapping schemes covering a wide range of extrinsic transfer characteristics were investigated. When using an appropriate bits-to-symbol mapping scheme and 10 detection iterations, gains of about 19.5 dB were obtained by the convolutional coded twin-antenna-aided DSTS-SP schemes over the identical-throughput uncoded DSTS-SP benchmark scheme discussed in Chapter 2. Furthermore, the AGM-1 based iteratively detected twin-antenna-aided DSTS-SP scheme is capable of performing within 2.3 dB from the maximum achievable rate limit obtained using EXIT charts at BER=10^{-5}.

Additionally, the chapter characterised the benefits of precoding, when concatenated with the outer channel code, suggesting that an E_b/N_0 gain of at least 1.2 dB can be obtained over the uncoded system at a BER of 10^{-6}, depending on the mapping scheme used. Explicitly, the four-antenna-aided DSTS-SP system employing no URC precoding attains a coding gain of 12 dB at a BER of 10^{-5} and performs within 1.82 dB from the maximum achievable rate limit. By contrast, the URC precoded system outperforms its non-precoded counterpart and operates within 0.92 dB from the maximum achievable rate limit obtained using EXIT charts.

DSTS (2Tx,1Rx) No URC precoding	Coding Gain	Distance from maximum achievable rate limit
SP L=16, GM	14.9 dB	6.9 dB
SP L=16, AGM-1	19.5 dB	2.3 dB
SP L=16, AGM-3	17.75 dB	4.05 dB
SP L=16, GM-8	15.9 dB	5.9 dB
QPSK, AGM	16.1 dB	5.7 dB
DSTS (4Tx,1Rx) No URC precoding	Coding Gain	Distance from maximum achievable rate limit
SP L=16, GM	9.5 dB	4.32 dB
SP L=16, AGM-1	12 dB	1.82 dB
SP L=16, AGM-3	10.9 dB	2.92 dB
SP L=16, GM-8	8.9 dB	4.92 dB
QPSK, AGM	9.2 dB	4.62 dB
DSTS (4Tx,1Rx) URC precoding	Coding Gain	Distance from maximum achievable rate limit
SP L=16, GM	12.9 dB	0.92 dB

Table 3.4: Iteratively-detected RSC-coded DSTS system coding gain and distance from maximum achievable rate limit at BER=10^{-5}.

3.5 Chapter Summary

In this chapter, two realisations of a novel iterative-detection aided DSTS-SP scheme were presented, namely an iteratively detected RSC-coded DSTS-SP scheme as well as an iteratively detected RSC-coded and URC precoded DSTS-SP arrangement. The iteratively detected RSC-coded DSTS-SP scheme was described in Section 3.2. In Section 3.2.1, we showed how the DSTS-SP demapper was modified for exploiting the *a priori* knowledge provided by the channel decoder, which is essential for the employment of iterative detection.

The concept of EXIT chart was introduced in Section 3.2.2 as a tool designed for studying iterative detection aided schemes. We proposed 9 different anti-Gray mapping (AGM) schemes in Figure 3.3 that were specifically selected from all the possible mapping schemes for L=16, in order to create the different extrinsic information transfer characteristics associated with different bit-to-SP-symbol mapping schemes. Both the Gray mapping as well as the various AGM mapping schemes considered in this chapter are detailed in Appendix A. In Section 3.2.2.2, we explained the procedure of computing the EXIT characteristics of an outer decoder in a serially concatenated scheme. Then, we proposed a novel technique for computing the maximum

DSTS (2Tx,1Rx) No URC precoding	Coding Gain	Distance from maximum achievable rate limit
SP L=16, GM	17.8 dB	8 dB
SP L=16, AGM-1	22.5 dB	3.3 dB
SP L=16, AGM-3	20.5 dB	5.3 dB
SP L=16, GM-8	18.4 dB	7.4 dB
QPSK, AGM	19 dB	6.8 dB
DSTS (4Tx,1Rx) No URC precoding	Coding Gain	Distance from maximum achievable rate limit
SP L=16, GM	13.7 dB	5.12 dB
SP L=16, AGM-1	16.7 dB	2.12 dB
SP L=16, AGM-3	14.8 dB	4.02 dB
SP L=16, GM-8	12.9 dB	5.92 dB
QPSK, AGM	13.5 dB	5.32 dB
DSTS (4Tx,1Rx) URC precoding	Coding Gain	Distance from maximum achievable rate limit
SP L=16, GM	17.9 dB	0.92 dB

Table 3.5: Iteratively-detected RSC-coded DSTS system coding gain and distance from maximum achievable rate limit at BER=10^{-6}.

achievable bandwidth efficiency of the system based on the EXIT charts in Section 3.2.3, followed by a discussion of the system's performance. Section 3.2.5 presented an application of the iteratively detected RSC-coded DSTS-SP system, where an Adaptive Multi-Rate WideBand (AMR-WB) source codec was employed by the system in order to demonstrate the attainable performance improvements.

In Section 3.3 we proposed an iteratively detected RSC-coded and URC-precoded DSTS-SP scheme that is capable of eliminating the error floor exhibited by the previous system, which hence performed closer to the system's achievable capacity. In Section 3.3.1 we presented an overview of the system operation, followed by a discussion of the results in Section 3.3.2. In Section 3.3.3 we presented an application of the proposed URC-precoded DSTS-SP system, while employing Irregular Variable Length Codes (IrVLC) as our outer code for the sake of achieving a near-capacity performance.

Finally, Tables 3.4 and 3.5 present the coding gains as well as the distance from the maximum achievable rate limit for the iteratively detected RSC-coded DSTS system, while employing SP as well as QPSK modulation schemes. The tables present the results for both the two- and four-antenna-aided DSTS scheme, when both systems optionally employ URC precoding.

The next chapter will consider the design of adaptive iteratively detected DSTS-SP schemes designed for attaining the highest possible system throughput, while maintaining a specific quality of service exemplified in terms of the attainable BER.

Chapter 4

Adaptive Differential Space-Time-Spreading-Assisted Iteratively-Detected Sphere Packing Modulation

4.1 Introduction

Mobile radio signals are subject to propagation path loss as well as small-scale fading and large-scale fading. Due to the nature of the fading channel, transmission errors occur in bursts, when the channel exhibits deep fades or when there is a sudden surge of multiple access interference or inter-symbol interference [25]. In mobile communication systems, power control techniques [240] are used to mitigate the effects of path loss and slow fading. However, in order to counteract the problem of fast fading and co-channel interference, agile power control algorithms are required [25, 241]. On the other hand, adaptive-rate transmission [242, 243] can be used to overcome these problems due to the time-variant fluctuations of the channel's quality or for mitigating the effects of shadow fading, when for example all the transmit diversity antennas experience correlated fading, as exemplified by the effects of large-bodied vehicles. In adaptive-rate transmission the information rate is varied according to the channel's quality rather than according to the users' requirements.

In recent years, the concept of intelligent multi-mode multimedia transceivers has emerged in the context of wireless systems [242]. The fundamental limitation of wireless systems is constituted by the time- and frequency-domain channel fading, that is exemplified in terms of the signal-to-interference-plus-noise ratio fluctuations experienced by wireless modems [242,

244]. Furthermore, the continued increase in demand for all types of wireless services including voice, data and multimedia increases the need for higher data rates. Therefore, no fixed mode transceiver may be expected to provide an attractive performance at a reasonable complexity and interleaver delay. Hence, advanced adaptive MIMO techniques, coded modulation as well as adaptive modulation and coding arrangements have to be invoked, which are capable of near-instantaneous High Speed Downlink Packet Access (HSDPA) style reconfiguration.

Adaptive modulation and coding techniques that track the time-varying characteristics of wireless channels can be used to significantly increase the data rate, reliability and spectrum efficiency of wireless communication systems. In recent years various adaptive coding and modulation arrangements have been proposed [25, 245, 246]. A whole range of different transmission parameters can be adapted, including the transmission power [247], the system bandwidth [248], the modulation scheme [245, 249], the spreading factor (SF) of DS-CDMA systems [250] in addition to the code rate or interleaver length of channel coded systems. The fundamental goal of near-instantaneous adaptation is to ensure that the most efficient mode is used in the face of rapidly-fluctuating time-variant channel conditions based on appropriate activation criteria. As a benefit, near-instantaneous adaptive systems are capable of achieving a higher effective throughput compared to their non-adaptive counterparts. When the channel quality is low, a lower information rate is chosen in order to reduce the number of errors. Conversely, when the channel quality is high, a higher information rate is used to increase the throughput of the system [242].

In [251], various multi-rate systems were compared, including variable SF based, multi-code and adaptive modulation aided schemes. According to the multi-code philosophy, the SF is kept constant for all users, but multiple spreading codes are assigned to users having higher bit-rate requirements. Multiple data rates can also be supported by a variable SF scheme, where the chip rate is kept fixed but the data rate is varied by varying the SF of different users. Hence, the lower the SF, the higher the data rate. Moreover, in [251] multilevel modulation schemes were investigated, where higher-rate users were assigned higher order modulation modes transmitting several bits per symbol. However, it was concluded that the performance experienced by users requiring higher rates was significantly worse than those requiring lower rates. Furthermore, the employment of L-ary orthogonal modulation supporting variable rate transmission was investigated in [252].

The transmission rate of each user can be adapted according to the channel quality in order to mitigate the effects of channel quality fluctuations. The performance of two different methods of combating the channel variations was analysed in [253]. More specifically, these two methods were based on either the adaptation of the transmission power in order to com-

pensate for the channel quality variations or on the switching of the information rate in order to suit the prevalent channel conditions. In [254], the authors investigated an adaptive packet transmission-based CDMA scheme, where the transmission rate is modified by varying both the channel code rate and the processing gain of the CDMA user, employing the carrier-to-interference-plus-noise-ratio as the channel quality parameter.

In this chapter, we also propose to vary the information rate in accordance with the channel quality. The instantaneous channel quality can be estimated at the receiver and the chosen information rate can then be communicated to the transmitter via explicit signalling in a closed loop scheme. Conversely, in an open loop scheme, by assuming reciprocity in the uplink and the downlink channel of Time Division Duplex (TDD) systems, the information rate for the downlink transmission is chosen according to the channel quality estimate related to the uplink and vice versa. Explicitly, in this chapter we investigate a novel adaptive DSTS-SP aided technique for supporting a wide range of bit rates, where the transmission of data from the four antennas is adapted by activating two different transmission schemes according to the near-instantaneous channel SNR conditions. Moreover, the transmission bit rate is adjusted with the aid of using a Variable Spreading Factor (VSF). More explicitly, given a fixed bandwidth and a fixed chip rate, the system enables a user to benefit from a higher bit rate while using a lower SF when the instantaneous SNR is sufficiently high. Furthermore, an iteratively-detected variable-rate RSC code is employed for further enhancing the system's attainable BER performance, where the code rate may be increased for the sake of increasing the achievable system throughput as the channel quality improves. As a further benefit, the proposed system exploits the implementation advantages of low-complexity differential encoding/decoding, although this is achieved at the cost of the typical SNR degradation of differential encoding. Therefore, the achievable integrity and bit rate enhancements of the system are determined by the following factors:

- *The specific transmission configuration used for transmitting data from the four antennas.*
- *The spreading factor used.*
- *The RSC encoder's code rate.*

This chapter is organised as follows. In Section 4.2, a brief system overview is presented. In Section 4.3 the adaptive DSTS-SP scheme varying the transmission configuration of the four antennas is detailed, followed by Section 4.4 that justifies the purpose of adapting the SF used. The iteratively detected variable code rate DSTS-SP system is discussed in Section 4.5. In Section 4.6, we quantify the performance of the proposed system and finally we conclude our findings in Section 4.7.

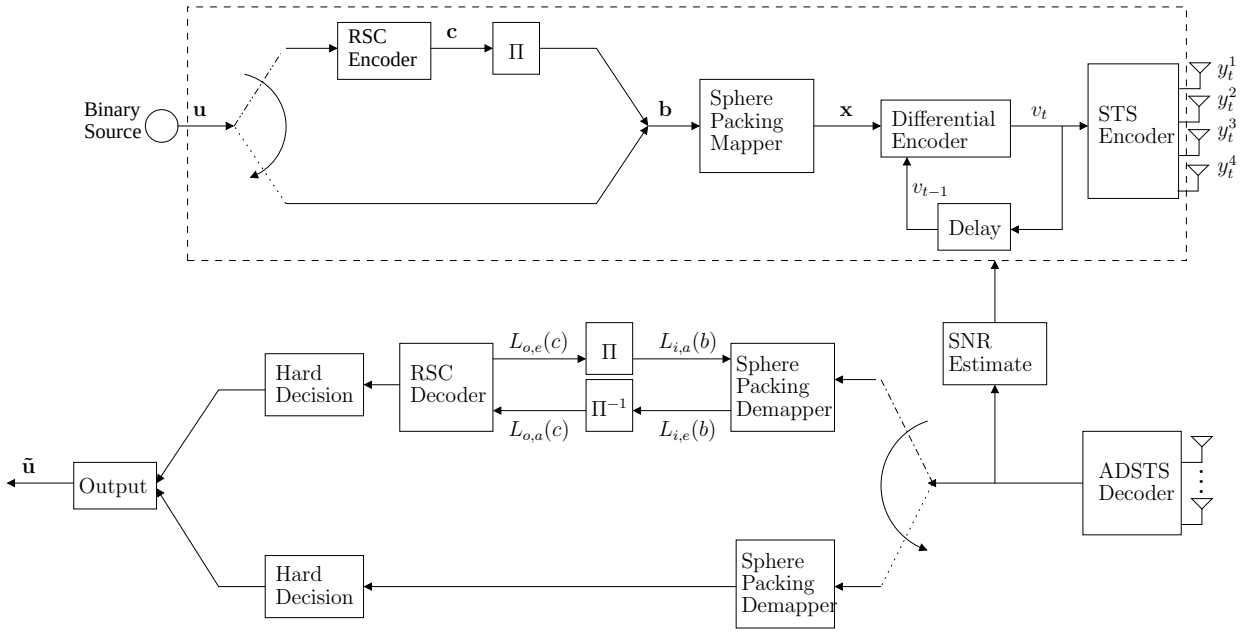

Figure 4.1: The proposed adaptive differential space-time spreading assisted iteratively detected SP aided system model.

4.2 System Overview

The adaptive DSTS system considered in this chapter employs four transmit antennas and a single receive antenna. A block diagram of the proposed system is shown in Figure 4.1, where four-dimensional SP modulation and real-valued orthogonal spreading were employed. A suitable transmission mode is selected according to the near-instantaneous channel conditions, which is quantified by the Signal-to-Noise Ratio (SNR) in our case. A low complexity technique of determining the channel conditions to be expected at the receiver in the context of TDD is that of exploiting the correlation between the fading envelope of the UpLink (UL) and the DownLink (DL), since the UL and the DL slots are transmitted at the same frequency and hence are likely to fade coincidentally, unless frequency-selective fading is encountered. Therefore, when transmitting a frame, transmitter A estimates the SNR of receiver B at the other end of the link based on the SNR estimate of receiver A and selects the most appropriate transmission mode accordingly. The proposed adaptive transceiver assumes the availability of a reliable modem-mode signalling link between the transmitter and the receiver, such as the control channel of the HSDPA system.

As shown in Figure 4.1, the transmitted source bits have two different paths to follow. In the upper path shown in the figure, the transmitted source bits are convolutionally encoded and then interleaved by a random bit interleaver. A variable rate RSC code is employed, where the code rate is varied between $R{=}\frac{1}{6}$ and $R{=}\frac{1}{2}$ depending on the near-instantaneous channel conditions. Moreover, when the channel SNR is sufficiently high for the target system

performance to be met without channel coding, the transmitted source bits are not channel coded at all. After deciding on whether to invoke channel coding or not, the SP mapper maps B_{sp} number of bits $\mathbf{b} = b_0, \ldots, b_{B_{sp}-1} \in \{0, 1\}$ to a SP symbol $\mathbf{s^l} \in \mathbf{S}$, $l = 0, 1, \ldots, L-1$, so that we have $\mathbf{s^l} = \text{map}_{sp}(\mathbf{b})$, where $B_{sp} = \log_2 L$ and L represents the number of modulated symbols in the SP signalling alphabet, as described in Chapter 2. Subsequently, each of the four components of a SP symbol is then transmitted using DSTS via four transmit antennas in two or four consecutive time slots, depending on the channel conditions, as detailed in Section 4.3. Furthermore, a VSF is employed by each user so that the system's effective bit rate can be enhanced along with any improvement in the channel conditions. Therefore, creating signalling modes that enable reliable communication even in poor channel conditions renders the system robust. By contrast, under good channel conditions the spectrally efficient modes are activated, in order to increase the effective throughput.

In this treatise, we consider transmissions over a correlated narrowband Rayleigh fading channel, associated with a normalised Doppler frequency of $f_D = f_d T_s = 0.01$, where f_d is the Doppler frequency and T_s is the symbol duration. The complex AWGN of $n = n_I + jn_Q$ contaminates the received signal, where n_I and n_Q are two independent zero-mean Gaussian random variables having a variance of $\sigma_n^2 = \sigma_{n_I}^2 = \sigma_{n_Q}^2 = N_0/2$ per dimension with $N_0/2$ representing the noise power spectral density expressed in W/Hz.

At the receiver side of Figure 4.1, the DSTS decoder decodes the received signal according to the received modem-mode side information or in other words according to the information fed back from the receiver to the transmitter before the transmission of the specific frame. More explicitly, the receiver has to decide whether the data was channel coded and what code rate was used for encoding. If no channel coding was employed, then the received signal will be directly demodulated by the SP demapper of Figure 4.1. By contrast, if channel coding was employed, then the decoder has to decide which code-rate was employed. As shown in Figure 4.1, the received complex-valued symbols are demapped to their Log-Likelihood Ratio (LLR) representation for each of the B_{sp} channel-coded bits per SP symbol. The *a priori* LLR values of the demodulator are subtracted from the *a posteriori* LLR values for the sake of generating the extrinsic LLR values $L_{i,e}(\mathbf{b})$ and then the extrinsic LLRs are deinterleaved by a soft-bit deinterleaver, again as seen in Figure 4.1. Next, the soft bits $L_{o,a}(\mathbf{c})$ are passed to the convolutional decoder in order to compute the *a posteriori* LLR values for all the channel-coded bits. During the last iteration, only the LLR values of the original uncoded systematic information bits are required, which are passed to the hard decision decoder of Figure 4.1 in order to determine the transmitted source bits.

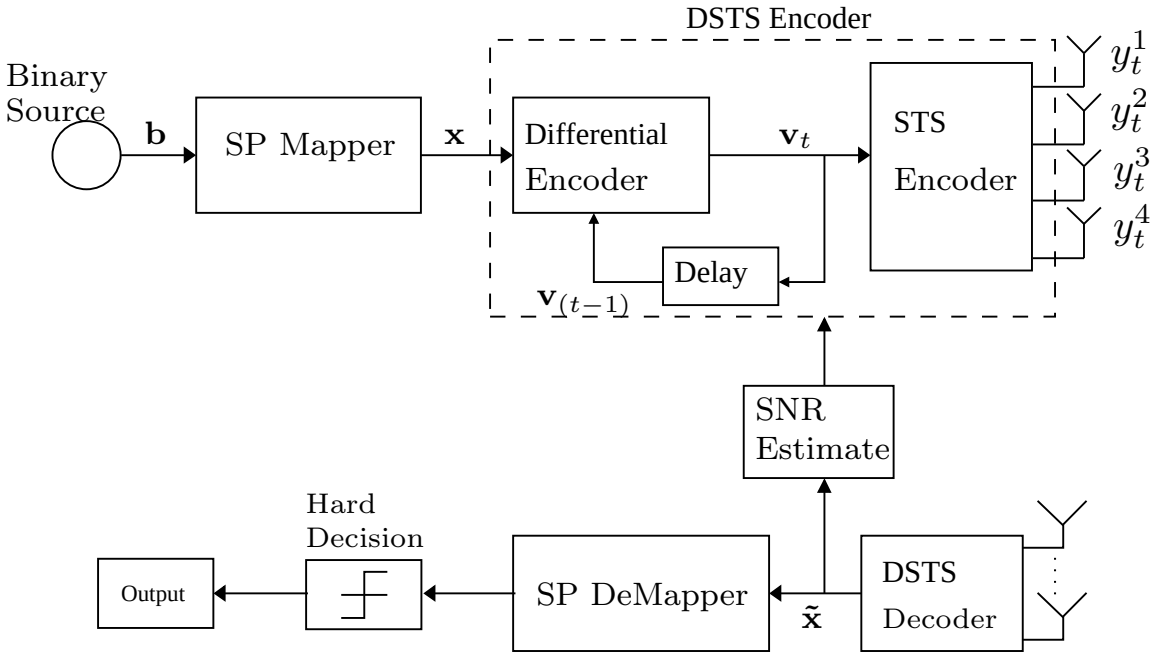

Figure 4.2: The proposed adaptive DSTS-assisted SP-aided system model.

4.3 Adaptive DSTS-Assisted Sphere Packing Modulation

The main philosophy of the proposed adaptive DSTS-SP scheme is that of the system's throughput maximisation while maintaining the required Quality of Service (QoS), namely the target BER performance. The scheme considered in this chapter consists of N_t=4 transmit antennas and N_r=1 receive antenna, although its extension to $N_r > 1$ antennas is straightforward. The transmitter schematic of the kth user and the receiver schematic of the reference user are shown in Figure 4.2, where SP modulation and real-valued spreading were employed.

The proposed adaptive system switches between two DSTS schemes depending on the channel's SNR. When a low channel quality is encountered and thus the short-term BER is higher than the required target BER, a high-diversity four-antenna-aided scheme is employed by the transceiver. However, as the channel quality improves and the system's BER performance becomes better than the target BER, then a lower-diversity higher-throughput twin-layer four-antenna-aided DSTS-SP configuration is used.

In the four-antenna-aided DSTS encoder, the data is serial-to-parallel converted to four substreams. The new bit duration of each parallel substream, which is referred to as the symbol duration, becomes T_s=4T_b as illustrated in Section 2.4 and in [25, 49]. The four-antenna-aided DSTS transmitter conveys one SP symbol in four time slots. Therefore, the DSTS-SP signalling rate becomes 1/4 and the effective throughput quantified in terms of the symbol rate is related to the number of bits-per-symbol B_{sp} as $B_{sp}/4$. However, this fixed-mode four-antenna-aided DSTS-SP system is unable to maximise the throughput as a function of the channel SNR

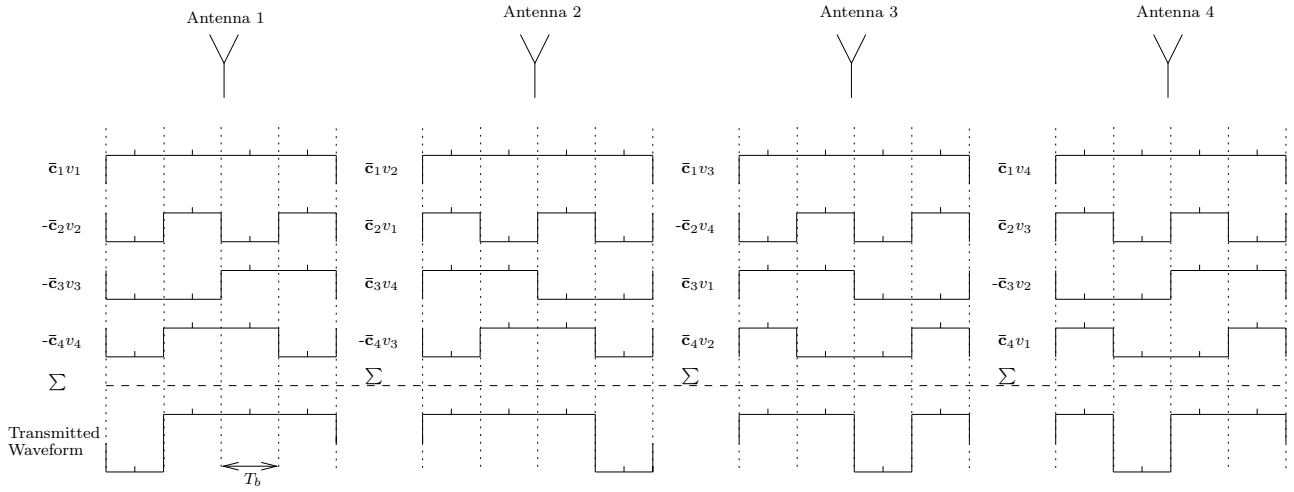

Figure 4.3: Illustration of STS using four transmit antennas transmitting 4 bits within $4T_b$ duration. v_1=v_2=v_3=v_4=1 were assumed and $\bar{\mathbf{c}}_1 = [+1+1+1+1+1+1+1+1]$, $\bar{\mathbf{c}}_2 = [+1+1-1-1+1+1-1-1]$, $\bar{\mathbf{c}}_3 = [+1+1+1+1-1-1-1-1]$ and $\bar{\mathbf{c}}_4 = [+1+1-1-1-1-1+1+1]$.

quality. For example, at a high SNR value, the system provides a lower BER than the target BER value, which imposes a low effective throughput. Thus, an intelligent high-efficiency DSTS system must be capable of monitoring the near-instantaneous channel quality and of adapting the DSTS scheme's mode of operation. When the channel SNR encountered is low and hence the resultant BER is higher than the target BER, a low-throughput DSTS transmitter mode is activated, which exhibits a high diversity gain. By contrast, when the channel quality is high, and hence the resultant BER is lower than the target BER, then a high-throughput DSTS-assisted transmitter mode having a lower transmit diversity gain is activated.

4.3.1 Single Layer Four-Antenna-Aided DSTS-SP System

The high-diversity four-antenna-aided DSTS-SP mode of operation acts as described in Section 2.4.3. At time instant t=0, the arbitrary reference symbols v_0^1, v_0^2, v_0^3 and v_0^4 are transmitted from the four antennas. At time instants $t \geq 1$, a block of B_{sp} bits arrives at the SP mapper of Figure 4.2, where the B_{sp} bits are mapped to a real-valued four dimensional SP symbol selected from the set $\mathbf{S}=\{\mathbf{s}^l = [a_{l,1}, a_{l,2}, a_{l,3}, a_{l,4}] \in \mathbb{R}^4 : 0 \leq l \leq L-1\}$, where L is the number of legitimate SP constellation points having a total energy of $E \triangleq \sum_{l=0}^{L-1}(|a_{l,1}|^2+|a_{l,2}|^2+|a_{l,3}|^2+|a_{l,4}|^2)$.

The differentially encoded symbols are then spread with the aid of the spreading codes $\bar{\mathbf{c}}_1$, $\bar{\mathbf{c}}_2$, $\bar{\mathbf{c}}_3$ and $\bar{\mathbf{c}}_4$, which are generated from the same user-specific spreading code $\bar{\mathbf{c}}$ by ensuring that they are orthogonal using the simple code-concatenation rule of Walsh-Hadamard codes, yielding longer codes and hence a proportionately reduced per antenna throughput.

The differentially encoded data is then divided into four quarter-rate substreams and the

four consecutive differentially encoded symbols are then spread to the four transmit antennas using the mapping of:

$$\mathbf{y}_t^1 = \frac{1}{\sqrt{4}}\left(\bar{\mathbf{c}}_1 \cdot v_t^1 - \bar{\mathbf{c}}_2 \cdot v_t^2 - \bar{\mathbf{c}}_3 \cdot v_t^3 - \bar{\mathbf{c}}_4 \cdot v_t^4\right) \quad (4.1)$$

$$\mathbf{y}_t^2 = \frac{1}{\sqrt{4}}\left(\bar{\mathbf{c}}_1 \cdot v_t^2 + \bar{\mathbf{c}}_2 \cdot v_t^1 + \bar{\mathbf{c}}_3 \cdot v_t^4 - \bar{\mathbf{c}}_4 \cdot v_t^3\right) \quad (4.2)$$

$$\mathbf{y}_t^3 = \frac{1}{\sqrt{4}}\left(\bar{\mathbf{c}}_1 \cdot v_t^3 - \bar{\mathbf{c}}_2 \cdot v_t^4 + \bar{\mathbf{c}}_3 \cdot v_t^1 + \bar{\mathbf{c}}_4 \cdot v_t^2\right) \quad (4.3)$$

$$\mathbf{y}_t^4 = \frac{1}{\sqrt{4}}\left(\bar{\mathbf{c}}_1 \cdot v_t^4 + \bar{\mathbf{c}}_2 \cdot v_t^3 - \bar{\mathbf{c}}_3 \cdot v_t^2 + \bar{\mathbf{c}}_4 \cdot v_t^1\right), \quad (4.4)$$

where $\bar{\mathbf{c}}_1$, $\bar{\mathbf{c}}_2$, $\bar{\mathbf{c}}_3$ and $\bar{\mathbf{c}}_4$ are four STS-related orthogonal codes having a period of $4T_b$. The transmitted signal's waveform corresponding to the four transmission antennas are shown in Figure 4.3, which shows that four real-valued symbols are jointly transmitted within a time duration of $4T_b$ with the aid of four transmit antennas. Hence, this scheme transmits one SP symbol during the interval of $4T_b$ and hence the effective transmission rate becomes R_b=1 $\times$ $1/(4T_b)$=$1/(4T_b)$.

4.3.2 Twin Layer Four-Antenna-Aided DSTS-SP System

Again, in its most robust but lowest-throughput mode, the above scheme transmits one SP symbol in $4T_b$ duration and hence the effective transmission rate becomes $1/(4T_b)$. By contrast, when the channel quality improves, the transmitter divides the four antennas into two groups of two antennas each for the sake of increasing the effective throughput by creating two independent second-order DSTS-aided subchannels. In this case, at time instants $t \geq 1$, a block of $2B_{sp}$ bits arrives at the SP mapper of Figure 4.2, where each of the B_{sp} bits is mapped to a four-dimensional SP symbol selected from the set $\mathbf{S} = \{\mathbf{s}^l = [a_{l,1}, a_{l,2}, a_{l,3}, a_{l,4}] \in \mathbb{R}^4 : 0 \leq l \leq L-1\}$. The four components of the four-dimensional SP symbol are combined according to Equation (2.21), where we have $\{x_t^1, x_t^2\} = \left\{a_{l,1} + ja_{l,2}, a_{l,3} + ja_{l,4}\right\}$ and $\{x_t^3, x_t^4\} = \left\{a_{l,5} + ja_{l,6}, a_{l,7} + ja_{l,8}\right\}$.

In this mode, the differential encoding is carried out as follows:

$$v_t^1 = \frac{(x_t^1 \cdot v_{t-1}^1 + x_t^2 \cdot v_{t-1}^{2*})}{\sqrt{|v_{t-1}^1|^2 + |v_{t-1}^2|^2}}$$
$$v_t^2 = \frac{(x_t^1 \cdot v_{t-1}^2 - x_t^2 \cdot v_{t-1}^{1*})}{\sqrt{|v_{t-1}^1|^2 + |v_{t-1}^2|^2}}$$

$$v_t^3 = \frac{(x_t^3 \cdot v_{t-1}^3 + x_t^4 \cdot v_{t-1}^{4*})}{\sqrt{|v_{t-1}^3|^2 + |v_{t-1}^4|^2}}$$
$$v_t^4 = \frac{(x_t^3 \cdot v_{t-1}^4 - x_t^4 \cdot v_{t-1}^{3*})}{\sqrt{|v_{t-1}^3|^2 + |v_{t-1}^4|^2}}. \quad (4.5)$$

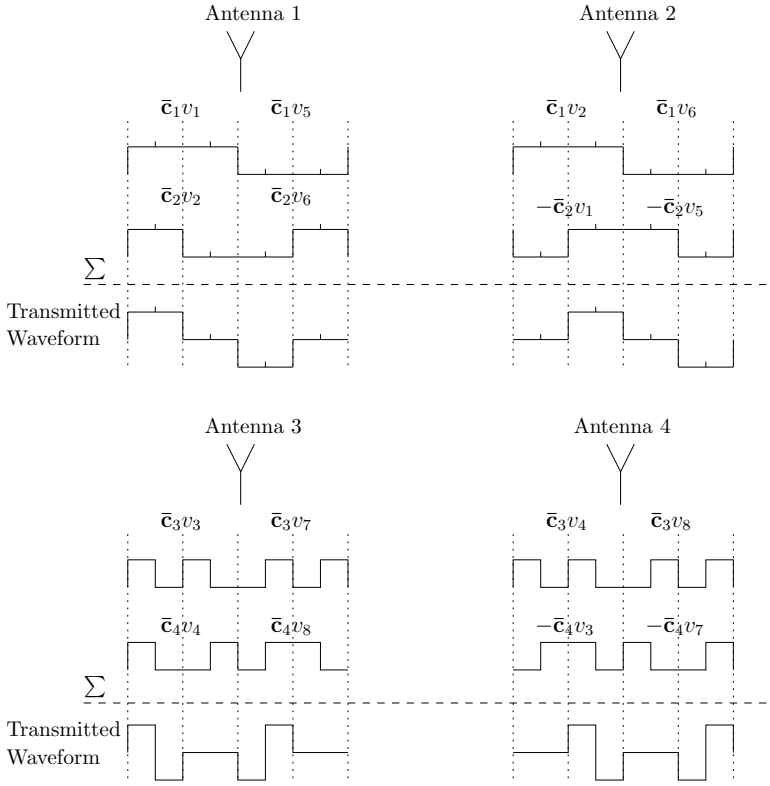

Figure 4.4: Illustration of STS using twin layer four transmit antennas transmitting 4 bits within $2T_b$ duration. v_1=v_2=v_3=v_4=1 and v_5=v_6=v_7=v_8=−1 were assumed and $\bar{\mathbf{c}} = [+1 + 1]$ and $\bar{\mathbf{c}}' = [+1 - 1]$.

The differentially encoded symbols are then spread with the aid of the spreading codes $\bar{\mathbf{c}}_1$, $\bar{\mathbf{c}}_2$, $\bar{\mathbf{c}}_3$ and $\bar{\mathbf{c}}_4$ to the transmit antennas. In this case, each user is assigned two spreading codes $\bar{\mathbf{c}}$, $\bar{\mathbf{c}}'$. The spreading codes used in this second-order diversity scenario are generated as follows:

$$\begin{aligned} \bar{\mathbf{c}}_1^T &= [\bar{\mathbf{c}} \quad \bar{\mathbf{c}}] \\ \bar{\mathbf{c}}_2^T &= [\bar{\mathbf{c}} \quad -\bar{\mathbf{c}}] \\ \bar{\mathbf{c}}_3^T &= [\bar{\mathbf{c}}' \quad \bar{\mathbf{c}}'] \\ \bar{\mathbf{c}}_4^T &= [\bar{\mathbf{c}}' \quad -\bar{\mathbf{c}}'], \end{aligned} \tag{4.6}$$

where $\bar{\mathbf{c}}_1$, $\bar{\mathbf{c}}_2$, $\bar{\mathbf{c}}_3$ and $\bar{\mathbf{c}}_4$ are the four DSTS-related orthogonal codes having a period of $2T_b$. The DSTS operation and the resultant transmitted waveforms from the four antennas are shown in Figure 4.4. Figure 4.4 shows that the first and second antennas transmit jointly one SP symbol within a time duration of $2T_b$, while the third and fourth antennas jointly transmit another SP symbol within the same $2T_b$ duration. However, the operation of the first and second antennas is independent of that of the third and fourth antennas.

The differentially encoded data is then spread to the transmit antennas and transmitted

using the mapping of:

$$\mathbf{y}_t^1 = \frac{1}{\sqrt{4}} \left(\bar{\mathbf{c}}_1 \cdot v_t^1 + \bar{\mathbf{c}}_2 \cdot v_t^{2*} \right) \tag{4.7}$$

$$\mathbf{y}_t^2 = \frac{1}{\sqrt{4}} \left(\bar{\mathbf{c}}_1 \cdot v_t^2 - \bar{\mathbf{c}}_2 \cdot v_t^{1*} \right) \tag{4.8}$$

$$\mathbf{y}_t^3 = \frac{1}{\sqrt{4}} \left(\bar{\mathbf{c}}_3 \cdot v_t^3 + \bar{\mathbf{c}}_4 \cdot v_t^{4*} \right) \tag{4.9}$$

$$\mathbf{y}_t^4 = \frac{1}{\sqrt{4}} \left(\bar{\mathbf{c}}_3 \cdot v_t^4 - \bar{\mathbf{c}}_4 \cdot v_t^{3*} \right). \tag{4.10}$$

The signal at the output of the single receiver antenna can be represented as:

$$\mathbf{r}_t = h_1 \cdot \mathbf{y}_t^1 + h_2 \cdot \mathbf{y}_t^2 + h_3 \cdot \mathbf{y}_t^3 + h_4 \cdot \mathbf{y}_t^4 + \mathbf{n}_t. \tag{4.11}$$

The received signal $\mathbf{r}_t$ is then correlated with $\bar{\mathbf{c}}_1$, $\bar{\mathbf{c}}_2$, $\bar{\mathbf{c}}_3$ and $\bar{\mathbf{c}}_4$ according to Section 2.3.2. Differential decoding is carried out by using the received data of two consecutive time slots in a similar fashion to Equation (2.13) in order to arrive at $\frac{1}{2} \cdot \sum_{i=1}^{2} |h_i|^2 \cdot \sqrt{\sum_{j=1}^{2} |v_t^j|^2} \cdot x_t^k + N_k$.

Based on the above, the twin-layer four-antenna-aided DSTS scheme transmits two SP symbols in $2T_b$ duration. Specifically, the first and second antennas transmit one SP symbol in the same fashion as Section 2.3 with the aid of $\bar{\mathbf{c}}_1$ and $\bar{\mathbf{c}}_2$ in two time slots, while the third and fourth transmit antennas transmit another SP symbol in the same time period with the aid of $\bar{\mathbf{c}}_3$ and $\bar{\mathbf{c}}_4$. Thus, this scheme transmits two SP symbols in $2T_b$ duration resulting in an effective transmission rate of $2 \times 1/2T_b = 1/T_b$, which is effectively four times that of the single layer four-antenna-aided DSTS-SP system. In other words, the twin-layer scheme transmits four SP symbols in $4T_b$ time duration compared to a single SP symbol in the single layer DSTS scheme of Section 4.3.1.

4.4 Variable Spreading Factor Based Adaptive Rate DSTS

In this section we discuss the employment of Variable Spreading Factor (VSF) codes in adaptive rate DSTS-SP systems, where the chip rate is kept constant and hence so is the bandwidth, while the effective bit rate is varied by varying the spreading factor over the course of transmission. For example, when stipulating a constant chip rate, the number of bits transmitted using a SF of 4 is half of that when employing SF=2.

When the channel quality is high, a low SF can be used in order to increase the throughput and conversely, when the channel conditions are hostile, a high SF is employed for maintaining the target BER performance [25]. To elaborate further, Figure 4.5 shows the BER performance of the DSTS-SP system versus the SNR in conjunction with different spreading factors. Figure 4.5 illustrates that using orthogonal VSFs does not affect the BER versus SNR=E_s/N_0

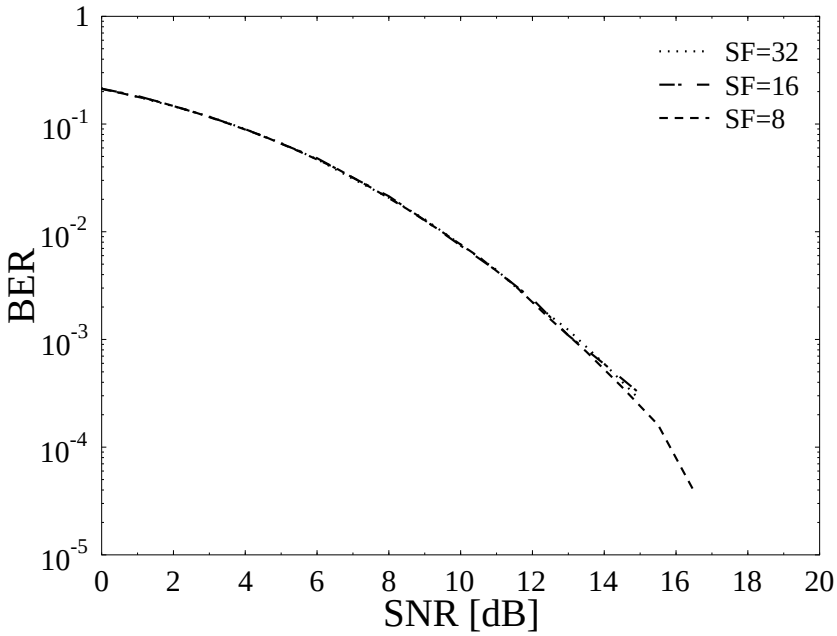

Figure 4.5: BER versus SNR performance of the DSTS-SP scheme in conjunction with L=16 and three different spreading factors.

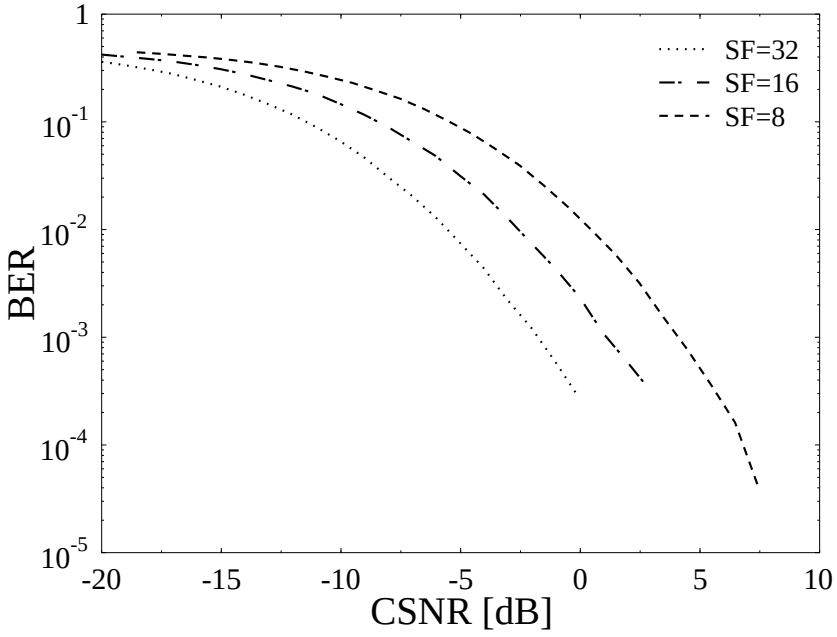

Figure 4.6: BER versus CSNR performance of the DSTS-SP scheme in conjunction with L=16 and three different spreading factors, where SNR = CSNR $\times$ SF.

performance, where E_s is the spread symbol's energy. Hence, no performance gain is attained when comparing the adaptive-rate scheme to a fixed-rate one [25]. However, Figure 4.6 demonstrates that plotting the BER curves versus the chip SNR (CSNR) defined as $E_s/N_0/SF$ results in SF dependent BER performance. Therefore, it can be concluded that upon accommodating the channel quality fluctuations using VSFs, the spread symbol's SNR is varied accordingly for the sake of maintaining a constant CSNR according to the expression SNR = CSNR × SF [25]. For example, when the channel quality is high and hence a low SF is used, the transmitter power -which is proportional to the SNR at a given fixed N_0 value- is also reduced. Therefore, the CSNR is always maintained at the specific value associated with the highest SF. In other words, the VSF regime accommodates the channel quality variations by adapting the SF according to the near-instantaneous channel quality without increasing the transmitted power above that associated with the highest SF [25]. When the SF is decreased, the SNR is proportionately decreased.

4.5 Variable Code Rate Iteratively Detected DSTS-SP System

As already discussed in Chapter 2, the detected DSTS signals can be represented by Equation (2.22), where a received SP symbol $\tilde{\mathbf{s}}$ is constructed from the estimates $\tilde{a}_1$, $\tilde{a}_2$, $\tilde{a}_3$ and $\tilde{a}_4$. In Chapter 3 we presented a detailed account of how iterative detection is carried out. The SP symbol $\tilde{\mathbf{s}}$ carries B_{sp} channel-coded bits $\mathbf{b} = b_0, \ldots, b_{B_{sp}-1} \in \{0, 1\}$, and the corresponding LLRs of the bits can be computed in a similar manner to that discussed in Chapter 3.

Naturally, the code rate of the RSC code employed affects both the system's performance as well as the throughput. More specifically, as the RSC code rate increases, the system's effective throughput increases at the expense of degrading the system's performance. Therefore, when the channel SNR is low and hence the resultant BER is higher than the target BER, a powerful low throughput low-rate RSC code is activated. By contrast, when the channel quality is high and hence the resultant BER is lower than the target BER, a higher throughput scheme corresponding to a higher-rate RSC code is activated.

4.6 Results and Discussions

We consider SP modulation associated with L=16 and DSTS employing four transmit antennas and a single receive antenna in order to demonstrate the performance improvements achieved by the proposed adaptive system. All simulation parameters are listed in Table 4.1, where BE represents the bandwidth efficiency of the system in bits/sec/Hz. The target BER of the system is selected to be 10^{-3}.

SP Modulation	L=16
Number of Tx Antennas	4
Number of Rx Antennas	1
Channel	Correlated Rayleigh Fading with f_D=0.01
Mode 1	Four Tx antennas DSTS-SP system SF=32, RSC code-rate=1/4, BE=0.25
Mode 2	Four Tx antennas DSTS-SP system SF=32, RSC code-rate=1/2, BE=0.5
Mode 3	Two Groups of two Tx antennas DSTS-SP system,SF=16, RSC code-rate=1/6,BE=4/3
Mode 4	Two Groups of two Tx antennas DSTS-SP system,SF=16, RSC code-rate=1/4,BE=2
Mode 5	Two Groups of two Tx antennas DSTS-SP system,SF=16, RSC code-rate=1/2,BE=4
Mode 6	Two Groups of two Tx antennas DSTS-SP system,SF=8, No channel coding,BE=16

Table 4.1: Proposed adaptive system parameters.

Figure 4.7 plots the BER as well as the bandwidth efficiency performance of the proposed adaptive iteratively detected DSTS-SP system. Due to employing time-variant modes, the performance results are plotted versus SNR on the x-axis. The SNR can be converted to E_b/N_0 value upon dividing the SNR by the bandwidth efficiency of the system. The performance of the adaptive system is evaluated by analysing the BER and the bandwidth efficiency expressed in bits/sec/Hz. The BER curve of the adaptive DSTS-SP system, which can be read by referring to the y-axis on the left of the figure, is plotted along with those of the non-adaptive modes. The system employs an interleaver depth ranging between $48,000$ bits and $16,000$ bits depending on the code rate of the RSC code employed. Moreover, six iterative detection iterations are employed in conjunction with the system parameters outlined in Table 4.1. The BER performance reaches the target BER around SNR =5 dB and it does not exceed the target BER for higher SNRs, while switching between the different transmission modes.

The y-axis at the right of Figure 4.8 plots the achievable effective bandwidth efficiency of the proposed adaptive iteratively detected DSTS-SP system, while employing an interleaver depth ranging from $48,000$ bits to $16,000$ bits depending on the transmission mode employed. Six iterative detection iterations and the system parameters outlined in Table 4.1 were invoked. Depending on the channel quality quantified in terms of the channel SNR, the transmitter activates one of the transmission modes outlined in Table 4.1. The bandwidth efficiency of the system varies from 0.25 bits/sec/Hz for the minimum-throughput mode to 16 bits/sec/Hz for the highest-throughput mode. For example, if we calculate the bandwidth efficiency of mode 1,

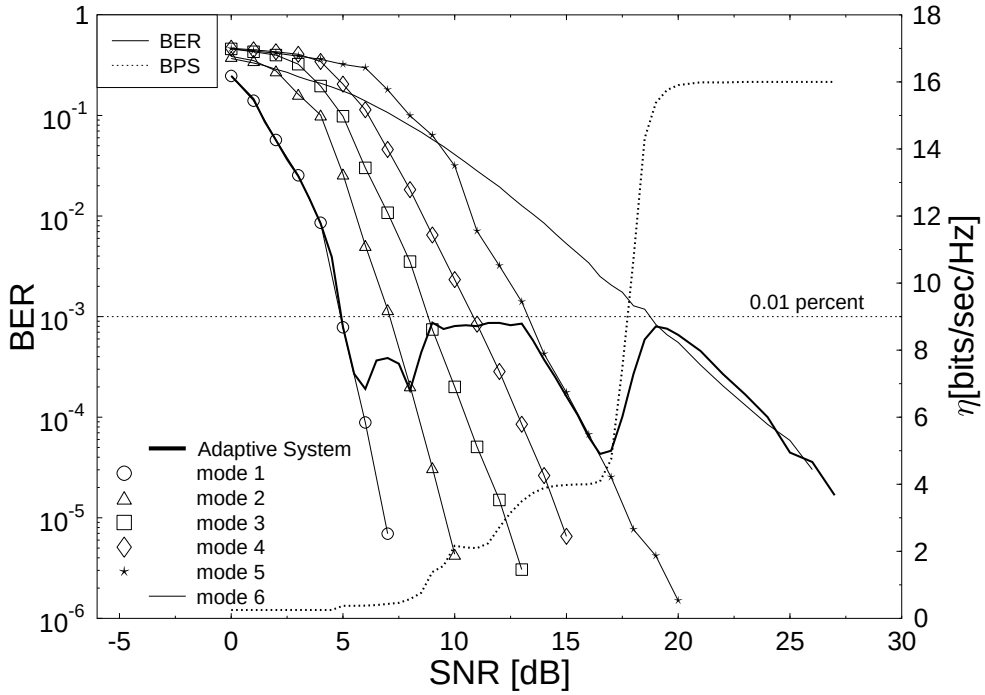

Figure 4.7: BER and throughput performance of the proposed iteratively detected adaptive DSTS-SP system for a target BER of 10^{-3}.

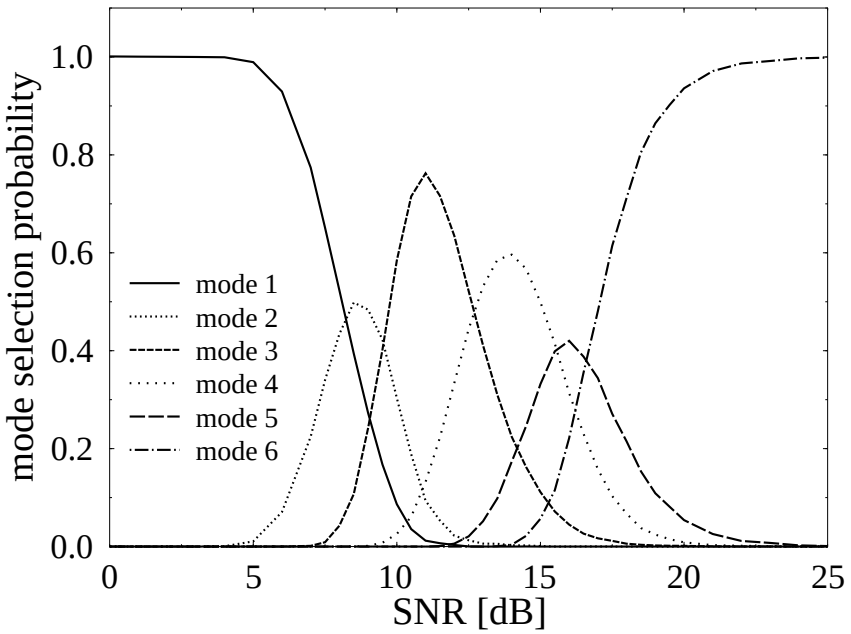

Figure 4.8: The mode selection probability of the proposed adaptive DSTS-SP system at a target BER of 10^{-3}.

employing the L=16 SP modulation scheme using SF=32 and an RSC code rate of 1/4 yields $4 \cdot 1/4 \cdot 1/4$=0.25 bit/sec/Hz, since each SP symbol is transmitted in four time slots. Similarly, for the highest-throughput mode using the L=16 SP modulation scheme, SF=8 and no channel coding, we arrive at $2 \cdot 4 \cdot 4 \cdot 1/2$=16 bit/sec/Hz, since two SP symbols are transmitted in two time slot.

Finally, Figure 4.8 portrays the mode selection probability of the proposed adaptive iteratively detected DSTS-SP system. It is clear from the figure that as the average SNR increases, the higher-throughput systems are employed more often.

4.7 Chapter Conclusion and Summary

In this chapter we proposed a novel adaptive DSTS system that exploits the advantages of differential encoding, iterative demapping as well as SP modulation, while adapting the system parameters for the sake of achieving the highest possible bandwidth efficiency as well as maintaining a given target BER. The proposed adaptive DSTS-SP scheme benefits from a substantial diversity gain, while using four transmit antennas without the need for pilot-assisted channel envelope estimation and coherent detection. The proposed scheme reaches the target BER of 10^{-3} at an SNR of about 5 dB and maintains it for SNRs in excess of this value, while increasing the effective throughput. The system's bandwidth efficiency varies from 0.25 bits/sec/Hz to 16 bits/sec/Hz.

Furthermore, in the presence of large-scale shadow fading, MIMO systems perform poorly, since the diversity gain that is based on the fact that the spatial channels fade independently, decreases in the presence of shadow fading. Therefore, the adaptive MIMO scheme presented constitutes a feasible design alternative in the presence of shadow fading.

Chapter 5

Layered Steered Space-Time Codes

5.1 Introduction

Time-varying multi-path fading imposes a fundamental limitation on wireless transmissions, which can be counteracted by employing Multiple-Input Multiple-Output (MIMO) schemes [26]. More explicitly, information theoretic studies of [33, 34] have revealed that a MIMO system attains a higher capacity than a single-input single-output system. In [81], Wolniansky *et al.* proposed the multi-layer MIMO structure known as the Vertical Bell Labs Layered Space-Time (V-BLAST) scheme, whose transceiver is capable of providing a tremendous increase of a specific user's effective bandwidth efficiency without the need for any increase in the transmitted power or in the system's bandwidth.

On the other hand, Space-Time Block Codes (STBC) [44,46] constitute a powerful transmit diversity scheme, which uses low-complexity linear processing at the receiver and is capable of achieving the maximum possible diversity gain. Since the V-BLAST structure is capable of achieving the maximum multiplexing gain, while the STBC scheme attains the maximum antenna diversity gain, it was proposed in [108] to combine the benefits of these two techniques for the sake of providing both antenna diversity as well as bandwidth efficiency gains. This hybrid scheme was improved in [109] by optimising the decoding order of the different antenna layers. Furthermore, beamforming [103] constitutes an effective technique of reducing the multiple-access interference, where the antenna gain is increased in the direction of the desired user whilst reducing the gain towards the interfering users. In order to achieve additional performance gains, beamforming has also been combined with STBC to attain a higher SNR gain [114].

The concept of combining orthogonal transmit diversity designs with the principle of Sphere Packing (SP) was introduced by Su *et al.* [55] in order to maximise the achievable coding ad-

vantage, where it was demonstrated that the proposed SP aided STBC scheme was capable of outperforming the conventional orthogonal design based STBC schemes of [44, 46]. A further advance was proposed in [58], where the SP demapper of [55] was modified for the sake of accepting the *a priori* information passed to it from the channel decoder as extrinsic information.

In [175], the employment of the iterative detection principle [163] was considered for iterative soft demapping in the context of multilevel modulation schemes combined with channel decoding, where a soft symbol-to-bit demapper was used between the multilevel demodulator and the binary channel decoder. It was also demonstrated in [183] that a recursive inner code is needed in order to maximise the interleaver gain and to avoid the formation of a BER floor, when employing iterative decoding. In [185], unity-rate inner codes were employed for designing low complexity iteratively detected schemes suitable for bandwidth and power limited systems having stringent BER requirements.

Recently, studying the convergence behaviour of iterative decoding has attracted considerable attention. In [186], ten Brink proposed the employment of the so-called Extrinsic Information Transfer (EXIT) characteristics between a concatenated decoder's output and input for describing the flow of extrinsic information through the soft-in soft-out constituent decoders. The concept of EXIT chart analysis has been extended to three-stage concatenated systems in [188, 193, 196].

The novelty and rationale of the proposed system can be summarised as follows:

1. *We amalgamate the merits of V-BLAST, STC and beamforming for the sake of achieving a multiplexing gain, a diversity gain as well as a beamforming gain. The resultant scheme is referred to here as a Layered Steered Space-Time Code (LSSTC). Additionally, the system is combined with multi-dimensional SP modulation, which is capable of maximising the coding advantage of the transmission scheme by jointly designing and detecting the sphere-packed space-time symbols.*

2. *We quantify the capacity of the LSSTC-SP scheme for transmission over both Rayleigh as well as Gaussian channels. Furthermore, we propose a novel technique for quantifying the maximum achievable rate of the system using EXIT charts.*

3. *We propose three near-capacity iteratively detected LSSTC-SP receiver structures, where iterative detection is carried out between an outer code's Decoder I, an intermediate code's Decoder II and an LSSTC-SP demapper. The three proposed schemes differ in the number of inner iterations employed between Decoder II and the SP demapper, as well as in the choice of the outer code which is either a regular Recursive Systematic Convolutional (RSC) code or an Irregular Convolutional Code (IrCC) [191, 194]. On the other hand, the intermediate code employed is a Unity-Rate Code (URC), which is capable of com-*

pletely eliminating the system's error-floor as well as of operating at the lowest possible turbo-cliff SNR without significantly increasing either the associated complexity or the interleaver delay. Furthermore, a comparison between the three iteratively-detected schemes reveals that a carefully designed two-stage[1] *iterative detection scheme is capable of operating sufficiently close to capacity at a lower complexity, when compared to a three-stage*[2] *system employing RSC or a two-stage system employing IrCC as an outer code.*

The rest of the chapter is organised as follows. In Section 5.2 we present the encoding and decoding algorithms of the novel LSSTC scheme and demonstrate how the scheme can be combined with conventional modulation as well as with multi-dimensional sphere packing modulation. In Section 5.3 we quantify the capacity of the LSSTC scheme, followed by a discussion about the iterative detection schemes invoked and the two-dimensional (2D) as well as three-dimensional (3D) EXIT charts employed in Section 5.4. The procedure of computing the maximum achievable rate of the LSSTC-SP scheme using EXIT charts is detailed in Section 5.4.3. The attainable performance of the proposed schemes is studied comparatively in Section 5.5, followed by our conclusions in Section 5.6. In Section 5.7 we provide a chapter summary discussing both the main contributions and the organisation of this chapter.

5.2 Layered Steered Space-Time Codes

5.2.1 Layered Steered Space-Time Codes Using Conventional Modulation

A block diagram of the proposed LSSTC scheme is illustrated in Figure 5.1. The antenna architecture employed in Figure 5.1 has N_t transmit Antenna Arrays (AA) spaced sufficiently far apart in order to experience independent fading and hence to achieve transmit diversity. The L_{AA} number of elements of each of the AAs are spaced at a distance of $d = \lambda/2$ for the sake of achieving a beamforming gain, where λ represents the carrier's wavelength. Furthermore, the receiver is equipped with $N_r \geqslant N_t$ antennas. According to Figure 5.1, a block of B input information symbols is serial-to-parallel converted to K groups of symbol streams of length B_1, B_2, $\cdots$, B_K, where $B_1 + B_2 + \cdots + B_K = B$. Each group of B_k symbols, $k \in [1, K]$, is then encoded by a component space-time code STC_k associated with m_k transmit AAs, where $m_1 + m_2 + \cdots + m_K = N_t$.

In this chapter, we consider transmissions over a temporally correlated narrowband Rayleigh

[1] A two-stage system employs iterations between the outer code's decoder and the intermediate code's decoder, but no iterations are employed between the intermediate code's decoder and the SP demapper.

[2] A three-stage system employs iterations between the SP demapper and the intermediate code's decoder, which we refer to as inner iterations, as well as between the outer code's decoder and the intermediate code's decoder, which are referred to as outer iterations.

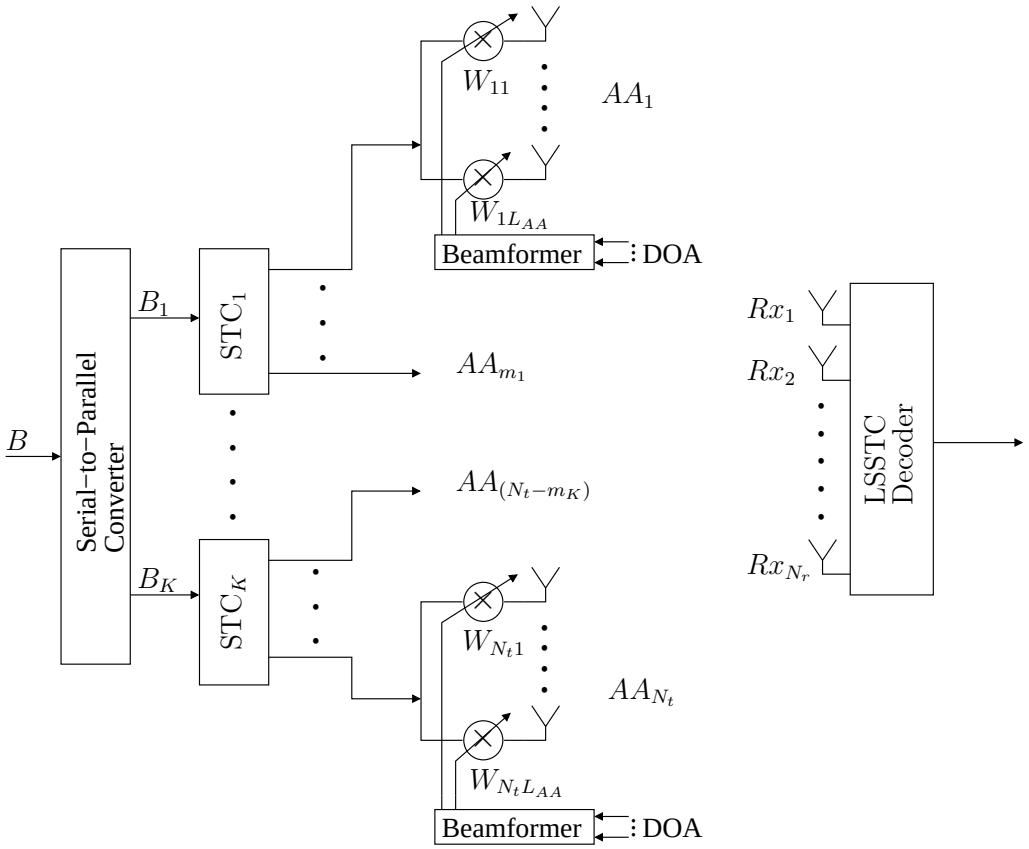

Figure 5.1: Layered steered space-time code system block diagram.

fading channel associated with a normalised Doppler frequency of $f_D = f_d T_s = 0.01$, with f_d being the Doppler frequency and T_s the symbol duration, while the spatial channel coefficients are independent. The complex Additive White Gaussian Noise (AWGN) of $n = n_I + jn_Q$ contaminates the received signal, where n_I and n_Q are two independent zero-mean Gaussian random variables having a variance of $N_0/2$ per dimension.

The L_{AA}-dimensional Spatial-Temporal (ST) Channel Impulse Response (CIR) vector spanning the mth transmitter AA, $m \in [1, \cdots, N_t]$, and the nth receiver antenna, $n \in [1, \cdots, N_r]$, can be expressed as

$$\mathbf{h}_{nm}(t) = \mathbf{a}_{nm}(t)\delta(t-\tau_k) = \left[a_{nm,0}(t), \ldots, a_{nm,(L_{AA}-1)}(t)\right]^T \delta(t-\tau_k), \tag{5.1}$$

where τ_k is the signal's delay and $a_{nm,l}(t)$ is the CIR with respect to the mnth link and the lth element of the mth AA. Based on the assumption that the array elements are separated by half a wavelength, we have

$$\mathbf{a}_{nm}(t) = \alpha_{nm}(t) \cdot \mathbf{d}_{nm}, \tag{5.2}$$

where $\alpha_{nm}(t)$ is a Rayleigh faded envelope,

$$\mathbf{d}_{nm} = [1, \exp(j[\pi \sin(\psi_{nm})]), \ldots, \exp(j[(L_{AA}-1)\pi \sin(\psi_{nm})])]^T \tag{5.3}$$

and ψ_{nm} is the nmth link's Direction Of Arrival (DOA). As for the AA specific DOA, we consider a scenario where the distance between the transmitter and the receiver is significantly higher than that between the AAs and thus we can assume that the signals arrive at the different AAs in parallel, i.e. the DOA at the different AAs is the same.

The received baseband data matrix $\mathbf{Y}$ can be expressed as

$$\mathbf{Y} = \mathbf{HWX} + \mathbf{N}, \tag{5.4}$$

where $\mathbf{X}$ represents the transmitted symbols matrix, $\mathbf{H}$ is an $(N_r \times N_t)$ matrix whose entries of $\mathbf{h}_{nm}$ are defined in Equation (5.1) and $\mathbf{N}$ denotes the AWGN matrix whose entries have a variance of $N_0/2$ per dimension. Furthermore, $\mathbf{W}$ is a diagonal AA weight matrix, whose diagonal entry $\mathbf{w}_{mn}$ is the L_{AA}-dimensional weight vector for the mth beamformer AA and the nth receive antenna. In this scenario, the MRC criterion based transmit beamformer, which constitutes an effective solution to maximising the antenna gain, is the optimum beamformer. Let

$$\mathbf{w}_{mn} = \mathbf{d}_{nm}^{\dagger}, \tag{5.5}$$

where the superscript † represents the Hermitian of the matrix. Then the received signal can be expressed as

$$\mathbf{Y} = L\widehat{\mathbf{H}}\mathbf{X} + \mathbf{N}, \tag{5.6}$$

where $\widehat{\mathbf{H}}$ is an $(N_r \times N_t)$ matrix, whose entries are α_{nm}. Moreover, $\mathbf{Y}$ can be written as

$$\mathbf{Y} = L\sum_{k=1}^{K} \widehat{\mathbf{H}}_k \mathbf{x}_k + \mathbf{N}, \tag{5.7}$$

where $\mathbf{x}_k$ represents the component STC used at layer k, with $k \in [1, \cdots, K]$.

The most beneficial decoding order of the STC layers is determined on the basis of detecting the highest-power layer first for the sake of a high correct detection probability. For simplicity, let us consider the case of $K = 2$ STBC layers and that layer 1 is detected first, which allows us to eliminate the interference caused by the signal of layer 2. However, the proposed concept is applicable to arbitrary STCs and to an arbitrary number of layers K. For this reason, the decoder of layer 1 has to compute a matrix $\mathbf{Q}$, so that we have $\mathbf{Q} \cdot \widehat{\mathbf{H}}_2 = 0$. Therefore, the decoder computes an orthonormal basis for the left null space of $\widehat{\mathbf{H}}_2$ and assigns the vectors of the basis to the rows of $\mathbf{Q}$. Multiplying $\mathbf{Q}$ by $\mathbf{Y}$ suppresses the interference of layer 2 originally imposed on layer 1 and generates a signal which can be decoded using maximum likelihood STBC detection. Then, the decoder subtracts the remodulated contribution of the decoded symbols of layer 1 from the composite twin-layer received signal $\mathbf{Y}$. Finally, the decoder applies direct STBC decoding to the second layer, since the interference imposed by the first layer has

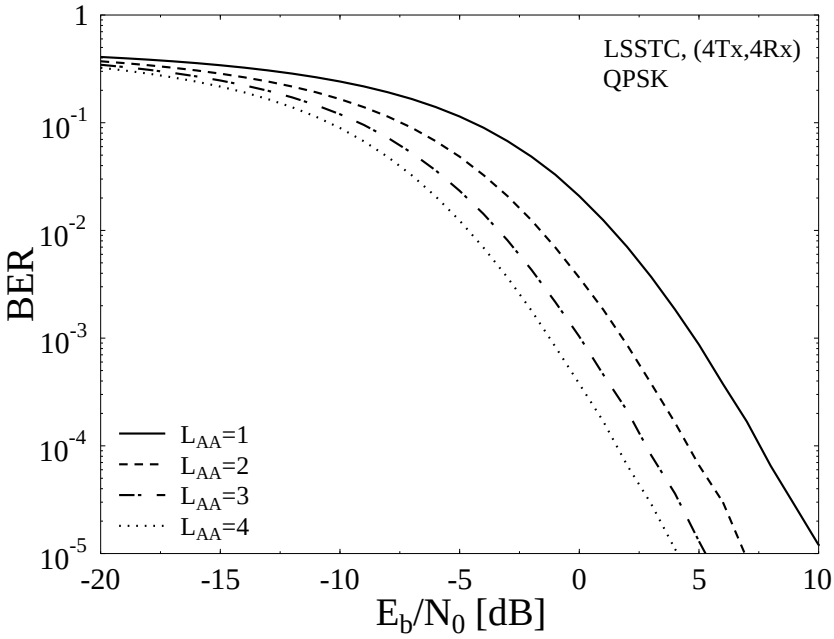

Figure 5.2: BER performance of a QPSK modulated $N_t \times N_r = 4 \times 4$ LSSTC system for variable number L_{AA} of elements per AA.

been eliminated. This group-interference cancellation procedure can be generalised to any N_t and K values.

We consider a system employing $N_t \times N_r = 4 \times 4$ antennas and $K = 2$ layers in order to demonstrate the performance improvements achieved by a DownLink (DL) scheme, where a BS employing $N_t = 4$ transmit antennas is communicating with a laptop receiver employing $N_r = 4$ back-plane antennas. The system employs QPSK modulation and considers transmission over a temporally correlated Rayleigh fading channel. Additionally, we assume that the channel state information is perfectly known at the receiver. We also assume that the transmitter has full knowledge of the DOA without any estimation or estimation errors. Figure 5.2 shows the DL BS beamforming gain achieved upon increasing the number of beam-steering elements L_{AA} in the AA, while maintaining the same total number of AAs. As shown in Figure 5.2, when the number of beam-steering elements L_{AA} increases, the achievable BER performance substantially improves.

5.2.2 Layered Steered Space-Time Codes Using Sphere Packing Modulation

According to the previous discussion, it becomes clear that the decoded signal represents a scaled version of the transmitted signal corrupted by noise. This observation implies that the diversity product of the LSSTC scheme is determined by the minimum Euclidean distance of all legitimate transmitted vectors. Hence, in order to maximise the achievable coding advantage, it was proposed in [55] to use SP schemes that maximise the minimum Euclidean distance

of the transmitted signal vectors. Our idea is to jointly design the legitimate m_k-component complex-valued vectors $(x^1,x^2,\cdots,x^{m_k})$ transmitted from layer k, $k \in [0,\cdots,K]$, so that they are represented by a single phasor point selected from a SP constellation corresponding to a $2m_k$-dimensional real-valued lattice having the best known minimum Euclidean distance in the $2m_k$-dimensional real-valued space $\mathbb{R}^{2m_k}$.

In what follows we assume that each layer is constituted by a twin-AA STBC scheme, i.e. we have $m_k = 2$, $\forall\, k \in [0, K]$, which means that the SP design required is $2m_k$=4-dimensional. To summarise, according to the previous discussion, x^1 and x^2 represent independent conventional PSK modulated symbols transmitted from the first and second transmit AA and no effort is made to jointly design a signal constellation for the various combinations of x^1 and x^2. By contrast, in the case of SP, these symbols are designed jointly in order to further increase the attainable coding advantage. Assuming that there are L legitimate vectors $(x^{l,1}, x^{l,2})$, $l = 0, 1, \ldots, L-1$, where L represents the number of sphere-packed modulated symbols, the transmitter then has to choose the modulated signal from these L legitimate symbols to be transmitted over the two AAs in layer $k \in [1,\cdots,K]$.

In the four-dimensional real-valued Euclidean space $\mathbb{R}^4$, the lattice D_4 is defined as a SP constellation having the best minimum Euclidean distance from all other $(L-1)$ legitimate 4-component constellation points in $\mathbb{R}^4$ [213]. More specifically, D_4 may be defined as a lattice that consists of all legitimate sphere-packed constellation points having integer coordinates $[a^{l,1}$ $a^{l,2}$ $a^{l,3}$ $a^{l,4}]$ subjected to the SP constraint of

$$a^{l,1} + a^{l,2} + a^{l,3} + a^{l,4} = \kappa, \tag{5.8}$$

where κ is an even integer [213]. Assuming that $\mathbf{S} = \{\mathbf{s}^l = [a^{l,1}, a^{l,2}, a^{l,3}, a^{l,4}] \in \mathbb{R}^4 : 0 \le l \le L-1\}$ constitutes a set of L legitimate constellation points from the lattice D_4 having a total energy of

$$E_{total} \stackrel{\triangle}{=} \sum_{l=0}^{L-1}(|a^{l,1}|^2 + |a^{l,2}|^2 + |a^{l,3}|^2 + |a^{l,4}|^2), \tag{5.9}$$

upon introducing the notation

$$\mathbf{C}_l = \{x^{l,1}, x^{l,2}\} = T_{sp}(a^{l,1}, a^{l,2}, a^{l,3}, a^{l,4}) = \left\{a^{l,1} + ja^{l,2}, a^{l,3} + ja^{l,4}\right\}, \tag{5.10}$$

we have a set of constellation symbols, $\{\mathbf{C}_l\colon\ 0 \le l \le L-1\}$, leading to the design of LSSTC signals, whose diversity product is determined by the minimum Euclidean distance of the set of L legitimate constellation points in $\mathbf{S}$.

Figure 5.3 depicts the BER performance of the SP modulated LSSTC scheme in conjunction with GM and $L = 16$, while employing $N_t = 4$, $N_r = 4$ and a variable number L_{AA} of elements per AA. The results in Figure 5.3 corresponds to the scenario, where the channel is assumed

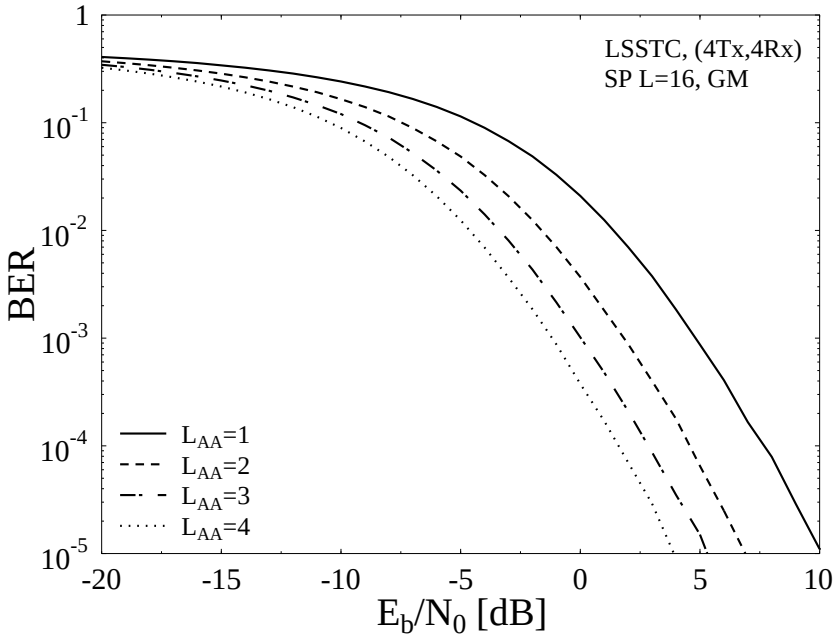

Figure 5.3: BER performance of the SP modulated $N_t \times N_r = 4 \times 4$ LSSTC system in conjunction with $L = 16$ for variable number L_{AA} of elements per AA.

to be perfectly known at the receiver. Figure 5.3 shows the DL BS beamforming gain achieved by increasing the number of beam-steering elements L_{AA} in the AA for the system employing $N_t \times N_r = 4 \times 4$ antennas and $K = 2$ layers, while maintaining the same total number of AAs. As shown in Figure 5.3, when the number of beam-steering elements L_{AA} increases, the achievable BER performance substantially improves.

5.3 Capacity of Layered Steered Space-Time Codes

Upon using the decoding order of $(1, 2, \cdots, K)$, group k will have a diversity order of $m_k \times (N_r - N_t + m_1 + m_2 + \cdots + m_k) = m_k \times N_{rk}$. Thus, the LSSTC decoded signal of layer k, *assuming perfect interference cancellation*, can be described as

$$\tilde{x}_k = L \sum_{r=1}^{N_{rk}} \sum_{t=1}^{m_k} \alpha_{rt} \cdot x_k + \Delta = \sum_{r=1}^{N_{rk}} \chi^2_{2m_k r} \cdot x_k + \Delta_k, \tag{5.11}$$

where $\chi^2_{2m_k r} = L \sum_{t=1}^{m_k} \alpha_{rt}$ represents a Chi-squared distributed random variable having $2m_k$ degrees of freedom and Δ_k is the AWGN after decoding, which has a variance of $\chi^2_{2m_k r} \cdot N_0/2$ per dimension.

The received sphere-packed symbol $\tilde{\mathbf{s}}_k$ at layer k is then constructed from the estimates $\tilde{x}^1_k$ and $\tilde{x}^2_k$ using the inverse function of T_{sp} introduced in Equation (5.10) as $\tilde{\mathbf{s}}_k = T^{-1}_{sp}(\tilde{x}^1_k, \tilde{x}^2_k)$, where we have $\tilde{\mathbf{s}} = [\tilde{a}^1\ \tilde{a}^2\ \tilde{a}^3\ \tilde{a}^4] \in \mathbb{R}^4$. Therefore, the received sphere-packed symbol $\tilde{\mathbf{s}}_k$ can be

written as

$$\tilde{\mathbf{s}}_k = \sum_{r=1}^{N_{rk}} \chi^2_{2m_k r} \mathbf{s}_k + \acute{\Delta}_k, \tag{5.12}$$

where we have $\acute{\Delta}_k = [\acute{\Delta}_{k1}\ \acute{\Delta}_{k2}\ \acute{\Delta}_{k3}\ \acute{\Delta}_{k4}] \in \mathbb{R}^4$, which is a four-dimensional real-valued Gaussian random variable having a covariance matrix of

$$\sigma^2_{\acute{\Delta}_k} \cdot \mathbf{I}_D = \sigma^2_{\Delta_k} \cdot \mathbf{I}_D = \chi^2_{2m_{k,r}} \cdot N_0/2 \cdot \mathbf{I}_D, \tag{5.13}$$

where we have $D = 4$, since the SP symbol constellation $\mathbf{S}$ is four-dimensional.

Let $\tilde{\mathcal{S}} = (\tilde{\mathbf{s}}_1, \tilde{\mathbf{s}}_2, \cdots, \tilde{\mathbf{s}}_K)^T$, $\mathcal{S} = (\mathbf{s}_1, \mathbf{s}_2, \cdots, \mathbf{s}_K)^T$ and note that in conjunction with K groups there are $M = (L)^K$ number of possible SP phasor combinations, where SP in conjunction with L is used for transmission. Thus, the achievable capacity of the MIMO system proposed for transmission over the Discrete-Input Continuous-Output Memoryless Channel (DCMC) can be derived from that of the discrete memoryless channel as [215, 217]:

$$\begin{aligned} C_{DCMC} &= \max_{p(\mathcal{S}^1),\cdots,p(\mathcal{S}^M)} \sum_{i=1}^{M} \underbrace{\int_{-\infty}^{\infty} \cdots \int_{-\infty}^{\infty}}_{D\text{–fold}} p(\tilde{\mathcal{S}}|\mathcal{S}_i) \cdot p(\mathcal{S}_i) \\ &\cdot \log_2 \left(\frac{p(\tilde{\mathcal{S}}|\mathcal{S}_i)}{\sum_{v=1}^{M} p(\tilde{\mathcal{S}}|\mathcal{S}_v) \cdot p(\mathcal{S}_v)} \right) \cdot d\tilde{\mathcal{S}} \ \ [\text{bit/sym}], \end{aligned} \tag{5.14}$$

where $p(\mathcal{S}_i)$ is the probability of occurrence for the transmitted symbol vector $\mathcal{S}_i$. Furthermore, since the components of the vectors $\mathcal{S}$ and $\tilde{\mathcal{S}}$ are independent, we have

$$p(\tilde{\mathcal{S}}|\mathcal{S}) = \prod_{k=1}^{K} p(\tilde{\mathbf{s}}_k|\mathbf{s}_k). \tag{5.15}$$

Furthermore, according to Equation (5.12), the conditional probability $p(\tilde{\mathbf{s}}_k|\mathbf{s}_k)$ of receiving a four-dimensional signal $\tilde{\mathbf{s}}_k$ at layer k is given by the following PDF:

$$p(\tilde{\mathbf{s}}_k|\mathbf{s}_k) = \frac{1}{\prod_{d=1}^{D=4} \sqrt{\pi N_0 \sum_{r=1}^{N_{rk}} \chi^2_{2m_k r}[d]}} \cdot \exp\left(\sum_{d=1}^{D=4} \sum_{r=1}^{N_{rk}} \frac{-\left(\tilde{\mathbf{s}}_k[d] - \chi^2_{2m_k r}[d] \cdot \mathbf{s}_k[d]\right)^2}{\chi^2_{2m_k r}[d] \cdot N_0} \right). \tag{5.16}$$

Moreover, C_{DCMC} in Equation (5.14) is maximised, when the transmitted symbols are equiprobably distributed, i.e. for $p(\mathcal{S}_i) = \frac{1}{M}$ [215]. Hence, we can write

$$\begin{aligned} \log_2 & \left(\frac{p(\tilde{\mathcal{S}}|\mathcal{S}_i)}{\sum_{v=1}^{M} p(\tilde{\mathcal{S}}|\mathcal{S}_v) \cdot p(\mathcal{S}_v)} \right) = \log_2 \left(\frac{p(\tilde{\mathcal{S}}|\mathcal{S}_i)}{\frac{1}{M} \cdot \sum_{v=1}^{M} p(\tilde{\mathcal{S}}|\mathcal{S}_v)} \right) \\ &= \log_2(M) - \log_2 \left(\sum_{v=1}^{M} \frac{p(\tilde{\mathcal{S}}|\mathcal{S}_v)}{p(\tilde{\mathcal{S}}|\mathcal{S}_i)} \right) = \log_2(M) - \log_2 \left(\sum_{v=1}^{M} \prod_{k=1}^{K} \frac{p(\tilde{\mathbf{s}}_k|\mathbf{s}_{kv})}{p(\tilde{\mathbf{s}}_k|\mathbf{s}_{ki})} \right) \\ &= \log_2(M) - \log_2 \left(\sum_{v=1}^{M} \prod_{k=1}^{K} \exp\left(\Psi_{k,vi}\right) \right), \end{aligned} \tag{5.17}$$

where the term $\Psi_{k,vi}$ is given by

$$\begin{aligned}\Psi_{k,vi} &= \sum_{d=1}^{D=4}\sum_{r=1}^{N_{rk}}\left(-\frac{\left(\tilde{\mathbf{s}}_k[d]-\chi^2_{2m_kr}[d]\mathbf{s}_{k,v}[d]\right)^2}{\chi^2_{2m_kr}[d]\cdot N_0}+\frac{\left(\tilde{\mathbf{s}}_k[d]-\chi^2_{2m_kr}[d]\mathbf{s}_{k,i}[d]\right)^2}{\chi^2_{2m_kr}[d]\cdot N_0}\right)\\ &= \sum_{d=1}^{D=4}\sum_{r=1}^{N_{rk}}\left(-\frac{\left(\chi^2_{2m_kr}[d]\left(\mathbf{s}_{k,i}[d]-\mathbf{s}_{k,v}[d]\right)+\acute{\Delta}_i[d]\right)^2}{\chi^2_{2m_kr}[d]\cdot N_0}+\frac{\left(\acute{\Delta}_i[d]\right)^2}{\chi^2_{2m_kr}[d]\cdot N_0}\right).\end{aligned} \tag{5.18}$$

Finally, Equation (5.14) can be simplified to

$$C_{DCMC}=\log_2(M)-\frac{1}{M}\sum_{i=1}^{M}\prod_{k=1}^{K}E\left[\log_2\left(\sum_{v=1}^{M}\prod_{k=1}^{K}\exp\left(\Psi_{k,vi}\right)\right)|\mathbf{s}_i\right]\quad[\text{bit/sym}], \tag{5.19}$$

where $E[A|B]$ is the expectation of A conditioned on B.

On the other hand, the Continuous-Input Continuous-Output Memoryless Channel (CCMC) capacity of the proposed LSSTC scheme can be expressed as [215, 217]:

$$C_{CCMC}=\sum_{k=1}^{K}E\left[\frac{D}{2}\log_2\left(1+\sum_{r=1}^{N_{rk}}\chi^2_{2m_k,r}\frac{SNR}{N_t}\right)\right]\quad[\text{bit/sym}]. \tag{5.20}$$

Finally, the bandwidth efficiency is related to the capacity according to [215]

$$\eta=\frac{C}{D/2}\quad[\text{bits/sec/Hz}]. \tag{5.21}$$

Figure 5.4 shows the DCMC capacity evaluated from Equation (5.19) for the QPSK assisted LSSTC, when employing $N_t = 4$ transmit antennas, $N_r = 4$ receive antennas as well as $L_{AA} = 1$, 2, 3 and 4 elements per transmit AA. The CCMC [35] capacity of the same multi-functional MIMO scheme was also plotted for comparison in Figures 5.4 based on Equation (5.20). Furthermore, Figure 5.5 compares the achievable bandwidth efficiency of the QPSK modulated LSSTC scheme in conjunction with $N_t \times N_r = 4 \times 4$ while varying the number of elements L_{AA} per AA. Figure 5.5 depicts that as the number of elements per AA increases the achievable bandwidth efficiency improves. Figure 5.5 also compares the achievable CCMC bandwidth efficiency for various L_{AA} values.

On the other hand, Figure 5.6 shows the DCMC capacity evaluated from Equation (5.19) for the LSSTC-SP scheme in conjunction with $L = 16$, when employing $N_t = 4$ transmit antennas, $N_r = 4$ receive antennas and a variable number of elements per AA L_{AA}. The CCMC [35] capacity of the same multi-functional MIMO scheme was also plotted for comparison in Figures 5.6 based on Equation (5.20). Furthermore, Figure 5.7 compares the achievable bandwidth efficiency of the LSSTC-SP scheme in conjunction with $L = 16$, $N_t \times N_r = 4 \times 4$,

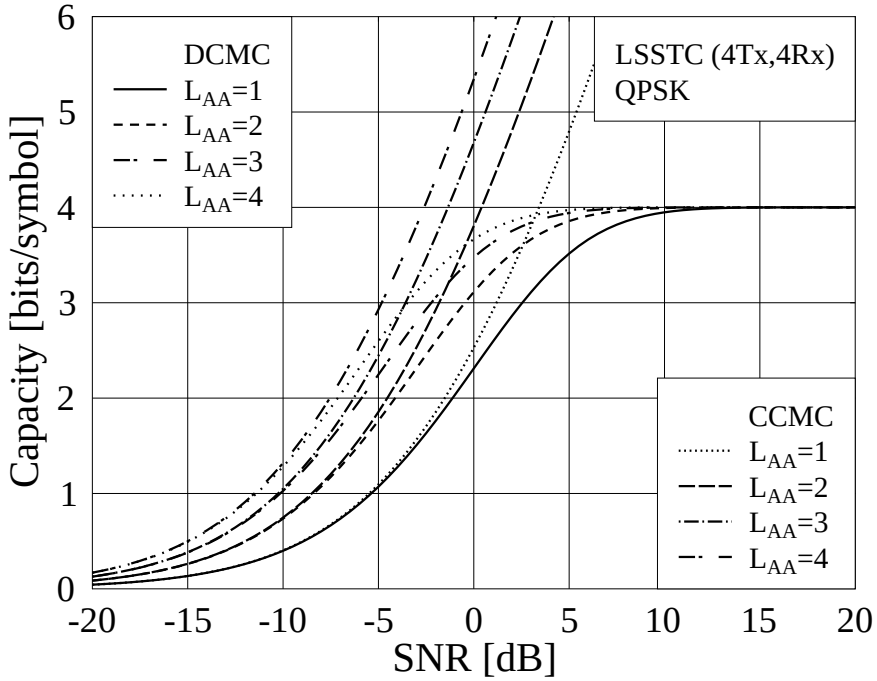

Figure 5.4: Capacity of a QPSK modulated $N_t \times N_r = 4 \times 4$ LSSTC scheme for variable L_{AA} values.

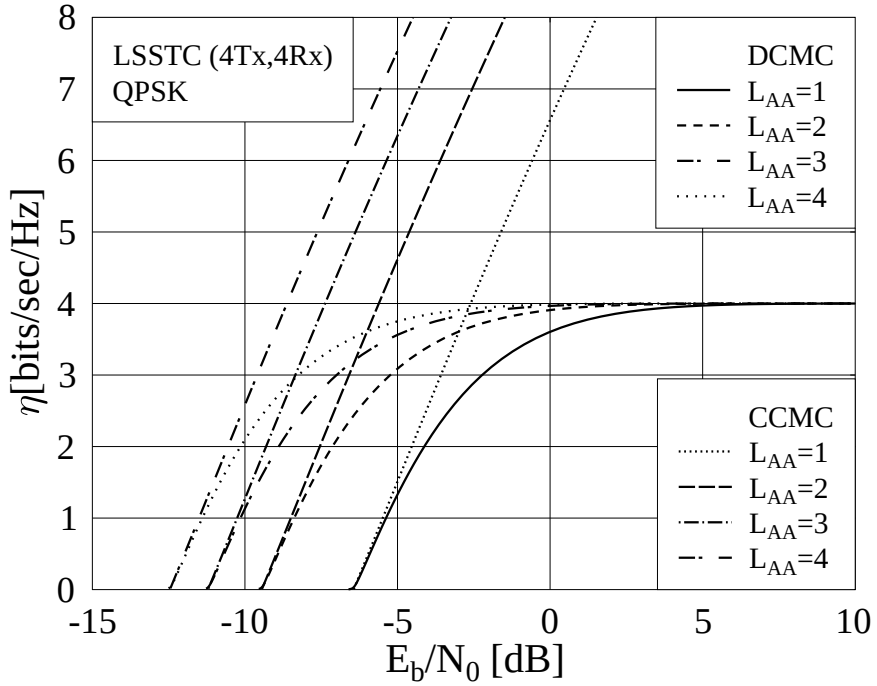

Figure 5.5: Bandwidth efficiency of a QPSK modulated $N_t \times N_r = 4 \times 4$ LSSTC scheme for variable L_{AA} values.

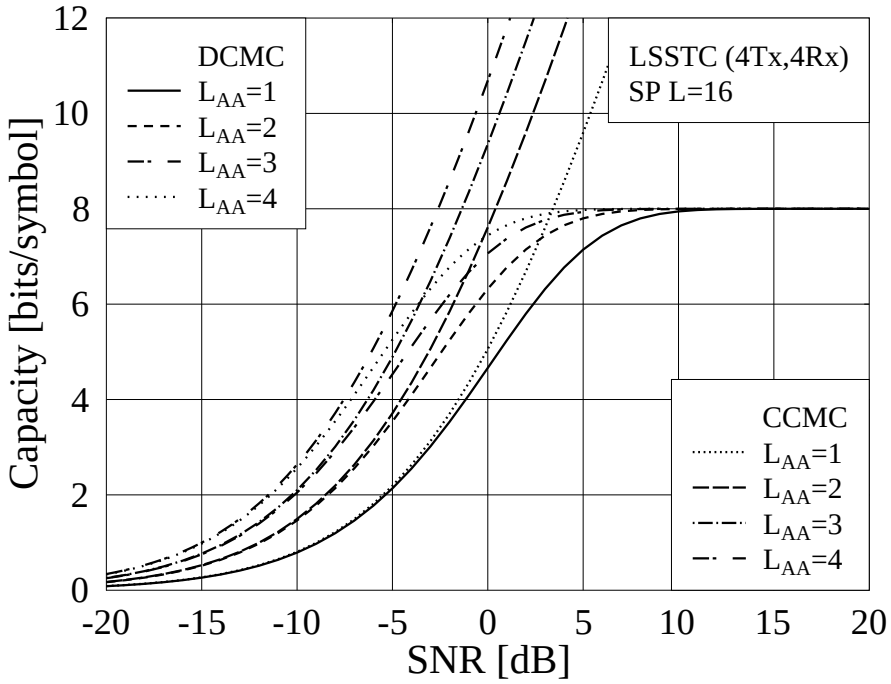

Figure 5.6: Capacity of the SP modulated $N_t \times N_r = 4 \times 4$ LSSTC scheme in conjunction with $L = 16$ for variable L_{AA} values.

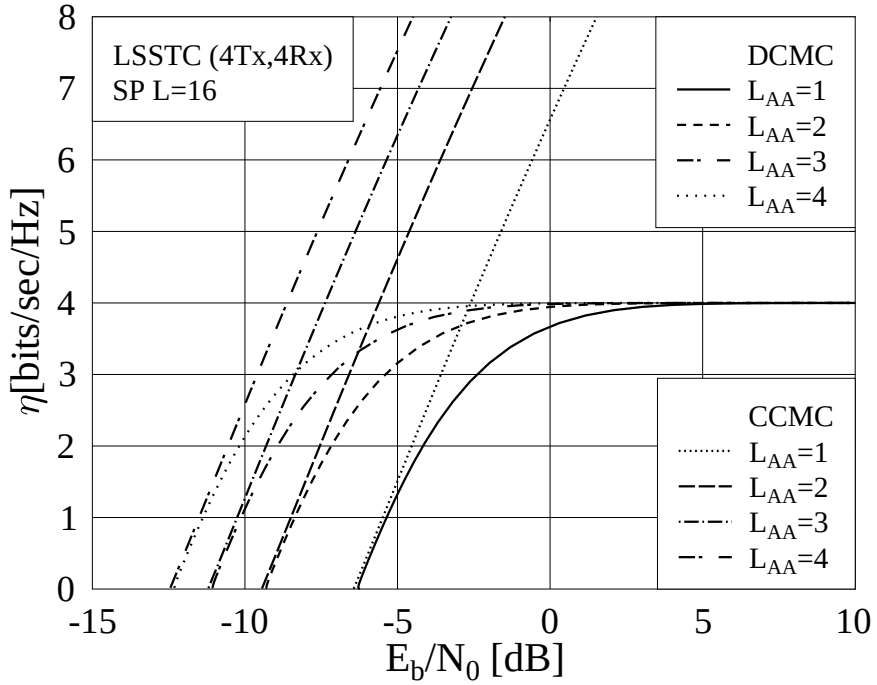

Figure 5.7: Bandwidth efficiency of the SP modulated $N_t \times N_r = 4 \times 4$ LSSTC scheme in conjunction with $L = 16$ for variable L_{AA} values.

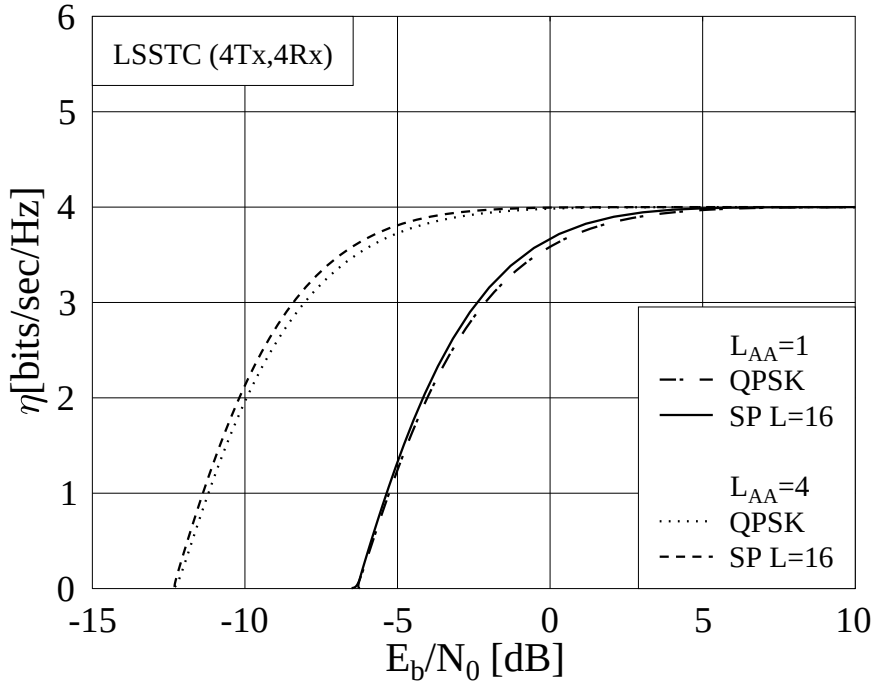

Figure 5.8: Comparison of the bandwidth efficiency of the QPSK and the SP aided scheme in conjunction with the $L = 16$, $N_t \times N_r = 4 \times 4$ based LSSTC scheme for $L_{AA} = 1$ and $L_{AA} = 4$.

while varying the number of elements L_{AA} per AA. Figure 5.7 demonstrates that as the number of elements per AA increases, the achievable bandwidth efficiency improves. Figure 5.7 also compares the achievable CCMC bandwidth efficiency for various L_{AA} values.

Finally, Figure 5.8 compares the attainable bandwidth efficiency of the LSSTC multi-functional MIMO scheme, when QPSK and SP in conjunction with $L = 16$ are employed. As seen in Figure 5.8, when $L_{AA} = 1$ was employed, the SP assisted system had a slightly higher bandwidth efficiency than the QPSK aided system. On the other hand, Figure 5.8 demonstrates that increasing the number of elements per AA to $L_{AA} = 4$ results in improving the bandwidth efficiency of the SP aided system compared to that of its QPSK assisted counterpart.

5.4 Iterative Detection and EXIT Chart Analysis

The block diagram of the LSSTC-aided iteratively detected SP modulation is shown in Figure 5.9. The transmitted source bits $\mathbf{u}_1$ are encoded by the outer channel Encoder I having a rate of R_I. The outer channel encoded bits $\mathbf{c}_1$ are then interleaved by a random bit interleaver Π_1, where the randomly permuted bits $\mathbf{u}_2$ are fed through the URC Encoder II. The encoded bits $\mathbf{c}_2$ at the output of the URC encoder are interleaved by a second random bit interleaver Π_2, producing the permuted bit stream $\mathbf{b}$. After bit interleaving, the SP mapper maps blocks of B_{sp} channel-coded bits $\mathbf{b} = b_0, \ldots, b_{B_{sp}-1} \in \{0, 1\}$ to the L number of legitimate four-dimensional

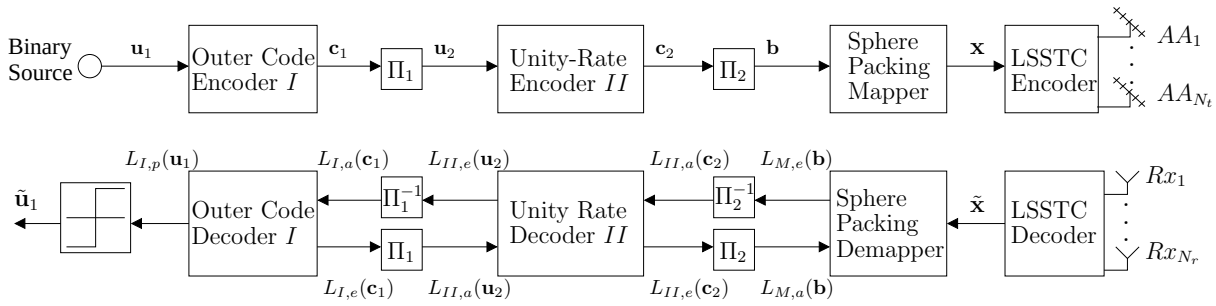

Figure 5.9: Block diagram of the layered steered space-time code employing SP modulation in conjunction with a unity-rate precoder and an outer code.

SP modulated symbols $\mathbf{s}^l \in \mathbf{S}$. The SP modulated symbols $\mathbf{s}$ are then transmitted using the LSSTC transmitter of Section 5.2.

At the receiver side, as shown in Figure 5.9, the received complex-valued symbols are first decoded by the LSSTC-SP decoder in order to produce the received SP soft-symbols $\tilde{\mathbf{s}}$. Then, iterative demapping/decoding is carried out between the SP demapper, the soft-in soft-out URC Decoder II and the soft-in soft-out Decoder I, where extrinsic information can be exchanged between the three constituent demapper/decoder modules.

More specifically, $L_{\cdot,a}(\cdot)$ in Figure 5.9 represents the *a priori* information, expressed in terms of the log-likelihood ratios (LLRs) of the corresponding bits, whereas $L_{\cdot,e}(\cdot)$ represents the *extrinsic* LLRs of the corresponding bits. The iterative process is performed for a number of consecutive iterations. During the last iteration, only the LLR values $L_{I,p}(\mathbf{u_1})$ of the original data information bits $\mathbf{u}_1$ are required, which are passed to a hard decision decoder in order to determine the estimated transmitted source bits $\tilde{\mathbf{u}}_1$, as shown in Figure 5.9.

In this chapter we present three iterative-detection-aided SP assisted LSSTC schemes. The first and second systems, referred to as System 1 and System 2 respectively, employ no iterations between the URC Decoder II and the SP demapper of Figure 5.9, i.e. no inner iterations. However, the two systems differ in the choice of the outer Encoder I, namely while System 1 employs a regular RSC code, System 2 uses an IrCC [191,194]. Finally, System 3 invokes three-stage iterative detection exchanging extrinsic information between the SP demapper, the URC Decoder II and the outer RSC Decoder I. In what follows, all the results presented characterise an LSSTC-SP scheme using $(N_t \times N_r) = (4 \times 4)$ and $L_{AA} = 4$ elements per AA in conjunction with the system parameters outlined in Table 5.1.

5.4.1 Two-Stage Iterative Detection Scheme

In this section, System 1 and System 2 are described, where the exchange of extrinsic information is carried out between the outer Decoder I and the URC Decoder II only, i.e. no iterations

Sphere Packing Modulation	L=16
Number of Transmitter AAs N_t	4
Number of Elements per AA L_{AA}	4
Number of Receiver Antennas N_r	4
Channel	Correlated Rayleigh Fading
Normalised Doppler frequency	0.01
Encoder I	
System 1	RSC(2,1,3), $(G_r, G) = (7, 5)_8$
System 2	Half-rate IrCC
System 3	RSC(2,1,2), $(G_r, G) = (3, 2)_8$
Encoder II	Unity-rate code
Generator	$(G_r, G) = (3, 2)_8$
Interleaver depth D_{int}	180,000 bits

Table 5.1: LSSTC aided iterative detection system parameters.

are carried out between the URC Decoder II and the SP demapper. As seen in Figure 5.10, the URC Decoder II processes the information forwarded by the SP demapper in conjunction with the *a priori* information $L_{II,a}(\mathbf{u}_2)$ in order to generate the *a posteriori* probability. The *a priori* LLR values of the URC decoder are subtracted from the *a posteriori* LLR values for the sake of generating the extrinsic LLR values $L_{II,e}(\mathbf{u}_2)$, as seen in Figure 5.10. Next, the soft bits $L_{I,a}(\mathbf{c}_1)$ are passed to the outer Decoder I of Figure 5.10 in order to compute the *a posteriori* LLR values for all the channel-coded bits. As seen in Figure 5.10, the extrinsic information $L_{I,e}(\mathbf{c}_1)$ is then fed back to the URC Decoder II as the *a priori* information $L_{II,a}(\mathbf{u}_2)$ after appropriately reordering them using the interleaver Π_1 of Figure 5.10. The soft-in soft-out Decoder II of Figure 5.10 exploits the *a priori* information for the sake of providing improved extrinsic LLR values, which are then passed to the outer Decoder I and then back to the Decoder II for further iterations.

5.4.1.1 2D EXIT Charts

As discussed in Chapter 3, the main objective of employing EXIT charts [186, 189] is to predict the convergence behaviour of the iterative decoding process by examining the evolution of the input/output Mutual Information (MI) exchange between the constituent decoders in consecutive iterations.

Let $I_{\cdot,a}(x)$, $0 \leq I_{\cdot,a}(x) \leq 1$, denote the MI between the *a priori* LLRs $L_{\cdot,a}(x)$ as well as the

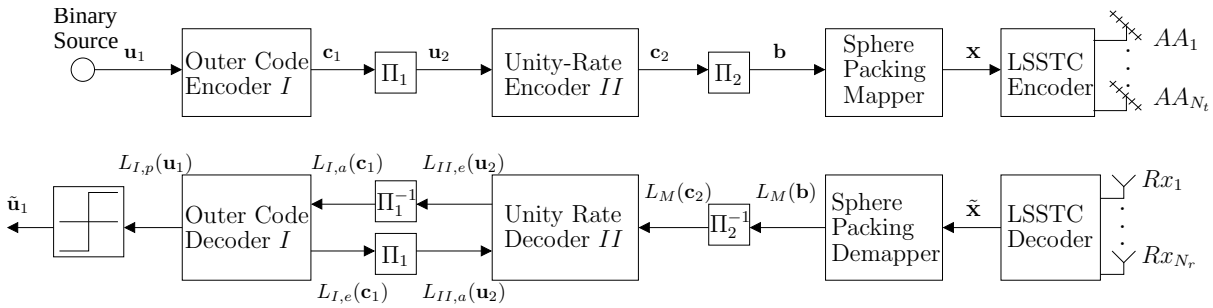

Figure 5.10: Block diagram of the layered steered space-time code employing SP modulation in conjunction with a unity-rate precoder and an outer code. The receiver employs iterative detection between the outer code's decoder and the precoder's decoder.

corresponding bits x and let $I_{\cdot,e}(x)$, $0 \leq I_{\cdot,e}(x) \leq 1$, denote the MI between the *extrinsic* LLRs $L_{\cdot,e}(x)$ and the corresponding bits x.

In the two-stage iterative detector of System 1 and System 2 of Figure 5.10, the EXIT characteristics of Decoders I and II can be described by the following two EXIT functions [186, 196]:

$$I_{I,e}(\mathbf{c}_1) = T_{I,c_1}\left[I_{I,a}(\mathbf{c}_1)\right] \tag{5.22}$$

$$I_{II,e}(\mathbf{u}_2) = T_{II,u_2}\left[I_{II,a}(\mathbf{u}_2), E_b/N_0\right]. \tag{5.23}$$

Figure 5.11 shows the EXIT chart of System 1 employing an iteratively detected RSC-coded LSSTC-SP system in conjunction with $L = 16$ and Gray mapping (GM), where iterations are carried out between the outer 1/2-rate RSC code and the inner URC decoders, while no iterations are invoked between the URC decoder and the SP demapper. The system employs a 1/2-rate memory-2 RSC code, denoted as RSC(2,1,3), in conjunction with an octal generator polynomial of $(G_r, G) = (7, 5)_8$, where G_r is the feedback polynomial. Encoder II is a simple URC scheme, described by the pair of octal generator polynomials $(G_r, G) = (3, 2)_8$. Furthermore, the EXIT chart of Figure 5.11 was generated for the LSSTC-SP system employing $(N_t, N_r) = (4, 4)$ using $L_{AA} = 4$ elements per AA in conjunction with the system parameters of Table 5.1. The GM was used in this case, because no iterations are invoked between the SP demapper and the decoders, hence it is better to use GM that results in a higher initial mutual information and hence a higher starting point for the EXIT curve. Observe from Figure 5.11 that an open convergence tunnel is formed around $E_b/N_0 = -8.5$ dB. This implies that according to the predictions of the EXIT chart seen in Figure 5.11, the iterative decoding process is expected to converge at $E_b/N_0 = -8.5$ dB. The EXIT chart based convergence predictions can be verified by the Monte-Carlo simulation based iterative decoding trajectory of Figure 5.12, where the trajectory was recorded at $E_b/N_0 = -8.5$ dB, while using an interleaver depth of $D_{int} = 180,000$ bits and the rest of the system parameters outlined in Table 5.1. The steps seen

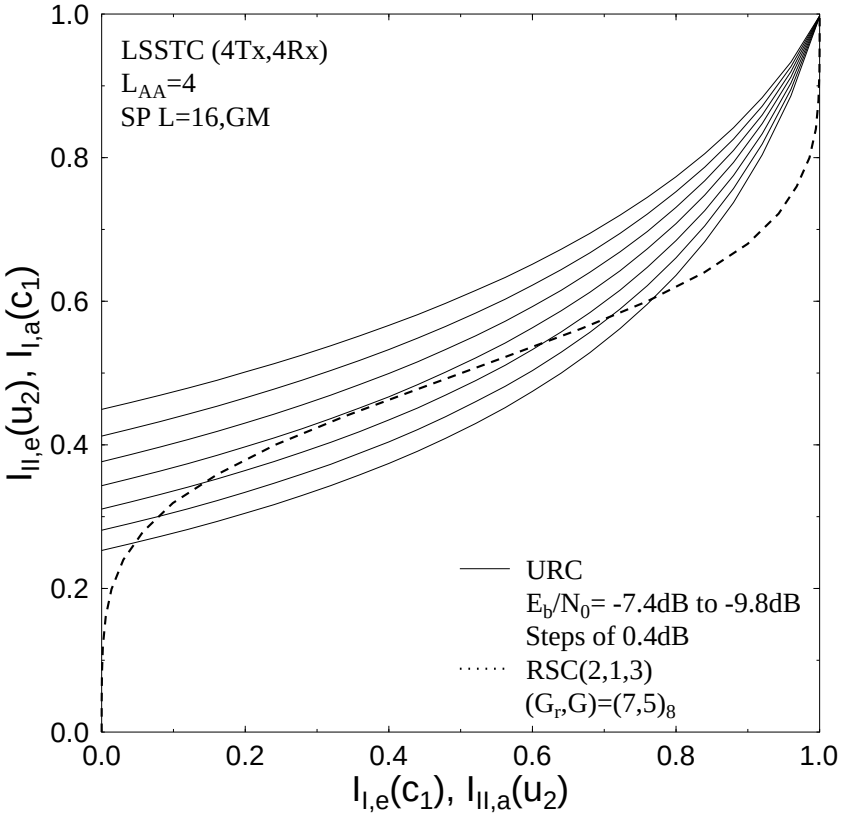

Figure 5.11: EXIT chart of a RSC-coded and URC-precoded LSSTC-SP System 1 employing GM in conjunction with $L = 16$ and the system parameters outlined in Table 5.1.

in the figure represent the actual extrinsic information exchange between the URC's decoder and the outer RSC channel decoder.

5.4.1.2 EXIT Tunnel-Area Minimisation for Near-Capacity Operation Using IrCCs

It is a well-understood property of the conventional 2D EXIT charts that a narrow but marginally open EXIT-tunnel represents a near-capacity performance [194]. Therefore, we invoke IrCCs for the sake of appropriately shaping the EXIT curves by minimising the area within the EXIT-tunnel using the procedure of [191, 194].

Let $\mathcal{A}_I$ and $\bar{\mathcal{A}}_I$ be the areas under the EXIT-curve of Decoder I and its inverse, respectively. Similarly, the area $\mathcal{A}_{II}$ is defined as that under the EXIT-curve of the URC Decoder II. It was observed in [191, 255] that for the APP-based outer Decoder I, the area $\bar{\mathcal{A}}_I$ may be approximated by $\bar{\mathcal{A}}_I \approx R_I$, where the equality $\bar{\mathcal{A}}_I = R_I$ was later shown in [229] for the family of Binary Erasure Channels (BECs). The area property of $\bar{\mathcal{A}}_I \approx R_I$ implies that the lowest SNR convergence threshold occurs, when we have $\mathcal{A}_{II} = R_I + \epsilon$, where ϵ is an infinitesimally small number, provided that the following convergence constraints hold [194]:

$$T_{II,u_2}(0) > 0,\ T_{II,u_2}(1) = 1,\ T_{II,u_2}(i) > T^{-1}_{I,c_1}(i),\ \forall i \in [0, 1). \tag{5.24}$$

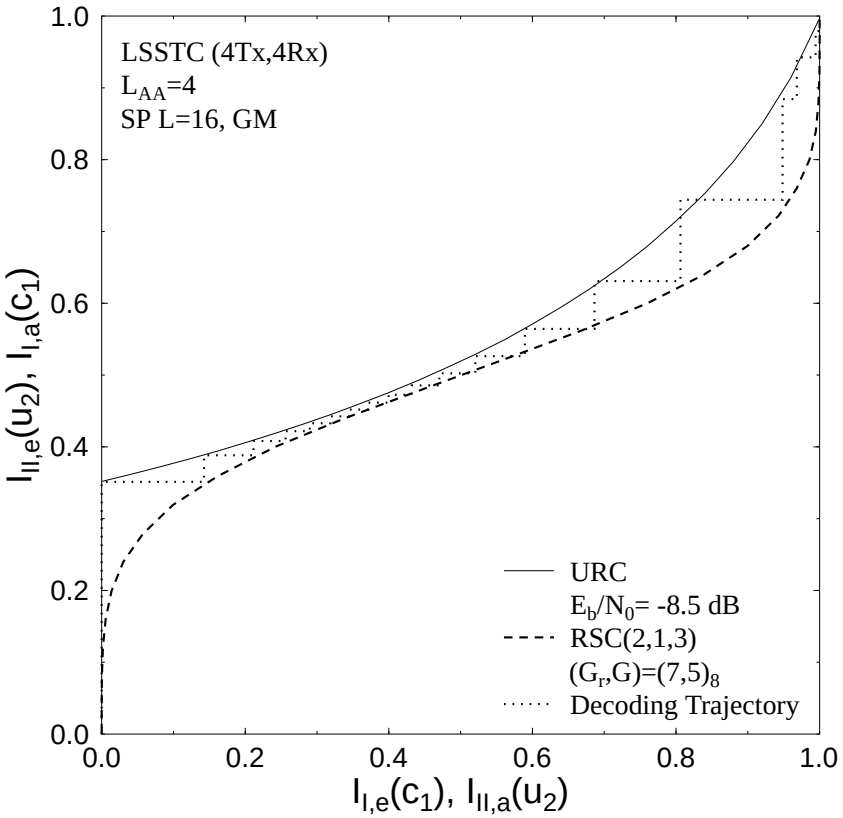

Figure 5.12: Decoding trajectory of the iteratively detected RSC-coded and URC-precoded LSSTC-SP System 1 employing GM in conjunction with $L = 16$ and the system parameters outlined in Table 5.1 while operating at $E_b/N_0 = -8.5$ dB.

Observe in Figure 5.12, however, that there is a wide tunnel between the EXIT curve $T_{II,u_2}(i)$ and the EXIT curve $T^{-1}_{I,c_1}(i)$ of the outer 1/2-rate RSC code at $E_b/N_0 = -8.5$ dB, especially when $i < 0.2$ and $i > 0.6$. This implies that the BER curve is farther from the achievable capacity than necessary. More quantitatively, the area under the EXIT curve $T_{II,u_2}(i)$ is $\mathcal{A}_{II} \approx 0.5625$ at $E_b/N_0 = -8.5$ dB, which is larger than the outer code rate of $R_I = 0.50$. Therefore, according to Figure 5.12 and to the area property of $\bar{\mathcal{A}}_I \approx R_I$, a lower E_b/N_0 convergence threshold may be attained, provided that the constraints outlined in Equation (5.24) are satisfied. In other words, the EXIT curve $T^{-1}_{I,c_1}(i)$ of the outer code should match the EXIT curve $T_{II,u_2}(i)$ of Figure 5.12 more closely. Hence we will invoke IrCCs as outer codes that exhibit flexible EXIT characteristics, which can be optimised for more closely matching the EXIT curve $T_{II,u_2}(i)$ of Figure 5.12, converting the near-capacity code optimisation to a simple curve-fitting problem.

An IrCC scheme constituted by a set of $P = 17$ subcodes was constructed in [194] from a systematic 1/2-rate memory-4 mother code defined by the octally represented generator polynomials $(G_r, G) = (31, 27)_8$. Each of the $P = 17$ subcodes have a different code rate R_I^i, $\forall i \in [1, 17]$, where puncturing was employed to obtain the rates of $R_I^i > 0.5$ and the code rates of $R_I^i < 0.5$ were created by adding more generators and by puncturing. The two

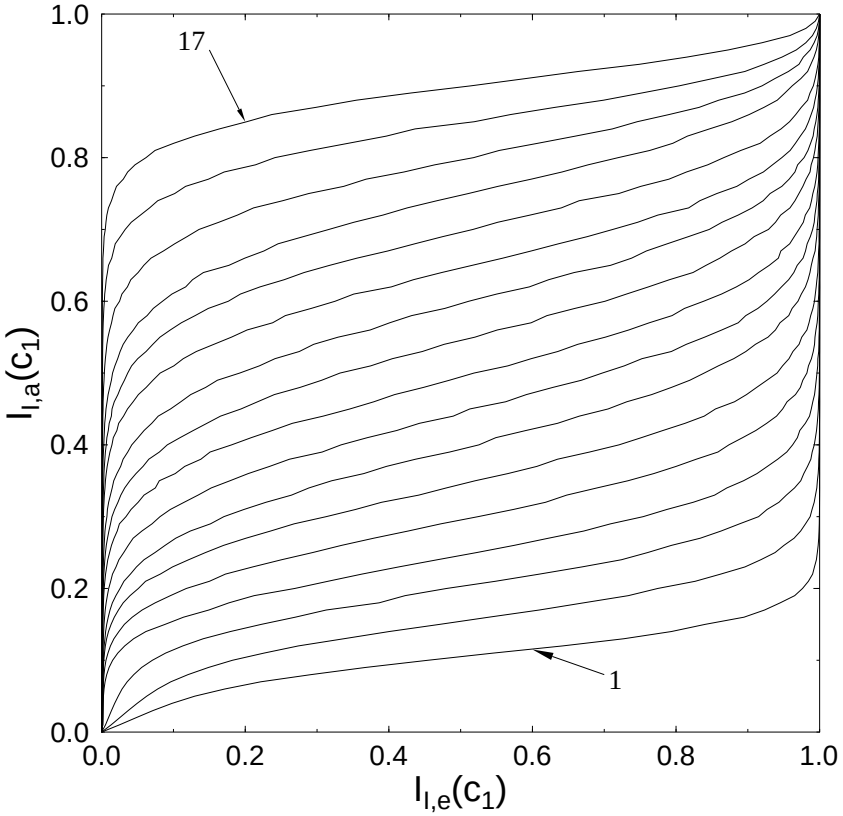

Figure 5.13: EXIT functions of the seventeen subcodes used in the IrCC.

additional generators employed in [194] are defined by the octally represented polynomials of $G_1 = (35)_8$ and $G_2 = (35)_8$, where the resultant $P = 17$ subcodes have coding rates spanning the range of $[0.1, 0.9]$. Each of the $P = 17$ subcodes encodes a specific fraction of the uncoded bits determined by the weighting coefficient α_i, $i = 1, \ldots, P$. Assuming an overall average code rate of $R_I = 0.5$, the following conditions must be satisfied:

$$\sum_{i=1}^{P} \alpha_i = 1, \quad R_I = \sum_{i=1}^{P} \alpha_i R_I^i, \quad \text{and} \quad \alpha_i \in [0, 1], \quad \forall i. \tag{5.25}$$

The EXIT function $T_{I,c_1}(I_{I,a}(c_1))$ corresponding to the IrCC may be constructed from the EXIT functions of the $P = 17$ subcodes, $T^i_{I,c_1}(I_{I,a}(c_1))$, $i = 1, \ldots, P$. More specifically, the EXIT function $T_{I,c_1}(I_{I,a}(c_1))$ of the IrCC is the weighted superposition of the $P = 17$ EXIT functions $T^i_{I,c_1}(I_{I,a}(c_1))$, $i = 1, \ldots, P$, as follows [194]

$$T_{I,c_1}(I_{I,a}(c_1)) = \sum_{i=1}^{P} \alpha_i T^i_{I,c_1}(I_{I,a}(c_1)). \tag{5.26}$$

Figure 5.13 shows the EXIT functions of the $P = 17$ subcodes used in [194]. Hence the coefficients α_i are optimised with the aid of the iterative algorithm of [191], so that the EXIT curve of the resultant IrCC closely matches the EXIT curve $T_{II,u_2}(i)$ at the specific E_b/N_0 value, where we have $\mathcal{A}_{II} \approx 0.50$. It is observed that $\mathcal{A}_{II} \approx 0.501$ at $E_b/N_0 = -9.4$ dB. However,

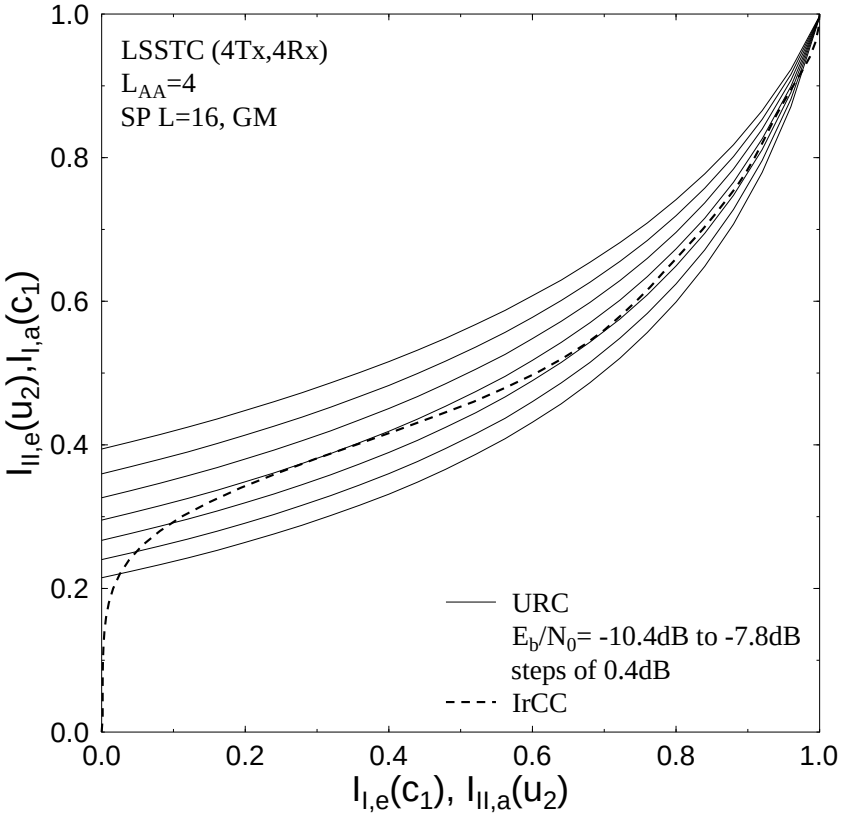

Figure 5.14: EXIT chart of a IrCC-coded and URC-precoded LSSTC-SP System 2 employing GM in conjunction with $L = 16$ and the system parameters outlined in Table 5.1.

observe in Figure 5.14 that we have an open tunnel at $E_b/N_0 = -9.2$ dB, indicating that this E_b/N_0 value is close to the lowest attainable convergence threshold, when employing a 1/2-rate outer code. Figure 5.14 also shows the EXIT curve of the resultant IrCC, where the optimised weighting coefficients are as follows:

$$\begin{aligned}[\alpha_1, \alpha_2, \ldots, \alpha_{16}, \alpha_{17}] \;=\; & [0,\ 0,\ 0,\ 0,\ 0,\ 0,\ 0.571927,\ 0.167114,\ 0,\\ & 0,\ 0,\ 0.0194083,\ 0.170044,\ 0,\ 0,\ 0,\ 0.0715566]. \end{aligned} \tag{5.27}$$

Figure 5.14 shows the EXIT chart of System 2 employing an iterative-detection aided IrCC-coded LSSTC-SP system using GM, where the iterations are carried out between the outer 1/2-rate IrCC code and the inner URC decoders, while no iterations are invoked between the URC decoder and the SP demapper. The system parameters of Table 5.1 are used for producing the EXIT curves of Figure 5.14. Observe from Figure 5.14 that an open convergence tunnel is formed around $E_b/N_0 = -9.2$ dB. This implies that according to the predictions of the EXIT chart of Figure 5.14, the iterative decoding process is expected to converge at $E_b/N_0 = -9.2$ dB. However, observe in Figure 5.14 that the open tunnel at $E_b/N_0 = -9.2$ dB is quite narrow and thus it requires a large number of iterations to converge at $E_b/N_0 = -9.2$ dB. This issue will be discussed further in the complexity analysis in Section 5.5.

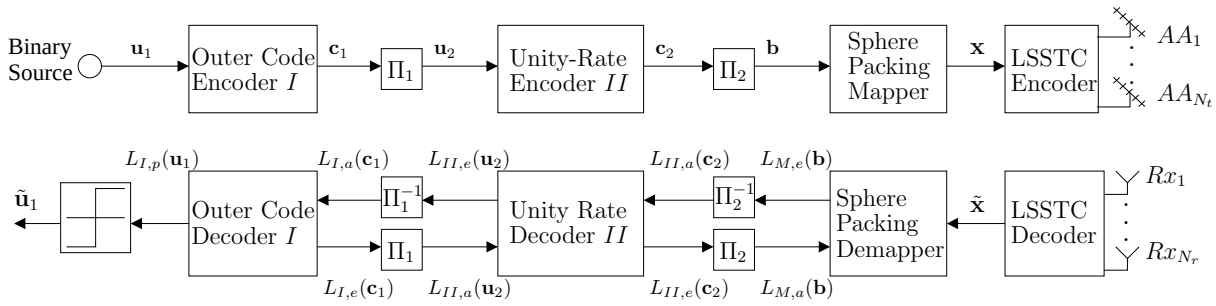

Figure 5.15: Block diagram of the layered steered space-time code employing SP modulation in conjunction with a unity-rate precoder and an outer code. The receiver employs iterative detection between the three constituent decoders, namely between the outer code decoder, the precoder's decoder and the SP demapper.

5.4.2 Three-Stage Iterative Detection Scheme

As shown in Figure 5.15, the received complex-valued symbols are first decoded by the LSSTC decoder in order to produce the received SP soft-symbols $\tilde{\mathbf{s}}$, where each SP symbol represents a block of B_{sp} coded bits as described in Section 5.2.2. Then, iterative demapping/decoding is carried out between the SP demapper, soft-in soft-out URC Decoder II and soft-in soft-out outer Decoder I, where extrinsic information is exchanged between the three constituent demapper/decoders. The iterative process is performed for a number of consecutive iterations. During the last iteration, only the LLR values $L_{I,p}(\mathbf{u_1})$ of the original uncoded systematic information bits $\mathbf{u}_1$ are required, which are passed to a hard decision decoder in order to determine the estimated transmitted source bits $\tilde{\mathbf{u}}_1$ as shown in Figure 5.15.

5.4.2.1 3D EXIT Charts

In this section System 3 is described, where iterative detection is employed by exchanging extrinsic information between the SP demapper, the URC Decoder II and the outer Decoder I. As seen from Figure 5.15, the input of Decoder II is constituted by the *a priori* input $L_{II,a}(\mathbf{c}_2)$ and the *a priori* input $L_{II,a}(\mathbf{u}_2)$ after appropriately ordering the data provided by the SP demapper and Decoder I, respectively. Therefore, the EXIT characteristics of Decoder II can be described by the following two EXIT functions [186, 196]:

$$I_{II,e}(\mathbf{c}_2) = T_{II,c_2}\left[I_{II,a}(\mathbf{u}_2), I_{II,a}(\mathbf{c}_2)\right] \quad (5.28)$$

$$I_{II,e}(\mathbf{u}_2) = T_{II,u_2}\left[I_{II,a}(\mathbf{u}_2), I_{II,a}(\mathbf{c}_2)\right], \quad (5.29)$$

which are illustrated by the 3D surfaces drawn in dotted lines in Figures 5.16 and 5.17, respectively. On the other hand, the EXIT characteristics of the SP demapper as well as those of Decoder I are each dependent on a single *a priori* input, namely on $L_{M,a}(\mathbf{b})$ and $L_{I,a}(\mathbf{c}_1)$, respectively, both of which are provided by the URC Decoder II after appropriately ordering the

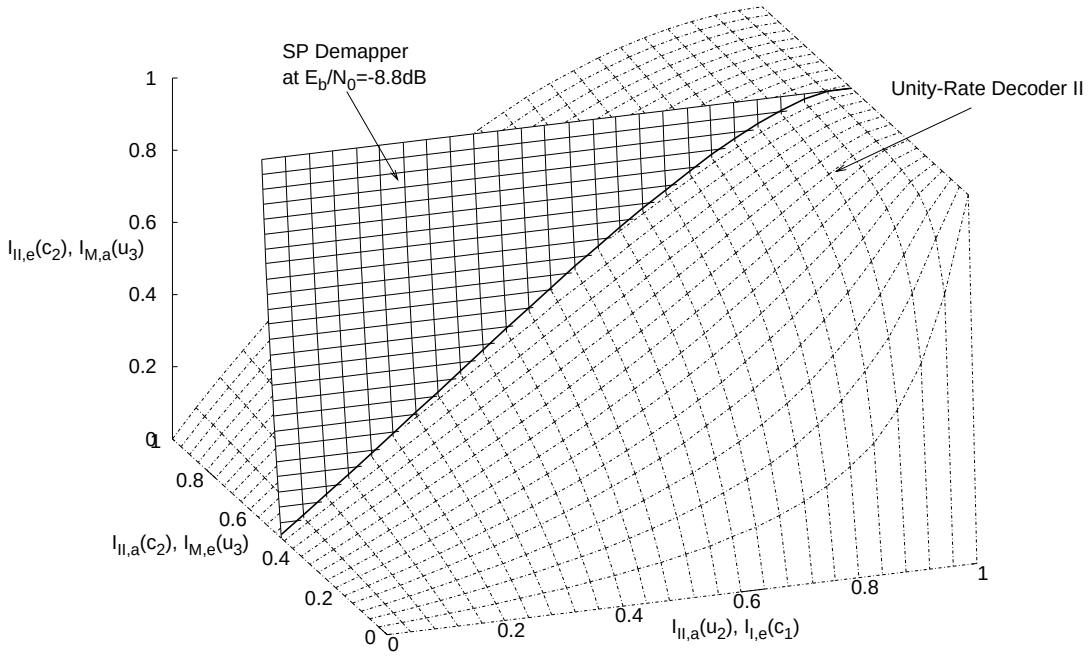

Figure 5.16: 3D EXIT chart of the URC Decoder II and the SP demapper at $E_b/N_0 = -8.8$ dB.

bits, as seen in Figure 5.15. The EXIT characteristics of the SP demapper are also dependent on the E_b/N_0 value. Consequently, the corresponding EXIT functions for the SP demapper and Decoder I, respectively, may be written as

$$I_{M,e}(\mathbf{b}) = T_{M,b}\left[I_{M,a}(\mathbf{b}), E_b/N_0\right], \tag{5.30}$$

$$I_{I,e}(\mathbf{c}_1) = T_{I,c_1}\left[I_{I,a}(\mathbf{c}_1)\right], \tag{5.31}$$

which are illustrated by the 3D surfaces drawn in solid lines in Figures 5.16 and 5.17, respectively.

Equations (5.28)-(5.31) can be represented with the aid of two 3D EXIT charts. More specifically, the 3D EXIT chart of Figure 5.16 is used to plot Equation (5.28) and Equation (5.30), which describe the EXIT relation between the SP demapper and Decoder II. Similarly, the 3D EXIT chart of Figure 5.17 can be used to describe the EXIT relation between Decoder II and Decoder I by plotting Equation (5.29) and Equation (5.31). Furthermore, for the sake of comparison we plot the 3D EXIT curves of the QPSK modulated LSSTC scheme employing a 3-stage iterative detection aided receiver and the same system parameters as the SP system of Figures 5.16 and 5.17. Figure 5.18 describes the EXIT relation between the QPSK demapper and the URC Decoder II, while Figure 5.19 describes the EXIT relation between Decoder II and Decoder I together with the EXIT projection from Figure 5.18.

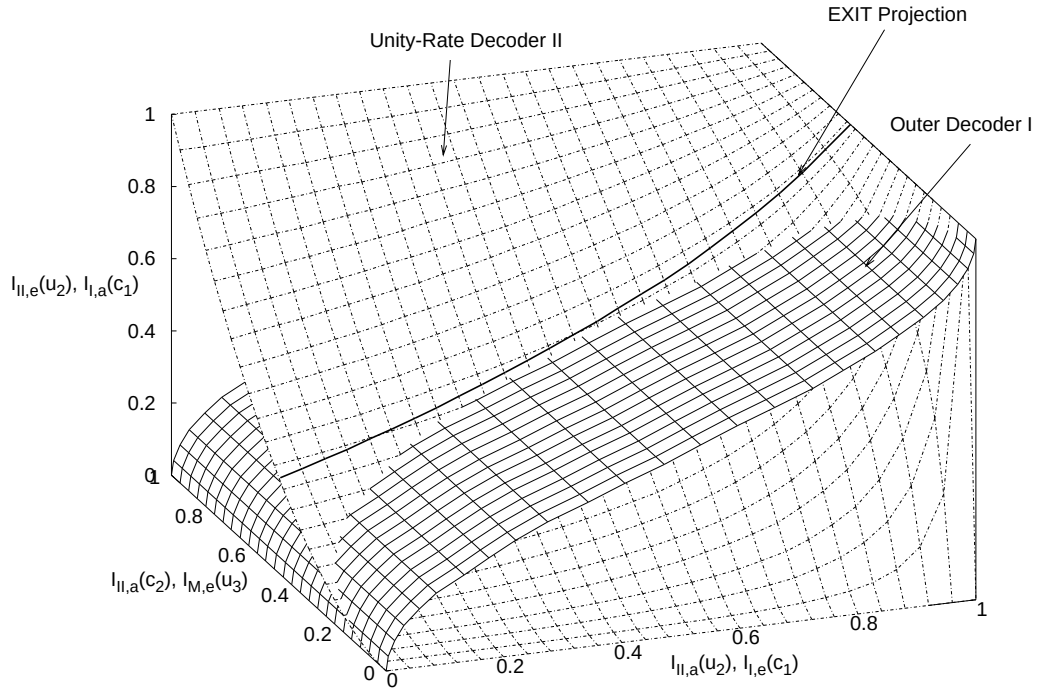

Figure 5.17: 3D EXIT chart of the URC Decoder II and the RSC Decoder I with projection from Figure 5.16.

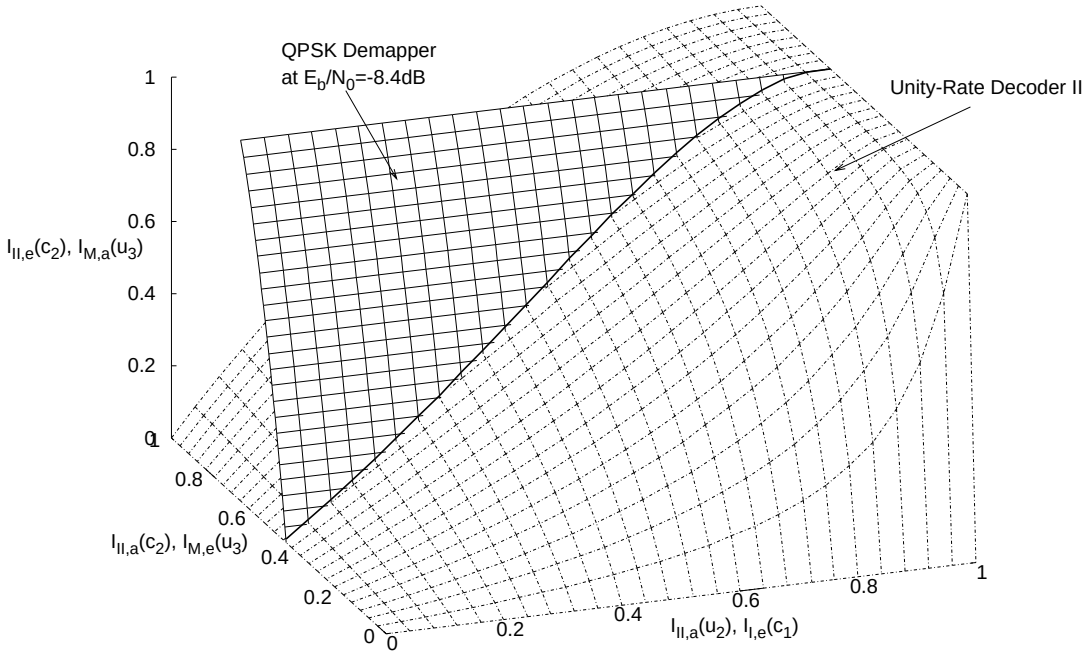

Figure 5.18: 3D EXIT chart of the URC Decoder II and the QPSK demapper at $E_b/N_0 = -7.8$ dB.

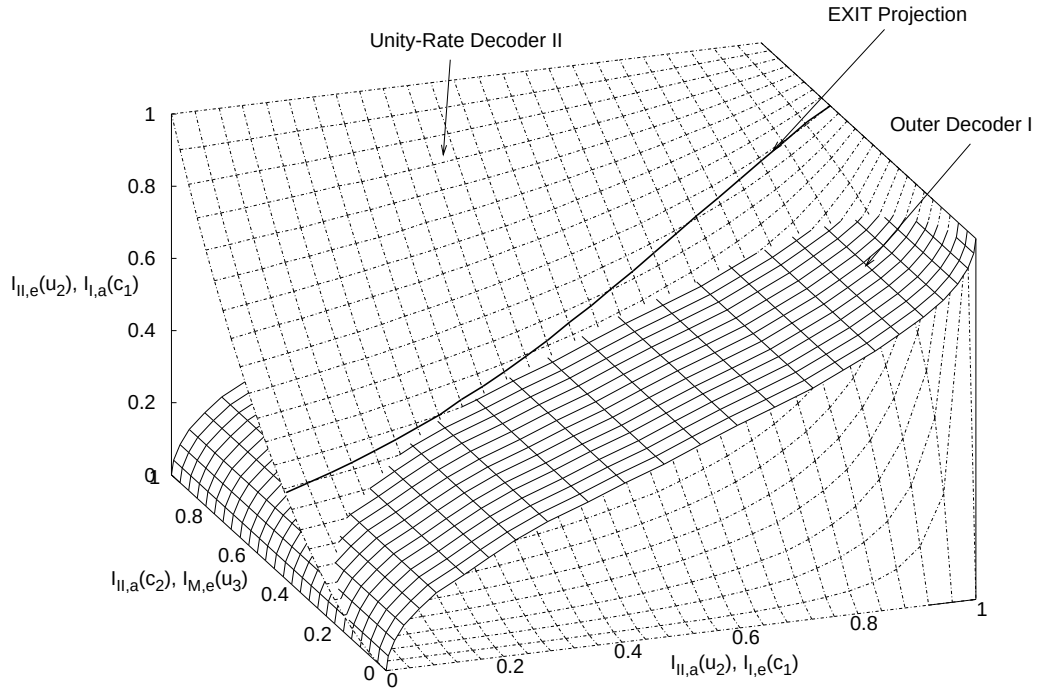

Figure 5.19: 3D EXIT chart of the URC Decoder II and the RSC Decoder I with projection from Figure 5.18.

5.4.2.2 2D EXIT Chart Projection

As observed in Figures 5.16 and 5.17, it is cumbersome to interpret the 3D EXIT charts. Hence in this section we derive their unique and unambiguous 2D representations, which may be interpreted more readily.

The intersection of the surfaces in Figure 5.16, shown as a thick solid line, portrays the achievable performance when exchanging mutual information between the SP demapper and the URC Decoder II for different fixed values of $I_{II,a}(\mathbf{u}_2)$ spanning the range of $[0, 1]$. Each $[I_{II,a}(\mathbf{u}_2),\ I_{II,a}(\mathbf{c}_2),\ I_{II,e}(\mathbf{c}_2)]$ point belonging to the intersection line of Figure 5.16 uniquely specifies a 3D point $[I_{II,a}(\mathbf{u}_2),\ I_{II,a}(\mathbf{c}_2),\ I_{II,e}(\mathbf{u}_2)]$ in Figure 5.17, according to the EXIT function of Equation (5.29). Therefore, the line corresponding to the $[I_{II,a}(\mathbf{u}_2), I_{II,a}(\mathbf{c}_2), I_{II,e}(\mathbf{c}_2)]$ points along the thick line of Figure 5.16 is projected to the solid line shown in Figure 5.17. The 2D projection of the solid line in Figure 5.17 at $I_{II,a}(\mathbf{c}_2) = 0$ onto the plane spanned by the lines $[I_{II,a}(\mathbf{u}_2), I_{II,e}(\mathbf{u}_2)]$ and $[I_{I,e}(\mathbf{c}_1), I_{I,a}(\mathbf{c}_1)]$ is shown in Figure 5.20 at $E_b/N_0 = -8.8$ dB for all possible SP AGM schemes of Appendix A. This projected EXIT curve may be written as

$$I_{II,e}(\mathbf{u}_2) = T^{p}_{II,u_2}\left[I_{II,a}(\mathbf{u}_2), E_b/N_0\right]. \tag{5.32}$$

Observe in Figure 5.20 the variety of curves that result from using different mapping schemes in the 3-stage iterative-detection-aided system. Figure 5.20 shows the 2-D EXIT projection at $E_b/N_0 = -8.8$ dB. As seen in the figure, an open tunnel exists at $E_b/N_0 = -8.8$ dB for

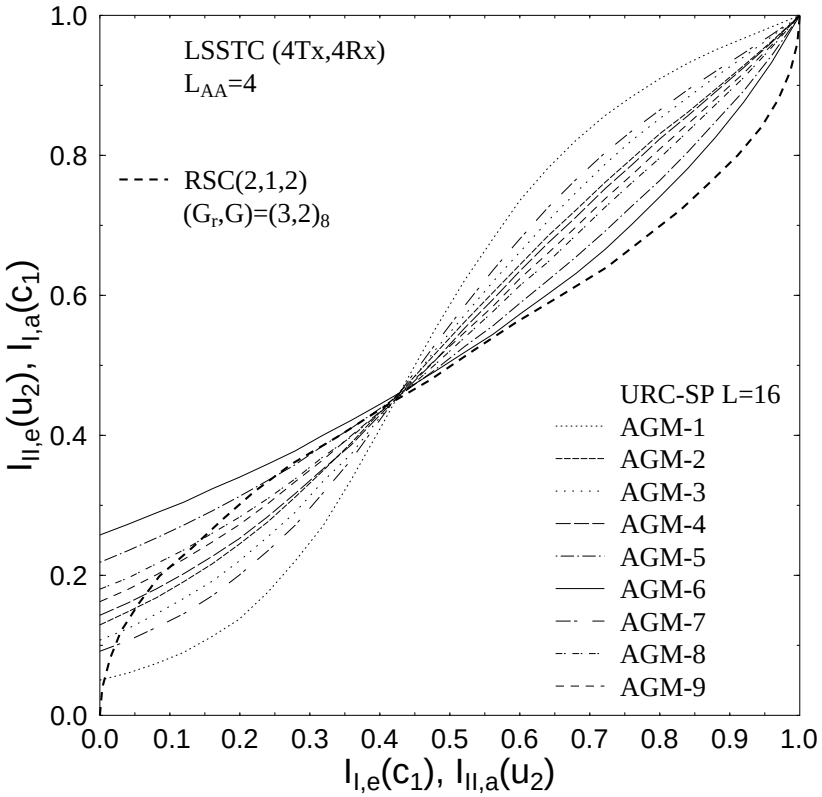

Figure 5.20: 2D projection of the EXIT charts of the three-stage RSC-coded LSSTC-SP System 3, when employing all possible anti-Gray mapping aided SP in conjunction with $L = 16$, while using an interleaver length of $D_{int} = 180,000$ bits and the system parameters outlined in Table 5.1 at E_b/N_0=−8.8 dB.

the system employing AGM-6, while an open tunnel exists for the other mapping schemes at different E_b/N_0 values higher than −8.8 dB. Therefore, according to the EXIT chart prediction, the system employing AGM-6 exhibits an open tunnel at $E_b/N_0 = -8.8$ dB and thus it is expected that the system employing AGM-6 exhibits an infinitesimally low BER at E_b/N_0 of −8.8 dB.

The intersection of the surfaces in Figure 5.16, shown as a thick solid line, portrays the *best achievable performance*, when exchanging mutual information between the SP demapper and the URC Decoder II for different fixed values of $I_{II,a}(\mathbf{u}_2)$ spanning the range of $[0, 1]$. The best achievable performance is the one corresponding to the AGM-6 assisted system, as portrayed in Figure 5.20. Therefore, the line corresponding to the $[I_{II,a}(\mathbf{u}_2), I_{II,a}(\mathbf{c}_2), I_{II,e}(\mathbf{c}_2)]$ points along the thick line of Figure 5.16 is projected to the solid line shown in Figure 5.17, while the 2D projection of the solid line in Figure 5.17 at $I_{II,a}(\mathbf{c}_2) = 0$ onto the plane spanned by the lines $[I_{II,a}(\mathbf{u}_2), I_{II,e}(\mathbf{u}_2)]$ and $[I_{I,e}(\mathbf{c}_1), I_{I,a}(\mathbf{c}_1)]$ is shown in Figure 5.21 at $E_b/N_0 = -8.8$ dB. Figure 5.21 shows the 2D-projected EXIT curve of the combined SP demapper and the URC Decoder II at $E_b/N_0 = -8.8$ dB, when employing the best possible Anti-Gray Mapping scheme, namely AGM-6. Figure 5.21 records the 2D-projected EXIT curves for a variable number of

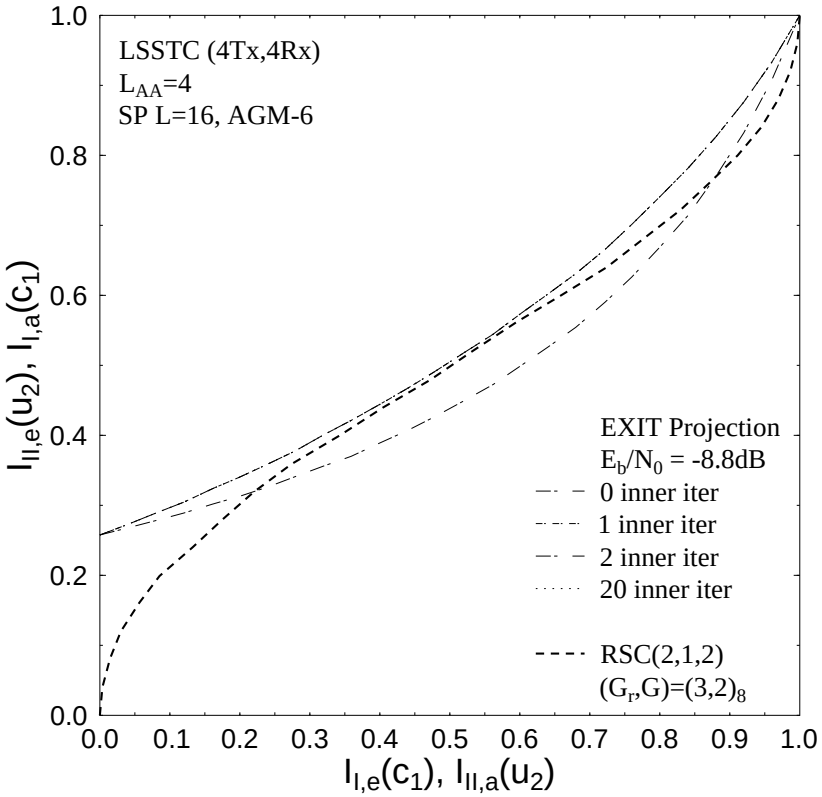

Figure 5.21: 2D projection of the EXIT charts of the three-stage RSC-coded LSSTC-SP scheme, when employing the best possible anti-Gray mapping AGM-6 aided SP in conjunction with $L = 16$, while using an interleaver depth of $D_{int} = 180,000$ bits and the system parameters outlined in Table 5.1.

inner iterations between the SP demapper and Decoder II. As observed from Figure 5.21, when no inner iterations are employed, the system becomes essentially a two-stage arrangement employing AGM instead of GM for System 1 and System 2. According to Figure 5.21, when no inner iterations are carried out, the system requires $E_b/N_0 > -8.8$ dB for maintaining an open tunnel. However, observe that when 1, 2 and 20 inner iterations are carried out, the open EXIT tunnel is formed at $E_b/N_0 = -8.8$ dB. Therefore, in our further investigations we use a single inner iteration that produces the same result and imposes the lowest complexity. This implies that according to the predictions of the 2D EXIT chart seen in Figure 5.21, the iterative decoding process is expected to converge to the $(1.0, 1.0)$ point and hence an infinitesimally low BER may be attained beyond $E_b/N_0 = -8.8$ dB. This expectation is confirmed by the decoding trajectory of Figure 5.22, which was recorded for an interleaver depth of $D_{int} = 180,000$ bits in conjunction with the system parameters outlined in Table 5.1.

Figure 5.23 shows the 2D-projected EXIT curve of the combined QPSK demapper and the URC Decoder II at $E_b/N_0 = -7.8$ dB, when employing the AGM scheme [256]. Figure 5.23 records the 2D-projected EXIT curves for a single inner iteration between the QPSK demapper and Decoder II. Observe in Figure 5.23 that no open tunnel exists between the EXIT projection and the outer code's EXIT curve at an E_b/N_0 below -7.8 dB. Therefore, a comparison between

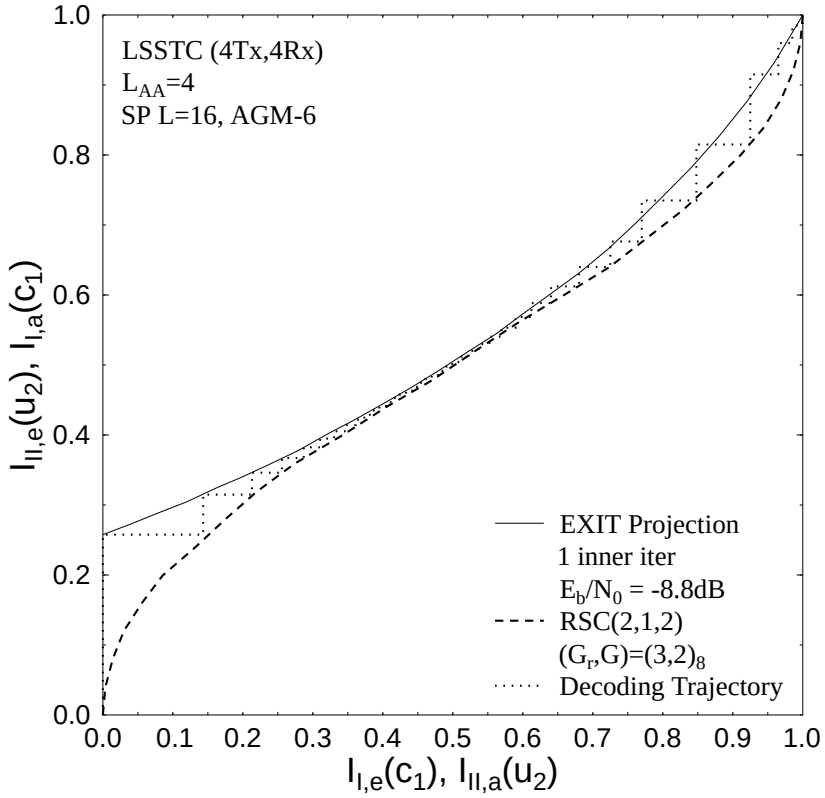

Figure 5.22: Decoding trajectory of the iteratively detected three-stage RSC-coded and URC-precoded LSSTC-SP System 3 employing GM in conjunction with $L = 16$ and the system parameters outlined in Table 5.1, while operating at $E_b/N_0 = -8.8$ dB.

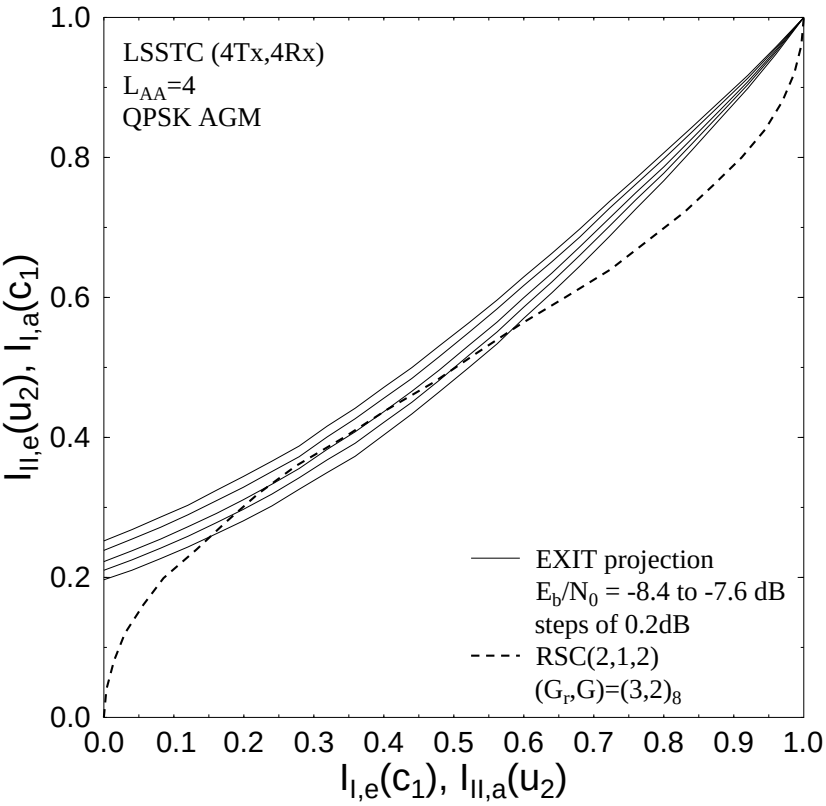

Figure 5.23: 2D projection of the EXIT charts of the three-stage RSC-coded LSSTC-QPSK scheme, when employing the AGM aided QPSK in conjunction with an interleaver depth of $D_{int} = 180,000$ bits and the system parameters outlined in Table 5.1.

Figure 5.23 and Figure 5.21 shows the flexibility that the multi-dimensional modulation scheme has in the choice of the mapping schemes compared to the two-dimensional QPSK scheme. Hence, according to the predictions of the 2D EXIT chart seen in Figure 5.23, the iterative decoding process is expected to converge to the $(1.0, 1.0)$ point and hence an infinitesimally low BER may be attained beyond $E_b/N_0 = -7.8$ dB.

5.4.3 Maximum Achievable Bandwidth Efficiency

The MIMO channel's bandwidth efficiency curves recorded for the four-dimensional SP modulation assisted LSSTC scheme in conjunction with $(N_t \times N_r) = (4 \times 4)$ and $L_{AA} = 4$ elements per AA are shown in Figure 5.24, portraying both the DCMC and CCMC bandwidth efficiency curves as well as the maximum achievable rate of the system derived from the EXIT curves according to the algorithm of Section 3.2.3. Observe the discrepancy between the two bandwidth efficiency curves shown in Figure 5.24 that are calculated using Equation (5.21) and Equation (3.21), which is due to the fact that Equation (5.21) was computed for the case where perfect interference cancellation is considered at the receiver. Therefore, Equation (5.21) constitutes an upper bound on the system's bandwidth efficiency, while Equation (3.21) constitutes a tighter bound on the maximum achievable bandwidth efficiency of the system considered in this chapter.

Similarly, we plot in Figure 5.25 the MIMO channel's bandwidth efficiency curves recorded for the QPSK modulation assisted LSSTC scheme in conjunction with $(N_t \times N_r) = (4 \times 4)$ and $L_{AA} = 4$ elements per AA. Figure 5.25 portrays both the DCMC and CCMC bandwidth efficiency curves as well as the maximum achievable rate of the system derived from the EXIT curves according to the algorithm of Section 3.2.3.

Figure 5.24 shows that at a bandwidth efficiency of $\eta = 2$ bits/sec/Hz, which is the bandwidth efficiency of the system employing the parameters of Table 5.1, the DCMC bandwidth efficiency limit seen for the LSSTC-SP scheme in Figure 5.25 is about $E_b/N_0 = -10.15$ dB, while the maximum achievable rate limit obtained using EXIT charts is at $E_b/N_0 = -9.45$ dB.

Figure 5.25 shows that at a bandwidth efficiency of $\eta = 2$ bits/sec/Hz the DCMC bandwidth efficiency limit seen for the LSSTC-SP scheme in Figure 5.25 is about $E_b/N_0 = -10$ dB, while the maximum achievable rate limit obtained using EXIT charts is at $E_b/N_0 = -9.34$ dB.

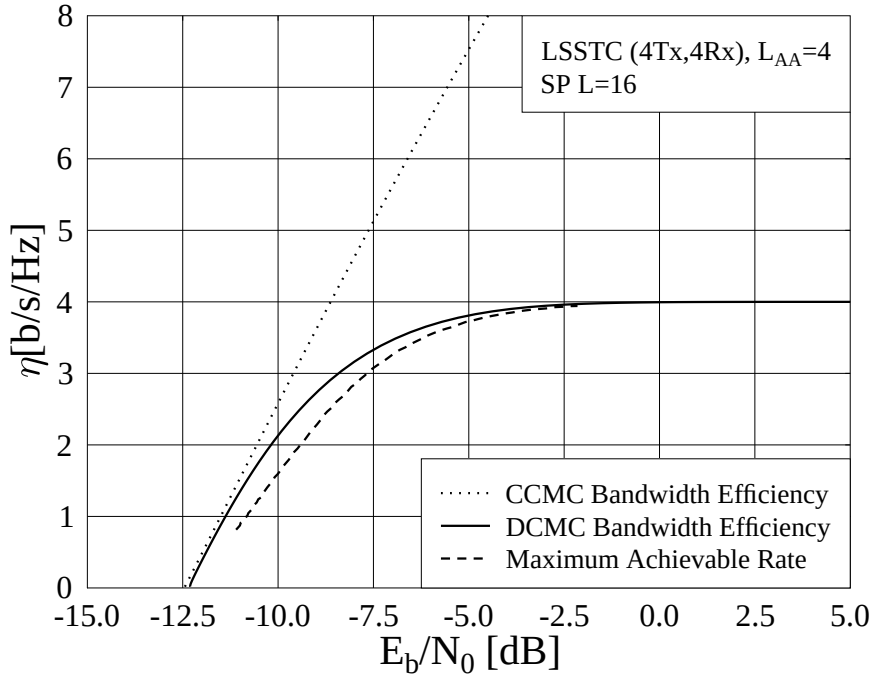

Figure 5.24: Bandwidth efficiency of the four-AAs aided LSSTC-SP system in conjunction with $L = 16$ employing four elements per AA for both DCMC and CCMC together with the maximum achievable rate obtained using EXIT charts.

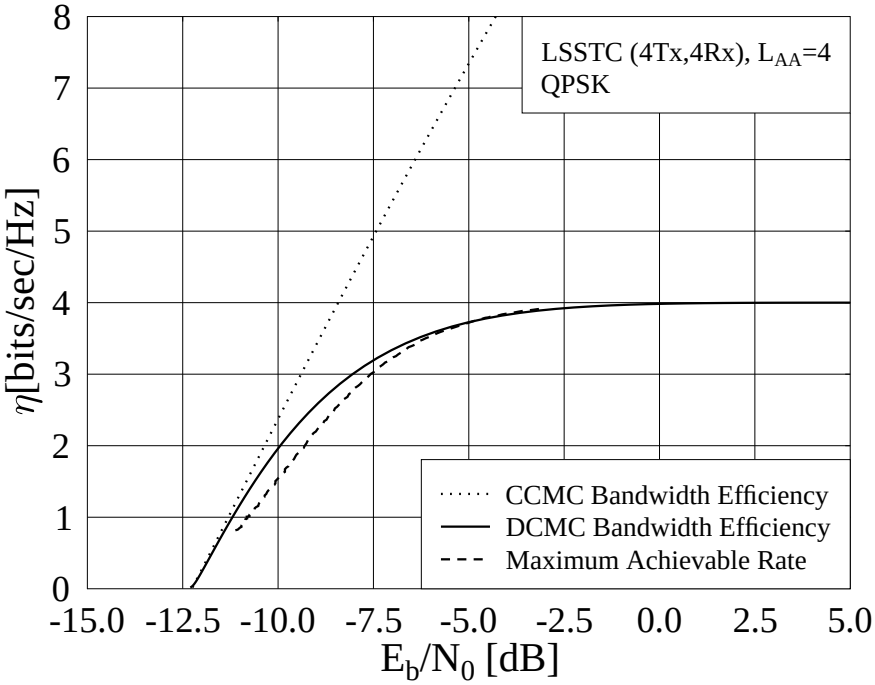

Figure 5.25: Bandwidth efficiency of the four-AAs aided LSSTC-QPSK system in conjunction with four elements per AA for both DCMC and CCMC together with the maximum achievable rate obtained using EXIT charts.

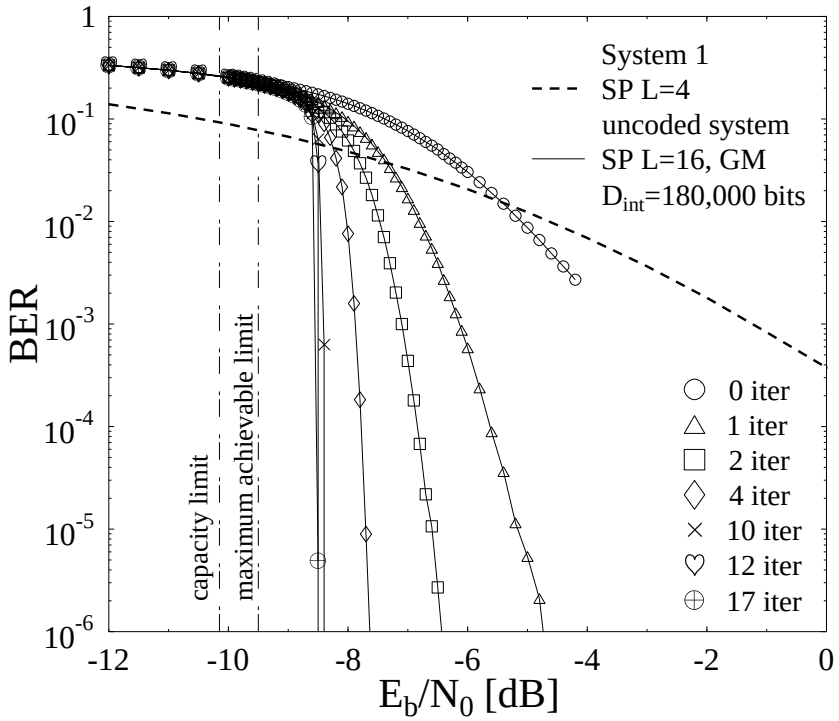

Figure 5.26: Performance comparison of the proposed LSSTC-SP aided System 1 employing iterative detection between a 1/2-rate RSC decoder and a URC decoder employing Gray mapping aided SP in conjunction with $L = 16$, while using an interleaver length of $D_{int} = 180,000$ bits and the system parameters outlined in Table 5.1 for a variable number of iterations.

5.5 Results and Discussion

In this section, we consider a LSSTC system associated with the system parameters outlined in Table 5.1 in order to demonstrate the performance improvements achieved by the proposed system. We employ SP in conjunction with $L = 16$ and QPSK modulation and hence the overall bandwidth efficiency of the system is 2 bits/sec/Hz. The results presented in this section correspond to the scenario where the channel is perfectly known at the receiver. We also assume that the transmitter has full knowledge of the DOA without any estimation or estimation errors.

Figure 5.26 compares the performance of the proposed System 1 employing the LSSTC-SP scheme in conjunction with $L = 16$ and GM together with the system parameters of Table 5.1 for different number of iterations against that of an uncoded LSSTC-SP scheme using $L = 4$, which has an identical bandwidth efficiency of 2 bits/sec/Hz. Figure 5.26 shows the performance of the iteratively detected RSC-coded LSSTC-SP scheme, when employing an interleaver depth of $D_{int} = 180,000$ bits and while communicating over a temporally correlated Rayleigh fading channel associated with a normalised Doppler frequency of $f_D = 0.01$. Explicitly, Figure 5.26 demonstrates that a coding advantage of about 16.5 dB was achieved at a BER of 10^{-6} after 17 iterations by System 1 over the equivalent-throughput uncoded LSSTC-SP scheme employing

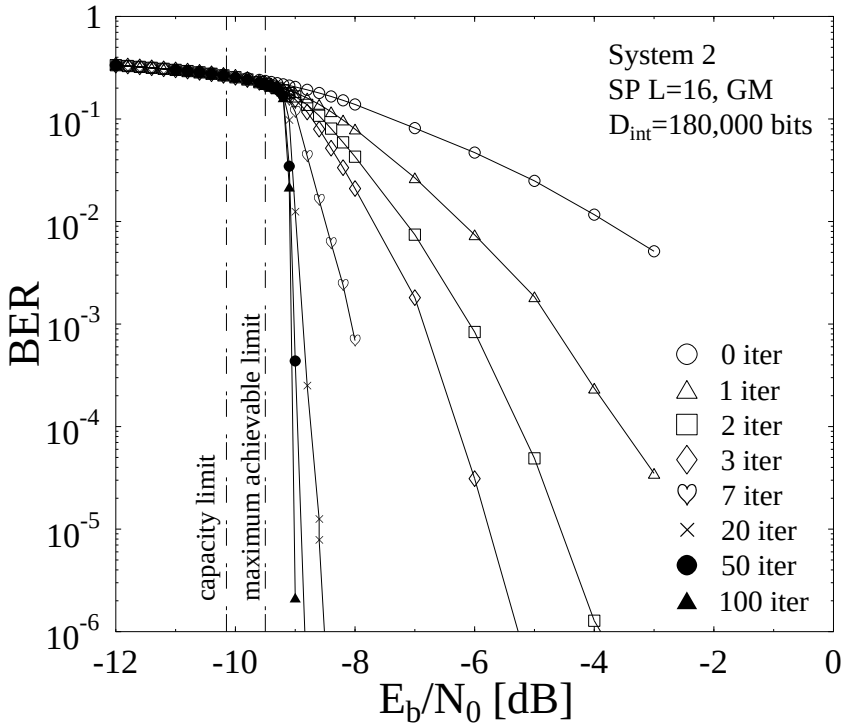

Figure 5.27: Performance comparison of the proposed LSSTC-SP aided System 2 employing iterative detection between a 1/2-rate IrCC decoder and a URC decoder employing Gray mapping aided SP in conjunction with $L = 16$, while using an interleaver length of $D_{int} = 180,000$ bits and the system parameters outlined in Table 5.1 for a variable number of iterations.

$L = 4$. Furthermore, Figure 5.26 demonstrates that the BER performance closely matches the EXIT chart based prediction of Figure 5.12, where the system approaches an infinitesimally low BER at $E_b/N_0 = -8.5$ dB after 17 iterations. Finally, according to Figure 5.26, System 1 performs within 0.9 dB from the maximum achievable rate limit of Figure 5.24 obtained using the EXIT chart and within 1.65 dB from the LSSTC-SP system's bandwidth efficiency limit.

On the other hand, Figure 5.27 compares the performance of the proposed System 2 employing the LSSTC-SP scheme in conjunction with $L = 16$ and GM, together with the system parameters of Table 5.1 for different number of iterations, where the system has a bandwidth efficiency of 2 bits/sec/Hz. The system of Figure 5.27 employs the IrCC of Figure 5.14 as an outer code and iterative detection is carried out between the IrCC decoder and the unity rate code's decoder. Furthermore, the system employs an interleaver depth of $D_{int} = 180,000$ bits and communicates over a temporally correlated Rayleigh fading channel associated with a normalised Doppler frequency of $f_D = 0.01$. Explicitly, Figure 5.27 demonstrates that the system approaches an infinitesimally low BER at $E_b/N_0 = -9.0$ dB after 100 iterations. However, according to the EXIT chart of Figure 5.14, it is predicted that the system's BER performance converges at $E_b/N_0 = -9.2$ dB. This is mainly due to the fact that the convergence tunnel in the EXIT chart of Figure 5.14 is quite narrow and the system requires more than 100 iterations for matching the EXIT chart prediction of maintaining an infinitesimally low BER at an E_b/N_0

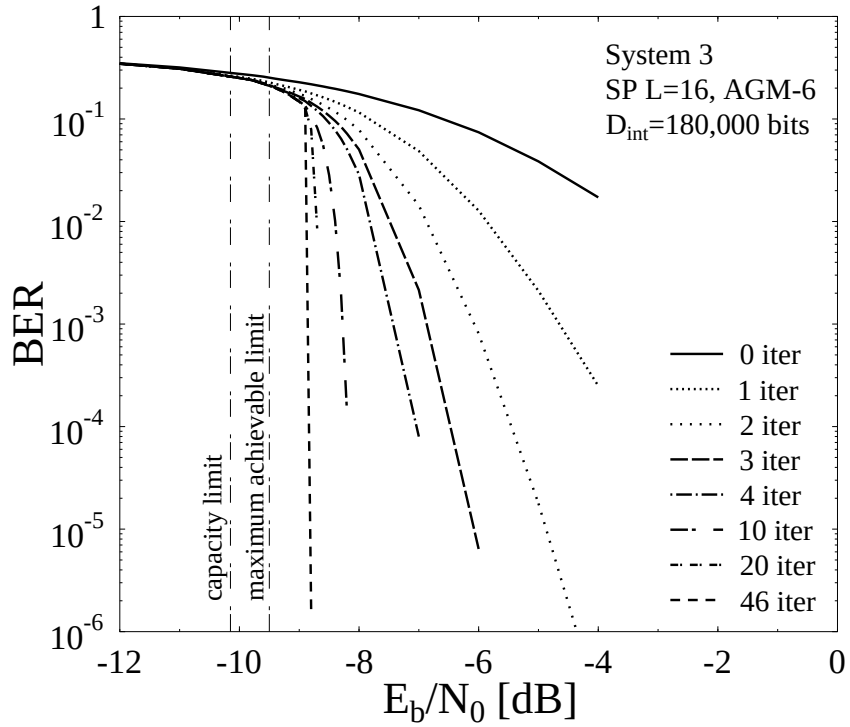

Figure 5.28: Performance comparison of the proposed LSSTC-SP aided System 3 employing three-stage iterative detection between a 1/2-rate RSC decoder, a URC decoder as well as SP demapper employing AGM aided SP in conjunction with $L = 16$, while using an interleaver depth of $D_{int} = 180,000$ bits and the system parameters outlined in Table 5.1 for a variable number of iterations.

value of -9.2 dB. Finally, according to Figure 5.27, System 2 performs within 0.4 dB from the maximum achievable rate limit obtained using the EXIT chart of Figure 5.24 and within 1.1 dB from the LSSTC-SP system's bandwidth efficiency limit.

Figure 5.28 compares the attainable performance of the proposed System 3 employing the LSSTC-SP scheme in conjunction with $L = 16$ and AGM-6 and the system parameters of Table 5.1 recorded for different number of iterations. In Figure 5.28, an interleaver depth of D_{int}=180,000 bits was employed for communication over a temporally correlated Rayleigh fading channel associated with a normalised Doppler frequency of 0.01. Figure 5.28 demonstrates that the BER performance closely matches the EXIT chart based prediction of Figure 5.22, where the system approaches an infinitesimally low BER at $E_b/N_0 = -8.8$ dB after 46 iterations. Finally, according to Figure 5.28, System 3 performs within 0.6 dB from the maximum achievable rate limit obtained using the EXIT chart of Figure 5.24 and within 1.35 dB from the LSSTC-SP system's bandwidth efficiency limit.

Furthermore, Figure 5.29 compares the attainable performance of the iteratively detected RSC-coded LSSTC scheme employing QPSK modulation in conjunction with the system parameters of Table 5.1 for different number of iterations. Figure 5.29 shows the BER curve for the three-stage system, where the decoder employs iterative detection exchanging extrinsic in-

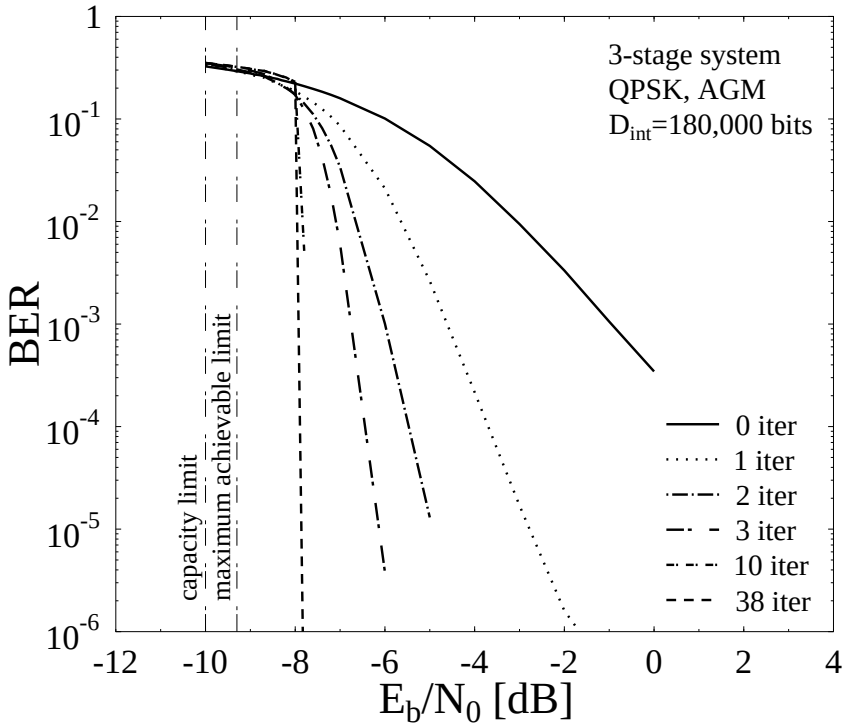

Figure 5.29: Performance comparison of the proposed LSSTC-QPSK aided System 3 employing iterative detection between a 1/2-rate RSC decoder, a URC decoder as well as QPSK demapper employing AGM aided QPSK, while using an interleaver depth of $D_{int} = 180,000$ bits and the system parameters outlined in Table 5.1 for a variable number of iterations.

formation between the three constituent decoders/demapper, namely the QPSK demapper, the URC Decoder II and the RSC Decoder I. Figure 5.29 demonstrates that the BER performance closely matches the EXIT chart based prediction of Figure 5.23, where the system approaches an infinitesimally low BER at $E_b/N_0 = -7.8$ dB after 38 iterations. Finally, according to Figure 5.29, the proposed QPSK modulated system performs within 1.54 dB from the maximum achievable rate limit obtained using the EXIT chart of Figure 5.24 and within 2.2 dB from the system's bandwidth efficiency limit.

A comparison between the three proposed SP modulated systems and the QPSK modulated three-stage iteratively detected system is presented in Figure 5.30. Figure 5.30 compares the *maximum achievable performance* of the proposed iterative detection aided LSSTC schemes, while employing an interleaver depth of $D_{int} = 180,000$ bits and the system parameters of Table 5.1. Observe that the performance of System 1 as well as that of the SP modulated and QPSK modulated System 3 matches the EXIT chart predictions of Figures 5.12, 5.22 and 5.23 after $I = 17$, $I = 46$ and $I = 38$ iterations, respectively. Explicitly, the SP modulated System 3 converges at E_b/N_0 of -8.8 dB, as predicted by the EXIT chart of Figure 5.22, while the QPSK modulated System 3 converges at E_b/N_0 of -7.8 dB, as predicted by the EXIT chart of Figure 5.23. Hence, the SP modulated System 3 performs within 0.6 dB from the maximum achievable rate limit obtained using the EXIT charts, while the QPSK modulated System

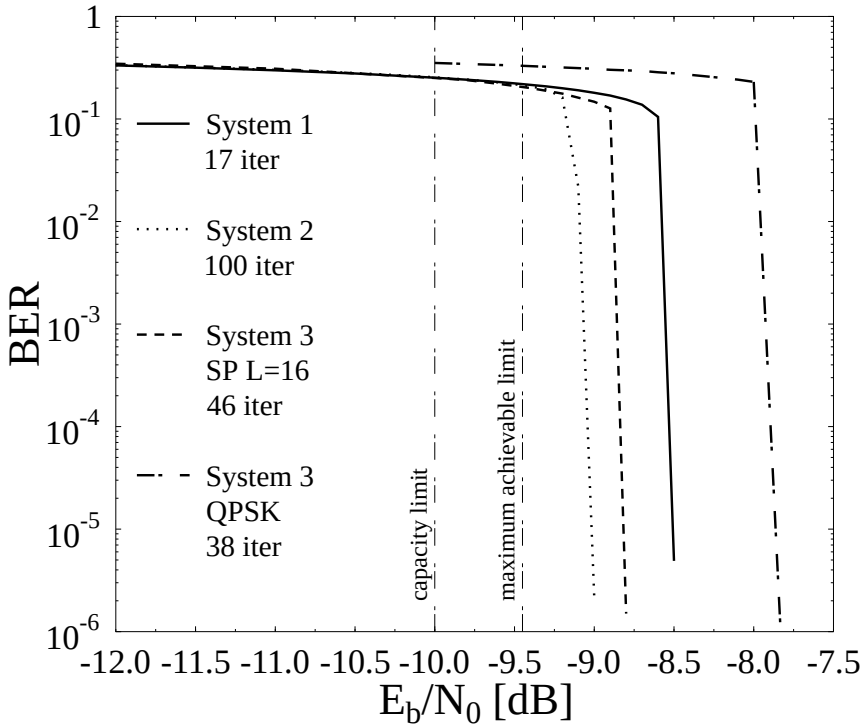

Figure 5.30: Performance comparison of the three proposed LSSTC-SP aided systems employing two-stage iteration between an outer code and a URC decoders, as well as three-stage iterative system between an outer RSC, intermediate URC decoders and an SP demapper. The figure also plots the BER performance of the three-stage system employing QPSK.

3 performs within 1.54 dB from the maximum achievable rate limit obtained using the EXIT charts. However, System 2 does not closely match the EXIT-chart based convergence prediction at $E_b/N_0 = -9.2$ dB even after $I = 100$ iterations, when employing an interleaver depth of $D_{int} = 180,000$ bits. This is due to the fact that at $E_b/N_0 = -9.2$ dB, the EXIT-tunnel of Figure 5.14 is narrow and thus requires a large number of iterations, which is significantly higher than $I = 100$. Thus, using the system parameters outlined in Table 5.1 and $I = 100$ decoding iterations, System 2 converges at $E_b/N_0 = -9.0$ dB, which is 0.4 dB from the maximum achievable rate obtained using the EXIT chart. Finally, System 1 performs within 0.9 dB from the maximum achievable rate limit.

Finally, Figure 5.31 shows the coding gain achieved at a BER of 10^{-5} for each system versus the detection complexity expressed in terms of the number of trellis states. Figure 5.31 demonstrates that System 1 employing the two-stage iteratively-detected system in conjunction with the RSC(2,1,3) code has the lowest complexity at a distance of 0.9 dB from the maximum achievable rate limit, where System 1 converges and hence approaches an infinitesimally low BER. System 3 is capable of performing equally well in BER terms, while operating 0.3 dB closer to the maximum achievable rate limit than System 1. However, this is achieved at the cost of almost doubling the complexity, as seen in Figure 5.31. On the other hand, in order to operate as close as $E_b/N_0 = 0.2$ dB from the maximum achievable rate limit, System 2 using IrCCs

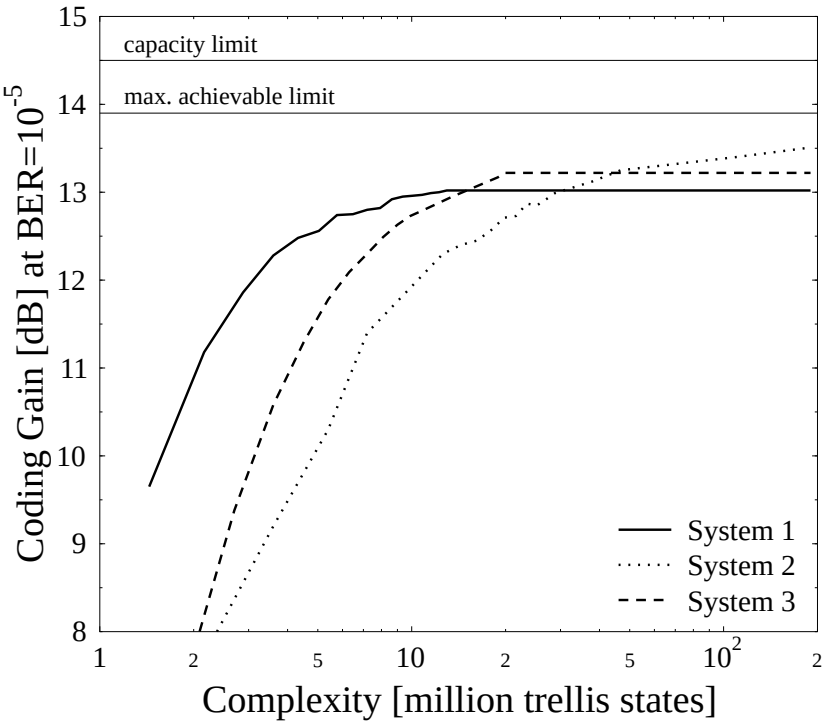

Figure 5.31: Comparison of the coding gain at a BER of 10^{-5} versus the complexity in terms of the number of trellis states of the three proposed LSSTC-SP aided systems while employing the system parameters in Table 5.1.

has to be employed in order to further reduce the EXIT tunnel's area. However, to match the EXIT chart predictions of Figure 5.14, the system requires a large number of iterations between Decoder I and Decoder II. When employing as many as 100 decoding iterations, System 2 becomes capable of performing within 0.4 dB from the maximum achievable rate limit, although this is achieved at the cost of a complexity that is 20 times that required for operating within 0.9 dB from the maximum achievable rate limit using System 1 and 10 times that necessitated by operating within 0.6 dB from the maximum achievable rate limit, when employing System 3. Note that the coding gain seen in Figure 5.31 for System 2 does not saturate and thus, provided that a higher number of iterations is affordable, a higher coding gain can be attained, as expected from the EXIT chart of Figure 5.14.

5.6 Chapter Conclusion

In this chapter, we proposed a novel multi-functional MIMO scheme that combines the benefits of STC, V-BLAST as well as beamforming. The system is also combined with multi-dimensional SP modulation facilitating the joint design of the AA's space-time signals and hence maximising the coding advantage of the transmission scheme. We also quantified the capacity of the LSSTC-SP scheme and computed an upper limit on the achievable bandwidth efficiency of

the system, which is based on EXIT charts. Furthermore, we proposed three near-capacity iteratively-detected LSSTC-SP schemes, where iterative detection is carried out between an outer code decoder, an intermediate code decoder and an LSSTC-SP demapper. The three proposed schemes differ in the number of inner iterations employed between Decoder II and the SP demapper, as well as in the choice of the outer code, which is either a regular RSC code or an IrCC. On the other hand, the intermediate code employed is a URC, which is capable of completely eliminating the system's error-floor as well as operating at the lowest possible turbo-cliff SNR without significantly increasing the associated complexity or interleaver delay. Explicitly, the system can operate within 0.9 dB, 0.6 dB and 0.4 dB from the maximum achievable rate limit. However, to operate within 0.6 dB from the maximum achievable rate limit, the system imposes twice the complexity compared to a system operating within 0.9 dB from this limit. On the other hand, to operate as close as 0.4 dB from the maximum achievable rate limit, the system imposes 20 times higher complexity as the one operating within 0.9 dB from the maximum achievable rate limit. The proposed design principles are applicable to an arbitrary number of antennas and diverse antenna configurations as well as modem schemes.

5.7 Chapter Summary

In this chapter, we proposed a multi-functional Multiple-Input Multiple-Output (MIMO) scheme, that combines the benefits of Vertical Bell Labs Layered Space-Time (V-BLAST) codes, of space-time codes as well as of beamforming. Thus, the proposed system benefits from the multiplexing gain of V-BLAST, from the diversity gain of space-time codes and from the SNR gain of the beamformer. This multi-functional MIMO scheme was referred to as a Layered Steered Space-Time Code (LSSTC). To further enhance the attainable system performance and to maximise the coding advantage of the proposed transmission scheme, the system was also combined with multi-dimensional SP modulation.

In Section 5.3 we quantified the capacity of the proposed multi-functional MIMO scheme and presented the capacity limits for a system employing $N_t = 4$ transmit antennas, $N_r = 4$ receive antennas and a variable number L_{AA} of elements per AA. Furthermore, in Section 5.4.3 we derived an upper bound of the achievable bandwidth efficiency for the system based on the EXIT charts obtained for the iteratively detected system.

To further enhance the achievable system performance, the proposed MIMO scheme was serially concatenated with an outer code combined with a URC, where three different receiver structures were presented by varying the iterative detection configuration of the constituent decoders/demapper as outlined in Table 5.1. In Section 5.4.1 we provided a brief description of the iteratively detected two-stage RSC-coded LSSTC-SP scheme, where extrinsic information was exchanged between the outer RSC decoder and the inner URC decoder, while no iterations

were carried out between the URC decoder and the SP demapper. The schematic of the system is shown in Figure 5.10. The convergence behaviour of the iterative-detection-aided system was analysed using EXtrinsic Information Transfer (EXIT) charts in Section 5.4.1.1. In Section 5.4.1.2, we employed the powerful technique of EXIT tunnel-area minimisation for near-capacity operation. More specifically, we exploited the well-understood properties of conventional 2D EXIT charts that a narrow but nonetheless open EXIT-tunnel represents a near-capacity performance. Consequently, we invoked IrCCs for the sake of appropriately shaping the EXIT curves by minimising the area within the EXIT-tunnel using the procedure of [191, 194].

In Section 5.4.2 we presented a three-stage iteratively detected RSC-coded LSSTC scheme, where extrinsic information was exchanged between the three constituent demapper/decoders, namely the outer RSC decoder, the inner URC decoder as well as the demapper. 3D EXIT charts were presented in Section 5.4.2.1, followed by Section 5.4.2.2 where the simplified 2D projections of the 3D EXIT charts were provided. In Figure 5.20 we portrayed the wide choice of the SP mapping schemes available and demonstrated that the system employing AGM-6 provided the best achievable performance amongst all possible mapping schemes. By contrast, QPSK modulation has only a single AGM scheme, which was characterised in Figure 5.23.

In Section 5.5 we discussed our performance results and characterised the three proposed iteratively detected LSSTC schemes, while employing the system parameters outlined in Table 5.1. Explicitly, the SP aided system can operate within 0.9 dB, 0.6 dB and 0.4 dB from the maximum achievable rate limit. However, when operating within 0.6 dB from the maximum achievable rate limit, the system imposes twice the complexity compared to a system operating within 0.9 dB from this limit. On the other hand, to operate as close as 0.4 dB from the maximum achievable rate limit, the system imposes a 20 times higher complexity as the one operating within 0.9 dB from the same limit. The proposed design principles are applicable to an arbitrary number of antennas and diverse antenna configurations as well as modem schemes. By contrast, the QPSK modulated iteratively detected three-stage system is capable of operating within 1.54 dB from the maximum achievable rate limit and thus the SP modulated system outperforms its QPSK aided counterpart by about 1 dB at a BER of 10^{-6}.

Chapter 6

Downlink Layered Steered Space-Time Spreading Aided Generalised MultiCarrier Direct Sequence Code Division Multiple Access

6.1 Introduction

In Chapter 5 we presented a multi-functional Multiple Input Multiple Output (MIMO) scheme that combines the benefits of space-time codes, of the Vertical Bell Labs Layered Space Time (V-BLAST) scheme as well as of beamforming. In other words, the Layered Steered Space-Time Code (LSSTC) of Chapter 5 benefits from a spatial diversity gain, multiplexing gain as well as beamforming gain. The correct decoding of the LSSTC of Chapter 5 requires that the number of receive antennas is higher than or equal to the number of transmit antennas. This condition makes the LSSTC scheme less practical, especially when we consider the DownLink (DL) scheme of a Base Station (BS) communicating with a Mobile Station (MS). The LSSTC scheme can however be conveniently applied for communicating between two BSs or between a BS and a laptop. To make the multi-functional MIMO presented in Chapter 5 more practical, we present in this chapter a multi-functional MIMO scheme employing four DL transmit and two receive antennas, which constitutes a rank-deficient scheme, where the channel matrix is non-invertible. However, we use linear decoding to decode the twin-antenna-based received signal. The proposed multi-functional MIMO combines the benefits of Space-Time Spreading (STS), V-BLAST, generalised MultiCarrier Direct Sequence Code Division Multiple Access (MC DS-CDMA) as well as beamforming. Therefore, the proposed scheme benefits from a

spatial diversity gain, a frequency diversity gain, a multiplexing gain as well as beamforming gain.

Alamouti [44] discovered a witty transmit diversity scheme using two transmit antennas, which was generalised by Tarokh *et al.* [46, 47] to an arbitrary number of transmit antennas, defining the concept of Space-Time Block Codes (STBC). Inspired by the philosophy of STBCs, Hochwald *et al.* [49] proposed the transmit diversity concept known as Space-Time Spreading (STS) for the downlink of Wideband Code Division Multiple Access (WCDMA) [25] that is capable of achieving the highest possible transmit diversity gain.

In [113] the authors presented a transmission scheme referred to as Double Space-Time Transmit Diversity (D-STTD), which consists of two Space-Time Block Code (STBC) layers at the transmitter that is equipped with four transmit antennas, while the receiver is equipped with two antennas. The decoding of D-STTD presented in [113] is based on a linear decoding scheme presented in [123], where the authors presented a broad overview of space-time coding and signal processing designed for high data rate wireless communications. In [123] a two-user scheme was presented, where each user is equipped with a two-antenna-aided STBC block transmitting at the same carrier frequency and in the same time slot. A two-antenna-aided receiver was implemented for the sake of decoding the users' data, while eliminating the interference imposed by the users on each others' data. A zero-forcing decoder designed for the D-STTD was presented in [120] for the sake of reducing the decoding complexity. Finally, [112, 124] present further results that compare the performance of STBC versus D-STTD and extends the applicability of the scheme to more than two STBC layers.

On the other hand, beamforming [103] constitutes an effective technique of reducing the multiple-access interference, where the antenna gain is increased in the direction of the desired user whilst reducing the gain towards the interfering users. Several attempts have been made to design hybrid MIMO schemes combining STBC with beamforming [114, 116–118, 125, 257]. In order to achieve additional performance gains, beamforming has also been combined with STBC to attain a higher SNR gain [114]. In [257] eigen-beamforming was combined with STBC while allocating the transmitted power equally between the different antenna elements. On the other hand, ideal beamforming was combined with STBCs in [125] for the sake of demonstrating the performance gains attained by such a combination.

Additionally, MultiCarrier Code Division Multiple Access (MC CDMA) [25, 258] is based on a combination of code division and multicarrier or Orthogonal Frequency Division Multiplexing (OFDM) techniques [258]. In [259] a generalised MC DS-CDMA scheme was proposed that includes the subclasses of both multi-tone [260] and orthogonal MC DS-CDMA [261] as special cases. Additionally, in [3, 12, 262] STS has been combined with beamforming and with

generalised MC DS-CDMA for the sake of combining the benefits of spatial diversity, frequency diversity as well as beamforming gain.

Furthermore, in [175], the employment of the iterative decoding principle [163] was considered for iterative soft demapping in the context of multilevel modulation schemes combined with channel decoding. It was also demonstrated in [183] that a recursive inner code is needed in order to maximise the interleaver gain and to avoid the formation of a BER floor, when employing iterative decoding. In [185], unity-rate inner codes were employed for designing low complexity iterative detection aided schemes suitable for bandwidth and power limited systems having stringent BER requirements. In [186], Brink proposed the employment of the so-called EXtrinsic Information Transfer (EXIT) characteristics between a concatenated decoder's input and output for describing the flow of extrinsic information through the soft-in soft-out constituent decoders.

In a nutshell, in this chapter we propose a system that combines the benefits STS, V-BLAST, beamforming as well as generalised MC DS-CDMA. The proposed system is referred to as Layered Steered Space-Time Spreading (LSSTS) aided generalised MC DS-CDMA. The system is characterised by the spatial diversity gain of the STS, the multiplexing gain of the V-BLAST, the frequency diversity gain of the generalised MC DS-CDMA as well as beamforming gain. In the generalised MC DS-CDMA scheme considered in this chapter, the subcarrier frequencies are arranged in a way that guarantees that the same STS signal is spread to and hence transmitted by the specific V number of subcarriers having the maximum possible frequency separation, so that they experience independent fading and achieve the maximum attainable frequency diversity. Therefore, the novelty and rationale of the proposed system can be summarised as follows:

1. *We amalgamate the merits of V-BLAST, STS, beamforming and generalised MC DS-CDMA for the sake of achieving a multiplexing gain, a spatial and frequency diversity gain as well as beamforming gain. We propose a transmission scheme equipped with four transmit and two receive antennas and employ a low-complexity linear receiver to decode the received signal.*

2. *We demonstrate that the number of users supported is substantially increased by invoking combined spreading in both the Time Domain (TD) and the Frequency Domain (FD). We also use a user-grouping technique for minimising the Multi-User Interference (MUI) imposed, when employing TD and FD spreading in the LSSTS-aided generalised MC DS-CDMA downlink scheme.*

3. *We propose three iteratively detected LSSTS schemes, where iterative detection is carried out by exchanging extrinsic information between two serially concatenated channel codes. We use EXIT charts to analyse the convergence behaviour of the proposed iterative detec-*

tion aided schemes and propose a novel Logarithm Likelihood Ratio (LLR) post-processing technique for improving the iteratively detected systems' performance. The three iterative detection aided schemes differ in the way the channel coding is implemented in the different STS layers. The overall code-rate of Systems 1-3 *is identical.*

(a) In the first scheme, referred to as System 1*, a single outer and a single inner channel code is used to encode the bits transmitted.*

(b) In the second scheme, namely System 2*, a single outer code is implemented, whose output is split into two substreams each of which are encoded using a separate inner code.*

(c) By contrast, in the third proposed scheme referred to as System 3*, the input data bit stream is first split into two different substreams, where a pair of different outer as well as inner codes are implemented in the different substreams.*

We will show that the three systems exhibit a similar complexity quantified in terms of the total number of trellis states encountered, which determines the number of Add-Compare-Select (ACS) arithmetic operations. Similarly, we will demonstrate that provided we employ sufficiently long interleavers, the three systems attain a similar BER performance. By contrast, when shorter interleavers are employed, System 1 *performs better than System* 2*, which in turn performs better than System* 3*. This is due to the fact that the interleaver depth of System* 2 *and System* 3 *is lower than that of System* 1 *since the bit stream is split into two substreams in System* 2 *and System* 3*, which constrains the interleaver to be shorter and hence the correlation in the extrinsic information becomes higher, which eventually decays the BER performance.*

The rest of the chapter is organised as follows. In Section 6.2 we present the encoding and decoding algorithms of the LSSTS aided generalised MC DS-CDMA scheme and demonstrate how the scheme benefits from the diversity gain, the multiplexing gain and the beamforming gain. In Section 6.3 we present how the TD and FD spreading can be combined in order to increase the number of users supported by the system and we introduce the user-grouping technique for reducing the MUI. Iterative detection of the proposed system is discussed in Section 6.4, where we introduce the LLR post-processing technique followed by a comparison of the attainable performance of the proposed schemes in Section 6.5. We present our conclusions in Section 6.6 followed by a brief chapter summary discussing both the main contributions and the organisation of this chapter in Section 6.7.

6.2 Layered Steered Space-Time Spreading Aided Generalised MC DS-CDMA

In this section we describe the proposed Layered Steered Space-Time Spreading (LSSTS) aided generalised MC DS-CDMA scheme designed for achieving spatial diversity gain, frequency diversity gain, multiplexing gain as well as beamforming gain. The antenna architecture employed in Figure 6.1 for the proposed scheme is equipped with N_t=4 transmit Antenna Arrays (AA) spaced sufficiently far apart in order to experience independent fading. The L_{AA} number of elements of each of the AAs are spaced at a distance of half the wavelength for the sake of achieving beamforming. Furthermore, the receiver is equipped with N_r=2 antennas. The system can support K users transmitting at the same time and using the same carrier frequencies, while they can be differentiated by the user-specific spreading code $\bar{\mathbf{c}}_k$, where $k \in [1, K]$. Additionally, in the generalised MC DS-CDMA considered, the subcarrier frequencies are arranged in a way that guarantees that the same STS signal is spread to and hence transmitted by the specific V number of subcarriers having the maximum possible frequency separation, so that they experience independent fading and achieve the maximum attainable frequency diversity.

6.2.1 Transmitter Model

The system considered employs the generalised MC DS-CDMA scheme of [259] using UV number of subcarriers. The transmitter schematic of the kth user is shown in Figure 6.1, where a block of UN_t data symbols $\mathbf{x}$ is Serial-to-Parallel (S/P) converted to U parallel sub-blocks. Afterwards, each set of N_t symbols is S/P converted to G=2 groups, where each group is encoded using the N_{tg}=2 antenna-aided Space-Time Spreading (STS) procedure of [49], where the transmitted signal is spread to N_{tg} transmit antennas with the aid of the orthogonal spreading codes of $\{\bar{\mathbf{c}}_{k,1}, \bar{\mathbf{c}}_{k,2}, \cdots, \bar{\mathbf{c}}_{k,N_{tg}}\}$, k=1, 2, ..., K.

The spreading codes $\bar{\mathbf{c}}_{k,1}$ and $\bar{\mathbf{c}}_{k,2}$ are generated from the same user-specific spreading code $\bar{\mathbf{c}}_k$ by ensuring that the two spreading codes $\bar{\mathbf{c}}_{k,1}$ and $\bar{\mathbf{c}}_{k,2}$ become orthogonal using the simple code-concatenation rule of Walsh-Hadamard codes, yielding longer codes and hence a proportionately reduced per-antenna throughput according to:

$$\bar{\mathbf{c}}_{k,1} = [\bar{\mathbf{c}}_k^T \quad \bar{\mathbf{c}}_k^T]^T \tag{6.1}$$

$$\bar{\mathbf{c}}_{k,2} = [\bar{\mathbf{c}}_k^T \quad -\bar{\mathbf{c}}_k^T]^T. \tag{6.2}$$

The discrete symbol duration of the orthogonal STS codes is $N_{tg}N_e$, where N_e represents the kth user's TD spreading factor. Each of the U sub-blocks is then divided into two half-rate substreams and the two consecutive symbols in each substream are then spread to both

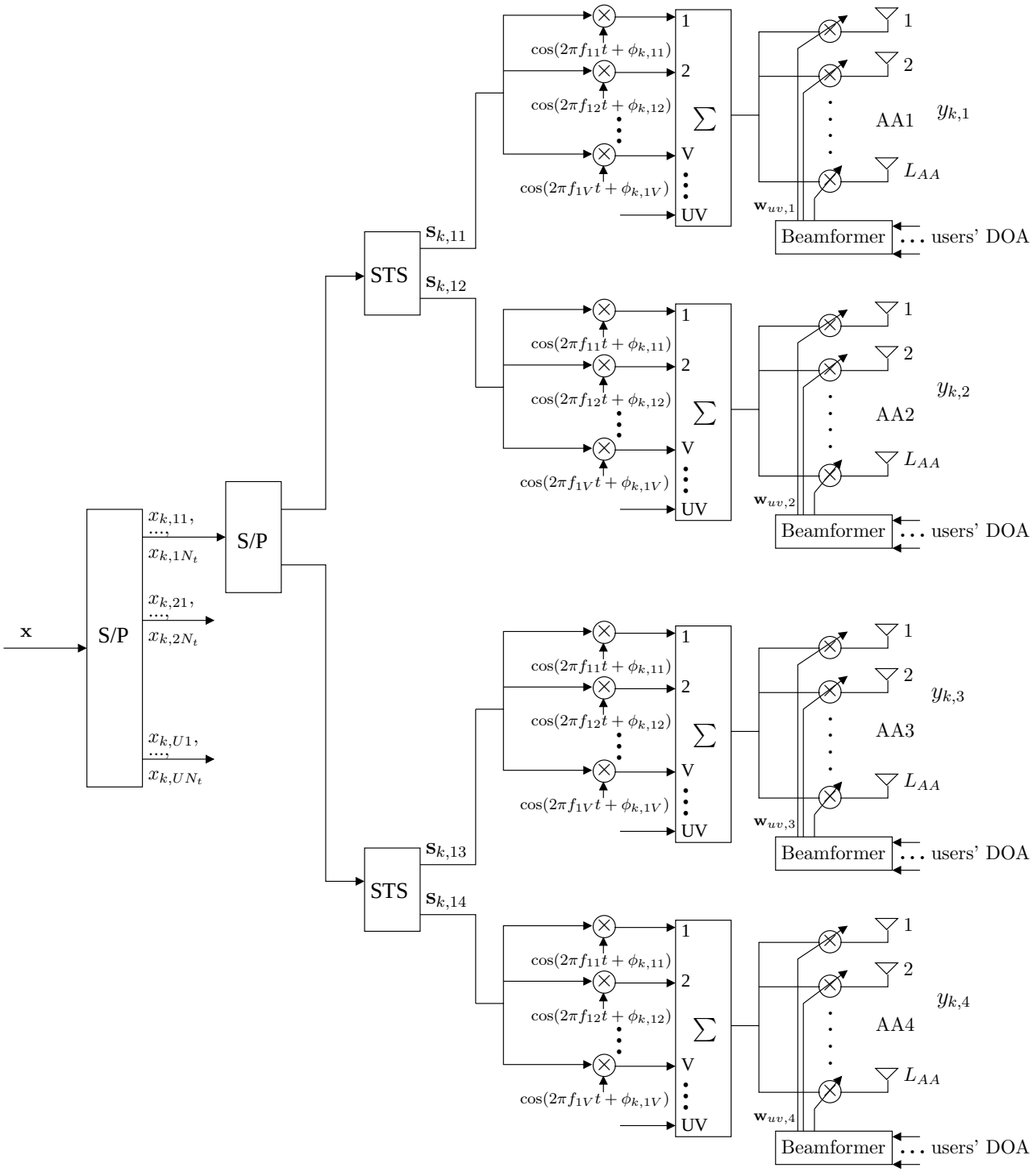

Figure 6.1: The k_{th} user's LSSTS aided Generalised MC DS-CDMA transmitter system model.

transmit antennas using the mapping of:

$$\mathbf{s}_{k,u1} = \left(\bar{\mathbf{c}}_{k,1} \cdot x_{k,u1} + \bar{\mathbf{c}}_{k,2} \cdot x^*_{k,u2}\right) \tag{6.3}$$

$$\mathbf{s}_{k,u2} = \left(\bar{\mathbf{c}}_{k,1} \cdot x_{k,u2} - \bar{\mathbf{c}}_{k,2} \cdot x^*_{k,u1}\right) \tag{6.4}$$

$$\mathbf{s}_{k,u3} = \left(\bar{\mathbf{c}}_{k,1} \cdot x_{k,u3} + \bar{\mathbf{c}}_{k,2} \cdot x^*_{k,u4}\right) \tag{6.5}$$

$$\mathbf{s}_{k,u4} = \left(\bar{\mathbf{c}}_{k,1} \cdot x_{k,u4} - \bar{\mathbf{c}}_{k,2} \cdot x^*_{k,u3}\right), \tag{6.6}$$

which is exemplified in simple graphical terms in Figure 2.3.

The UN_t outputs of the UG number of STS blocks modulate a group of subcarrier frequencies $\{f_{u,1}, f_{u,2}, ..., f_{u,V}\}$. Since each of the U sub-blocks is spread to and hence conveyed with the aid of V subcarriers, a total of UV number of subcarriers are required in the MC DS-CDMA system considered. The UV number of subcarrier signals are superimposed on each other in order to form the complex modulated signal. The subcarrier frequencies are arranged in a way that guarantees that the same STS signal is spread to and hence transmitted by the specific V subcarriers having the maximum possible frequency separation, so that they experience independent fading and achieve the maximum attainable frequency diversity. Finally, according to the kth user's channel information, the UVN_t signals of the kth user are weighted by the transmit weight vector $\mathbf{w}^{(k)}_{uv,n}$ determined for the uvth subcarrier of the kth user, which is generated for the nth AA.

The k_{th} user's transmitted signal can be written as follows:

$$\mathbf{y}_{k,1} = \sum_{u=1}^{U}\sum_{v=1}^{V}\sqrt{\frac{2P_k}{VL_{AA}}\frac{1}{N_tN_{tg}}}(\mathbf{w}^k_{uv,1} \otimes I_{2N_e}) \cdot \mathbf{s}_{k,u1} \tag{6.7}$$

$$\mathbf{y}_{k,2} = \sum_{u=1}^{U}\sum_{v=1}^{V}\sqrt{\frac{2P_k}{VL_{AA}}\frac{1}{N_tN_{tg}}}(\mathbf{w}^k_{uv,2} \otimes I_{2N_e}) \cdot \mathbf{s}_{k,u2} \tag{6.8}$$

$$\mathbf{y}_{k,3} = \sum_{u=1}^{U}\sum_{v=1}^{V}\sqrt{\frac{2P_k}{VL_{AA}}\frac{1}{N_tN_{tg}}}(\mathbf{w}^k_{uv,3} \otimes I_{2N_e}) \cdot \mathbf{s}_{k,u3} \tag{6.9}$$

$$\mathbf{y}_{k,4} = \sum_{u=1}^{U}\sum_{v=1}^{V}\sqrt{\frac{2P_k}{VL_{AA}}\frac{1}{N_tN_{tg}}}(\mathbf{w}^k_{uv,4} \otimes I_{2N_e}) \cdot \mathbf{s}_{k,u4}, \tag{6.10}$$

where $\otimes$ represents the Hadamard product, P_k/V represents the transmitted power of each subcarrier, the factor L_{AA} in the denominator is due to beamforming and the factor N_tN_{tg} in the denominator suggests that the STS scheme using N_t transmit antennas and N_{tg} orthogonal spreading codes distributes its power proportionally in space and time.

The bandwidth efficiency of the proposed system can be formulated as follows. Assuming that the system employs a modulation scheme transmitting B bits-per-symbol, then the bandwidth efficiency of the LSSTS aided Generalised MC DS-CDMA is given by $2UB$ bits-per-channel-use.

6.2.2 Receiver Model

Let us assume that there are N_t number of transmit AAs at the Base Station (BS), which are located sufficiently far apart from each other, having an antenna-spacing of about 10λ, where λ represents the carriers wavelength. The channel impulse response vector $\mathbf{h}_{uv,nm}$ spanning the nth transmit antenna array, $n \in [1, N_t]$, and the mth receive antenna, $m \in [1, N_r]$, while employing the uvth subcarrier can be expressed as:

$$\begin{aligned} \mathbf{h}^k_{uv,nm} &= \left[h^k_{uv,nm0}, h^k_{uv,nm1}, \ldots, h^k_{uv,nm(L_{AA}-1)}\right]^T \\ &= \mathbf{a}^k_{uv,nm} \\ &= \left[a^k_{uv,nm0}, a^k_{uv,nm1}, \ldots, a^k_{uv,nm(L_{AA}-1)}\right]^T, \end{aligned} \tag{6.11}$$

where $a_{uv,nml}$ is the CIR with respect to the nmth link, uvth subcarrier and the lth element of the nth AA. Based on the assumption that the array elements are separated by half a wavelength, we can simplify $\mathbf{a}^k_{uv,nm}$ according to

$$\begin{aligned} \mathbf{a}^k_{uv,nm} &= \alpha^k_{uv,nm} \cdot \mathbf{d}^k_{nm} \\ &= \alpha^k_{uv,nm} \left[1, \exp(j[\pi \sin(\psi^k_{nm})]), \ldots, \exp(j[(L_{AA}-1)\pi \sin(\psi^k_{nm})])\right]^T, \end{aligned} \tag{6.12}$$

where α_{nm} is a Rayleigh faded envelope,

$$\mathbf{d}^k_{nm} = \left[1, \exp(j[\pi \sin(\psi^k_{nm})]), \ldots, \exp(j[(L_{AA}-1)\pi \sin(\psi^k_{nm})])\right]^T, \tag{6.13}$$

and ψ_{nm} is the nmth link's Direction Of Arrival (DOA). As for the AA specific DOA, we consider a scenario where the distance between the transmitter and the receiver is significantly higher than that between the AAs and thus we can assume that the signals arrive at the different AAs in parallel, i.e. the DOA at the different AAs is the same.

Assuming that the K users' data expressed in the form of Equations (6.7)-(6.10) are transmitted synchronously over a dispersive Rayleigh fading channel characterised by the CIR of Equation (6.11), the complex-valued received signal of user 1 over the two receive antennas can be expressed as

$$\begin{aligned} \mathbf{z}^1_1 &= \sum_{k=1}^{K}\sum_{u=1}^{U}\sum_{v=1}^{V} \big((\mathbf{h}_{uv,11} \otimes I_{2N_e})^T \cdot \mathbf{y}_{k,uv1} + (\mathbf{h}_{uu,21} \otimes I_{2N_e})^T \cdot \mathbf{y}_{k,uv2} \\ &+ (\mathbf{h}_{uv,31} \otimes I_{2N_e})^T \cdot \mathbf{y}_{k,uv3} + (\mathbf{h}_{uv,41} \otimes I_{2N_e})^T \cdot \mathbf{y}_{k,uv4}\big) + \mathbf{n}_1, \end{aligned} \tag{6.14}$$

$$\begin{aligned} \mathbf{z}^1_2 &= \sum_{k=1}^{K}\sum_{u=1}^{U}\sum_{v=1}^{V} \big((\mathbf{h}_{uv,12} \otimes I_{2N_e})^T \cdot \mathbf{y}_{k,uv1} + (\mathbf{h}_{uv,22} \otimes I_{2N_e})^T \cdot \mathbf{y}_{k,uv2} \\ &+ (\mathbf{h}_{uv,32} \otimes I_{2N_e})^T \cdot \mathbf{y}_{k,uv3} + (\mathbf{h}_{uv,42} \otimes I_{2N_e})^T \cdot \mathbf{y}_{k,uv4}\big) + \mathbf{n}_2. \end{aligned} \tag{6.15}$$

In Equations (6.7)-(6.10), $\mathbf{w}^k_{uv,nm}$ represents the weight vector of the desired user derived from the nmth antenna link and the uvth subcarrier, which is generated by the MRC beam-

former [242] with the aid of channel state information. Let $\mathbf{w}^1_{uv,nm}$=$\mathbf{d}^{1\dagger}_{nm}$, then the k=1st user's received signal for the uvth subcarrier can be simplified to

$$\mathbf{z}^1_{uv,1} = L_{AA}\left[\alpha_{uv,11}\mathbf{y}_{1,uv1} + \alpha_{uv,21}\mathbf{y}_{1,uv2} + \alpha_{uv,31}\mathbf{y}_{1,uv3} + \alpha_{uv,41}\mathbf{y}_{1,uv4}\right] + \mathbf{n}_{uv,1}, \tag{6.16}$$

$$\mathbf{z}^1_{uv,2} = L_{AA}\left[\alpha_{uv,12}\mathbf{y}_{1,uv1} + \alpha_{uv,22}\mathbf{y}_{1,uv2} + \alpha_{uv,32}\mathbf{y}_{1,uv3} + \alpha_{uv,42}\mathbf{y}_{1,uv4}\right] + \mathbf{n}_{uv,2}. \tag{6.17}$$

The two received signals $\mathbf{z}_{uv,1}$ and $\mathbf{z}_{uv,2}$, corresponding to the first and second receive antennas, respectively, are then correlated with $\bar{\mathbf{c}}_{1,1}$ and $\bar{\mathbf{c}}_{1,2}$ of Equations (6.1) and (6.2) according to the following operations:

$$\begin{aligned} r^1_{uv,11} &= \bar{\mathbf{c}}^\dagger_{1,1} \cdot \mathbf{z}^1_{uv,1} \qquad (6.18)\\ &= \sqrt{\frac{2P_1}{VL_{AA}}\frac{1}{N_tN_{tg}}}L_{AA}\left[\alpha_{uv,11}x_{1,u1} + \alpha_{uv,21}x_{1,u2} + \alpha_{uv,31}x_{1,u3} + \alpha_{uv,41}x_{1,u4}\right]\\ &\quad + \bar{\mathbf{c}}^\dagger_{1,1} \cdot \mathbf{n}_{uv,1}\\ r^1_{uv,12} &= \bar{\mathbf{c}}^\dagger_{1,2} \cdot \mathbf{z}^1_{uv,1} \qquad (6.19)\\ &= \sqrt{\frac{2P_1}{VL_{AA}}\frac{1}{N_tN_{tg}}}L_{AA}\left[-\alpha_{uv,11}x^*_{1,u2} + \alpha_{uv,21}x^*_{1,u1} - \alpha_{uv,31}x^*_{1,u4} + \alpha_{uv,41}x^*_{1,u3}\right]\\ &\quad + \bar{\mathbf{c}}^\dagger_{1,2} \cdot \mathbf{n}_{uv,1}\\ r^1_{uv,21} &= \bar{\mathbf{c}}^\dagger_{1,1} \cdot \mathbf{z}^1_{uv,2} \qquad (6.20)\\ &= \sqrt{\frac{2P_1}{VL_{AA}}\frac{1}{N_tN_{tg}}}L_{AA}\left[\alpha_{uv,12}x_{1,u1} + \alpha_{uv,22}x_{1,u2} + \alpha_{uv,32}x_{1,u3} + \alpha_{uv,42}x_{1,u4}\right]\\ &\quad + \bar{\mathbf{c}}^\dagger_{1,1} \cdot \mathbf{n}_{uv,2}\\ r^1_{uv,22} &= \bar{\mathbf{c}}^\dagger_{1,2} \cdot \mathbf{z}^1_{uv,2} \qquad (6.21)\\ &= \sqrt{\frac{2P_1}{VL_{AA}}\frac{1}{N_tN_{tg}}}L_{AA}\left[-\alpha_{uv,12}x^*_{1,u2} + \alpha_{uv,22}x^*_{1,u1} - \alpha_{uv,32}x^*_{1,u4} + \alpha_{uv,42}x^*_{1,u3}\right]\\ &\quad + \bar{\mathbf{c}}^\dagger_{1,2} \cdot \mathbf{n}_{uv,2}. \end{aligned}$$

The received and despread signals of Equations (6.18)-(6.21) can be written in a matrix form as follows:

$$\mathbf{r}_{uv}^{1} = \begin{bmatrix} r_{uv,11}^{1} \\ r_{uv,12}^{1*} \\ r_{uv,21}^{1} \\ r_{uv,22}^{1*} \end{bmatrix} \tag{6.22}$$

$$= \sqrt{\frac{2P_1 L_{AA}}{V} \frac{1}{N_t N_{tg}}} \begin{bmatrix} \alpha_{uv,11} & \alpha_{uv,21} & \alpha_{uv,31} & \alpha_{uv,41} \\ \alpha_{uv,21}^{*} & -\alpha_{uv,11}^{*} & \alpha_{uv,41}^{*} & -\alpha_{uv,31}^{*} \\ \alpha_{uv,12} & \alpha_{uv,22} & \alpha_{uv,32} & \alpha_{uv,42} \\ \alpha_{uv,22}^{*} & -\alpha_{uv,12}^{*} & \alpha_{uv,42}^{*} & -\alpha_{uv,32}^{*} \end{bmatrix} \cdot \begin{bmatrix} x_{1,u1} \\ x_{1,u2} \\ x_{1,u3} \\ x_{1,u4} \end{bmatrix} + \begin{bmatrix} \bar{\mathbf{c}}_{1,1}^{\dagger} \cdot \mathbf{n}_1 \\ (\bar{\mathbf{c}}_{1,2}^{\dagger} \cdot \mathbf{n}_1)^{*} \\ \bar{\mathbf{c}}_{1,1}^{\dagger} \cdot \mathbf{n}_2 \\ (\bar{\mathbf{c}}_{1,2}^{\dagger} \cdot \mathbf{n}_2)^{*} \end{bmatrix}.$$

Therefore, the received and despread signal matrix $\mathbf{r}$ can be written as[1]:

$$\mathbf{r} = \mathbf{H} \cdot \mathbf{X} + \mathbf{N}. \tag{6.23}$$

The channel matrix $\mathbf{H}$ can be represented as:

$$\mathbf{H} = \begin{bmatrix} \mathbf{H}_1 & \mathbf{H}_2 \\ \mathbf{G}_1 & \mathbf{G}_2 \end{bmatrix}, \tag{6.24}$$

where $\mathbf{H}_1 = \begin{bmatrix} \alpha_{uv,11} & \alpha_{uv,21} \\ \alpha_{uv,21}^{*} & -\alpha_{uv,11}^{*} \end{bmatrix}$, $\mathbf{H}_2 = \begin{bmatrix} \alpha_{uv,31} & \alpha_{uv,41} \\ \alpha_{uv,41}^{*} & -\alpha_{uv,31}^{*} \end{bmatrix}$, $\mathbf{G}_1 = \begin{bmatrix} \alpha_{uv,12} & \alpha_{uv,22} \\ \alpha_{uv,22}^{*} & -\alpha_{uv,12}^{*} \end{bmatrix}$ and $\mathbf{G}_2 = \begin{bmatrix} \alpha_{uv,32} & \alpha_{uv,42} \\ \alpha_{uv,42}^{*} & -\alpha_{uv,32}^{*} \end{bmatrix}$.

Additionally, the transmitted symbol matrix can be written as $\mathbf{X} = \begin{bmatrix} \mathbf{X}_1 \\ \mathbf{X}_2 \end{bmatrix}$, where $\mathbf{X}_1 = \begin{bmatrix} x_{1,u1} \\ x_{1,u2}^{*} \end{bmatrix}$ and $\mathbf{X}_2 = \begin{bmatrix} x_{1,u3} \\ x_{1,u4}^{*} \end{bmatrix}$.

Hence, the received and despread signal can be represented as:

$$\mathbf{r} = \begin{bmatrix} \mathbf{r}_1 \\ \mathbf{r}_2 \end{bmatrix} = \begin{bmatrix} \mathbf{H}_1 & \mathbf{H}_2 \\ \mathbf{G}_1 & \mathbf{G}_2 \end{bmatrix} \cdot \begin{bmatrix} \mathbf{X}_1 \\ \mathbf{X}_2 \end{bmatrix} + \begin{bmatrix} \mathbf{N}_1 \\ \mathbf{N}_2 \end{bmatrix}. \tag{6.25}$$

The decoding is carried out in two steps, first the interference cancellation is performed according to [113, 123] followed by the STS decoding procedure of [49]. The interference cancellation employed completely eliminates the interference of the two layers on each other as follows. The received and despread signal matrix $\mathbf{r}$ is multiplied by a matrix $\mathbf{Q}$ yielding:

$$\mathbf{Q} \cdot \mathbf{r} = \begin{bmatrix} \widetilde{\mathbf{r}}_1 \\ \widetilde{\mathbf{r}}_2 \end{bmatrix} = \begin{bmatrix} \widetilde{\mathbf{H}} & \mathbf{0} \\ \mathbf{0} & \widetilde{\mathbf{G}} \end{bmatrix} \cdot \begin{bmatrix} \mathbf{X}_1 \\ \mathbf{X}_2 \end{bmatrix} + \begin{bmatrix} \widetilde{\mathbf{N}}_1 \\ \widetilde{\mathbf{N}}_2 \end{bmatrix}. \tag{6.26}$$

[1] In the following analysis we remove the subscript uv for simplicity of notation.

According to Equation (6.26) the modified received signal $\tilde{\mathbf{r}}_1$ depends only on signals transmitted from the first STS layer and the modified received signal $\tilde{\mathbf{r}}_2$ depends only on signals transmitted from the second STS layer. It was shown in [123] that a solution for $\mathbf{Q}$ is given by:

$$\mathbf{Q} = \begin{bmatrix} \mathbf{I}_2 & -\mathbf{G}_1\mathbf{G}_2^{-1} \\ -\mathbf{H}_2\mathbf{H}_1^{-1} & \mathbf{I}_2 \end{bmatrix}, \tag{6.27}$$

where $\mathbf{I}_2$ is the identity matrix of dimension 2×2.

Hence, $\widetilde{\mathbf{H}}$ and $\widetilde{\mathbf{G}}$ can be expressed as

$$\widetilde{\mathbf{H}} = \mathbf{H}_1 - \mathbf{G}_1\mathbf{G}_2^{-1}\mathbf{H}_2 \tag{6.28}$$

$$\widetilde{\mathbf{G}} = \mathbf{G}_2 - \mathbf{H}_2\mathbf{H}_1^{-1}\mathbf{G}_1. \tag{6.29}$$

An important observation is that the matrices $\widetilde{\mathbf{H}}$ and $\widetilde{\mathbf{G}}$ have the same structure as that of the channel matrix $\mathbf{H}_1$. Hence, the above process will transform the decoding of the LSSTS signal into two separate problems that can be solved by the simple decoding process of STS [49].

Finally, after combining the k=1st user's identical replicas of the same signal transmitted by spreading over V number of subcarriers, the decision variables corresponding to the symbols transmitted in the uth sub-block can be expressed as

$$\widetilde{x}_{1,u} = \sum_{v=1}^{V} \widetilde{x}_{1,uv}. \tag{6.30}$$

The decoded signal can be expressed as

$$\widetilde{x} = \sqrt{\frac{2P_1L_{AA}}{V}\frac{1}{N_tN_{tg}}} \sum_{v=1}^{V} \left(|\widetilde{\alpha}_{uv,1}|^2 + |\widetilde{\alpha}_{uv,2}|^2\right) x + \eta. \tag{6.31}$$

Therefore, according to Equation (6.31) the decoded signal has a diversity order of $2V$. More explicitly, second order spatial diversity is attained from the STS operation and a diversity order of V is achieved as a benefit of spreading by the generalised MC DS-CDMA scheme, where the subcarrier frequencies are arranged in a way that guarantees that the same STS signal is spread to and hence transmitted by the specific V number of subcarriers having the maximum possible frequency separation, so that they experience as independent fading as possible.

We consider a system employing BPSK modulation, L_{AA} number of elements per AA, V number of subcarriers and a TD spreading factor of N_e=32 for the sake of demonstrating the performance improvements achieved by the proposed system. The transmitter is equipped with N_t=4 AAs, while the receiver has N_r=2 antennas. We assume the availability of perfect channel knowledge both at the receiver and at the beamformer. The resultant per-user throughput is 2 bits-per-channel-use. Figure 6.2 portrays the benefits of the different components employed

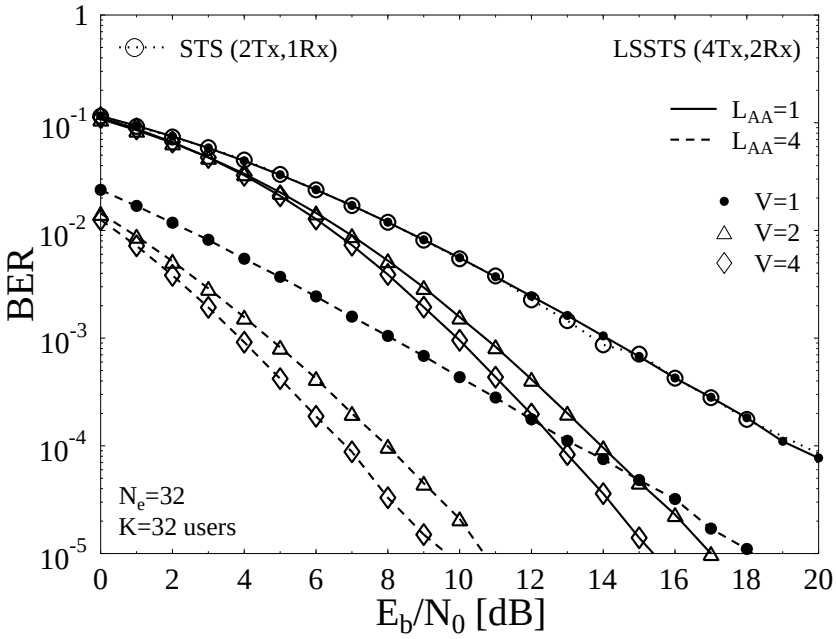

Figure 6.2: BER performance of the proposed system in Figure 6.1 employing N_t=4 AAs and N_r=2 antennas in conjunction with a varying number of L_{AA} elements per AA as well as a varying number of subcarriers V, while employing K=32 users and a spreading factor N_e=32. The per-user throughput is 2 bits-per-channel-use.

in the system, namely the MC DS-CDMA, the beamforming, the STS and the V-BLAST components. When a single carrier is employed, i.e. we have $V = 1$, and $L_{AA} = 1$ element per AA, the system's performance is identical to that of the STS scheme of [49]. Therefore, the system has a diversity order of two, while the bandwidth efficiency of the proposed system is twice that of the STS scheme of [49]. Additionally, Figure 6.2 shows the beamforming gain achieved upon increasing the number of beam-steering elements L_{AA} in the AA, while maintaining the same total number of AAs. As shown in the figure, when the number of beam-steering elements L_{AA} increases, the achievable BER performance substantially improves. Furthermore, to increase the achievable diversity order, the system employs $V > 1$ number of subcarriers, as shown in Figure 6.2. Hence, the proposed system has a diversity order of $2V$ due to the employment of LSSTS aided generalised MC DS-CDMA and the throughput becomes twice that of a system employing only a single STS block, which is a benefit of the V-BLAST structure. Figure 6.2 quantifies the advantages of increasing both L_{AA} and V in the proposed system, where increasing L_{AA} increases the SNR gain of the system while increasing V improves the attainable diversity order.

6.3 Increasing the Number of Users by Employing Time and Frequency Domain Spreading

In the previous section, the DS spreading used by the generalised MC DS-CDMA system was carried out in the Time-Domain (TD) only based on orthogonal Walsh-Hadamard codes. It was proposed in [259, 263–265] to employ spreading in the Frequency-Domain (FD) for the MC-CDMA schemes for the sake of exploiting the attainable diversity gain in the FD. In the generalised MC DS-CDMA scheme considered, the transmitted data stream can be spread in both the TD and FD in order to support more users or to achieve the maximum attainable frequency diversity gain [266]. When FD spreading is employed, the FD spreading is applied after STS TD spreading in Figure 6.1 by multiplying the data symbols of the V subcarriers by the V number of chip values of a spreading code invoked for spreading the data in the FD across the V number of subcarriers. Hence, the spreading factor of the FD spreading code is equal to the number of subcarriers V. The resultant bandwidth in this case is identical to that when the TD-only spreading is considered. Therefore, in this case the system benefits from TD as well as FD spreading, which allows increasing the number of users, as it will be described in Section 6.3.1.

At the receiver side, the received signal is first despread in the TD and then despread by the FD spreading code of length V. Furthermore, the number of users supported by employing generalised MC DS-CDMA using both TD and FD spreading is equal to $N_e \cdot V$. In other words, the N_e users spread in the TD will have a unique spreading code in the FD and the users having a different FD spreading code can share the same TD spreading code. Hence, the complexity of implementing separate TD and FD Multi-User Detectors (MUD) for short spreading codes is expected to be significantly lower than that of a single TD MUD designed for long codes, as exemplified by comparing a 64-chip TD-only scheme to that using 8-chip TD and 8-chip FD spreading. The total number of users supported becomes $V \cdot \mathcal{K}_{max} = V \cdot N_e$, which is V times the number of users supported by the scheme employing TD-only spreading.

6.3.1 Transmitter Model

The transmitter schematic of the proposed system employing TD and FD spreading is shown in Figure 6.1, which has been presented as the system model in Section 6.2 in conjunction with TD-only spreading. The transmitter model is the same as in figure 6.1, except that the V-depth FD repetition scheme in Figure 6.1 is replaced by the V-depth FD spreading arrangement of Figure 6.3. Let us assume that the kth user's FD spreading code can be represented as $\bar{\mathbf{c}}'_k = \{c'_k[1], c'_k[2], \cdots, c'_k[V]\}$. Additionally, the TD spreading code is denoted by $\bar{\mathbf{c}}_k$ as in Section 6.2.1.

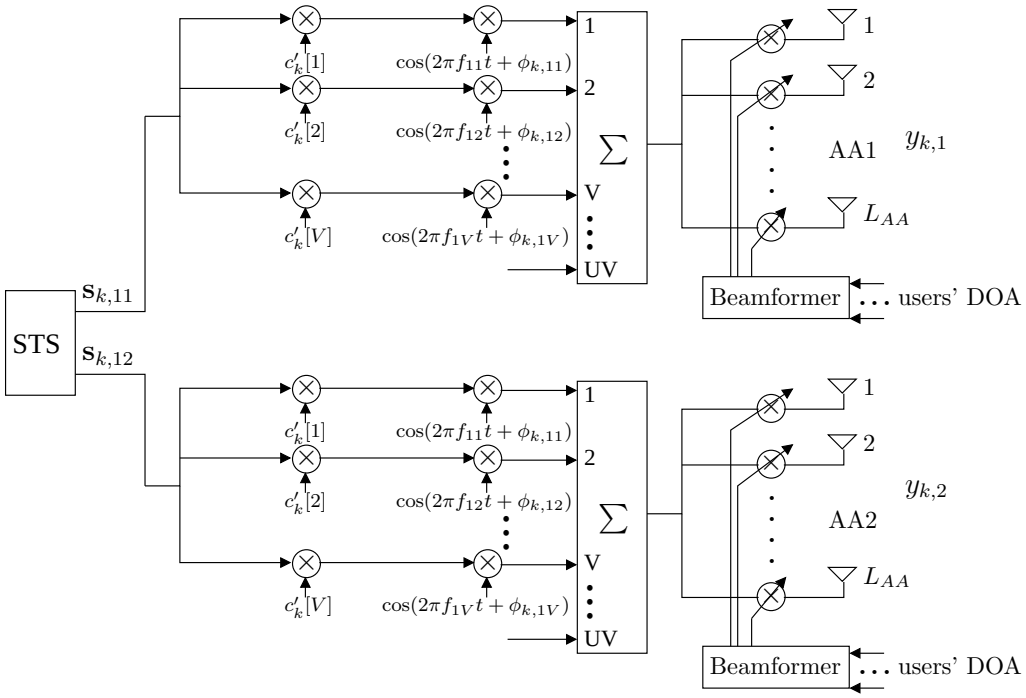

Figure 6.3: The first STS block of Figure 6.1 employing TD and FD spreading.

As shown in Figure 6.1 and as discussed in Section 6.2, the data stream of duration T_b is S/P converted to U parallel sub-streams. Afterwards, each set of N_t symbols is S/P converted to G=2 groups, where each group is encoded using the N_{tg}=2 antenna-aided STS procedure using the spreading code $\bar{\mathbf{c}}_k$, as described in Equations (6.3)-(6.6). Afterwards, when employing TD and FD spreading, instead of using data repetition over V subcarriers as shown in Figure 6.1, the U number of sub-blocks generated after the TD spreading are now further spread across the FD using the previously introduced FD spreading codes $\bar{\mathbf{c}}'$, as depicted in Figure 6.3. When employing TD-only spreading, the number of users $\mathcal{K}_{max}$ that can be supported by the system is equal to the spreading factor of the TD spreading code used, i.e. $\mathcal{K}_{max}$=N_e. On the other hand, the total number of orthogonal codes that can be used for the FD spreading is equal to V. This implies that if V number of users share the same TD spreading code, they can be distinguished by their FD spreading codes. Hence, employing TD and FD spreading increases the number of users to $V \cdot \mathcal{K}_{max}$, as compared to $\mathcal{K}_{max}$ for the system employing TD-only spreading.

The TD and FD orthogonal spreading codes can be assigned as follows. If the number of users is still less than $\mathcal{K}_{max}$, the users will be assigned different TD spreading codes, while sharing the same FD spreading code. The resultant scheme in this case is equivalent to that described in Section 6.2. When the number of users is in the range of $v \cdot \mathcal{K}_{max} \leq K \leq (v+1) \cdot \mathcal{K}_{max}$, where $v = 1, 2, \cdots, V-1$, then the same TD orthogonal spreading code will be assigned to v users, where these users sharing the same TD code will be assigned different

FD orthogonal spreading codes. Hence, the users sharing the same TD spreading code can be distinguished by their corresponding FD spreading code.

Since the subcarrier signals are transmitted over independently fading channels, the orthogonality of the FD spreading codes cannot be retained in frequency-selective fading channels. Hence, Multi-User Interference (MUI) is inevitably introduced, which degrades the attainable BER performance, when the number of users sharing the same TD spreading code increases.

When employing TD and FD spreading, the kth user's transmitted signals can be expressed as

$$\mathbf{y}_{k,n} = \sum_{u=1}^{U}\sum_{v=1}^{V}\sqrt{\frac{2P_k}{VL_{AA}}\frac{1}{N_tN_{tg}}}(\mathbf{w}_{uv,n}^{k}\otimes I_{2N_e})\cdot\mathbf{s}_{k,un}c'_k[v], \tag{6.32}$$

where $n \in [1, N_t]$ represents the number of transmit antenna, P_k/V represents the transmitted power of each subcarrier, the factor L_{AA} in the denominator is due to beamforming and the factor N_tN_{tg} in the denominator suggests that the STS scheme using N_t transmit antennas and N_{tg} orthogonal spreading codes distributes its power proportionally in space and time.

6.3.2 Receiver Model

Let us assume that there are $1 \leq K' \leq V$ number of users sharing the same TD spreading code but are distinguished by their FD spreading codes. Then, when the $K'\mathcal{K}_{max}$ number of users' signals are transmitted over frequency selective fading channels, the complex-valued received signal of user 1 can be expressed as

$$\begin{aligned}\mathbf{z}_m^1 &= \sum_{k=1}^{K'\mathcal{K}_{max}}\sum_{u=1}^{U}\sum_{v=1}^{V}\sum_{n=1}^{N_t}(\mathbf{h}_{uv,nm}\otimes I_{2N_e})^T\cdot\mathbf{y}_{k,uvn}+\mathbf{n}_m \\ &= \sqrt{\frac{2P_k}{VL_{AA}}\frac{1}{N_tN_{tg}}}\sum_{k=1}^{K'\mathcal{K}_{max}}\sum_{u=1}^{U}\sum_{v=1}^{V}\sum_{n=1}^{N_t}(\mathbf{a}_{uv,nm}^T\cdot\mathbf{w}_{uv,n}^1)\otimes I_{2N_e}\cdot\mathbf{s}_{k,un}c'_k[v]+\mathbf{n}_m.\end{aligned} \tag{6.33}$$

Since orthogonal multicarrier signals and orthogonal TD STS spreading codes are used for the synchronous downlink transmission over per-subcarrier Rayleigh flat-fading, there is no interference between the users employing different TD spreading codes or using different subcarrier signals. The receiver in this case performs two main operations. The first operation consists mainly of multicarrier demodulation followed by STS decoding, which is similar to the decoding process of Section 6.2.2. The first part of the decoding operation provides V number of outputs corresponding to the V number of subcarriers conveying the same data. The second operation in this case corresponds to FD despreading of the V number of subcarrier outputs by the FD orthogonal spreading code.

Following the multicarrier demodulation and the TD despreading operations of Equation (6.33), the k=1st user's data mapped to the uvth subcarrier can be expressed as

$$\begin{aligned} r^1_{uv,mg} &= \bar{\mathbf{c}}^{\dagger}_{1,g} \cdot \mathbf{z}^1_{uv,m} \qquad (6.34)\\ &= \sum_{k=1}^{K'} \sqrt{\frac{2P_1}{VL_{AA}} \frac{1}{N_t N_{tg}}} \left[(\mathbf{a}^T_{uv,1m} \cdot \mathbf{w}^1_{uv,1m}) \otimes I_{2N_e} e_{k,u1} + (\mathbf{a}^T_{uv,2m} \cdot \mathbf{w}^1_{uv,2m}) \otimes I_{2N_e} e_{k,u2} \right.\\ &\qquad \left. + (\mathbf{a}^T_{uv,3m} \cdot \mathbf{w}^1_{uv,3m}) \otimes I_{2N_e} e_{k,u3} + (\mathbf{a}^T_{uv,4m} \cdot \mathbf{w}^1_{uv,4m}) \otimes I_{2N_e} e_{k,u4} \right] \cdot c'_k[v]\\ &\quad + \bar{\mathbf{c}}^{\dagger}_{1,g} \cdot \mathbf{n}_{uv,m}, \end{aligned}$$

where $e_{k,ui}$ may assume the values of $x_{k,u1}$, $x_{k,u2}$, $x_{k,u3}$, $x_{k,u4}$ or their conjugates as compared to Equations (6.18)-(6.21).

In Equation (6.34), $\mathbf{w}^k_{uv,nm}$ represents the weight vector of the desired user derived from the nmth antenna link and the uvth subcarrier, which is generated by the MRC beamformer [242] with the aid of channel state information. Let $\mathbf{w}^1_{uv,nm} = \mathbf{d}^{1\dagger}_{nm}$, where $\mathbf{d}^1_{nm}$ is defined in Equation (6.13), then Equation (6.34) can be simplified to

$$\begin{aligned} r^1_{uv,mg} &= \sqrt{\frac{2P_1}{VL_{AA}} \frac{1}{N_t N_{tg}}} \left[L_{AA} \left(\alpha_{uv,1m} e_{k,u1} + \alpha_{uv,2m} e_{k,u2} + \alpha_{uv,3m} e_{k,u3} + \alpha_{uv,4m} e_{k,u4} \right) \cdot c'_k[v] \right.\\ &+ \sum_{k=2}^{K'} \Big(\alpha_{uv,1m} \mathbf{d}^{k\dagger}_{1m} \cdot \mathbf{d}^1_{1m} e_{k,u1} + \alpha_{uv,2m} \mathbf{d}^{k\dagger}_{2m} \cdot \mathbf{d}^1_{2m} e_{k,u2}\\ &\qquad \left. + \alpha_{uv,3m} \mathbf{d}^{k\dagger}_{3m} \cdot \mathbf{d}^1_{3m} e_{k,u3} + \alpha_{uv,4m} \mathbf{d}^{k\dagger}_{4m} \cdot \mathbf{d}^1_{4m} e_{k,u4} \Big) \cdot c'_k[v] \right]\\ &+ \bar{\mathbf{c}}^{\dagger}_{1,g} \cdot \mathbf{n}_{uv,m}. \qquad (6.35) \end{aligned}$$

By employing the decoding scheme of Section 6.2.2 and after despreading the V number of decision variables with the aid of the V-chip FD spreading code $\bar{\mathbf{c}}'$, we arrive at

$$\widetilde{x} = \sqrt{\frac{2P_1}{VL_{AA}} \frac{1}{N_t N_{tg}}} \left[L_{AA} \sum_{v=1}^{V} \left(|\widetilde{\alpha}_{uv,1}|^2 + |\widetilde{\alpha}_{uv,2}|^2 \right) x + \bar{\mathbf{c}}'_1 \mathbf{i} \right] + \eta, \qquad (6.36)$$

where $\mathbf{i}$ represents a V-dimensional interference vector and η represents the noise term after STS demodulation and FD despreading.

We observe from Equation (6.36) that MUI is inevitably introduced, since the orthogonality of the FD spreading codes cannot be retained over frequency-selective fading channels. Observe that the desired user's signal is not interfered by the signals of the users employing different orthogonal TD spreading codes, when assuming synchronous downlink transmission as well as flat-fading of the individual subcarriers. The users sharing the same TD spreading code and employing different FD spreading codes interfere with each other. Therefore, the MUI can be

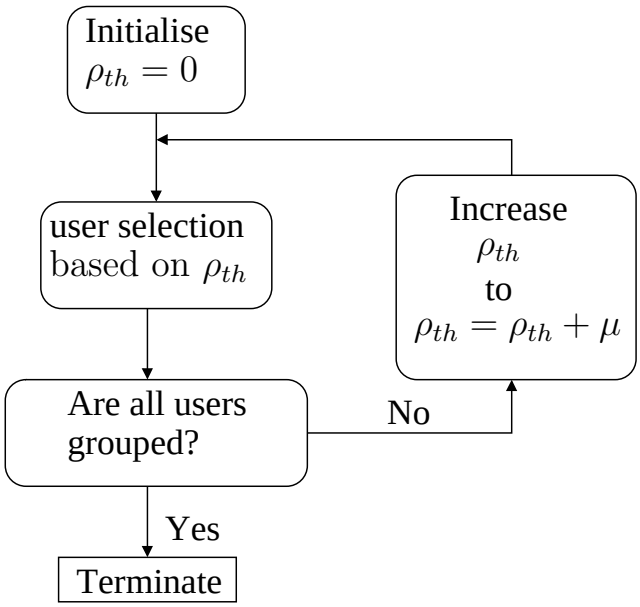

Figure 6.4: Block diagram of the user grouping technique © Hu *et al.* [262], 2006.

reduced, if we carefully select the $(K' - 1)$ potentially interfering users, namely those which have the lowest FD interference coefficient with respect to the desired user, from the entire set of all the $K'\mathcal{K}_{max}$ users [3, 262]. More explicitly, when selecting the specific users for the sake of sharing the same TD spreading code with the desired user, it must be ensured that their FD interference remains low and hence they remain distinguishable. The user grouping technique will be discussed in the following section.

6.3.3 User Grouping Technique

As mentioned in the previous section, some MUI is inevitably imposed, when communicating over frequency-selective fading channels. However, the MUI can be reduced, if the $(K'-1)$ users are carefully grouped, so that the specific-users, having the lowest FD interference coefficient with respect to the desired user, share the same TD spreading code with the desired user. More explicitly, the users sharing the same TD spreading code are carefully selected from the entire set of all the $K'\mathcal{K}_{max}$ users. The user grouping algorithm [3, 262] used is suboptimal, yet its performance improvements justify its employment, as we will show in Figure 6.5.

The above-mentioned interference coefficient can be defined as ρ_{1k}=$\mathbf{d}^k\mathbf{d}^{1\dagger}$, which can be evaluated before transmission ensues, based on the assumption that the users' DOAs are perfectly known at the beamformer [3, 262]. The user grouping technique can be represented by the block diagram of Figure 6.4 and operates as follows.

In the absence of any prior knowledge, the initial value of ρ_{th} is set to 0, where ρ_{th} represents a threshold interference coefficient. The users having an FD interference coefficient of $\rho_{k_1k_2} < \rho_{th}$

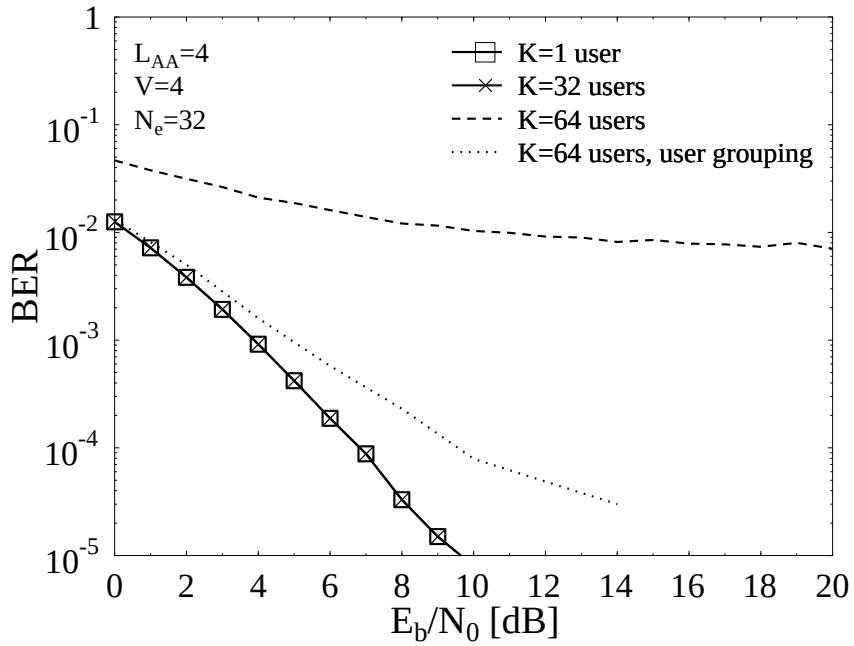

Figure 6.5: BER performance of the proposed system in conjunction with a varying number of users, where both TD and FD spreading as well as user grouping were employed to improve the achievable system performance, while suppressing the MUI. The per-user throughput is 2 bits-per-channel-use.

are deemed to be the users interfering with each other. Furthermore, when the k_1th user shares the same TD spreading code with the k_2th user, they belong to the same TD group and are differentiated by their FD spreading codes. The algorithm aims for ensuring that the users sharing the same TD sequence have the lowest possible FD interference coefficient. The selection procedure will continue, until all the users have been grouped. However, if the threshold value ρ_{th} was set too low, some users cannot be allocated to any of the TD user groups owing to imposing an FD interference coefficient lower than ρ_{th}. In this scenario, ρ_{th} is increased by a given step size of $0 < \mu < L_{AA}$. Based on the increased threshold value, another user allocation attempt is initiated. The process continues until all the users are grouped. Following this user-grouping procedure, the effect of the interfering signals imposed on the desired user's signal becomes less pronounced. Therefore, the achievable BER performance is improved. Additionally, when a new user joins or leaves the communication system, then the user grouping has to be updated [3, 262].

In Figure 6.5 we plot the BER performance of the proposed DL LSSTS aided generalised MC DS-CDMA system using N_t=4 transmit AAs, N_r=2 receive antennas, V=4 subcarriers, L_{AA}=4 elements per AA and a TD spreading factor N_e=32. The system also employs BPSK modulation for K=1, 32 and 64 users. We assume having perfect channel knowledge at both the receiver and at the beamformer. The resultant per-user throughput is 2 bits-per-channel-use. Figure 6.5 shows that the performance of the system supporting K=32 users is identical

to that of the system serving a single user, since no interference is encountered by the K=32 users employing different orthogonal 32-chip Walsh codes as their TD DS spreading in the synchronous DL. Let us now consider TD and FD spreading, which is employed for the sake of supporting K=64 users. Consequently, MUI is inevitably introduced among the users sharing the same TD spreading code. This becomes clear in Figure 6.5 for the case of K=64 users when no user grouping was employed, since the performance of the system supporting K=64 users is significantly worse than that supporting a single user or even K=32 users. However, when user grouping is employed by the LSSTS system for the sake of reducing the MUI imposed, the performance of the system supporting K=64 users substantially improves. Consequently, as a benefit of the user grouping technique, the BER performance of the 64-user system is only slightly inferior in comparison to that serving a single user.

6.4 Iterative Detection and EXIT Chart Analysis

In this section we design an iteratively detected receiver for the proposed system using iterative detection of serially concatenated Recursive Systematic Convolutional (RSC) codes and Unity Rate Codes (URC) combined with the QPSK assisted LSSTS aided generalised MC DS-CDMA scheme. We present three different transceiver structures referred to as System 1, System 2 and System 3, as shown in Figures 6.6, 6.7 and 6.8, respectively.

In the structure of System 1 seen in Figure 6.6 the transmitted source bits $\mathbf{u}_1$ are encoded by the outer RSC code's Encoder I having a rate of R_I=1/2. The outer channel encoded bits $\mathbf{c}_1$ are then interleaved by a random bit interleaver Π_1, where the randomly permuted bits $\mathbf{u}_2$ are fed through the URC Encoder II. The encoded bits $\mathbf{c}_2$ at the output of the URC encoder are interleaved by a second random bit interleaver Π_2, producing the permuted bit stream $\mathbf{b}$. The interleaver Π_2 is used in order to mitigate the correlation in the soft data sequence $L_M(\mathbf{b})$. After bit interleaving, the QPSK modulator maps blocks of B channel-coded bits to their legitimate symbols, which are then transmitted using the transmitter structure of Figure 6.1.

At the receiver side, the soft-in soft-out RSC decoder iteratively exchanges extrinsic information with the URC decoder, as shown in Figure 6.6. The extrinsic soft information, represented in the form of Logarithmic Likelihood Ratios (LLR) [226], is iteratively exchanged between the URC and the RSC decoders for the sake of assisting each other's operation, as detailed in [227]. In Figure 6.6, $L(\cdot)$ denotes the LLRs of the bits concerned, where the subscript I indicates the RSC decoder, while II corresponds to inner URC decoder. Additionally, the subscripts a, p and e denote the dedicated role of the LLRs, with a, p and e indicating *a priori*, *a posteriori* and extrinsic information, respectively. Furthermore, the LLR $L_M(\mathbf{b})$ denotes the soft output

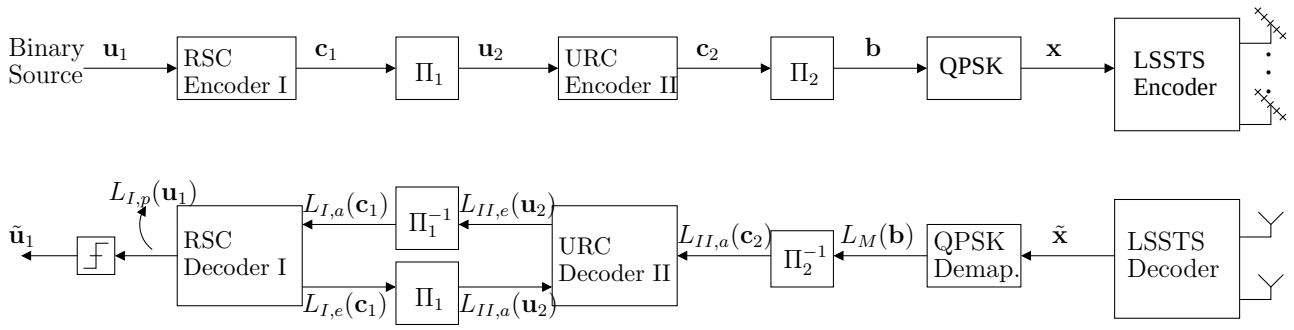

Figure 6.6: Block diagram of the proposed DL System 1 employing QPSK modulation in series with a unity-rate precoder and an outer RSC code.

of the QPSK demapper.

As shown in Figure 6.6, the received and decoded complex-valued symbol stream $\tilde{\mathbf{x}}$ is then fed into the QPSK demapper. The output of the demapper represents the LLR metric $L_M(\mathbf{b})$ passed from the QPSK demapper to the URC decoder. As seen in Figure 6.6, the URC decoder processes the information forwarded by the demapper in conjunction with the *a priori* information in order to generate the *a posteriori* probability. The *a priori* LLR values of the URC decoder are subtracted from the *a posteriori* LLR values for the sake of generating the extrinsic LLR values $L_{II,e}(\mathbf{u}_2)$ and then the LLRs $L_{II,e}(\mathbf{u}_2)$ are deinterleaved by a soft-bit deinterleaver, as seen in Figure 6.6. Next, the soft bits $L_{I,a}(\mathbf{c}_1)$ are passed to the RSC decoder of Figure 6.6 in order to compute the *a posteriori* LLR values $L_{II,p}(\mathbf{c}_1)$ provided by the Log-MAP algorithm [182] for all the channel-coded bits $\mathbf{c}_1$. During the last iteration, only the LLR values $L_{I,p}(\mathbf{u}_1)$ of the original uncoded systematic information bits are required, which are passed to the hard decision decoder of Figure 6.6 in order to determine the estimated transmitted source bits. As seen in Figure 6.6, the extrinsic information $L_{I,e}(\mathbf{c}_1)$, is fed back to the URC decoder as the *a priori* information $L_{I,a}(\mathbf{u}_2)$ after appropriately reordering them using the interleaver of Figure 6.6. The URC decoder exploits the *a priori* information for the sake of providing improved *a posteriori* LLR values, which are then passed to the 1/2-rate RSC decoder and then back to the URC decoder for further iterations.

In the structure of Figure 6.7 denoted as System 2, the transmitted source bits $\mathbf{u}_1$ are encoded by the outer RSC code's Encoder I having a rate of R_I=1/2. The outer channel encoded bits $\mathbf{c}_1$ are then S/P converted to two parallel streams $\mathbf{c}_{11}$ and $\mathbf{c}_{12}$. Each bit stream is then interleaved by a random bit interleaver, where the interleaved bits in each stream are then encoded by a corresponding URC encoder. Note that the URC encoders in each stream are identical. The URC encoded bits in each stream are then interleaved by random bit interleavers to be then mapped to QPSK symbols and transmitted using steered STS. Similarly to the URC encoders, the QPSK modulators I and II are identical. The two STS blocks transmit different

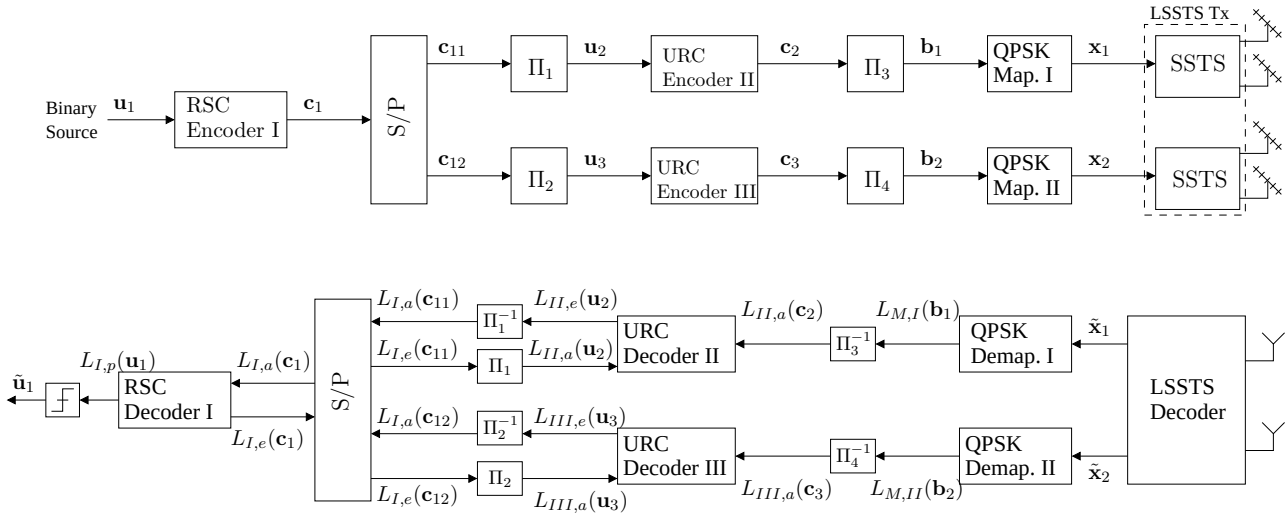

Figure 6.7: Block diagram of the proposed DL System 2 employing an RSC code in series with two parallel branches corresponding to a URC encoder in series with a QPSK mapper transmitting through two steered STS blocks.

data at the same time and employ the same subcarriers for the generalised MC DS-CDMA as described in Section 6.2.

At the receiver side, the decoding process of Section 6.2.2 is employed, where the decoded symbols are passed to their corresponding branch as shown in Figure 6.7. In each branch, the decoded symbols are passed to the QPSK demapper to produce the corresponding LLR $L_{M,i}(\mathbf{b}_i)$, $i = 1, 2$, values. The demapper's soft output is deinterleaved by a soft bit deinterleaver and passed to the URC decoders as *a priori* information. The URC decoder utilises the LLR information passed to it from the demapper as well as the RSC decoder to produce the extrinsic LLR values $L_{i,e}(\mathbf{u}_i)$, $i = 2, 3$. The extrinsic output of the URC decoders is deinterleaved and then Parallel-to-Serial (P/S) converted to be passed to the RSC decoder as *a priori* information. The RSC decoder utilises the information passed from the URC decoders to produce the extrinsic LLR $L_{I,e}(\mathbf{c}_1)$. The extrinsic output of the RSC decoder is then S/P converted to be passed to the URC decoders of each branch, which in turn exploits the *a priori* information for the sake of providing improved *a posteriori* LLR values, which are then passed to the 1/2-rate RSC decoder and then back to the URC decoders for further iterations.

Finally, in the structure of Figure 6.8 referred to as System 3, the transmitted source bits $\mathbf{u}_1$ are first S/P converted to two parallel substreams $\mathbf{u}_{11}$ and $\mathbf{u}_{12}$. Each substream is encoded by the outer RSC code's Encoder having a rate of R_I=1/2. The outer channel encoded bits $\mathbf{c}$ of each bit stream are then interleaved by a random bit interleaver, where the interleaved bits in each stream are then encoded by a corresponding URC encoder. The URC encoded bits in each stream are then interleaved by random bit interleavers to be finally mapped to QPSK symbols and transmitted using steered STS. Note that the RSC encoders I and II are

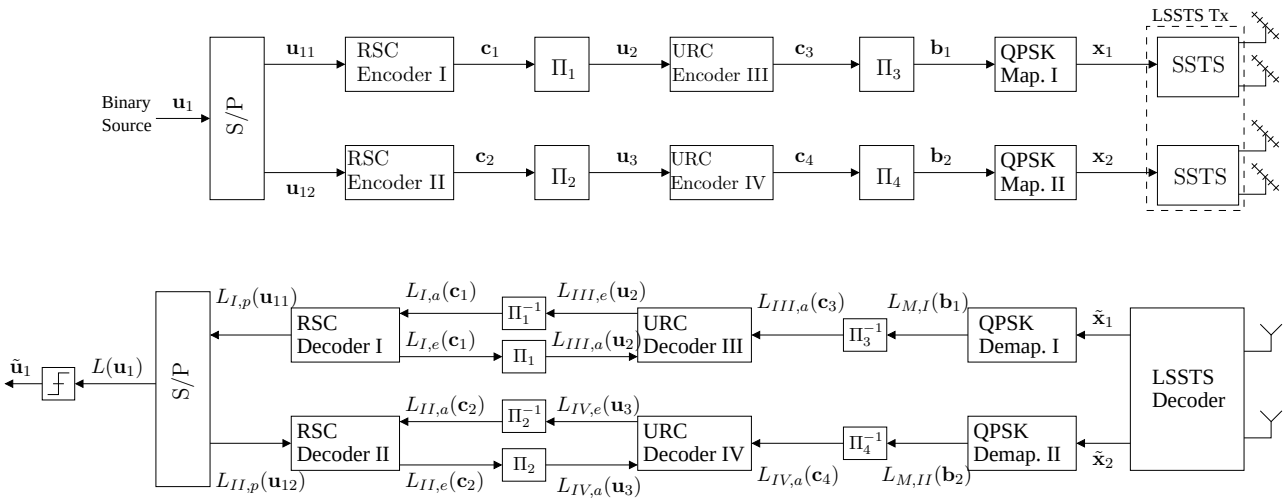

Figure 6.8: Block diagram of the proposed DL System 3 employing two parallel branches of RSC encoder in series with a URC encoder and transmitting through a QPSK aided steered STS.

identical, the URC encoders III and IV are identical as well as the QPSK modulators I and II are identical.

At the receiver side of System 3 seen in Figure 6.8, the decoding process of Section 6.2.2 is employed, where the decoded symbols are passed to their corresponding branch, as shown in Figure 6.8. Each branch then applies iterative detection exchanging extrinsic information between the corresponding RSC and URC decoders, as shown in Figure 6.8. The output $L_{I,p}(\mathbf{u}_{11})$ and $L_{II,p}(\mathbf{u}_{12})$ of the RSC decoders is then P/S converted to produce a single stream $L(\mathbf{u}_1)$, which is passed to the hard-decision decoder of Figure 6.8.

6.4.1 EXIT Charts and LLR Post-processing

As discussed in Chapter 3, the main objective of employing EXIT charts [186, 189] is to predict the convergence behaviour of the iterative decoding process by examining the evolution of the input/output Mutual Information (MI) exchange between the constituent decoders in consecutive iterations. Again, the application of EXIT charts is based on two main assumptions, which are realistic when using high interleaver depths, namely that the *a priori* LLR values are uncorrelated and that they satisfy the consistency condition.

Let $I_{\cdot,a}(x)$, $0 \leq I_{\cdot,a}(x) \leq 1$, denote the MI between the *a priori* LLRs $L_{\cdot,a}(x)$ as well as the corresponding bits x and let $I_{\cdot,e}(x)$, $0 \leq I_{\cdot,e}(x) \leq 1$, denote the MI between the *extrinsic* LLRs $L_{\cdot,e}(x)$ and the corresponding bits x.

Figure 6.9 shows the EXIT chart of System 1 depicted in Figure 6.6 employing an iteratively detected RSC-coded and URC precoded LSSTS system in conjunction with Gray Mapping (GM) aided QPSK modulation, where iterations are carried out between the outer 1/2-rate RSC

Modulation Scheme	QPSK
Mapping	Gray Mapping
Number of Transmitter AAs N_t	4
Number of Elements per AA	L_{AA}
Number of Receiver Antennas N_r	2
Number of Subcarriers V	4
TD Spreading Factor N_e	4
FD Spreading Factor	V
Number of Users	K
Outer Encoder	RSC(2,1,3),
Generator	$(G_r, G) = (7, 5)_8$
Inner Encoder	Unity-rate code
Generator	$(G_r, G) = (3, 2)_8$
Interleaver Depth	D_{int} bits

Table 6.1: System parameters.

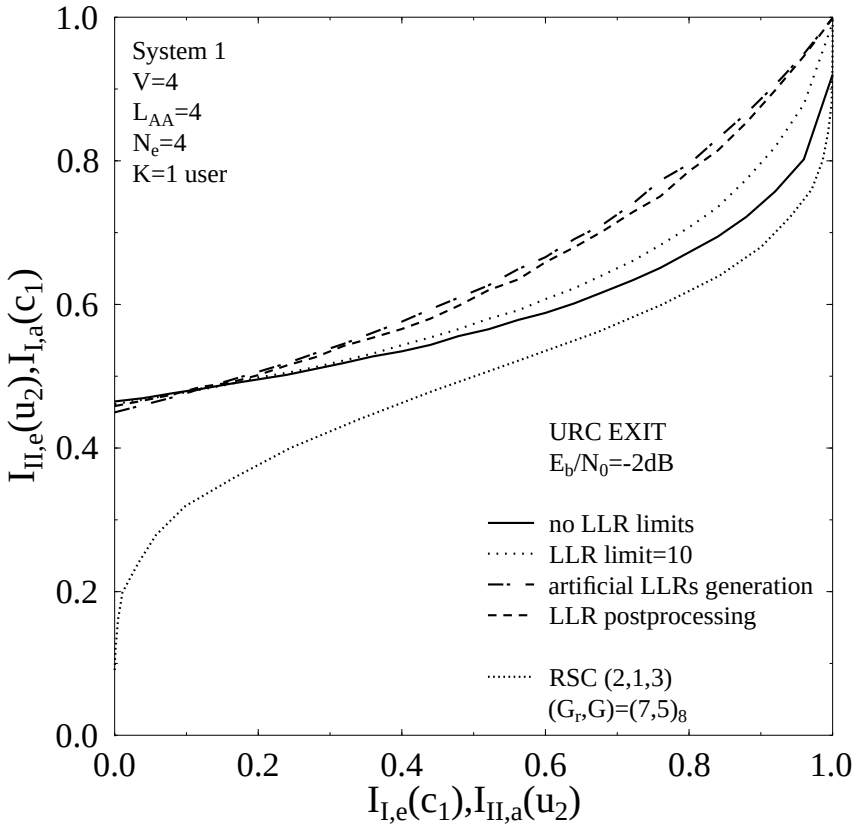

Figure 6.9: EXIT chart of a RSC-coded and URC-precoded proposed System 1 of Figure 6.6 employing GM aided QPSK in conjunction with N_t=4, N_r=2, V=4, L_{AA}=4, K=1 user, $E_b/N_0 = -2$ dB and the remaining system parameters outlined in Table 6.1.

code and the inner URC decoders, while no iterations are invoked between the URC decoder and the QPSK demapper. The system employs a 1/2-rate memory-2 RSC code, denoted as RSC(2,1,3), in conjunction with an octal generator polynomial of $(G_r, G)=(7,5)_8$, where G_r is the feedback polynomial and G is the feedforward polynomial. Encoder II is a URC encoder, described by the pair of octal generator polynomials $(G_r, G)=(3,2)_8$. Furthermore, the EXIT chart of Figure 6.9 was generated for the system employing N_t=4 transmit AAs and N_r=2 antennas, while using L_{AA}=4 elements per AA in conjunction with V=4 subcarriers and the system parameters outlined in Table 6.1.

Observe in Figure 6.9 that there are several EXIT curves for the URC decoder for the same E_b/N_0 value. Let us first consider the dark line marked by the legend "no LLR limits". This EXIT curve corresponds to the URC decoder of Figure 6.6, which has a recursive encoder at the transmitter and hence it is expected that the EXIT curve of the URC decoder will reach the $(1.0, 1.0)$ point of perfect convergence in the EXIT curve while using sufficiently long interleavers, as discussed in Section 3.2.4. However, the EXIT curve of the proposed System 1 characterised in Figure 6.9 shows that the EXIT curves of the URC decoder do not reach the $(1.0, 1.0)$ point. As a first step in circumventing this problem, we attempted to limit the maximum and minimum of the LLR values $L_M(\mathbf{b})$ for the sake of avoiding the problem of numerical overflow in the computer's memory. Limiting the LLR values allowed the URC EXIT curve to reach the $(1.0, 1.0)$ point, as shown in Figure 6.9 by the dotted line associated with the legend "LLR limit=10". On the other hand, for the sake of testing the accuracy of the URC EXIT curve, while imposing a limit on the LLR values, we generated artificial Gaussian distributed and uncorrelated LLRs $L_M(\mathbf{b})$, that satisfy the consistency condition. The resultant EXIT curve in this case is represented by the dotted line having the legend "artificial LLRs generation". The artificial LLRs are generated assuming the transmitted bits are known at the receiver and it is used as a benchmark for testing the accuracy of our results. As shown in Figure 6.9, the curves corresponding to the case where the LLR's dynamic range is limited and where the artificial LLRs are generated are quite different. Therefore, limiting the LLR values does not solve the problem.

In order to understand this problem, let us return to the basics of the LLR and mutual information. The soft information pertaining to bits is typically represented using the LLRs within the receiver. Here, the particular LLR $L_M(b_i)$ in the frame $L_M(\mathbf{b})$ that pertains to the bit b_i from the frame $\mathbf{b}$ is specified according to

$$L_M(b_i) = \log\left(\frac{P(b_i=1)}{P(b_i=0)}\right), \tag{6.37}$$

where $P(b_i) \in [0,1]$ is the probability that the bit b_i has the logical value 0 or 1 within the transmitter. Note that the logarithmic domain is employed since it provides symmetry resulting

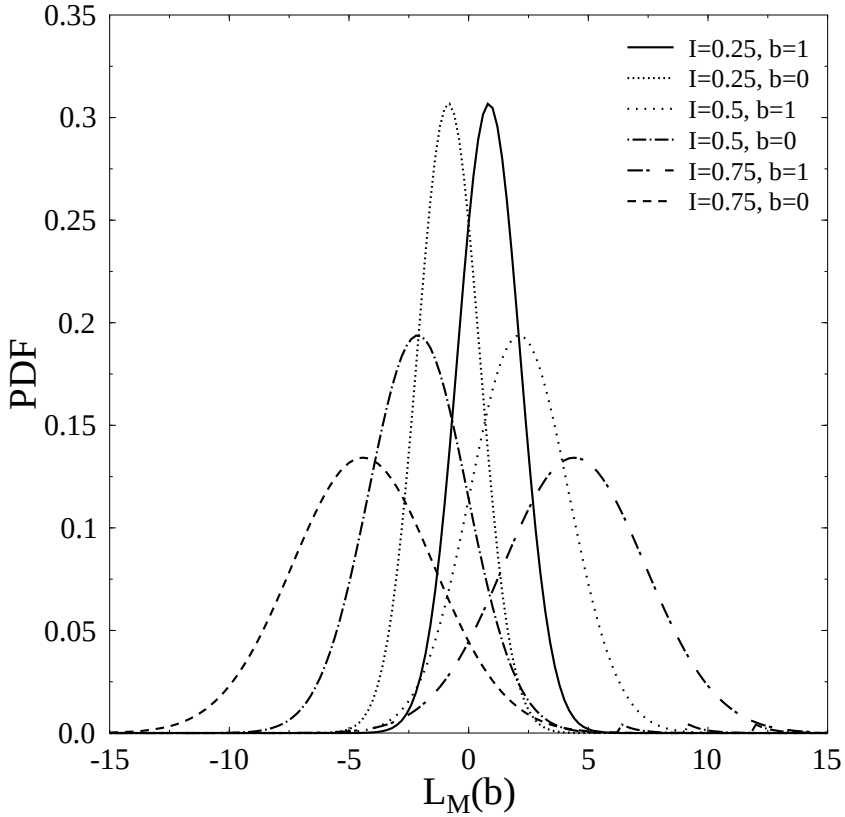

Figure 6.10: Gaussian distributed LLRs $L_M(b)$ corresponding to logical zero- and one-valued bits **b** for various mutual informations I.

in LLRs having a positive or negative sign, when there is a higher confidence in a logical one- or a logical zero-valued bit, respectively. Furthermore, the level of this confidence increases with the LLR's magnitude.

On the other hand, as described in [267], the mutual information between an LLR frame $L(\mathbf{b})$ and the corresponding bit stream **b** depends on the distribution of the LLR values. More specifically, if the distribution of the LLR values that correspond to logical zero-valued bits is equal to that of the LLR values pertaining to logical one-valued bits, then the mutual information will be zero. In this case, the LLR values are unreliable and the hard decision based on the LLR values will result in an error rate of 50%.

As the reliability of the LLR values increases, the LLR distributions corresponding to the bits 1 and bits 0 will move apart, as shown in Figure 6.10. As the MI I increases, the two LLR distributions will move apart and will overlap only at the tails of the distributions, giving a higher mutual information value. This results in a high confidence in the hard decoding based on the LLR values and a reduced probability of bit errors at the receiver. In Figure 6.10 the LLRs can be seen to have Gaussian distributions, although other distributions may be encountered in practice, depending on the transmission channel employed.

Observe in Figure 6.10 that the LLR abscissa value along the x-axis can be calculated by

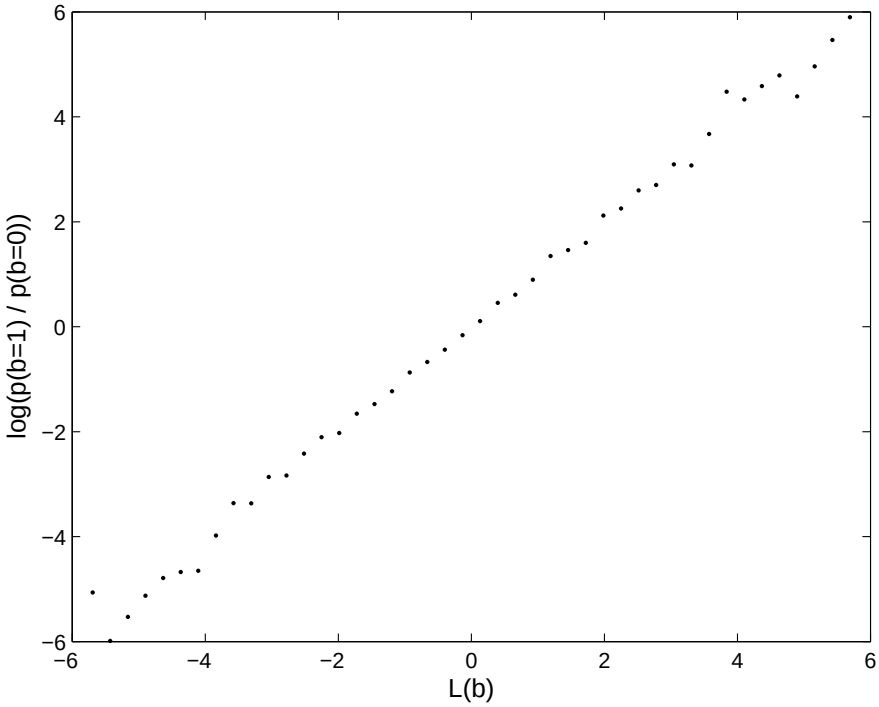

Figure 6.11: Logarithm of the probabilities in Figure 6.10 versus the corresponding QPSK demapper LLR output $L_M(\mathbf{b})$ for the DSTS system of Chapter 2.

computing $\log\left(\frac{P(b=1)}{P(b=0)}\right)$, where $P(b)$ can be computed from the y-axis of the figure. This property has been tested for the LLR $L_M(\mathbf{b})$ in the iteratively detected DSTS system of Section 3.3 and for the proposed System 1 of Figure 6.6. For the DSTS system, we have shown that this property is true when we plotted the $\log\left(\frac{P(b=1)}{P(b=0)}\right)$ versus $L_M(\mathbf{b})$ in Figure 6.11. As shown in Figure 6.11, the result is a diagonal line, which means that $L_M(b_i) = \log\left(\frac{P(b_i=1)}{P(b_i=0)}\right)$ as expected.

The same experiment has been carried out for the proposed System 1 of Figure 6.6. We plotted the $\log\left(\frac{P(b=1)}{P(b=0)}\right)$ versus $L_M(\mathbf{b})$ and the result is shown in Figure 6.12. Theoretically, the result should be identical to Figure 6.11, where we have a diagonal line. However, we observe in Figure 6.12 that the result is a non-linear function. The reason for this behaviour is the fact that the input $\tilde{\mathbf{x}}$ of the QPSK demapper is not Gaussian distributed, although we calculate the LLR values $L_M(\mathbf{b})$ assuming that the input data stream $\tilde{\mathbf{x}}$ is Gaussian distributed. A trivial solution to this problem is to try to find the probability distribution of the LSSTS decoder's output $\tilde{\mathbf{x}}$ and compute the LLRs in the QPSK demapper using the correct PDF. However, it is not straightforward to find a mathematical formula to model the PDF of $\tilde{\mathbf{x}}$. On the other hand, it is possible to compute the LLRs based on the histogram of the received and decoded data $\tilde{\mathbf{x}}$. However, computing the histogram for every received frame is a complex and time-consuming process.

By considering the specific relationship between the probabilities and LLR values seen in

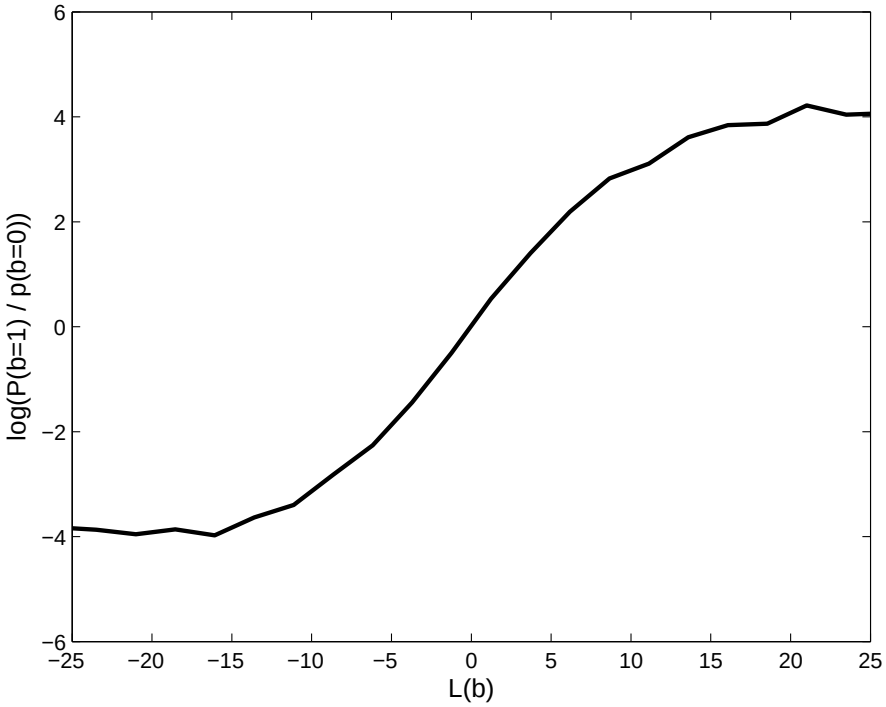

Figure 6.12: Logarithm of the probabilities in Figure 6.10 versus the corresponding QPSK demapper LLR output $L_M(\mathbf{b})$ for the proposed System 1 shown in Figure 6.6.

Figure 6.12 we can find a relationship that can transform the result of Figure 6.12 into that seen in Figure 6.11. The y-axis of Figure 6.12 is the correct LLR value and hence we have to transform the x-axis LLR value into its corresponding y-axis value. An empirical transformation of the $L_M(\mathbf{b})$ LLR values has been computed for the sake of correcting the relationship between the LLR values and their corresponding probabilities. The transformation is applied to the LLR values at the output of the QPSK demapper and hence it is referred to as LLR post-processing. The empirical transformation can be expressed as:

$$\text{LLR}_{out} = \frac{L_M(\mathbf{b})}{1.25\left(\log_2(V)+1\right) - 0.75\lceil \frac{K}{N_e} - 1 \rceil} \ , \tag{6.38}$$

where LLR_{out} represents the LLR passed from the QPSK demapper to the deinterleaver Π_2 of Figure 6.6 after the transformation of the LLRs. This transformation is referred to as LLR post-processing, since it is applied at the receiver side after computing the LLRs in the QPSK demapper.

Figure 6.9 also shows the EXIT curve of the inner URC decoder after the LLR post-processing technique was employed. As shown in Figure 6.9, the EXIT curve of the system where the post-processing is employed is similar to that where the artificial LLRs were considered. Hence, the proposed LLR post-processing technique solves the problem of the non-Gaussian decoded data passed from the MIMO decoder to the QPSK demapper and at the same time eliminates the complexity of the histogram estimation for every received frame.

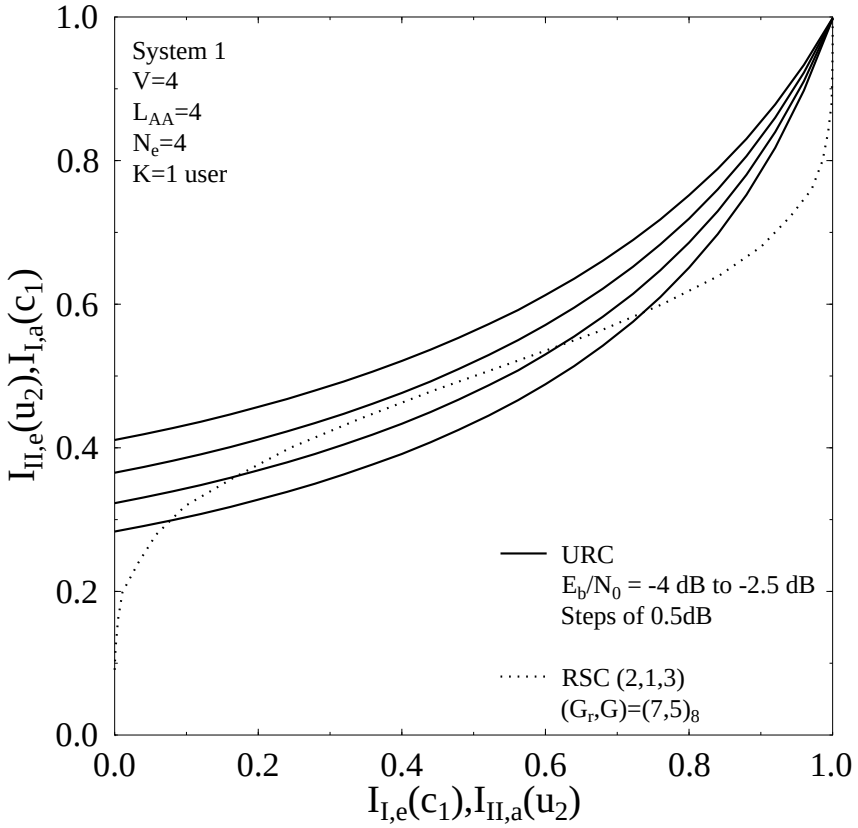

Figure 6.13: EXIT chart of the RSC-coded and URC-precoded System 1 of Figure 6.6 employing an interleaver depth of D_{int}=160,000 bits, V=4 subcarriers, L_{AA}=4 elements per AA, N_e=4, K=1 user in conjunction with the system parameters outlined in Table 6.1.

Observe from Figure 6.13 that an open EXIT chart convergence tunnel is formed around E_b/N_0=−3 dB for System 1 employing V=4 subcarriers, L_{AA}=4 elements per AA, N_e=4 and supporting K=1 user, while using the remaining system parameters outlined in Table 6.1. This implies that according to the predictions of the EXIT chart seen in Figure 6.13, the iterative decoding process is expected to converge at an E_b/N_0 of at least −3 dB. The EXIT chart based convergence predictions can be verified by the Monte-Carlo simulation based iterative decoding trajectory of Figure 6.14, where the trajectory was recorded at E_b/N_0=−2.8 dB, while using an interleaver depth of D_{int}=160,000 bits, V=4 subcarriers, L_{AA}=4 elements per AA, N_e=4, K=1 user in conjunction with the system parameters outlined in Table 6.1. The steps seen in Figure 6.14 represent the actual extrinsic information exchange between the URC's decoder and the outer RSC channel decoder.

On the other hand, increasing the number of users beyond the TD spreading factor N_e and employing both TD as well as FD spreading combined with the user grouping technique of Section 6.3.3 degrades the system's performance, as shown in Figure 6.5. The TD and FD spreading as well as the user grouping technique have been applied to System 1 of Figure 6.6. Iterative detection has been carried out by exchanging extrinsic information between the RSC decoder and the URC decoder at the receiver side in addition to the LLR post-processing

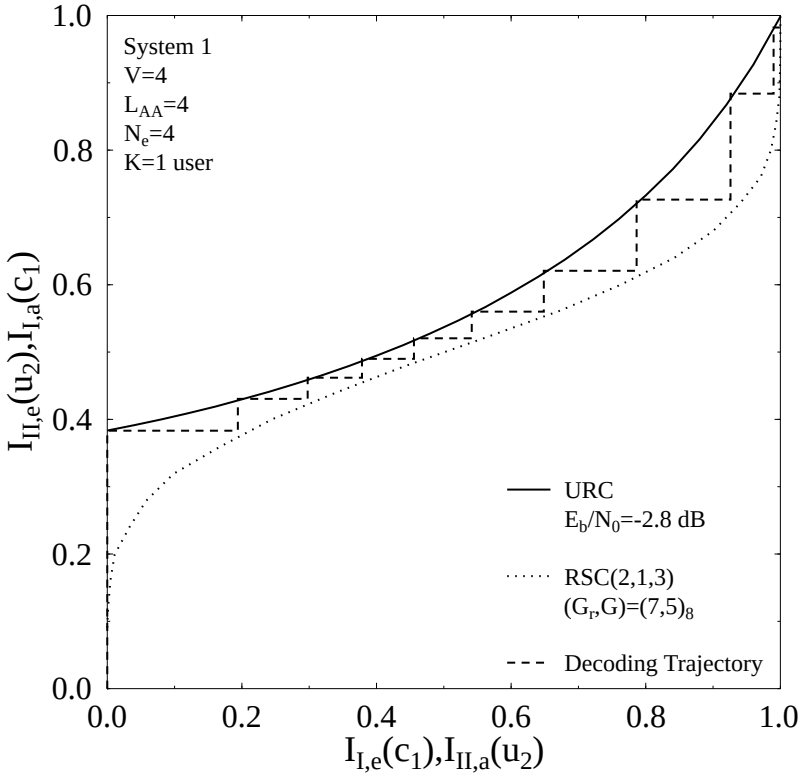

Figure 6.14: Decoding trajectory of the iteratively detected RSC-coded and URC-precoded System 1 seen in Figure 6.6 employing an interleaver depth of D_{int}=160,000 bits, V=4 subcarriers, L_{AA}=4 elements per AA, N_e=4 and K=1 user, while operating at E_b/N_0=−2.8 dB in conjunction with the system parameters outlined in Table 6.1.

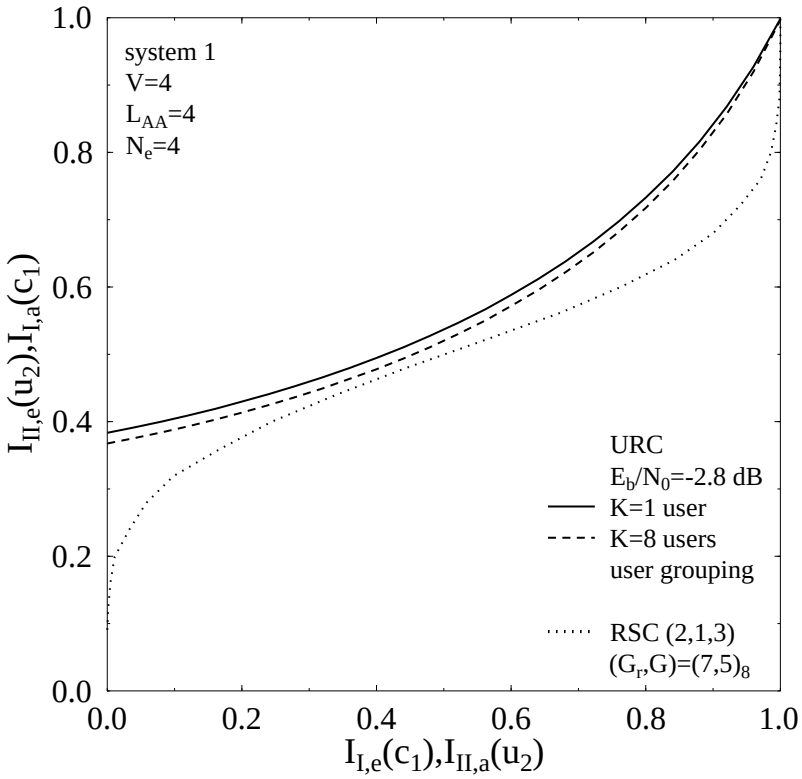

Figure 6.15: EXIT chart of a RSC-coded and URC-precoded System 1 of Figure 6.6 employing an interleaver depth of D_{int}=160,000 bits, V=4 subcarriers, L_{AA}=4 elements per AA, N_e=4 and K=1, 8 users in conjunction with the system parameters outlined in Table 6.1.

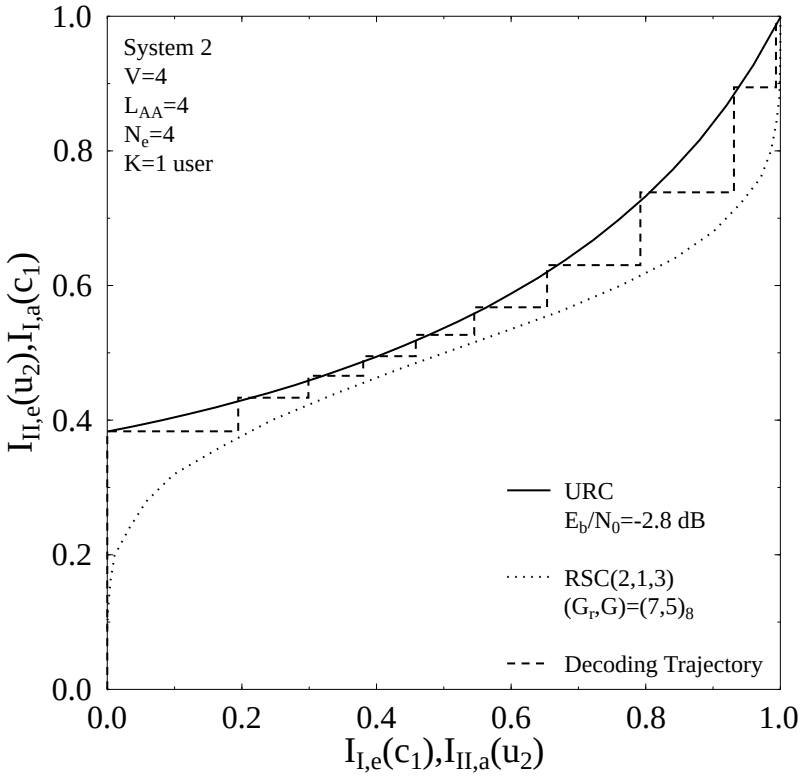

Figure 6.16: Decoding trajectory of the iteratively detected System 2 of Figure 6.7 employing an interleaver depth of D_{int}=160,000 bits, V=4 subcarriers, L_{AA}=4 elements per AA, N_e=4 and K=1 user, while operating at E_b/N_0=−2.8 dB in conjunction with the system parameters outlined in Table 6.1. The inner decoders EXIT curve was generated for one branch of the system seen in Figure 6.7.

technique, which was applied for the sake of correcting the LLR output of the QPSK demapper. The resultant EXIT chart is shown in Figure 6.15, where a comparison between the EXIT curves of the URC decoder is offered for both K=1 and K=8 users. Figure 6.15 portrays the EXIT chart of a system employing N_t=4 transmit AAs, N_r=2 receive antennas, V=4 subcarriers, L_{AA}=4 elements per AA, N_e=4 and the system parameters outlined in Table 6.1. As shown in Figure 6.15, it is expected that the single-user system outperforms the overloaded eight-user system by E_b/N_0 of about 0.2 dB.

Figure 6.16 shows the EXIT chart of the iteratively detected System 2 of Figure 6.7. The EXIT curve of the inner URC decoder was recorded for one of the two substreams seen in Figure 6.7. The EXIT curve of the two substreams is identical, since the interference cancellation scheme of Section 6.2.2 completely eliminates the interference imposed by one of the STS layers on the other. The EXIT chart of Figure 6.16 was recorded for the system employing V=4 subcarriers, L_{AA}=4 elements per AA, N_e=4, K=1 user and the remaining system parameters outlined in Table 6.1. The EXIT chart based convergence predictions can be verified by the Monte-Carlo simulation based iterative decoding trajectory of Figure 6.16, where the trajectory was recorded at E_b/N_0=−2.8 dB, while using an interleaver depth of D_{int}=160,000 bits.

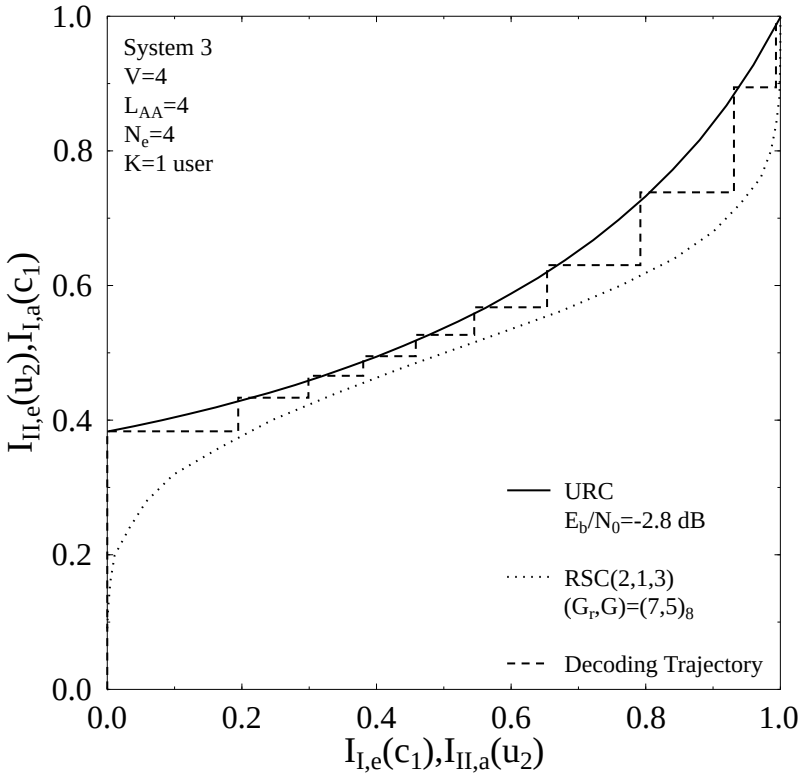

Figure 6.17: Decoding trajectory of the iteratively detected System 3 of Figure 6.8 employing an interleaver depth of D_{int}=160,000 bits, V=4 subcarriers, L_{AA}=4 elements per AA, N_e=4 and K=1 user, while operating at E_b/N_0=−2.8 dB in conjunction with the system parameters outlined in Table 6.1. The inner and outer EXIT curve was generated for one branch of the system in Figure 6.8.

The steps seen in Figure 6.16 represent the actual extrinsic information exchange between the URCs' decoders and the outer RSC channel decoder.

On the other hand, Figure 6.17 shows the EXIT chart of the iteratively detected System 3 of Figure 6.8. The EXIT curves of the inner URC decoder as well as the outer RSC code's decoder were recorded for one of the two substreams seen in Figure 6.8. Again, the EXIT curve of the two substreams is identical since the interference cancellation scheme of Section 6.2.2 completely cancels the interference imposed by one of the STS layers on the other. The EXIT chart of Figure 6.17 was recorded for the system employing V=4 subcarriers, L_{AA}=4 elements per AA, N_e=4, K=1 user and the system parameters outlined in Table 6.1. The EXIT chart based convergence predictions can be verified by the Monte-Carlo simulation based iterative decoding trajectory of Figure 6.17, where the trajectory was recorded at E_b/N_0=−2.8 dB, while using an interleaver depth of D_{int}=160,000 bits.

As observed in Figures 6.14, 6.16 and 6.17, the three systems, namely System 1, System 2 and System 3 may be expected to have a similar BER performance based on these EXIT chart predictions. This is due to the fact that the interference cancellation operation of the proposed system outlined in Section 6.2.2 completely eliminates any interference imposed by one of the STS layers on the other layer. Therefore, the iteratively detected Systems 1-3, have

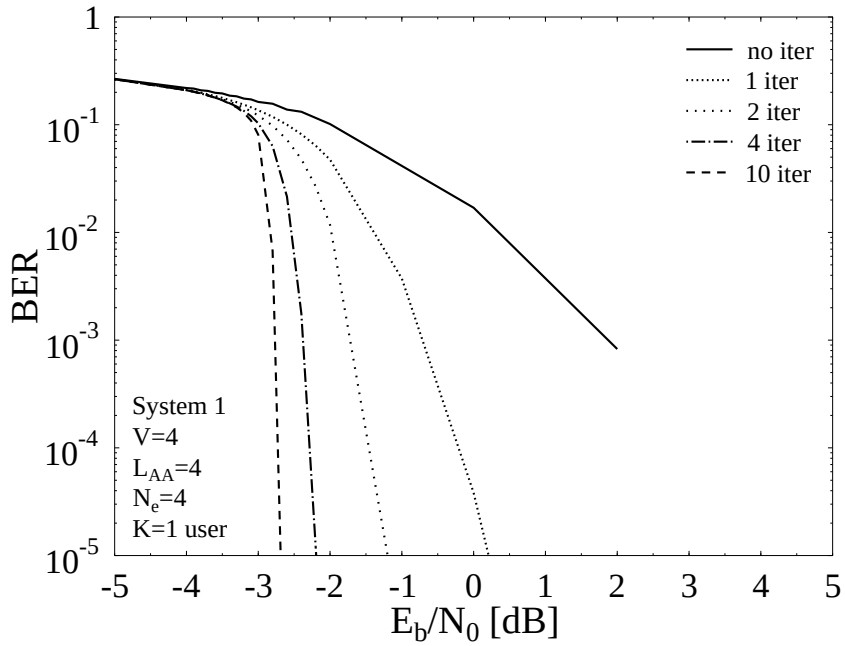

Figure 6.18: Performance comparison of the GM-based RSC-coded and URC precoded System 1 of Figure 6.6 in conjunction with V=4 subcarriers, L_{AA}=4 elements per AA, N_e=4 and K=1 user and the system parameters outlined in Table 6.1, when using an interleaver depth of D_{int}=160,000 bits for a variable number of iterations.

similar BER performances according to our EXIT chart prediction provided that we employ sufficiently long interleavers which are capable of eliminating the correlation of the extrinsic information.

6.5 Results and Discussions

In this section, we consider a LSSTS system associated with N_t=4 transmit AAs, N_r=2 receive antennas, V=4 subcarriers, L_{AA}=4 elements per AA, N_e=4 and the system parameters outlined in Table 6.1 in order to demonstrate the performance improvements achieved by the proposed systems, namely System 1, System 2 and System 3. We employ Gray Mapping (GM) aided QPSK modulation. Additionally, perfect channel knowledge is assumed at both the receiver as well as at the transmit beamformer.

Figure 6.18 compares the BER performance of the proposed System 1 supporting K=1 user in conjunction with GM aided QPSK for different number of iterations. Figure 6.18 portrays the performance of the iteratively detected RSC-coded and URC precoded System 1, when employing an interleaver depth of D_{int}=160,000 bits. Figure 6.18 demonstrates that the BER performance closely matches the EXIT chart based prediction of Figure 6.14, where the system approaches an infinitesimally low BER at E_b/N_0=−2.8 dB after 10 iterations. On the other hand, Figure 6.19 compares the BER performance of the iterative detection aided System 1,

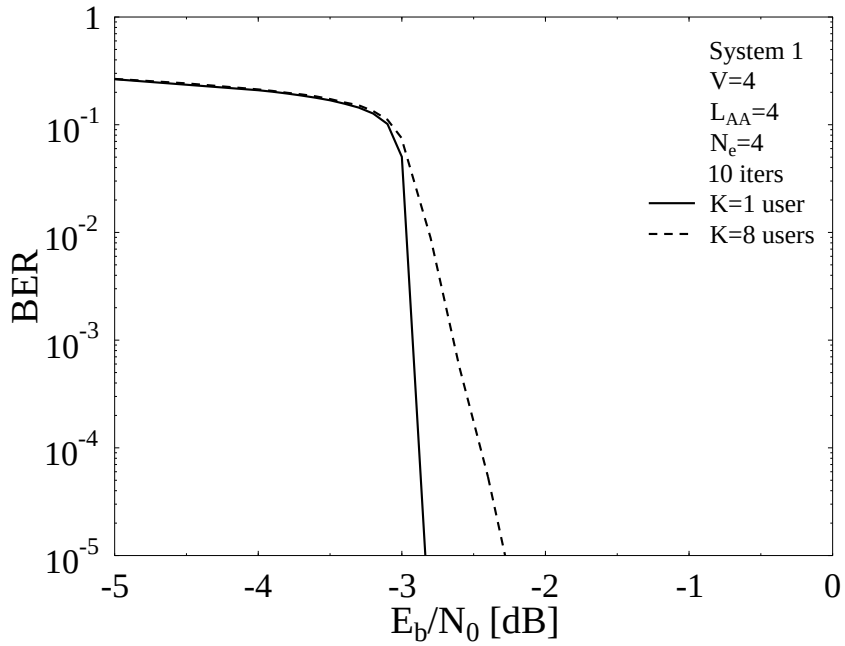

Figure 6.19: Performance comparison of the GM-based RSC-coded and URC precoded System 1 of Figure 6.6 in conjunction with V=4 subcarriers, L_{AA}=4 elements per AA, N_e=4 and 10 iterations and the system parameters outlined in Table 6.1, when using an interleaver depth of D_{int}=160,000 bits for K=1 and K=8 users.

while employing V=4 subcarriers, L_{AA}=4 elements per AA, N_e=4 and 10 decoding iterations in conjunction with GM aided QPSK for K=1 and K=8 users. The system of Figure 6.19 employs TD and FD spreading for the sake of increasing the number of users to K=8, which is twice the TD spreading factor, i.e. twice the number of users supported by employing TD-only spreading, in addition to applying the user grouping technique of Section 6.3.3. Furthermore, we employ the LLR post-processing technique of Equation (6.38) for the sake of correcting the LLR output of the QPSK demapper. According to the EXIT chart predictions seen in Figure 6.15, the system employing K=1 and K=8 users has an E_b/N_0 requirement difference of about 0.2 dB. According to Figure 6.19, when the system employs an interleaver depth of D_{int}=160,000 bits and 10 decoding iterations, the system supporting a single user outperforms that supporting K=8 users by about 0.45 dB at a BER of 10^{-5}.

As discussed previously, according to the EXIT chart prediction of Figures 6.14, 6.16 and 6.17 the BER performance of Systems 1-3 is identical, when employing a long interleaver as well as a sufficient number of decoding iterations. Observe from Figures 6.6, 6.7 and 6.8 that the interleaver depth for System 2 and System 3 is half of that for System 1 when considering the same frame length for the input data bit stream $\mathbf{u}_1$. This is due to the fact that the input bit stream in System 2 and System 3 are split into two parallel equal length bit streams. In what follows we refer to the interleaver Π_1 depth of System 1 in Figure 6.6 as D_{int} and it is equal to the RSC code rate R times the input bit stream frame length. Hence the

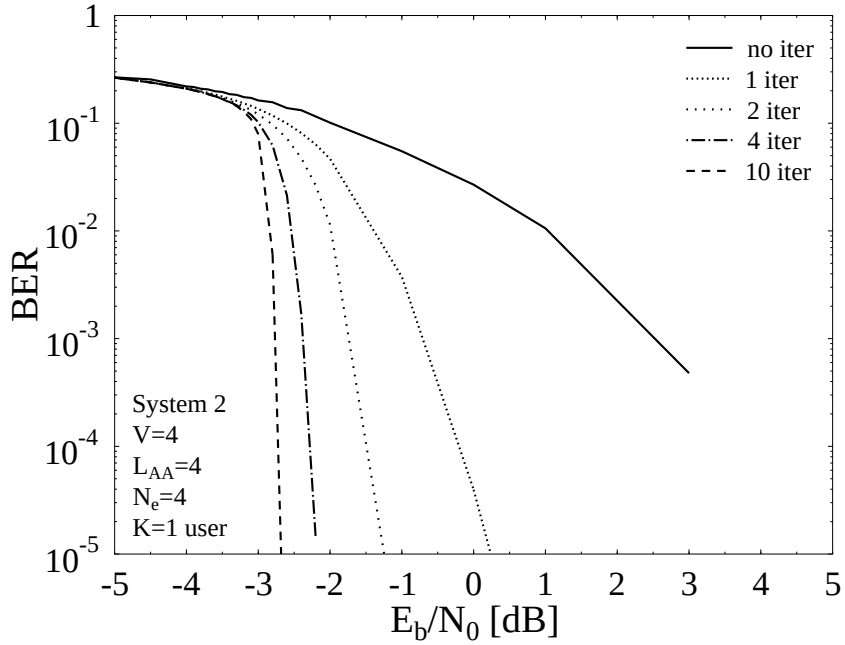

Figure 6.20: Performance comparison of the GM-based RSC-coded and URC precoded System 2 of Figure 6.7 in conjunction with V=4 subcarriers, L_{AA}=4 elements per AA, N_e=4, K=1 user and the system parameters outlined in Table 6.1, when using an interleaver depth of D_{int}=160,000 bits for a variable number of iterations.

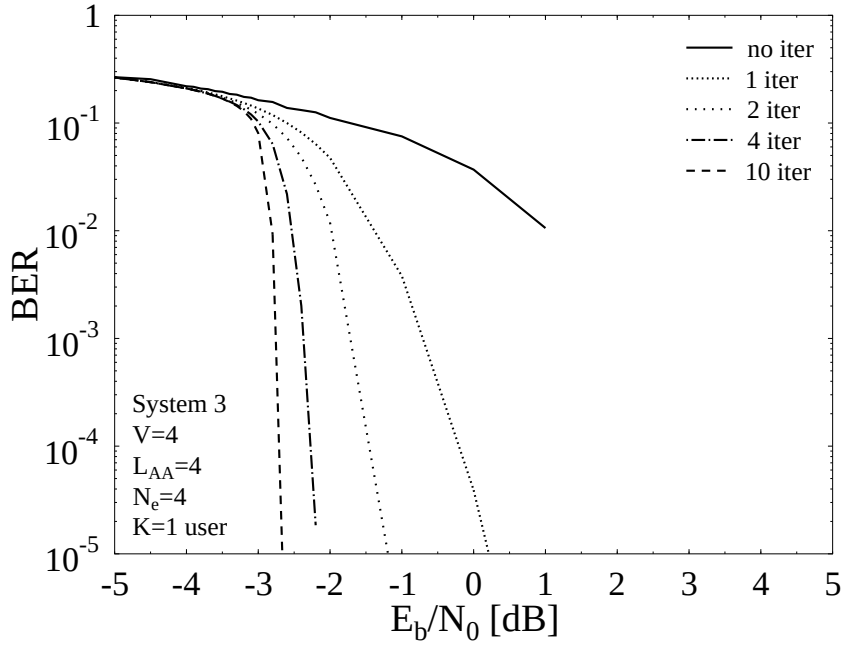

Figure 6.21: Performance comparison of the GM-based RSC-coded and URC precoded System 3 of Figure 6.8 in conjunction with V=4 subcarriers, L_{AA}=4 elements per AA, N_e=4 and K=1 user and the system parameters outlined in Table 6.1, when using an interleaver depth of D_{int}=160,000 bits for a variable number of iterations.

interleaver Π_1 depth of System 2 and System 3 in Figures 6.7 and 6.8 is $D_{int}/2$. Figure 6.20 compares the BER performance of the proposed System 2 employing V=4 subcarriers, L_{AA}=4 elements per AA, N_e=4 and supporting K=1 user in conjunction with GM aided QPSK for different number of iterations. The figure shows the performance of the iteratively detected RSC-coded and URC precoded System 2, when employing a bit sequence $\mathbf{u}_1$ having a length of $80,000$ bits, i.e. D_{int}=$160,000$ bits. This means that the interleaver Π_1 of Figure 6.7 has a depth of $80,000$ bits. Figure 6.20 demonstrates that the BER performance closely matches the EXIT chart based predictions of Figure 6.16, where the system approaches a BER below 10^{-5} at E_b/N_0 in excess of -2.8 dB after 10 iterations. Similarly, we plot in Figure 6.21 the BER performance comparison of the proposed System 3 employing V=4 subcarriers, L_{AA}=4 elements per AA, N_e=4 and K=1 user in conjunction with GM aided QPSK for different number of iterations and employing an interleaver Π_1 of Figure 6.8 having depth of $80,000$ bits, i.e. D_{int}=$160,000$ bits. Figure 6.21 demonstrates that the BER performance closely matches the EXIT chart based predictions of Figure 6.17, where the system performance approaches a BER below 10^{-5} at E_b/N_0 in excess of -2.8 dB after 10 iterations.

To comment briefly on the associated complexity, for an interleaver depth of D_{int} and after I number of iterations, System 1 encounters $(I+1)(4D_{int}-16)$ number of trellis states, while System 2 invokes $(I+1)(4D_{int}-17)$ number of trellis states. On the other hand, System 3 has $(I+1)(4D_{int}-32)$ trellis states. Hence, for the system parameters of Table 6.1 employed in the above investigations, i.e. for D_{int}=$160,000$ bits and I=10 iterations, System 1 encounters a total of $7,039,824$ trellis states, System 2 employs $7,039,813$ trellis states and finally System 3 requires $7,039,648$ trellis states. Therefore, we may conclude that the three systems also have a similar complexity, although System 3 is the least complex in terms of the number of trellis states used throughout the iterative decoding process, which determines the number of Add-Compare-Select (ACS) arithmetic operations. Note that System 2 employs one more mapper and URC encoder and decoder blocks than System 1, while System 3 employs one more mapper, one URC encoder/decoder as well as an extra RSC encoder/decoder in comparison to System 1.

We have shown that while employing a high interleaver depth $D_{int} = 160,000$ bits, Systems 1-3 have both a similar performance and a similar complexity, although Systems 2 and 3 use more encoder and decoder components than System 1. On the other hand, splitting the bit stream into two parallel substreams in Systems 2 and 3 implies that their interleaver depth becomes lower than that of System 1, while considering the same number of input bits. Hence, in what follows we study the effect of the interleaver depth on the achievable performance of the three systems.

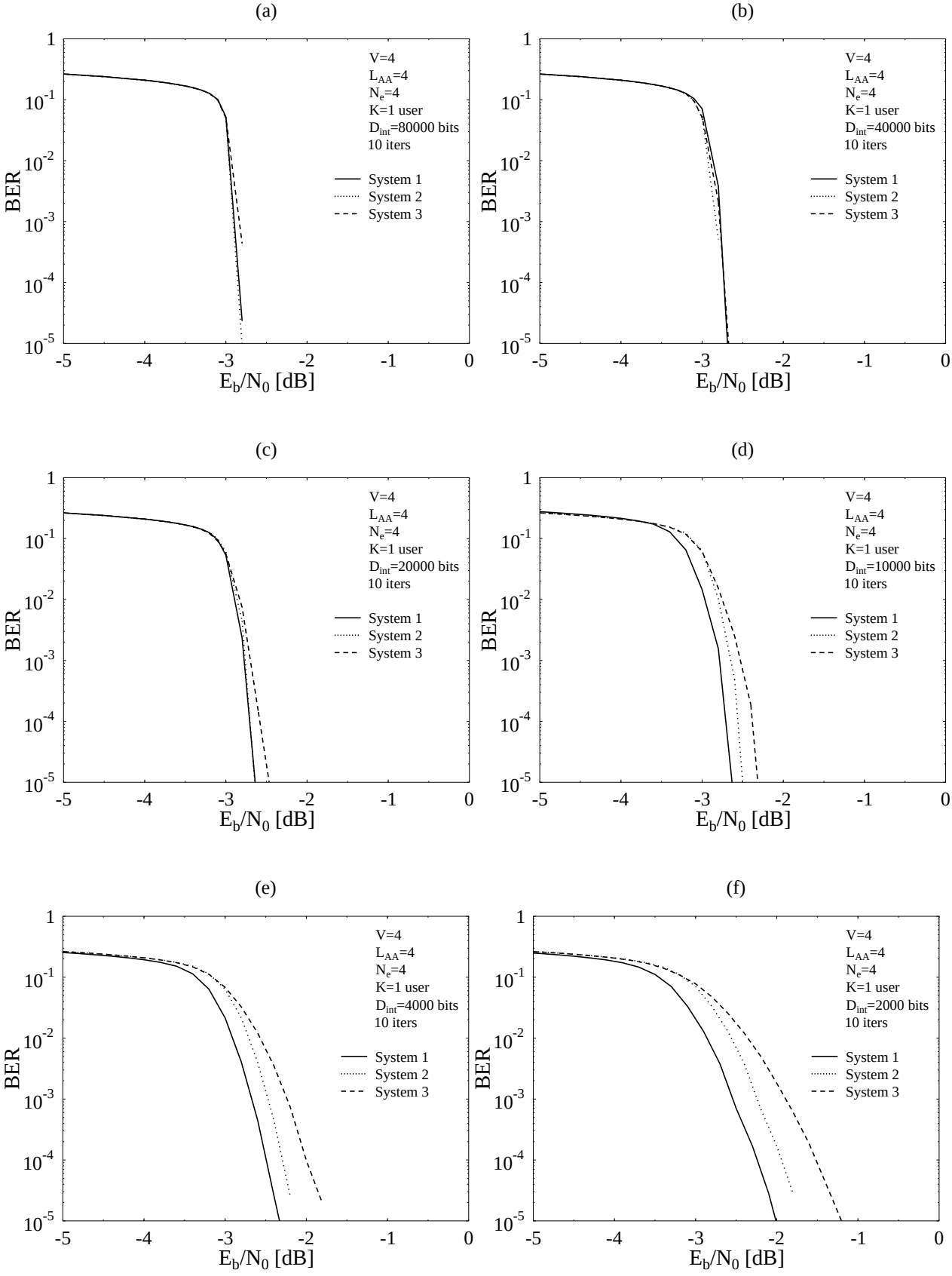

Figure 6.22: Performance comparison of GM-based RSC-coded and URC precoded Systems 1, 2 and 3 in conjunction with V=4 subcarriers, L_{AA}=4 elements per AA, N_e=4 and K=1 user and the system parameters outlined in Table 6.1, when varying the interleaver depth for 10 decoding iterations.

Figure 6.22 shows the BER performance comparison of Systems 1-3 while employing different interleaver depths D_{int} varying between 80,000 bits and 2,000 bits. Figure 6.22 compares the achievable BER performance of the proposed systems employing V=4 subcarriers, L_{AA}=4 elements per AA, N_e=4 and supporting K=1 user in conjunction with GM aided QPSK after I=10 decoding iterations. Observe in Figures 6.18-6.21 and in Figures 6.22 (a) and (b) that when long interleavers are employed, i.e. when the interleaver Depth is D_{int}=160,000 bits, 80,000 bits and 40,000 bits, the three systems have a similar BER performance. However, when we employ shorter interleavers, we can observe from Figure 6.22 that the BER performance of System 3 becomes inferior to that of System 2, which in turn performs worse than System 1. This is due to the fact that the interleaver depth of Systems 2 and 3 is half of that of System 1, which implies that the extrinsic information remains more correlated and hence prevents the decoding trajectory from reaching the (1.0, 1.0) point of perfect convergence, as discussed in Section 3.2.4. Observe also in Figure 6.22 that the performance of System 3 is lower than that of System 2 and this is due to the fact that the trellis of the RSC decoder in System 2 is longer than that of System 3 and hence a high LLR value will improve the attainable performance right across the entire trellis in System 2, while it will only benefit one of the two RSC constituent trellises in System 3.

Therefore, we may conclude that although Systems 1-3, have a similar overall complexity in terms of the number of their trellis states encountered, the BER performance of the three systems remains similar only when an interleaver depth of $D_{int} \geqslant 40,000$ bits is employed. By contrast, if we employ shorter interleavers, we can observe from Figure 6.22 that the BER performance of System 1 degrades to a lesser extent in comparison to System 2, which in turn performs better than System 3, as portrayed in Figure 6.22.

6.6 Chapter Conclusion

In this chapter, we proposed a novel multi-functional downlink MIMO scheme that combines the benefits of STC, V-BLAST, generalised MC DS-CDMA as well as beamforming. The system proposed in this chapter differs from that of Chapter 5 in terms of the decoding procedure that allows the receiver of this chapter to have less receive antennas than the number of transmit antenna arrays. Hence, the system proposed in this chapter can be applied where relatively small handsets are used at the receiver. The proposed system employing N_t=4 transmit antenna arrays has a per-user throughput that is twice that of a system employing only a single STS block, which was the case in [49]. On the other hand, employing generalised MC DS-CDMA and assuming that the subcarrier frequencies are arranged in a way that guarantees that the same STS signal is spread to and hence transmitted by the specific V number of subcarriers having the

maximum possible frequency separation, the diversity order of the system employing V number of subcarriers increases V fold compared to that employing a single subcarrier. Additionally, in order to increase the number of users so that the system can support more than N_e number of users, where N_e is the TD spreading factor, TD and FD spreading was employed. We also employed a user-grouping technique for the sake of minimising the multiuser interference imposed by the users sharing the same TD spreading code on each other. In order to improve the performance of the proposed system, we presented three iterative detection aided structures of Figure 6.6, 6.7 and 6.8.

The three iterative detection aided systems ultimately resulted in a similar BER performance and also had a similar complexity provided that we employ an interleaver depth of $D_{int} \geqslant 40,000$ bits. Explicitly, after 10 decoding iterations and employing an interleaver depth of $D_{int} = 160,000$ bits, the three systems attained a BER below 10^{-5} at E_b/N_0 values in excess of -2.8 dB. On the other hand, System 1 of Figure 6.6 had $7,039,824$ trellis states, System 2 of Figure 6.7 employed $7,039,813$ number of trellis states and finally System 3 of Figure 6.8 required $7,039,648$ trellis states, when considering D_{int}=$160,000$ bits and I=10 decoding iterations. On the other hand, if we employ interleavers having a depth shorter than $40,000$ bits, we can observe from Figure 6.22 that System 1 performs better than Systems 2 and 3, since the interleaver depth of Systems 2 and 3 is half that employed in System 1. Finally, the single-user iteratively detected System 1 employing N_e=4 and V=4 outperformed the K=8-user system by an E_b/N_0 of about 0.45 dB at a BER of 10^{-5}.

6.7 Chapter Summary

In this chapter, we proposed a multi-functional multiuser MIMO scheme that combined the benefits of V-BLAST, of space-time codes, of generalised MC DS-CDMA and of beamforming. Thus, the proposed system benefits from the multiplexing gain of V-BLAST, from the spatial diversity gain of space-time codes, from the frequency diversity gain of the generalised MC DS-CDMA and from the SNR gain of the beamformer. This multi-functional MIMO scheme was referred to as LSSTS aided generalised MC DS-CDMA.

In Section 6.2 we introduced the proposed MIMO scheme, where we illustrated how the transmitter of the different users was constructed. Then, we outlined the decoding process that takes place at the receiver side, where two-stage decoding was employed. First, the interference cancellation was carried out, where the interference imposed by one of the STS blocks on the other was perfectly cancelled by the interference cancellation technique employed. Afterwards, STS decoding was carried out in the same way as proposed in [49]. In order to increase the

number of users supported by the system, FD spreading was applied in the generalised MC DS-CDMA in addition to the TD spreading of the STS. In this case, the users can share the same TD spreading code and then they are distinguished by their FD spreading code. This results in the users sharing the same TD spreading code imposing multiuser interference on each other. Hence, we employed a user grouping technique that minimises the FD interference coefficient for the users in the same TD group. The user grouping technique was described in Section 6.3.3.

To further enhance the achievable system performance, the proposed MIMO scheme was serially concatenated with an outer code combined with a URC, where three different iteratively detected systems were presented, referred to as System 1, System 2 and System 3. System 1, shown in Figure 6.6 employed the serial concatenation of an RSC encoder and a URC encoder with the proposed QPSK modulated LSSTS scheme. At the receiver side, iterative detection was carried out between the RSC decoder and the URC decoder. Additionally, in the structure of Figure 6.7 denoted as System 2, the transmitted source bits were encoded by the outer RSC code's encoder. The outer channel encoded bits were then S/P converted to two parallel streams. Each bit stream was then encoded by a corresponding URC encoder followed by a QPSK modulator in each substream. The data in each stream was then transmitted using SSTS. At the receiver side of System 2, iterative detection was carried out between the RSC decoder and the two URC decoders, where the LLRs were S/P converted from the RSC decoder to the URC decoders and they were then P/S converted, when passed from the URC decoders to the RSC decoder. Finally, in the structure of Figure 6.8 denoted as System 3, the transmitted source bits were first S/P converted to two parallel substreams, where each substream was encoded by the outer RSC code's Encoder followed by the URC encoder. The URC encoded bits in each stream were then mapped to QPSK symbols and transmitted using SSTS. At the receiver side of System 3 seen in Figure 6.8, the decoding process of Section 6.2.2 was employed, where the decoded symbols were passed to their corresponding branch as shown in Figure 6.8. Each branch then applied iterative detection exchanging extrinsic information between the corresponding RSC and URC decoders, as shown in Figure 6.8. The extrinsic output of the RSC decoders was then P/S converted to produce an LLR stream, which was passed to the hard-decision decoder of Figure 6.8.

We used EXIT charts in order to study the convergence behaviour of the proposed systems and in Section 6.4.1 we proposed an LLR post-processing scheme for the soft output of the QPSK demapper, in order to improve the achievable system performance. In Section 6.5 we discussed our performance results and characterised the three proposed iteratively detected schemes, while employing N_t=4 transmit AAs, N_r=2 receive antennas, L_{AA} number of elements per AA, V number of subcarriers and K users. We demonstrated that the three pro-

posed systems attain a BER lower than 10^{-5} at E_b/N_0 in excess of -2.8 dB, while employing D_{int}=160,000 bits and I=10 iterations. Finally, for the system employing N_e=4 and V=4, the single user iteratively detected System 1 outperformed the eight-users system by an E_b/N_0 of about 0.45 dB at a BER of 10^{-5}.

Chapter 7

Distributed Turbo Coding

7.1 Introduction

As discussed in Chapter 1, wireless channels suffer from multipath propagation of signals, that results in a variation in the received signal strength. During severe fading of a specific propagation path, the received signal cannot be correctly decoded, unless some less attenuated multipath versions of it are available at the decoder side. This can be arranged by introducing transmit diversity for example, as discussed in Chapter 1. In conventional MIMO systems constituted by colocated MIMO elements, transmit diversity is generated by transmitting different versions of the signal from different antennas located at the same BS or MS. Transmit diversity results in a significantly improved BER performance, when the different transmit antennas are positioned sufficiently far apart to ensure that the signal from each antenna to the destination experience independent fading.

The antenna spacing in colocated MIMOs is assumed to be sufficiently large so that the assumption of statistical independence of the different paths from the different antennas is justified. However, satisfying the assumption of a sufficient high antenna spacing may be impractical for shirt-pocket-sized wireless devices, which are typically limited in size and hardware complexity to a single transmit antenna. On the other hand, spatial fading correlations caused by insufficient antenna spacing at the transmitter or receiver of a MIMO system result in a degraded capacity as well as BER performance for MIMO systems, as shown in Figure 7.1 for a twin-antenna-aided STBC system [44]. Spatial correlation is typically introduced as a result of large-scale shadow fading that affects the transmission links between the different transmit and receive antennas [31]. Figure 7.1 compares the BER performance of a single-transmit and single-receive antenna system with that of a twin-antenna-aided STBC system affected by the large-scale shadow fading. As shown in Figure 7.1, the performance of MIMO systems degrades

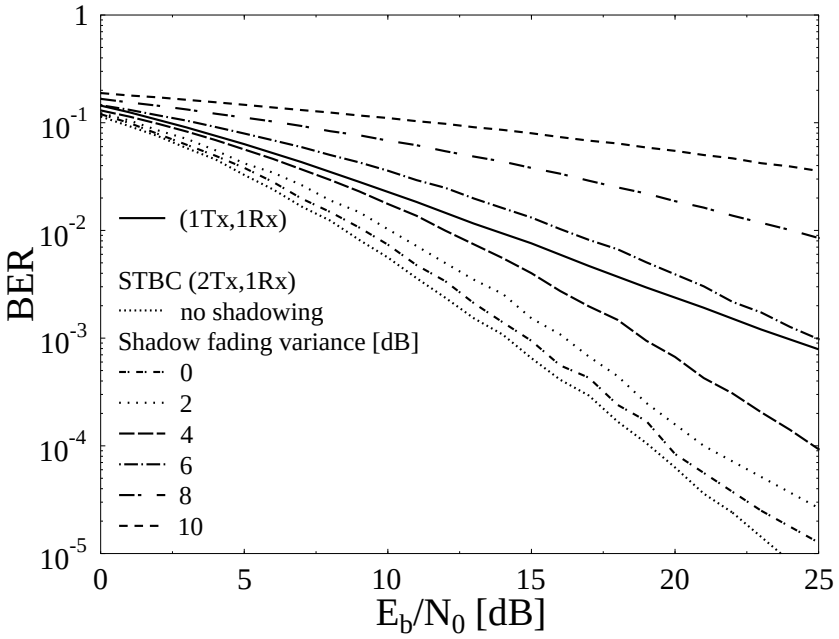

Figure 7.1: Effect of large-scale shadow fading on the performance of twin-antenna-aided STBC system.

as the variance of the shadow fading increases and the single-antenna aided system succeed in outperforming a MIMO system, when the shadow fading variance is higher than 5 dB.

Hence, we can surmise that transmit diversity methods are not readily applicable to compact wireless communicators owing to the size as well as complexity constraints that limit the use of multiple transmit antennas. For example, in wireless mobile systems the size of the mobile unit is a limiting factor in incorporating several antennas that are sufficiently far apart for attaining statistically uncorrelated fading between the different transmit and receive antennas. Recently, cooperative communication techniques [36, 37, 268] were proposed for eliminating correlation amongst the diversity paths by cooperatively activating the single antenna of several MSs, hence effectively creating a distributed MIMO scheme. In other words, single-antenna aided users support each other by "sharing their antennas" and thus generate a virtual multi-antenna environment [137]. Again, in cooperative communications it is possible to guarantee that the cooperating users are sufficiently far apart, in order to attain independent fading. Since the signals transmitted from different users undergo independent fading, spatial diversity can be achieved by the concerted action of the cooperating partners' antennas.

In this chapter we design a Distributed Turbo Coding (DTC) scheme, where two users cooperate in a two-phase cooperation scheme. During the first phase of cooperation, each user sends his/her own data to the other user, followed by the second phase where both users transmit their own data as well as the data of the other user after interleaving and channel coding. The two users employ multidimensional Sphere Packing (SP) modulation and then transmit their data simultaneously. The receiver applies interference cancellation for the sake of eliminating

the interference imposed by one user's data on the other. We employ SP modulation for the sake of attaining further iteration gains, as described in Chapter 3. The data transmitted from the second user's transmitter is an interleaved version of the bit stream transmitted from the first user's transmitter. Hence, at the receiver side, the interference canceller outputs two data streams corresponding to the data transmitted from the first and the second users' transmitters, respectively. Afterwards, iterative detection is employed between the SP demapper and the channel decoder in each data stream (or decoding branch) as well as between the two channel decoders of the two branches, hence forming a distributed turbo code. Additionally, we study the effects of different Inter-User Channel (IUC) characteristics on the attainable BER performance of the proposed DTC system, where we compare the attainable BER performance, when the IUC is perfect, Gaussian, Ricean and Rayleigh faded.

The rest of the chapter is organised as follows. In Section 7.2 we present an overview of cooperative communications, followed by the description of the proposed DTC system in Section 7.3. In Section 7.4 we characterise the DTC aided system with the aid of simulation results, while considering different IUC characteristics. We conclude in Section 7.5 and present a brief chapter summary in Section 7.6.

7.2 Background of Cooperative Communications

In this section we present a brief literature overview of cooperative communications and introduce the basic ideas behind the concept of user cooperation.

The basic idea behind cooperative communications can be traced back to the idea of the relay channel, which was introduced in 1971 by Van der Meulen [131]. Cover and El Gamal characterised the relay channel from an information theoretic point of view in [132]. The relay model is comprised of three components: a source transmitting data, a destination receiving the data from the source and a relay receiving the data from the source and then transmitting it to the destination. Cooperative communications may be interpreted as a generalisation of the relay channel, where the source and the relay transmit their own data as well as the other's data, which results in the destination receiving multiple copies of the same data from both the source as well as from the relays, hence benefitting from a spatial diversity gain and eventually from an improved BER performance for the two users. Cooperative techniques benefit from the broadcast nature of wireless signals, where the signal transmitted from a specific user to a specific destination can be "overheard" by neighbouring users.

In [134] Sendonaris *et al.* generalised the relay model to multiple nodes that transmit their own data as well as serve as relays for each other. The scheme proposed in [134] was referred

to as "user cooperation diversity", where the authors examined the achievable rate regions and outage probabilities for this particular scheme. In [36, 37] Sendonaris *et al.* presented a simple user-cooperation methodology based on a Decode-and-Forward (DF) signalling scheme using Code Division Multiple Access (CDMA). The orthogonality of the different spreading codes of the different users makes it possible for the intended receiver to distinguish between the information transmitted from different cooperating users. In [135] the authors reported the gains achieved in terms of an improved data rate and reduced sensitivity to channel variations, where it was concluded that cooperation effectively mimics a multi-antenna scenario with the aid of single-antenna terminals.

Cooperative communications has been shown to offer significant performance gains in terms of various performance metrics including diversity gains [138, 141, 161] as well as multiplexing gains [145]. In the following sections we review the main-stream cooperative methods used for signalling the data between the different users and the destination.

7.2.1 Amplify-and-Forward

Each user receives a noise-contaminated version of the other users' signals. In the case of an Amplify-and-Forward (AF) signalling strategy [135], the relay simply amplifies the noisy version of the signal without improving its SNR and retransmits it to the destination. The destination then combines the information sent by the source as well as the relay and makes a final decision on the transmitted bits [269]. Although the relay amplifies the noise in addition to amplifying the desired signal, the destination still observes two independently faded version of the signal, thus benefitting from a diversity gain as compared to non-cooperative schemes.

AF was first proposed and analysed by Laneman *et al.* in [135], where the authors have shown that in the case of two-user cooperation, AF is capable of achieving a diversity order of two. In the scheme of [135], it was assumed that the destination has perfect knowledge of the IUC so that optimal decoding can be performed, where the IUC knowledge was assumed to be acquired by exchanging this IUC information between the nodes with the aid of side-information signalling or by blind estimation [269]. More elaborate AF algorithms and more general linear relaying schemes have been considered in [142, 270].

7.2.2 Decode-and-Forward

In the Decode-and-Forward (DF) signalling scheme the relay decodes the partners' signals and then re-encodes the detected bits before their retransmission [269]. The destination combines the signal received from both the source as well as the relay, hence creating spatial diversity. A witty low-complexity DF signalling strategy can be found in [36, 37], where two users were

paired to cooperate with each other using CDMA. Each signalling period is divided into three time slots, where in the first and second time slots each user transmits his/her own data. Each user's data is broadcast and hence can be detected by the other user. In the second time slot, each user detects the other user's data. In the third time slot, both users transmit a linear combination of their own second time slot data and the partners' second time slot data, each multiplied by the appropriate spreading code. The allocation of transmitted power for the three time slots is determined by the average power constraint of each user. Explicitly, when the IUC has a high SNR, more power can be allocated to cooperation. Otherwise, less power is assigned for cooperation. The advantage of this signalling regime is its appealing simplicity and adaptability to channel variations. Additionally, it is required that the destination has acquired the knowledge of the Channel Impulse Response (CIR) of the IUC for the sake of optimal decoding [269].

In order to avoid the problem of error propagation, selection DF was proposed by Laneman *et al.* in [141], where the relay detects the signal from the source and only forwards the signal when the instantaneous SNR for the IUC is below a certain threshold. Otherwise, the source continues its transmission to the destination in the form of repetition or more powerful codes [269]. If the measured SNR falls below the threshold, the relay transmits what it receives from the source using either AF or DF, in order to attain a diversity gain. Another signalling strategy is referred to as incremental relaying [141], which can be viewed as an extension to incremental redundancy or Hybrid Automatic-Repeat-reQuest (HARQ). In this case, the relay retransmits in case the destination provides a negative acknowledgement in an attempt to attain a diversity gain.

7.2.3 Coded Cooperation

Coded cooperation [136,149] combines the concept of cooperative communications with channel coding. Coded cooperation maintains the same information rate, code rate, bandwidth as well as transmit power as a comparable non-cooperative system. The basic idea is that each user attempts to transmit incremental redundancy for his/her partner. Whenever the IUC is not favourable, the users automatically revert to a non-cooperative mode [269]. The key to the efficiency of coded cooperation is that all this is managed automatically with the aid of sophisticated code design, with no feedback between the users [269].

Each user encodes his/her data bits using a Cyclic Redundancy Check (CRC) followed by a specific code from a family of Rate Compatible Punctured Convolutional (RCPC) codes [136]. Each user's encoded codeword is divided into two segments containing N_1 and N_2 bits, where $N_1 + N_2 = N$ and N is the total codeword length of the encoded sequence. In the first time slot,

each user transmits his/her own first set of N_1 bits, where the encoded codeword is punctured to N_1 bits and hence the N_1 bits transmitted constitute a valid or legitimate codeword. The remaining N_2 bits are the punctured bits. Each user then attempts to decode the transmission of the other user. If this attempt is deemed to be successful based on the CRC code, the user computes and transmits the N_2 bits of the other user in the second time slot. Otherwise, the user transmits his/her own N_2 bits. Thus, each user always transmits a total of $N = N_1 + N_2$ bits per source block over the two time slots [136, 269].

The users act independently in the second time slot, with no knowledge of whether their own first frame was correctly decoded. As a result, there are four possible cases for the transmission of the second frame: both users cooperate, neither user cooperates, user 1 cooperates and user 2 does not or vice versa. It was suggested in [143] that the destination successively decodes according to all possibilities and checks the CRC code's success for each case. If the CRC fails for all possibilities, then the destination will select the specific codeword with the lowest path metric from the Viterbi algorithm.

Additionally, it was proposed in [138] to use distributed space-time codes for the relay channel, demonstrating its benefits from an information theoretic point of view. In [143] Janani *et al*. proposed space-time cooperation in addition to implementing turbo coding by exchanging extrinsic information between the data received from the source and the relay. Furthermore, a method designed for achieving cooperative diversity using rate compatible punctured codes was proposed in [136, 149]. In [139, 140], it was proposed to employ distributed turbo codes by exchanging extrinsic information between the data received from the source and that received from the relay, where the relay applies interleaving for the data received from the source and then uses an appropriate channel code before retransmission.

7.3 Distributed Turbo Coding

In this section we propose a specific DTC scheme based on the system architecture shown in Figure 7.2, where the users u_1 and u_2 cooperate in a two-phase cooperation scenario. The difference between our proposed system and those presented in [136, 139, 140, 143, 149] is that the two users in our design transmit their own data in addition to the other user's data, while the systems in [136, 139, 140, 143, 149] have a single active user and a relay transmitting the data of the active user only. Additionally, in our proposed system we study the effect of the IUC characteristics on the attainable performance of the proposed DTC system. As shown in Figure 7.2 two users cooperate in order to communicate with a Base Station (BS). This way the users achieve a diversity gain in case the two users transmit in a space-time coded manner or attain a multiplexing gain, if they transmit in a BLAST-like scheme. In the proposed scheme,

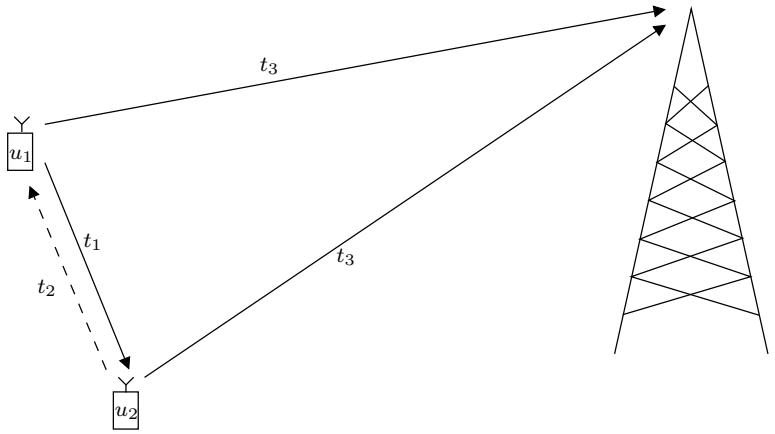

Figure 7.2: Distributed turbo coding system model.

the two users cooperate in two phases, where they exchange their data in the first cooperation phase and then they both transmit simultaneously their own data as well as the data of the other user in the second phase of cooperation.

The proposed system operates in a half-duplex mode, where none of the transceivers can transmit and receive at the same time. The transceivers operate in a Time Division Duplex (TDD) mode, where different transmitters transmit in different time slots. As shown in Figure 7.2, in time slot t_1 user 1 transmits his/her data to user 2. Similarly, in time slot t_2 user 2 shares his/her data with user 1. Hence, the first two time slots, i.e. time slots t_1 and t_2, comprise the first phase of cooperation. In the second phase of cooperation, i.e. in time slot t_3, the two users transmit their data simultaneously to the BS after appropriate interleaving and channel coding.

A more detailed block diagram of the proposed scheme is shown in Figure 7.3. In time slot t_1, user 1 transmits his/her data bit stream $\mathbf{a}_1$ to user 2, where the received and decoded estimate of $\mathbf{a}_1$ is denoted by $\widetilde{\mathbf{a}}_1$. Hence, the DF signalling strategy is used in the proposed DTC scheme. Similarly, user 2 transmits his/her data bit stream $\mathbf{a}_2$ to user 1, where the received and decoded bit stream in denoted by $\widetilde{\mathbf{a}}_2$. There are several scenarios for the inter-user communication, i.e. for the phase-one cooperation. The simplest phase-one cooperation, where each user transmits the source bits directly without any channel coding and the other user applies hard decision decoding of the received signal. Another possible scenario is, where each user encodes his/her data using a channel code of a specific code rate and then the receiver decodes the received stream by passing it through the modulated symbol to channel-coded bits demapper as well as the channel decoder and may employ iterative detection by exchanging extrinsic information between the demapper and the channel decoder.

After inter-user communication phase was concluded during time slots t_1 and t_2, the two users now have both their own data as well as an estimate of the data of the other user.

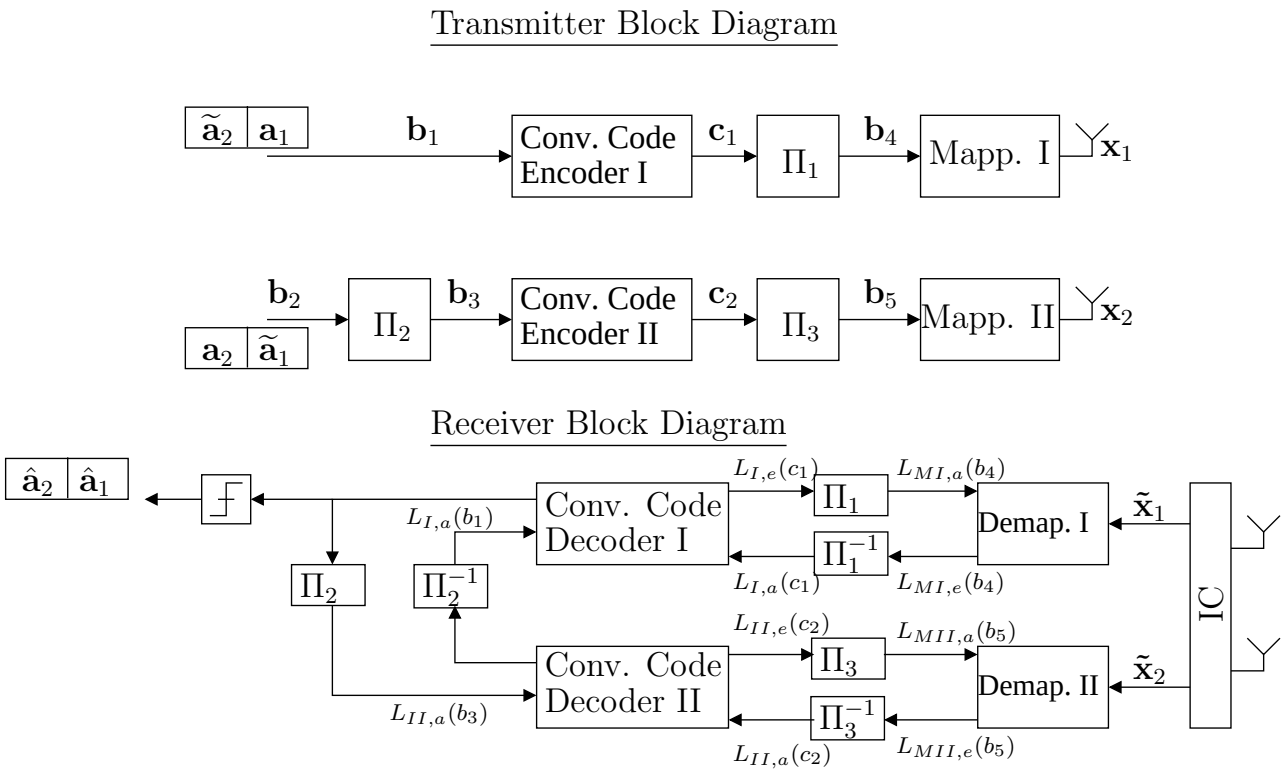

Figure 7.3: Block diagram of the two users' transmitters and the BS receiver.

Both users concatenate their own data with the estimate of the other user's data, as shown in Figure 7.3 and detailed as follows. The first user appends the estimate of the second user's data $\widetilde{\mathbf{a}}_2$ with his/her own data $\mathbf{a}_1$ and then encodes the resultant bit stream $\mathbf{b}_1$ by a Recursive Systematic Convolutional (RSC) code. The channel coded bit stream $\mathbf{c}_1$ is interleaved by the random bit interleaver Π_1 of Figure 7.3 and then the interleaved bits $\mathbf{b}_4$ are modulated by the SP Mapper I of Figure 7.3. Similarly, user 2 appends his/her own data $\mathbf{a}_2$ to the estimate of the user 1 data $\widetilde{\mathbf{a}}_1$ and then interleaves the resultant bit frame $\mathbf{b}_2$ by the bit interleaver Π_2 of Figure 7.3. The interleaved bit stream $\mathbf{b}_3$ is channel coded by a RSC code and then the encoded bit stream $\mathbf{c}_2$ is interleaved. Finally, the interleaved bit stream $\mathbf{b}_5$ is modulated by the SP Mapper II of Figure 7.3.

The two users simultaneously transmit their SP modulated symbol streams $\mathbf{x}_1$ and $\mathbf{x}_2$ assuming that there is perfect synchronisation between the two users' MSs. The two users' MSs normalise their transmit power so that the transmit power in the two phases of cooperation is equivalent to the case when there is no cooperation.

At the BS, low-complexity Zero Forcing (ZF) Interference Cancellation (IC) is applied, as described in [81]. The IC decoder outputs the two streams of decoded data $\widetilde{\mathbf{x}}_1$ and $\widetilde{\mathbf{x}}_2$ corresponding to the data transmitted by user 1 and user 2, respectively, as shown in Figure 7.3. After the IC stage, estimates of the transmitted data streams $\widetilde{\mathbf{x}}_1$ and $\widetilde{\mathbf{x}}_2$ are passed to the SP

demappers of Figure 7.3. The SP demappers I and II of Figure 7.3 utilise the data received from the IC together with the *a priori* information $L_{MI,a}(\mathbf{b}_4)$ and $L_{MII,a}(\mathbf{b}_5)$ passed to them from the RSC decoders for the sake of providing the improved *extrinsic* information $L_{MI,e}(\mathbf{b}_4)$ and $L_{MII,e}(\mathbf{b}_5)$, which is then passed to the RSC decoders as the *a priori* information $L_{I,a}(\mathbf{c}_1)$ and $L_{II,a}(\mathbf{c}_2)$. Afterwards, iterative detection is carried out by exchanging extrinsic information between the two RSC decoders of the two branches. The two RSC decoders employ iterative detection for the sake of providing improved *extrinsic* information to the SP demappers of Figure 7.3. The iterations employed between the two RSC decoders is similar in its concept to that employed in classic turbo codes [26, 271], which motivates the terminology of distributed turbo coding.

Figure 7.4 shows the EXIT chart of the proposed DTC system. In Figure 7.4 we plot the EXIT curve of the inner SP demappers in conjunction with L=16 and the Anti-Gray Mapping AGM-1 listed in Appendix A. The EXIT curves of the inner SP demappers seen in Figure 7.4 are shown for E_b/N_0 between 0 dB and 6 dB in steps of 0.5 dB. Figure 7.4 also shows the inverted EXIT curve of the outer DTC. The outer codes applied are 1/2-rate memory-2 RSC codes in conjunction with an octal generator polynomial of $(G_r, G) = (7, 5)_8$, where G is the feedforward polynomial and G_r is the feedback polynomial. We plot two curves corresponding to the outer DTC in Figure 7.4, where one, represented by the dashed-dotted line evolving mostly above the dashed curve, corresponds to two iterations between the two outer RSC codes' decoders, while the other curve marked by the dashed line corresponds to six iterations between the two RSC codes' decoders. In this case, in the first phase of cooperation, each user modulates the source bits and transmits the QPSK modulated symbols to the other user without incorporating any channel coding. Additionally, the EXIT curves are plotted for the system where the IUC is considered to be perfect. As shown in Figure 7.4, an open convergence tunnel is formed around E_b/N_0=3.0 dB. This implies that according to the predictions of the EXIT chart seen in Figure 7.4, the iterative decoding process is expected to converge for $E_b/N_0 > 3.0$ dB. On the other hand, observe in Figure 7.4 that the point of intersection between the EXIT curves of the inner and the outer codes approaches the 1.0 mutual information points of the x-axis, as the number of outer iterations or distributed turbo coding iterations increases from I_{out}=2 to 6. Hence, it is expected that employing I_{out}=6 outer iterations between the RSC decoders will result in a better performance than the system employing two decoding iterations between the outer RSC codes.

On the other hand, Figure 7.5 shows the EXIT curve of the benchmark scheme, where two users cooperate by transmitting their own data simultaneously without transmitting the other user's data. In other words, each user encodes his/her own bit stream by an outer RSC code and then the encoded bit stream in interleaved by a random bit interleaver. Afterwards, the

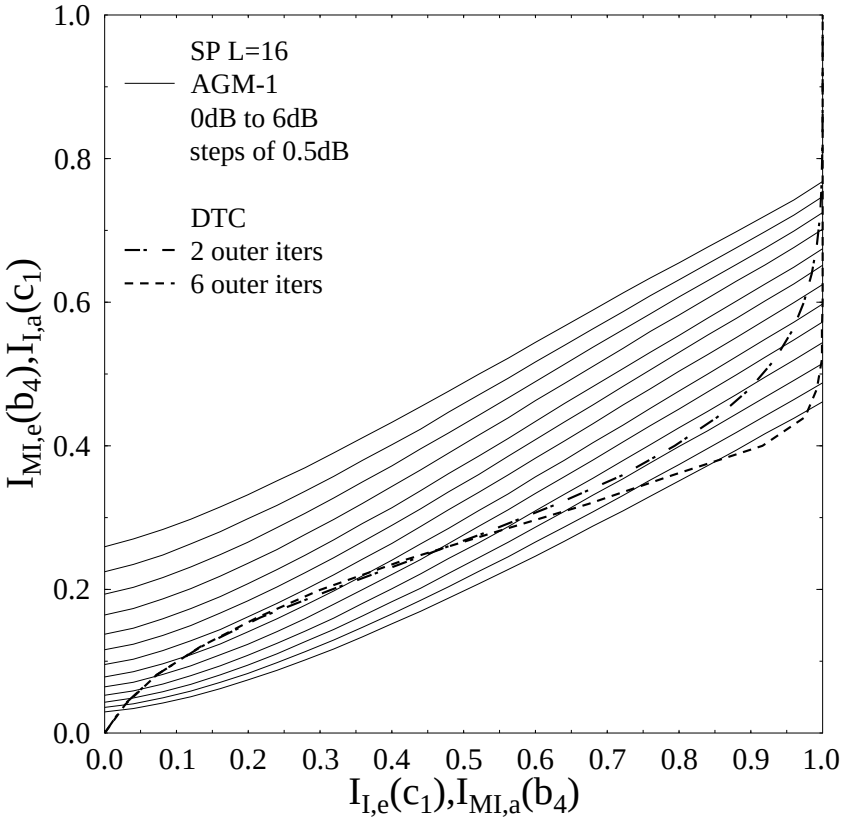

Figure 7.4: EXIT chart of the DTC system, where cooperation is employed between two users employing 1/2-rate RSC codes while uplink communication is performed over a narrowband Rayleigh fading channel.

interleaved bit stream is modulated by a SP mapper and then transmitted from the users' single-antenna-aided MS. At the receiver side, IC is employed in order to eliminate the interference imposed by each of the users' data on the other user's data. Iterative detection is then carried out between the outer RSC decoder and the inner SP demapper in each branch and no iterations are employed between the two outer RSC codes' decoders, since the data in the two branches of Figure 7.3 in this case are different. Figure 7.5 shows the EXIT chart of the benchmark scheme in conjunction with an inner SP demapper employing L=16 and AGM-1 of Appendix A for E_b/N_0 between 0 dB and 6 dB in steps of 0.5 dB. The outer code in this case is a 1/2-rate memory-2 RSC code in conjunction with an octal generator polynomial of $(G_r, G) = (7, 5)_8$. As shown in Figure 7.5, an open convergence tunnel is formed around E_b/N_0=4.0 dB. This implies that according to the predictions of the EXIT chart seen in Figure 7.5, the iterative decoding process is expected to converge at $E_b/N_0 > 4.0$ dB. Additionally, a comparison between Figure 7.4 and Figure 7.5 shows that the benchmark scheme exhibits a higher error floor as compared to an error floor at low BER values for the proposed DTC scheme.

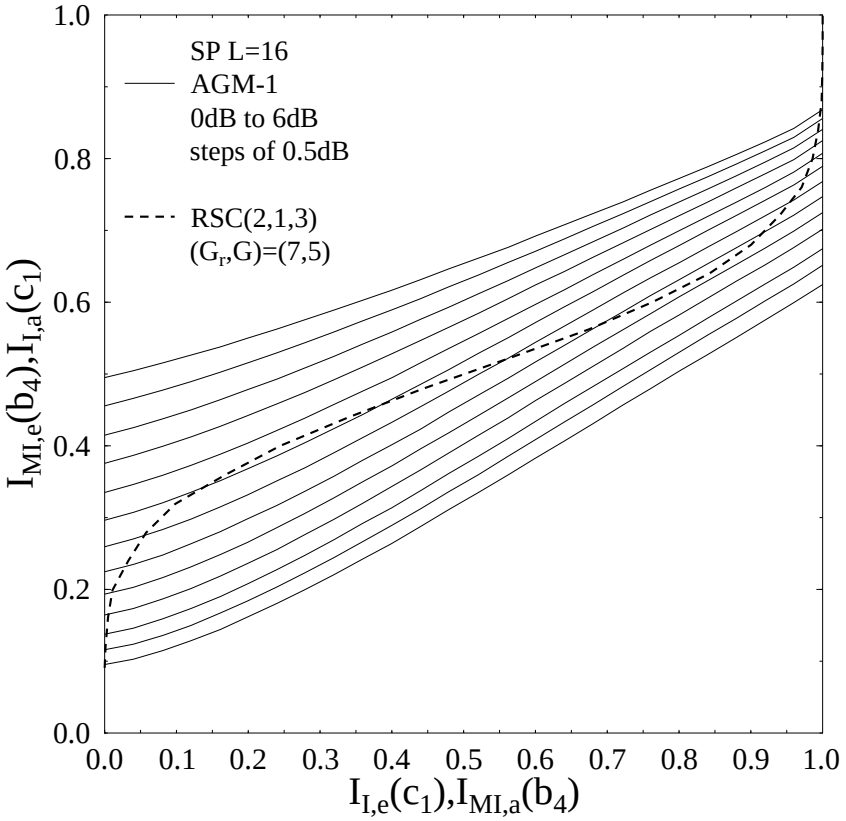

Figure 7.5: EXIT chart of the benchmark scheme where iterative detection is carried out between the outer RSC decoder and the inner SP demapper of each user without employing any iteration between the RSC decoders of the two users. In this case, each user transmits his/her own data only and hence there is no inter-user communication involved.

7.4 Results and Discussions

In this section, we consider the achievable performance of the proposed DTC system, where two users cooperate in order to simultaneously transmit their data and then apply the ZF IC at the receiver for the sake of eliminating the interference imposed by each of the users' data on the other user's data. Each user's MS is equipped with a single antenna and each applies a 1/2-rate memory-2 RSC code for coding the bits, which are then mapped to symbols using a SP mapper in conjunction with L=16 and AGM-1. In this section, we consider uplink transmissions over a narrowband uncorrelated Rayleigh fading channel, where coherent detection is applied at the receiver side. It is also assumed that the receiver has perfect knowledge of the uplink channel impulse response.

The proposed DTC scheme corresponds to a cooperation between two users, where each user is equipped with a single-antenna terminal. The system operates in a TDD mode, where the two users exchange their data in two time slots and then they transmit their joint data to the BS. Each user encodes his/her bit stream by an outer RSC code and then maps the encoded bits to SP symbols using an SP mapper. At the BS, ZF IC is applied, where the

decoder outputs two data streams corresponding to the data received from user 1 and user 2. The decoded symbols are demapped to soft LLR values by the SP demappers of Figure 7.3. The SP demapper of each branch exchanges soft information with the RSC decoder in the same branch after appropriate interleaving and deinterleaving. Afterwards, the RSC decoders of the two branches exchange extrinsic information in order to provide improved information for the SP demappers, which in turn pass extrinsic information to the RSC decoders. As shown in Figure 7.4, in order to arrive as low an error floor as possible, it is required to employ I_{out}=6 outer iterations between the two RSC decoders. Hence, in what follows, we refer to an iteration as a system iteration I_{sys}, where the SP demappers exchange extrinsic information with the RSC decoders once in an inner iteration, followed by I_{out}=6 outer decoding iterations between the two parallel RSC decoders, before passing the improved extrinsic information back to the SP demappers.

The benchmark scheme for our proposed system is also a cooperative scheme exchanging extrinsic information between single-antenna-aided users. However, in the benchmark scheme, the two users do not exchange their information, rather each user transmits his/her own data after channel coding, interleaving and then SP mapping. The two users transmit their data simultaneously and then ZF IC is applied at the receiver, where each user's data is passed to a separate branch of iterative detection between the SP demapper and the outer RSC decoder. In this case, no iterative detection is carried out by exchanging extrinsic information between the two RSC decoders, since the two branches have different data.

The bandwidth efficiency of the proposed DTC scheme can be analysed as follows. During the first time slot t_1, user 1 transmits his/her data to user 2, followed by time slot t_2, where user 2 transmits his/her data to user 1. Afterwards, during the second phase of cooperation, each user has to transmit the data of the two users, which requires two time slots. Hence, a total of four time slots are required for the transmission of the two users' data to the BS. By contrast, the benchmark scheme requires only a single time slot for the transmission of the same amount of data to the BS by the two users. Hence, the proposed scheme has a factor of four lower throughput compared to the benchmarker, but as a benefit, the proposed scheme attains a better BER performance according to the EXIT chart predictions of Figure 7.4 and 7.5, which will be demonstrated in Figure 7.7.

Figure 7.6 shows the BER performance of a V-BLAST system having colocated MIMO elements, where the transmitter has two antennas and the receiver is also equipped with two antennas, while communicating over narrowband Rayleigh fading channels also affected by large-scale shadow fading. The source bits are encoded by a 1/2-rate RSC code and then interleaved by a random bit interleaver, where the interleaved bits are mapped to SP symbols

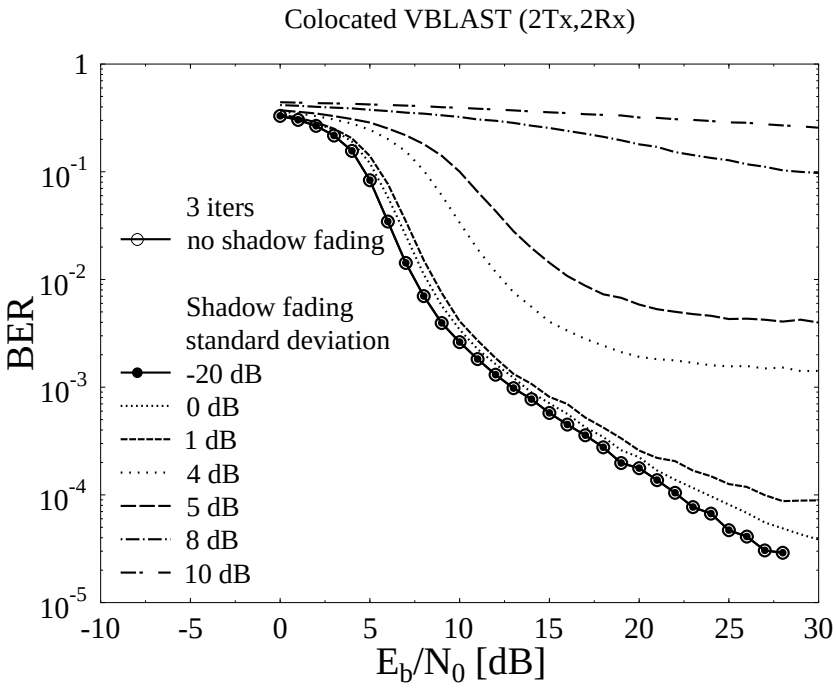

Figure 7.6: BER performance of a V-BLAST scheme employing two transmit and two receive antennas in conjunction with iterative detection between an outer RSC decoder and a SP demapper at the receiver side. The figure shows the effect of shadow fading on the attainable performance.

before transmission. At the receiver side, iterative detection is carried out by exchanging extrinsic information between the outer RSC code and the SP demapper. Figure 7.6 shows the effect of shadow fading on the attainable performance of MIMO scheme having colocated elements, where the shadow fading imposes correlation on the impulse response of the channels between the two transmit antennas and the receive antennas. In Figure 7.6 the RSC code used is a 1/2-rate memory-2 code with an octal generator polynomial of $(G_r, G)=(5, 7)_8$ and the BER curves correspond to $I_{inner}=3$ decoding iterations between the SP demapper and the RSC decoder. As shown in Figure 7.6, when the shadow fading standard deviation increases, the attainable BER performance degrades. Therefore, distributed MIMO or cooperative communications represent an intelligent way of retaining the gains of the MIMO systems having independently fading colocated elements without being affected by the shadow fading, while relying on single-antenna-aided MSs.

Figure 7.7 compares the attainable BER performance of both the proposed DTC scheme and of the benchmark scheme, while considering uplink transmissions over a narrowband Rayleigh fading channel. In this case, the IUC is considered to be perfect, i.e. the data exchanged between the two users is perfectly recovered without any errors. In Figure 7.7 an interleaver depth of $D_{int}=80,000$ bits was employed and SP modulation in conjunction with $L=16$ and AGM-1 is used. Observe in Figure 7.7 that the benchmark scheme suffers from a fairly pronounced error floor and that no iteration gain may be obtained after employing more than one inner iteration between the SP demapper and the RSC decoder in each branch. This result confirms the EXIT

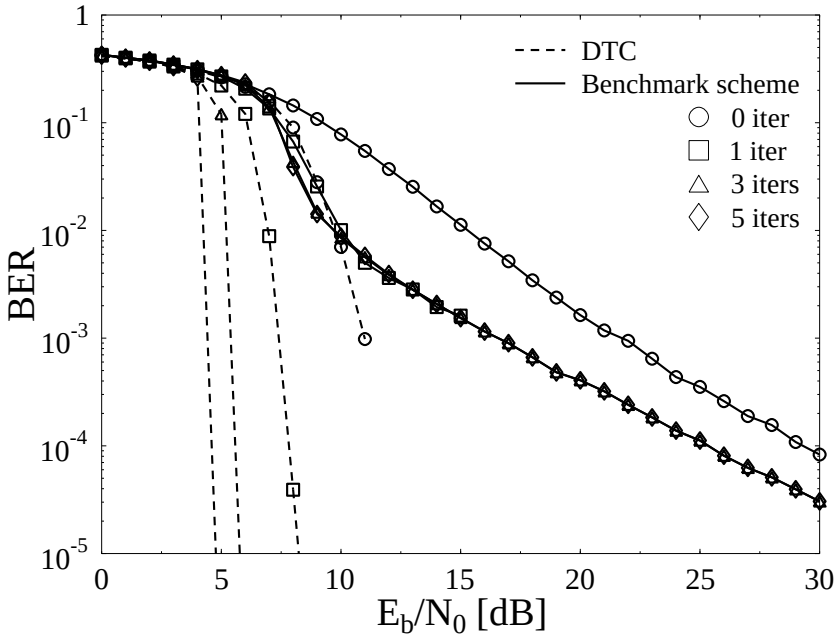

Figure 7.7: BER performance comparison of the proposed distributed turbo coded system and the benchmark scheme in conjunction with an interleaver depth of D_{int}=80,000 bits for a variable number of system iterations I_{sys}, where two users are cooperating and communication over an narrowband uplink Rayleigh fading channel. The IUC in this case is considered to be perfect.

chart predictions of Figure 7.5, where the EXIT curves of the inner and outer codes intersect for E_b/N_0=6.0 dB at a point different from the 1.0 point on the x-axis indicating the lack of convergence to an infinitesimally low BER. On the other hand, observe in Figure 7.7 that the attainable BER performance of the proposed DTC aided system exhibits no error floor. This can be explained from the EXIT chart of Figure 7.4, where the EXIT curves of the inner and outer codes intersect at the 1.0 point on the x-axis, when there is an open tunnel. The 1.0 point on the x-axis corresponds to the case, where the outer decoder has perfect extrinsic information available at its output. This means that for the E_b/N_0 values where there is an open tunnel, the EXIT curves of the inner and outer codes intersect at the 1.0 point of perfect convergence, i.e. at the point where the outer decoder has perfect extrinsic information at its output, which results in an infinitesimally low BER. Again, for the proposed DTC scheme, a system iteration I_{sys} is constituted by a single inner iteration between the SP demapper and the RSC decoder of each branch, followed by I_{outer}=6 iterations between the two RSC decoders in the two branches. Explicitly, the proposed DTC system outperforms its benchmark scheme by E_b/N_0 of about 25 dB at a BER of 10^{-5} after employing I_{sys}=5 system iterations.

Figure 7.8 shows the attainable BER performance of the proposed DTC scheme, while considering uplink transmission over a narrowband Rayleigh fading channel, where the IUC considered is a Line-Of-Sight (LOS) AWGN channel, i.e. Gaussian noise is added to the received data without any amplitude or phase attenuation. In Figure 7.8 an interleaver depth of

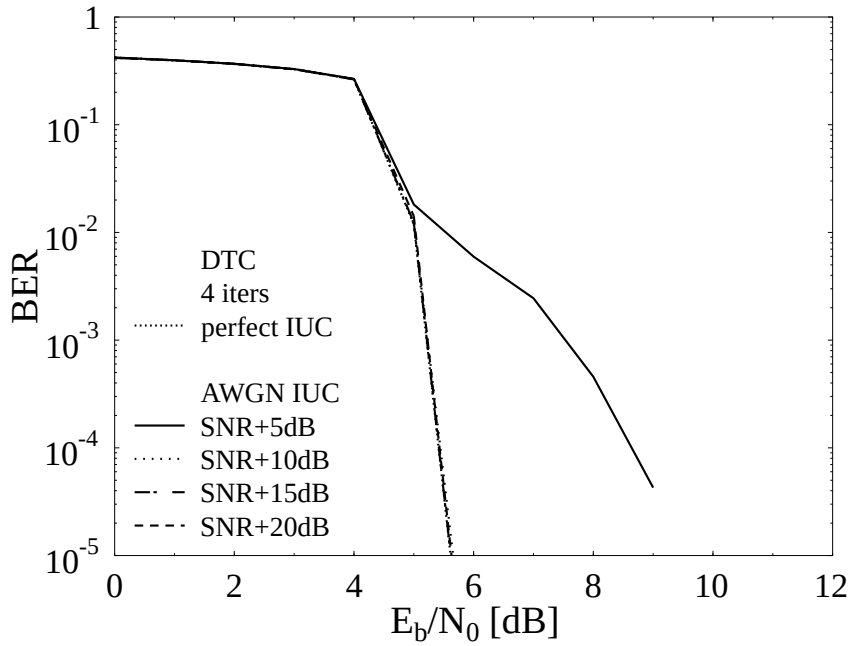

Figure 7.8: Comparison of the attainable BER performance of the proposed distributed turbo coding scheme, while considering a AWGN IUC for variable IUC SNR values. The figure corresponds to I_{sys}=4 iterations in conjunction with an interleaver depth of D_{int}=80,000 bits.

D_{int}=80,000 bits was employed and SP modulation in conjunction with L=16 and AGM-1 is used. Figure 7.8 also shows the BER performance of the DTC system, when a perfect IUC is considered. The BER curves seen in Figure 7.8 correspond to the system where I_{sys}=4 system iterations are employed. The notation SNR+10 dB in Figure 7.8 means that the IUC SNR is 10 dB higher than the uplink channel SNR, where SNR represents the uplink channel SNR. Observe in Figure 7.8 that the attainable BER performance of the DTC system, when the IUC is constituted by an AWGN channel having a 10 dB higher SNR than that of the uplink channel, is equivalent to that of the system considering a perfect IUC. However, when the IUC SNR is 5 dB higher than the uplink channel SNR, an error floor is formed in Figure 7.8. This is due to the fact that the iterative detection at the receiver side assumes that the data in the two RSC decoders is identical, while the inter-user communication induces errors in the data available at the users' terminals, and hence results in a discrepancy in the data transmitted from the two users' terminals, which results in the error floor of Figure 7.8.

Figure 7.9 shows the attainable BER performance of the proposed DTC scheme, while considering uplink transmission over a narrowband Rayleigh fading channel, when the IUC considered is a Ricean channel. In Figure 7.9 an interleaver depth of D_{int}=80,000 bits was employed and SP modulation in conjunction with L=16 and AGM-1 is used. Figure 7.9 also shows the BER performance of the DTC aided system, when a perfect IUC is considered. The BER curves in Figure 7.9 correspond to the system where I_{sys}=4 system iterations are employed. Observe in Figure 7.9 that the attainable BER performance of the DTC assisted

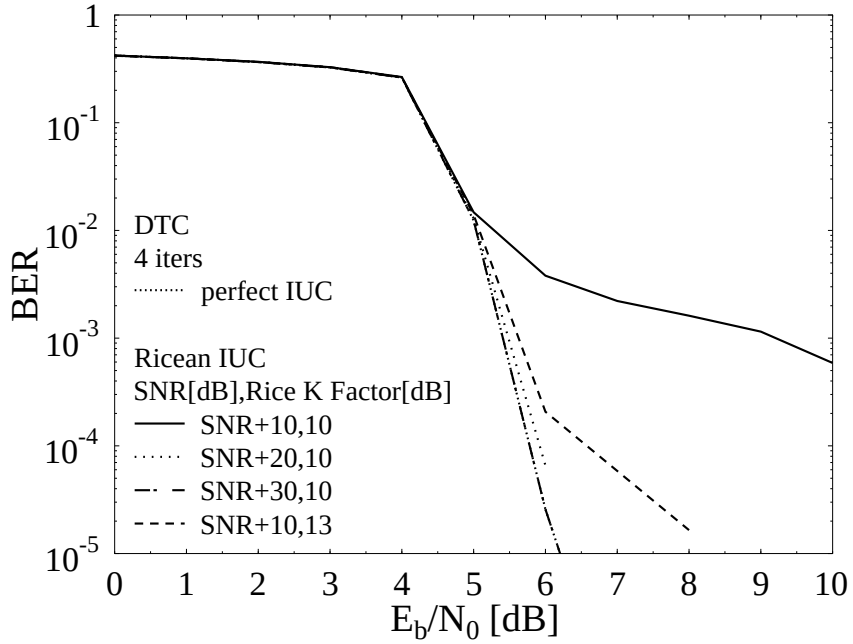

Figure 7.9: Comparison of the attainable BER performance of the proposed distributed turbo coding scheme, while considering a Ricean IUC for a variable IUC SNR having different Ricean K-factor. The figure corresponds to I_{sys}=4 iterations in conjunction with an interleaver depth of D_{int}=80,000 bits.

system is equivalent to that of the system considering a perfect IUC, when the Ricean K-factor is 10 dB and the IUC SNR is 30 dB higher than the uplink channel SNR. However, when the IUC SNR becomes less than 20 dB higher than the uplink channel SNR, the BER performance degrades, where an error floor is formed. As the Ricean K-factor increases to 13 dB, no error floor is formed in the BER curve even for an IUC SNR of 10 dB higher than the uplink channel SNR. On the other hand, in Figure 7.10 a Rayleigh faded IUC is considered for the DTC aided system. Observe in Figure 7.10 that an error floor is formed for all IUC SNR values, even when the IUC SNR goes as high as 50 dB above the uplink channel SNR. This is due to the fact that transmission over Rayleigh fading channels imposes errors in the data received by the two users from each other and hence this means that there will be a difference between the data transmitted from the two users, which affects the turbo detection process at the receiver side.

Figures 7.7-7.10 show the BER performance of the proposed DTC aided system, while considering different IUC characteristics. Explicitly, Figure 7.8 shows the BER performance of the uplink transmission, while the IUC is considered to be AWGN with variable IUC SNR values. Figure 7.9 shows the same BER performance, while the IUC is Ricean with a variable Ricean K-factor and a variable IUC SNR. Additionally, in Figure 7.10 we show the uplink BER performance of the DTC scheme, while considering a Rayleigh IUC with variable IUC SNR values. Observe in the figures that an error floor is formed at a specific IUC SNR value, depending on the different IUC characteristics. To understand this phenomenon further, in Figure 7.11 we plot the BER performance of a single-input single-output QPSK modulated

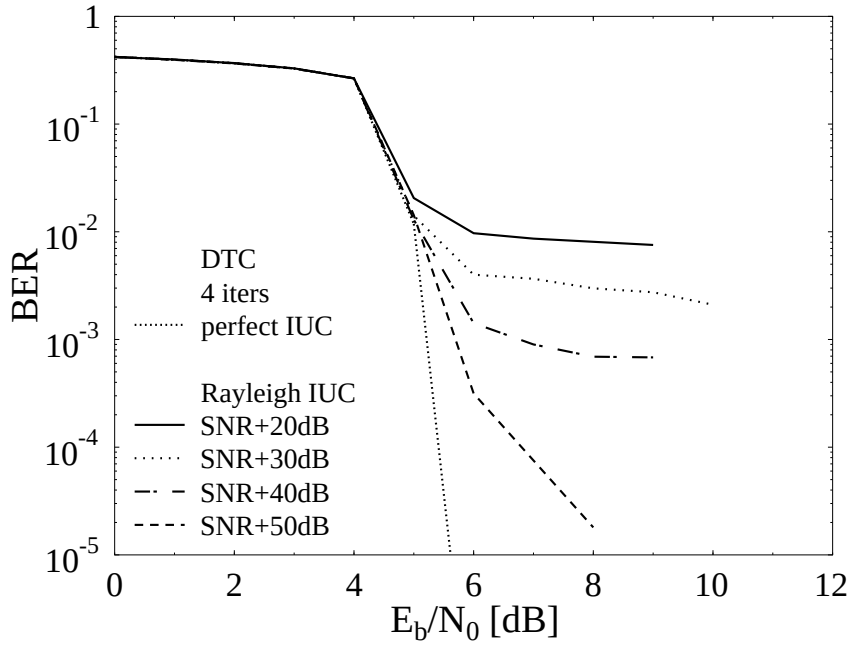

Figure 7.10: Comparison of the attainable BER performance of the proposed distributed turbo coding scheme, while considering a Rayleigh IUC for variable IUC SNR values. The figure corresponds to I_{sys}=4 iterations in conjunction with an interleaver depth of D_{int}=80,000 bits.

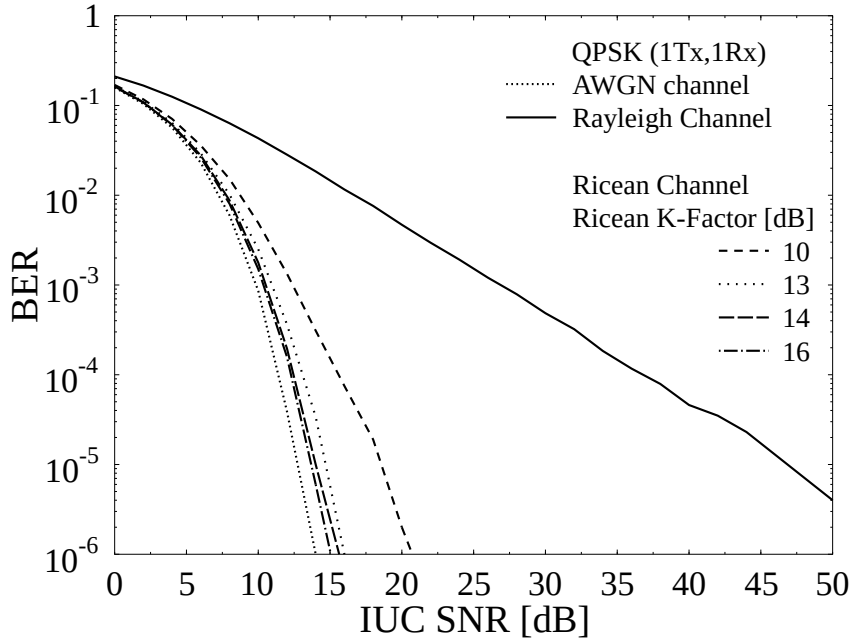

Figure 7.11: Attainable BER performance of a single-input single-output QPSK modulated system, while considering inter-user transmission over AWGN channel, Rayleigh channel and Ricean channel with a variable Ricean K-factor.

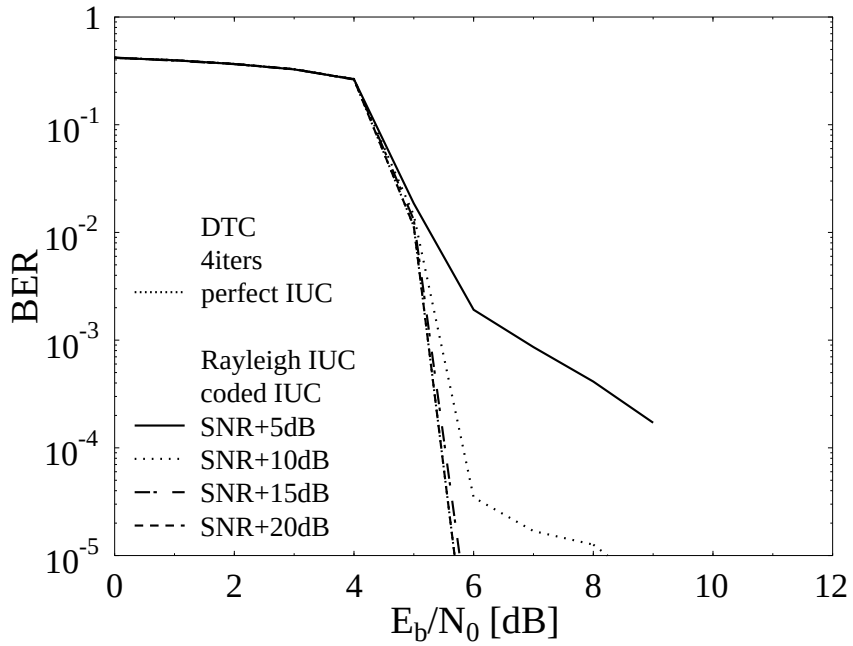

Figure 7.12: Comparison of the attainable BER performance of the proposed distributed turbo coding scheme, while considering a Rayleigh IUC for variable IUC SNR values as well as employing RSC channel coding for inter-user communications. The figure corresponds to I_{sys}=4 iterations in conjunction with an interleaver depth of D_{int}=80,000 bits.

system, while considering inter-user transmissions over AWGN, Rayleigh as well as Ricean channels. Observe in Figures 7.8-7.10 that an error floor is formed for the uplink transmission of the proposed DTC scheme, when transmission over the IUC induces error in the data exchanged between the two users. It can be shown that for the proposed DTC scheme to attain a reasonable BER performance with no error floor, the inter-user BER should be less than 10^{-6}.

The previous results outlined in Figure 7.7-7.10 show that the proposed DTC scheme attains a good BER performance without any error floor, provided that the inter-user communications can maintain a BER below 10^{-6}. Observe in the BER results of Figures 7.10 that an error floor in formed for inter-user transmission over a Rayleigh IUC for all IUC SNR values. All the previous results correspond to the system, where no channel coding was employed in the inter-user communication, i.e. each user maps the source bits to QPSK symbols and transmits them to the other user. In order to improve the performance of the inter-user communication, especially when the IUC is Rayleigh faded, each user can benefit from the RSC code it is equipped with and then encode the data bits, before mapping the encoded bits to QPSK symbols for transmission. This improves the BER performance of the IUC and allows the attainable BER performance of the DTC uplink scheme to improve, as shown in Figure 7.12 when compared to Figure 7.10. In Figure 7.12 the two users employ a 1/2-rate RSC code for the exchange of their data. Observe in Figure 7.12 that the DTC uplink scheme attains a BER performance with no error floor, when the IUC SNR is 15 dB higher than the uplink channel

SNR, while for the uncoded inter-user communications scenario, an error floor was formed even when the inter-user Rayleigh channel had an SNR 50 dB higher than the uplink channel SNR.

7.5 Chapter Conclusion

In this chapter, we proposed a distributed turbo coding scheme, where two users cooperate in order to improve their attainable BER performance. Each user's single-antenna aided transmitter is constituted by a RSC code, an interleaver and a SP mapper. In the first phase of cooperation, the two users exchange their data by transmission over the inter-user channel. Each user then has his/her own data as well as the other user's data. In the second phase of cooperation, each user concatenates his/her own data and the other user's data. The first user applies RSC channel coding to the resultant data bit stream and then the channel coded bits are interleaved by a random bit interleaver. The interleaved bits are then mapped to 4-bit symbols by a SP mapper, where the symbols are transmitted from a single antenna. The second user applies the same procedure, but interleaves the data bit stream before channel encoding. The receiver applies the zero forcing interference cancellation algorithm of [81] and outputs two data streams that are passed to two branches, where each branch has a SP demapper, deinterleaver and a RSC decoder. Iterative detection is carried out by exchanging extrinsic information between the SP demappers and the RSC decoders in each branch as well as between the two RSC decoders of the two branches, thus forming a turbo code.

The proposed DTC scheme is benchmarked against another cooperative scheme, where the two users do not exchange their data. In the benchmark scheme, each user encodes his/her own data bits by an RSC encoder, interleaves the coded bits and then the interleaved bits are mapped to SP symbols for transmission from a single antenna. In the benchmark scheme, the iterative detection is carried out by exchanging extrinsic information between the SP demapper and the RSC decoder of each branch without employing any iterations between the RSC decoders of the two branches.

The proposed DTC scheme attained a throughput that is four times less than that of the benchmark scheme. However, the proposed scheme attained an E_b/N_0 gain of about 25 dB at BER of 10^{-5}, when compared to the benchmark scheme, while considering perfect IUC and employing I_{sys}=5 system iterations in conjunction with an interleaver depth of D_{int}=80,000 bits, where a system iteration corresponds to a single inner iteration between the SP demapper and the RSC decoder of each branch, followed by I_{outer}=6 iterations between the RSC decoders of the two branches.

Additionally, a study of the inter-user channel characteristics effects on the performance

of the proposed uplink DTC scheme was conducted. First, in phase one of the cooperation, each user transmits his/her own data to the other user by mapping the source bits to QPSK symbols and then transmit them through a single antenna. When the users exchange their data over an AWGN channel with IUC SNR being 10 dB higher than the uplink channel SNR, the attainable BER performance of the DTC scheme is similar to that when the inter-user channel is assumed to be perfect. Furthermore, while considering a Rayleigh faded inter-user channel, an error floor is formed for the attainable BER performance of the proposed scheme even for IUC SNR as high as 50 dB higher than the uplink channel SNR. It was shown in Figure 7.11 that in order to eliminate the error floor in the BER performance of the proposed scheme, the BER performance of the inter-user channel is required to be less than 10^{-6}. Hence, in order to improve the attainable system performance, it is suggested to use channel coding, while the users are exchanging their data during the first phase of cooperation.

7.6 Chapter Summary

In this chapter, we proposed a novel cooperative communication scheme referred to as distributed turbo coding. In the proposed scheme, two users are cooperating, where each user's transmitter constitutes of a RSC code then an interleaver followed by a SP mapper. The two users exchange their data in the first phase of cooperation followed by the second phase, which is the uplink transmission of the combined data from the two users' antennas, protected by channel coding and interleaving. The second user interleaves the data bits before channel coding, so that at the receiver side iterative detection can be applied by exchanging extrinsic information between the two channel decoders after appropriately arranging the bits in the required order by interleaving and deinterleaving.

In Section 7.2 we provided an overview of cooperative communications, elaborating on the major cooperative signalling schemes, including Amplify-and-Forward, Decode-and-Forward and coded cooperation. In Section 7.3 we presented our distributed turbo coding scheme, where we proposed a two-phase cooperation scheme. In the first phase, the two users exchange their data, while in the second phase they simultaneously transmit their data to the base station. In Section 7.4 we presented our performance results and compared the proposed scheme to a benchmark scheme employing no exchange of the users' data, i.e. each user only transmits his/her own data. In Section 7.4 we studied the effect of varying the inter-user channel characteristics on the performance of the uplink DTC scheme, where we showed that the inter-user channel BER should not be higher than 10^{-6} in order to avoid the formation of an error floor in the uplink. In Section 7.4 it was shown that an error floor is formed when the inter-user channel considered is Rayleigh-faded even if the IUC SNR is as high as 50 dB higher than the

uplink channel SNR, as shown in Figure 7.10. In order to improve the system performance, it was shown in Figure 7.12 that the attainable BER performance can be improved when the users exchange their data over a Rayleigh channel, if the users employ channel coding in the first phase of cooperation.

In Section 7.4, we have shown that the data exchanged between the two users in the first phase of cooperation requires the IUC BER to be lower than 10^{-6} in order to eliminate any error floor in the uplink performance of the DTC aided system. We tackled this problem by using channel coding in the first phase of cooperation, where each user's data is channel coded and then interleaved before mapping the bits to QPSK symbols for transmission. Observe in Figure 7.12 that using channel coding in the first phase of cooperation does not entirely eliminate the error floor for IUC SNR being 10 dB higher than the uplink channel SNR. Therefore, another solution has to be devised in order to improve the attainable performance, when there are errors in the data exchanged between the users in the first phase of cooperation.

In the proposed scheme, DF signalling was used in the first phase of cooperation, where hard decision was performed on the received data. In [146], it was argued that the DF signalling loses the benefit of soft information. Hence, in [146] the employment of soft DF signalling was proposed, where all operations are performed in a soft-input soft-output fashion. It was shown in [146] that the soft DF outperforms the hard-decoded DF and the AF signalling schemes. In [154] soft DF was used, where the soft information was quantised, encoded and transmitted using superimposed modulation to the destination. The scheme proposed in [154] is a practical method devised for encoding the soft information without the need for reducing the system's throughput or without increasing the system's bandwidth. In [146, 151, 154] soft information has been used in diverse systems, where there are errors in the first phase of cooperation and it was shown that soft DF attains a better performance than hard DF. Therefore, a potential improvement of our proposed system is to employ soft DF, where the MAP decoder used at the BS has to be modified in order to decode the data received from the two users.

Chapter 8

Conclusions and Future Research

8.1 Conclusions

In this treatise, we characterised a suite of Multiple-Input Multiple-Output (MIMO) transceivers operating in narrowband Rayleigh fading channels, where iterative detection has been employed in order to achieve a near-capacity performance for the proposed transceivers.

More specifically, we reported the following major findings:

- In Chapter 2, a Differential Space-Time Spreading (DSTS) scheme was proposed, which is advocated for the sake of achieving a high transmit diversity gain, while eliminating the potentially high complexity of MIMO channel estimation. Additionally, the system was combined with multi-dimensional Sphere Packing (SP) modulation, which is capable of maximising the coding advantage of the transmission scheme by jointly designing and detecting the sphere-packed DSTS symbols. We also quantified the capacity of the DSTS-SP scheme for transmission over both Rayleigh as well as Gaussian channels.

- Iteratively detected DSTS-SP schemes were proposed in Chapter 3, where EXIT charts were used in order to analyse the attainable convergence behaviour. A unity-rate precoder was introduced, which is capable of completely eliminating the system's error-floor that was formed in the systems, where the SP demapper was used as an inner code. It was demonstrated that the URC precoded system outperforms its non-precoded counterpart and operates within 0.92 dB from the maximum achievable rate limit obtained using EXIT charts.

- An algorithm devised for computing the maximum achievable rate of the iteratively detected system using EXIT charts was proposed in Chapter 3, where it was shown that the maximum achievable rate obtained using EXIT charts matches closely with the analytical capacity limits.

- Furthermore, in order to maximise the DSTS-SP system's throughput in Chapter 4, we proposed an adaptive scheme that is capable of adapting the transmission configuration, the spreading factor as well as the RSC encoder's code rate according to the near-instantaneous channel quality.

- In Chapter 5 we amalgamated the merits of V-BLAST, STC and beamforming for the sake of achieving a multiplexing gain, a diversity gain as well as a beamforming gain. We then analytically quantified the capacity of the LSSTC-SP scheme. Furthermore, in order to characterise the system, three near-capacity iteratively detected LSSTC-SP receiver structures were proposed, where iterative detection was carried out by exchanging extrinsic information between an outer code's decoder, an intermediate code's decoder and an LSSTC-SP demapper. Our comparison between the three iteratively-detected schemes revealed that a carefully designed two-stage iterative detection scheme is capable of operating sufficiently close to capacity at a lower complexity, when compared to a three-stage system employing RSC or a two-stage system employing an IrCC as an outer code.

- On the other hand, in order to allow the receiver of the system in Chapter 5 to accommodate less receiver antennas than the number of transmit antennas and still provide a good performance, in Chapter 6 we amalgamated the merits of V-BLAST, STC, beamforming as well as generalised MC DS-CDMA for the sake of achieving a multiplexing gain, a spatial and frequency diversity gain as well as beamforming gain. We demonstrated that the number of users supported can be substantially increased by invoking combined spreading in both the Time Domain (TD) and the Frequency Domain (FD). We also used a user-grouping technique for minimising the multi-user interference imposed, when employing TD and FD spreading.

- In Section 6.4 We proposed three iteratively detected LSSTS schemes, where iterative detection was carried out by exchanging extrinsic information between two serially concatenated channel codes' decoders. We used EXIT charts to analyse the convergence behaviour of the proposed iterative detection aided schemes and proposed a novel Logarithm Likelihood Ratio (LLR) post-processing technique for improving the iteratively detected systems' performance.

- Finally, in Chapter 7 we designed a Distributed Turbo Coding (DTC) scheme that combines cooperative communications with the concept of turbo coding, where turbo coding is employed between the decoders of the cooperating users.

In the following we will summarise the main findings of our investigations presented in this treatise. Additionally, a range of ideas concerning our future research is presented in Section 8.2.

8.1.1 Differential Space-Time Spreading

DSTS employing either two or four transmit antennas was proposed in Chapter 2 as a non-coherent MIMO scheme that eliminates the potentially high complexity of MIMO channel estimation at the expense of a 3 dB performance loss compared to the corresponding coherently detected system using perfect channel knowledge at the receiver. DSTS is capable of providing transmit diversity gains, while at the same time supporting multiple users employing different spreading codes. DSTS was designed to work with real- as well as complex-valued conventional modulation schemes including BPSK, QPSK and 16-QAM. Additionally, DSTS was combined with multidimensional SP modulation in order to attain a higher coding gain, since SP has the best known Minimum Euclidean Distance (MED) in the $2(k+1)$-dimensional real-valued Euclidean space $\mathbb{R}^{2(k+1)}$ [213].

In Section 2.3, we outlined both the encoding and decoding algorithms of the twin-antenna-aided DSTS scheme, when combined with conventional modulation. Afterwards, in Section 2.3.3, the philosophy of DSTS using SP modulation, referred to as DSTS-SP, was introduced based on the fact that the diversity product of the DSTS design is improved by maximising the MED of the DSTS symbols [210]. This was motivated by the fact that SP has the best known MED in the real-valued space. Additionally, the capacity of the DSTS scheme employing $N_t = 2$ transmit antennas was derived in Section 2.3.6, where it was shown that the DSTS-SP scheme attains a higher bandwidth efficiency than that of the conventional DSTS scheme dispensing with SP. The performance characterisation of a twin-antenna-aided DSTS scheme was provided in Section 2.3.7, demonstrating that the DSTS scheme is capable of providing both a full diversity gain and a multi-user capability. In addition to that, the results demonstrated that DSTS-SP schemes are capable of outperforming DSTS schemes that employ conventional modulation, as shown in Table 8.1, which summarises the coding gains of DSTS-SP over conventional modulated DSTS schemes at a SP Symbol Error Rate (SP-SER) of 10^{-4}, when communicating over a correlated narrowband Rayleigh fading channel. Observe in Figure 8.1 that there is no gain for the DSTS-SP system over the conventional DSTS system for the 2 BPS case. This is due to the fact that the QPSK modulation is a special case of the SP modulation, as discussed in Section 2.3.7.

The four-antenna-aided DSTS design was characterised in Section 2.4, where it was demonstrated that the DSTS scheme can be combined with both conventional real- and complex-valued modulated constellations as well as with SP modulation. It was also shown that the

	1 BPS	2 BPS	3 BPS
$1Rx$	0.20 dB	0.0 dB	0.70 dB
$2Rx$	0.25 dB	0.0 dB	0.90 dB
$3Rx$	0.30 dB	0.0 dB	0.95 dB
$4Rx$	0.30 dB	0.0 dB	1.00 dB

Table 8.1: Coding gains of SP modulation over conventional modulation at SP-SER of 10^{-4} for the schemes of Figures 2.21, 2.23, 2.25 and 2.27, when employing twin-antenna-aided DSTS and communicating over a correlated Rayleigh fading channel associated with $f_D = 0.01$.

four-dimensional SP modulation scheme is constructed differently in the case of two transmit antennas than when employing four transmit antennas. The capacity analysis of the four-antenna-aided DSTS-SP scheme was also derived for systems having a different bandwidth efficiency, while employing a variable number of receive antennas in Section 2.4.5. Finally, in Section 2.4.6 we presented the simulation results obtained for the four-antenna-aided DSTS scheme, when combined with both conventional as well as SP modulation.

Further performance improvements can be attained by the DSTS system, when combined with channel coding and employing iterative detection at the receiver by exchanging extrinsic information between the constituent decoders/demappers. In Chapter 3, two realisations of a novel iterative-detection aided DSTS-SP scheme were presented, namely an iteratively detected Recursive Systematic Convolutional (RSC) coded DSTS-SP scheme as well as an iteratively detected RSC-coded and Unity Rate Code (URC) based precoded DSTS-SP arrangement. The iteratively detected RSC-coded DSTS-SP scheme was described in Section 3.2. In Section 3.2.1 we showed how the DSTS-SP demapper was modified for exploiting the *a priori* knowledge provided by the channel decoder, which is essential for the employment of iterative detection.

The concept of EXIT charts was introduced in Section 3.2.2 as a semi-analytical tool for analysing the convergence behaviour of iterative detection aided schemes. We have used several different Anti-Gray Mapping (AGM) schemes, whose EXIT curves are shown in Figure 8.1, which were specifically selected from all the possible mapping schemes for $L = 16$. Both the Gray Mapping (GM) as well as the various AGM schemes considered in Figure 8.1 are detailed in Appendix A. We have analysed different iteratively detected schemes using EXIT charts and shown how EXIT charts allow us to satisfy diverse design objectives. For example, we can design a system having the lowest possible turbo-cliff-SNR, but tolerating the formation of an error floor. Alternatively, we can design a system having no error floor, but having a slightly higher turbo-cliff-SNR. To elaborate further, the BER performance of the iteratively detected 1/2-rate RSC-coded DSTS-SP scheme recorded in conjunction with two transmit antennas and different GM and AGM mapping schemes is shown in Figure 8.2, when applying I=10 iterations.

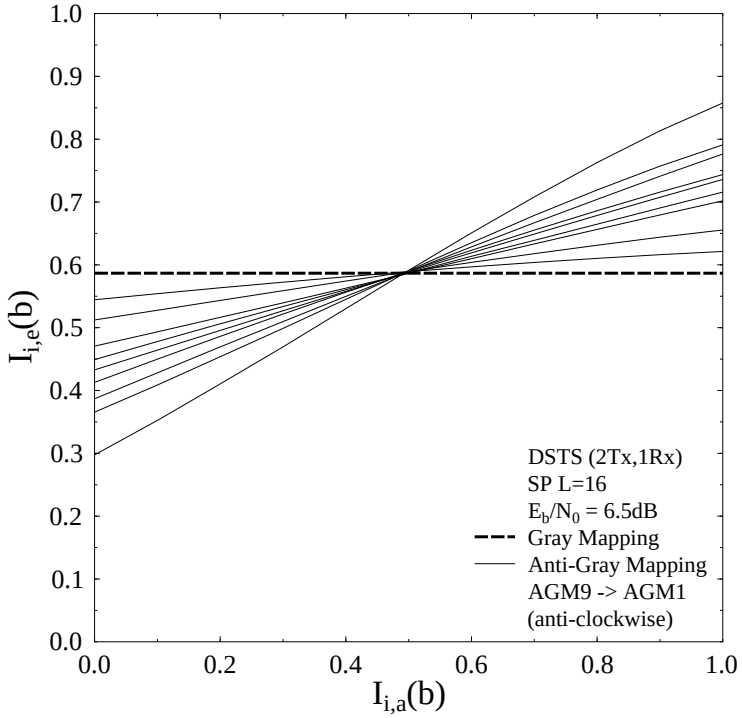

Figure 8.1: SP demapper extrinsic information transfer characteristics for different bits to SP symbol mappings at $E_b/N_0 = 6.5$ dB for $L = 16$, while considering transmissions using the twin-antenna-aided DSTS scheme.

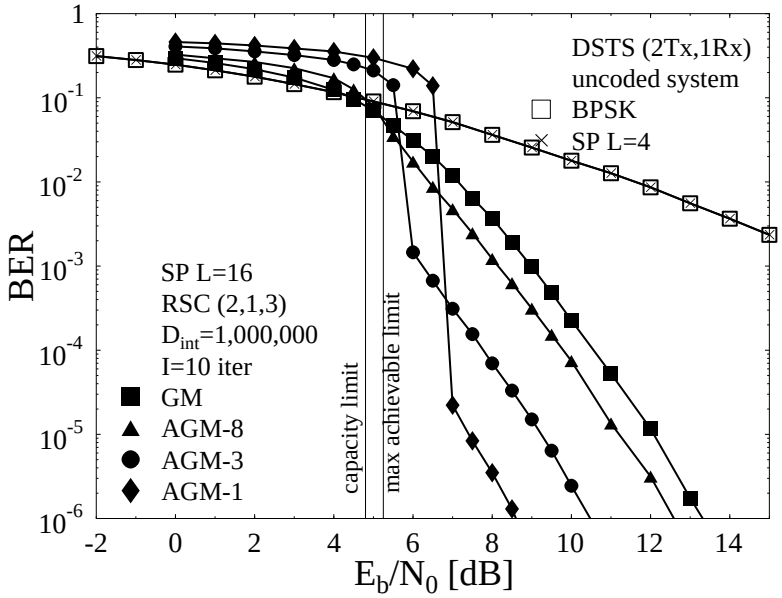

Figure 8.2: Performance comparison of different AGM- and GM-based iteratively detected RSC-coded two transmit antennas DSTS-SP schemes in conjunction with $L = 16$ against an identical spectral efficiency of 1 bit-per-channel-use uncoded DSTS-SP scheme using $L = 4$ and against the conventional DSTS-BPSK scheme, when employing an interleaver depth of $D_{int} = 1,000,000$ bits after $I = 10$ iterations.

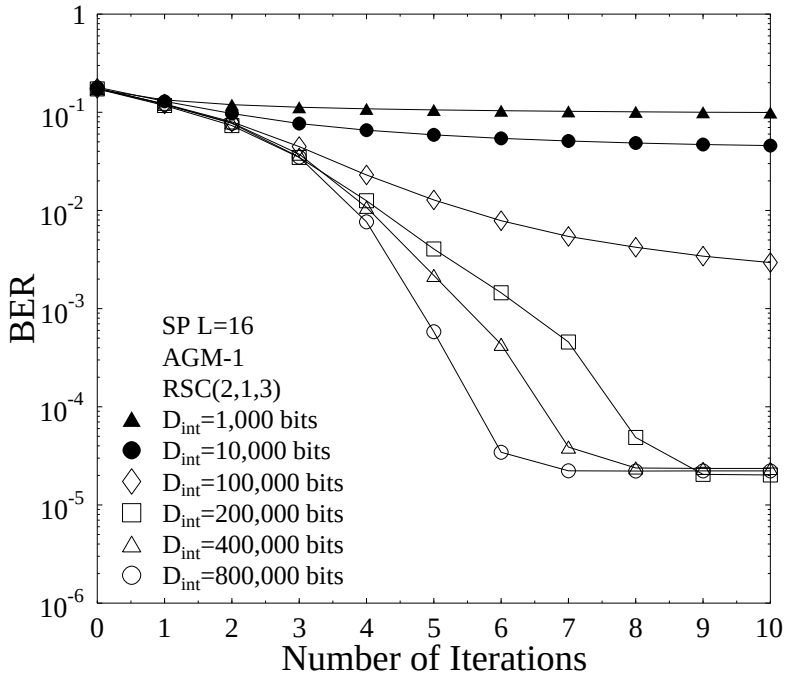

Figure 8.3: Comparison of the BER performance versus the number of iterations for the iteratively detected 1/2-rate RSC-coded DSTS-SP scheme in conjunction with two transmit antennas and AGM-1 of Figure 8.1, while employing different interleaver depths recorded at E_b/N_0 of 7.0 dB.

Observe in Figure 8.2 that the GM and AGM-8 based systems have a similar performance and this can be justified by referring to the EXIT chart of Figure 8.1, where the EXIT curves of the GM and AGM-8 based systems have similar slopes. On the other hand, observe in Figure 8.2 that the AGM-3 based system exhibits a turbo cliff at an E_b/N_0 value lower than the AGM-1 based system, while the AGM-1 aided system attains a lower error floor than its AGM-3 counterpart.

On the other hand, in order to show the effects of the interleaver depth on the performance of iteratively detected schemes, Figure 8.3 compares the BER performance of the iteratively detected RSC-coded DSTS-SP scheme employing AGM-1 versus the number of iterations, while using different interleaver depths ranging from D_{int}=1,000 bits to D_{int}=800,000 bits and operating at E_b/N_0=7.0 dB. The plot investigates the BER performance versus the complexity of the system quantified in terms of the number of iterations. As shown in the figure, when using short interleavers, increasing the number of iterations results in no significant BER performance improvement, which is the case for the interleavers with depths of D_{int}=1,000 bits and D_{int}=10,000 bits. However, as the interleaver becomes longer, i.e. as the correlation of the extrinsic LLRs is reduced, the achievable system performance improves upon increasing the number of iterations. Moreover, as the interleaver depth increases, the system requires less iterations to achieve its best attainable performance, as shown in Figure 8.3. For example, for the case of an interleaver depth of D_{int}=800,000 bits, it is shown in Figure 8.3 that after I=7

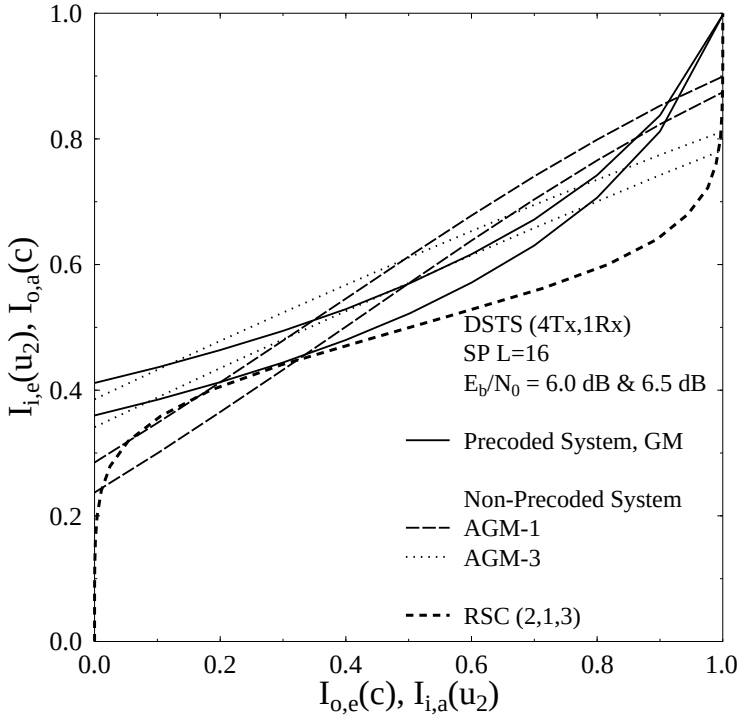

Figure 8.4: Comparison of the convergence behaviour of both the precoded and non-precoded DSTS-SP systems employing GM and AGM in conjunction with $L = 16$, based on their EXIT characteristics while operating at E_b/N_0 of 6 dB and 6.5 dB.

iterations, there is no more improvement in the attainable system performance, while the system employing D_{int}=400,000 bits requires one more iteration, before the system's performance saturates.

We also proposed a novel technique for computing the maximum achievable bandwidth efficiency of the system based on EXIT charts in Section 3.2.3, where it was shown that the maximum achievable bandwidth efficiency based on EXIT charts closely matches with the analytical calculation carried out in Chapter 2 for the bandwidth efficiency of the DSTS-SP system.

In order to eliminate the error floor exhibited by the iteratively detected system discussed previously, in Section 3.3 we proposed an iteratively detected RSC-coded and URC-precoded DSTS-SP scheme, which performed closer to the system's achievable rate. This is due to the fact that the URC has a recursive encoder and hence, when applying a sufficiently long interleaver, the EXIT chart of the URC decoder is capable of reaching the point of perfect convergence at $(1.0, 1.0)$. Figure 8.4 compares the EXIT chart of the iteratively detected four-antenna-aided DSTS-SP scheme, while applying the non-precoded AGM-1 and AGM-3 SP as well as the precoded GM-aided SP modulation schemes. As shown in Figure 8.4, the non-precoded scheme's inner decoder EXIT curves do not reach the point of perfect convergence at $(1.0, 1.0)$ and hence an error floor will be formed, where there is no error floor in the BER of the precoded

DSTS (2Tx,1Rx) No URC precoding	Coding Gain	Distance from maximum achievable rate limit
SP L=16, GM	14.9 dB	6.9 dB
SP L=16, AGM-1	19.5 dB	2.3 dB
SP L=16, AGM-3	17.75 dB	4.05 dB
SP L=16, GM-8	15.9 dB	5.9 dB
QPSK, AGM	16.1 dB	5.7 dB
DSTS (4Tx,1Rx) No URC precoding	Coding Gain	Distance from maximum achievable rate limit
SP L=16, GM	9.5 dB	4.32 dB
SP L=16, AGM-1	12 dB	1.82 dB
SP L=16, AGM-3	10.9 dB	2.92 dB
SP L=16, GM-8	8.9 dB	4.92 dB
QPSK, AGM	9.2 dB	4.62 dB
DSTS (4Tx,1Rx) URC precoding	Coding Gain	Distance from maximum achievable rate limit
SP L=16, GM	12.9 dB	0.92 dB

Table 8.2: Iteratively-detected RSC-coded DSTS system coding gain and distance from maximum achievable rate limit at BER=10^{-5}, when employing an interleaver depth of D_{int}=1,000,000 bits.

system, since the EXIT curve of the URC decoder reaches the point of perfect convergence at $(1.0, 1.0)$.

Explicitly, when using an appropriate bits-to-symbol mapping scheme and 10 turbo detection iterations, gains of about 19.5 dB were obtained by the RSC-coded twin-antenna-aided DSTS-SP schemes over the identical-throughput uncoded DSTS-SP benchmark scheme described in Chapter 2. Furthermore, the AGM-1 based iteratively detected twin-antenna-aided DSTS-SP scheme is capable of performing within 2.3 dB from the maximum achievable rate limit obtained using EXIT charts at BER=10^{-5}, when employing an interleaver depth of D_{int}=1,000,000 bits. Additionally, Chapter 3 characterised the benefits of precoding, when concatenated with the outer channel code, suggesting that an E_b/N_0 gain of at least 1.2 dB can be obtained over the non-precoded system at a BER of 10^{-5}, depending on the mapping scheme used. Explicitly, the four-antenna-aided DSTS-SP system employing no URC precoding attains a coding gain of 12 dB at a BER of 10^{-5} and performs within 1.82 dB from the maximum achievable rate limit, when employing an interleaver depth of D_{int}=1,000,000 bits. By contrast, the URC aided precoded system outperforms its non-precoded counterpart and operates within 0.92 dB from the maximum achievable rate limit obtained using EXIT charts,

DSTS (2Tx,1Rx) No URC precoding	Coding Gain	Distance from maximum achievable rate limit
SP L=16, GM	17.8 dB	8 dB
SP L=16, AGM-1	22.5 dB	3.3 dB
SP L=16, AGM-3	20.5 dB	5.3 dB
SP L=16, GM-8	18.4 dB	7.4 dB
QPSK, AGM	19 dB	6.8 dB
DSTS (4Tx,1Rx) No URC precoding	Coding Gain	Distance from maximum achievable rate limit
SP L=16, GM	13.7 dB	5.12 dB
SP L=16, AGM-1	16.7 dB	2.12 dB
SP L=16, AGM-3	14.8 dB	4.02 dB
SP L=16, GM-8	12.9 dB	5.92 dB
QPSK, AGM	13.5 dB	5.32 dB
DSTS (4Tx,1Rx) URC precoding	Coding Gain	Distance from maximum achievable rate limit
SP L=16, GM	17.9 dB	0.92 dB

Table 8.3: Iteratively-detected RSC-coded DSTS system coding gain and distance from maximum achievable rate limit at BER=10^{-6}, when employing an interleaver depth of D_{int}=1,000,000 bits.

when employing an interleaver depth of D_{int}=1,000,000 bits.

Finally, Tables 8.2 and 8.3 present the coding gains as well as the distance from the maximum achievable rate limit for the iteratively detected RSC-coded DSTS system, while employing SP as well as QPSK modulation schemes. The coding gain is measured against the performance of the identical-throughput uncoded DSTS-SP system. The tables present the results for both the two- and four-antenna-aided DSTS scheme, when both systems optionally employ URC precoding at BER=10^{-5} and 10^{-6}, while employing an interleaver depth of D_{int}=1,000,000 bits.

On the other hand, in order to maximise the throughput of the DSTS-SP scheme, while maintaining a certain target Quality of Service (QoS), an adaptive DSTS-SP system was proposed in Chapter 4. The proposed adaptive DSTS-SP system exploits the advantages of differential encoding, iterative decoding as well as SP modulation, while adapting the system parameters for the sake of achieving the highest possible spectral efficiency, as well as maintaining a given target BER. The proposed adaptive DSTS-SP scheme benefits from a substantial diversity gain, while using four transmit antennas without the need for pilot-assisted channel estimation and coherent detection. The proposed scheme reaches the target BER of 10^{-3} at an SNR of about 5 dB and maintains it for SNRs in excess of this value, while increasing

the effective throughput. The system's bandwidth efficiency varies from 0.25 bits/sec/Hz to 16 bits/sec/Hz.

The achievable integrity and bit rate enhancements of the adaptive DSTS-SP system are determined by the following factors: the specific transmission configuration used for transmitting data from the four antennas, the spreading factor used and the RSC encoder's code rate.

8.1.2 Multi-functional MIMO

In Chapter 5, we proposed a multi-functional Multiple-Input Multiple-Output (MIMO) scheme that combines the benefits of the Vertical Bell Labs Layered Space-Time (V-BLAST) scheme, of space-time codes as well as of beamforming. Thus, the proposed system benefits from the multiplexing gain of the V-BLAST, from the diversity gain of the space-time codes and from the SNR gain of beamforming. The multi-functional MIMO scheme was referred to as a Layered Steered Space-Time Code (LSSTC). To further enhance the attainable system performance and to maximise the coding advantage of the proposed transmission scheme, the system was combined with multidimensional SP modulation.

Figure 8.5 compares the attainable BER performances of a single input single output system, of a twin-antenna aided STBC system and of a four transmit four receive antenna aided LSSTC system. The multiplexing gain of the LSSTC scheme is exemplified by the fact that the LSSTC system used in Figure 8.5 has a throughput that is twice that of a system employing a twin-antenna aided STBC scheme. Additionally, observe in Figure 8.5 that the LSSTC scheme attains a diversity gain that is exemplified in terms of the gain attained by the LSSTC scheme over a single-antenna-aided system as well as over the twin-antenna aided STBC scheme. On the other hand, notice that an increased SNR gain is obtained by the LSSTC scheme, when more beamforming elements per Antenna Array (AA) are used. Therefore, Figure 8.5 shows the diversity gain as well as the beamforming gain of the proposed LSSTC scheme and the multiplexing gain is exemplified by the fact that the LSSTC's throughput is higher than that of a twin-antenna aided STBC scheme.

In Section 5.3 we quantified the capacity of the proposed LSSTC scheme and presented the capacity limits for a system employing $N_t = 4$ transmit AAs, $N_r = 4$ receive antennas and a variable number L_{AA} of elements per AA. Furthermore, in Section 5.4.3 we quantified an upper bound for the achievable bandwidth efficiency of the system based on the EXIT charts obtained for the iteratively detected system. It was shown that there is a discrepancy between the maximum achievable rate limit obtained using EXIT chart and the analytical bandwidth efficiency. This is due to the fact that the capacity of the LSSTC scheme was analysed for the case where perfect interference cancellation was assumed, while the proposed system employed

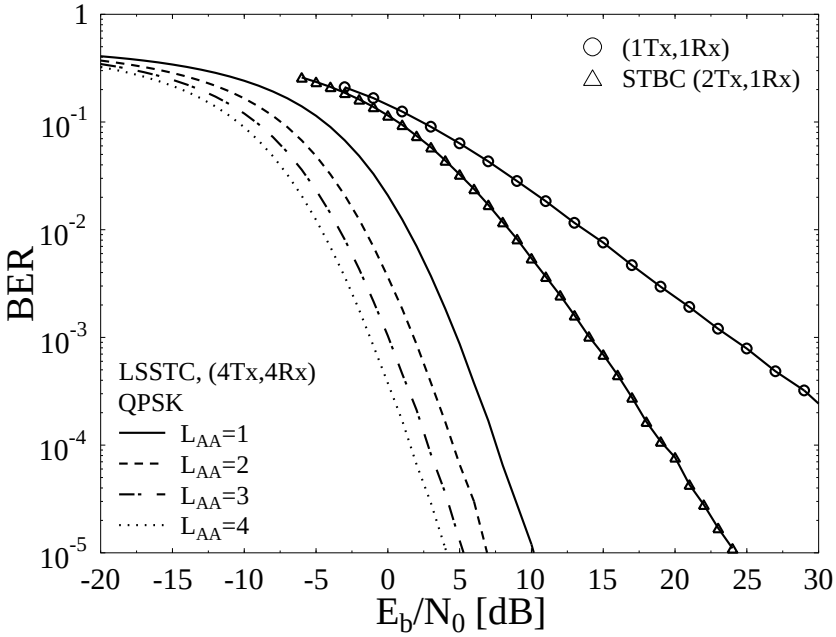

Figure 8.5: Comparison of the attainable BER performance of a QPSK modulated $N_t \times N_r = 4 \times 4$ LSSTC system for variable L_{AA} values, with that of the twin-antenna aided STBC scheme and the single transmit single receive antenna aided scheme.

a low-complexity, but error-prone zero forcing interference cancellation scheme.

In order to further enhance the achievable system performance, the proposed LSSTC scheme was serially concatenated with both an outer code and a URC, where three different receiver structures were created by varying the iterative detection configuration of the constituent decoders/demapper. As a benchmark scheme, we proposed a two-stage iteratively detected RSC-coded LSSTC-SP scheme, where extrinsic information was exchanged between the outer RSC decoder and the inner URC decoder, while no iterations were carried out between the URC decoder and the GM-based SP demapper. This system was referred to as System 1. The convergence behaviour of the iterative-detection-aided system was analysed using EXIT charts.

In Section 5.4.1.2, we employed the powerful technique of EXIT tunnel-area minimisation for near-capacity operation. More specifically, we exploited the well-understood properties of EXIT charts that a narrow but nonetheless open EXIT-tunnel represents a near-capacity performance. Consequently, we invoked Irregular Convolutional Codes (IrCC) for the sake of appropriately shaping the EXIT curves by minimising the area within the EXIT-tunnel using the procedure of [191, 194]. The IrCC aided system was referred to as System 2.

In Section 5.4.2 we presented a three-stage iteratively detected RSC-coded LSSTC scheme, where extrinsic information was exchanged between the three constituent decoders/demapper, namely the outer RSC decoder, the inner URC decoder as well as the SP demapper. The three-stage system was referred to as System 3.

Explicitly, the SP aided LSSTC system, employing N_t=4 transmit antennas, N_r=4 receive

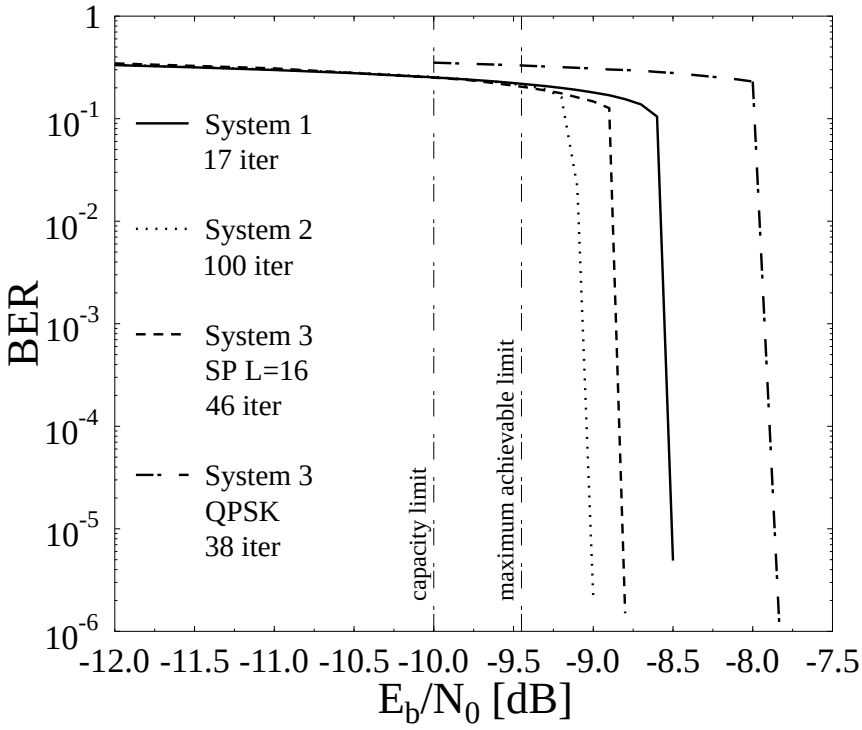

Figure 8.6: Performance comparison of the three proposed LSSTC-SP aided systems employing two-stage iteration between an outer code and a URC decoder, as well as that of the three-stage iterative information exchange between an outer RSC decoder, an intermediate URC decoder and an SP demapper.

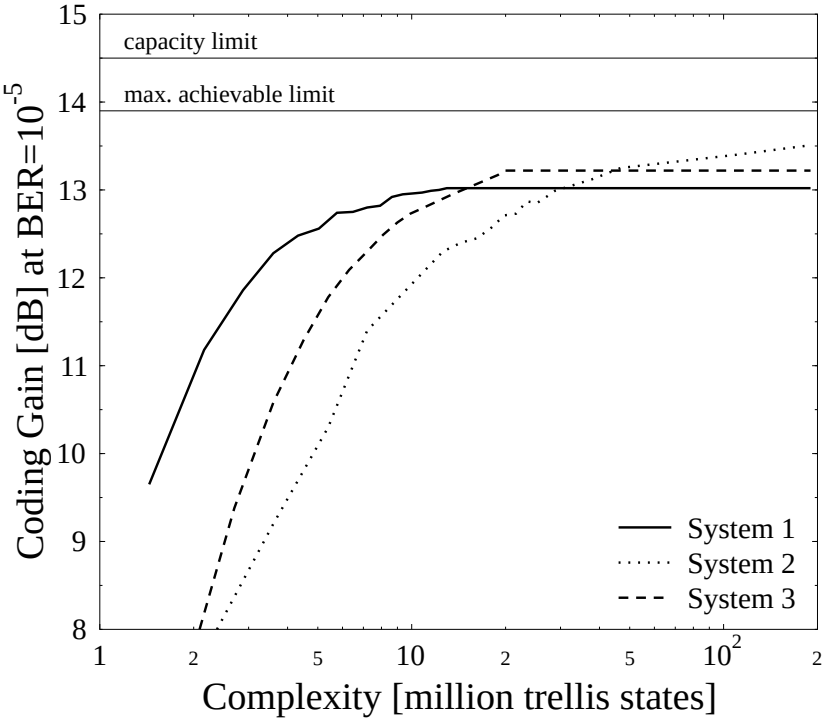

Figure 8.7: Comparison of the coding gain at a BER of 10^{-5} versus the complexity in million trellis states of the three proposed LSSTC-SP aided systems.

LSSTC (4Tx,4Rx) L_{AA}=4	Coding Gain	Distance from maximum achievable rate limit
System 1	14.5 dB	0.9 dB
System 2	15.0 dB	0.4 dB
SP-aided System 3	14.8 dB	0.6 dB
QPSK-aided System 3	13.1 dB	1.6 dB

Table 8.4: Iteratively-detected LSSTC system coding gain and distance from maximum achievable rate limit at BER=10^{-6} in conjunction with N_t=4 transmit AAs, N_r=4 receive antennas, L_{AA}=4 elements per AA and D_{int}=180,000 bits.

antennas and L_{AA}=4 elements per AA, is capable of operating within 0.9 dB, 0.6 dB and 0.4 dB from the maximum achievable rate limit, as shown in Figure 8.6. However, to operate within 0.6 dB from the maximum achievable rate limit, the system imposes twice the complexity compared to a system operating within 0.9 dB from this limit. On the other hand, to operate as close as 0.4 dB from the maximum achievable rate limit, the system imposes a 20 times higher complexity as the one operating within 0.9 dB from the maximum achievable rate limit. By contrast, the QPSK modulated three-stage iteratively detected system is capable of operating within 1.54 dB from the maximum achievable rate limit and thus the SP modulated system outperforms its QPSK aided counterpart by about 1 dB at a BER of 10^{-6}. The proposed design principles are applicable to an arbitrary number of antennas and diverse antenna configurations as well as to various modem schemes. The complexity of the proposed schemes is compared in Figure 8.7, where the coding gain attained by the different schemes at a BER of 10^{-5} has been plotted versus the corresponding complexity expressed in terms of the number of trellis states, which is directly proportional to the number of Add-Compare-Select (ACS) operations.

Finally, Table 8.4 presents the coding gains as well as the distance from the maximum achievable rate limit for the proposed iteratively detected systems, namely the SP-aided Systems 1-3 and the QPSK-aided System 3. The table presents the results for the LSSTC system at BER=10^{-6}, while employing an interleaver depth of D_{int}=180,000 bits.

The LSSTC scheme of Chapter 5 is characterised by a diversity gain, a multiplexing gain as well as a beamforming gain. However, a drawback of the design is that it requires the number of receive antennas to be at least the same as the number of transmit AAs. Therefore, for a system employing four transmit AAs, the receiver requires four antennas for correct decoding, which implies that the LSSTC scheme cannot be used in a downlink transmission from a base station to a shirt-pocket-sized mobile phone due to the size limitation of implementing four antennas. The LSSTC scheme can however be conveniently applied for communicating between two BSs or between a BS and a laptop. In order to make the LSSTC scheme more practical, in Chapter 6

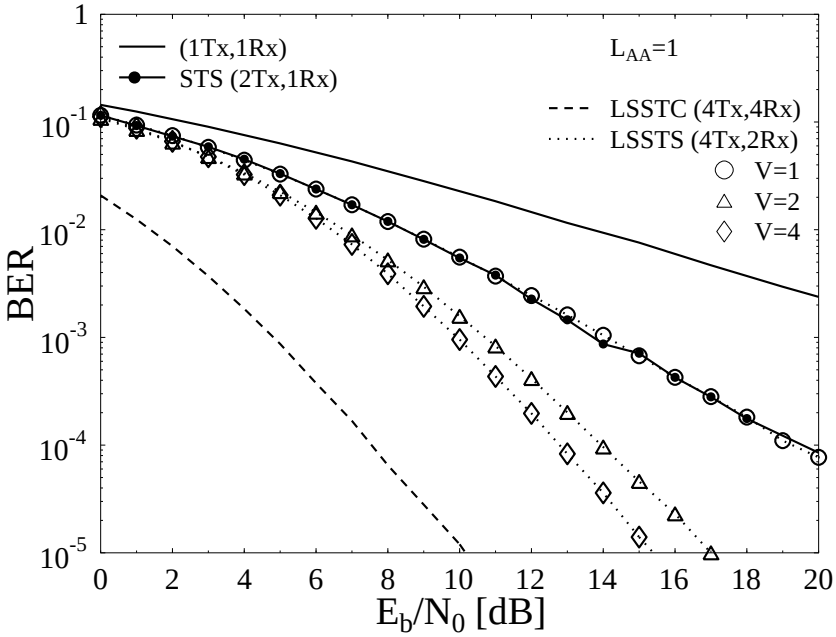

Figure 8.8: Comparison of the attainable BER performance of a QPSK modulated LSSTS assisted generalised MC DS-CDMA and LSSTC systems with that of the twin-antenna aided STBC scheme and the single transmit single receive antenna aided scheme.

we presented a multi-functional MIMO scheme employing four DL transmit and two receive antennas. The proposed multi-functional MIMO scheme of Chapter 6 combines the benefits of Space-Time Spreading (STS), V-BLAST, generalised MultiCarrier Direct Sequence Code Division Multiple Access (MC DS-CDMA) as well as beamforming. The proposed scheme of Chapter 6 is referred to as Layered Steered Space-Time Spreading (LSSTS). The LSSTS scheme benefits from a spatial diversity gain, a frequency diversity gain, a multiplexing gain as well as a beamforming gain.

Figure 8.8 compares the attainable BER performance of LSSTS assisted generalised MC DS-CDMA with that of the LSSTC scheme. The figure also shows the BER performance of the twin-antenna aided STS and the single-input single-output benchmark systems. The LSSTS scheme employs four transmit AAs and two receive antennas, while the LSSTC scheme of Figure 8.8 employs four transmit AAs and four receive antennas. Observe in Figure 8.8 that the BER performance of the LSSTS scheme is identical to that of the STBC scheme, when a single subcarrier is used. This means that the LSSTS scheme attains a spatial diversity gain of 2, while attaining a multiplexing gain that is twice that of a twin-antenna aided STBC scheme. Additionally, increasing the number of subcarriers V improves the attainable BER performance as shown in Figure 8.8 for the LSSTS scheme. Hence, the LSSTS scheme is also capable of attaining frequency diversity gain, when the subcarrier frequencies are arranged in a way that guarantees that the same STS signal is spread to and hence transmitted by the specific V subcarriers having the maximum possible frequency separation, so that they experience independent fading. On the other hand, comparing the BER performance of the

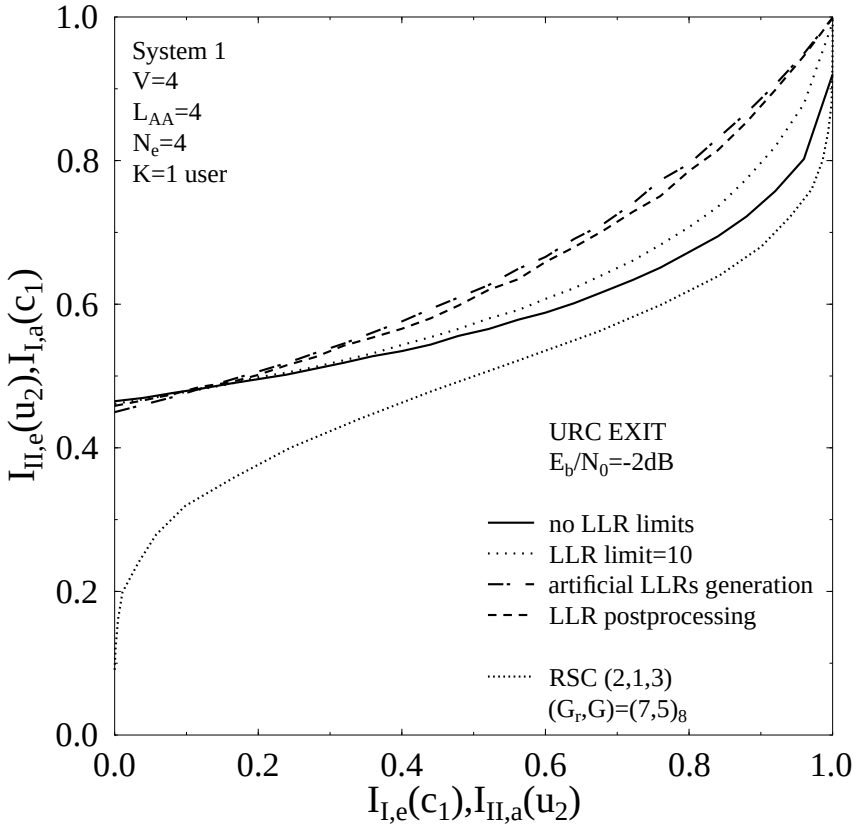

Figure 8.9: EXIT chart of a RSC-coded and URC-precoded proposed System 1 of Figure 6.6 employing GM aided QPSK in conjunction with N_t=4, N_r=2, V=4, L_{AA}=4, K=1 user and $E_b/N_0 = -2$ dB.

LSSTS scheme employing V=1 subcarrier with that of the LSSTC scheme shows that the LSSTC scheme attains a better BER performance. This is due to the fact that the LSSTC scheme employs more receive antennas than the LSSTS scheme and hence the LSSTC scheme is capable of attaining a higher spatial diversity gain.

In Section 6.3 we demonstrated that the number of users supported by the LSSTS scheme can be substantially increased by invoking combined spreading in both the Time Domain (TD) and the Frequency Domain (FD). We also used a novel user-grouping technique for minimising the multi-user interference imposed, when employing both TD and FD spreading in the LSSTS-aided generalised MC DS-CDMA downlink scheme.

Furthermore, in order to further improve the attainable performance of the LSSTS assisted generalised MC DS-CDMA, we proposed three iteratively detected LSSTS schemes, where iterative detection was carried out by exchanging extrinsic information between two serially concatenated channel codes. We used EXIT charts to analyse the convergence behaviour of the proposed iterative detection aided schemes and proposed a novel Logarithm Likelihood Ratio (LLR) post-processing technique for improving the iteratively detected systems' performance.

In order to elaborate a little further on the LLR post-processing technique, observe in Figure 8.9 that there are several EXIT curves for the URC decoder at the same E_b/N_0 value.

Let us first consider the dark line marked by the legend "no LLR limits". This EXIT curve corresponds to a URC decoder, which has a recursive encoder at the transmitter and hence it is expected that the EXIT curve of the URC decoder will indeed reach the $(1.0, 1.0)$ point of perfect convergence in the EXIT curve, as discussed in [1]. However, Figure 8.9 also shows that the EXIT curve of the URC decoder does not reach the $(1.0, 1.0)$ point. Limiting the maximum and minimum of the LLR values allowed the URC EXIT curve to reach the $(1.0, 1.0)$ point, as shown in Figure 8.9 by the dotted line associated with the legend "LLR limit=10".

On the other hand, for the sake of testing the accuracy of the URC EXIT curve, while imposing a limit on the LLR values, we generated artificial Gaussian distributed and uncorrelated LLRs, where the resultant EXIT curve is represented by the dotted line having the legend "artificial LLR generation". As shown in Figure 8.9, the curves corresponding to the case where the LLRs' dynamic range is limited and where the artificial LLRs are generated are quite different. Therefore, limiting the LLR values did not solve the problem. The reason for this behaviour is the fact that the output of the LSSTS decoder that is passed to the QPSK demapper is not Gaussian distributed, although the LLR values in the demapper are calculated assuming Gaussian distribution. Therefore, in order to eliminate the complexity of computing an analytical formula for the Probability Density Functions (PDF) of the LSSTS decoded data or computing the LLRs based on the histogram of the data, we devised LLR post-processing technique of Section 6.4.1 as a transformation for the output LLR of the demapper. Figure 8.9 shows that the system employing the LLR post-processing technique attains a similar EXIT curve to the case where artificial LLRs were generated.

The three iterative detection aided LSSTS schemes differed in the way the channel coding was implemented in the different STS layers, while the overall code-rate of three systems was kept identical.

1. In the first scheme, referred to as System 1, a single outer and a single inner channel code was used to encode the bits transmitted.

2. In the second scheme, namely System 2, a single outer code was implemented, whose output was split into two substreams, each of which were encoded using a separate inner code.

3. By contrast, in the third proposed scheme referred to as System 3, the input data bit stream was first split into two different substreams, where a pair of different outer as well as inner codes were implemented in the different substreams.

It was shown in Chapter 6 that the three systems exhibit a similar complexity quantified in terms of the total number of trellis states encountered, which determines the number of Add-

Compare-Select (ACS) arithmetic operations. Similarly, we demonstrated that, provided we employed sufficiently long interleavers, the three systems attained a similar BER performance. By contrast, when shorter interleavers were employed, System 1 performed better than System 2, which in turn performed better than System 3. This is due to the fact that the interleaver depth of System 2 and System 3 is lower than that of System 1, since the bit stream is split into two substreams in System 2 and System 3, which constrains the interleaver to be shorter and hence the correlation in the extrinsic information becomes higher, which eventually degrades the BER performance.

8.1.3 Distributed Turbo Coding

The MIMO schemes presented in Sections 8.1.1 and 8.1.2 are considered to be colocated MIMOs, i.e. the multiple antennas at the transmitter and receiver are connected physically to the same station. Additionally, in order to attain a diversity gain, it is required that the channel impulse response between the different transmit antennas and the receive antenna be uncorrelated or statistically independent. This is possible if the antenna spacing is sufficiently large so that the assumption of statistical independence of the different paths from the different antennas is justified. However, the assumption of sufficient antenna spacing may be impractical for shirt-pocket-sized wireless devices, which are typically limited in size and hardware complexity to a single transmit antenna.

On the other hand, spatial fading correlations caused by insufficient antenna spacing at the transmitter or receiver of a MIMO system results in degradation in the capacity as well as the BER performance of MIMO systems as shown in Figure 8.10 for a twin-antenna STBC system [44]. Correlation is likely to be introduced as a result of large-scale shadow fading that affects the transmission links between the different transmit and receive antennas [31]. Figure 8.10 compares the BER performance of a single-transmit and single-receive antenna system with that of a twin-antenna aided STBC system affected by the large-scale shadow fading. As shown in Figure 8.10, the performance of MIMO systems degrades, as the shadow fading effects increase and the single-antenna aided system performs better than a MIMO system, when the shadow fading variance is higher than 5 dB.

Cooperative communications were recently introduced for attaining spatial diversity, where it is typically possible to guarantee the spatial separation of the transmit antennas. This is due to the fact that the different antennas belong to different mobile stations, which are assumed to be far enough to attain statistically independent fading from the different antennas. Therefore, since the signals transmitted from different users undergo independent fading, spatial diversity can be achieved with the aid of the cooperating partners' antennas.

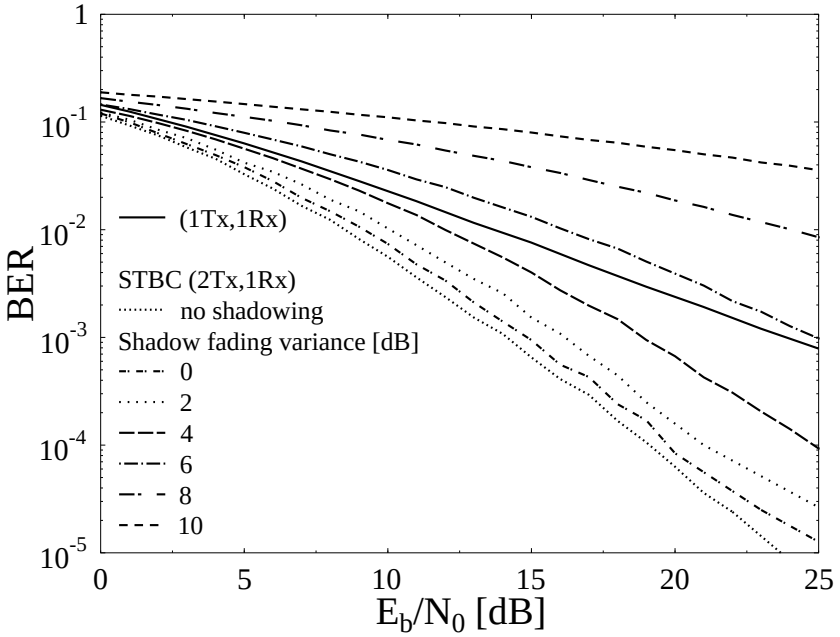

Figure 8.10: Effect of large-scale shadow fading on the performance of STBC systems.

In Chapter 7 we proposed a Distributed Turbo Coding (DTC) scheme, where two users cooperate by appropriately sending their own data coupled with the other user's data after interleaving and channel coding. Cooperation in the proposed DTC scheme is carried out in two phases. During the first phase of cooperation, the two users exchange their data in two time slots. Hence, after the first phase of cooperation the two users have their own data as well as the data of the other user. Then, during the second phase of cooperation, each user employs channel coding and interleaving before mapping the bits to multidimensional SP symbols that are then simultaneously transmitted from the two users' antennas. At the receiver side, interference cancellation is applied to the received data, where two branches of decoded data are output from the interference canceller. Afterwards, iterative detection is carried out both between the demapper and the channel code's decoder in each branch as well as between the channel codes' decoders in the two branches.

The proposed DTC is compared against a benchmark scheme, where no exchange of data is carried out between the two users. By contrast, each user transmits his/her own data after channel coding and interleaving. At the receiver side, interference cancellation is performed on the received signal and then iterative detection is carried out between the demapper and the channel code's decoder in each branch of the decoded signal.

The DTC scheme has a four times lower throughput than the benchmark scheme. However, the DTC scheme is capable of attaining an E_b/N_0 gain of more than 25 dB at a BER of 10^{-5} over the benchmark scheme due to the fact that the benchmark scheme has an error floor, while the DTC scheme does not.

Additionally, in Section 7.4 we studied the effect of errors induced in the data exchanged

between the different users in the first phase of cooperation on the performance of the uplink transmission in the second phase of cooperation. We considered transmission over AWGN, Rayleigh and Ricean inter-user channels and studied the effects of transmission over the different channels on the performance of the DTC scheme. It was shown in Section 7.4 that an error rate higher than 10^{-6} in the inter-user communication results in an error floor in the attainable BER performance of the cooperative uplink transmission. Therefore, it was proposed to consider soft data relaying in the DTC scheme and this will be further discussed in Section 8.2 in terms of our future work ideas.

8.2 Future Work

The research presented in this thesis can be extended in several ways. In this section we present some ideas of our proposed future work and briefly elaborate on each idea.

8.2.1 Differential Multi-functional MIMO

As discussed in Chapter 2, the channel estimation complexity increases with the product of the number of transmit and receive antennas. Additionally, channel estimation errors degrade the performance of the MIMO systems when coherent detection is employed. A solution for eliminating the complexity of MIMO channel estimation is to employ non-coherent detection dispensing with channel estimation.

The multi-functional MIMOs presented in Chapters 5 and 6 use coherent detection, while assuming perfect channel knowledge at the receiver. However, channel estimation, which is a complex process, includes channel estimation errors that degrades the attainable BER performance of the system. Figure 8.11 compares the attainable BER performance of the LSSTC scheme of Chapter 5 both when considering perfect channel knowledge and when modelling the channel estimation error as Gaussian noise imposed on the channel impulse response at the receiver side. Observe that as the noise variance increases, i.e. as the channel estimation error increases, the BER performance degrades and an error floor is formed. Therefore, an attractive way of eliminating the potentially high-complexity channel estimation as well as the performance degradation due to channel estimation errors is to design non-coherent receivers that do not require any channel knowledge. Differential schemes, such as DSTS, employ non-coherent detectors at the expense of 3 dB performance degradation compared to the coherent scheme using perfect channel knowledge.

Therefore, as a further extension to the multi-functional MIMO schemes of Chapters 5 and 6, we can design differential multi-functional MIMO schemes that do not require any channel

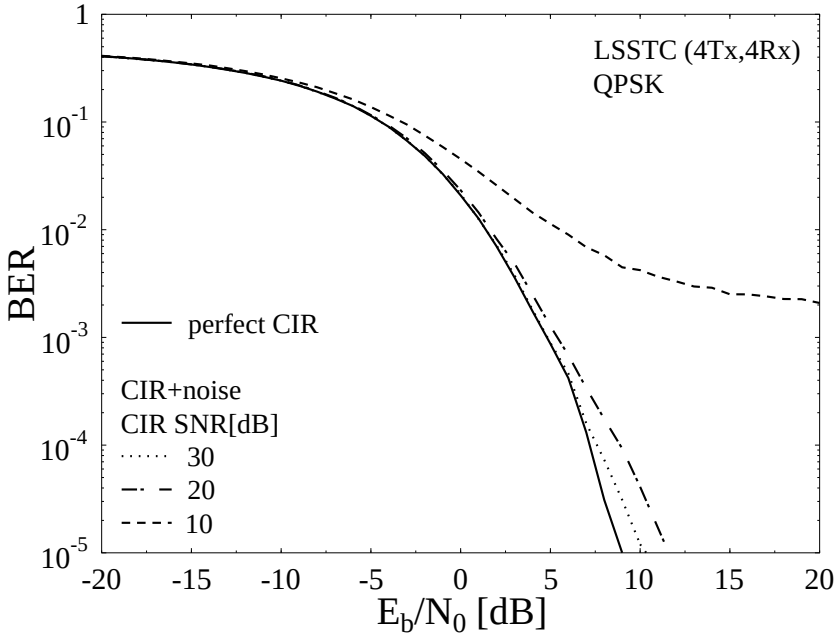

Figure 8.11: Effect of channel estimation error on the performance of the LSSTC scheme of Chapter 5. Gaussian noise was added to the channel impulse response at the receiver for the sake of inducing errors in the channel knowledge.

knowledge. Additionally, it is expected that the differential scheme will have a 3 dB performance degradation when compared to the coherent scheme assuming perfect channel knowledge at the receiver. However, when channel estimation is employed, differential detection eliminates the complexity of channel estimation and we may even attain a better BER performance than that of the coherent scheme, when the channel estimation is not reliable.

8.2.2 Multi-functional Cooperative Communication Systems

MIMO systems require more than one transmit antenna, but satisfying this need may be impractical for shirt-pocket-sized wireless devices, which are typically limited in both size and hardware complexity to a single transmit antenna. Furthermore, as most wireless systems support multiple users, user cooperation [36, 37, 268] can be employed, where users support each other by "sharing their antennas" and thus generate a virtual multiple antenna environment [137]. Since the signals transmitted from different users undergo independent fading, spatial diversity can be achieved with the aid of the cooperating partners' antennas.

Several cooperative communication schemes have been proposed in the literature [10, 36, 37, 135, 137, 138, 141, 145, 161, 268], where cooperative communications have been shown to offer significant performance gains in terms of various performance metrics, including diversity gains as well as multiplexing gains. Hence, a potential research idea is to investigate the design of cooperative communication schemes that are characterised by diversity gain, multiplexing gain as well as beamforming gain. In other words, we are proposing to design multi-functional

cooperative communication schemes. An uplink scheme can be implemented, where each Mobile Station (MS) may be equipped with a single antenna or a single antenna array. Users can be combined in a way that the nearest users can transmit in a Space-Time Code (STC) manner, where the channels from the different MSs to the uplink receiver are assumed to be statistically independent. Additionally, different groups of users employing STC may transmit their data at the same time and using the same carrier frequency, like V-BLAST, in order to increase the attainable throughput of the system.

On the other hand, the user cooperation is usually implemented as two-phase cooperation. The first phase corresponds to the phase, where the users exchange their data so that they can assists each other in the second phase of cooperation, where the users communicate with the base station. Hence, the total throughput of the system depends on the number of time-slots as well as on the way the different users exchange their data. Additionally, the performance of the system depends on the signalling scheme used by the different users for relaying the data of the other users. Therefore, the multi-functional cooperative communication scheme can be designed and studied in the context of completely different signalling schemes, evaluating their effect on the attainable BER performance as well as on the attainable throughput.

On the other hand, instead of considering a cooperative uplink scheme, where the different users communicate with a BS, it is possible to consider an ad-hoc network, where the different users cooperate with other users. In this case, the receiving users can also cooperate in order to reliably decode their received signals and hence each receiving user can decode his/her own data. The receivers have to exchange their received signals as well as the CIRs of the channels between the transmitting users and each receiving user. This can be carried out in a single time slot for each receiving user using CDMA spreading, where each receiving user transmits at the same time its received signal with the CIRs from the transmitting users.

8.2.3 Soft Relaying and Power Optimisation in Distributed Turbo Coding

In Chapter 7 we proposed a Distributed Turbo Coding (DTC) scheme that combines the concepts of cooperative communications and turbo coding. In the proposed scheme, we considered equal power allocation for the two phases of cooperation as well as for the two users. However, in a practical scenario, the two cooperating users must be closer to each other than to the Base Station (BS). Hence, power can be allocated more efficiently so that less power can be allocated for the first phase of cooperation and more power can be allocated to the second phase, while keeping the total transmit power in the two phases of cooperation constant. Additionally, the transmit power can be optimally shared between the two users so that the user with the better channel conditions can transmit more power.

Half-rate channel coding has been used in the first phase of communication in the DTC scheme of Chapter 7 in order to improve the attainable BER performance of the uplink transmission. The results presented in Chapter 7 were considered for the system, where the 1/2-rate codes were employed in the two phases of cooperation. This means that the system is wasting the available bandwidth. Hence, it is possible to distribute the code rate between the two phases of cooperation so that the system utilises the available bandwidth as efficiently as possible, while providing a good BER performance. Additionally, iterative detection can be carried out during the phase-one of cooperation, where the number of iterations can be adapted depending on the Inter-User Channel (IUC) SNR. In other words, when the IUC SNR is high enough, no iterations may be applied and then as the IUC SNR decreases, the number of decoding iterations can be increased in order to maintain a good BER performance in the first phase of cooperation, which eventually affects the performance of the transmission in the second phase of cooperation.

On the other hand, soft relaying has been proposed as a method for combining the main advantages of both Amplify-and-Forward (AF) and Decode-and-Forward (DF) signalling strategies. In [146] soft DF has been shown to outperform the DF and AF signalling, where it was argued that the DF signalling loses soft information and hence all operations were performed in a LLR domain. A more detailed study on the soft DF was carried out in [154], where it was shown how the soft information can be quantised, encoded and then modulated using superimposed modulation in order to maintain the system's throughput and bandwidth constant. Soft information relaying has also been used in [151] in order to pass soft information from the relay to the BS using BPSK modulation. Furthermore, in [147, 152] distributed source coding techniques have been adopted for employment in wireless cooperative communications in order to improve the inter-user performance. Therefore, based on the performance improvements reported in the literature while using soft information relaying and based on the fact that the performance of the DTC scheme of Chapter 7 is highly dependent on the inter-user channel characteristics, it is of potential research interest to investigate the effect of using soft information relaying. In other words, in the DTC scheme the two users transmit soft estimates of the other users' data instead of performing hard decoding and losing the advantage of soft information.

Appendix A

Gray and Anti-Gray Mapping Schemes for Sphere Packing Modulation of Size $L = 16$

In this appendix, Gray mapping and the 9 different Anti-Gray mapping schemes introduced in Chapter 3 for DSTS-SP signals of size $L = 16$ are described in detail. More specifically, for all mapping schemes, constellation points of the lattice D_4 are given for each integer index $l = 0, 1, \ldots, 15$. Observe that all mapping schemes use the same 16 constellation points. The normalisation factor of these constellation points is $\sqrt{\frac{2L}{E_{total}}} = 1$ as described in Equation (2.21). The constellation points corresponding to each mapping scheme are given in Tables A.1 to A.10.

	Points from D_4			
Integer Index	a_1	a_2	a_3	a_4
0	-1	-1	0	0
1	0	-1	-1	0
2	0	-1	$+1$	0
3	$+1$	-1	0	0
4	-1	0	0	$+1$
5	0	0	-1	$+1$
6	0	0	$+1$	$+1$
7	$+1$	0	0	$+1$

	Points from D_4			
Integer Index	a_1	a_2	a_3	a_4
8	-1	0	0	-1
9	0	0	-1	-1
10	0	0	$+1$	-1
11	$+1$	0	0	-1
12	-1	$+1$	0	0
13	0	$+1$	-1	0
14	0	$+1$	$+1$	0
15	$+1$	$+1$	0	0

Table A.1: Gray mapping.

	Points from D_4			
Integer Index	a_1	a_2	a_3	a_4
0	$+1$	-1	0	0
1	0	-1	-1	0
2	0	-1	$+1$	0
3	-1	-1	0	0
4	-1	0	0	$+1$
5	0	0	-1	$+1$
6	0	0	$+1$	$+1$
7	$+1$	0	0	$+1$

	Points from D_4			
Integer Index	a_1	a_2	a_3	a_4
8	-1	0	0	-1
9	0	0	-1	-1
10	0	0	$+1$	-1
11	$+1$	0	0	-1
12	-1	$+1$	0	0
13	0	$+1$	-1	0
14	0	$+1$	$+1$	0
15	$+1$	$+1$	0	0

Table A.2: Anti-Gray mapping AGM-1.

	Points from D_4			
Integer Index	a_1	a_2	a_3	a_4
0	+1	+1	0	0
1	0	−1	−1	0
2	0	−1	+1	0
3	+1	−1	0	0
4	−1	0	0	+1
5	0	0	−1	+1
6	0	0	+1	+1
7	+1	0	0	+1

	Points from D_4			
Integer Index	a_1	a_2	a_3	a_4
8	−1	0	0	−1
9	0	0	−1	−1
10	0	0	+1	−1
11	+1	0	0	−1
12	−1	+1	0	0
13	0	+1	−1	0
14	0	+1	+1	0
15	−1	−1	0	0

Table A.3: Anti-Gray mapping AGM-2.

	Points from D_4			
Integer Index	a_1	a_2	a_3	a_4
0	+1	0	0	−1
1	+1	0	0	+1
2	−1	0	0	−1
3	0	0	+1	+1
4	0	−1	+1	0
5	+1	−1	0	0
6	0	0	+1	−1
7	0	+1	+1	0

	Points from D_4			
Integer Index	a_1	a_2	a_3	a_4
8	0	−1	−1	0
9	0	0	−1	+1
10	−1	−1	0	0
11	−1	0	0	+1
12	0	0	−1	−1
13	0	+1	−1	0
14	+1	+1	0	0
15	−1	+1	0	0

Table A.4: Anti-Gray mapping AGM-3.

	Points from D_4			
Integer Index	a_1	a_2	a_3	a_4
0	0	0	−1	+1
1	0	0	−1	−1
2	−1	+1	0	0
3	−1	0	0	−1
4	+1	0	0	+1
5	+1	+1	0	0
6	0	+1	−1	0
7	0	+1	+1	0

	Points from D_4			
Integer Index	a_1	a_2	a_3	a_4
8	+1	−1	0	0
9	0	0	+1	−1
10	−1	0	0	+1
11	−1	−1	0	0
12	0	−1	−1	0
13	+1	0	0	−1
14	0	−1	+1	0
15	0	0	+1	+1

Table A.5: Anti-Gray mapping AGM-4.

	Points from D_4			
Integer Index	a_1	a_2	a_3	a_4
0	0	+1	+1	0
1	0	0	+1	−1
2	−1	0	0	−1
3	−1	+1	0	0
4	0	−1	+1	0
5	+1	+1	0	0
6	0	0	+1	+1
7	+1	0	0	−1

	Points from D_4			
Integer Index	a_1	a_2	a_3	a_4
8	−1	0	0	+1
9	−1	−1	0	0
10	0	0	−1	+1
11	0	−1	−1	0
12	+1	−1	0	0
13	0	0	−1	−1
14	+1	0	0	+1
15	0	+1	−1	0

Table A.6: Anti-Gray mapping AGM-5.

	Points from D_4			
Integer Index	a_1	a_2	a_3	a_4
0	-1	0	0	$+1$
1	0	-1	-1	0
2	0	0	$+1$	-1
3	0	$+1$	-1	0
4	0	0	-1	$+1$
5	$+1$	-1	0	0
6	$+1$	$+1$	0	0
7	$+1$	0	0	-1

	Points from D_4			
Integer Index	a_1	a_2	a_3	a_4
8	0	0	$+1$	$+1$
9	-1	0	0	-1
10	0	-1	$+1$	0
11	0	$+1$	$+1$	0
12	-1	-1	0	0
13	-1	$+1$	0	0
14	$+1$	0	0	$+1$
15	0	0	-1	-1

Table A.7: Anti-Gray mapping AGM-6

	Points from D_4			
Integer Index	a_1	a_2	a_3	a_4
0	-1	-1	0	0
1	-1	$+1$	0	0
2	$+1$	-1	0	0
3	$+1$	$+1$	0	0
4	0	-1	-1	0
5	0	-1	$+1$	0
6	0	$+1$	-1	0
7	0	$+1$	$+1$	0

	Points from D_4			
Integer Index	a_1	a_2	a_3	a_4
8	0	0	-1	-1
9	0	0	-1	$+1$
10	0	0	$+1$	-1
11	0	0	$+1$	$+1$
12	-1	0	0	-1
13	-1	0	0	$+1$
14	$+1$	0	0	-1
15	$+1$	0	0	$+1$

Table A.8: Anti-Gray mapping AGM-7.

	Points from D_4			
Integer Index	a_1	a_2	a_3	a_4
0	0	−1	−1	0
1	−1	−1	0	0
2	−1	0	0	−1
3	0	0	−1	−1
4	0	−1	+1	0
5	−1	+1	0	0
6	−1	0	0	+1
7	0	0	−1	+1

	Points from D_4			
Integer Index	a_1	a_2	a_3	a_4
8	0	+1	+1	0
9	+1	+1	0	0
10	+1	0	0	+1
11	0	0	+1	+1
12	0	+1	−1	0
13	+1	−1	0	0
14	+1	0	0	−1
15	0	0	+1	−1

Table A.9: Anti-Gray mapping AGM-8.

	Points from D_4			
Integer Index	a_1	a_2	a_3	a_4
0	+1	+1	0	0
1	+1	0	0	−1
2	+1	0	0	+1
3	−1	+1	0	0
4	0	+1	+1	0
5	0	0	−1	+1
6	0	0	−1	−1
7	0	−1	+1	0

	Points from D_4			
Integer Index	a_1	a_2	a_3	a_4
8	0	+1	−1	0
9	0	0	+1	+1
10	0	0	+1	−1
11	0	−1	−1	0
12	+1	−1	0	0
13	−1	0	0	−1
14	−1	0	0	+1
15	−1	−1	0	0

Table A.10: Anti-Gray mapping AGM-9.

Glossary

AA	Antenna Array
ACS	Add-Compare-Select Arithmetic Operation
AF	Amplify-and-Forward
AGM	Anti-Gray Mapping
AMR-WB	Adaptive MultiRate Wideband
AWGN	Additive White Gaussian Noise
BCJR	Bahl-Cocke-Jelinek-Raviv
BER	Bit Error Ratio
BICM	Bit Interleaved Coded Modulation
BPS	Bits Per Modulated Symbol
BPSK	Binary Phase Shift Keying
BS	Base Station
CCMC	Continuous-Input Continuous-Output Memoryless Channel
CDMA	Code Division Multiple Access
CIR	Channel Impulse Response
CRC	Cyclic Redundancy Check
CSI	Channel State Information
CSNR	Chip Signal-to-Noise Ratio

D-STTD	Double Space-Time Transmit Diversity
DCMC	Discrete-Input Continuous-Output Memoryless Channel
DF	Decode-and-Forward
DL	DownLink
DOA	Direction Of Arrival
DPSK	Differential Phase Shift Keying
DSTBC	Differential Space-Time Block Codes
DSTS	Differential Space-Time Spreading
DSTS-SP	Differential Space-Time Spreading using Sphere Packing Modulation
DTC	Distributed Turbo Code
EXIT	Extrinsic Information Transfer
FD	Frequency Domain
GM	Gray Mapping
HARQ	Hybrid Automatic-Repeat-reQuest
HSDPA	High Speed Downlink Packet Access
i.i.d.	Independent and Identically Distributed
IC	Interference Cancellation
IrCC	Irregular Convolutional Code
IrVLC	Irregular Variable Length Code
ISCD	Iterative Source and Channel Decoding
ISI	InterSymbol Interference
IUC	Inter-User Channel
LLR	Logarithmic Likelihood Ratio
LM	Lloyd-Max
LSSTC	Layered Steered Space-Time Codes

LSSTS	Layered Steered Space-Time Spreading
LST	Layered Space-Time
MAP	Maximum A Posteriori
MC CDMA	Multi-Carrier Code Division Multiple Access
MC DS-CDMA	Multi-Carrier Direct Sequence Code Division Multiple Access
MED	Minimum Euclidean Distance
MI	Mutual Information
MIMO	Multiple-Input Multiple-Output
ML	Maximum Likelihood
MS	Mobile Station
MUD	Multi-User Detection
MUI	Multi-User Interference
OFDM	Orthogonal Frequency Division Multiplexing
P/S	Parallel-to-Serial Conversion
PAM	Pulse Amplitude Modulation
PDF	Probability Density Function
PSK	Phase Shift Keying
QAM	Quadrature Amplitude Modulation
QoS	Quality of Service
QPSK	Quadrature Phase Shift Keying
RCPC	Rate Compatible Punctured Convolutional
RSC	Recursive Systematic Convolutional
S/P	Serial-to-Parallel Conversion
SF	Spreading Factor
SIC	Successive Interference Cancellation

SINR	Signal to Interference plus Noise Ratio
SNR	Signal to Noise Ratio
SP	Sphere Packing
SP-SER	Sphere Packing Symbol Error Ratio
ST	Space-Time
STBC	Space-Time Block Coding
STC	Space-Time Coding
STS	Space-Time Spreading
STTC	Space-Time Trellis Codes
TCM	Trellis Coded Modulation
TD	Time Domain
TDD	Time Division Duplex
UL	UpLink
URC	Unity Rate Code
V-BLAST	Vertical Bell Labs Layered Space-Time
VAA	Virtual Antenna Array
VSF	Variable Spreading Factor
WCDMA	Wideband Code Division Multiple Access
ZF	Zero Forcing

Bibliography

[1] M. El-Hajjar, O. Alamri, S. X. Ng and L. Hanzo, "Turbo detection of precoded sphere packing modulation using four transmit antennas for differential space-time spreading," *IEEE Transactions on Wireless Communications*, vol. 7, pp. 943–952, March 2008.

[2] M. El-Hajjar and L. Hanzo, "Layered steered space-time codes and their capacity," *Electronics Letters*, vol. 43, pp. 680–682, June 2007.

[3] M. El-Hajjar, B. Hu, L.-L. Yang and L. Hanzo, "Coherent and differential downlink space-time steering aided generalised multicarrier DS-CDMA," *IEEE Transactions on Wireless Communications*, vol. 6, pp. 3857–3863, November 2007.

[4] M. El-Hajjar, O. Alamri, J. Wang, S. Zummo and L. Hanzo, "Layered steered space-time codes using multi-dimensional sphere-packing modulation," *accepted for publication in IEEE Transactions on Wireless Communications*, 2008.

[5] N. Othman, M. El-Hajjar, O. Alamri and L. Hanzo, "Iterative AMR-WB source and channel-decoding of differential space-time spreading assisted sphere packing modulation," *accepted for publication in IEEE Transactions on Vehicular Technology*, 2008.

[6] M. El-Hajjar, O. Alamri, R.G. Maunder and L. Hanzo, "Layered steered space-time spreading using generalised MC DS-CDMA," *submitted to IEEE Signal Processing Letters*, April 2008.

[7] M. El-Hajjar, O. Alamri and L. Hanzo, "Differential space-time spreading using iteratively detected sphere packing modulation and two transmit antennas," in *Wireless Communications and Networking Conference (WCNC)*, vol. 3, pp. 1664–1668, April 2006.

[8] M. El-Hajjar, O. Alamri and L. Hanzo, "Differential space-time spreading using four transmit antennas and iteratively detected sphere packing modulation," in *IEEE Ninth International Symposium on Spread Spectrum Techniques and Applications*, (Manaus-Amazon), pp. 322–326, August 2006.

[9] M. El-Hajjar, O. Alamri and L. Hanzo, "Adaptive differential space-time-spreading-assisted turbo-detected sphere packing modulation," in *IEEE Wireless Communications and Networking Conference*, pp. 645–649, March 2007.

[10] M. El-Hajjar, S. Zummo and L. Hanzo, "Near-instantaneously adaptive cooperative schemes based on space-time block codes and V-BLAST," in *IEEE Vehicular Technology Conference (VTC2007-Spring)*, pp. 2200–2204, April 2007.

[11] N. Othman, M. El-Hajjar, O. Alamri and L. Hanzo, "Soft-bit assisted iterative AMR-WB source-decoding and turbo-detection of channel-coded differential space-time spreading using sphere packing modulation," in *IEEE Vehicular Technology Conference (VTC)*, pp. 2010–2014, April 2007.

[12] M. El-Hajjar, R.Y.S. Tee, H. Bin, L.-L. Yang and L. Hanzo, "Downlink steered space-time spreading assisted generalised Multicarrier DS-CDMA using sphere packing aided multilevel coding," in *IEEE 66th Vehicular Technology Conference*, (Baltimore, MD, USA), pp. 472–476, September 2007.

[13] M. El-Hajjar, R. G. Maunder, O. Alamri, S. X. Ng and L. Hanzo, "Iteratively detected irregular variable length coding and sphere packing modulation aided differential space-time spreading," in *IEEE 66th Vehicular Technology Conference*, (Baltimore, MD, USA), pp. 1238–1242, September 2007.

[14] M. El-Hajjar, O. Alamri and L. Hanzo, "Layered steered space-time codes using iterative detection," in *IEEE Workshop on Signal Processing Systems*, (Shanghai, China), pp. 35–39, October 2007.

[15] N. Sahal, M. El-Hajjar and L. Hanzo, "Downlink steered space-time spreading for multi-carrier transmission over frequency selective channels," in *IEEE Vehicular Technology Conference*, (Marina Bay, Singapore), pp. 943–947, May 2008.

[16] R.A. Riaz, M. El-Hajjar, Q.Z. Ahmed, S.X. Ng, S. Chen and L. Hanzo, "Convergence analysis of iteratively detected time hopping and DS-CDMA ultrawide bandwidth systems by EXIT charts," in *IEEE Vehicular Technology Conference*, (Marina Bay, Singapore), pp. 1127–1131, May 2008.

[17] N.S. Othman, M. El-Hajjar, A.Q. Pham, O. Alamri, S.X. Ng and L. Hanzo, "Over-complete source-mapping aided AMR-WB MIMO transceiver using three-stage iterative detection," in *IEEE International Conference on Communications*, (Beijing, China), pp. 751–755, May 2008.

[18] T.D. Nguyen, M. El-Hajjar, L.-L. Yang and L. Hanzo, "A systematic Luby transform coded V-BLAST system," in *IEEE International Conference on Communications*, (Beijing, China), pp. 775–779, May 2008.

[19] L. Xu, M. El-Hajjar, O. Alamri, S. Chen and L. Hanzo, "Iteratively detected sphere packing modulated OFDM: An EXIT chart perspective," in *IEEE International Conference on Communications*, (Beijing, China), pp. 631–635, May 2008.

[20] M. El-Hajjar, O. Alamri and L. Hanzo, "Iteratively detected three-stage multi-dimensional sphere packing modulation aided multi-functional MIMO," in *submitted to IEEE Global Communications Conference*, 2008.

[21] Nasruminallah, M. El-Hajjar, N.S. Othman, A.P. Quang and L. Hanzo, "Over-complete mapping aided soft-bit assisted iterative unequal error protection H.264 joint source and channel decoding," in *accepted for publication in IEEE Vehicular Technology Conference*, September 2008.

[22] R.A. Riaz, M. El-Hajjar, S.X. Ng, S. Chen and L. Hanzo, "EXIT chart aided design of DS-CDMA ultrawide bandwidth systems using iterative decoding," in *accepted for publication in the Proceedings of IEEE Vehicular Technology Conference*, September 2008.

[23] C. E. Shannon, "A mathematical theory of communication," *Bell Systems Technical Journal*, vol. 27, pp. 623–656, October 1948.

[24] B. Vucetic and J. Yuan, *Space-time coding*. Wiley, 2003.

[25] L. Hanzo, L.-L. Yang, E.-L. Kuan and K. Yen, *Single and multi-carrier DS-CDMA: Multi-user detection, space-time spreading, synchronisation, networking and standards*. Chichester, England: John Wiley and Sons Ltd and IEEE Press, 2003.

[26] L. Hanzo, T.H. Liew and B.L. Yeap, *Turbo coding, turbo equalisation and space time coding for transmission over fading channels*. Chichester, UK: Wiley: IEEE Press, 2002.

[27] L. Hanzo, S.X. Ng, T. Keller and W. Webb, *Quadrature amplitude modulation: From basics to adaptive trellis-coded, turbo equalised and space-time coded OFDM, CDMA and MC-CDMA systems, 2nd Edition*. Chichester, England: John Wiley and Sons Ltd and IEEE Press, 2004.

[28] G.J. Foschini, D. Chizhik, M.J. Gans, C. Papadias and R.A. Valenzuela, "Analysis and performance of some basic space-time architectures," *IEEE Journal on Selected Areas in Communications*, vol. 21, no. 3, pp. 303–320, 2003.

[29] S. Siwamogsatham and M. Fitz, "Robust space-time coding for correlated Rayleigh fading channels," *IEEE Transactions on Signal Processing*, vol. 50, pp. 2408–2416, October 2002.

[30] H. Jafarkhani, *Space-time coding: Theory and practice*. Cambridge University Press, 2005.

[31] T. S. Rappaport, *Wireless communications: Principles and practice*. Prentice Hall, 1996.

[32] J. Winters, "On the capacity of radio communication systems with diversity in a Rayleigh fading environment," *IEEE Journal on Selected Areas in Communications*, vol. 5, pp. 871–878, June 1987.

[33] E. Telatar, "Capacity of multi-antenna Gaussian channels," *European Transactions on Telecommunications*, vol. 10, pp. 585–595, November/December 1999.

[34] G.J. Foschini and M.J. Gans, "On limits of wireless communications in a fading environment when using multiple antennas," *Kluwer Academic Publishers, Wireless Personal Communications*, pp. 311–335, 1998.

[35] J.G. Proakis, *Digital communications*. McGraw-Hill, 2001.

[36] A. Sendonaris, E. Erkip and B. Aazhang, "User cooperation diversity Part I: System description," *IEEE Transactions on Communications*, vol. 51, no. 11, pp. 1927–1938, 2003.

[37] A. Sendonaris, E. Erkip and B. Aazhang, "User cooperation diversity Part II: Implementation aspects and performance analysis," *IEEE Transactions on Communications*, vol. 51, no. 11, pp. 1939–1948, 2003.

[38] D.G. Brennan, "Linear diversity combining techniques," in *Proceedings of the IRE*, vol. 47, pp. 1075–1102, June 1959.

[39] A. Wittneben, "Base station modulation diversity for digital simulcast," in *41st IEEE Vehicular Technology Conference Gateway to the Future Technology in Motion*, (St. Louis, MO), pp. 848–853, May 1991.

[40] A. Wittneben, "A new bandwidth efficient transmit antenna modulation diversity scheme for linear digital modulation," in *IEEE International Conference on Communications*, vol. 3, (Geneva), pp. 1630–1634, May 1993.

[41] N. Seshadri and J.H. Winters, "Two signaling schemes for improving the error performance of frequency-division-duplex transmission systems using transmitter antenna diversity," in *IEEE Vehicular Technology Conference*, (Secaucus, NJ), pp. 508–511, May 1993.

[42] J.H. Winters, "The diversity gain of transmit diversity in wireless systems with Rayleigh fading," in *IEEE International Conference on Communications*, (New Orleans, LA), pp. 1121–1125, May 1994.

[43] T. Eng, N. Kong and L.B. Milstein, "Comparison of diversity combining techniques for Rayleigh-fading channels," *IEEE Transactions on Communications*, vol. 44, pp. 1117–1129, September 1996.

[44] S.M. Alamouti, "A simple transmit diversity technique for wireless communications," *IEEE Journal on Selected Areas in Communications*, vol. 16, no. 8, pp. 1451–1458, 1998.

[45] V. Tarokh, N. Seshadri and A.R. Calderbank, "Space-time codes for high data rate wireless communication: performance criterion and code construction," *IEEE Transactions on Information Theory*, vol. 44, pp. 744–765, March 1998.

[46] V. Tarokh, H. Jafarkhani and A.R. Calderbank, "Space-time block codes from orthogonal designs," *IEEE Transactions on Information Theory*, vol. 45, no. 5, pp. 1456–1467, 1999.

[47] V. Tarokh, H. Jafarkhani and A.R. Calderbank, "Space-time block coding for wireless communications: performance results," *IEEE Journal on Selected Areas in Communications*, vol. 17, no. 3, pp. 451–460, 1999.

[48] J.-C. Guey, M.P. Fitz, M.R. Bell and W.-Y. Kuo, "Signal design for transmitter diversity wireless communication systems over Rayleigh fading channels," *IEEE Transactions on Communications*, vol. 47, pp. 527–537, April 1999.

[49] B. Hochwald, T.L. Marzetta and C.B. Papadias, "A transmitter diversity scheme for wideband CDMA systems based on space-time spreading," *IEEE Journal on Selected Areas in Communications*, vol. 19, no. 1, pp. 48–60, 2001.

[50] H. Jafarkhani, "A quasi-orthogonal space-time block code," *IEEE Transactions on Communications*, vol. 49, no. 1, pp. 1–4, 2001.

[51] B. Hassibi and B.M. Hochwald, "High-rate codes that are linear in space and time," *IEEE Transactions on Information Theory*, vol. 48, pp. 1804–1824, July 2002.

[52] P. Stoica and G. Ganesan, "Space-time block codes: trained, blind and semi-blind detection," in *IEEE International Conference on Acoustics, Speech and Signal Processing*, vol. 2, (Orlando, FL), pp. 1609–1612, 2002.

[53] D.G. Brennan, "Linear diversity combining techniques," *Proceedings of the IEEE*, vol. 91, pp. 331–356, February 2003.

[54] H. Wang and X.-G. Xia, "Upper bounds of rates of complex orthogonal space-time block codes," *IEEE Transactions on Information Theory*, vol. 49, pp. 2788–2796, October 2003.

[55] W. Su, Z. Safar and K.J.R. Liu, "Space-time signal design for time-correlated Rayleigh fading channels," in *IEEE International Conference on Communications*, vol. 5, pp. 3175–3179, 2003.

[56] H. Zhang and T.A Gulliver, "Capacity and error probability analysis for orthogonal space-time block codes over fading channels," *IEEE Transactions on Wireless Communications*, vol. 4, pp. 808–819, March 2005.

[57] T.-H. Liew and L. Hanzo, "Space-time trellis and space-time block coding versus adaptive modulation and coding aided OFDM for wideband channels," *IEEE Transactions on Vehicular Technology*, vol. 55, pp. 173–187, January 2006.

[58] O. Alamri, B.L. Yeap and L. Hanzo, "A turbo detection and sphere-packing-modulation-aided space-time coding scheme," *IEEE Transactions on Vehicular Technology*, vol. 56, pp. 575–582, March 2007.

[59] P. Luo and H. Leib, "Class of full-rank space-time codes combining orthogonal designs with delay diversity," *IEEE Transactions on Vehicular Technology*, vol. 57, pp. 260–272, January 2008.

[60] J.H. Winters, "The diversity gain of transmit diversity in wireless systems with Rayleigh fading," *IEEE Transactions on Vehicular Technology*, vol. 47, pp. 119–123, February 1998.

[61] V. Tarokh, A. Naguib, N. Seshadri and A.R. Calderbank, "Space-time codes for high data rate wireless communication: performance criteria in the presence of channel estimation errors, mobility and multiple paths," *IEEE Transactions on Communications*, vol. 47, pp. 199–207, February 1999.

[62] V. Tarokh, S.M. Alamouti and P. Poon, "New detection schemes for transmit diversity with no channel estimation," in *IEEE International Conference on Universal Personal Communications*, vol. 2, pp. 917–920, October 1998.

[63] V. Tarokh and H. Jafarkhani, "A differential detection scheme for transmit diversity," in *IEEE Wireless Communications and Networking Conference*, vol. 3, pp. 1043–1047, September 1999.

[64] B.M. Hochwald and W. Sweldens, "Differential unitary space-time modulation," *IEEE Transactions on Communications*, vol. 48, no. 12, pp. 2041–2052, 2000.

[65] B.L. Hughes, "Differential space-time modulation," *IEEE Transactions on Information Theory*, vol. 46, pp. 2567–2578, November 2000.

[66] H. Jafarkhani and V. Tarokh, "Multiple transmit antenna differential detection from generalized orthogonal designs," *IEEE Transactions on Information Theory*, vol. 47, no. 6, pp. 2626–2631, 2001.

[67] R. Schober and L. Lampe, "Noncoherent receivers for differential space-time modulation," *IEEE Transactions on Communications*, vol. 50, pp. 768–777, May 2002.

[68] C.-S. Hwang, S.H. Nam, J. Chung and V. Tarokh, "Differential space time block codes using QAM constellations," in *14th IEEE Proceedings on Personal, Indoor and Mobile Radio Communications*, vol. 2, pp. 1693–1697, 2003.

[69] C.-S. Hwang, S.H. Nam, J. Chung and V. Tarokh, "Differential space time block codes using nonconstant modulus constellations," *IEEE Transactions on Signal Processing*, vol. 51, no. 11, pp. 2955–2964, 2003.

[70] S.H. Nam, C.-S. Hwang, J. Chung and V. Tarokh, "Differential space time block codes using QAM for four transmit antennas," in *IEEE International Conference on Communications*, vol. 2, pp. 952–956, 2004.

[71] Y. Zhu and H. Jafarkhani, "Differential modulation based on quasi-orthogonal codes," *IEEE Transactions on Wireless Communications*, vol. 4, no. 6, pp. 3005–3017, 2005.

[72] L.-Y. Song and A.G. Burr, "General differential modulation scheme for quasi-orthogonal space-time block codes with partial or full transmit diversity," *IET Communications*, vol. 1, pp. 256–266, April 2007.

[73] V. Tarokh and H. Jafarkhani, "A differential detection scheme for transmit diversity," *IEEE Journal on Selected Areas in Communications*, vol. 18, no. 7, pp. 1169–1174, 2000.

[74] B.M. Hochwald and T.L. Marzetta, "Unitary space-time modulation for multiple-antenna communications in Rayleigh flat fading," *IEEE Transactions on Information Theory*, vol. 46, pp. 543–564, March 2000.

[75] E. Biglieri, G. Taricco and A. Tulino, "Performance of space-time codes for a large number of antennas," *IEEE Transactions on Information Theory*, vol. 48, pp. 1794–1803, July 2002.

[76] A.J. Paulraj, D.A. Gore, R.U. Nabar and H. Bolcskei, "An overview of MIMO communications - a key to gigabit wireless," *Proceedings of the IEEE*, vol. 92, pp. 198–218, February 2004.

[77] E. Viterbo and J. Boutros, "A universal lattice code decoder for fading channels," *IEEE Transactions on Information Theory*, vol. 45, no. 5, pp. 1639–1642, 1999.

[78] O. Damen, A. Chkeif and J.-C. Belfiore, "Lattice code decoder for space-time codes," *IEEE Communications Letters*, vol. 4, pp. 161–163, May 2000.

[79] E. Agrell, T. Eriksson, A. Vardy and K. Zeger, "Closest point search in lattices," *IEEE Transactions on Information Theory*, vol. 48, pp. 2201–2214, August 2002.

[80] G.J. Foschini, "Layered space-time architecture for wireless communication in a fading environment when using multiple antennas," *Bell Laboratories Technical Journal*, vol. 1, pp. 41–59, Autumn 1996.

[81] P.W. Wolniansky, G.J. Foschini, G.D. Golden and R.A. Valenzuela, "V-BLAST: an architecture for realizing very high data rates over the rich-scattering wireless channel," in *International Symposium on Signals, Systems and Electronics*, (Pisa), pp. 295–300, September 1998.

[82] G.D. Golden, C.J. Foschini, R.A. Valenzuela and P.W. Wolniansky, "Detection algorithm and initial laboratory results using V-BLAST space-time communication architecture," *Electronics Letters*, vol. 35, pp. 14–16, January 1999.

[83] A. Benjebbour, H. Murata and S. Yoshida, "Comparison of ordered successive receivers for space-time transmission," in *IEEE Vehicular Technology Conference*, vol. 4, (Atlantic City, NJ), pp. 2053–2057, October 2001.

[84] M. Sellathurai and S. Haykin, "Turbo-BLAST for wireless communications: theory and experiments," *IEEE Transactions on Signal Processing*, vol. 50, pp. 2538–2546, October 2002.

[85] D. Wubben, R. Bohnke, V. Kuhn and K.-D. Kammeyer, "MMSE extension of V-BLAST based on sorted QR decomposition," in *IEEE Vehicular Technology Conference*, vol. 1, pp. 508–512, October 2003.

[86] H. Zhu, Z. Lei and F.P.S. Chin, "An improved square-root algorithm for BLAST," *IEEE Signal Processing Letters*, vol. 11, pp. 772–775, September 2004.

[87] Y. Huang, J. Zhang and P.M. Djuric, "Bayesian detection for BLAST," *IEEE Transactions on Signal Processing*, vol. 53, pp. 1086–1096, March 2005.

[88] S. Verdu, *Multiuser Detection.* Cambridge University Press, 2003.

[89] B. Hassibi, "An efficient square-root algorithm for BLAST," in *IEEE International Conference on Acoustics, Speech and Signal Processing*, vol. 2, (Istanbul), June 2000.

[90] D. Wubben, R. Bohnke, J. Rinas, V. Kuhn and K.D. Kammeyer, "Efficient algorithm for decoding layered space-time codes," *Electronics Letters*, vol. 37, pp. 1348–1350, October 2001.

[91] W. Zha and S.D. Blostein, "Modified decorrelating decision-feedback detection of BLAST space-time system," in *IEEE International Conference on Communications*, vol. 1, (New York), pp. 335–339, April/May 2002.

[92] T. Xiaofeng, Y. Zhuizhuan, Q. Haiyan, Z. Ping, H. Haas and E. Costa, "New sub-optimal detection algorithm of layered space-time code," in *IEEE Vehicular Technology Conference*, vol. 4, pp. 1791–1794, May 2002.

[93] J. Choi, "A bi-directional zero-forcing BLAST receiver," *IEEE Transactions on Signal Processing*, vol. 52, pp. 2670–2673, September 2004.

[94] H. Zhu, Z. Lei and F.P.S. Chin, "An improved square-root algorithm for BLAST," *IEEE Signal Processing Letters*, vol. 11, pp. 772–775, September 2004.

[95] W.-J. Choi, K.-W. Cheong and J.M. Cioffi, "Iterative soft interference cancellation for multiple antenna systems," in *IEEE Wireless Communications and Networking Conference*, vol. 1, (Chicago, IL), pp. 304–309, September 2000.

[96] S. Baro, G. Bauch, A. Pavlic and A. Semmler, "Improving BLAST performance using space-time block codes and turbo decoding," in *IEEE Global Telecommunications Conference (GLOBECOM)*, vol. 2, (San Francisco, CA), pp. 1067–1071, 2000.

[97] X. Jing, H. Wang, C. Ming and S. Cheng, "A novel BLAST detection algorithm based instantaneous error ordering," in *IEEE International Conference on Communications*, vol. 5, pp. 3056–3060, May 2003.

[98] C. Shen, H. Zhuang, L. Dai and S. Zhou, "Detection algorithm improving V-BLAST performance over error propagation," *Electronics Letters*, vol. 39, pp. 1007–1008, June 2003.

[99] H. Yao and G.W. Wornell, "Lattice-reduction-aided detectors for MIMO communication systems," in *IEEE Global Telecommunications Conference*, vol. 1, pp. 424–428, November 2002.

[100] D. Wubben, R. Bohnke, V. Kuhn and K.-D. Kammeyer, "Near-maximum-likelihood detection of MIMO systems using MMSE-based lattice reduction," in *IEEE International Conference on Communications*, vol. 2, pp. 798–802, June 2004.

[101] A. Elkhazin, K. Plataniotis and S. Pasupathy, "Group MAP BLAST detector," in *IEEE International Conference on Acoustics, Speech and Signal Processing*, vol. 4, pp. 785–788, May 2004.

[102] M. Sellathurai and S. Haykin, "T-BLAST for wireless communications: first experimental results," *IEEE Transactions on Vehicular Technology*, vol. 52, pp. 530–535, May 2003.

[103] J. Blogh and L. Hanzo, *Third-generation systems and intelligent wireless networking: smart antennas and adaptive modulation*. John Wiley & Sons - IEEE Press, 2002.

[104] R.T. Compton, *Adaptive antennas: concepts and performance*. Englewood Cliffs (NJ): Prentice-Hall, 1988.

[105] L.C. Godara, "Applications of antenna arrays to mobile communications I: Performance improvement, feasibility and system considerations," *Proceedings of the IEEE*, vol. 85, pp. 1031–1060, July 1997.

[106] L.C. Godara, "Application of antenna arrays to mobile communications II: Beam-forming and direction-of-arrival considerations," *Proceedings of the IEEE*, vol. 85, pp. 1195–1245, August 1997.

[107] M. Chryssomallis, "Smart antennas," *IEEE Antennas and Propagation Magazine*, vol. 42, pp. 129–136, June 2000.

[108] V. Tarokh, A. Naguib, N. Seshadri and A.R. Calderbank, "Combined array processing and space-time coding," *IEEE Transactions on Information Theory*, vol. 45, no. 4, pp. 1121–1128, 1999.

[109] M. Tao and R.S. Cheng, "Generalized layered space-time codes for high data rate wireless communications," *IEEE Transactions on Wireless Communications*, vol. 3, no. 4, pp. 1067–1075, 2004.

[110] A.F. Naguib, N. Seshadri and A.R. Calderbank, "Applications of space-time block codes and interference suppression for high capacity and high data rate wireless systems," in *Conference Record of the Thirty-Second Asilomar Conference on Signals, Systems and Computers*, vol. 2, (Pacific Grove, CA), pp. 1803–1810, 1998.

[111] H. Huang and H. Viswanathan, "Multiple antennas and multiuser detection in high data rate CDMA systems," in *IEEE 51st Vehicular Technology Conference Proceedings*, vol. 1, (Tokyo), pp. 556–560, May 2000.

[112] A. Stamoulis, N. Al-Dhahir and A. Calderbank, "Further results on interference cancellation and space-time block codes," in *Conference Record of the Thirty-Fifth Asilomar Conference on Signals, Systems and Computers*, vol. 1, (Pacific Grove, CA), pp. 257–261, November 2001.

[113] E.N. Onggosanusi, A.G. Dabak and T.A. Schmidl, "High rate space-time block coded scheme: performance and improvement in correlated fading channels," in *IEEE Wireless Communications and Networking Conference*, vol. 1, pp. 194–199, March 2002.

[114] G. Jongren, M. Skoglund and B. Ottersten, "Combining beamforming and orthogonal space-time block coding," *IEEE Transactions on Information Theory*, vol. 48, pp. 611–627, March 2002.

[115] H. Huang, H. Viswanathan and G.J. Foschini, "Multiple antennas in cellular CDMA systems: transmission, detection and spectral efficiency," *IEEE Transactions on Wireless Communications*, vol. 1, pp. 383–392, July 2002.

[116] R.A. Soni, R.M. Buehrer and R.D. Benning, "Intelligent antenna system for CDMA2000," *IEEE Signal Processing Magazine*, vol. 19, pp. 54–67, July 2002.

[117] J. Liu and E. Gunawan, "Combining ideal beamforming and Alamouti space-time block codes," *Electronics Letters*, vol. 39, pp. 1258–1259, August 2003.

[118] F. Zhu and M.S. Lim, "Combined beamforming with space-time block coding using double antenna array group," *Electronics Letters*, vol. 40, pp. 811–813, June 2004.

[119] L. Zhao and V.K. Dubey, "Detection schemes for space-time block code and spatial multiplexing combined system," *IEEE Communications Letters*, vol. 9, pp. 49–51, January 2005.

[120] H. Lee, E.J. Powers and J. Kang, "Low-complexity ZF detector for D-STTD systems in time-selective fading channels," in *IEEE 62nd Vehicular Technology Conference*, vol. 3, pp. 2043–2047, September 2005.

[121] M. Sellathurai, T. Ratnarajah and P. Guinand, "Multirate layered space-time coding and successive interference cancellation receivers in quasi-static fading channels," *IEEE Transactions on Wireless Communications*, vol. 6, pp. 4524–4533, December 2007.

[122] S. Ekbatani and H. Jafarkhani, "Combining beamforming and space-time coding using quantized feedback," *IEEE Transactions on Wireless Communications*, vol. 7, pp. 898–908, March 2008.

[123] A.F. Naguib, N. Seshadri and A.R. Calderbank, "Increasing data rate over wireless channels," *IEEE Signal Processing Magazine*, vol. 17, pp. 76–92, May 2000.

[124] N. Al-Dhahir, C. Fragouli, A. Stamoulis, W. Younis and R. Calderbank, "Space-time processing for broadband wireless access," *IEEE Communications Magazine*, vol. 40, pp. 136–142, September 2002.

[125] W. Meng, L. Gu and C. Li, "The combined beamforming and space-time block coding technique for downlink transmission," in *International Conference on Wireless Networks, Communications and Mobile Computing*, vol. 1, pp. 481–486, June 2005.

[126] K.-H. Li and M.A. Ingram, "Space-time block-coded OFDM systems with RF beamformers for high-speed indoor wireless communications," *IEEE Transactions on Communications*, vol. 50, pp. 1899–1901, December 2002.

[127] R. Negi, A.M. Tehrani and J.M. Cioffi, "Adaptive antennas for space-time codes in outdoor channels," *IEEE Transactions on Communications*, vol. 50, pp. 1918–1925, December 2002.

[128] R. Nabar, H. Bolcskei and A.J. Paulraj, "Transmit optimization for spatial multiplexing in the presence of spatial fading correlation," in *IEEE Global Telecommunications Conference (GLOBECOM)*, vol. 1, (San Antonio, TX), pp. 131–135, November 2001.

[129] Z. Hong, K. Liu, R.W. Jr. Heath and A.M. Sayeed, "Spatial multiplexing in correlated fading via the virtual channel representation," *IEEE Journal on Selected Areas in Communications*, vol. 21, pp. 856–866, June 2003.

[130] H. Kim and J. Chun, "MIMO structure which combines the spatial multiplexing and beamforming," in *IEEE Vehicular Technology Conference*, vol. 1, pp. 108–112, May 2004.

[131] E.C. Van der Meulen, "Three-terminal communication channels," *Advanced Applied Probability*, vol. 3, no. 1, pp. 120–154, 1971.

[132] T. Cover and A. El Gamal, "Capacity theorems for the relay channel," *IEEE Transactions on Information Theory*, vol. 25, no. 5, pp. 572–584, 1979.

[133] F. Willems, "The discrete memoryless multiple access channel with partially cooperating encoders," *IEEE Transactions on Information Theory*, vol. 29, no. 3, pp. 441–445, 1983.

[134] A. Sendonaris and E. Erkip and B. Aazhang, "Increasing uplink capacity via user cooperation diversity," in *IEEE International Symposium on Information Theory*, (Cambridge, MA), August 1998.

[135] J.N. Laneman, G.W. Wornell and D.N.C. Tse, "An efficient protocol for realizing cooperative diversity in wireless networks," in *IEEE International Symposium on Information Theory*, (Washington, DC), 2001.

[136] T.E. Hunter and A. Nosratinia, "Cooperation diversity through coding," in *IEEE International Symposium on Information Theory*, 2002.

[137] M. Dohler, E. Lefranc and H. Aghvami, "Space-time block codes for virtual antenna arrays," in *The 13th IEEE International Symposium on Personal, Indoor and Mobile Radio Communications*, vol. 1, pp. 414–417, September 2002.

[138] J.N. Laneman and G.W. Wornell, "Distributed space-time-coded protocols for exploiting cooperative diversity in wireless networks," *IEEE Transactions on Information Theory*, vol. 49, no. 10, pp. 2415–2425, 2003.

[139] M.C. Valenti and B. Zhao, "Distributed turbo codes: towards the capacity of the relay channel," in *IEEE Vehicular Technology Conference VTC-Fall*, vol. 1, pp. 322–326, October 2003.

[140] B. Zhao and M.C. Valenti, "Distributed turbo coded diversity for relay channel," *Electronics Letters*, vol. 39, pp. 786–787, May 2003.

[141] J.N. Laneman, D.N. Tse and G.W. Wornell, "Cooperative diversity in wireless networks: Efficient protocols and outage behavior," *IEEE Transactions on Information Theory*, vol. 50, pp. 3062–3080, December 2004.

[142] R.U. Nabar, H. Bolcskei and F.W. Kneubuhler, "Fading relay channels: performance limits and space-time signal design," *IEEE Journal on Selected Areas in Communications*, vol. 22, pp. 1099–1109, August 2004.

[143] M. Janani, A. Hedayat, T. Hunter and A. Nosratinia, "Coded cooperation in wireless communications: space-time transmission and iterative decoding," *IEEE Transactions on Signal Processing*, vol. 52, pp. 362–371, February 2004.

[144] A. Stefanov and E. Erkip, "Cooperative coding for wireless networks," *IEEE Transactions on Communications*, vol. 52, pp. 1470–1476, September 2004.

[145] K. Azarian, H. El Gamal and P. Schniter, "On the achievable diversity-multiplexing tradeoff in half-duplex cooperative channels," *IEEE Transactions on Information Theory*, vol. 51, pp. 4152–4172, December 2005.

[146] H. Sneessens and L. Vandendorpe, "Soft decode and forward improves cooperative communications," in *6th IEE International Conference on 3G and Beyond*, (Washington, DC), pp. 1–4, November 2005.

[147] R. Hu and J. Li, "Exploiting Slepian-Wolf codes in wireless user cooperation," in *IEEE 6th Workshop on Signal Processing Advances in Wireless Communications*, pp. 275–279, June 2005.

[148] M. Yu and J. Li, "Is amplify-and-forward practically better than decode-and-forward or vice versa?," in *IEEE International Conference on Acoustics, Speech and Signal Processing*, vol. 3, March 2005.

[149] T.E. Hunter and A. Nosratinia, "Diversity through coded cooperation," *IEEE Transactions on Wireless Communications*, vol. 5, pp. 283–289, February 2006.

[150] T.E. Hunter, S. Sanayei and A. Nosratinia, "Outage analysis of coded cooperation," *IEEE Transactions on Information Theory*, vol. 52, pp. 375–391, February 2006.

[151] Y. Li, B. Vucetic, T.F. Wong and M. Dohler, "Distributed turbo coding with soft information relaying in multihop relay networks," *IEEE Journal on Selected Areas in Communications*, vol. 24, pp. 2040–2050, November 2006.

[152] R. Hu and J. Li, "Practical compress-forward in user cooperation: Wyner-Ziv Cooperation," in *IEEE International Symposium on Information Theory*, (Seattle, WA), pp. 489–493, July 2006.

[153] A. Host-Madsen, "Capacity bounds for cooperative diversity," *IEEE Transactions on Information Theory*, vol. 52, pp. 1522–1544, April 2006.

[154] T. Bui and J. Yuan, "A decode and forward cooperation scheme with soft relaying in wireless communication," in *IEEE 8th Workshop on Signal Processing Advances in Wireless Communications (SPAWC)*, (Helsinki), pp. 1–5, June 2007.

[155] M.N. Khormuji and E.G. Larsson, "Improving collaborative transmit diversity by using constellation rearrangement," in *IEEE Wireless Communications and Networking Conference*, (Kowloon), pp. 803–807, March 2007.

[156] X. Bao and J. Li, "Efficient message relaying for wireless user cooperation: Decode-Amplify-Forward (DAF) and Hybrid DAF and coded-cooperation," *IEEE Transactions on Wireless Communications*, vol. 6, pp. 3975–3984, November 2007.

[157] L. Xiao, T. Fuja, J. Kliewer and D. Costello, "A network coding approach to cooperative diversity," *IEEE Transactions on Information Theory*, vol. 53, pp. 3714–3722, October 2007.

[158] G. Yue, X. Wang, Z. Yang and A. Host-Madsen, "Coding schemes for user cooperation in low-power regimes," *IEEE Transactions on Signal Processing*, vol. 56, pp. 2035–2049, May 2008.

[159] W. Zhang, Y. Li, X.-G. Xia, P.C. Ching and K. Ben Letaief, "Distributed space-frequency coding for cooperative diversity in broadband wireless Ad Hoc networks," *IEEE Transactions on Wireless Communications*, vol. 7, pp. 995–1003, March 2008.

[160] T. Wang and G.B. Giannakis, "Complex field network coding for multiuser cooperative communications," *IEEE Journal on Selected Areas in Communications*, vol. 26, pp. 561–571, April 2008.

[161] P. Mitran, H. Ochiai and V. Tarokh, "Space-time diversity enhancements using collaborative communications," *IEEE Transactions on Information Theory*, vol. 51, pp. 2041–2057, June 2005.

[162] G. Forney, *Concatenated codes*. Cambridge: MIT Press, 1966.

[163] C. Berrou, A. Glavieux and P. Thitimajshima, "Near Shannon limit error-correcting coding and decoding: Turbo-codes. 1," in *IEEE International Conference on Communications*, vol. 2, (Geneva), pp. 1064–1070, May 1993.

[164] D. Divsalar and F. Pollara, "Multiple turbo codes for deep-space communications," Telecommunications and Data Acquisition Progress Report 42-121, Jet Propulsion Laboratory, Pasadena, CA, May 1995.

[165] S. Benedetto and G. Montorsi, "Iterative decoding of serially concatenated convolutional codes," *Electronics Letters*, vol. 32, pp. 1186–1188, June 1996.

[166] S. Benedetto, D. Divsalar, G. Montorsi and F. Pollara, "Analysis, design and iterative decoding of double serially concatenated codes with interleavers," *IEEE Journal on Selected Areas in Communications*, vol. 16, pp. 231–244, February 1998.

[167] D. Raphaeli and Y. Zarai, "Combined turbo equalization and turbo decoding," in *Proceedings of IEEE Global Telecommunications Conference (GLOBECOM)*, vol. 2, (Phoenix, AZ), pp. 639–643, November 1997.

[168] D. Raphaeli and Y. Zarai, "Combined turbo equalization and turbo decoding," *IEEE Communications Letters*, vol. 2, pp. 107–109, April 1998.

[169] M. Toegel, W. Pusch and H. Weinrichter, "Combined serially concatenated codes and turbo-equalization," in *2nd International Symposium on Turbo Codes*, (Brest, France), pp. 375–378, September 2000.

[170] R. Ramamurthy and W.E. Ryan, "Convolutional double accumulate codes (or double turbo DPSK)," *IEEE Communications Letters*, vol. 5, pp. 157–159, April 2001.

[171] C. Douillard, M. Jezequel, C. Berrou, A. Picart, P. Didier and A. Glavieux, "Iterative correction of intersymbol interference: turbo equalization," *European Transaction on Telecommunications*, vol. 6, pp. 507–511, September/October 1995.

[172] S. Benedetto, D. Divsalar, G. Montorsi and F. Pollara, "A soft-input soft-output APP module for iterative decoding of concatenated codes," *IEEE Communications Letters*, vol. 1, pp. 22–24, January 1997.

[173] G. Caire, G. Taricco and E. Biglieri, "Bit-interleaved coded modulation," in *Proceedings of IEEE International Symposium on Information Theory (ISIT)*, (Ulm, Germany), p. 96, June/July 1997.

[174] G. Caire, G. Taricco and E. Biglieri, "Bit-interleaved coded modulation," *IEEE Transactions on Information Theory*, vol. 44, pp. 927–946, May 1998.

[175] S. ten Brink, J. Speidel and R.-H. Yan, "Iterative demapping and decoding for multi-level modulation," in *IEEE Global Telecommunications Conference (GLOBCOM)*, vol. 1, (Sydney,NSW), pp. 579–584, 1998.

[176] X. Li and J. A. Ritcey, "Bit-interleaved coded modulation with iterative decoding," *IEEE Communications Letters*, vol. 1, pp. 169–171, November 1997.

[177] X. Li and J. A. Ritcey, "Bit-interleaved coded modulation with iterative decoding using soft feedback," *IEE Electronics Letters*, vol. 34, pp. 942–943, May 1998.

[178] X. Li and J. A. Ritcey, "Trellis-coded modulation with bit interleaving and iterative decoding," *IEEE Journal on Selected Areas in Communications*, vol. 17, pp. 715–724, April 1999.

[179] X. Wang and H. V. Poor, "Iterative (turbo) soft interference cancellation and decoding for coded CDMA," *IEEE Transactions on Communications*, vol. 47, pp. 1046–1061, July 1999.

[180] A. Sezgin, D. Wuebben and V. Kuehn, "Analysis of mapping strategies for turbo-coded space-time block codes," in *Proceedings of IEEE Information Theory Workshop*, (Paris, France), pp. 103–106, March/April 2003.

[181] L. Bahl, J. Cocke, F. Jelinek and J. Raviv, "Optimal decoding of linear codes for minimizing symbol error rate," *IEEE Transactions on Information Theory*, vol. 20, no. 2, pp. 284–287, 1974.

[182] P. Robertson, E. Villebrun and P. Hoeher, "A comparison of optimal and sub-optimal MAP decoding algorithms operating in the Log domain," in *Proceedings of International Conference on Communications*, (Seattle, USA), pp. 1009–1013, June 1995.

[183] S. Benedetto, D. Divsalar, G. Montorsi and F. Pollara, "Serial concatenation of interleaved codes: performance analysis, design and iterative decoding," *IEEE Transactions on Information Theory*, vol. 44, pp. 909–926, May 1998.

[184] D. Divsalar, S. Dolinar and F. Pollara, "Low complexity turbo-like codes," in *2nd International Symposium on Turbo Codes and Related Topics*, (Brest, France), pp. 73–80, September 2000.

[185] D. Divsalar, S. Dolinar and F. Pollara, "Serial concatenated trellis coded modulation with rate-1 inner code," in *IEEE Global Telecommunications Conference (GLOBECOM)*, vol. 2, (San Francisco, CA), pp. 777–782, 2000.

[186] S. ten Brink, "Designing iterative decoding schemes with the extrinsic information transfer chart," *AEÜ International Journal of Electronics and Communications*, vol. 54, pp. 389–398, November 2000.

[187] I. Lee, "The effect of a precoder on serially concatenated coding systems with an ISI channel," *IEEE Transactions on Communications*, vol. 49, pp. 1168–1175, July 2001.

[188] S. ten Brink, "Convergence of multidimensional iterative decoding schemes," in *Conference Record of the Thirty-Fifth Asilomar Conference on Signals, Systems and Computers*, vol. 1, (Pacific Grove, CA, USA), pp. 270–274, 2001.

[189] S. ten Brink, "Convergence behavior of iteratively decoded parallel concatenated codes," *IEEE Transactions on Communications*, vol. 49, no. 10, pp. 1727–1737, 2001.

[190] H. El Gamal and A.R. Hammons, "Analyzing the turbo decoder using the Gaussian approximation," *IEEE Journal on Selected Areas in Communications*, vol. 47, pp. 671–686, February 2001.

[191] M. Tüchler and J. Hagenauer, "EXIT charts of irregular codes," in *Conference on Information Science and Systems*, (Princtone, NJ), pp. 748–753, March 2002.

[192] M. Tüchler, S. ten Brink and J. Hagenauer, "Measures for tracing convergence of iterative decoding algorithms," in *Proceedings of the 4th International ITG Conference on Source and Channel Coding*, (Berlin, Germany), pp. 53–60, January 2002.

[193] M. Tüchler, "Convergence prediction for iterative decoding of threefold concatenated systems," in *IEEE Global Telecommunications Conference (GLOBECOM)*, vol. 2, pp. 1358–1362, November 2002.

[194] M. Tüchler, "Design of serially concatenated systems depending on the block length," *IEEE Transactions on Communications*, vol. 52, no. 2, pp. 209–218, 2004.

[195] L. Lifang, D. Divsalar and S. Dolinar, "Iterative demodulation, demapping and decoding of coded non-square QAM," in *IEEE Transactions on Communications*, vol. 53, pp. 16–19, January 2005.

[196] F. Brännström, L.K. Rasmussen and A.J. Grant, "Convergence analysis and optimal scheduling for multiple concatenated codes," *IEEE Transactions on Information Theory*, vol. 51, no. 9, pp. 3354–3364, 2005.

[197] R.G. Maunder, J. Wang, S.X. Ng, L.-L. Yang and L. Hanzo, "On the performance and complexity of irregular variable length codes for near-capacity joint source and channel coding," *IEEE Transactions on Wireless Communications*, vol. 7, pp. 1338–1347, April 2008.

[198] S. Benedetto, D. Divsalar, G. Montorsi and F. Pollara, "Serial concatenation of interleaved codes: performance analysis, design and iterative decoding," *IEEE Transactions on Information Theory*, vol. 44, pp. 909–926, May 1998.

[199] K.R. Narayanan, "Effect of precoding on the convergence of turbo equalization for partial response channels," *IEEE Journal on Selected Areas in Communications*, vol. 19, pp. 686–698, April 2001.

[200] J. Hagenauer, "The EXIT chart - Introduction to extrinsic information transfer in iterative processing," in *European Signal Processing Conference*, (Vienna, Austria), pp. 1541–1548, September 2004.

[201] J. Kliewer, S.X. Ng and L. Hanzo, "Efficient computation of EXIT functions for nonbinary iterative decoding," *IEEE Transactions on Communications*, vol. 54, pp. 2133–2136, December 2006.

[202] J. Liu, J. Li and E.G. Larsson, "Differential space-time block code modulation for DS-CDMA systems," *EURASIP Journal on Applied Signal Processing*, vol. 3, pp. 289–296, 2002.

[203] N. Seshadri, V. Tarokh and A.R. Calderbank, "Space-time codes for wireless communication: code construction," in *IEEE Vehicular Technology Conference*, vol. 2, (Phoenix, AZ), pp. 637–641, 1997.

[204] B.M. Hochwald, G. Caire, B. Hassibi and T.L. Marzetta, "The academic and industrial embrace of space-time methods," in *IEEE Transactions on Information Theory*, vol. 49, pp. 2329–2331, October 2003.

[205] B.M. Hochwald, G. Caire, B. Hassibi and T.L. Marzetta, "Special Issue on Space-Time Transmission, Reception, Coding and Signal Processing," *IEEE Transactions on Information Theory*, pp. 2329–2806, October 2003.

[206] G. Ganesan and P. Stoica, "Utilizing space-time diversity for wireless communications," *Wireless Personal Communications*, vol. 18, pp. 149–163, 2001.

[207] G. Ganesan and P. Stoica, "Space-time diversity using orthogonal and amicable orthogonal designs," *Wireless Personal Communications*, vol. 18, pp. 165–178, 2001.

[208] G. Ganesan, P. Stoica and E. Larsson, "Orthogonal space-time block codes with feedback," *Wireless Personal Communications*, vol. 28, pp. 287–312, 2004.

[209] L. Hanzo, M. Münster, B.J. Choi and T. Keller, *OFDM and MC-CDMA for broadband multi-user communications, WLANs and broadcasting*. Chichester, UK: Wiley, 2003.

[210] O. Alamri, *Turbo detection of sphere packing modulation aided space-time coding schemes*. PhD thesis, School of Electronics and Computer Science, University of Southampton, September 2006.

[211] O. Alamri, B.L. Yeap and L. Hanzo, "Turbo detection of channel-coded space-time signals using sphere packing modulation," in *Prodeedings of IEEE Vehicular Technology Conference*, vol. 4, (Los Angeles, USA), pp. 2498–2502, September 2004.

[212] A. Shokrollahi, B. Hassibi, B.M. Hochwald and W. Sweldens, "Representaion theory for high-rate multiple-antenna code design," *IEEE Transactions on Information theory*, vol. 47, pp. 2335–2367, September 2001.

[213] J.H. Conway and N.J. Sloane, *Sphere packings, lattices and groups*. Springer-Verlag, 1999.

[214] C. E. Shannon, "A mathematical theory of communication," *Bell Systems Technical Journal*, vol. 27, pp. 379–423, July 1948.

[215] S.X. Ng and L. Hanzo, "On the MIMO channel capacity of multidimensional signal sets," *IEEE Transactions on Vehicular Technology*, vol. 55, no. 2, pp. 528–536, 2006.

[216] H. Shin and J.H. Lee, "Capacity of multiple-antenna fading channels: spatial fading correlation, double scattering and keyhole," *IEEE Transactions on Information Theory*, vol. 49, no. 10, pp. 2636–2647, 2003.

[217] R. Gallager, *Information theory and reliable communication*. New York: Wiley, 1968.

[218] J.M. Wozencraft and I. M. Jacobs, *Pinciples of communication engineering*. John Wiley & Sons, NY, USA, 1965.

[219] P.E. McIllree, "Channel capacity calculations for M-ary N-dimensional signal sets." M.S. thesis, School of Electronic Engineering, University of South Australia, Adelaide, Australia, 1995.

[220] T.J. Richardson and R. Urbanke, "The capacity of low-density parity-check codes under message-passing decoding," *IEEE Transactions on Information Theory*, vol. 47, pp. 599–618, February 2001.

[221] T.J. Richardson, A. Shokrollahi and R. Urbanke, "Design of capacity-approaching low-density parity-check codes," *IEEE Transactions on Information Theory*, vol. 47, pp. 619–637, February 2001.

[222] S.Y. Chung, G.D. Forney, T.J. Richardson and R. Urbanke, "On the design of low-density parity-check codes within 0.0045 dB of the Shannon limit," *IEEE Communication Letter*, vol. 5, pp. 58–60, February 2001.

[223] M. Peleg, I. Sason, S. Shamai and A. Elia, "On interleaved differentially encoded convolutional codes," *IEEE Transactions on Information Theory*, vol. 45, pp. 2572–2582, November 1999.

[224] S. ten Brink, J. Speidel and R.-H. Han, "Iterative demapping for QPSK modulation," *Electronics Letters*, vol. 34, no. 15, pp. 1459–1460, 1998.

[225] V.B. Balakirsky, "Joint source-channel coding with variable length codes," in *IEEE International Symposium on Information Theory*, (Ulm, Germany), p. 419 , June 1997.

[226] J. Hagenauer, E. Offer and L. Papke, "Iterative decoding of binary block and convolutional codes," *IEEE Transactions on Information Theory*, vol. 42, no. 2, pp. 429–445, 1996.

[227] S. Benedetto, G. Montorsi, "Serial concatenation of block and convolutional codes," *Electronics Letters*, vol. 32, pp. 887–888, May 1996.

[228] T.M. Cover and J.A. Thomas, *Elements of information theory.* New York: Wiley, 1991.

[229] A. Ashikhmin, G. Kramer and S. ten Brink, "Extrinsic information transfer functions: model and erasure channel properties," *IEEE Transactions on Information Theory*, vol. 50, no. 11, pp. 2657–2673, 2004.

[230] L. Hanzo, F.C. Somerville and J. P. Woodard, *Voice compression and communications: Principles and applications for fixed wireless channels.* IEEE Press-John Wiley & Sons, 2001.

[231] L. Hanzo, P.J. Cherriman and J. Streit, *Wireless video communications: second to third generation and beyond.* IEEE Press-John Wiley & Sons, 2001.

[232] T. Fingscheidt and P. Vary, "Speech decoding with error concealment using residual source redundancy," *IEEE Workshop on Speech Coding for Telecommunication*, pp. 91–92, September 1997.

[233] T. Fingscheidt and P. Vary, "Softbit speech decoding: A new approach to error concealment," *IEEE Transactions on Speech and Audio Processing*, vol. 9, pp. 240–251, March 2001.

[234] M. Adrat, P. Vary and J. Spittka, "Iterative source-channel decoder using extrinsic information from softbit-source decoding," *IEEE International Conference on Acoustics, Speech and Signal Processing*, pp. 2653–2656, May 2001.

[235] T. Clevorn, J. Brauers, M. Adrat and P. Vary, "Turbo decodulation: Iterative combined demodulation and source-channel decoding," *IEEE Communications Letters*, vol. 9, pp. 820–822, September 2005.

[236] B. Bessette, R. Salami, R. Lefebvre, M. Jelinek, J. Rotola-Pukkila, J. Vainio, H. Mikkola, K. Jarvinen, "The adaptive multirate wideband speech codec (AMR-WB)," *IEEE Transactions on Speech and Audio Processing*, vol. 10, pp. 620–636, November 2002.

[237] T. Hindelang, T. Fingscheidt, N. Seshadri and R.V. Cox, "Combined source/channel (de-)coding: can a priori information be used twice?," *IEEE International Conference on Communications*, pp. 1208–1212, June 2000.

[238] S. Lloyd, "Least squares quantization in PCM," *IEEE Transaction on Information Theory*, vol. 28, pp. 129–137, March 1982.

[239] V. Buttigieg and P.G. Farrell, "Variable-length error-correcting codes," *IEE Proceedings-Communications*, vol. 147, pp. 211–215, August 2000.

[240] N. Dimitriou, R. Tafazolli and G. Sfikas, "Quality of service for multimedia CDMA," *IEEE Communications Magazine*, vol. 38, pp. 88–94, July 2000.

[241] K.S. Gilhousen, I.M. Jacobs, R. Padovani, A.J. Viterbi, L.A. Jr. Weaver and C.E. Wheatley, "On the capacity of a cellular CDMA system," *IEEE Transactions on Vehicular Technology*, vol. 40, pp. 303–312, May 1991.

[242] L. Hanzo, C.H. Wong and M.S. Yee, *Adaptive wireless transceivers: turbo-coded, turbo-equalized and space-time coded TDMA, CDMA and OFDM systems*. Chichester, UK: John Wiley and Sons, 2002.

[243] P.A. Bello, "Sample size required in error-rate measurement on fading channels," *Proceedings of the IEEE*, vol. 86, pp. 1435–1441, July 1998.

[244] L.-L. Yang and L. Hanzo, "Adaptive space-time-spreading-assisted wideband CDMA systems communicating over dispersive Nakagami-m fading channels," *EURASIP Journal on Wireless Communications and Networking*, vol. 2, pp. 216–230, April 2005.

[245] W.T. Webb and R. Steele, "Variable rate QAM for mobile radio," *IEEE Transactions on Communications*, vol. 43, no. 7, pp. 2223–2230, 1995.

[246] A.J. Goldsmith and S.-G. Chua, "Variable-rate variable-power MQAM for fading channels," *IEEE Transactions on Communications*, vol. 45, pp. 1218–1230, 1997.

[247] J. Hayes, "Adaptive feedback communications," *IEEE Transactions on Communications*, vol. 16, pp. 29–34, 1968.

[248] J. Cavers, "Variable-rate transmission for Rayleigh fading channels," *IEEE Transactions on Communications*, vol. 20, no. 1, pp. 15–22, 1972.

[249] B.-J. Choi and L. Hanzo, "Optimum mode-switching-assisted constant-power single- and multi-carrier adaptive modulation," *IEEE Transactions on Vehicular Technology*, vol. 52, no. 3, pp. 536–560, 2003.

[250] L.-L. Yang and L. Hanzo, "Adaptive rate DS-CDMA systems using variable spreading factors," *IEEE Transactions on Vehicular Technology*, vol. 53, no. 1, pp. 72–81, 2004.

[251] T. Ottosson and A. Svensson, "On schemes for multirate support in DS-CDMA systems," *Wireless Personal Communications, Kluwer Academic Publisher*, vol. 6, pp. 265–287, March 1998.

[252] T. Ojanpera and R. Prasad, *Wideband CDMA for third generation mobile communications*. Artech House Publishers, 1998.

[253] S.W. Kim, "Adaptive rate and power DS-CDMA communications in fading channels," *IEEE Communications Letters*, vol. 3, pp. 85–87, April 1999.

[254] S. Abeta, S. Sampei and N. Morinaga, "Channel activation with adaptive coding rate and processing gain control for cellular DS-CDMA systems," in *IEEE 46th Vehicular Technology Conference*, vol. 2, (Atlanta, GA), pp. 1115–1119, April/May 1996.

[255] A. Ashikhmin, G. Kramer and S. ten Brink, "Extrinsic information transfer functions: A model and two properties," in *36th Annual Conference on Information Sciences and Systems (CISS)*, (Princeton, NJ, USA), March 2002.

[256] G. Ungerboeck, "Channel coding with multilevel/phase signals," *IEEE Transactions on Information Theory*, vol. 28, no. 1, pp. 55–67, 1982.

[257] L. Linnan, K. Jingming and F. Zesong, "Combining Eigen-beamforming and space-time block coding with equal power allocation," in *International Conference on Communication Technology (ICCT)*, (Guilin, China), pp. 1–4, November 2006.

[258] L. Hanzo and T. Keller, *OFDM and MC-CDMA: A Primer*. IEEE Press-John Wiley & Sons, April 2006.

[259] L.-L. Yang and L. Hanzo, "Performance of generalized multicarrier DS-CDMA over Nakagami-m fading channels," *IEEE Transactions on Communications*, vol. 50, pp. 956–966, June 2002.

[260] L. Vandendorpe, "Multitone spread spectrum multiple access communications system in a multipath Rician fading channel," *IEEE Transactions on Vehicular Technology*, vol. 44, pp. 327–337, May 1995.

[261] E.A. Sourour and M. Nakagawa, "Performance of orthogonal multicarrier CDMA in a multipath fading channel," *IEEE Transactions on Communications*, vol. 44, pp. 356–367, March 1996.

[262] Bin Hu, *Multicarrier DS-CDMA communication systems using smart antennas*. PhD thesis, School of Electronics and Computer Science, University of Southampton, April 2006.

[263] C.W. You and D.S. Hong, "Multicarrier CDMA systems using time-domain and frequency-domain spreading codes," *IEEE Transactions on Communications*, vol. 51, pp. 17–21, January 2003.

[264] X. Gui and T.S. Ng, "Performance of asynchronous orthogonal multicarrier CDMA system in frequency selective fading channel," *IEEE Transactions on Communications*, vol. 47, pp. 1084–1091, July 1999.

[265] S. Hara and R. Prasad, "Overview of multicarrier CDMA," *IEEE Communications Magazine*, vol. 35, pp. 126–133, December 1997.

[266] L.-L. Yang and L. Hanzo, "Performance of broadband multicarrier DS-CDMA using space-time spreading-assisted transmit diversity," *IEEE Transactions on Wireless Communications*, vol. 4, no. 3, pp. 885–894, 2005.

[267] S. ten Brink, "Convergence of iterative decoding," *Electronics Letters*, vol. 35, no. 13, pp. 1117–1119, 1999.

[268] G. Scutari and S. Barbarossa, "Distributed space-time coding for regenerative relay networks," *IEEE Transactions on Wireless Communications*, vol. 4, pp. 2387–2399, September 2005.

[269] A. Nosratinia, T.E. Hunter and A. Hedayat, "Cooperative communication in wireless networks," *IEEE Communications Magazine*, vol. 42, no. 10, pp. 74–80, 2004.

[270] Y. Jing and B. Hassibi, "Wireless networks, diversity and space-time codes," in *IEEE Information Theory Workshop*, pp. 463–468, October 2004.

[271] C. Berrou, A. Glavieux, "Near optimum error correcting coding and decoding: turbo-codes," *IEEE Transactions on Communications*, vol. 44, pp. 1261–1271, October 1996.

Index

W

Z

Author Index

C

D

E

F

G

H

I

J

K

L

M

N

O

T